frontiers | Research Topics

Novel mechanisms involved in aging and neurodegeneration: Seeking potential therapeutic targets for neurodegenerative diseases.

Edited by
Natalia Salvadores, Yasmina Manso, Claudio Soto and Mario Sanhueza

Published in
Frontiers in Aging Neuroscience

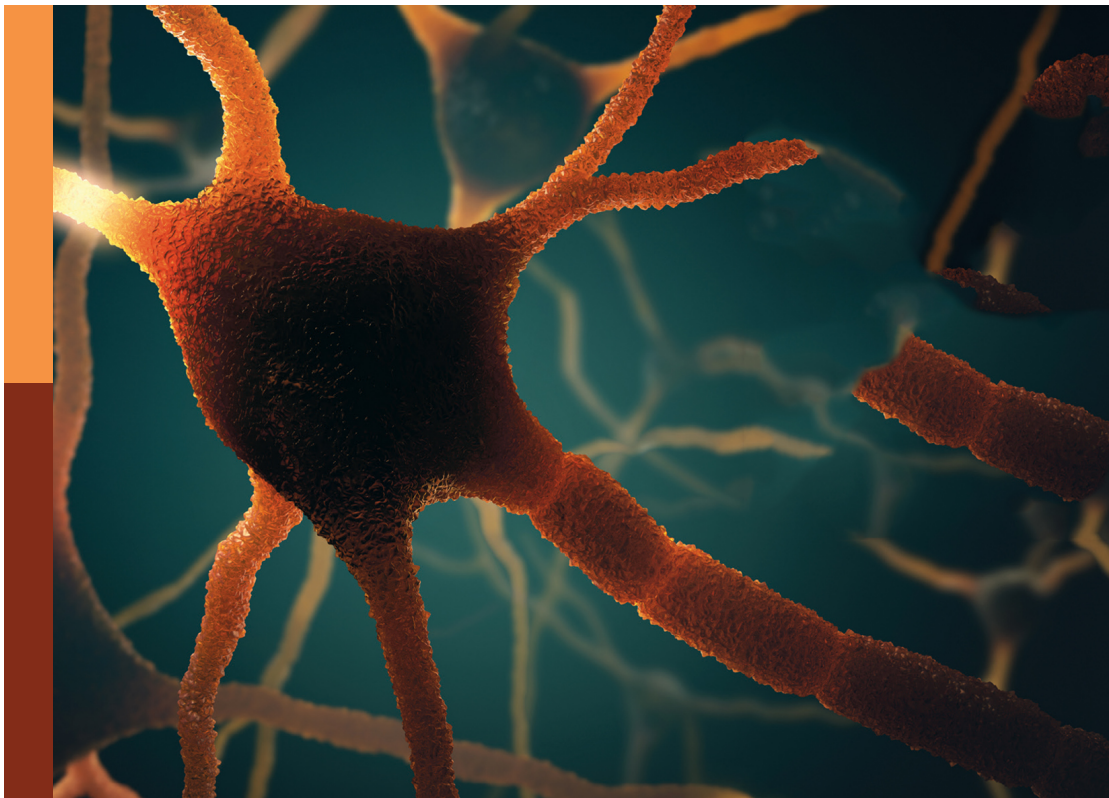

ISSN 1664-8714
ISBN 978-2-83251-126-8
DOI 10.3389/978-2-83251-126-8

About Frontiers

Frontiers is more than just an open access publisher of scholarly articles: it is a pioneering approach to the world of academia, radically improving the way scholarly research is managed. The grand vision of Frontiers is a world where all people have an equal opportunity to seek, share and generate knowledge. Frontiers provides immediate and permanent online open access to all its publications, but this alone is not enough to realize our grand goals.

Frontiers journal series

The Frontiers journal series is a multi-tier and interdisciplinary set of open-access, online journals, promising a paradigm shift from the current review, selection and dissemination processes in academic publishing. All Frontiers journals are driven by researchers for researchers; therefore, they constitute a service to the scholarly community. At the same time, the *Frontiers journal series* operates on a revolutionary invention, the tiered publishing system, initially addressing specific communities of scholars, and gradually climbing up to broader public understanding, thus serving the interests of the lay society, too.

Dedication to quality

Each Frontiers article is a landmark of the highest quality, thanks to genuinely collaborative interactions between authors and review editors, who include some of the world's best academicians. Research must be certified by peers before entering a stream of knowledge that may eventually reach the public - and shape society; therefore, Frontiers only applies the most rigorous and unbiased reviews. Frontiers revolutionizes research publishing by freely delivering the most outstanding research, evaluated with no bias from both the academic and social point of view. By applying the most advanced information technologies, Frontiers is catapulting scholarly publishing into a new generation.

What are Frontiers Research Topics?

Frontiers Research Topics are very popular trademarks of the *Frontiers journals series*: they are collections of at least ten articles, all centered on a particular subject. With their unique mix of varied contributions from Original Research to Review Articles, Frontiers Research Topics unify the most influential researchers, the latest key findings and historical advances in a hot research area.

Find out more on how to host your own Frontiers Research Topic or contribute to one as an author by contacting the Frontiers editorial office: frontiersin.org/about/contact

Novel mechanisms involved in aging and neurodegeneration: Seeking potential therapeutic targets for neurodegenerative diseases.

Topic editors

Natalia Salvadores — Universidad Mayor, Chile

Yasmina Manso — Center for Biomedical Research on Neurodegenerative Diseases (CIBERNED), Spain

Claudio Soto — University of Texas Health Science Center at Houston, United States

Mario Sanhueza — Major University, Chile

Citation

Salvadores, N., Manso, Y., Soto, C., Sanhueza, M., eds. (2023). *Novel mechanisms involved in aging and neurodegeneration: Seeking potential therapeutic targets for neurodegenerative diseases.*. Lausanne: Frontiers Media SA.

doi: 10.3389/978-2-83251-126-8

Table of contents

frontiers | Frontiers in Aging Neuroscience

TYPE Editorial
PUBLISHED 09 December 2022
DOI 10.3389/fnagi.2022.1104647

OPEN ACCESS

EDITED AND REVIEWED BY
Agustin Ibanez,
Latin American Brain Health Institute (BrainLat), Chile

*CORRESPONDENCE
Natalia Salvadores
natalia.salvadores@umayor.cl

SPECIALTY SECTION
This article was submitted to Alzheimer's Disease and Related Dementias, a section of the journal Frontiers in Aging Neuroscience

RECEIVED 21 November 2022
ACCEPTED 28 November 2022
PUBLISHED 09 December 2022

CITATION
Sanhueza M, Manso Y, Soto C and Salvadores N (2022) Editorial: Novel mechanisms involved in aging and neurodegeneration: Seeking potential therapeutic targets for neurodegenerative diseases. *Front. Aging Neurosci.* 14:1104647. doi: 10.3389/fnagi.2022.1104647

Editorial: Novel mechanisms involved in aging and neurodegeneration: Seeking potential therapeutic targets for neurodegenerative diseases

Mario Sanhueza[1], Yasmina Manso[2,3], Claudio Soto[4] and Natalia Salvadores[1]*

[1]Center for Resilience, Adaptation and Mitigation, Universidad Mayor, Temuco, Chile, [2]Department of Cell Biology, Physiology, and Immunology, Faculty of Biology, Institute of Neurosciences, Universitat de Barcelona, Barcelona, Spain, [3]Centro de Investigación Biomédica en Red Enfermedades Neurodegenerativas, Instituto de Salud Carlos III, Madrid, Spain, [4]Mitchell Center for Alzheimer's Disease, Department of Neurology, McGovern Medical School, The University of Texas Health Science Center at Houston, Houston, TX, United States

KEYWORDS

aging, neurodegeneration, therapeutic targets, protein aggregation, Alzheimer's disease, Parkinson's disease

Editorial on the Research Topic
Novel mechanisms involved in aging and neurodegeneration: Seeking potential therapeutic targets for neurodegenerative diseases

During the past decades, the world's demographics have changed considerably, with an aging global population that is expected to keep rising due to constant progress in biomedical research. Aging constitutes the main risk factor for chronic diseases including neurodegenerative conditions and therefore, the incidence of brain diseases associated with aging is growing, constituting a major health issue worldwide (GBD 2017 US Neurological Disorders Collaborators et al., 2021). Although neurodegenerative disorders have different clinical manifestations, several pathogenic processes are common to these diseases. These include cerebral accumulation of misfolded protein aggregates, inflammation, altered proteostasis, changes in response to cellular stress, altered intercellular communication, damage to the synaptic network, mitochondrial dyshomeostasis, and cellular senescence (Habib et al., 2018). This Research Topic comprises 12 articles, involving 98 authors across the globe, which describe new evidence connecting molecular, cellular, and physiological mechanisms with the development of neurodegenerative disorders.

Sleep disruption is a common feature in several neurodegenerative disorders (Mander et al., 2016). The orexinergic system is essential for sleep-wake state regulation, and dysregulation of this system is thought to contribute to neurodegenerative disease pathogenesis (Asai et al., 2009; Fatemi et al., 2016; Liguori, 2017). A comprehensive review by Wang et al. describes evidence for the role of the orexinergic system in Alzheimer's disease (AD), Parkinson's disease (PD), Huntington's

disease (HD), and multiple sclerosis (MS). The authors of this manuscript highlight the orexinergic system as a potential target for disease treatment.

AD represents the most common neurodegenerative disease (Alzheimer's Association, 2022). This devastating neurological condition has no cure yet, and many efforts are currently underway to identify novel targets for AD treatment. In this context, the N-methyl-D-aspartate (NMDA) receptor is a critical molecule for synaptic plasticity and cognitive function, both altered in AD. Using the APP/PS1 model of AD, Xu et al. found alterations in NMDA receptor function, paralleled by reduced expression of synaptic proteins, decreased dendritic complexity, and dendritic spine density. The authors conclude that these changes might underlie the electrophysiological and synaptic plasticity impairments observed in the hippocampus of this model, which may in turn lead to the age-related cognitive deficits observed. The presence of the APOEε4 and Trem2*R47H alleles, constitute two of the most powerful risk factors for late-onset AD (Cacace et al., 2016). Using a novel mouse model of AD expressing these genes, Kotredes et al. carried out a compelling characterization, identifying behavioral, transcriptomic, metabolic, and neuropathological alterations, including disruption of glycolytic metabolism and vascular perfusion in this new model.

Cerebral vascular disease is a known contributor to vascular cognitive impairment (VCI) and AD (Gorelick et al., 2011). Investigating the possible mechanisms involved, Li et al. used a model in which Tg-SwDI mice were subjected to bilateral common carotid stenosis (BCAS), a well-characterized murine model of VCI. The researchers observed that mice that underwent BCAS exhibited impaired glymphatic drainage as well as reduced vascular pulsation unveiling potential targets for VCI treatment. Another feature shared by vascular dementia (VaD) and AD is neuronal cytoskeleton disruption characterized by microtubule destabilization (Mukaetova-Ladinska et al., 2015; Zhang et al., 2015). In this context, Santiago-Mujika et al. summarized current knowledge on posttranslational modifications of tubulin that affect microtubule dynamics and discuss why restoring the microtubule network might be critical to stopping the progression of neurodegeneration in the context of AD and VaD.

Diagnosis of mild cognitive impairment (MCI) is crucial for identifying subjects at high risk of AD. In this line, the development of biomarkers for MCI has been the focus of intense research, which is the issue reviewed by Ogonowski et al.. In this manuscript, the authors cover literature regarding diagnostic criteria in MCI, traditional and new biomarkers in the diagnosis of MCI and then focus on microRNAs as potential biomarkers. This systematic review identified five miRNA expression profiles, which may be exploited as fluid biomarkers of early-stage AD.

PD is the second most prevalent neurodegenerative disease, characterized by progressive loss of motor function. Current treatments can only slightly decrease the symptoms but do not stop the process of neurodegeneration (Kalia and Lang, 2015). Using a novel *C. elegans* PD model expressing α-Synuclein in DA neurons, Vozdek et al. performed a GWAS for a functional search of PD risk genes. The researchers identified several modulators of α-Synuclein toxicity and provided the basis for follow-up studies aimed at further characterizing the role of these genes in PD, which may represent new potential therapeutic targets for synucleinopathies. Growing evidence has shown the benefits of exercise in PD patients (Fox et al., 2018). Yet, the potential mechanisms underlying exercise-associated improvements in PD remain unknown, which is the focus of the study by Shi et al.. In this article, the authors show that exercise intervention alleviates motor deficits in a rat PD model based on 6-OHDA administration. Researchers provide evidence that exercise treatment regulates brain plasticity in this PD model by suppressing the overexcitability of local field potentials (LFP) and minimizing spike-LFP synchronization in the motor cortex. The loss of parvalbumin-positive (PV+) neurons in the substantia nigra pars reticulata (SNR) has been demonstrated in animal models of PD and postmortem PD brains (Hardman et al., 1996; Pamukcu et al., 2020). To investigate the progression of PV+ neuron loss, Zheng et al. used a transgenic PD mouse model previously developed by the research group (Jiao et al., 2020). Histopathological analyses of these aged mice revealed increased accumulation of α-synuclein in the SNR which was concomitant with neurodegeneration and progressive apoptosis activation, providing evidence of the interplay between Tau and α-synuclein in the mechanism of neuronal loss.

Given the fact that amyloid aggregates constitute a histopathological hallmark of most neurodegenerative diseases, the role of amyloids in the development of these disorders has been widely studied (Soto and Pritzkow, 2018). In this line, many studies have centered on the molecular properties of these proteins. In his review, Diaz-Espinoza presents state-of-the-art progress on the amyloid structures reported for amyloid-β, tau, and α-synuclein, which has been facilitated by the use of solid-state nuclear magnetic resonance and cryogenic-electron microscopy. The author further discusses the potential of these models for the design of novel therapies against neurodegenerative diseases.

The study by Zhao et al. uncovers evidence of NLRP3 as a modulator of hyperphosphorylated Tau toxicity. Employing a traumatic brain injury and a tau hyperphosphorylation mouse model, the researchers were able to demonstrate an increase in NLRP3 in response to tau overexpression, which was associated with neurodegeneration. Moreover, NLRP3 knockout prevented the upregulation of HMGB1 and pTau levels. Interestingly, treatment with an HMGB1 inhibitor resulted in improvements

in the cognitive performance of tau-overexpressing mice, unveiling HMGB1 as a potential target for tauopathies.

Myotonic dystrophy type 1 (DM1) is a multisystem disorder that affects muscles, as well as the eye, heart, endocrine system, and central nervous system (Nguyen and Campbell, 2016). The manuscript by Liu et al. summarizes the evidence around the central nervous system deficits in DM1, highlighting potential therapeutic strategies for the disease.

The studies presented in this Research Topic expand the current understanding of the mechanisms contributing to neurodegeneration. Importantly, the increased knowledge regarding the pathways involved in the processes underlying neurodegenerative diseases will be key to uncovering new therapies for brain disorders.

Author contributions

MS, YM, CS, and NS have contributed to manuscript writing and editing. MS coordinated, reviewed, and checked the final version. All authors have made a substantial intellectual contribution to this manuscript and approved it for publication.

Funding

This work was funded by the following agencies: MS: ANID Fondecyt 11200981. NS: ANID FONIS SA22I0041. CS: NIH Grants R01AG059321 and R01AG061069.

Conflict of interest

The authors declare that the research was conducted in the absence of any commercial or financial relationships that could be construed as a potential conflict of interest.

Publisher's note

References

Alzheimer's Association. (2022). "Alzheimer's disease facts and figures," in *Alzheimer's & Dementia*.

Asai, H., Hirano, M., Furiya, Y., Udaka, F., Morikawa, M., Kanbayashi, T., et al. (2009). Cerebrospinal fluid-orexin levels and sleep attacks in four patients with Parkinson's disease. *Clin. Neurol. Neurosurg.* 111, 341–344.

Cacace, R., Sleegers, K., and van Broeckhoven, C. (2016). Molecular genetics of early-onset Alzheimer's disease revisited. *Alzheimers Dement.* 12, 733–748.

Fatemi, I., Shamsizadeh, A., Ayoobi, F., Taghipour, Z., Sanati, M. H., Roohbakhsh, A., et al. (2016). Role of orexin-A in experimental autoimmune encephalomyelitis. *J. Neuroimmunol.* 291, 101–109.

Fox, S. H., Katzenschlager, R., Lim, S. Y., Barton, B., de Bie, R. M. A., Seppi, K., et al. (2018). International Parkinson and movement disorder society evidence-based medicine review: Update on treatments for the motor symptoms of Parkinson's disease. *Mov. Disord.* 33, 1248–1266.

GBD 2017 US Neurological Disorders Collaborators, Feigin, V. L., Vos, T., Alahdab, F., Amit, A. M. L., Bärnighausen, T. W., et al. (2021). Burden of neurological disorders across the US from 1990-2017: a global burden of disease study. *JAMA Neurol.* 78, 165–176. doi: 10.1001/jamaneurol.2020.4152

Gorelick, P. B., Scuteri, A., Black, S. E., Decarli, C., Greenberg, S. M., Iadecola, C., et al. (2011). Vascular contributions to cognitive impairment and dementia: a statement for healthcare professionals from the american heart association/american stroke association. *Stroke.* 42, 2672–2713.

Habib, R., Noureen, N., and Nadeem, N. (2018). Decoding common features of neurodegenerative disorders: From differentially expressed genes to pathways. *Curr. Genomics.* 19, 300–312.

Hardman, C. D., McRitchie, D. A., Halliday, G. M., Cartwright, H. R., Morris, J. G. (1996). Substantia nigra pars reticulata neurons in Parkinson's disease. *Neurodegeneration.* 5, 49–55.

Jiao, L., Zheng, M., Duan, J., Wu,T., Li, Z., Liu, L., et al. (2020). Tau knockout exacerbates degeneration of parvalbumin-positive neurons in substantia nigra pars reticulata in Parkinson's disease-related α-synuclein A53T mice. *FASEB J.* 34, 12239–12254.

Kalia, L. V., and Lang, A. E. (2015). Parkinson's disease. *Lancet.* 386, 896–912.

Liguori, C. (2017). Orexin and alzheimer's disease. *Curr. Top. Behav. Neurosci.* 33, 305–322.

Mander, B. A., Winer, J. R., Jagust, W. J., and Walker, M. P. (2016). Sleep: A novel mechanistic pathway, biomarker, and treatment target in the pathology of alzheimer's disease? *Trends Neurosci.* 39, 552–566.

Mukaetova-Ladinska, E. B., Abdel-All, Z., Mugica, E. S., Li, M., Craggs, L. J. L., Oakley, A. E., et al. (2015). Tau proteins in the temporal and frontal cortices in patients with vascular dementia. *J. Neuropathol. Exp. Neurol.* 74, 148–157.

Nguyen, C. E., and Campbell, C. (2016). Myotonic dystrophy type 1. *CMAJ.* 188:1033. doi: 10.1503/cmaj.151384

Pamukcu, A., Cui, Q., Xenias, H. S., Berceau, B. L., Augustine, E. C., Fan, I., et al. (2020). Parvalbumin(+) and Npas1(+) pallidal neurons have distinct circuit topology and function. *J. Neurosci.* 40, 7855–7876.

Soto, C., and Pritzkow, S. (2018). Protein misfolding, aggregation, and conformational strains in neurodegenerative diseases. *Nat. Neurosci.* 21, 1332–1340.

Zhang, F., Su, B., Wang, C., Siedlak, S. L., Mondragon-Rodriguez, S., Lee, H. G, et al. (2015). Posttranslational modifications of α-tubulin in alzheimer disease. *Transl. Neurodegener.* 4, 9.

frontiers in Aging Neuroscience

ORIGINAL RESEARCH
published: 14 June 2021
doi: 10.3389/fnagi.2021.695108

Exercise Improves Movement by Regulating the Plasticity of Cortical Function in Hemiparkinsonian Rats

Kaixuan Shi[1,2], *Xiaoli Liu*[2]*, *Lijuan Hou*[2], *Decai Qiao*[2] and *Yuan Peng*[1]

[1] Department of Physical Education, China University of Geosciences, Beijing, China, [2] College of Physical Education and Sports, Beijing Normal University, Beijing, China

Aberrant cortical spike-local field potential (LFP) coupling leads to abnormal basal ganglia activity, disruption of cortical function, and impaired movement in Parkinson's disease (PD). Here, the primary motor cortex mediated plasticity mechanism underlying behavioral improvement by exercise intervention was investigated. Exercise alleviates motor dysfunction and induces neuroplasticity in PD. In this study, Sprague-Dawley (SD) rats were injected with 6-hydroxydopamine (6-OHDA) to induce unilateral nigrostriatal dopamine depletion. Two weeks later, a 4-week exercise intervention was initiated in the PD + exercise (Ex) group. Multichannel recording technology recorded spikes and LFPs in rat motor cortices, and balanced ability tests evaluated behavioral performance. The balanced ability test showed that the total crossing time/front leg error/input latency time was significantly lower in PD + Ex rats than in PD rats ($P < 0.05$). Scalograms and LFP power spectra indicated increased beta-range LFP power in lesioned hemispheres, with exercise reducing LFP power spectral density. Spike-triggered LFP waveform averages showed strong phase-locking in PD motor cortex cells, and exercise reduced spike-LFP synchronization. Our results suggest that exercise can suppress overexcitability of LFPs and minimize spike-LFP synchronization in the motor cortex, leading to motor-improving effects in PD.

Keywords: Parkinson's disease, exercise, motor cortex, local field potential, synchronization

OPEN ACCESS

Edited by:
Natalia Salvadores, Universidad Mayor, Chile

Reviewed by:
Oliver Schmitt, University of Rostock, Germany
Ao Zhang, Emory University, United States

***Correspondence:**
Xiaoli Liu
xiaolil@bnu.edu.cn

Received: *14 April 2021*
Accepted: *17 May 2021*
Published: *14 June 2021*

Citation:
Shi K, Liu X, Hou L, Qiao D and Peng Y (2021) Exercise Improves Movement by Regulating the Plasticity of Cortical Function in Hemiparkinsonian Rats. Front. Aging Neurosci. 13:695108. doi: 10.3389/fnagi.2021.695108

INTRODUCTION

Parkinson's disease (PD) is a progressive neurodegenerative disease characterized by cell death of dopaminergic neurons in the basal ganglia (BG) (Kalia and Lang, 2015). Development of motor impairments, including bradykinesia, rest tremor, rigidity, and lack of coordination, have been associated with exaggerated synchronized oscillation of the beta band (13–35 Hz) in the corticostriatal circuit of patients with PD (Jankovic, 2008; Tinkhauser et al., 2018). These cortical beta oscillations, which may reflect active inhibition of movement and are related to maintenance of postural tone, are abnormally enhanced with dopamine (DA) depletion and coincide with the emergence of akinesia and bradykinesia (Pogosyan et al., 2009; Leventhal et al., 2012). Furthermore, after levodopa administration or deep brain stimulation (DBS), electrophysiological signal acquisition from the motor cortex and BG of PD patients shows reductions in this coherent beta frequency activity, with motor improvement (Kuhn et al., 2008; Babiloni et al., 2019; Wiest et al., 2020). Unfortunately, these pharmacological and surgical therapies often lead to side effects, including levodopa-induced dyskinesia (Huot et al., 2013; Antosik-Wojcinska et al., 2017).

Exercise can complement pharmacological therapies in these patients and has been used for rehabilitative management of PD since the 1990s (Duchesne et al., 2015; Pedersen and Saltin, 2015; Fox et al., 2018). While studies of exercise and physical therapy in PD have demonstrated clear improvements in motor performance, substantially less is known about the functional neuroplasticity resulting from long-term exercise interventions (Jakowec et al., 2016; Ferrazzoli et al., 2018). Thus, to explore the potential mechanisms underlying exercise-associated improvements in PD, cortical spikes and local field potentials (LFPs) were recorded simultaneously in control and lesioned rats (created by 6-hydroxydopamine [6-OHDA] injection into the medial forebrain bundle [MFB]), and spike-LFP relationships were investigated.

MATERIALS AND METHODS

Animals and Experimental Procedures

Sprague-Dawley (SD) rats (male, 230–250 g, 8 weeks old, from Beijing Vital River Laboratory Animal Technological Company, Beijing, China) were housed in a controlled environment, with a 12/12-h light/dark cycle (lights on at 18:00) and *ad libitum* access to food and water. The Beijing Normal University Committee for Animal Care approved all experimental procedures, and this study complied with the guidelines set forth by the National Institutes of Health.

All rats were initially randomly assigned to three groups: ① control group ($n = 11$), ② PD group ($n = 14$), and ③ PD with exercise (PD + Ex) group ($n = 14$). As shown in **Figure 1**, rats in the PD + Ex group were placed on a treadmill, and all rats practiced using the automatic foot-fault equipment to familiarize them with the study procedures. The baseline behavioral level was evaluated after 1 week of habituation.

Then, animals in the control and PD groups (including the PD and PD + Ex groups) were administered vehicle or 6-OHDA, respectively. At 7 days after surgery, rats were tested for their rotational behavior using apomorphine (APO; 0.5 mg/kg, subcutaneous (s.c.); Sigma-Aldrich, St. Louis, MI, USA), with a total net number of rotations of ≥100 per 30 min indicating rats represented a model of Parkinson's disease, as described previously (Shi et al., 2017a). Subsequently, electrophysiological recording and automatic foot-fault testing were performed once per week. Starting during Week 1, rats in the PD + Ex group began a 4-week exercise intervention. At the end of Week 4, histological localization of electrodes and biochemical assays were performed.

Nigrostriatal Lesions and Electrode Implantation

Each rat was anesthetized with chloral hydrate (350 mg/kg) and then placed on a stereotaxic frame (Stoelting, Chicago, IL, USA) fitted with atraumatic ear bars to level the skull in the dorsal-ventral plane (mouth bar was set at −3.3 mm). A small hole was made in the skull at the right MFB coordinate (Paxinos and Watson, 2007) (AP: −4.3 mm, ML: −1.5 mm, and DV: 7.6–7.8 mm), and an 8-μg solution of 6-OHDA (4 μL in total, per μL in 0.2% ascorbic acid and 0.9% saline, Sigma-Aldrich) was injected into this hole to lesion nigral dopaminergic cells, with an injection rate of 1 μL/min and slow syringe withdrawal (1 mm/min) over 5 min. Control animals received an equal volume of a solution of 0.2% ascorbic acid and 0.9% saline in the same manner.

Electrode implantation was conducted after 6-OHDA or vehicle injection. A chronic 16-channel microwire electrode array, which consisted of 4 × 4 rows of electrodes with an additional ground wire serving as a local reference (Stablohm 675, MicroProbes, USA; tip diameter = 35 μm, spacing = 300 μm), was implanted into the right primary motor cortex (M1) layers 5/6 (AP: 1.8∼3.0 mm, ML: 2.3∼3.3 mm, DV: 1.4–1.6 mm) (Paxinos and Watson, 2007). Finally, five stainless steel screws were anchored to the skull and wrapped with a reference wire. Dental cement (A-M Systems, WA, USA) was added to secure the skull screws.

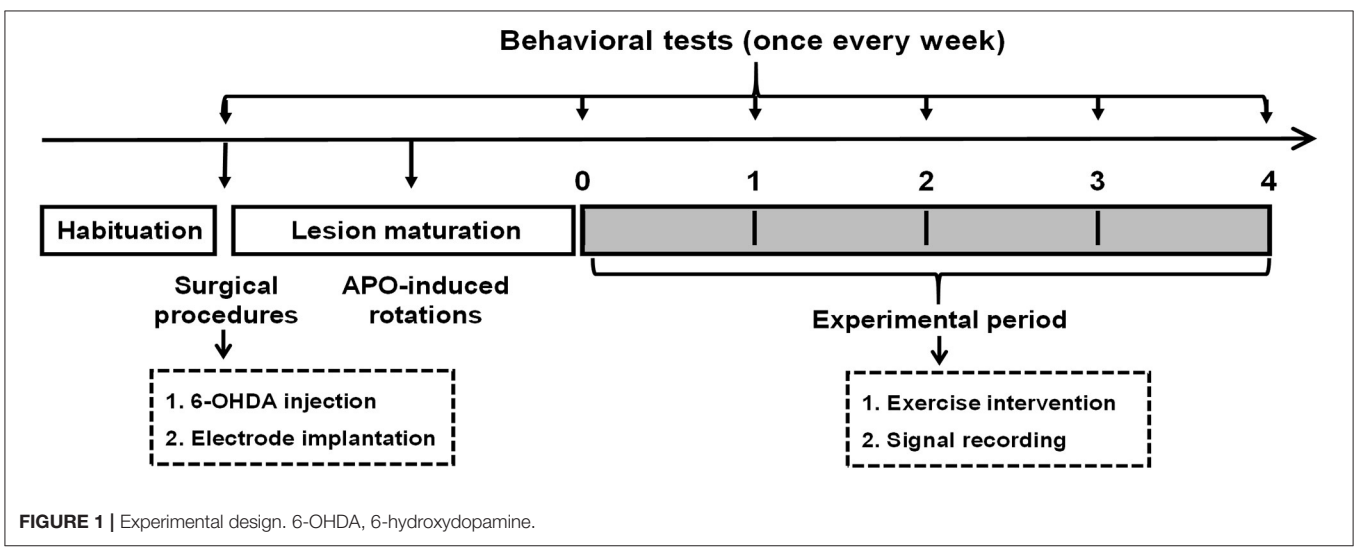

FIGURE 1 | Experimental design. 6-OHDA, 6-hydroxydopamine.

Exercise Protocol

Before undergoing surgery, all animals were adapted to the treadmill with a speed limit of 11 m/min. Two weeks after 6-OHDA injections, the sustained mandatory treadmill protocol (11 m/min, 30 min per day) was performed 5 days/week for 4 weeks (Tajiri et al., 2010; Chen et al., 2017) without electrical shock and at a 0° inclination. Meanwhile, rats in both the control and PD groups were placed on an unmoving treadmill for 30 min at a time.

Behavioral Testing

To evaluate sensorimotor function, an automatic foot fault test was carried out before and after the 6-OHDA lesion was induced. One week before surgery, rats were placed at the departure box and trained to walk spontaneously across a horizontal scale with 77 bars to the arrival box. Rats underwent three training trials per day for 3 days, after which they could reliably walk from the departure box to the arrival box with fewer than five errors. Infrared beams and a sensor device (LocotronicH, Bioseb, Vitrolles, France; L × W × H: 128 cm × 28 cm × 20 cm) detected the movement of rats along the length of the ladder and were used to recognize and record the exact position and duration of errors in motor coordination (missteps or paw slips between any two rungs). The included software identified input latency times, front errors, and total crossing times. Each rat performed the test two times per day on Weeks 0, 1, 2, 3, and 4, with a rest of 5 min between two trials.

Electrophysiological Data Acquisition and Analysis

The raw neural signals from each microwire of the electrode were amplified and recorded using the Cerebus^{TM} 128-Channel Data Acquisition System (Cyberkinetics Inc., Salt Lake City, UT, USA). Low-pass, filtered, LFP channels were amplified by 1000×, sampled at 1 kHz, and filtered under 250 Hz. Meanwhile, high-pass, filtered, waveform channels were amplified by 20,000×, digitized at 30 kHz, and bandpass-filtered between 250 and 5000 Hz. Spike detection and sorting were carried out automatically in real-time using the Centre software of the Cerebus^{TM} system. Simultaneously, the rat's automatic activities were tracked and recorded by the Neuromotive^{TM} system (Cyberkinetics Inc., Salt Lake City, UT, USA). Videotaped motor behavior was used to identify a sedentary behavioral state.

All recorded data were stored for additional offline analyses. Off-line Sorter software version 4.2.0 (Plexon, Dallas, TX, USA), Neuroexplorer software version 5 (Nex Technologies, Littleton, MA, USA), and custom-written MATLAB routines were used for these analyses.

Power Spectral Density Analysis of LFPs

Epochs of 300 LFP recordings (according to the rat's behavioral rest state) were captured, and the trapped filter was set to 50 Hz to remove power line interference and other high-frequency noises. Next, the spectrum value was normalized as the log of the raw power spectral density (PSD) from 0 to 80 Hz, which was constructed using a fast Fourier transform (FFT) with a based analysis and a 1-s moving window. The PSD and frequency blocks were set at 1,024 and 512 points at 0.2 Hz, respectively.

Spike Sorting and Cell-Type Classification

Spike waveforms recorded from M1 were required to satisfy the following conditions: ① the threshold was three times the standard deviation; ② the signal-to-noise ratio was more than 2.5; and ③ the interspike interval (ISI) histogram reflected spikes that did not occur within the assumed refractory period of 1.2 ms. Next, single-unit spikes were sorted using a principal component analysis (PCA) and a K-means cluster analysis to measure action potential widths and the frequency of spike trains. PC1 and PC2 (x and y axes) were plotted against time (z-axis) to isolate each unit in 2D and 3D PC space, as shown in **Figure 2A**. The F, J3, and Davis-Bouldin (DB) statistics were also calculated to determine whether the classification was qualified. **Figure 2B** shows the three identified units (a, b, and c) according to the spike waveform characteristics (top) and the ISI histograms (bottom).

Based on several studies comparing morphology with electrophysiological characteristics in M1, spikes were classified into two different neuronal subpopulations (Li et al., 2012; Lacey et al., 2014). One neuron type exhibited relatively long action potential widths (0.5–0.8 ms) and low discharge frequencies (<10 Hz) and were categorized as pyramidal neurons (PNs). Conversely, another neuron type had shorter action potential widths (0.2–0.5 ms) and higher spontaneous discharge frequencies (8–45 Hz) and was presumed to be interneurons (INs).

Spike-Triggered Waveform Analysis

Spike-triggered LFP waveform averages (STWA) were calculated to assess the degree of entrainment between spontaneous spike potentials of distinct neurons and LFP oscillations (**Figure 3**). LFPs were bandpass-filtered (beta band, 10–30 Hz) using the MATLAB signal-processing toolbox. STWAs were calculated as follows: 0 ms denoted the spike timestamp for a certain spike train, and filtered beta bands were averaged from two 200-ms epochs (unshuffled STWA). Subsequently, the original inter-spike intervals were randomly shuffled to produce different STWA. This process was repeated 1,000 times to provide a mean value for the beta band (shuffled STWA). Spikes were deemed to be related to beta oscillations when the unshuffled STWA exceeded the 96% confidence interval for the mean of the 1,000 shuffled spike trains at the timestamp (0 ms). Thus, the percentage of correlated neurons was calculated. The ratio of the mean unshuffled to the mean shuffled STWA was also calculated to estimate the proportion of synchronized neurons. When this ratio was close to 1, it indicated no phase locking between spikes and beta oscillations (Denker et al., 2011; Brazhnik et al., 2016; Wilson et al., 2018).

Histology and Immunohistochemistry

After electrophysiological recordings were complete, the rats (control, $n = 9$; PD, $n = 11$; PD + Ex, $n = 13$) were deeply anesthetized by an intraperitoneal (i.p.) injection of chloral hydrate (450 mg/kg) and transcardially perfused with

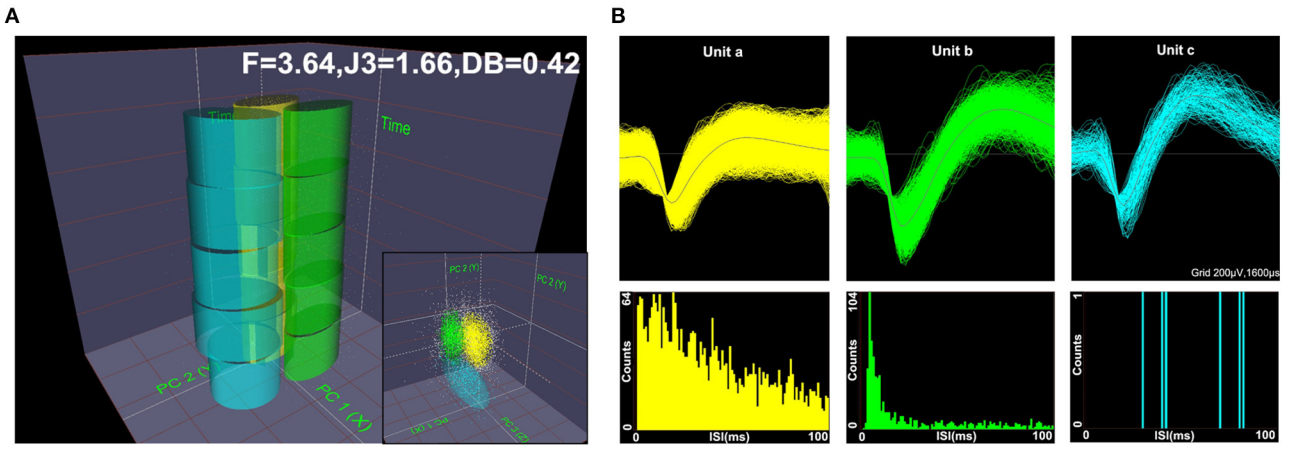

FIGURE 2 | Diagram of offline unit sorting by principal component analysis (PCA) and the quality metrics of F, J3, and Davis-Bouldin (DB). Spikes were sorted using PCA in 2D and 3D PC spaces, **(A)** and the three units (a, b, c) were well-isolated based on their respective spike waveforms and interspike interval (ISI) histograms **(B)**.

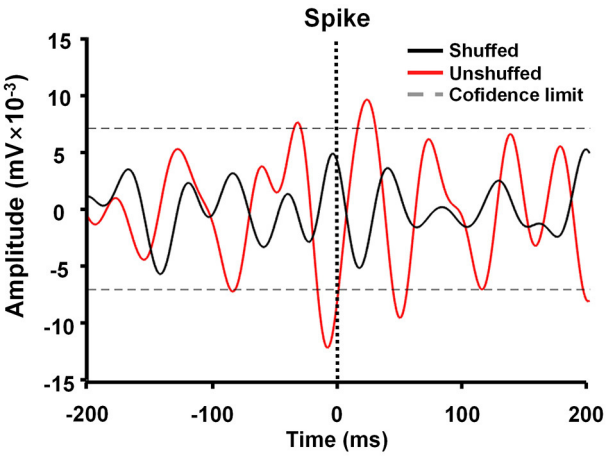

FIGURE 3 | Example of M1 spike-triggered 10–30-Hz waveform averages. The unshuffled spike train (red) exceeded the 96% confidence interval of the shuffled spike train (black) and represented spike-local field potential (LFP) synchronization in the 10–30 Hz range.

saline followed by 4% paraformaldehyde (PFA) in phosphate-buffered saline (0.1 M, pH 7.4). Brains were dissected and fixed in 4% PFA overnight at 4°C. Coronal sections were cut at M1 (50 μm), the substantia nigra pars compacta (SNc; 30 μm), and the striatum (30 μm) using a freezing microtome. The sections for recording electrode targets were mounted on glass slides and stained with cresyl violet. To assess dopaminergic denervation in PD models, sections from the SNc and striatum were analyzed by tyrosine hydroxylase (TH) immunohistochemistry, as described previously (Shi et al., 2019). The number of TH-immunoreactive neurons in the SNc and the optical density of TH-immunoreactive fibers in the striatum were evaluated. Results were normalized in each rat by values obtained on the right and left sides using the following formula: lesioned/unlesioned.

Data Analysis

All data are presented as the mean ± standard error of the mean (SEM). Multiple comparisons were performed by one-way (before vs. after exercise intervention, i.e., "pre- vs. post" comparisons) or two-way (between two different groups) repeated-measures analysis of variance (ANOVA) followed by Student-Newman-Keuls *post-hoc* testing. All analyses were carried out using SPSS 21.0 (IBM Corp., Armonk, NY, USA) and Sigmaplot 13.0 (Systat Software, Inc, Richmond, CA, USA). A P-value of ≤ 0.05 was considered statistically significant.

RESULTS

Behavioral Results

Rats were placed on the automatic foot fault device (**Figure 4D**), and 6-ODHA-lesioned rats were shown to have deficits in the adjusting step test. In the control and PD groups, the three test indicators showed no significant changes compared to Week 0 ($P > 0.05$, **Figures 4A–C**). For the total crossing time (% baseline), exercise improved the performance of PD rats by enhancing vigor and reducing the duration of time required to cross the beam at Weeks 2, 3, and 4 (at Weeks 2 and 3, $P < 0.05$; at Week 4, $P < 0.01$, **Figure 4A**) compared to Week 0. Input latency times showed the same trend (at Week 2, $P < 0.05$; at Weeks 3 and 4, $P < 0.01$, **Figure 4C**), whereas deficits in front leg errors were reduced at Week 3 ($P < 0.05$) and remained relatively stable at Week 4 ($P < 0.01$).

Histological and TH-Immunoreactivity Results

APO-induced rotation showed that 24 rats were successfully modeled in the PD and PD + Ex groups, with net rotations consistent with the criterion for the PD model (165.43 ± 17.67 r/30 min > 100 r/30 min). Failed modeling occurred in four rats that had net rotations <60 r/30 min.

Histological staining with cresyl violet confirmed correct placement of the recording electrode array in M1 (layer 5)

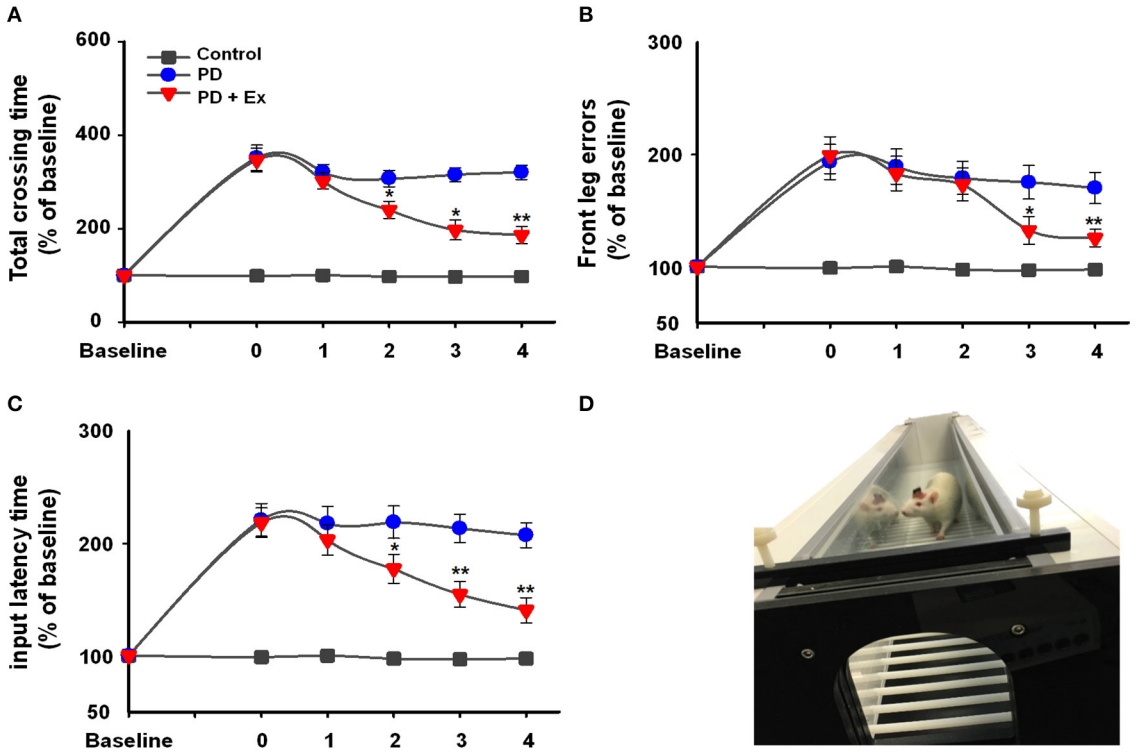

FIGURE 4 | Automatic foot fault test **(D)** results in the control, Parkinson's disease (PD), and PD + exercise (Ex) groups. Time course of the automatic foot test and the percentages of baseline for total crossing time **(A)**, front leg error **(B)**, and input latency time **(C)**. Compared with the Week 0 standard *: $P < 0.05$, **: $P < 0.01$.

on coronal sections (**Figure 5A**). **Figures 5B,C** shows immunostaining for TH in rat SNc and striatum, with obviously lower numbers of TH-immunoreactive cells and fibers on the lesioned side relative to the unlesioned side. Compared with the control group, 6-OHDA-lesioned rats had significantly reduced nigrostriatal projections in both the PD and PD + Ex groups ($P < 0.01$). The exercise intervention was unable to significantly reverse the nigrostriatal depletion in these groups ($P > 0.05$, **Figures 5D,E**).

Time-Dependent Changes in Spontaneous Firing Rates in M1 Correlates With the Efficacy of Exercise

As described in section Spike Sorting and Cell-Type Classification, PNs and INs have distinct electrophysiological characteristics. Based on the electrophysiological properties of spontaneous firing rate and spike width (**Figure 6**), PNs and INs can be distinguished explicitly. The proportions of these two types of neurons in the study groups are summarized in **Table 1**.

An intergroup analysis of the spontaneous firing activity of PNs and INs at Week 4 indicated that the mean firing rate was different after induction of 6-ODHA lesions. As shown in **Figure 7A**, the mean firing rate of PNs was significantly lower in the PD group than in the control group (3.427 ± 0.703 vs. 2.569 ± 0.79 Hz, $P < 0.01$). Compared with the PD group, the mean frequency of PN firing in the PD + Ex group was obviously increased (3.033 ± 0.77, $P < 0.01$) but was still significantly lower than in the Control group ($P < 0.01$). The average frequency of firing for INs, however, did not significantly differ between the three groups ($P > 0.05$).

Intragroup comparisons of mean firing rates showed that these two types of neurons did not have significant alterations at Weeks 0, 1, 2, 3, or 4, either in the control group or PD group ($P > 0.05$, **Figures 7B,C**). For the PD + Ex group, however, the mean firing rate of PNs was significantly increased from Week 3 to 4 compared with Week 0 ($P < 0.05$), though there were no changes in INs during exercise training ($P > 0.05$; **Figure 7D**).

Exercise Attenuates Cortical Beta Oscillatory LFP Power in 6-ODHA-Lesioned Rats

In this study, hemiparkinsonian rats (PD and PD + Ex groups) exhibited higher cortical LFP power in the 10–30 Hz range than control rats in the resting state ($P < 0.01$ and $P < 0.05$, respectively, **Figures 8A,B**). The PSDs of beta LFPs were significantly higher in the PD + Ex group than in the PD group ($P < 0.05$, **Figure 8C**), and this change was time-dependent, which has been confirmed in our previous study (Shi et al., 2017b).

Exercise Disrupts the Pathological Synchrony Between M1 Neurons and Beta Oscillations

The spike–LFP relationship was examined in M1 to determine whether changes in spike timing correlated with the increases

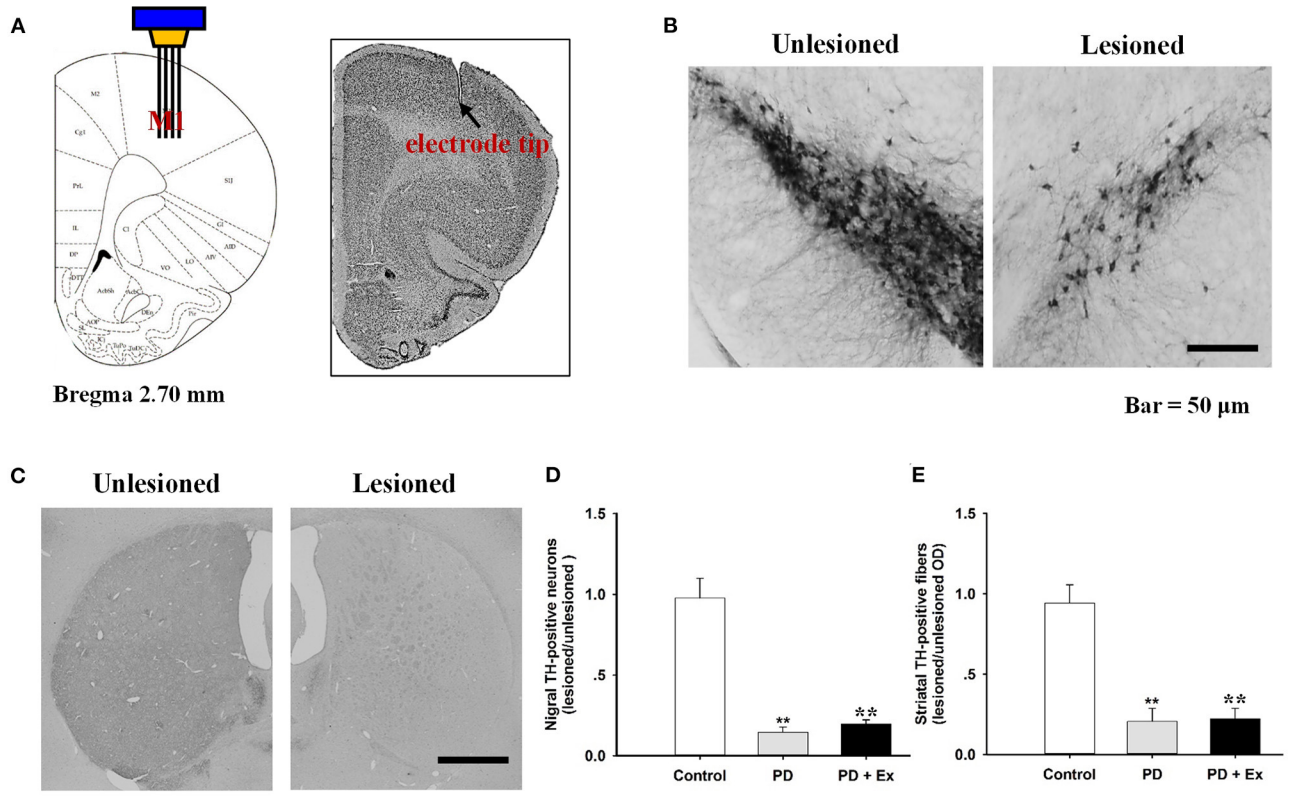

FIGURE 5 | Histological results in the M1 and tyrosine hydroxylase (TH)-immunostaining results in the substantia nigra pars compacta (SNc). The recording electrode site at M1 was confirmed on the coronal section and adapted from Paxinos and Watson (2007) **(A)**. TH-immunostaining results in the SNc **(B)** and striatum **(C)** from both unlesioned and lesioned sides. There were significantly lower numbers of TH-positive neurons in the Parkinson's disease (PD) and PD + exercise (Ex) groups than in the Control group (**: $P < 0.01$); however, there was no significant difference between the PD and PD + Ex groups ($P > 0.01$) **(D,E)**.

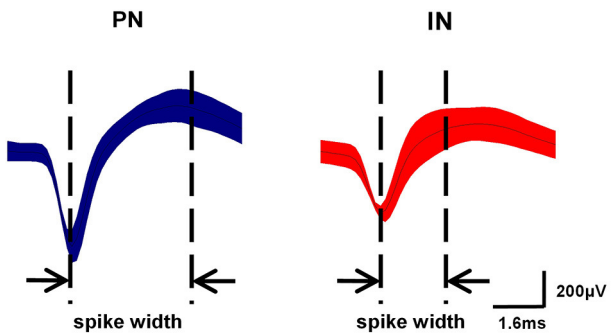

FIGURE 6 | Classification of neurons in M1. Waveform examples of pyramidal neuron (PN) (blue) and interneuron (IN) (red) subtypes in M1. PNs exhibited relatively long action potential widths (0.5–0.8 ms) and low spontaneous firing rates (<10 Hz), while INs had shorter action potential widths (0.2–0.5 ms) and higher spontaneous firing rates (8–45 Hz).

in LFP beta-range (10–30 Hz) activity observed in 6-OHDA-lesioned rats. As described in section Data Analysis, increases in the LFP power in the 10–30-Hz range in the lesioned hemisphere have been associated with an increased synchronization of spikes and LFP oscillations in the same frequency range.

TABLE 1 | Proportions of pyramidal neurons (PN) and interneurons (IN) in the motor cortices of rats in the control, Parkinson's disease (PD), and Parkinson's disease + exercise (PD + Ex) groups.

Group	Total neurons	PN (%)	IN (%)
Control ($n = 9$)	113	86 (76.1%)	27 (23.9%)
PD ($n = 11$)	147	104 (70.7%)	43 (29.3%)
PD + Ex ($n = 13$)	156	123 (78.8%)	33 (21.2%)

Figure 9A shows STWA without obvious phase locking, and **Figure 9B** depicts typical STWA synchronization. The mean ratios of unshuffled-to-shuffled STWA peak-to-trough amplitudes (STWA ratios) of cortical neurons in the 10–30-Hz band were compared between the three groups. **Figure 9C** shows that the STWA ratio was higher in PD models than in control rats (compared to the control group, PD: $P < 0.01$, PD + Ex: $P < 0.05$). Following the exercise intervention, phase-locking of spikes with beta-band oscillations was reduced in the PD + Ex group compared to the PD group ($P < 0.05$). In the control group, PNs and INs did not show notable synchronization of spiking with the beta band. The percentage of neurons (both PNs and INs) entrained to STWA was significantly increased

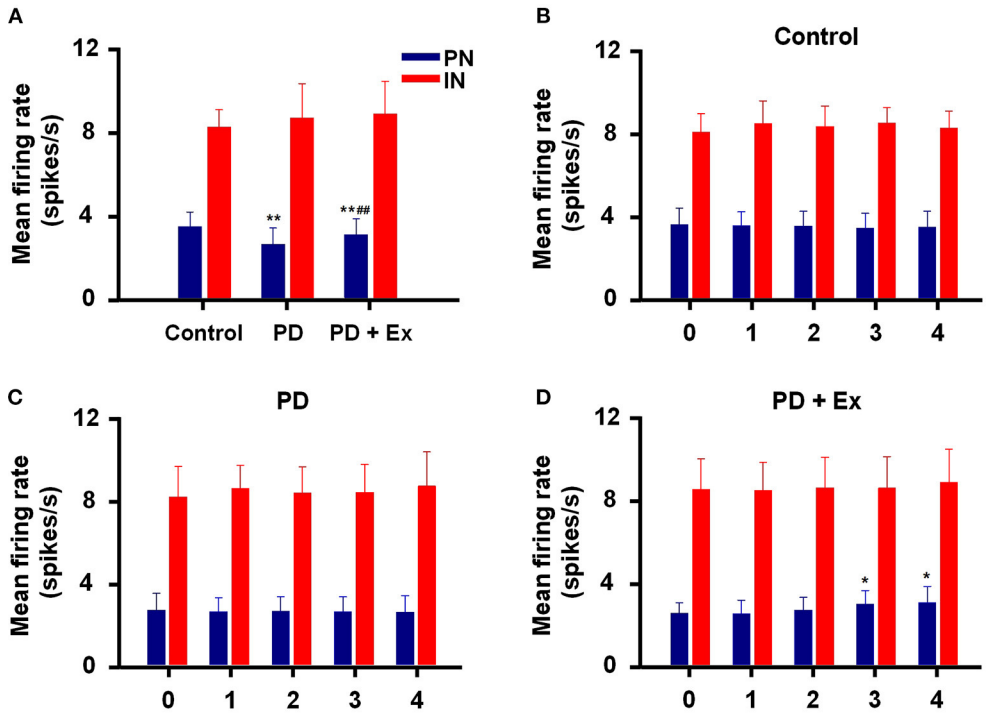

FIGURE 7 | Inter- and intragroup comparisons of the mean firing rates of pyramidal neurons (PNs) and interneurons (INs) in M1. The intergroup analysis of PNs (blue) and INs (red) at Week 4 is shown in **(A)**. The mean firing rates of PNs and INs varied with time in the Control **(B)**, Parkinson's disease (PD) **(C)**, and PD + exercise (Ex) **(D)** groups. Compared with the Control group or Week 0 data, *: $P < 0.05$, **: $P < 0.01$; and compared with the PD group, #: $P < 0.05$, ##: $P < 0.01$.

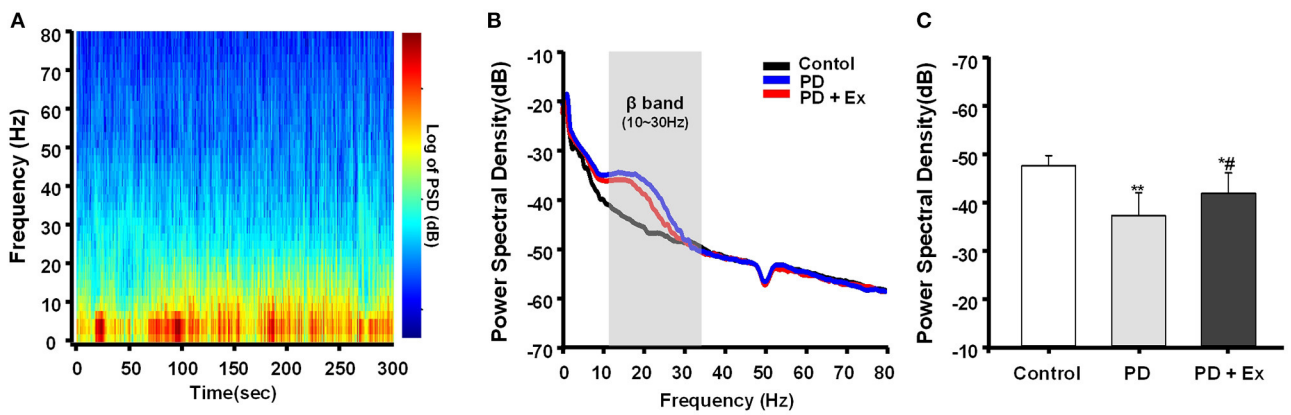

FIGURE 8 | Power spectral density (PSD) of β local field potentials (LFPs) recorded in M1. A representative fast Fourier transform (FFT)-based spectrogram depicts the time-frequency spectral power of motor cortex LFPs during 5-min epochs of rest **(A)**. Linear graphs show averaged LFP power (0–80 Hz) spectra for the Control, Parkinson's disease (PD), and PD + exercise (Ex) groups **(B)**, with the gray area showing that the beta band in the 10–30 Hz range of LFP power was significantly increased in 6-hydroxydopamine (6-OHDA)-lesioned rats. The average PSDs of the three groups are shown in **(C)**. The PSD of the beta band was increased in the PD group compared to the Control group. For the PD + Ex group, the PSD of the beta band was decreased compared to the PD group but was still higher than in the Control group. Compared with the Control group, *: $P < 0.05$, **: $P < 0.01$; and compared with the PD group, #: $P < 0.05$.

in PD model rats compared to control rats (compared to the control group, percent PNs and INs in PD: $P < 0.01$, percent PNs and INs in PD + Ex: $P < 0.01$). After the exercise intervention, the percentage of these neurons was smaller than in the PD group (percent PNs: $P < 0.01$; percent INs: $P < 0.05$; **Figure 9D**). The polar plots in **Figure 9E** show the distribution of STWA phases from spike trains in the M1 with cortical LFP 10–30-Hz oscillations. The phase angles between spikes and beta oscillations appeared random in control rats; however, the STWA of spike trains in PD rats showed strong phase-locking at

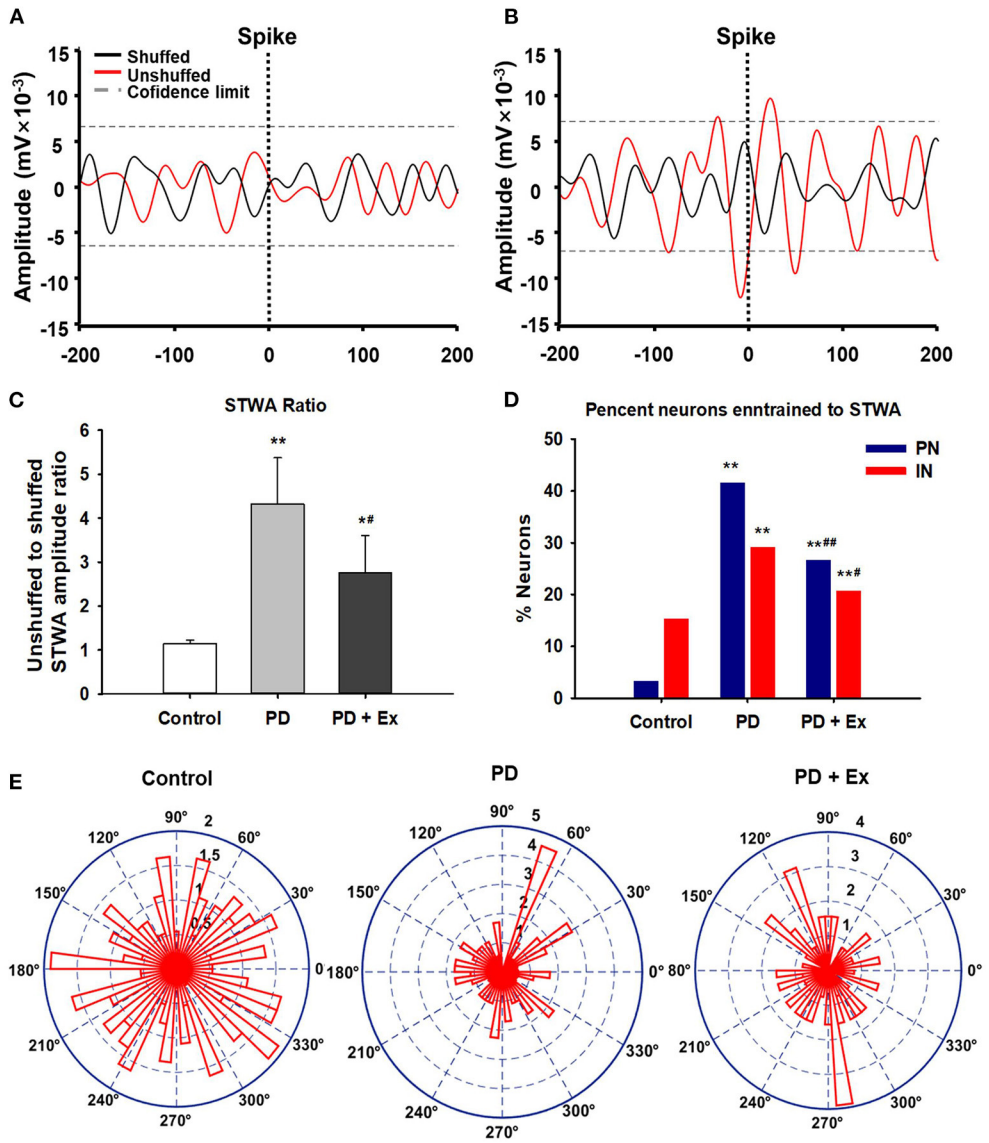

FIGURE 9 | Phase locking of cortical spiking with 10–30 Hz local field potentials (LFPs) in the three groups. Unsynchronized spike-triggered LFP waveform averages (STWA) **(A)**. Example STWA for a typical cortical spike train paired with an LFP in the 10–30 Hz range **(B)**. The ratio of STWA-based unshuffled-to-shuffled spike trains indicating cortical spike-LFP synchronization **(C)**. Bar graphs show the proportions of pyramidal neurons (PNs) and interneurons (INs) significantly synchronized with 10–30 Hz LFP oscillations **(D)**. To assess STWA, mean phase angles between spikes and cortical LFP oscillations were significantly clustered around different phases of cortical 10–30 Hz LFP oscillations, as the polar plots show in **(E)**. Compared with the Control group, *: $P < 0.05$, **: $P < 0.01$; and compared with the PD group, #: $P < 0.05$; ##: $P < 0.01$.

about 60°. The STWA of cortical neurons in the PD + Ex group seemed to be relatively scattered but still presented with obvious phase-locking consistent with the STWA ratio results.

DISCUSSION

Previous studies have demonstrated that exercise training can modulate activity in the cortical motor areas of PD patients, as well as in animal models of parkinsonism (Wang et al., 2015; Alberts et al., 2016; Ginanneschi et al., 2021). In this study, multichannel electrode arrays were implanted into the M1, and spike trains of neurons and LFPs were recorded and analyzed in hemiparkinsonian rats during a therapeutically effective exercise intervention. This approach allowed us to address several key questions related to the role of functional changes in M1 on PD, providing insights into the mechanism of exercise-induced neuroplasticity.

This study identified increases in spiking discharges and beta-band oscillations, which was consistent with the results of previous studies conducted in humans and PD animal models, including rodents and non-human primates (Hammond et al., 2007; Zhuang et al., 2018; Holt et al., 2019). Abnormal spike and beta LFP activity at various levels of the cortical-basal ganglia-thalamocortical circuit have been observed in PD individuals (patients and animal models), though the origin of these changes remains unknown (Goldberg et al., 2004; Dejean et al., 2008; Stein and Bar-Gad, 2013). It is generally hypothesized that pathological changes in the motor cortex may contribute to the motor dysfunction observed in parkinsonian conditions. Li et al. (2012) have confirmed that exaggerated spike trains and beta oscillations can deteriorate motor control and lead to the development of akinesia and bradykinesia. Furthermore, several studies focusing on the mechanisms of subthalamic nuclei DBS or L-3, 4-dihydroxyphenylalanine (L-DOPA) treatment have shown that L-DOPA administration reduces the cortical power in the beta range and that STN-DBS induces reductions in the synchronization of oscillations in the cortex-basal ganglia circuit.

Although M1 is a crucial basal ganglia output area that transforms neurophysiological signals into motion instructions, there have only been a few previous studies related to exercise-induced plasticity of cortical neural activity (e.g., electrophysiological evaluations) at the cellular level in PD patients (Bonavita, 2020; Feng et al., 2020). Wang et al. (2013) analyzed regional cerebral blood flow-related tissue radioactivity in three-dimensionally reconstructed brains by statistical parametric mapping to explore the neural substrates underlying exercise-based neurorehabilitation. The results of that study highlighted exercise-dependent functional reorganization both in the motor (M1) and limbic circuits (dorsal striatum). In this study, we also found direct evidence of neural plasticity in M1 cells in PD rats following exercise induction.

Our results confirmed exaggerated beta-range LFP activity in cortical cells of 6-ODHA-lesioned rats, which was effectively eliminated by exercise. Exercise was also able to increase the mean firing rate of PNs; however, the mean firing rates of INs and all cells were not significantly changed. A few factors may have contributed to this result. First, firing rates of PNs and INs vary in different animal models and with different signal acquisition methods (Degenetais et al., 2002; Xu and Baker, 2018). The majority of previous studies have identified a reduced firing rate in PNs without obvious changes in INs, which may reflect a compensatory change after DA depletion (Pasquereau and Turner, 2011; Shepherd, 2013). Another possibility is that exercise-induced improvements in motor function might modulate the degree of coupling between spikes and LFP oscillations. Multiple studies have shown that spike trains tend to be phase-locked to overactive beta bands in various nuclei and motor cortices (Brazhnik et al., 2012, 2014). In this study, we used multichannel recording technology to simultaneously record spikes and LFPs, which allowed us to analyze the level of synchrony between them. The results showed that the STWA ratio and the percentage of neurons were increased in 6-OHDA-lesioned rats, contributing to movement disorders. Exercise likely induces a critical reduction in the synchronization of spike and beta-range oscillations in M1.

Exercise modalities such as treadmill training, Tai Chi, tango dancing, boxing, and forced cycling incorporating both motor skill learning and aerobic training; they may work synergistically to facilitate neuroplasticity and functional restoration to drive motor and cognitive behavioral improvement in PD. Treadmill can be easily adjusted for exercise elements (include speed and gradient) and its training in subjects with PD has been proved in multiple studies to promote behavioral performances (Da Silva et al., 2018; Dauwan et al., 2021). Forced treadmill and wheel running approaches used to drive movement improvement in patients with PD and finding in animal studies that support the potential mechanism (Ferrazzoli et al., 2018). It should be noted that the dopaminergic depletion of the nigrostriatal system was unable to be reversed by the exercise intervention, as has previously been reported (Sconce et al., 2015; Hood et al., 2016; Shi et al., 2019). This finding might be attributed to the fact that the exercise intervention was started 14 days after the 6-OHDA injection, at which point DA depletion may have been completed. Moreover, the behavioral improvements appeared after 2 or 3 weeks exercise intervention. This time-dependence on training might due to the PD rats being in the advanced stage, which affects the cognitive elements and needs more repetitively practice to restoration. Despite the 6-OHDA-induced injury severity, other factors also influence exercise-mediated neuroprotection, including the exercise initiated time, the exercise intervention administrated pre or at mild stage of PD may facilitate neuroprotection or an alternative process for behavioral recovery involve neuroplasticity (Jakowec et al., 2016; Ferrazzoli et al., 2018).

Indeed, numerous studies have shown that chronic exercise cannot reverse dopaminergic cell death and that improvements in motor performance are related to other compensatory mechanisms (O'Dell et al., 2007; Churchill et al., 2017; Hou et al., 2017). Moreover, studies with PD animal models have shown that exercise decreases excessive striatal glutamate content, restores glutamatergic receptors, and inhibits glutamate-mediated excitotoxicity, thereby contributing to a functional reorganization of the corticostriatal pathway (Van Leeuwen et al., 2010; Toy et al., 2014). Thus, it is likely that the efficacy of the exercise intervention was dependent on plastic changes in the glutamate-mediated corticostriatal pathway, which affected the activity of cortical neurons and led to changes in motor symptoms.

In conclusion, this study provides evidence that a treadmill exercise administration can effectively alleviate motor deficits in PD rats. This exercise-induced behavioral improvement involved the disruption of abnormal neural activity in the M1 region of PD rats. The synchronization of spike firing and beta oscillations in this model may hold the key to this process, and the functional consequences of this synchrony on exercise-induced neuroplasticity in PD rats need to be verified.

DATA AVAILABILITY STATEMENT

The raw data supporting the conclusions of this article will be made available by the authors, without undue reservation.

ETHICS STATEMENT

The animal study was reviewed and approved by Beijing Normal University Committee for Animal Care.

AUTHOR CONTRIBUTIONS

XL, KS, and DQ: conceived and designed the experiments. KS and LH: performed the experiments. KS, LH, and YP: analyzed the data and wrote the paper. All authors contributed to the article and approved the submitted version.

FUNDING

This work was supported by the National Natural Science Foundation of China (32000833).

ACKNOWLEDGMENTS

In addition to the listed authors, assistance was provided by Xiangming Lin, Ru Song, and Gang Zhao. We would like to thank Editage (www.editage.cn) for English language editing.

REFERENCES

Alberts, J. L., Phillips, M., Lowe, M. J., Frankemolle, A., Thota, A., Beall, E. B., et al. (2016). Cortical and motor responses to acute forced exercise in Parkinson's disease. *Parkinsonism Relat. Disord.* 24, 56–62. doi: 10.1016/j.parkreldis.2016.01.015

Antosik-Wojcinska, A., Swiecicki, L., Dominiak, M., Soltan, E., Bienkowski, P., and Mandat, T. (2017). Impact of STN-DBS on mood, drive, anhedonia, and risk of psychiatric side-effects in the population of PD patients. *J. Neurol. Sci.* 375, 342–347. doi: 10.1016/j.jns.2017.02.020

Babiloni, C., Del Percio, C., Lizio, R., Noce, G., Lopez, S., Soricelli, A., et al. (2019). Levodopa may affect cortical excitability in Parkinson's disease patients with cognitive deficits as revealed by reduced activity of cortical sources of resting state electroencephalographic rhythms. *Neurobiol. Aging* 73, 9–20. doi: 10.1016/j.neurobiolaging.2018.08.010

Bonavita, S. (2020). Exercise and Parkinson's disease. *Adv. Exp. Med. Biol.* 1228, 289–301. doi: 10.1007/978-981-15-1792-1_19

Brazhnik, E., Cruz, A. V., Avila, I., Wahba, M. I., Novikov, N., Ilieva, N. M., et al. (2012). State-dependent spike and local field synchronization between motor cortex and substantia nigra in hemiparkinsonian rats. *J. Neurosci.* 32, 7869–7880. doi: 10.1523/JNEUROSCI.0943-12.2012

Brazhnik, E., McCoy, A. J., Novikov, N., Hatch, C. E., and Walters, J. R. (2016). Ventral medial thalamic nucleus promotes synchronization of increased high beta oscillatory activity in the basal ganglia-thalamocortical network of the hemiparkinsonian rat. *J. Neurosci.* 36, 4196–4208. doi: 10.1523/JNEUROSCI.3582-15.2016

Brazhnik, E., Novikov, N., McCoy, A. J., Cruz, A. V., and Walters, J. R. (2014). Functional correlates of exaggerated oscillatory activity in basal ganglia output in hemiparkinsonian rats. *Exp. Neurol.* 261, 563–577. doi: 10.1016/j.expneurol.2014.07.010

Chen, W., Qiao, D. C., Liu, X. L., and Shi, K. X. (2017). Treadmill exercise improves motor dysfunction and hyperactivity of the corticostriatal glutamatergic pathway in rats with 6-OHDA-induced Parkinson's disease. *Neural Plast.* 2017:2583910. doi: 10.1155/2017/2583910

Churchill, M. J., Pflibsen, L., Sconce, M. D., Moore, C., Kim, K., and Meshul, C. K. (2017). Exercise in an animal model of Parkinson's disease: motor recovery but not restoration of the nigrostriatal pathway. *Neuroscience* 359, 224–247. doi: 10.1016/j.neuroscience.2017.07.031

Da Silva, F. C., Iop, R. D. R., de Oliveira, L. C., Boll, A. M., de Alvarenga, J. G. S., Gutierres, P. J., et al. (2018). Effects of physical exercise programs on cognitive function in Parkinson's disease patients: a systematic review of randomized controlled trials of the last 10 years. *PLoS ONE* 13:e0193113. doi: 10.1371/journal.pone.0193113

Dauwan, M., Begemann, M. J. H., Slot, M. I. E., Lee, E. H. M., Scheltens, P., and Sommer, I. E. C. (2021). Physical exercise improves quality of life, depressive symptoms, and cognition across chronic brain disorders: a transdiagnostic systematic review and meta-analysis of randomized controlled trials. *J. Neurol.* 268, 1222–1246. doi: 10.1007/s00415-019-09493-9

Degenetais, E., Thierry, A. M., Glowinski, J., and Gioanni, Y. (2002). Electrophysiological properties of pyramidal neurons in the rat prefrontal cortex: an *in vivo* intracellular recording study. *Cereb. Cortex* 12, 1–16. doi: 10.1093/cercor/12.1.1

Dejean, C., Gross, C. E., Bioulac, B., and Boraud, T. (2008). Dynamic changes in the cortex-basal ganglia network after dopamine depletion in the rat. *J. Neurophysiol.* 100, 385–396. doi: 10.1152/jn.90466.2008

Denker, M., Roux, S., Linden, H., Diesmann, M., Riehle, A., and Grun, S. (2011). The local field potential reflects surplus spike synchrony. *Cereb. Cortex* 21, 2681–2695. doi: 10.1093/cercor/bhr040

Duchesne, C., Lungu, O., Nadeau, A., Robillard, M. E., Bore, A., Bobeuf, F., et al. (2015). Enhancing both motor and cognitive functioning in Parkinson's disease: aerobic exercise as a rehabilitative intervention. *Brain Cogn.* 99, 68–77. doi: 10.1016/j.bandc.2015.07.005

Feng, Y. S., Yang, S. D., Tan, Z. X., Wang, M. M., Xing, Y., Dong, F., et al. (2020). The benefits and mechanisms of exercise training for Parkinson's disease. *Life Sci.* 245:117345. doi: 10.1016/j.lfs.2020.117345

Ferrazzoli, D., Ortelli, P., Madeo, G., Giladi, N., Petzinger, G. M., and Frazzitta, G. (2018). Basal ganglia and beyond: the interplay between motor and cognitive aspects in Parkinson's disease rehabilitation. *Neurosci. Biobehav. Rev.* 90, 294–308. doi: 10.1016/j.neubiorev.2018.05.007

Fox, S. H., Katzenschlager, R., Lim, S. Y., Barton, B., de Bie, R. M. A., Seppi, K., et al. (2018). International Parkinson and Movement Disorder Society evidence-based medicine review: update on treatments for the motor symptoms of Parkinson's disease. *Mov. Disord.* 33, 1248–1266. doi: 10.1002/mds.27372

Ginanneschi, F., Messa, L. V., Battisti, C., and Rossi, A. (2021). Changes in corticomotor pathway excitability after exercise training in Parkinson's disease. *Neurol. Sci.* doi: 10.1007/s10072-020-04960-y. [Epub ahead of print].

Goldberg, J. A., Rokni, U., Boraud, T., Vaadia, E., and Bergman, H. (2004). Spike synchronization in the cortex-basal ganglia networks of parkinsonian primates reflects global dynamics of the local field potentials. *J. Neurosci.* 24, 6003–6010. doi: 10.1523/JNEUROSCI.4848-03.2004

Hammond, C., Bergman, H., and Brown, P. (2007). Pathological synchronization in Parkinson's disease: networks, models, and treatments. *Trends Neurosci.* 30, 357–364. doi: 10.1016/j.tins.2007.05.004

Holt, A. B., Kormann, E., Gulberti, A., Potter-Nerger, M., McNamara, C. G., Cagnan, H., et al. (2019). Phase-dependent suppression of beta oscillations in Parkinson's disease patients. *J. Neurosci.* 39, 1119–1134. doi: 10.1523/JNEUROSCI.1913-18.2018

Hood, R. L., Liguore, W. A., Moore, C., Pflibsen, L., and Meshul, C. K. (2016). Exercise intervention increases spontaneous locomotion but fails to attenuate dopaminergic system loss in a progressive MPTP model in aged mice. *Brain Res.* 1646, 535–542. doi: 10.1016/j.brainres.2016.06.032

Hou, L. J., Chen, W., Liu, X. L., Qiao, D. C., and Zhou, F. M. (2017). Exercise-induced neuroprotection of the nigrostriatal dopamine system in Parkinson's disease. *Front. Aging Neurosci.* 9:35810. doi: 10.3389/fnagi.2017.00358

Huot, P., Johnston, T. H., Koprich, J. B., Fox, S. H., and Brotchie, J. M. (2013). The pharmacology of L-DOPA-induced dyskinesia in

Parkinson's disease. *Pharmacol. Rev*. 65, 171–222. doi: 10.1124/pr.111.005678

Jakowec, M. W., Wang, Z., Holschneider, D., Beeler, J., and Petzinger, G. M. (2016). Engaging cognitive circuits to promote motor recovery in degenerative disorders. Exercise as a learning modality. *J. Hum. Kinet*. 52, 35–51. doi: 10.1515/hukin-2015-0192

Jankovic, J. (2008). Parkinson's disease: clinical features and diagnosis. *J. Neurol. Neurosurg. Psychiatry* 79, 368–376. doi: 10.1136/jnnp.2007.131045

Kalia, L. V., and Lang, A. E. (2015). Parkinson's disease. *Lancet* 386, 896–912. doi: 10.1016/S0140-6736(14)61393-3

Kuhn, A. A., Kempf, F., Brucke, C., Doyle, L. G., Martinez-Torres, I., Pogosyan, A., et al. (2008). High-frequency stimulation of the subthalamic nucleus suppresses oscillatory beta activity in patients with Parkinson's disease in parallel with improvement in motor performance. *J. Neurosci.* 28, 6165–6173. doi: 10.1523/JNEUROSCI.0282-08.2008

Lacey, M. G., Gooding-Williams, G., Prokic, E. J., Yamawaki, N., Hall, S. D., Stanford, I. M., et al. (2014). Spike firing and IPSPs in layer V pyramidal neurons during beta oscillations in rat primary motor cortex (M1) *in vitro*. *PLoS ONE* 9:e85109. doi: 10.1371/journal.pone.0085109

Leventhal, D. K., Gage, G. J., Schmidt, R., Pettibone, J. R., Case, A. C., and Berke, J. D. (2012). Basal ganglia beta oscillations accompany cue utilization. *Neuron* 73, 523–536. doi: 10.1016/j.neuron.2011.11.032

Li, Q., Ke, Y., Chan, D. C. W., Qian, Z. M., Yung, K. K. L., Ko, H., et al. (2012). Therapeutic deep brain stimulation in parkinsonian rats directly influences motor cortex. *Neuron* 76, 1030–1041. doi: 10.1016/j.neuron.2012.09.032

O'Dell, S. J., Gross, N. B., Fricks, A. N., Casiano, B. D., Nguyen, T. B., and Marshall, J. F. (2007). Running wheel exercise enhances recovery from nigrostriatal dopamine injury without inducing neuroprotection. *Neuroscience* 144, 1141–1151. doi: 10.1016/j.neuroscience.2006.10.042

Pasquereau, B., and Turner, R. S. (2011). Primary motor cortex of the parkinsonian monkey: differential effects on the spontaneous activity of pyramidal tract-type neurons. *Cereb. Cortex* 21, 1362–1378. doi: 10.1093/cercor/bhq217

Paxinos, G., and Watson, C. (2007). *The Rat Brain in Stereotaxic Coordinates*. Amsterdam: Elsevier.

Pedersen, B. K., and Saltin, B. (2015). Exercise as medicine–evidence for prescribing exercise as therapy in 26 different chronic diseases. *Scand. J. Med. Sci. Sports* 25, 1–72. doi: 10.1111/sms.12581

Pogosyan, A., Gaynor, L. D., Eusebio, A., and Brown, P. (2009). Boosting cortical activity at beta-band frequencies slows movement in humans. *Curr. Biol*. 19, 1637–1641. doi: 10.1016/j.cub.2009.07.074

Sconce, M. D., Churchill, M. J., Greene, R. E., and Meshul, C. K. (2015). Intervention with exercise restores motor deficits but not nigrostriatal loss in a progressive MPTP mouse model of Parkinson's disease. *Neuroscience* 299, 156–174. doi: 10.1016/j.neuroscience.2015.04.069

Shepherd, G. M. G. (2013). Corticostriatal connectivity and its role in disease. *Nat. Rev. Neurosci*. 14, 278–291. doi: 10.1038/nrn3469

Shi, K. X., Liu, X. L., Hou, L. J., Qiao, D. C., and Lin, X. M. (2019). Effects of exercise on mGluR-mediated glutamatergic transmission in the striatum of hemiparkinsonian rats. *Neurosci. Lett*. 705, 143–150. doi: 10.1016/j.neulet.2019.04.052

Shi, K. X., Liu, X. L., Qiao, D. C., Chen, Y. X., and Zhang, L. T. (2017b). Treadmill exercise modulates abnormal β oscillation of M1 in the hemiparkinsonian rat. *J. Xi'an Phys. Educ. Univ.* 34, 590–598. doi: 10.16063/j.cnki.issn1001-747x.2017.05.014

Shi, K. X., Liu, X. L., Qiao, D. C., and Hou, L. J. (2017a). Effects of treadmill exercise on spontaneous firing activities of striatal neurons in a rat model of Parkinson's disease. *Motor Control* 21, 58–71. doi: 10.1123/mc.2015-0065

Stein, E., and Bar-Gad, I. (2013). Beta oscillations in the cortico-basal ganglia loop during parkinsonism. *Exp. Neurol.* 245, 52–59. doi: 10.1016/j.expneurol.2012.07.023

Tajiri, N., Yasuhara, T., Shingo, T., Kondo, A., Yuan, W. J., Kadota, T., et al. (2010). Exercise exerts neuroprotective effects on Parkinson's disease model of rats. *Brain Res.* 1310, 200–207. doi: 10.1016/j.brainres.2009.10.075

Tinkhauser, G., Torrecillos, F., Duclos, Y., Tan, H., Pogosyan, A., Fischer, P., et al. (2018). Beta burst coupling across the motor circuit in patients with Parkinson's disease. *Neurobiol. Dis.* 117, 217–225. doi: 10.1016/j.nbd.2018.06.007

Toy, W. A., Petzinger, G. M., Leyshon, B. J., Akopian, G. K., Walsh, J. P., Hoffman, M. V., et al. (2014). Treadmill exercise reverses dendritic spine loss in direct and indirect striatal medium spiny neurons in the 1-methyl-4-phenyl-1,2,3,6-tetrahydropyridine (MPTP) mouse model of Parkinson's disease. *Neurobiol. Dis.* 63, 201–209. doi: 10.1016/j.nbd.2013.11.017

Van Leeuwen, J. E., Petzinger, G. M., Walsh, J. P., Akopian, G. K., Vuckovic, M., and Jakowec, M. W. (2010). Altered AMPA receptor expression with treadmill exercise in the 1-Methyl-4-Phenyl-1,2,3,6-Tetrahydropyridine-lesioned mouse model of basal ganglia injury. *J. Neurosci. Res.* 88, 650–668. doi: 10.1002/jnr.22216

Wang, Z., Guo, Y. M., Myers, K. G., Heintz, R., and Holschneider, D. P. (2015). Recruitment of the prefrontal cortex and cerebellum in Parkinsonian rats following skilled aerobic exercise. *Neurobiol. Dis.* 77, 71–87. doi: 10.1016/j.nbd.2015.02.020

Wang, Z., Myers, K. G., Guo, Y. M., Ocampo, M. A., Pang, R. D., Jakowec, M. W., et al. (2013). Functional reorganization of motor and limbic circuits after exercise training in a rat model of bilateral parkinsonism. *PLoS ONE* 8:e80058. doi: 10.1371/journal.pone.0080058

Wiest, C., Tinkhauser, G., Pogosyan, A., Bange, M., Muthuraman, M., Groppa, S., et al. (2020). Local field potential activity dynamics in response to deep brain stimulation of the subthalamic nucleus in Parkinson's disease. *Neurobiol. Dis.* 143:105019. doi: 10.1016/j.nbd.2020.105019

Wilson, C. J., Higgs, M. H., Simmons, D. V., and Morales, J. C. (2018). Oscillations and spike entrainment. *F1000Res.* 7:F1000. doi: 10.12688/f1000research.16451.1

Xu, W., and Baker, S. N. (2018). *In vitro* characterization of intrinsic properties and local synaptic inputs to pyramidal neurons in macaque primary motor cortex. *Eur. J. Neurosci.* 48, 2071–2083. doi: 10.1111/ejn.14076

Zhuang, Q. X., Li, G. Y., Li, B., Zhang, C. Z., Zhang, X. Y., Xi, K., et al. (2018). Regularizing firing patterns of rat subthalamic neurons ameliorates parkinsonian motor deficits. *J. Clin. Invest.* 128, 5413–5427. doi: 10.1172/JCI99986

Conflict of Interest: The authors declare that the research was conducted in the absence of any commercial or financial relationships that could be construed as a potential conflict of interest.

frontiers in Aging Neuroscience

MINI REVIEW
published: 17 August 2021
doi: 10.3389/fnagi.2021.713201

Orexinergic System in Neurodegenerative Diseases

*Qinqin Wang[1,2], Fei Cao[1] and Yili Wu[3,4]**

[1] Shandong Collaborative Innovation Center for Diagnosis, Treatment & Behavioral Interventions of Mental Disorders, Institute of Mental Health, Jining Medical University, Jining, China, [2] Shandong Key Laboratory of Behavioral Medicine, School of Mental Health, Jining Medical University, Jining, China, [3] Key Laboratory of Alzheimer's Disease of Zhejiang Province, Institute of Aging, School of Mental Health and The Affiliated Kangning Hospital, Wenzhou Medical University, Wenzhou, China, [4] Oujiang Laboratory, Wenzhou, China

Orexinergic system consisting of orexins and orexin receptors plays an essential role in regulating sleep–wake states, whereas sleep disruption is a common symptom of a number of neurodegenerative diseases. Emerging evidence reveals that the orexinergic system is disturbed in various neurodegenerative diseases, including Alzheimer's disease (AD), Parkinson's disease (PD), Huntington's disease (HD), and multiple sclerosis (MS), whereas the dysregulation of orexins and/or orexin receptors contributes to the pathogenesis of these diseases. In this review, we summarized advanced knowledge of the orexinergic system and its role in sleep, and reviewed the dysregulation of the orexinergic system and its role in the pathogenesis of AD, PD, HD, and MS. Moreover, the therapeutic potential of targeting the orexinergic system for the treatment of these diseases was discussed.

Keywords: orexinergic system, Alzheimer's disease, Parkinson's disease, Huntington's disease, multiple sclerosis

OPEN ACCESS

Edited by:
Yasmina Manso, Center for Biomedical Research on Neurodegenerative Diseases (CIBERNED), Spain

Reviewed by:
Marian Henryk Lewandowski, Jagiellonian University, Poland
Jim R. Fadel, University of South Carolina, United States

***Correspondence:**
Yili Wu
yili_wu2004@yahoo.ca;
wuyili@wmu.edu.ca

Received: *22 May 2021*
Accepted: *20 July 2021*
Published: *17 August 2021*

Citation:
Wang Q, Cao F and Wu Y (2021) Orexinergic System in Neurodegenerative Diseases. Front. Aging Neurosci. 13:713201. doi: 10.3389/fnagi.2021.713201

INTRODUCTION

Orexinergic system is essential for the maintenance of various physiological processes including sleep–wake states (Gamble et al., 2019; Yukitake et al., 2019; Zhang et al., 2019). Emerging evidence reveals that the orexinergic system is disturbed in various neurodegenerative diseases, such as Alzheimer's disease (AD), Parkinson's disease (PD), Huntington's disease (HD), and multiple sclerosis (MS), whereas the dysregulation of the orexinergic system plays a pivotal role in the pathogenesis of these diseases (Petersen et al., 2005; Asai et al., 2009; Fatemi et al., 2016; Mander et al., 2016; Liguori, 2017). To gain a better understanding of the therapeutic potential of targeting the orexinergic system for the treatment of these diseases, we extensively reviewed the characteristics of the orexinergic system, its function in sleep–wake states, and its role in the pathogenesis of the neurodegenerative diseases and underlying mechanisms.

OVERVIEW OF OREXINERGIC SYSTEM

Orexinergic system consists of orexins and their receptors. Orexin, also named as hypocretin, includes two isoforms, namely, orexin A (OXA) or hypocretin-1 (HCRT-1) and orexin B (OXB) or hypocretin-2 (HCRT-2) (de Lecea et al., 1998; Sakurai et al., 1998; Soya and Sakurai, 2020). OXA and OXB are generated from the same prepro-orexin precursor *via* differential hydrolysis (Gotter et al., 2012). OXA is a ∼3.5 kDa peptide with 33 amino acids, whereas OXB is a ∼2.9 kDa peptide

with 28 amino acids. Both of them are highly conserved in mammalian species (Sakurai et al., 1998; Dyer et al., 1999; Spinazzi et al., 2006). Orexins are mainly expressed in lateral hypothalamic neurons (Wang et al., 2018). Orexin receptors, including orexin 1 receptor (OX1R) and orexin 2 receptor (OX2R), are G-protein-coupled receptors (GPCRs) (de Lecea et al., 1998; Sakurai et al., 1998; Soya and Sakurai, 2020). OX1R is mainly expressed in ventromedial hypothalamic nucleus, dorsal raphe, locus coeruleus, and hippocampus, whereas OX2R is highly expressed in nucleus accumbens, anterior pretectal nucleus, and cerebral cortex (Trivedi et al., 1998; Soya et al., 2013). Both of them are highly conserved in mammals, for example, human OX1R and OX2R share 94 and 95% identity with rat OX1R and OX2R, respectively. Human OX1R and OX2R consist of 425 and 444 amino acids, respectively, and they share approximately 64% sequence identity (Spinazzi et al., 2006). OXA binds to both OX1R and OX2R with similar affinity (Gotter et al., 2012; Wang et al., 2018), whereas OXB prefers to bind to OX2R (Gotter et al., 2012; Wang et al., 2018).

The main function of the orexinergic system is to regulate sleep–wake states (Adamantidis et al., 2007; Gamble et al., 2019; Yukitake et al., 2019; Zhang et al., 2019). Orexin deficiency is the proximal cause of human narcolepsy with cataplexy, which has been comprehensively studied and reviewed (Bassetti et al., 2019; Nepovimova et al., 2019). Consistently, OX2R agonist YNT-185 ameliorates narcolepsy symptoms in a mouse model of narcolepsy-cataplexy (Irukayama-Tomobe et al., 2017). Photostimulation of orexin neurons induces the transition of sleep to wake in mice, indicating that orexin neurons play a key role in promoting sleep-to-wake transition (Adamantidis et al., 2007). Activation of orexin neurons leads to a marked increase of wakefulness time and a reduction of sleep time including both rapid eye movement (REM) sleep and non-REM (NREM) sleep in mice (Sasaki et al., 2011). Consistently, OX2R agonist YNT-185 markedly increases wakefulness time in mice (Irukayama-Tomobe et al., 2017).

OREXINERGIC SYSTEM IN NEURODEGENERATIVE DISEASEs

Orexinergic System in AD

AD, the most common neurodegenerative disease, is characterized by the clinical manifestations such as progressive memory loss, cognitive deficits, and sleep disruption. Neuritic plaques, neurofibrillary tangles, and neuronal loss are the neuropathological hallmarks of AD. β-Amyloid (Aβ) and hyperphosphorylated Tau are the core components of neuritic plaques and neurofibrillary tangles, respectively (Lane et al., 2018; Qiu et al., 2019).

Although studies indicate that the orexin levels in cerebrospinal fluid (CSF) are associated with circadian alteration in AD and the OXA levels are positively correlated with the cognitive function in AD (Liguori et al., 2020; Shimizu et al., 2020), the dysregulation of the orexinergic system in AD remains inconclusive. For example, a significant reduction of OXA positive neurons and the levels of OXA were observed in patients with AD (Fronczek et al., 2012), whereas both Slats et al. and Liguori et al. reported that there was no difference of OXA in CSF of patients with AD and healthy controls (Slats et al., 2012; Liguori et al., 2014). In addition, Gabelle et al. reported that OXA was increased in AD (Gabelle et al., 2017). The inconsistent results might result from the different methods and sample sizes. For example, studies by Fronczek et al. and Gabelle et al. were performed in postmortem ventricular CSF and the stored CSF samples, respectively (Fronczek et al., 2012; Gabelle et al., 2017), whereas the participants were awaked in studies performed by Slats et al. and Liguori et al., respectively (Slats et al., 2012; Liguori et al., 2014). Moreover, increased orexin along with more fragmented sleep was observed in patients with AD with neuropsychiatric symptoms compared with that in patients with AD without neuropsychiatric symptoms (Liguori et al., 2018).

Orexinergic system is implicated in Aβ pathology. First, the levels of OXA were correlated with the level of $A\beta_{42}$ in patients with AD (Slats et al., 2012; Gabelle et al., 2017; **Figure 1A**). Importantly, orexin deficiency markedly decreased Aβ pathology in AD model mice, amyloid precursor protein/presenilin 1 (APP/PS1) transgenic mice (Roh et al., 2014). Moreover, sleep disruption, a common symptom of AD, facilitated Aβ accumulation, contributing to neurodegeneration in AD, which might be correlated with the alteration of the orexinergic system (Mander et al., 2016; Liguori, 2017; **Figure 1A**). Reduced $A\beta_{1-42}$ was correlated with the decrease of REM sleep and sleep efficiency in AD, whereas the increase of OXA in CSF was correlated with the decrease of REM and sleep efficiency in AD (Liguori et al., 2014). The diurnal variation of Aβ levels in interstitial fluid (ISF) was observed in human. Consistently, the Aβ levels in ISF were positively correlated with the awaked time and negatively correlated with the asleep time in mice (Kang et al., 2009; **Figure 1A**). In addition, the rate of $A\beta_{1-40}$ clearance was much faster in sleeping mice than that in awaked mice (Xie et al., 2013). Furthermore, the administration of orexin significantly increased the Aβ levels in ISF during the light phase and orexin receptors antagonist led to the inhibition of the diurnal fluctuation of Aβ in ISF of AD model mice (Kang et al., 2009). On the other hand, increased Aβ contributes to the dysregulation of the orexinergic system and sleep disruption. For example, the administration of $A\beta_{25-35}$ markedly increased awaked time and reduced NREM sleep in AD mice (Liu et al., 2019; **Figure 1A**). $A\beta_{25-35}$ significantly increased the level of OXA in AD mice (Liu et al., 2019; **Figure 1A**).

The orexinergic signaling is associated with Tau pathology in AD (Deuschle et al., 2014; Liguori et al., 2014; Liguori, 2017). The level of OXA in CSF was correlated with Tau and phosphorylated Tau (pTau) in patients with AD (Deuschle et al., 2014; **Figure 1A**). Consistently, the level of OXA in CSF exhibited an evidently positive correlation with Tau and pTau in patients with moderate to severe AD (Liguori et al., 2014), and even in control subjects (Shimizu et al., 2020). Importantly, the OXA downregulation dramatically decreased the levels of Tau and pTau induced by $A\beta_{25-35}$ *in vitro* (Liu et al., 2019; **Figure 1A**). Moreover, studies show that the levels of pTau were correlated with stage 1 of NREM sleep in AD (Liguori et al., 2014; **Figure 1A**). It indicates that the

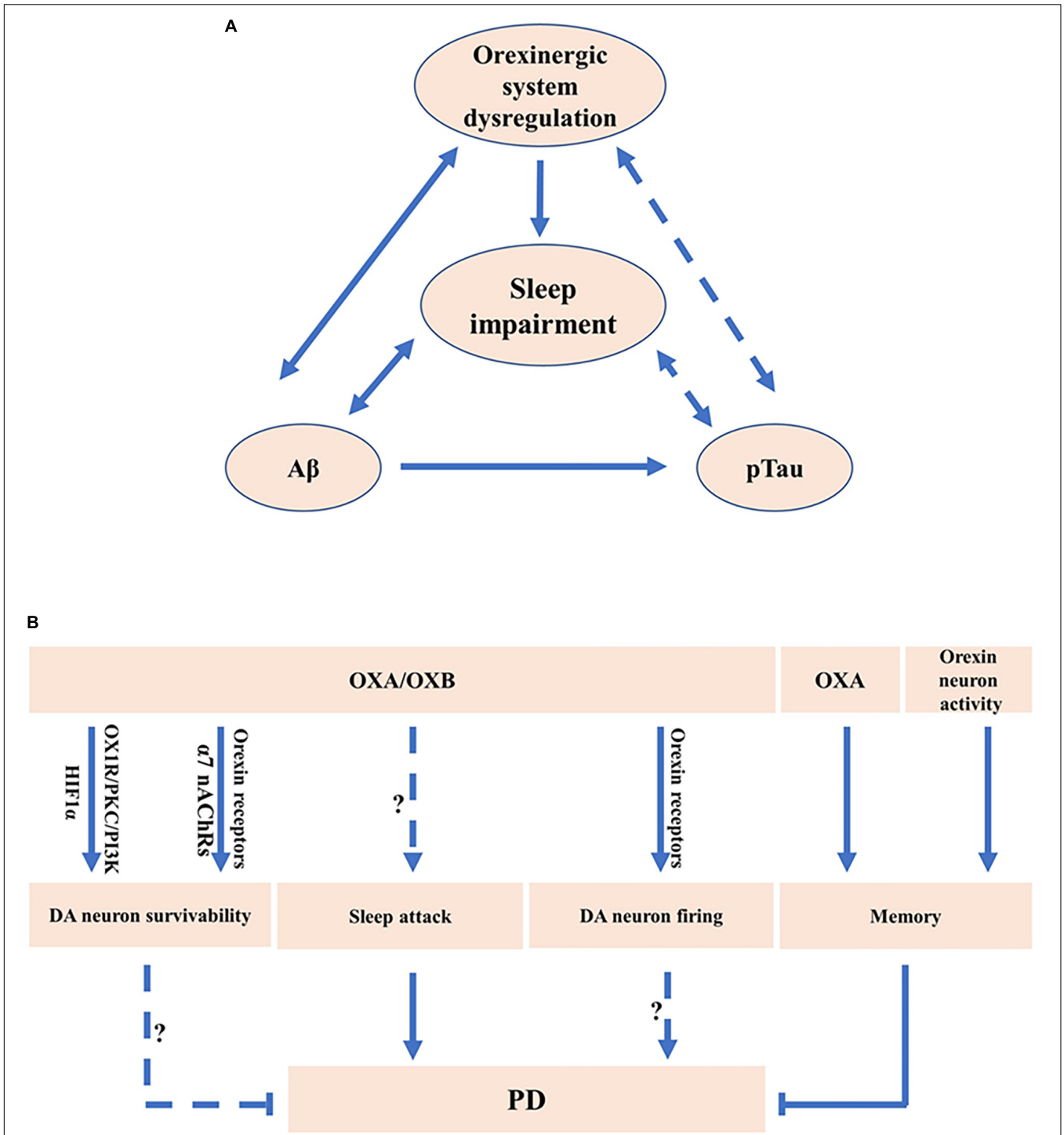

FIGURE 1 | The potential roles of orexinergic system in Alzheimer's disease (AD) and Parkinson's disease (PD). **(A)** The potential roles of orexinergic system in AD. Orexinergic system is involved in the regulation of sleep–wake states. Sleep disruption facilitated Aβ accumulation in AD. Orexin A (OXA) is associated with Aβ. Evidence also suggests a potential relationship between Aβ levels and sleep–wake states. Moreover, OXA in cerebrospinal fluid (CSF) was correlated with pTau. The levels of pTau were correlated with stage 1 of NREM sleep. More experiments are needed to clarify the correlation between pTau and orexinergic system-related sleep dysfunction. **(B)** The potential roles of orexinergic system in PD. OXA exerted the neuroprotective roles in PD cell model *via* regulating HIF-1α or orexin 1 receptor (OX1R)/protein kinase C (PKC)/PI3-kinase (PI3K) signaling. Orexin 2 receptor (OX2R) and α7 nAChRs were involved in the promotion of the survivability of DA neurons regulated by orexin B (OXB). OXA treatment or enhancement of orexin neurons activity markedly decreased the memory impairment in PD mice. OXA and OXB significantly increased the rate of spontaneous firing of dopaminergic (DA) neurons *via* OX1R and OX2R. Sleep attack has been observed in PD. Orexinergic system was involved in sleep disorders, indicating the potential roles of orexinergic system in regulating PD-related sleep disorders.

role of orexinergic signaling in Tau pathology may be related to sleep dysfunction.

Dysregulation of orexinergic signaling may be associated with neurodegeneration and neuronal loss in AD. First, AD was primarily associated with the loss of basal forebrain cholinergic neurons (Zajo et al., 2016). Basal forebrain was one of the major projection targets of orexin neurons (Li and de Lecea, 2020). Orexin receptors were expressed in the basal forebrain (Li and de Lecea, 2020), while orexin neurons directly communicated with the cholinergic neurons in the basal forebrain through synapses (Li and de Lecea, 2020). Moreover, the administration of OXA in basal forebrain ameliorated distracter-induced attention deficiency in rats (Zajo et al., 2016). These results indicate that the orexinergic system may be involved in AD pathology by regulating the cholinergic pathway in the basal forebrain.

Orexinergic System in PD

PD is characterized by the selective loss of dopaminergic (DA) neurons in the substantia nigra (SN) and the formation of Lewy body (Kalia and Lang, 2015; Reich and Savitt, 2019). The clinical symptoms include both motor symptoms such as resting tremor and bradykinesia and non-motor symptoms such as pain, sleep disorder, and cognition dysfunction (Kalia and Lang, 2015).

The dysregulation of the orexinergic system in PD is inconclusive as the number of studies is limited. First, it was reported that the level of OXA was significantly decreased in ventricular CSF of patients with advanced PD compared with controls (Drouot et al., 2003). Consistently, the number of orexin neurons was markedly decreased in patients with PD compared with that in controls (Fronczek et al., 2007). However, the level of OXA was within the normal range in CSF obtained from patients with PD by lumbar puncture (Yasui et al., 2006).

Orexinergic system is implicated in the neuroprotective effect on DA neurons (Cui et al., 2010; Feng et al., 2014; Guerreiro et al., 2015; Hadadianpour et al., 2017; Pasban-Aliabadi et al., 2017; Liu M. F. et al., 2018). The number of OXA positive neurons tended to be decreased in hypothalamus of PD model rats (Cui et al., 2010). OXA significantly ameliorated 1-methyl-4-phenylpyridinium (MPP^+)-induced injury in SH-SY5Y cells, which was mediated by hypoxia inducible factor-1 alpha (HIF-1α) (Feng et al., 2014; **Figure 1B**). Moreover, OXA significantly attenuated 6-hydroxydopamine (6-OHDA)-induced cell toxicity in SH-SY5Y cells, which was mediated by OX1R/protein kinase C (PKC)/PI3-kinase (PI3K) signaling (Pasban-Aliabadi et al., 2017; **Figure 1B**). In addition, OXA significantly attenuated 1-methyl-4-phenyl-1, 2, 3, 6-tetrahydropyridine (MPTP)-induced DA neuron loss in the SN of mice, contributing to the improvement of cognitive and motor ability (Liu M. F. et al., 2018), whereas OX1R antagonist SB334867 could inhibit the protective effect (Liu M. F. et al., 2018; **Figure 1B**). Consistently, OXA significantly ameliorated 6-OHDA-induced impairments of locomotor function, sensorimotor function, and muscle tone in rats (Hadadianpour et al., 2017). Furthermore, OXB increased the survivability of DA neurons mediated by OX2R but not by OX1R, whereas nicotine markedly improved the neuroprotective effects of OXB on DA neuron *via* the activation of α7 nicotinic acetylcholine receptors (α7 nAChRs) (Guerreiro et al., 2015; **Figure 1B**). The above evidence indicates that orexins and orexin receptors are involved in the protective effect on DA neurons in PD models.

Sleep disruption is a common symptom in PD (Asai et al., 2009; Nie et al., 2019). Most of these patients suffer from excessive sleepiness during daytime and some of them present the sleep attack (Tracik and Ebersbach, 2001; Brodsky et al., 2003; Asai et al., 2009). Some characteristics of sleep attack in patients with PD are similar to narcolepsy symptoms (Arnulf et al., 2000; Asai et al., 2009). Dopamine agonists were one of the major factors influencing the emergence of sleep attack, suggesting the close correlation between DA system and sleep attack in PD (Paus et al., 2003; **Figure 1B**). Electrophysiological analysis revealed that the administration of OXA and OXB observably enhanced the rate of spontaneous firing of DA neurons in the SN of rats and inhibition of OX1R and OX2R significantly decreased the firing rate of DA neurons in the SN, implying the roles of the orexinergic pathway in regulating DA system (Liu C. et al., 2018; **Figure 1B**). Moreover, OXA application in the hippocampus or chemogenetic activation of orexin neurons significantly ameliorated the memory impairment in A53T transgenic mice, a PD model mice (Stanojlovic et al., 2019; **Figure 1B**). It indicates that the orexinergic system plays a key role in sleep disruption and memory defects in patients with PD.

Orexinergic System in HD

HD, a kind of polyglutamine disorder described first by George Huntington, presents autosomal dominant inheritance and is characterized by a progressive decline of cognition, motor, and behavioral functions (Wyant et al., 2017; Ghosh and Tabrizi, 2018; Croce and Yamamoto, 2019). Given that the molecular mechanisms underlying HD pathogenesis remain unclear, there is no effective treatment for HD (Ghosh and Tabrizi, 2018). Orexinergic system is involved in the pathogenesis of HD. A significant reduction of orexin neurons in the LH and hypothalamus was observed in patients with HD compared with that in controls (Petersen et al., 2005; Gabery et al., 2010; **Figure 2A**). Consistently, a significant decrease of OXA and OXB was observed in HD model mice (Petersen et al., 2005; **Figure 2A**).

The abnormal sleep characteristics were observed in HD model mice, including a shorter slow-wave sleep (SWS) duration, more episodes of every vigilance state during the periods of light and dark cycle, and a particular β rhythm with the frequency of 20–35 Hz (Jeantet et al., 2013; Lebreton et al., 2015). Promoting sleep with the pharmacological method effectively slowed the decline of cognition performance in HD mice (Pallier et al., 2007). Imposing a drug-induced relative regular rhythm of wake–sleep contributed to the enhancement of cognition ability in HD mice (Pallier and Morton, 2009). In addition, the administration of OX1R and OX2R antagonist significantly attenuated the β activity during the sleep stage of SWS and REM, reduced sleep–wake rhythm deficiency, and efficiently improved the behavioral performance in HD mice (Cabanas et al., 2019; **Figure 2A**). These results indicate that modulating orexinergic system may have a therapeutic potential for the improvement of sleep and cognitive performance in HD.

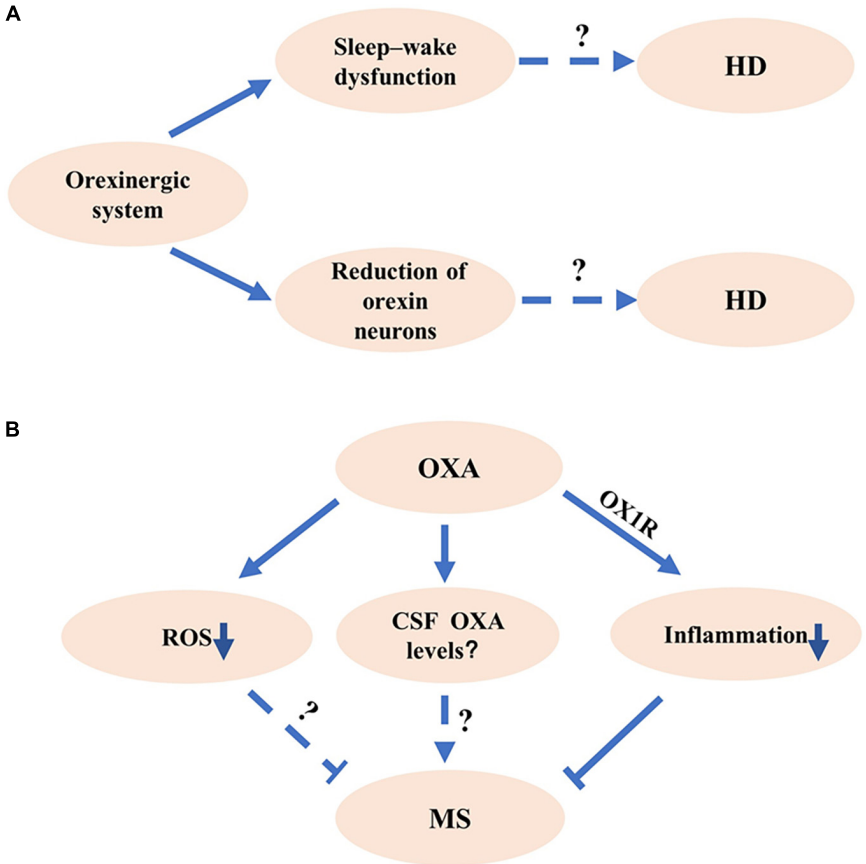

FIGURE 2 | The potential roles of orexinergic system in Huntington's disease (HD) and multiple sclerosis (MS). **(A)** The potential roles of orexinergic system in HD. Studies show that the number of OX neurons decreased in HD. Abnormal sleep existed in HD. The details of orexinergic signaling in HD need to be further investigated. **(B)** The potential roles of orexinergic system in MS. The OXA/OX1R signaling significantly decreased the inflammation and pathological processes in EAE mice. Moreover, OXA could markedly reduce the reactive oxygen species (ROS) and microglial activation, indicating that the orexinergic system might involve in MS pathology by regulating ROS and microglial activation. More experiments are needed to determine the relationship between orexin levels and MS pathology at different courses.

Dorsal striatum is the major pathological region in HD (Page et al., 2000). OXA increased the surface levels of α-amino-3-hydroxy-5-methyl-4-isoxazolepropioinc acid (AMPA) receptor in the striatum, leading to the functional changes of striatum circuits (Shin et al., 2009). Both OX1R and OX2R were expressed in dorsal striatum (Zhang et al., 2007). It suggests that orexinergic system may involve in HD pathology by regulating the activity of striatum circuits. Thus, modulating orexinergic system in dorsal striatum-related circuits may be a potential target for the HD treatment.

Orexinergic System in MS

MS is a kind of long-term inflammation-related autoimmune disease with the major characteristic of demyelinating in the central nervous system, ultimately leading to the neurodegeneration (Correale et al., 2017; Gencer et al., 2019). As the progress of MS is variable, MS is classified into relapsing remitting MS (RRMS), secondary progressive MS (SPMS), primary progressive form of MS (PPMS), and progressive relapsing form of MS (PRMS) (Lublin and Reingold, 1996; Correale et al., 2017; Hughes et al., 2018). The major characteristic of patients with RRMS is experiencing partial or complete recovery from the emergence of recurring symptoms of the disease (Antel et al., 2012; Correale et al., 2017). After periods of years, some of the patients slowly turn into gradual deterioration, the stage called SPMS (Antel et al., 2012; Correale et al., 2017). About 15% of the patients present a progressive decline of neurological function without obvious relapses, which is called PPMS (Antel et al., 2012; Correale et al., 2017). A group of patients with MS who undergo episodes of distinct clinical relapse are taken as PRMS (Hughes et al., 2018). Although environmental element, inflammation, and genetic factors are implicated in MS pathology, the precise mechanisms of MS remain unclear (Correale et al., 2017).

Sleep disturbance is a trigger of relapse in MS, indicating the potential roles of the orexinergic pathway in MS (Sahraian et al., 2017). A significant decrease of OXA in CSF was observed in a female MS patient with hypersomnia (Oka et al., 2004). However, Constantinescu et al. showed that there was no significant deficiency of OXA in patients with MS compared

with controls with other inflammatory-related brain disorders or non-inflammatory brain diseases (Constantinescu et al., 2011; Burfeind et al., 2016). A recent study showed that serum OXA was remarkably decreased in patients with MS compared with that in healthy cases (Gencer et al., 2019). Moreover, serum OXA was robustly lower in patients with SPMS than that in patients with RRMS, indicating the serum OXA may correlate with the progression of MS (Gencer et al., 2019). Given the complexity and variety of the pathological courses of MS, further investigation is necessary to determine the orexin levels in CSF of patients with MS at different courses (**Figure 2B**).

Evidence indicates that neuroinflammation and glial activation are the important pathological features of MS (Datta et al., 2017; Grajchen et al., 2018). Experimental autoimmune encephalomyelitis (EAE) was a commonly used animal model of MS (Becquet et al., 2019). OXA significantly reduced the formation of reactive oxygen species (ROS) in primary cultured microglia (Tunisi et al., 2019; **Figure 2B**). Moreover, the intraperitoneal injection of OXA decreased lipopolysaccharide (LPS)-induced activation of microglia in the prefrontal cortex, which was blocked by OX1R antagonist SB334867 (Tunisi et al., 2019), indicating the regulation role of the orexinergic system in neuroinflammation (**Figure 2B**). In addition, the OXA treatment significantly reduced the inflammation and decreased the pathological scores in EAE mice, which was inhibited by SB334867 (Fatemi et al., 2016; **Figure 2B**). Consistently, the administration of OXA dramatically reduced clinical symptoms, decreased neuroinflammation, and alleviated demyelinating and glial activation in EAE mice (Becquet et al., 2019; **Figure 2B**). All the above studies indicate that the orexinergic system exerts the neuroprotection roles by inhibiting the neuroinflammation in MS (Becquet et al., 2019).

PERSPECTIVE OF TARGETING OREXINERGIC SYSTEM

Given the dysfunction of orexinergic pathway is implicated in the pathogenesis of AD, PD, HD, and MS, the orexinergic system may be a potential therapeutic target for the treatment of these diseases (Petersen et al., 2005; Asai et al., 2009; Fatemi et al., 2016; Mander et al., 2016; Liguori, 2017). Dysfunction of sleep–wake, abnormal protein aggregation, and neuroinflammation are the common features of these diseases (Glass et al., 2010; Correale et al., 2017; Illarioshkin et al., 2018). First, dysregulation of the orexinergic system is implicated in the disruption of the sleep–wake process in AD, PD, HD, and MS (Asai et al., 2009; Mander et al., 2016; Liguori, 2017; Sahraian et al., 2017; Cabanas et al., 2019; Turkoglu et al., 2020). On the one hand, sleep disruption contributes to neurodegeneration by facilitating disease-associated protein accumulation such as Aβ (Mander et al., 2016; Liguori, 2017). On the other hand, sleep disruption also attenuates the clearance of Aβ, whereas sleeping facilitates Aβ clearance in AD model mice (Xie et al., 2013). Moreover, abnormal protein aggregation-induced neuroinflammation aggravates the neurodegeneration and neuronal loss in AD and PD (Glass et al., 2010). Thus, targeting the orexinergic system might ameliorate sleep impairment attenuating abnormal protein aggregation and subsequent neuroinflammation and neurodegeneration.

CONCLUSION

Mounting evidence shows that the orexinergic system is involved in the sleep–wake process, whereas sleep disruption is a common symptom of many neurodegenerative diseases including AD, PD, HD, and MS. Moreover, dysfunction of the orexinergic pathway is implicated in the pathogenesis of AD, PD, HD, and MS, which is associated with sleep impairment, pathogenic protein aggregation, neuronal loss, and activation of neuroinflammation (**Figures 1**, **2**). However, the exact roles of the orexinergic system in the above diseases and underlying mechanisms are still not fully understood. Thus, it is essential to further investigate the dysregulation of the orexinergic system in neurodegenerative diseases and its role in the pathogenesis of these diseases.

AUTHOR CONTRIBUTIONS

QW and FC wrote the manuscript. YW conceived and revised the manuscript. All the authors approved the final manuscript.

FUNDING

This work was funded by the Research Fund for Lin He's Academician Workstation of New Medicine and Clinical Translation in Jining Medical University (No. JYHL2018MS03), Technology Development Project of Shandong Province Medicine and Health Science (No. 202002081082), NSFC cultivation project of Jining Medical University (No. JYP2019KJ20), A Project of Shandong Province Higher Educational Science and Technology Program (No. J18KA124), and Research Fund for the Doctoral Program of Jining Medical University, the National Natural Science Foundation of China (NSFC) (Grant Nos. 81771147 and 81971019) to YW.

REFERENCES

Adamantidis, A. R., Zhang, F., Aravanis, A. M., Deisseroth, K., and de Lecea, L. (2007). Neural substrates of awakening probed with optogenetic control of hypocretin neurons. *Nature* 450, 420–424. doi: 10.1038/nature06310

Antel, J., Antel, S., Caramanos, Z., Arnold, D. L., and Kuhlmann, T. (2012). Primary progressive multiple sclerosis: part of the MS disease spectrum or separate disease entity? *Acta Neuropathol.* 123, 627–638. doi: 10.1007/s00401-012-0953-0

Arnulf, I., Bonnet, A. M., Damier, P., Bejjani, B. P., Seilhean, D., Derenne, J. P., et al. (2000). Hallucinations, REM sleep, and Parkinson's disease: a medical hypothesis. *Neurology* 55, 281–288. doi: 10.1212/wnl.55.2.281

Asai, H., Hirano, M., Furiya, Y., Udaka, F., Morikawa, M., Kanbayashi, T., et al. (2009). Cerebrospinal fluid-orexin levels and sleep attacks in four patients

with Parkinson's disease. *Clin. Neurol. Neurosurg.* 111, 341–344. doi: 10.1016/j.clineuro.2008.11.007

Bassetti, C. L. A., Adamantidis, A., Burdakov, D., Han, F., Gay, S., Kallweit, U., et al. (2019). Narcolepsy–clinical spectrum, aetiopathophysiology, diagnosis and treatment. *Nat. Rev. Neurol.* 15, 519–539. doi: 10.1038/s41582-019-0226-9

Becquet, L., Abad, C., Leclercq, M., Miel, C., Jean, L., Riou, G., et al. (2019). Systemic administration of orexin a ameliorates established experimental autoimmune encephalomyelitis by diminishing neuroinflammation. *J. Neuroinflammation* 16:64. doi: 10.1186/s12974-019-1447-y

Brodsky, M. A., Godbold, J., Roth, T., and Olanow, C. W. (2003). Sleepiness in Parkinson's disease: a controlled study. *Mov. Disord.* 18, 668–672. doi: 10.1002/mds.10429

Burfeind, K. G., Yadav, V., and Marks, D. L. (2016). Hypothalamic dysfunction and multiple sclerosis: implications for fatigue and weight dysregulation. *Curr. Neurol. Neurosci. Rep.* 16:98. doi: 10.1007/s11910-016-0700-3

Cabanas, M., Pistono, C., Puygrenier, L., Rakesh, D., Jeantet, Y., Garret, M., et al. (2019). Neurophysiological and behavioral effects of anti-orexinergic treatments in a mouse model of Huntington's disease. *Neurotherapeutics* 16, 784–796. doi: 10.1007/s13311-019-00726-3

Constantinescu, C. S., Niepel, G., Patterson, M., Judd, A., Braitch, M., Fahey, A. J., et al. (2011). Orexin A (hypocretin-1) levels are not reduced while cocaine/amphetamine regulated transcript levels are increased in the cerebrospinal fluid of patients with multiple sclerosis: no correlation with fatigue and sleepiness. *J. Neurol. Sci.* 307, 127–131. doi: 10.1016/j.jns.2011.04.024

Correale, J., Gaitan, M. I., Ysrraelit, M. C., and Fiol, M. P. (2017). Progressive multiple sclerosis: from pathogenic mechanisms to treatment. *Brain* 140, 527–546. doi: 10.1093/brain/aww258

Croce, K. R., and Yamamoto, A. (2019). A role for autophagy in Huntington's disease. *Neurobiol. Dis.* 122, 16–22. doi: 10.1016/j.nbd.2018.08.010

Cui, L. B., Li, B. W., Jin, X. H., Zhao, L., and Shi, J. (2010). Progressive changes of orexin system in a rat model of 6-hydroxydopamine-induced Parkinson's disease. *Neurosci. Bull.* 26, 381–387. doi: 10.1007/s12264-010-0410-9

Datta, G., Colasanti, A., Rabiner, E. A., Gunn, R. N., Malik, O., Ciccarelli, O., et al. (2017). Neuroinflammation and its relationship to changes in brain volume and white matter lesions in multiple sclerosis. *Brain* 140, 2927–2938. doi: 10.1093/brain/awx228

de Lecea, L., Kilduff, T. S., Peyron, C., Gao, X., Foye, P. E., Danielson, P. E., et al. (1998). The hypocretins: hypothalamus-specific peptides with neuroexcitatory activity. *Proc. Natl. Acad. Sci. U.S.A.* 95, 322–327. doi: 10.1073/pnas.95.1.322

Deuschle, M., Schilling, C., Leweke, F. M., Enning, F., Pollmacher, T., Esselmann, H., et al. (2014). Hypocretin in cerebrospinal fluid is positively correlated with Tau and pTau. *Neurosci. Lett.* 561, 41–45. doi: 10.1016/j.neulet.2013.12.036

Drouot, X., Moutereau, S., Nguyen, J. P., Lefaucheur, J. P., Creange, A., Remy, P., et al. (2003). Low levels of ventricular CSF orexin/hypocretin in advanced PD. *Neurology* 61, 540–543. doi: 10.1212/01.wnl.0000078194.53210.48

Dyer, C. J., Touchette, K. J., Carroll, J. A., Allee, G. L., and Matteri, R. L. (1999). Cloning of porcine prepro-orexin cDNA and effects of an intramuscular injection of synthetic porcine orexin-B on feed intake in young pigs. *Domest. Anim. Endocrinol.* 16, 145–148. doi: 10.1016/s0739-7240(99)00011-9

Fatemi, I., Shamsizadeh, A., Ayoobi, F., Taghipour, Z., Sanati, M. H., Roohbakhsh, A., et al. (2016). Role of orexin-A in experimental autoimmune encephalomyelitis. *J. Neuroimmunol.* 291, 101–109. doi: 10.1016/j.jneuroim.2016.01.001

Feng, Y., Liu, T., Li, X. Q., Liu, Y., Zhu, X. Y., Jankovic, J., et al. (2014). Neuroprotection by orexin-A via HIF-1alpha induction in a cellular model of Parkinson's disease. *Neurosci. Lett.* 579, 35–40. doi: 10.1016/j.neulet.2014.07.014

Fronczek, R., Overeem, S., Lee, S. Y., Hegeman, I. M., van Pelt, J., van Duinen, S. G., et al. (2007). Hypocretin (orexin) loss in Parkinson's disease. *Brain* 130(Pt 6), 1577–1585. doi: 10.1093/brain/awm090

Fronczek, R., van Geest, S., Frolich, M., Overeem, S., Roelandse, F. W., Lammers, G. J., et al. (2012). Hypocretin (orexin) loss in Alzheimer's disease. *Neurobiol. Aging* 33, 1642–1650. doi: 10.1016/j.neurobiolaging.2011.03.014

Gabelle, A., Jaussent, I., Hirtz, C., Vialaret, J., Navucet, S., Grasselli, C., et al. (2017). Cerebrospinal fluid levels of orexin-A and histamine, and sleep profile within the Alzheimer process. *Neurobiol. Aging* 53, 59–66. doi: 10.1016/j.neurobiolaging.2017.01.011

Gabery, S., Murphy, K., Schultz, K., Loy, C. T., McCusker, E., Kirik, D., et al. (2010). Changes in key hypothalamic neuropeptide populations in Huntington disease revealed by neuropathological analyses. *Acta Neuropathol.* 120, 777–788. doi: 10.1007/s00401-010-0742-6

Gamble, M. C., Katsuki, F., McCoy, J. G., Strecker, R. E., and McKenna, J. T. (2019). The dual orexinergic receptor antagonist DORA-22 improves the sleep disruption and memory impairment produced by a rodent insomnia model. *Sleep* 43:zsz241. doi: 10.1093/sleep/zsz241

Gencer, M., Akbayir, E., Sen, M., Arsoy, E., Yilmaz, V., Bulut, N., et al. (2019). Serum orexin-a levels are associated with disease progression and motor impairment in multiple sclerosis. *Neurol. Sci.* 40, 1067–1070. doi: 10.1007/s10072-019-3708-z

Ghosh, R., and Tabrizi, S. J. (2018). Huntington disease. *Handb. Clin. Neurol.* 147, 255–278. doi: 10.1016/B978-0-444-63233-3.00017-8

Glass, C. K., Saijo, K., Winner, B., Marchetto, M. C., and Gage, F. H. (2010). Mechanisms underlying inflammation in neurodegeneration. *Cell* 140, 918–934. doi: 10.1016/j.cell.2010.02.016

Gotter, A. L., Webber, A. L., Coleman, P. J., Renger, J. J., and Winrow, C. J. (2012). International union of basic and clinical pharmacology. LXXXVI. OREXIN receptor function, nomenclature and pharmacology. *Pharmacol. Rev.* 64, 389–420. doi: 10.1124/pr.111.005546

Grajchen, E., Hendriks, J. J. A., and Bogie, J. F. J. (2018). The physiology of foamy phagocytes in multiple sclerosis. *Acta Neuropathol. Commun.* 6:124. doi: 10.1186/s40478-018-0628-8

Guerreiro, S., Florence, C., Rousseau, E., Hamadat, S., Hirsch, E. C., and Michel, P. P. (2015). The sleep-modulating peptide orexin-B protects midbrain dopamine neurons from degeneration, alone or in cooperation with nicotine. *Mol. Pharmacol.* 87, 525–532. doi: 10.1124/mol.114.095703

Hadadianpour, Z., Fatehi, F., Ayoobi, F., Kaeidi, A., Shamsizadeh, A., and Fatemi, I. (2017). The effect of orexin-A on motor and cognitive functions in a rat model of Parkinson's disease. *Neurol. Res.* 39, 845–851. doi: 10.1080/01616412.2017.1352185

Hughes, J., Jokubaitis, V., Lugaresi, A., Hupperts, R., Izquierdo, G., Prat, A., et al. (2018). Association of inflammation and disability accrual in patients with progressive-onset multiple sclerosis. *JAMA Neurol.* 75, 1407–1415. doi: 10.1001/jamaneurol.2018.2109

Illarioshkin, S. N., Klyushnikov, S. A., Vigont, V. A., Seliverstov, Y. A., and Kaznacheyeva, E. V. (2018). Molecular pathogenesis in Huntington's disease. *Biochemistry* 83, 1030–1039. doi: 10.1134/S0006297918090043

Irukayama-Tomobe, Y., Ogawa, Y., Tominaga, H., Ishikawa, Y., Hosokawa, N., Ambai, S., et al. (2017). Nonpeptide orexin type-2 receptor agonist ameliorates narcolepsy-cataplexy symptoms in mouse models. *Proc. Natl. Acad. Sci. U.S.A.* 114, 5731–5736. doi: 10.1073/pnas.1700499114

Jeantet, Y., Cayzac, S., and Cho, Y. H. (2013). Beta oscillation during slow wave sleep and rapid eye movement sleep in the electroencephalogram of a transgenic mouse model of Huntington's disease. *PLoS One* 8:e79509. doi: 10.1371/journal.pone.0079509

Kalia, L. V., and Lang, A. E. (2015). Parkinson's disease. *Lancet* 386, 896–912. doi: 10.1016/S0140-6736(14)61393-3

Kang, J. E., Lim, M. M., Bateman, R. J., Lee, J. J., Smyth, L. P., Cirrito, J. R., et al. (2009). Amyloid-beta dynamics are regulated by orexin and the sleep-wake cycle. *Science* 326, 1005–1007. doi: 10.1126/science.1180962

Lane, C. A., Hardy, J., and Schott, J. M. (2018). Alzheimer's disease. *Eur. J. Neurol.* 25, 59–70. doi: 10.1111/ene.13439

Lebreton, F., Cayzac, S., Pietropaolo, S., Jeantet, Y., and Cho, Y. H. (2015). Sleep physiology alterations precede plethoric phenotypic changes in R6/1 Huntington's disease mice. *PLoS One* 10:e0126972. doi: 10.1371/journal.pone.0126972

Li, S. B., and de Lecea, L. (2020). The hypocretin (orexin) system: from a neural circuitry perspective. *Neuropharmacology* 167:107993. doi: 10.1016/j.neuropharm.2020.107993

Liguori, C. (2017). Orexin and Alzheimer's disease. *Curr. Top. Behav. Neurosci.* 33, 305–322. doi: 10.1007/7854_2016_50

Liguori, C., Mercuri, N. B., Nuccetelli, M., Izzi, F., Bernardini, S., and Placidi, F. (2018). Cerebrospinal fluid orexin levels and nocturnal sleep disruption in

Alzheimer's disease patients showing neuropsychiatric symptoms. *J. Alzheimers Dis.* 66, 993–999. doi: 10.3233/JAD-180769

Liguori, C., Romigi, A., Nuccetelli, M., Zannino, S., Sancesario, G., Martorana, A., et al. (2014). Orexinergic system dysregulation, sleep impairment, and cognitive decline in Alzheimer disease. *JAMA Neurol.* 71, 1498–1505. doi: 10.1001/jamaneurol.2014.2510

Liguori, C., Spanetta, M., Izzi, F., Franchini, F., Nuccetelli, M., Sancesario, G. M., et al. (2020). Sleep-wake cycle in Alzheimer's disease is associated with tau pathology and orexin dysregulation. *J. Alzheimers Dis.* 74, 501–508. doi: 10.3233/JAD-191124

Liu, C., Xue, Y., Liu, M. F., Wang, Y., Liu, Z. R., Diao, H. L., et al. (2018). Orexins increase the firing activity of nigral dopaminergic neurons and participate in motor control in rats. *J. Neurochem.* 147, 380–394. doi: 10.1111/jnc.14568

Liu, M. F., Xue, Y., Liu, C., Liu, Y. H., Diao, H. L., Wang, Y., et al. (2018). Orexin-A exerts neuroprotective effects via OX1R in Parkinson's disease. *Front. Neurosci.* 12:835. doi: 10.3389/fnins.2018.00835

Liu, Z., Wang, F., Tang, M., Zhao, Y., and Wang, X. (2019). Amyloid beta and tau are involved in sleep disorder in Alzheimer's disease by orexin A and adenosine A(1) receptor. *Int. J. Mol. Med.* 43, 435–442. doi: 10.3892/ijmm.2018.3935

Lublin, F. D., and Reingold, S. C. (1996). Defining the clinical course of multiple sclerosis: results of an international survey. national multiple sclerosis society (USA) advisory committee on clinical trials of new agents in multiple sclerosis. *Neurology* 46, 907–911. doi: 10.1212/wnl.46.4.907

Mander, B. A., Winer, J. R., Jagust, W. J., and Walker, M. P. (2016). Sleep: a novel mechanistic pathway, biomarker, and treatment target in the pathology of Alzheimer's disease? *Trends Neurosci* 39, 552–566. doi: 10.1016/j.tins.2016.05.002

Nepovimova, E., Janockova, J., Misik, J., Kubik, S., Stuchlik, A., Vales, K., et al. (2019). Orexin supplementation in narcolepsy treatment: a review. *Med. Res. Rev.* 39, 961–975. doi: 10.1002/med.21550

Nie, K., Gao, Y., Mei, M., Guo, M., Huang, Z., Wang, L., et al. (2019). The clinical characteristics and cognitive features of mild cognitive impairment in Parkinson's disease and the analysis of relevant factors. *J. Clin. Neurosci.* 63, 142–148. doi: 10.1016/j.jocn.2019.01.021

Oka, Y., Kanbayashi, T., Mezaki, T., Iseki, K., Matsubayashi, J., Murakami, G., et al. (2004). Low CSF hypocretin-1/orexin-A associated with hypersomnia secondary to hypothalamic lesion in a case of multiple sclerosis. *J. Neurol.* 251, 885–886. doi: 10.1007/s00415-004-0442-z

Page, K. J., Besret, L., Jain, M., Monaghan, E. M., Dunnett, S. B., and Everitt, B. J. (2000). Effects of systemic 3-nitropropionic acid-induced lesions of the dorsal striatum on cannabinoid and mu-opioid receptor binding in the basal ganglia. *Exp. Brain Res.* 130, 142–150. doi: 10.1007/s002210050016

Pallier, P. N., Maywood, E. S., Zheng, Z., Chesham, J. E., Inyushkin, A. N., Dyball, R., et al. (2007). Pharmacological imposition of sleep slows cognitive decline and reverses dysregulation of circadian gene expression in a transgenic mouse model of Huntington's disease. *J. Neurosci.* 27, 7869–7878. doi: 10.1523/JNEUROSCI.0649-07.2007

Pallier, P. N., and Morton, A. J. (2009). Management of sleep/wake cycles improves cognitive function in a transgenic mouse model of Huntington's disease. *Brain Res.* 1279, 90–98. doi: 10.1016/j.brainres.2009.03.072

Pasban-Aliabadi, H., Esmaeili-Mahani, S., and Abbasnejad, M. (2017). Orexin-A protects human neuroblastoma SH-SY5Y cells against 6-hydroxydopamine-induced neurotoxicity: involvement of PKC and PI3K signaling pathways. *Rejuvenation Res.* 20, 125–133. doi: 10.1089/rej.2016.1836

Paus, S., Brecht, H. M., Koster, J., Seeger, G., Klockgether, T., and Wullner, U. (2003). Sleep attacks, daytime sleepiness, and dopamine agonists in Parkinson's disease. *Mov. Disord.* 18, 659–667. doi: 10.1002/mds.10417

Petersen, A., Gil, J., Maat-Schieman, M. L., Bjorkqvist, M., Tanila, H., Araujo, I. M., et al. (2005). Orexin loss in Huntington's disease. *Hum. Mol. Genet.* 14, 39–47. doi: 10.1093/hmg/ddi004

Qiu, K., Zhang, X., Wang, S., Li, C., Wang, X., Li, X., et al. (2019). TMP21 in Alzheimer's disease: molecular mechanisms and a potential target. *Front. Cell. Neurosci.* 13:328. doi: 10.3389/fncel.2019.00328

Reich, S. G., and Savitt, J. M. (2019). Parkinson's disease. *Med. Clin. North Am.* 103, 337–350. doi: 10.1016/j.mcna.2018.10.014

Roh, J. H., Jiang, H., Finn, M. B., Stewart, F. R., Mahan, T. E., Cirrito, J. R., et al. (2014). Potential role of orexin and sleep modulation in the pathogenesis of Alzheimer's disease. *J. Exp. Med.* 211, 2487–2496. doi: 10.1084/jem.20141788

Sahraian, M. A., Rezaali, S., Hosseiny, M., Doosti, R., Tajik, A., and Naser Moghadasi, A. (2017). Sleep disorder as a triggering factor for relapse in multiple sclerosis. *Eur. Neurol.* 77, 258–261. doi: 10.1159/000470904

Sakurai, T., Amemiya, A., Ishii, M., Matsuzaki, I., Chemelli, R. M., Tanaka, H., et al. (1998). Orexins and orexin receptors: a family of hypothalamic neuropeptides and G protein-coupled receptors that regulate feeding behavior. *Cell* 92, 573–585. doi: 10.1016/s0092-8674(02)09256-5

Sasaki, K., Suzuki, M., Mieda, M., Tsujino, N., Roth, B., and Sakurai, T. (2011). Pharmacogenetic modulation of orexin neurons alters sleep/wakefulness states in mice. *PLoS One* 6:e20360. doi: 10.1371/journal.pone.0020360

Shimizu, S., Takenoshita, N., Inagawa, Y., Tsugawa, A., Hirose, D., Kaneko, Y., et al. (2020). Positive association between cognitive function and cerebrospinal fluid orexin a levels in Alzheimer's disease. *J. Alzheimers Dis.* 73, 117–123. doi: 10.3233/JAD-190958

Shin, H. S., Cho, H. S., Sung, K. W., and Yoon, B. J. (2009). Orexin-A increases cell surface expression of AMPA receptors in the striatum. *Biochem. Biophys. Res. Commun.* 378, 409–413. doi: 10.1016/j.bbrc.2008.11.051

Slats, D., Claassen, J. A., Lammers, G. J., Melis, R. J., Verbeek, M. M., and Overeem, S. (2012). Association between hypocretin-1 and amyloid-beta42 cerebrospinal fluid levels in Alzheimer's disease and healthy controls. *Curr. Alzheimer Res.* 9, 1119–1125. doi: 10.2174/156720512804142840

Soya, S., and Sakurai, T. (2020). Evolution of orexin neuropeptide system: structure and function. *Front. Neurosci.* 14:691. doi: 10.3389/fnins.2020.00691

Soya, S., Shoji, H., Hasegawa, E., Hondo, M., Miyakawa, T., Yanagisawa, M., et al. (2013). Orexin receptor-1 in the locus coeruleus plays an important role in cue-dependent fear memory consolidation. *J. Neurosci.* 33, 14549–14557. doi: 10.1523/JNEUROSCI.1130-13.2013

Spinazzi, R., Andreis, P. G., Rossi, G. P., and Nussdorfer, G. G. (2006). Orexins in the regulation of the hypothalamic-pituitary-adrenal axis. *Pharmacol. Rev.* 58, 46–57. doi: 10.1124/pr.58.1.4

Stanojlovic, M., Pallais, J. P., Lee, M. K., and Kotz, C. M. (2019). Pharmacological and chemogenetic orexin/hypocretin intervention ameliorates Hipp-dependent memory impairment in the A53T mice model of Parkinson's disease. *Mol. Brain* 12:87. doi: 10.1186/s13041-019-0514-8

Tracik, F., and Ebersbach, G. (2001). Sudden daytime sleep onset in Parkinson's disease: polysomnographic recordings. *Mov. Disord.* 16, 500–506. doi: 10.1002/mds.1083

Trivedi, P., Yu, H., MacNeil, D. J., Van der Ploeg, L. H., and Guan, X. M. (1998). Distribution of orexin receptor mRNA in the rat brain. *FEBS Lett.* 438, 71–75. doi: 10.1016/s0014-5793(98)01266-6

Tunisi, L., Forte, N., Fernandez-Rilo, A. C., Mavaro, I., Capasso, R., D'Angelo, L., et al. (2019). Orexin-A prevents lipopolysaccharide-induced neuroinflammation at the level of the intestinal barrier. *Front. Endocrinol.* 10:219. doi: 10.3389/fendo.2019.00219

Turkoglu, R., Benbir, G., Ozyurt, S., Arsoy, E., Akbayir, E., Turan, S., et al. (2020). Sleep disturbance and cognitive decline in multiple sclerosis patients with isolated optic neuritis as the first demyelinating event. *Int. Ophthalmol.* 40, 151–158. doi: 10.1007/s10792-019-01157-x

Wang, C., Wang, Q., Ji, B., Pan, Y., Xu, C., Cheng, B., et al. (2018). The orexin/receptor system: molecular mechanism and therapeutic potential for neurological diseases. *Front. Mol. Neurosci.* 11:220. doi: 10.3389/fnmol.2018.00220

Wyant, K. J., Ridder, A. J., and Dayalu, P. (2017). Huntington's disease-update on treatments. *Curr. Neurol. Neurosci. Rep.* 17:33. doi: 10.1007/s11910-017-0739-9

Xie, L., Kang, H., Xu, Q., Chen, M. J., Liao, Y., Thiyagarajan, M., et al. (2013). Sleep drives metabolite clearance from the adult brain. *Science* 342, 373–377. doi: 10.1126/science.1241224

Yasui, K., Inoue, Y., Kanbayashi, T., Nomura, T., Kusumi, M., and Nakashima, K. (2006). CSF orexin levels of Parkinson's disease, dementia with Lewy bodies, progressive supranuclear palsy and corticobasal degeneration. *J. Neurol. Sci.* 250, 120–123. doi: 10.1016/j.jns.2006.08.004

Yukitake, H., Fujimoto, T., Ishikawa, T., Suzuki, A., Shimizu, Y., Rikimaru, K., et al. (2019). TAK-925, an orexin 2 receptor-selective agonist, shows robust wake-promoting effects in mice. *Pharmacol. Biochem. Behav.* 187:172794. doi: 10.1016/j.pbb.2019.172794

Zajo, K. N., Fadel, J. R., and Burk, J. A. (2016). Orexin A-induced enhancement of attentional processing in rats: role of basal forebrain neurons. *Psychopharmacology* 233, 639–647. doi: 10.1007/s00213-015-4139-z

Zhang, B., Guo, D., Han, L., Rensing, N., Satoh, A., and Wong, M. (2019). Hypothalamic orexin and mechanistic target of rapamycin activation mediate sleep dysfunction in a mouse model of tuberous sclerosis complex. *Neurobiol. Dis.* 134:104615. doi: 10.1016/j.nbd.2019.104615

Zhang, G. C., Mao, L. M., Liu, X. Y., and Wang, J. Q. (2007). Long-lasting up-regulation of orexin receptor type 2 protein levels in the rat nucleus accumbens after chronic cocaine administration. *J. Neurochem.* 103, 400–407. doi: 10.1111/j.1471-4159.2007.04748.x

Conflict of Interest: The authors declare that the research was conducted in the absence of any commercial or financial relationships that could be construed as a potential conflict of interest.

frontiers in Aging Neuroscience

ORIGINAL RESEARCH
published: 03 September 2021
doi: 10.3389/fnagi.2021.721474

NLRP3 Inflammasome-Dependent Increases in High Mobility Group Box 1 Involved in the Cognitive Dysfunction Caused by Tau-Overexpression

Yan Zhao[1,2†], Si-Wei Tan[1†], Zhi-Zhong Huang[1], Fa-Bo Shan[1], Ping Li[1,2], Ya-Lei Ning[1,2], Shi-Yang Ye[1], Zi-Ai Zhao[3], Hao Du[1], Ren-Ping Xiong[1], Nan Yang[1], Yan Peng[1], Xing Chen[1] and Yuan-Guo Zhou[1,2]*

[1] Department of Army Occupational Disease, State Key Laboratory of Trauma, Burns and Combined Injury, Research Institute of Surgery, Daping Hospital, Army Medical University, Chongqing, China, [2] Institute of Brain and Intelligence, Army Medical University, Chongqing, China, [3] Department of Neurology, General Hospital of Northern Theater Command, Shenyang, China

OPEN ACCESS

Edited by:
Natalia Salvadores,
Universidad Mayor, Chile

Reviewed by:
Bora Taştan,
Dokuz Eylul University, Turkey
Yang Chen,
Guangzhou University of Chinese Medicine, China
Bo-Zong Shao,
General Hospital of Chinese PLA, China

***Correspondence:**
Yuan-Guo Zhou
ygzhou@tmmu.edu.cn;
yuanguo.zhou@gmail.com

[†] These authors have contributed equally to this work and share first authorship

Received: 07 June 2021
Accepted: 10 August 2021
Published: 03 September 2021

Citation:
Zhao Y, Tan S-W, Huang Z-Z, Shan F-B, Li P, Ning Y-L, Ye S-Y, Zhao Z-A, Du H, Xiong R-P, Yang N, Peng Y, Chen X and Zhou Y-G (2021) NLRP3 Inflammasome-Dependent Increases in High Mobility Group Box 1 Involved in the Cognitive Dysfunction Caused by Tau-Overexpression. Front. Aging Neurosci. 13:721474. doi: 10.3389/fnagi.2021.721474

Tau hyperphosphorylation is a characteristic alteration present in a range of neurological conditions, such as traumatic brain injury (TBI) and neurodegenerative diseases. Treatments targeting high-mobility group box protein 1 (HMGB1) induce neuroprotective effects in these neuropathologic conditions. However, little is known about the interactions between hyperphosphorylated tau and HMGB1 in neuroinflammation. We established a model of TBI with controlled cortical impacts (CCIs) and a tau hyperphosphorylation model by injecting the virus encoding human P301S tau in mice, and immunofluorescence, western blotting analysis, and behavioral tests were performed to clarify the interaction between phosphorylated tau (p-tau) and HMGB1 levels. We demonstrated that p-tau and HMGB1 were elevated in the spatial memory-related brain regions in mice with TBI and tau-overexpression. Animals with tau-overexpression also had significantly increased nucleotide-binding oligomerization domain-like receptor pyrin domain-containing protein 3 (NLRP3) inflammasome activation, which manifested as increases in apoptosis-associated speck-like protein containing a caspase recruitment domain (ASC), activating caspase-1 and interleukin 1 beta (IL-1β) levels. In addition, NLRP3$^{-/-}$ mice and the HMGB1 inhibitor, glycyrrhizin, were used to explore therapeutic strategies for diseases with p-tau overexpression. Compared with wild-type (WT) mice with tau-overexpression, downregulation of p-tau and HMGB1 was observed in NLRP3$^{-/-}$ mice, indicating that HMGB1 alterations were NLRP3-dependent. Moreover, treatment with glycyrrhizin at a late stage markedly reduced p-tau levels and improved performance in the Y- and T-mazes and the ability of tau-overexpressing mice to build nests, which revealed improvements in spatial memory and advanced hippocampal function. The findings identified that p-tau has a triggering role in the modulation of neuroinflammation and spatial memory in an NLRP3-dependent manner, and suggest that treatment with HMGB1 inhibitors may be a better therapeutic strategy for tauopathies.

Keywords: traumatic brain injury, high mobility group box-1, tau, NLRP3 inflammasome, spatial memory, hippocampus

INTRODUCTION

The accumulation of phosphorylated tau is a characteristic change in tauopathy and other neurodegenerative diseases. Accumulating research has revealed that tau plays a crucial role in the severity and progression of cognitive impairments (Furman et al., 2017), and that the immunological inhibition of tau has beneficial effects in the therapy of degenerative diseases (Albert et al., 2019; Takeda, 2019; Colin et al., 2020). The hyperphosphorylation of tau is consistently observed in secondary tauopathies, such as chronic traumatic encephalopathy (CTE), traumatic brain injury (TBI), and Alzheimer's disease (AD; Edwards et al., 2017; Johnson et al., 2017; Rubenstein et al., 2017; VanItallie, 2019), and is regarded as a risk factor for AD and CTE (Washington et al., 2016; Collins-Praino and Corrigan, 2017; Kulbe and Hall, 2017). Recent evidence has shown that behavioral disorders are more closely associated with a high level of p-tau after TBI than with amyloid-beta (Aβ; Chen et al., 2009; Huber et al., 2013; Tweedie et al., 2013; Takahata et al., 2017). These abnormalities related to tau occur as early as several months to years after trauma; thus, hyperphosphorylated tau is considered the "trigger" of AD (Bramlett and Dietrich, 2015; Johnson et al., 2017). In addition, the p-tau level has a dose-dependent effect on the severity and frequency of trauma, suggesting that tau hyperphosphorylation may be a key factor for the early onset or rapid progression of cognitive impairments (Edwards et al., 2017). However, the distribution and spread of p-tau in brain regions varies depending on the type of neurodegenerative disease (Kaufman et al., 2016), and the mechanisms by which abnormal tau leads to neuropathological alterations and cognitive damage have not been fully clarified.

Neuroinflammation is a typical pathological change seen with neurodegenerative diseases, and the relationship between neuroinflammation and characteristic pathological impairments (neurofibrillary tangles caused by tau hyperphosphorylation and senile plaques caused by Aβ) has received much attention from neuroscientists. In particular, the NLRP3 inflammasome, which is involved in both infectious and sterile inflammation, has recently been considered a potential therapeutic target for cognitive impairments such as AD (White et al., 2017; Swanson et al., 2019). A large body of research has shown that NLRP3 inhibition reduces the release of proinflammatory factors and inhibits the activation of microglia in experimental animals in the acute phase after TBI (Kuwar et al., 2019; Yi et al., 2019). A variety of pathogen-associated molecular patterns (PAMPs) and damage-associated molecular patterns (DAMPs) can activate the (Kaufman et al., 2016) NLRP3 inflammasome and cause significant increases in proinflammatory factors such as IL-1β. Recently, it has been found that Aβ is also an activator of NLRP3 (Halle et al., 2008); however, there are limited studies on whether phosphorylated tau (monomer or oligomer) could activate the NLRP3 inflammasome, and the underlying mechanisms remain to be clarified. The activation of the NLRP3 inflammasome leads to neuroinflammation not only by activating caspase-1 to produce interleukin 1 beta (IL-1β) and interleukin-18 (IL-18) but also by releasing high mobility group box-1 (HMGB1) to initiate a cascade of inflammation that can lead to neuroinflammatory responses. Many studies have reported that HMGB1, as an important late-stage inflammatory mediator, is an important therapeutic target for infectious diseases such as sepsis-associated encephalopathy and autoimmune encephalomyelitis (Uzawa et al., 2013) at an early stage. It has been reported that the expression of HMGB1 increases approximately 12 h following TBI, spinal cord injury, and cerebral hemorrhage, and that anti-HMGB1 therapy can reduce brain edema, inhibit neuroinflammation, and restore neurological dysfunction (Okuma et al., 2012; Haruma et al., 2016; Wang et al., 2017; Kobayashi et al., 2018). However, HMGB1 almost returned to the baseline level 2–4 weeks after injury according to published data (Kigerl et al., 2018). It is not clear whether HMGB1 increases in the late period after brain injury. However, HMGB1 is closely related to cognitive impairment in the chronic period after injury. For instance, prolonged increase in HMGB1 is associated with cognitive impairment in intensive care unit survivors (Bruck et al., 2020), suggesting that HMGB1 is an important factor that exacerbates the progression of cognitive impairments. However, the reason for the increase in HMGB1 at a delayed stage and the interaction between the increased p-tau and HMGB1 are not fully understood. Therefore, we tried to identify the effect of hyperphosphorylated tau on the activation of the NLRP3 inflammasome and HMGB1 levels in different brain regions using animals with tau-overexpression and NLRP3 knockout. In addition, we explored the therapeutic strategy of HMGB1 inhibitors to elicit neuroprotective effects in neurodegenerative diseases with tau overexpression. This research paves the way for the multiple-target treatment of neurodegenerative diseases and offers insight into the complexity of p-tau-HMGB1 interactions.

MATERIALS AND METHODS

Animals

Adult male mice (10–11 weeks old), purchased from the Shanghai Laboratory Animal Research Center (Shanghai, China), were housed in a 12-h light/dark cycle facility and allowed free access to food and water. Global NLRP3 knockout mice on a C57BL/6J background were provided by Professor Lei Li from Army Medical University. All the animal experiments were approved by the Laboratory Animal Welfare and Ethics Committee of the Army Medical University (AMUWEC20191822), and complied with the NIH Guide for the Care and Use of Laboratory Animals.

Traumatic Brain Injury Models

The animal model of moderate TBI was established by controlled cortical impact (CCI) according to a published article (Zhao et al., 2017b). Briefly, the mice were anesthetized using 50 mg/kg pentobarbital sodium. TBI was induced using a head trauma contusion device with a pneumatic impactor (TBI-0310, PSI, Hampton, United States) after craniotomy was performed over the left parietal cortex. The impact parameters were a velocity of 3.5 m/s, diameter of 3 mm, and depth of 1.5 mm (**Figure 1A**). The mice were then placed on an electric blanket until they woke up

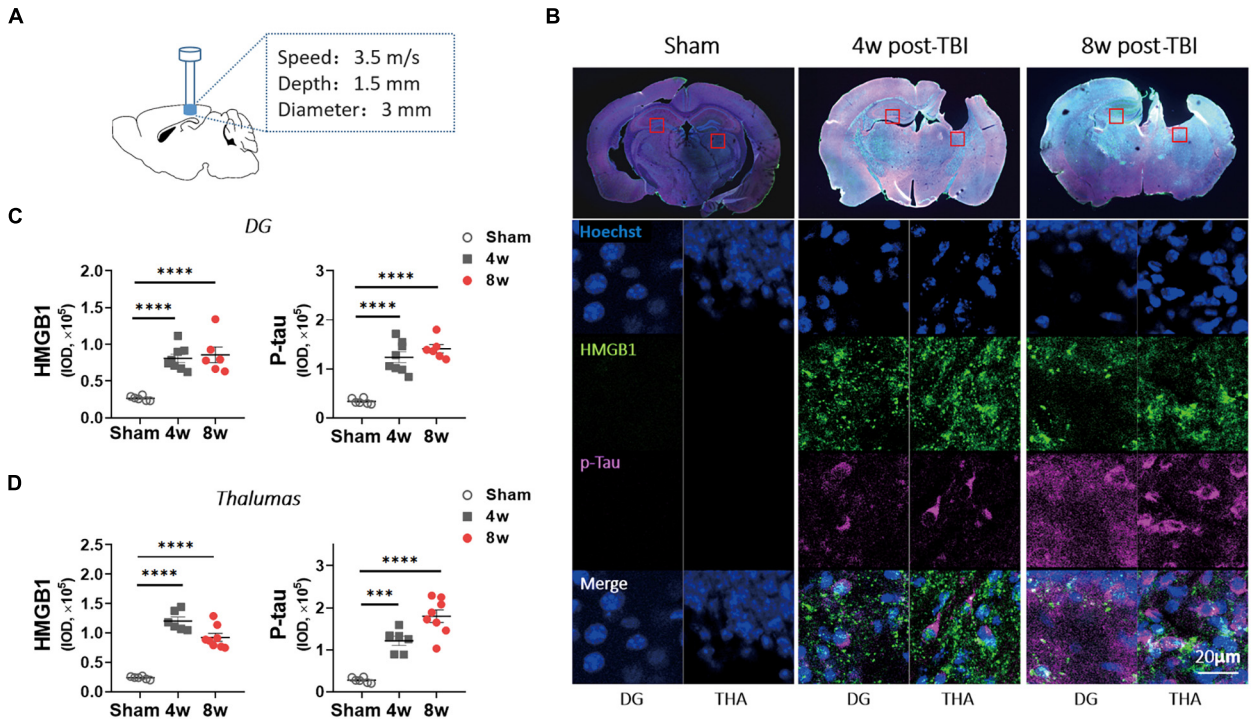

FIGURE 1 | Levels of p-tau and high mobility group box-1 (HMGB1) were increased in wild-type (WT) mice with traumatic brain injury (TBI). **(A)** An experimental mouse model of TBI. **(B)** Representative images showed the increased immunoreactivities for HMGB1 and p-tau (ser404) in ipsilateral thalamus (THA) (close to lesion location) and contralateral dentate gyrus (DG) at 4 and 8 weeks (w) post-TBI. **(C,D)** HMGB1 and p-tau immunoreactivities were quantified with fluorescence intensity in **(C)** DG and **(D)** thalamus 4 and 8 weeks post TBI. One-way analysis of variance (ANOVA) was performed followed by Dunnett's multiple comparisons test. ***$p < 0.001$, ****$p < 0.0001$.

and then returned to their home cages. In the sham group, only anesthesia and craniotomy were performed in animals.

Overexpression of Tau P301S

The adeno-associated virus (AAV) encoding human P301S tau under the control of the neuron-specific CaMKII promoter (AAV2/9-CaMKII-hTau^{P301S}-GFP, AAV-tau hereafter) and a control virus (AAV2/9-CamkII-GFP, AAV-GFP hereafter) were created by Hanbio Biotechnology Co. Ltd. (Shanghai, China). The mice were anesthetized, and craniotomy was performed using a.5 mm diameter drill over the left parietal cortex (AP: −2 ML: −1 DV: −1.5). The animals were stereotaxically injected with 1 μl of normal saline (Sham), AAV-tau, or AAV-GFP (viral titers 1.8×10^{12} vg/ml) into the hippocampus at a rate of 200 nl/min, and the needle was kept in place for 5 min before retraction. Then, the mice were removed from the stereotaxic frame and returned to their home cages.

Drugs

Glycyrrhizin, an HMGB1 inhibitor (GZ, Selleck, Shanghai, China), was dissolved in 2% dimethyl sulfoxide (DMSO) + 30% polyethylene glycol (PEG) 300 + 2% Tween 80 + ddH_2O according to the recommendation of the manufacturer. The mice were injected intraperitoneally with a volume of 100 μl GZ at a dose of 25 mg/kg. The drug was administered once daily for 7 days. Then, the drug was administered once a week for 3 weeks. The total treatment duration was 4 weeks (**Figure 7A**).

Behavioral Experiments

The behavioral tests of mice were performed at the indicated time points (**Figures 2A**, **7A**) and analyzed by the EthoVision XT system (Version 11.5; Noldus, Wageningen, Netherlands). All the tests were conducted by experimenters blinded to the animal groups.

The Y-maze was used to assess short-term spatial memory, as previously described (Webster et al., 2019a). In brief, each trial consisted of a 5-min acquisition phase (novel arms were blocked), an intertrial interval (30 min), and a final 5-min test phase (all arms were open). The total amount of time spent in each arm was recorded, and the percentage of time spent in the novel arm was used to reflect the spatial memory of mice (McAllister et al., 2018). It was calculated as [the time in novel arm/(the time in novel arm + the time in familiar arm)] × 100.

We used the T-maze to assess the working memory of the animals. There were two phases in the current paradigm: a sample phase and a choice phase with a 1-min interval (Deacon and Rawlins, 2006). The animals were placed in the start area, allowed to choose a goal arm, and confined in the chosen arm for 1 min. Then, the animals were returned to the start arm to undergo another choice, and a different choice against the former was

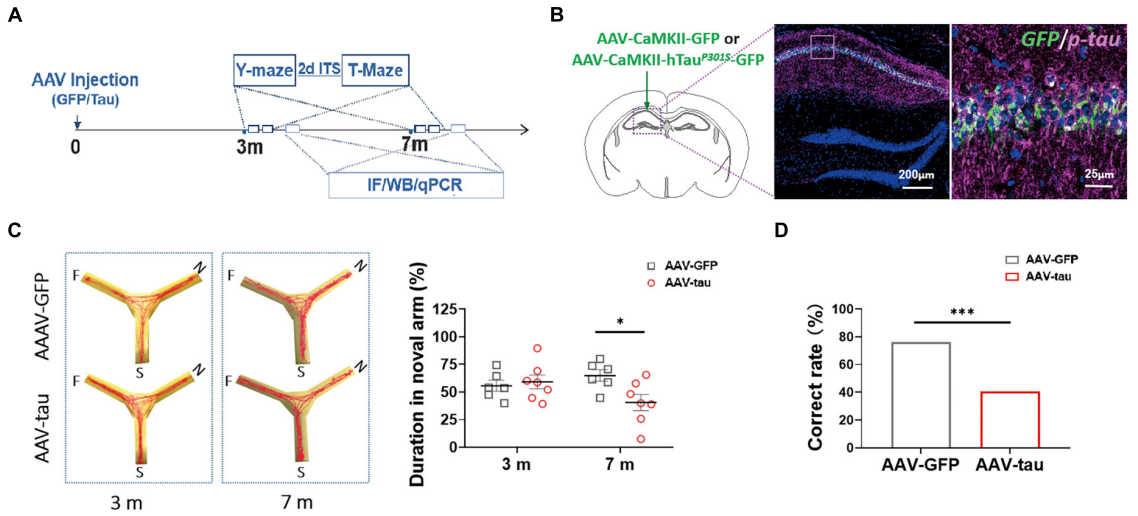

FIGURE 2 | Overexpression of p-tau induced cognitive dysfunction in mice with adeno-associated virus (AAV)-tau injection. **(A)** Experimental paradigm. **(B)** Representative images of the ipsilateral hippocampus taken from mice injected with AAV2/9-CaMKII-hTau^{P301S}-GFP (called AAV-tau) into the hippocampus. The positive staining for phosphorylated tau at ser404 (purple) indicated successful animal model with p-tau overexpression. **(C)** Representative moving tracks (left) and the percentages of time spent in the novel arm (right) of mice that received AAV-tau (n = 8) or AAV-GFP (n = 6) injections in Y-maze at 3 and 7 months time points. **(D)** Working memory of mice was assessed by the total correct rate of six trials at 3 (n = 10) and 7 months (n = 7 and 12, AAV-GFP and AAV-tau) post-injection in a T-maze test. Two-way ANOVA was performed followed by Bonferroni's multiple comparisons test. Pearson chi-square test was also performed, $^{*}p < 0.05$, $^{***}p < 0.001$.

recorded as correct. We performed the test twice a day for three consecutive days. The total percentage of correct responses was calculated to measure the performances in this behavioral testing.

The capacity of nest building reflected advanced hippocampus cognition. Briefly, the mice were housed individually, and a piece of cotton material was placed in each cage overnight for them to build nests. Then, the nests were assessed the next morning by weighing untorn cotton pieces (Deacon, 2006). A higher percentage of untorn material indicated nest building performances that were worse.

Immunofluorescence Staining

The mice were anesthetized with 1.5% sodium pentobarbital and perfused transcardially with phosphate-buffered saline (PBS), followed by 4% paraformaldehyde (PFA). Their brains were dissected and fixed in 4% PFA for 24 h, and coronal cryosections (30 μm thick) were obtained from the experimental animals. Anti-tau Ser404 (ab92676) and anti-HMGB1 (ab18256) antibodies were purchased from Abcam (Cambridge, United Kingdom), and anti-NLRP3 (AG-20B-0014-C100), anti-ASC (AG-25B-0006-C100), and anti-caspase-1 (P20) (AG-20B-0042-C100) antibodies were purchased from AdipoGen Life Sciences (San Diego, CA, United States) (detailed information in **Supplementary Table 1**). Fluorescence images were acquired using a laser scanning confocal fluorescence microscope (TCS SP8; Leica, Wetzlar, Germany). The fluorescence images were converted to 8-bit images, and then the stained area was quantified using the ImageJ software. Detection of the background staining was eliminated by setting the same threshold to all the images.

Western Blotting

The mouse brains were rapidly dissected on ice, and the hippocampal and prefrontal cortices were removed for western blotting. The tissues were homogenized using T-PER Tissue Protein Extraction Reagent (Thermo Fisher Scientific, Waltham, MA, United States) plus Pierce Protease and Phosphatase Inhibitor Mini Tablets (Thermo Fisher Scientific, Waltham, MA, United States). The proteins were separated by 10% sodium dodecyl sulfate-polyacrylamide gel electrophoresis (SDS-PAGE) electrophoresis, transferred onto polyvinylidene difluoride (PVDF) membranes, and incubated overnight in primary antibodies. Except for the anti-tau 5 (ab80579; Abcam, Cambridge, United Kingdom) and anti-glyceraldehyde 3-phosphate dehydrogenase (GAPDH) (Bioworld, St. Louis, Park, MN, United States) antibodies, the rest were the same as those in immunofluorescence experiments. The bands were analyzed using the ImageJ software.

Quantitative Reverse Transcription Polymerase Chain Reaction

Total RNA was extracted using an Eastep® Super Total RNA Extraction Kit (Promega, Madison, WI, United States) and then reverse transcribed to cDNA (GoScript™ Reverse Transcription System; Promega, Madison, WI, United States) according to the instructions of the manufacturer. Quantitative polymerase chain reaction (qPCR) was performed in a Stratagene Mx3000P system (Stratagene, La Jolla, CA, United States). The primer sequences were as follows (detailed information in **Supplementary Table 2**): IL-1β: acggaccccaaaagatgaag and ttctccacagccacaatgag; IL-18: gcctcaaaccttccaaatcac and

gttgtctgattccaggtctcc; tumor necrosis factor α (TNF-α): cttctgtctactgaacttcggg and caggcttgtcactcgaattttg; GAPDH: ctttgtcaagctcatttcctgg and tcttgctcagtgtccttgc. The results presented are normalized to sham.

Statistical Analysis

Two-tailed unpaired Student's *t*-test was performed to compare the two groups. One- or two-way ANOVA was performed for experiments containing more than two groups, followed by Bonferroni's multiple comparisons test. Data are shown as mean ± standard error of mean (SEM). Pearson chi-square test was performed for rate comparison. Differences were considered to be statistically significant at $p < 0.05$. All the data were analyzed using the Prism 5.0 software.

RESULTS

Traumatic Brain Injury Causes Persistent Increases in HMGB1 and p-Tau Levels

To confirm the role of HMGB1 in the delayed period (4–8 weeks post injury), a period during which cognitive disorders appeared after TBI, immunofluorescence examination was performed in the mice with moderate TBI. Although the ipsilateral hippocampus was lacking, a significant increase in HMGB1 immunoactivity was observed at 4 weeks post injury in the contralateral dentate gyrus (DG) and ipsilateral thalamus compared with the sham group, and this change existed for 8 weeks after the brain injury (**Figures 1B–D**). As the previous study found that p-tau (Ser404) increased obviously after TBI in mice, we investigated p-tau and found that it increased significantly in the above two brain regions at 4 and 8 weeks post injury (**Figures 1B–D**). Similar trends in p-tau and HMGB1 changes led to speculation that p-tau may cause elevation of HMGB1.

Overexpression of Phosphorylated Tau Induces Late-Onset Cognitive Dysfunction

To understand whether hyperphosphorylated tau following TBI alters HMGB1 levels independently, we established a tau-overexpressing (mostly phosphorylated) model by AAV-tau injection. The immunofluorescence staining revealed obvious elevations in endogenous (only p-tau positive) and exogenous p-tau proteins (both p-tau and GFP positive) in the left hippocampus ipsilateral to the injection site 3 m after injection (**Figure 2B**).

In the Y-maze, no significant differences were detected between the tau-overexpressing group and the GFP control at 3 m after injection. At 7 m, the tau-overexpressing mice displayed significant spatial cognitive impairment, with reduced percentage of exploration time spent with the novel arm compared with the control (**Figure 2C**). As with the T-maze test, the tau-overexpressing animals showed worse performance at 7 m, suggesting that working memory deficits occurred at a relatively late period post injection (**Figure 2D**).

Overexpression of p-Tau in the Hippocampus Leads to Elevations in HMGB1

To determine whether the increased p-tau prompted the alteration in HMGB1 expression, this experiment detected HMGB1 levels in spatial memory-related regions, the hippocampus and prefrontal cortex (PFC). Compared with the GFP control, HMGB1 levels were elevated in the ipsilateral hippocampal CA1 region and PFC at both 3 and 7 months post injection in the AAV-tau groups (**Figures 3A–F**). Moreover, the expression of total tau (tau 5) and p-tau (Ser404) was significantly increased in the hippocampus (**Figures 3C,D**) and PFC (**Figures 3E,F**) at a relatively late stage of 7 months. Of note, the levels of the above proteins increased over time, and the increases were more pronounced at 7 months post injection when cognitive impairments were present, implying the underlying relationship between elevated HMGB1 induced by p-tau overexpression and spatial memory disorders.

p-Tau Overexpression Causes Activation of the NLRP3 Inflammasome

Studies have shown that the activation of inflammasomes is related to the release of HMGB1 (Yu et al., 2019). Therefore, the most extensively explored NLRP3 inflammasome, which is well known to affect cognition, was detected by immunofluorescence staining and western blot. We detected components of the NLRP3 inflammasome, such as NLRP3, ASC, caspase-1, and its active isomer P20.

There were no significant differences in NLRP3 immunoactivity between the AAV-tau and AAV-GFP groups in the hippocampus and prefrontal cortex at 7 m. In contrast to NLRP3, mice with AAV-tau displayed considerable increases in ASCs in the hippocampus and PFC by immunoactivity and western blot analyses (**Figures 4A,B**). In addition, NLRP3 expression was significantly increased in the PFC at 3 and 7 m but not in the hippocampus (**Figures 4C–F**).

To evaluate the activation of the NLRP3 inflammasome, P20 (cleaved caspase-1) and proinflammatory factors were detected. The results revealed that P20 levels were dramatically elevated in the hippocampus and PFC at 7 m (**Figures 5A–F**). The mice with tau overexpression displayed a significant increase in IL-1β compared with the AAV-GFP control, but no significant change was observed in the messenger RNA (mRNA) level of IL-18 at 7 m post injection (**Figure 5G**).

NLRP3 Knockout Reduces Elevations in HMGB1 and p-Tau Levels

We next confirmed whether the increased HMGB1 levels in the hippocampus and PFC after tau overexpression were caused by the activation of the NLRP3 inflammasome in the NLRP3$^{-/-}$ mice. The results showed that the NLRP3 staining was almost invisible in the hippocampus and PFC after NLRP3 gene knockout, indicating success of the animal model (**Figures 6A,B**), and the expression of HMGB1 in mice receiving AAV-tau virus was also significantly lower than that in their wild-type (WT) littermates in these two brain regions 3 m post

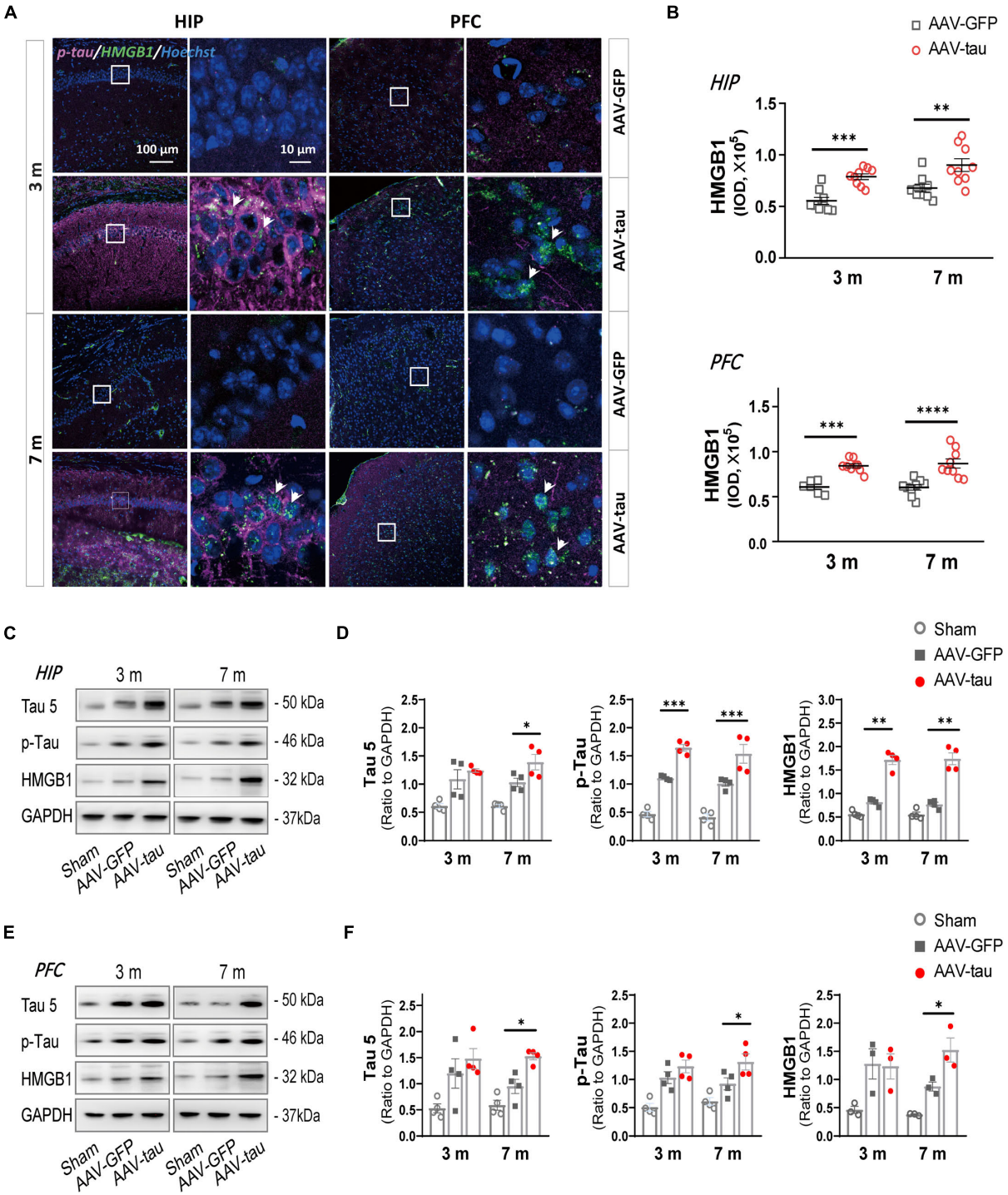

FIGURE 3 | Overexpression of p-tau led to increases in HMGB1 and tau expressions. **(A)** Representative images of HMGB1 (green) and p-tau (ser404) (purple) in the ipsilateral hippocampus (HIP) and prefrontal cortex (PFC) taken from mice injected with AAV-tau or AAV-GFP 3 and 7 months after injection. Right columns of HIP and PFC are higher magnification sections of the dashed squares in the left columns, and white arrows indicate positive staining for p-tau or HMGB1. **(B)** Quantification of HMGB1 with fluorescence intensity (nine regions of interest from three mice for every group) showed significant increases in HMGB1 levels in the HIP (top) and PFC (bottom). **(C–F)** Representative western blots of tau 5 (total tau), p-tau (ser404), and HMGB1 in **(C)** the ipsilateral hippocampus and **(E)** PFC. Quantifications by the integrated optical density showed increased immunoreactivities for tau 5 (left), p-tau (middle), and HMGB1 (right) in the **(D)** HIP and **(F)** PFC of mice with AAV-tau or AAV-GFP 3 and 7 months after virus injection, and data were normalized to glyceraldehyde 3-phosphate dehydrogenase (GAPDH), $n = 3$–4 per group. Two-way ANOVA was performed followed by Bonferroni's multiple comparisons test for behavioral analysis, $^{*}p < 0.05$, $^{**}p < 0.01$, $^{***}p < 0.001$, $^{****}p < 0.0001$.

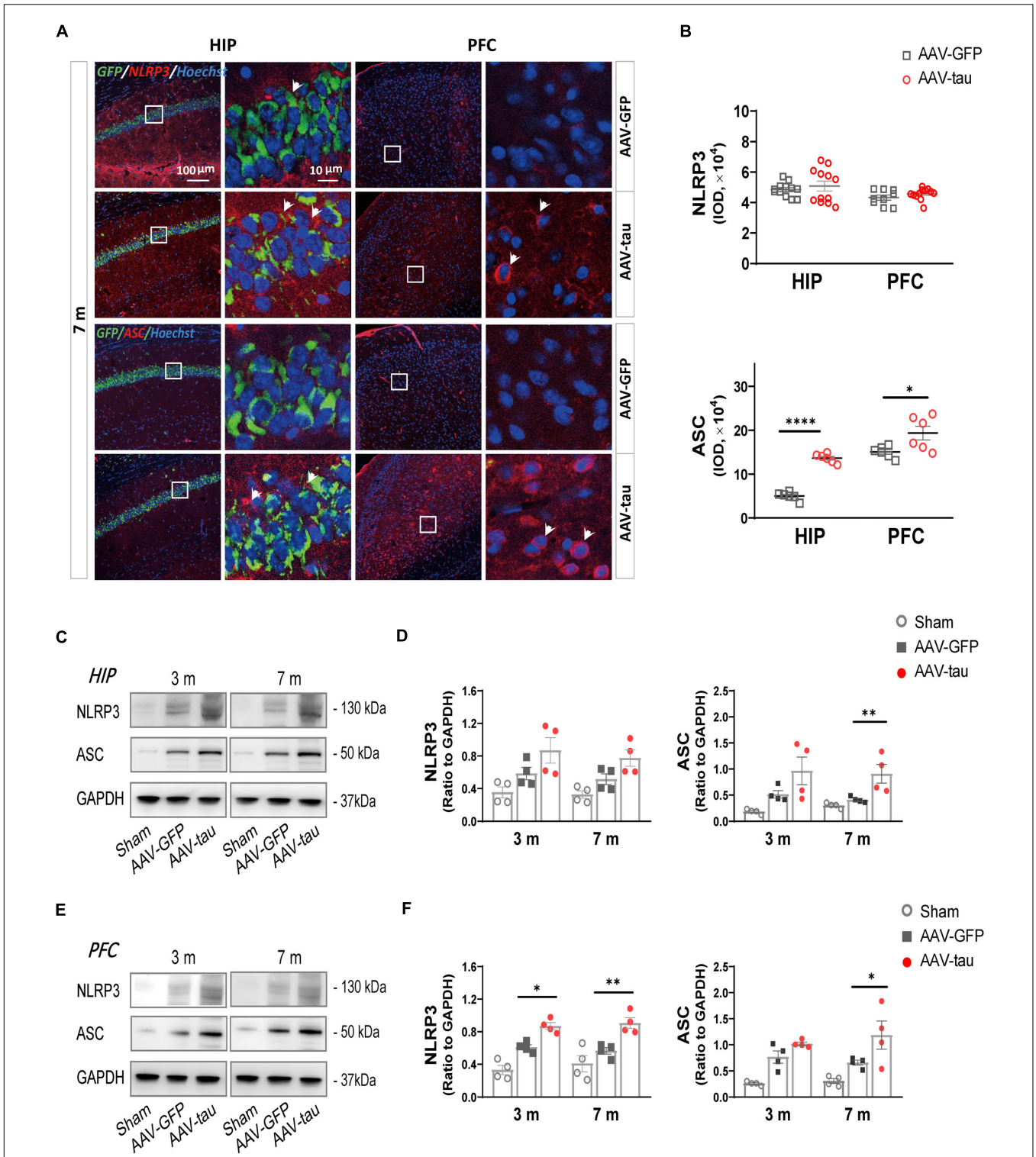

FIGURE 4 | Overexpression of p-tau caused elevations in ASC expression in the hippocampus and PFC. **(A)** Representative images of nucleotide-binding oligomerization domain (NOD)-like receptor pyrin domain-containing protein 3 (NLRP3) (red) and ASC (red) in the ipsilateral HIP and PFC taken from mice injected with AAV-tau or AAV-GFP 3 and 7 months after injection. White arrows indicate positive staining for NLRP3 or ASC. **(B)** Quantifications of NLRP3 (top) and ASC (bottom) immunoactivities shown in the previous panel (6–12 ROIs from three mice for every group). **(C–F)** Representative western blots of NLRP3 and ASC in the **(C)** ipsilateral HIP and **(E)** PFC, and quantifications of the immunoreactivities for NLRP3 (left) and ASC (right) in the **(D)** HIP and **(F)** PFC. Data were normalized to GAPDH, $n = 4$ per group. **(D,F)** Two-way ANOVA and **(B)** unpaired t-test were performed, $^{*}p < 0.05$, $^{**}p < 0.01$, $^{****}p < 0.0001$.

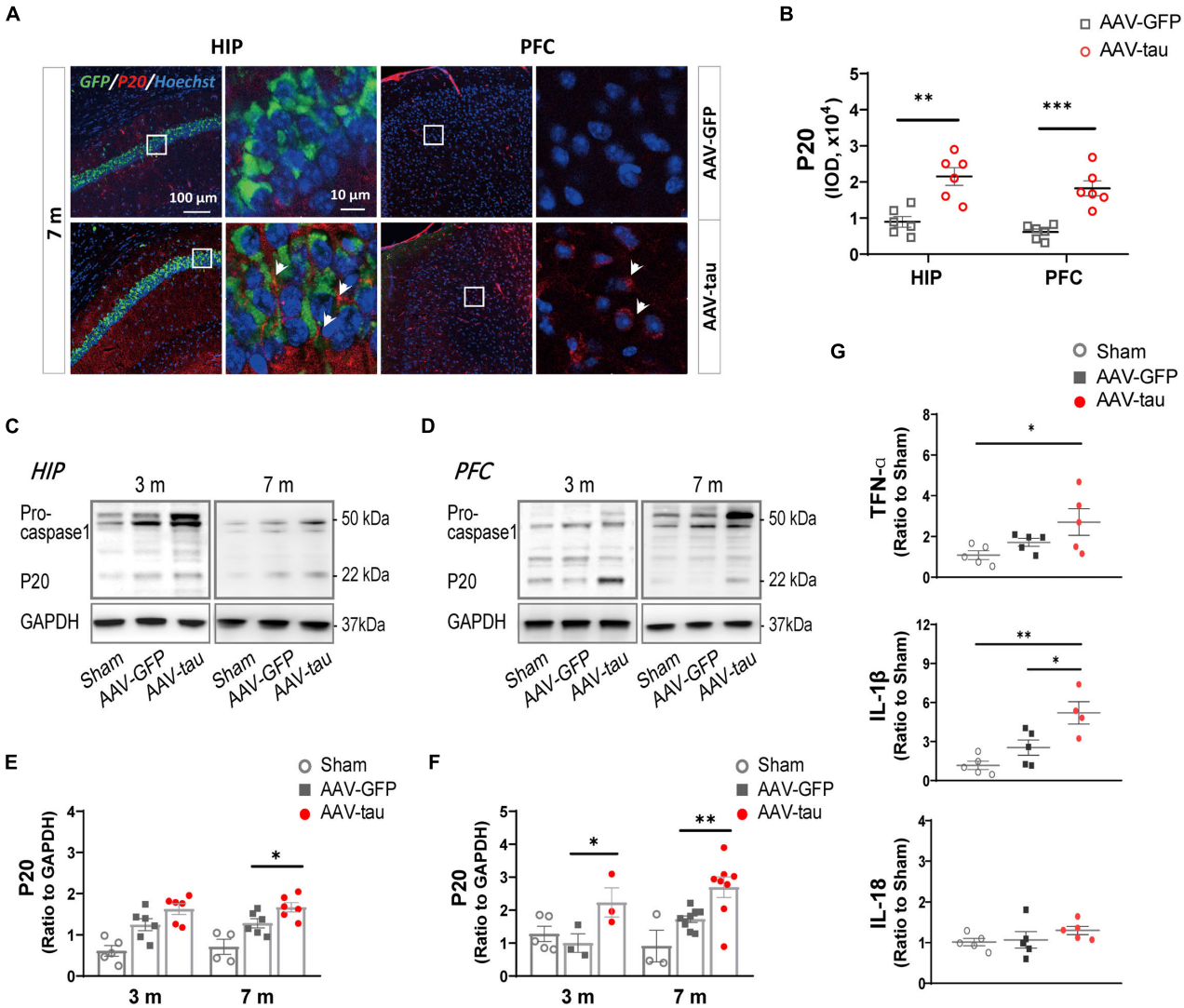

FIGURE 5 | Overexpression of p-tau caused the activation of NLRP3 inflammasome in the hippocampus and PFC. **(A)** Representative images and **(B)** quantifications of P20 immunostainings (six ROIs from three mice for every group) in the HIP and PFC in mice injected with AAV-tau or AAV-GFP 7 months after injection. White arrows indicate positive staining for P20. **(C,D)** Representative western blots of P20 and their quantifications by the integrated optical density in the **(E)** HIP and **(F)** PFC from mice receiving AAV-tau or AAV-GFP control 3 and 7 months after injection. Data were normalized to GAPDH, $n = 3$–8 per group. **(G)** Messenger RNA (mRNA) expression of tumor necrosis factor α (TNF-α) (top), interleukin 1 beta (IL-1β) (middle), and interleukin-18 (IL-18) (bottom) in the HIP of mice injected with AAV-tau or AAV-GFP 7 months after injection, $n = 4$–5 per group. **(B)** Unpaired *t*-test (b), **(G)** one-way ANOVA, and **(E,F)** two-way ANOVA were performed, $^{*}p < 0.05$, $^{**}p < 0.01$, $^{***}p < 0.001$.

injection (**Figures 6A,C**). Importantly, p-tau immunoactivities were significantly decreased in both the hippocampus and PFC of the NLRP3$^{-/-}$ mice relative to the WT mice (**Figures 6A,D**).

Glycyrrhizin Treatment Prevents Pathological Alterations of Tau and Alleviates Neurobehavioral Deficits in Tau-Overexpressing Mice

We next examined the effect of the HMGB1 inhibitor GZ on cognitive disorders in the delayed period following virus injection. The GZ treatment was initiated 2 months (m) post injection and maintained for 1 month. This therapeutic strategy reduced the immunofluorescence staining for HMGB1 compared with vehicle-treated controls in the hippocampus and PFC of tau-overexpressing mice 7 m post injection. Surprisingly, the treatment also decreased the p-tau staining at the above regions at 7 m (**Figures 7B–D**), implying that the inhibition of HMGB1 was beneficial to rescue the elevated p-tau in the hippocampus and PFC. The next behavioral tests demonstrated that the GZ treatment significantly improved the spatial short-term memory of the animals in the AAV-tau group compared with the vehicle-treated mice by the Y-maze task (**Figures 7E,F**), and that the performance of the HMGB1-administered mice in

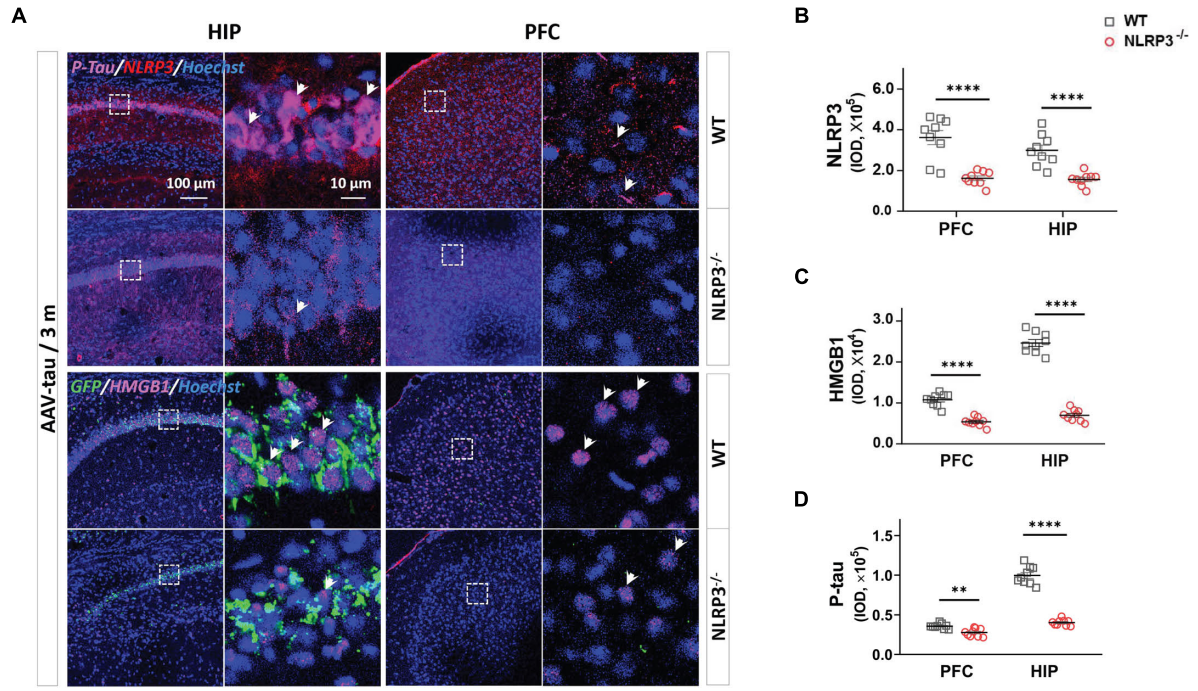

FIGURE 6 | NLRP3$^{-/-}$ mice displayed the lower levels of p-tau and HMGB1 after AAV-tau injection. **(A)** Representative images and quantifications of **(B)** NLRP3, **(C)** HMGB1, and **(D)** p-tau (ser404) immunostainings in the HIP and PFC (nine ROIs from three mice for every group) of mice injected with AAV-tau or AAV-GFP 3 months after injection. White arrows indicate positive staining for p-tau or HMGB1. Unpaired *t*-test was performed for immunohistochemical analysis, $^{**}p < 0.01$, $^{****}p < 0.0001$. WT, wild-type.

the T-maze task was also better than that of the vehicle-treated ones, suggesting restored hippocampal-spatial working memory (**Figure 7G**). In addition, nest building activity, considered to be a manifestation of advanced hippocampal cognition, was recovered after the GZ treatment (**Figures 7H,I**).

DISCUSSION

Elevated p-Tau and HMGB1 Levels in Spatial Memory-Related Brain Regions Post-TBI Associated With Late-Onset Cognitive Deficits

High mobility group box-1, as a late inflammatory factor and immunoregulatory molecule, has been reported to be elevated during the acute and subacute phases (3–12 h) of brain injury and to gradually return to normal levels up to 4 weeks post injury (Kigerl et al., 2018; Webster et al., 2019b). In this study, it was found that HMGB1 increased 4 and 8 weeks after TBI, which was consistent with the temporal and spatial distribution of increased p-tau at Ser404, suggesting that increased HMGB1 in a delayed period was closely related to tau hyperphosphorylation. Mounting evidence has revealed that TBI induces increases in p-tau levels *via* a variety of factors, such as detachment of p-tau from microtubules induced by mechanical forces, dissociation caused by hyperphosphorylation (Collins-Praino and Corrigan, 2017), and neuroinflammation resulting from axonal injury (Smith et al., 2003). An increasing number of studies have highlighted how elevated p-tau results in neuropathological changes and cognitive impairments and whether endogenous immune-related molecules are involved in the detrimental roles of p-tau in cognition. Although the accumulating literature has reported that HMGB1 is closely related to cognitive dysfunction caused by a variety of reasons, such as neurodegenerative diseases (Hei et al., 2018; Okuma et al., 2019), surgery (Kong et al., 2017), and sepsis (Chavan et al., 2012), the association between p-tau and HMGB1 in a delayed period post injury remains undefined. Here, we found that HMGB1 and p-tau (Ser404) increased simultaneously during the period when spatial memory impairment occurred, suggesting that the overexpression of p-tau may be mainly responsible for an earlier onset of spatial cognitive dysfunction in patients with TBI rather than in elderly patients with AD through the promotion HMGB1 levels in spatial memory-related brain regions.

p-Tau Is an Independent Factor for Increased HMGB1 and Decreased Cognition

It has been well demonstrated that sterile and infectious threats can cause an increase in HMGB1 levels in the central nervous system, which is associated with the activation of microglia and astrocytes, and the release of proinflammatory cytokines, such as TNF-α and IL-1β. Considering the influence of various stimuli on HMGB1 after TBI, this study established

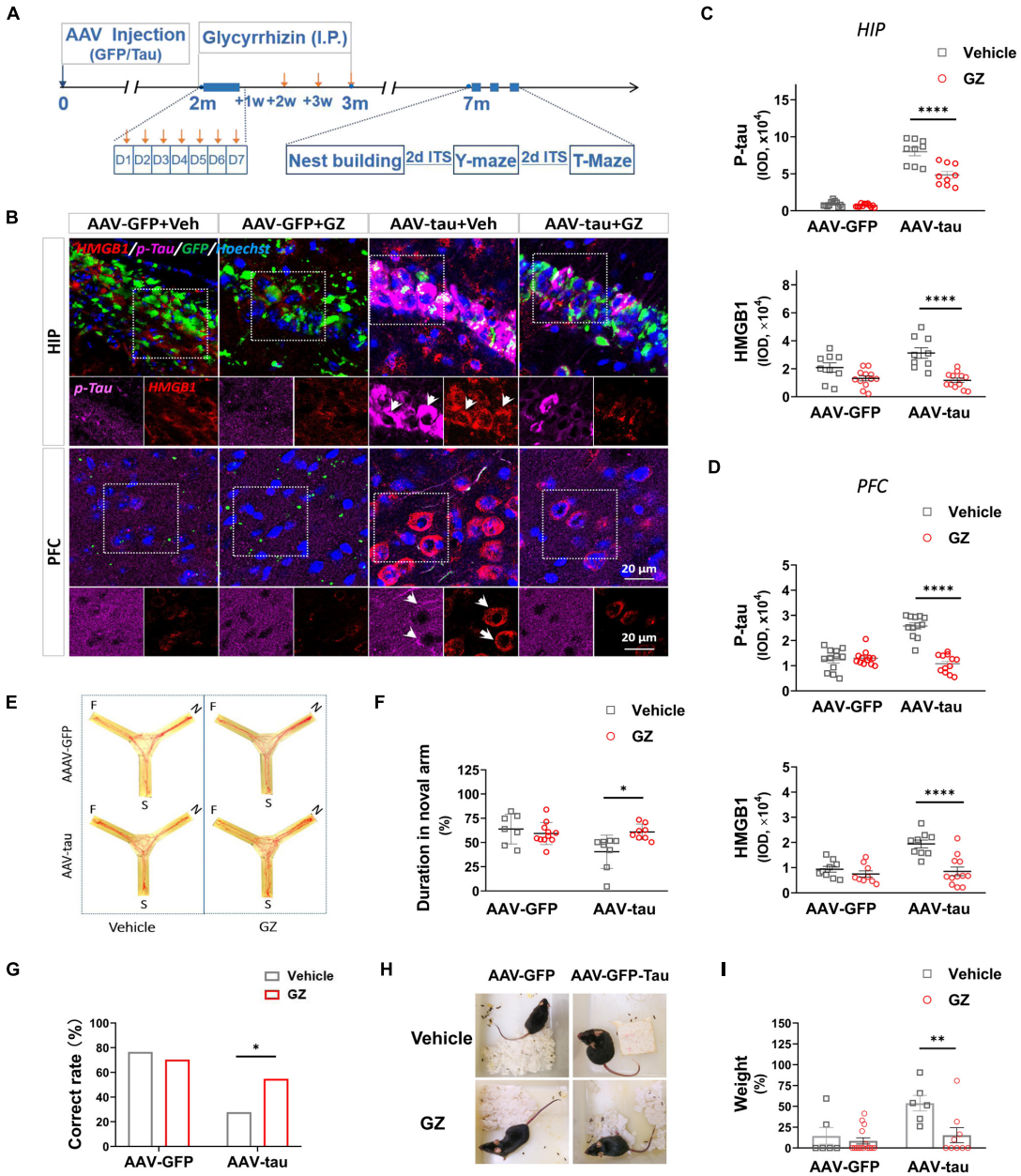

FIGURE 7 | High mobility group box-1 inhibitor alleviated tau pathology and improved spatial cognition in mice with p-tau overexpression. **(A)** Experimental procedure and drug administration schemes. Glycyrrhizin (GZ, 25 mg/kg i.p.), a pharmacological inhibitor of HMGB1, or vehicle was administered 2 months after virus injection, and orange arrows indicate the injection time. **(B)** Representative images of p-tau (ser404) and HMGB1 in the HIP and PFC from mice receiving AAV-tau or AAV-GFP 7 months after injection. White arrows indicate positive staining for p-tau or HMGB1. **(C,D)** Quantifications of p-tau (top) and HMGB1 (bottom) immunostainings (9∼12 ROIs from three mice for every group) in the **(C)** HIP and **(D)** PFC shown in panel **(B)**. **(E)** Representative moving tracks and the percentages of duration in **(F)** novel arm in GZ or vehicle-treated mice that received AAV-tau (n = 8) or AAV-GFP (n = 7 for vehicle and n = 11 for GZ) injections in the Y-maze test. **(G)** GZ improved the performance of p-tau-overexpressed mice in the T-maze test. **(H)** Representative nest pictures and **(I)** weight analysis of the cotton pads used for nest building showed GZ decreased the weight percentage of untorn cotton in mice that received AAV-tau injections. **(G)** Two-way ANOVA and **(C,D,F,I)** Pearson chi-square test were performed,*$p < 0.05$,**$p < 0.01$, ****$p < 0.0001$.

an animal model with high expression of p-tau by injecting AAV-tau into the hippocampus of mice to clarify the influence of p-tau on HMGB1. Behavioral tests indicated that tau-overexpressing animals presented spatial cognitive dysfunction 7 m post injection, and most importantly, alterations in total tau, p-tau, and HMGB1 appeared in the spatial memory-related brain regions, hippocampus and PFC at the same time point. Of note, the increase in the phosphorylation of tau at

Ser404 was obvious after TBI, which has been demonstrated in the previously published article (Zhao et al., 2017a). Tau phosphorylation at Ser404 occurs more frequently after TBI than in neurodegenerative diseases such as AD, in which the phosphorylation sites at Thr205, Thr181, Ser262, and Tyr396 are much more common (Katsumoto et al., 2019; Barthelemy et al., 2020). Several pieces of evidence have demonstrated that Ser404 phosphorylation is involved in the aggregation and mislocalization of tau; thus, we speculated that Ser404 phosphorylation may be facilitated by the disassociation of tau from microtubules in injured axons following TBI. Importantly, we found that endogenous tau phosphorylation at Ser404 was also markedly increased in animals that received P301S mutant human tau. These results suggest that p-tau may act as an independent factor causing neuropathologic changes.

High mobility group box-1, regarded as a late proinflammatory cytokine, triggers inflammatory response through several receptors, such as toll-like receptor-4 (TLR4), TLR2, and the receptor for advanced glycation end product (RAGE). It is also a non-histone chromatin DNA-binding protein that, therefore, regulates transcription factor recruitment. HMGB1 is mainly expressed in the nucleus of hippocampal neurons (Faraco et al., 2007). In this study, HMGB1 was obviously increased in the hippocampus and PFC, regions tightly associated with spatial cognition, suggesting that HMGB1 may act as a detrimental downstream factor of p-tau in the cognitive impairment caused by tau overexpression. We, therefore, speculated that p-tau might be an initiator that triggers a series of neuropathological alterations in tauopathies.

Increases in HMGB1 Induced by Tau-Overexpression Were Dependent on the Activation of NLRP3 Inflammasome

Recent evidence indicates that the activation of the nucleotide-binding oligomerization domain-like receptor pyrin domain-containing protein 3 inflammasome is one of the most important factors for the release of high mobility group box-1 and is widely involved in cognitive dysfunction in patients with AD and animal models (Singhal et al., 2014; Pennisi et al., 2017; Thawkar and Kaur, 2019). The NLRP3 inflammasome is composed of three components: a cytosolic pattern recognition receptor (NLRP3), an adaptor protein (ASC), and an effector component (caspase-1). In this study, the increases in ASC specks showed that more constituent proteins were assembled into the complete NLRP3 inflammasome, and the formation of P20 and the elevation of the downstream proinflammatory factor IL-1β suggested the activation of the NLRP3 inflammasome. Many studies have reported that the NLRP3 inflammasome is involved in HMGB1 elevation in sepsis (Lamkanfi et al., 2010), inflammatory kidney disease (Zhang et al., 2020), acute lung injury (Hou et al., 2018), and other infectious diseases (Willingham et al., 2009; Yu et al., 2019), and most studies have focused on immune cells such as macrophages and microglia.

In the central nervous system, Aβ activates the nucleotide-binding oligomerization domain-like receptor pyrin domain-containing protein 3 inflammasome in microglia and further aggravates the phosphorylation of tau (Ising et al., 2019; Lempriere, 2020). However, Aβ was only found in 30% of postmortem acute TBI cases and 40–45% of CTE cases (Edwards et al., 2017). A recent study revealed an exacerbating role of the ASC-NLRP3 axis in seeded tau pathology in primary microglia and in tau mice (Stancu et al., 2019), but it is still unclear whether the overexpression of p-tau in the cytoplasm could cause the alteration of HMGB1 and the activation of the NLRP3 inflammasome before they spread through the extracellular space or innervated nerve fibers to other brain regions. In this study, the alteration of NLRP3 levels was not obvious, but the NLRP3 inflammasome was activated 7 m post injection, and cognitive impairment appeared, indicating that it may be a major contributor to the elevation in HMGB1 and abnormal cognition resulting from tau overexpression. By the injection of AAV-tau into the NLRP3$^{-/-}$ mice, HMGB1 levels were significantly decreased in the hippocampus and PFC, implying that tau overexpression induced increases in HMGB1 levels, at least partially through the activation of NLRP3. Interestingly, the NLRP3 knockout blocked not only the upregulation of HMGB1 but also the hyperphosphorylation of tau, which suggested that increased HMGB1 could in turn affect tau phosphorylation. HMGB1 promotes tau pathology through the activation of major tau kinases, such as glycogen synthase kinase-3β (GSK-3β), by binding to its receptors (Li et al., 2012; Chen et al., 2014). Therefore, the interaction between p-tau and HMGB1 leads to a vicious cycle in which p-tau causes an increase in HMGB1, and elevated HMGB1 in turn enhances the phosphorylation of tau and ultimately impairs spatial cognition.

HMGB1 Inhibitor Reduced p-Tau Levels and Alleviated Cognitive Dysfunction

Given the significant increase in HMGB1 caused by p-tau and possible mutual enhancement between these two proteins, we explored the therapeutic effects and optimal administration (timing of treatment initiation and duration) of the HMGB1 inhibitor on behavioral outcomes and neuropathological consequences. HMGB1 levels continued to increase at a late stage, which provided a longer time window for treatment than with most of the inflammatory factors, such as TNF-α and IL-1β. In addition, GZ was revealed to pass through the blood-brain barrier and exert neuroprotective roles by reducing extracellular and intracellular HMGB1 levels. Here, we found that GZ reduced p-tau and HMGB1 levels simultaneously in spatial memory-associated regions, the hippocampus and PFC, and alleviated cognitive dysfunction, suggesting a close association between tau and HMGB1 in the development of cognitive impairment.

Several lines of evidence have indicated that the HMGB1 inhibitor GZ has a good therapeutic effect at doses of 10–50 mg/kg in the early stages after TBI (Sun et al., 2018; Thakur et al., 2020). Based on these data, we utilized a dose of 25 mg/kg in the mice that received AAV-tau and a longer period of treatment (once daily for 7 days followed by once a week for 3 weeks) in this study. We found that the cognitive deficits were alleviated, manifesting as improved abilities of nest building, prolonged times with the novel arm, and higher performances in the Y-maze

by this treatment regime. These results suggest that the time window of GZ may not be limited to the acute or subacute phases, and that the delayed administration of GZ can still play a good therapeutic role under tau-overexpression conditions. Moreover, the reduced HMGB1 was accompanied by decreases in p-tau levels after the treatment, which may account for the beneficial effects of the GZ treatment on cognitive impairments. It is plausible to believe that GZ plays a multi-target role in the treatment of tauopathies.

The elevation in HMGB1 levels was observed not only in the animal model of tau overexpression but also in other neurodegenerative diseases. For example, recent studies found that Aβ-induced increases in HMGB1 levels in experimental animals or cultured microglial cells (Nan et al., 2019), but therapy targeting Aβ was not always effective in cognitive disorders. Several studies revealed that Aβ caused the phosphorylation of tau after severe TBI (Tran et al., 2011; Bloom, 2014); therefore, we postulated that the alteration of HMGB1 and the enhancement of the interaction between HMGB1 and p-tau caused by increased p-tau might be key factors responsible for the ineffectiveness of the Aβ antibody. Moreover, Tran et al. found that the elevation in p-tau levels did not recover after the administration of an Aβ antibody (Tran et al., 2011), which supports the hypothesis of the authors. Of note, there might be crosstalk between neurons and glial cells, which affects the interactions between HMGB1 and p-tau, which is worthy of consideration in future studies.

Study Limitations and Perspectives

Accelerated neurodegeneration after TBI occurs with a complex interplay of pathological mechanisms. The lack of experimental data on neuron- or microglial-specific NLRP3 knockout makes it difficult to draw definitive conclusions regarding the mechanisms by which p-tau overexpression leads to cognitive impairment, which is worthy of further research in the future. In addition, there is some evidence that the biological and behavioral responses to TBI may differ between sexes, and male mice have more intense activation of the NLRP3 inflammasome (Kodama et al., 2020; O'Brien et al., 2020). Therefore, further experimental confirmation in females is needed to identify the effectiveness of HMGB1 antagonists.

CONCLUSION

To the best knowledge of the authors, this study is the first to reveal that tau overexpression causes a long-lasting increase in HMGB1 levels through activation of the nucleotide-binding oligomerization domain-like receptor pyrin domain-containing protein 3 inflammasome. In this study, both the HMGB1 inhibitor and the NLRP3 knockout markedly alleviated cognitive deficits. This study provides experimental evidence for the delayed treatment of diseases mainly manifested as hyperphosphorylation of tau, such as CTE, TBI, and frontotemporal dementia, which may better control the progress of the diseases and offer new insight into cognitive impairment.

DATA AVAILABILITY STATEMENT

The original contributions presented in the study are included in the article/**Supplementary Material**, further inquiries can be directed to the corresponding author.

ETHICS STATEMENT

The animal study was reviewed and approved by the Laboratory Animal Welfare and Ethics Committee of the Army Medical University.

AUTHOR CONTRIBUTIONS

YZ and S-WT conceived and designed the research. Z-ZH and F-BS performed the experiments. PL and Y-LN interpreted the results of experiments. S-YY, Z-AZ, and HD analyzed the data. NY, YP, and XC prepared the figures. Y-GZ drafted, edited, and revised the manuscript. All the authors read and approved the final version of the manuscript.

FUNDING

This study was funded by the National Natural Science Foundation of China (Grant No. 31771118) and Talent Innovation Training Program of Army Medical Center (2019CXJSB003).

SUPPLEMENTARY MATERIAL

The Supplementary Material for this article can be found online at: https://www.frontiersin.org/articles/10.3389/fnagi.2021.721474/full#supplementary-material

REFERENCES

Albert, M., Mairet-Coello, G., Danis, C., Lieger, S., Caillierez, R., Carrier, S., et al. (2019). Prevention of tau seeding and propagation by immunotherapy with a central tau epitope antibody. *Brain* 142, 1736–1750. doi: 10.1093/brain/awz100

Barthelemy, N. R., Li, Y., Joseph-Mathurin, N., Gordon, B. A., Hassenstab, J., Benzinger, T. L. S., et al. (2020). A soluble phosphorylated tau signature links tau, amyloid and the evolution of stages of dominantly inherited Alzheimer's disease. *Nat. Med.* 26, 398–407. doi: 10.1038/s41591-020-0781-z

Bloom, G. S. (2014). Amyloid-beta and tau: the trigger and bullet in Alzheimer disease pathogenesis. *JAMA Neurol.* 71, 505–508. doi: 10.1001/jamaneurol.2013.5847

Bramlett, H. M., and Dietrich, W. D. (2015). Long-Term consequences of traumatic brain injury: current status of potential mechanisms of injury and neurological outcomes. *J. Neurotrauma* 32, 1834–1848. doi: 10.1089/neu.2014.3352

Bruck, E., Lasselin, J., Group, H. S., Andersson, U., Sackey, P. V., and Olofsson, P. S. (2020). Prolonged elevation of plasma HMGB1 is associated with cognitive impairment in intensive care unit survivors. *Intensive Care Med.* 46, 811–812. doi: 10.1007/s00134-020-05941-7

Chavan, S. S., Huerta, P. T., Robbiati, S., Valdes-Ferrer, S. I., Ochani, M., Dancho, M., et al. (2012). HMGB1 mediates cognitive impairment in sepsis survivors. *Mol. Med.* 18, 930–937. doi: 10.2119/molmed.2012.00195

Chen, S., An, F.-M., Yin, L., Liu, A.-R., Yin, D.-K., Yao, W.-B., et al. (2014). Glucagon-Like Peptide-1 protects hippocampal neurons against advanced glycation end product-induced tau hyperphosphorylation. *Neuroscience* 256, 137–146. doi: 10.1016/j.neuroscience.2013.10.038

Chen, X. H., Johnson, V. E., Uryu, K., Trojanowski, J. Q., and Smith, D. H. (2009). A lack of amyloid beta plaques despite persistent accumulation of amyloid beta in axons of long-term survivors of traumatic brain injury. *Brain Pathol.* 19, 214–223.

Colin, M., Dujardin, S., Schraen-Maschke, S., Meno-Tetang, G., Duyckaerts, C., Courade, J. P., et al. (2020). From the prion-like propagation hypothesis to therapeutic strategies of anti-tau immunotherapy. *Acta Neuropathol.* 139, 3–25. doi: 10.1007/s00401-019-02087-9

Collins-Praino, L. E., and Corrigan, F. (2017). Does neuroinflammation drive the relationship between tau hyperphosphorylation and dementia development following traumatic brain injury? *Brain Behav. Immun.* 60, 369–382. doi: 10.1016/j.bbi.2016.09.027

Deacon, R. M. (2006). Assessing nest building in mice. *Nat. Protoc.* 1, 1117–1119. doi: 10.1038/nprot.2006.170

Deacon, R. M., and Rawlins, J. N. (2006). T-maze alternation in the rodent. *Nat. Protoc.* 1, 7–12. doi: 10.1038/nprot.2006.2

Edwards, G. III, Moreno-Gonzalez, I., and Soto, C. (2017). Amyloid-beta and tau pathology following repetitive mild traumatic brain injury. *Biochem. Biophys. Res. Commun.* 483, 1137–1142. doi: 10.1016/j.bbrc.2016.07.123

Faraco, G., Fossati, S., Bianchi, M. E., Patrone, M., Pedrazzi, M., Sparatore, B., et al. (2007). High mobility group box 1 protein is released by neural cells upon different stresses and worsens ischemic neurodegeneration in vitro and in vivo. *J. Neurochem.* 103, 590–603. doi: 10.1111/j.1471-4159.2007.04788.x

Furman, J. L., Vaquer-Alicea, J., White, C. L. III, Cairns, N. J., Nelson, P. T., and Diamond, M. I. (2017). Widespread tau seeding activity at early braak stages. *Acta Neuropathol.* 133, 91–100. doi: 10.1007/s00401-016-1644-z

Halle, A., Hornung, V., Petzold, G. C., Stewart, C. R., Monks, B. G., Reinheckel, T., et al. (2008). The NALP3 inflammasome is involved in the innate immune response to amyloid-beta. *Nat. Immunol.* 9, 857–865. doi: 10.1038/ni.1636

Haruma, J., Teshigawara, K., Hishikawa, T., Wang, D., Liu, K., Wake, H., et al. (2016). Anti-high mobility group box-1 (HMGB1) antibody attenuates delayed cerebral vasospasm and brain injury after subarachnoid hemorrhage in rats. *Sci. Rep.* 6:37755.

Hei, Y., Chen, R., Yi, X., Long, Q., Gao, D., and Liu, W. (2018). HMGB1 neutralization attenuates hippocampal neuronal death and cognitive impairment in rats with chronic cerebral hypoperfusion via suppressing inflammatory responses and oxidative stress. *Neuroscience* 383, 150–159. doi: 10.1016/j.neuroscience.2018.05.010

Hou, L., Yang, Z., Wang, Z., Zhang, X., Zhao, Y., Yang, H., et al. (2018). NLRP3/ASC-mediated alveolar macrophage pyroptosis enhances HMGB1 secretion in acute lung injury induced by cardiopulmonary bypass. *Lab. Invest.* 98, 1052–1064. doi: 10.1038/s41374-018-0073-0

Huber, B. R., Meabon, J. S., Martin, T. J., Mourad, P. D., Bennett, R., Kraemer, B. C., et al. (2013). Blast exposure causes early and persistent aberrant phospho- and cleaved-tau expression in a murine model of mild blast-induced traumatic brain injury. *J. Alzheimers. Dis.* 37, 309–323.

Ising, C., Venegas, C., Zhang, S., Scheiblich, H., Schmidt, S. V., Vieira-Saecker, A., et al. (2019). NLRP3 inflammasome activation drives tau pathology. *Nature* 575, 669–673.

Johnson, V. E., Stewart, W., Arena, J. D., and Smith, D. H. (2017). Traumatic brain injury as a trigger of neurodegeneration. *Adv. Neurobiol.* 15, 383–400. doi: 10.1007/978-3-319-57193-5_15

Katsumoto, A., Takeuchi, H., and Tanaka, F. (2019). Tau pathology in chronic traumatic encephalopathy and Alzheimer's disease: similarities and differences. *Front. Neurol.* 10:980. doi: 10.3389/fneur.2019.00980

Kaufman, S. K., Sanders, D. W., Thomas, T. L., Ruchinskas, A. J., Vaquer-Alicea, J., Sharma, A. M., et al. (2016). Tau prion strains dictate patterns of cell pathology, progression rate, and regional vulnerability in vivo. *Neuron* 92, 796–812. doi: 10.1016/j.neuron.2016.09.055

Kigerl, K. A., Lai, W., Wallace, L. M., Yang, H., and Popovich, P. G. (2018). High mobility group box-1 (HMGB1) is increased in injured mouse spinal cord and can elicit neurotoxic inflammation. *Brain Behav. Immun.* 72, 22–33. doi: 10.1016/j.bbi.2017.11.018

Kobayashi, M., Tamari, K., Al Salihi, M. O., Nishida, K., and Takeuchi, K. (2018). Anti-high mobility group box 1 antibody suppresses local inflammatory reaction and facilitates olfactory nerve recovery following injury. *J. Neuroinflammation* 15:124.

Kodama, L., Guzman, E., Etchegaray, J. I., Li, Y., Sayed, F. A., Zhou, L., et al. (2020). Microglial microRNAs mediate sex-specific responses to tau pathology. *Nat. Neurosci.* 23, 167–171. doi: 10.1038/s41593-019-0560-7

Kong, Z. H., Chen, X., Hua, H. P., Liang, L., and Liu, L. J. (2017). The oral pretreatment of glycyrrhizin prevents surgery-induced cognitive impairment in aged mice by reducing neuroinflammation and alzheimer's-related pathology via HMGB1 inhibition. *J. Mol. Neurosci.* 63, 385–395. doi: 10.1007/s12031-017-0989-7

Kulbe, J. R., and Hall, E. D. (2017). Chronic traumatic encephalopathy-integration of canonical traumatic brain injury secondary injury mechanisms with tau pathology. *Prog. Neurobiol.* 158, 15–44. doi: 10.1016/j.pneurobio.2017.08.003

Kuwar, R., Rolfe, A., Di, L., Xu, H., He, L., Jiang, Y., et al. (2019). A novel small molecular NLRP3 inflammasome inhibitor alleviates neuroinflammatory response following traumatic brain injury. *J. Neuroinflammation* 16:81.

Lamkanfi, M., Sarkar, A., Vande Walle, L., Vitari, A. C., Amer, A. O., Wewers, M. D., et al. (2010). Inflammasome-dependent release of the alarmin HMGB1 in endotoxemia. *J. Immunol.* 185, 4385–4392. doi: 10.4049/jimmunol.1000803

Lempriere, S. (2020). NLRP3 inflammasome activation implicated in tau pathology. *Nat. Rev. Neurol.* 16:4. doi: 10.1038/s41582-019-0299-5

Li, X. H., Lv, B. L., Xie, J. Z., Liu, J., Zhou, X. W., and Wang, J. Z. (2012). AGEs induce Alzheimer-like tau pathology and memory deficit via RAGE-mediated GSK-3 activation. *Neurobiol. Aging* 33, 1400–1410. doi: 10.1016/j.neurobiolaging.2011.02.003

McAllister, B. B., Wright, D. K., Wortman, R. C., Shultz, S. R., and Dyck, R. H. (2018). Elimination of vesicular zinc alters the behavioural and neuroanatomical effects of social defeat stress in mice. *Neurobiol. Stress* 9, 199–213. doi: 10.1016/j.ynstr.2018.10.003

Nan, K., Han, Y., Fang, Q., Huang, C., Yu, L., Ge, W., et al. (2019). HMGB1 gene silencing inhibits neuroinflammation via down-regulation of NF-kappaB signaling in primary hippocampal neurons induced by Abeta25-35. *Int. Immunopharmacol.* 67, 294–301. doi: 10.1016/j.intimp.2018.12.027

O'Brien, W. T., Pham, L., Symons, G. F., Monif, M., Shultz, S. R., and Mcdonald, S. J. (2020). The NLRP3 inflammasome in traumatic brain injury: potential as a biomarker and therapeutic target. *J. Neuroinflammation* 17:104.

Okuma, Y., Liu, K., Wake, H., Zhang, J., Maruo, T., Date, I., et al. (2012). Anti-high mobility group box-1 antibody therapy for traumatic brain injury. *Ann. Neurol.* 72, 373–384. doi: 10.1002/ana.23602

Okuma, Y., Wake, H., Teshigawara, K., Takahashi, Y., Hishikawa, T., Yasuhara, T., et al. (2019). Anti-High mobility group Box 1 antibody therapy may prevent cognitive dysfunction after traumatic brain injury. *World Neurosurg.* 122, e864–e871.

Pennisi, M., Crupi, R., Di Paola, R., Ontario, M. L., Bella, R., Calabrese, E. J., et al. (2017). Inflammasomes, hormesis, and antioxidants in neuroinflammation: role of NRLP3 in Alzheimer disease. *J. Neurosci. Res.* 95, 1360–1372. doi: 10.1002/jnr.23986

Rubenstein, R., Chang, B., Yue, J. K., Chiu, A., Winkler, E. A., Puccio, A. M., et al. (2017). Comparing plasma phospho tau, total tau, and phospho tau-total tau ratio as acute and chronic traumatic brain injury biomarkers. *JAMA Neurol.* 74, 1063–1072. doi: 10.1001/jamaneurol.2017.0655

Singhal, G., Jaehne, E. J., Corrigan, F., Toben, C., and Baune, B. T. (2014). Inflammasomes in neuroinflammation and changes in brain function: a focused review. *Front. Neurosci.* 8:315. doi: 10.3389/fnins.2014.00315

Smith, D. H., Meaney, D. F., and Shull, W. H. (2003). Diffuse axonal injury in head trauma. *J. Head Trauma Rehabil.* 18, 307–316. doi: 10.1097/00001199-200307000-00003

Stancu, I. C., Cremers, N., Vanrusselt, H., Couturier, J., Vanoosthuyse, A., Kessels, S., et al. (2019). Aggregated Tau activates NLRP3-ASC inflammasome

exacerbating exogenously seeded and non-exogenously seeded Tau pathology in vivo. *Acta Neuropathol.* 137, 599–617. doi: 10.1007/s00401-018-01957-y

Sun, Y., Chen, H., Dai, J., Wan, Z., Xiong, P., Xu, Y., et al. (2018). Glycyrrhizin protects mice against experimental autoimmune encephalomyelitis by inhibiting high-mobility group Box 1 (HMGB1) expression and neuronal HMGB1 release. *Front. Immunol.* 9:1518. doi: 10.3389/fimmu.2018.01518

Swanson, K. V., Deng, M., and Ting, J. P. (2019). The NLRP3 inflammasome: molecular activation and regulation to therapeutics. *Nat. Rev. Immunol.* 19, 477–489. doi: 10.1038/s41577-019-0165-0

Takahata, K., Kimura, Y., Shimada, H., Ichise, M., Tabuchi, H., Kitamura, S., et al. (2017). Delayed-Onset psychosis following TBI is associated with tau depositions in the neocortex but not with β-Amyloid depositions: a pet study with [11C]PBB3 and [11C]PiB. *Biol. Psychiatry* 81, S277–S413.

Takeda, S. (2019). Tau propagation as a diagnostic and therapeutic target for dementia: potentials and unanswered questions. *Front. Neurosci.* 13:1274. doi: 10.3389/fnins.2019.01274

Thakur, V., Sadanandan, J., and Chattopadhyay, M. (2020). High-Mobility group Box 1 protein signaling in painful diabetic neuropathy. *Int. J. Mol. Sci.* 21:881.

Thawkar, B. S., and Kaur, G. (2019). Inhibitors of NF-kappaB and P2X7/NLRP3/Caspase 1 pathway in microglia: novel therapeutic opportunities in neuroinflammation induced early-stage Alzheimer's disease. *J. Neuroimmunol.* 326, 62–74. doi: 10.1016/j.jneuroim.2018.11.010

Tran, H. T., Laferla, F. M., Holtzman, D. M., and Brody, D. L. (2011). Controlled cortical impact traumatic brain injury in 3xTg-AD mice causes acute intra-axonal amyloid-beta accumulation and independently accelerates the development of tau abnormalities. *J. Neurosci.* 31, 9513–9525. doi: 10.1523/jneurosci.0858-11.2011

Tweedie, D., Rachmany, L., Rubovitch, V., Zhang, Y., Becker, K. G., Perez, E., et al. (2013). Changes in mouse cognition and hippocampal gene expression observed in a mild physical- and blast-traumatic brain injury. *Neurobiol. Dis.* 54, 1–11. doi: 10.1016/j.nbd.2013.02.006

Uzawa, A., Mori, M., Taniguchi, J., Masuda, S., Muto, M., and Kuwabara, S. (2013). Anti-high mobility group box 1 monoclonal antibody ameliorates experimental autoimmune encephalomyelitis. *Clin. Exp. Immunol.* 172, 37–43. doi: 10.1111/cei.12036

VanItallie, T. B. (2019). Traumatic brain injury (TBI) in collision sports: Possible mechanisms of transformation into chronic traumatic encephalopathy (CTE). *Metabolism* 100S:153943. doi: 10.1016/j.metabol.2019.07.007

Wang, D., Liu, K., Wake, H., Teshigawara, K., Mori, S., and Nishibori, M. (2017). Anti-high mobility group box-1 (HMGB1) antibody inhibits hemorrhage-induced brain injury and improved neurological deficits in rats. *Sci. Rep.* 7:46243.

Washington, P. M., Villapol, S., and Burns, M. P. (2016). Polypathology and dementia after brain trauma: does brain injury trigger distinct neurodegenerative diseases, or should they be classified together as traumatic encephalopathy? *Exp. Neurol.* 275(Pt 3), 381–388. doi: 10.1016/j.expneurol.2015.06.015

Webster, K. M., Shultz, S. R., Ozturk, E., Dill, L. K., Sun, M., Casillas-Espinosa, P., et al. (2019a). Targeting high-mobility group box protein 1 (HMGB1) in pediatric traumatic brain injury: chronic neuroinflammatory, behavioral, and epileptogenic consequences. *Exp. Neurol.* 320:112979. doi: 10.1016/j.expneurol.2019.112979

Webster, K. M., Sun, M., Crack, P. J., O'brien, T. J., Shultz, S. R., and Semple, B. D. (2019b). Age-dependent release of high-mobility group box protein-1 and cellular neuroinflammation after traumatic brain injury in mice. *J. Comp. Neurol.* 527, 1102–1117. doi: 10.1002/cne.24589

White, C. S., Lawrence, C. B., Brough, D., and Rivers-Auty, J. (2017). Inflammasomes as therapeutic targets for Alzheimer's disease. *Brain Pathol.* 27, 223–234. doi: 10.1111/bpa.12478

Willingham, S. B., Allen, I. C., Bergstralh, D. T., Brickey, W. J., Huang, M. T., Taxman, D. J., et al. (2009). NLRP3 (NALP3, Cryopyrin) facilitates in vivo caspase-1 activation, necrosis, and HMGB1 release via inflammasome-dependent and -independent pathways. *J. Immunol.* 183, 2008–2015. doi: 10.4049/jimmunol.0900138

Yi, H. J., Lee, J. E., Lee, D. H., Kim, Y. I., Cho, C. B., Kim, I. S., et al. (2019). The role of NLRP3 in traumatic brain injury and its regulation by pioglitazone. *J. Neurosurg.* Online ahead of print.

Yu, S., Wang, D., Huang, L., Zhang, Y., Luo, R., Adah, D., et al. (2019). The complement receptor C5aR2 promotes protein kinase R expression and contributes to NLRP3 inflammasome activation and HMGB1 release from macrophages. *J. Biol. Chem.* 294, 8384–8394. doi: 10.1074/jbc.ra118.006508

Zhang, K., Fan, C., Cai, D., Zhang, Y., Zuo, R., Zhu, L., et al. (2020). Contribution of TGF-Beta-Mediated NLRP3-HMGB1 activation to tubulointerstitial fibrosis in rat with angiotensin II-Induced chronic kidney disease. *Front. Cell Dev. Biol.* 8:1. doi: 10.3389/fcell.2020.00001

Zhao, Z. A., Li, P., Ye, S. Y., Ning, Y. L., Wang, H., Peng, Y., et al. (2017a). Perivascular AQP4 dysregulation in the hippocampal CA1 area after traumatic brain injury is alleviated by adenosine A2A receptor inactivation. *Sci. Rep.* 7:2254.

Zhao, Z. A., Ning, Y. L., Li, P., Yang, N., Peng, Y., Xiong, R. P., et al. (2017b). Widespread hyperphosphorylated tau in the working memory circuit early after cortical impact injury of brain (Original study). *Behav. Brain Res.* 323, 146–153. doi: 10.1016/j.bbr.2017.02.002

Conflict of Interest: The authors declare that the research was conducted in the absence of any commercial or financial relationships that could be construed as a potential conflict of interest.

Publisher's Note: All claims expressed in this article are solely those of the authors and do not necessarily represent those of their affiliated organizations, or those of the publisher, the editors and the reviewers. Any product that may be evaluated in this article, or claim that may be made by its manufacturer, is not guaranteed or endorsed by the publisher.

frontiers in Aging Neuroscience

ORIGINAL RESEARCH
published: 11 October 2021
doi: 10.3389/fnagi.2021.735524

Uncovering Disease Mechanisms in a Novel Mouse Model Expressing Humanized APOEε4 and Trem2*R47H

Kevin P. Kotredes[1], Adrian Oblak[2], Ravi S. Pandey[1], Peter Bor-Chian Lin[2], Dylan Garceau[1], Harriet Williams[1], Asli Uyar[1], Rita O'Rourke[1], Sarah O'Rourke[1], Cynthia Ingraham[2], Daria Bednarczyk[1], Melisa Belanger[1], Zackary Cope[3], Kate E. Foley[1], Benjamin A. Logsdon[4], Lara M. Mangravite[4], Stacey J. Sukoff Rizzo[3], Paul R. Territo[2], Gregory W. Carter[1], Michael Sasner[1], Bruce T. Lamb[2] and Gareth R. Howell[1]**

[1]The Jackson Laboratory, Bar Harbor, ME, United States, [2]Stark Neurosciences Research Institute, School of Medicine, Indiana University Bloomington, Indianapolis, IN, United States, [3]Department of Medicine—Aging Institute, University of Pittsburgh School of Medicine, Pittsburgh, PA, United States, [4]Sage Bionetworks, Seattle, WA, United States

Late-onset Alzheimer's disease (AD; LOAD) is the most common human neurodegenerative disease, however, the availability and efficacy of disease-modifying interventions is severely lacking. Despite exceptional efforts to understand disease progression *via* legacy amyloidogenic transgene mouse models, focus on disease translation with innovative mouse strains that better model the complexity of human AD is required to accelerate the development of future treatment modalities. LOAD within the human population is a polygenic and environmentally influenced disease with many risk factors acting in concert to produce disease processes parallel to those often muted by the early and aggressive aggregate formation in popular mouse strains. In addition to extracellular deposits of amyloid plaques and inclusions of the microtubule-associated protein tau, AD is also defined by synaptic/neuronal loss, vascular deficits, and neuroinflammation. These underlying processes need to be better defined, how the disease progresses with age, and compared to human-relevant outcomes. To create more translatable mouse models, MODEL-AD (Model Organism Development and Evaluation for Late-onset AD) groups are identifying and integrating disease-relevant, humanized gene sequences from public databases beginning with *APOEε4* and *Trem2*R47*H, two of the most powerful risk factors present in human LOAD populations. Mice expressing endogenous, humanized *APOEε4* and *Trem2*R47*H gene sequences were extensively aged and assayed using a multi-disciplined phenotyping approach associated with and relative to human AD pathology. Robust analytical pipelines measured behavioral, transcriptomic, metabolic, and neuropathological phenotypes in cross-sectional cohorts for progression of disease

OPEN ACCESS

Edited by:
Mario Sanhueza, Universidad Mayor, Chile

Reviewed by:
Huaibin Cai, National Institutes of Health (NIH), United States
Rafael Posada-Duque, University of Antioquia, Colombia

***Correspondence:**
Gareth R. Howell
gareth.howell@jax.org
Bruce T. Lamb
btlamb@iu.edu

Received: *02 July 2021*
Accepted: *06 September 2021*
Published: *11 October 2021*

Citation:
*Kotredes KP, Oblak A, Pandey RS, Lin PB-C, Garceau D, Williams H, Uyar A, O'Rourke R, O'Rourke S, Ingraham C, Bednarczyk D, Belanger M, Cope Z, Foley KE, Logsdon BA, Mangravite LM, Sukoff Rizzo SJ, Territo PR, Carter GW, Sasner M, Lamb BT and Howell GR (2021) Uncovering Disease Mechanisms in a Novel Mouse Model Expressing Humanized APOEε4 and Trem2*R47H. Front. Aging Neurosci. 13:735524. doi: 10.3389/fnagi.2021.735524*

Abbreviations: AD, Alzheimer's disease; ADGC, Alzheimer's Disease Genetics Consortium; ADNI, Alzheimer's Disease Neuroimaging Initiative; ADSP, Alzheimer's Disease Sequencing Project; AMP-AD, Accelerating Medicines Partnership—Alzheimer's Disease; B6, C57BL/6J; BBB, Blood-brain barrier; CNS, Central nervous system; DEG, Differentially expressed genes; FP, frontal pole brain regions; HDL, high-density lipoproteins; IGAP, International Genomics of Alzheimer's Project; LOAD, Late-onset Alzheimer's disease; LDL, low-density lipoproteins; M^2OVE-AD, Molecular Mechanisms of the Vascular Etiology of Alzheimer's Disease; MRI, Magnetic resonance imaging; PET, Positron emission tomography; PHG, parahippocampal gyrus; ROS/MAP, Religious Orders Study and Memory and Aging Project.

hallmarks at all life stages. *In vivo* PET/MRI neuroimaging revealed regional alterations in glycolytic metabolism and vascular perfusion. Transcriptional profiling by RNA-Seq of brain hemispheres identified sex and age as the main sources of variation between genotypes including age-specific enrichment of AD-related processes. Similarly, age was the strongest determinant of behavioral change. In the absence of mouse amyloid plaque formation, many of the hallmarks of AD were not observed in this strain. However, as a sensitized baseline model with many additional alleles and environmental modifications already appended, the dataset from this initial MODEL-AD strain serves an important role in establishing the individual effects and interaction between two strong genetic risk factors for LOAD in a mouse host.

Keywords: ApoE4, TREM2, mouse model, MODEL-AD, late-onset AD

INTRODUCTION

Alzheimer's disease (AD) is the most common form of dementia, currently affecting 5.8 million patients in the United States (Alzheimer's Association, 2020), ∼95% of which are late-onset (LOAD; Cacace et al., 2016). Unfortunately for patients and their families, interventions approved to delay or reverse AD-related neurodegeneration have yet to materialize (U.S. Department of Health and Human Services, 2021), despite promising new therapies aimed at decreasing amyloid burden (U.S. Food and Drug Administration, 2021). LOAD is a heterogeneous disease defined by a few widely accepted hallmarks: extracellular amyloid plaques, intracellular tau tangles, vascular dysfunction, immune activation, synapse loss, neuron death, and cognitive decline (Blennow et al., 2006). Dissecting the etiology of these properties in animal models has provided key insights into our understanding of the disease and strategies to treat AD, however, human clinical trials of resultant therapeutics have not yielded an approvable drug.

In 2015, the National Institutes on Aging (NIA) aimed to accelerate the AD drug testing pipeline by promoting the design of more predictive preclinical studies that better translate to human disease (U.S. Department of Health and Human Services, 2021). Current popular animal models of AD rely on the expression of transgenic alleles to promote the aggregation of amyloid plaques or neurofibrillary tangles as drivers of subsequent disease processes, notably during adolescence and early adulthood (Sasaguri et al., 2017). Therefore, these overexpression models do not fully capitulate the breadth of the disease observed in human patients, particularly elderly populations; many underlying biological pathways affected in human disease are not observed in these mice (Logsdon et al., 2019). From this need, the MODEL-AD (Model Organism Development and Evaluation for Late-onset AD) consortium was established to provide the research community with the next generation of AD animal models (Oblak et al., 2020). In an effort to design and validate novel mouse models of LOAD that better mimic human disease, we opted to create knock-in humanized coding and non-coding LOAD risk variants expressed at endogenous levels. To implement these considerations in the development of a new generation of preclinical animal models, candidate humanized gene variants or SNPs from a number of public data repositories (ADSP, AMP-AD, ADGC, ADNI, ROS/MAP, IGAP, M^2OVE-AD, Resilience-AD, ACT) are being identified and engineered into existing mouse genes under endogenous promoters (Karch and Goate, 2015). As a heterogenous disease, it is unlikely that a single genetic alteration will promote the complex set of endophenotypes observed in humans. Rather, a combination of genetic and/or environmental risk factors is likely needed to phenocopy human disease and a better understanding of the effects of the complex interrelationships between risk factors is required to identify prospective therapeutic avenues. To this end, new mouse strains and conditions better replicating human LOAD are needed to improve the clinical translation of mouse therapies in human patients.

To date, approximately 40 loci have been identified through genetic and genome-wide association studies that increase the risk for AD (Dourlen et al., 2019; Andrews et al., 2020; Bellenguez et al., 2020). The strongest of these risk factors include the ε4 allele of apolipoprotein E (*APOE*) and point mutations in triggering receptor expressed on myeloid cells 2 (*TREM2)* locus (Allen et al., 2016; Cacace et al., 2016; Wang et al., 2018; Logsdon et al., 2019; Andrews et al., 2020; Bellenguez et al., 2020). These mutations were characterized in C57BL/6J mice alone and each correlated by gene-expression analysis to human transcripts to predict risk. Furthermore, by expressing both risk alleles in concert, genetic interaction and parallel molecular pathways could be investigated for dominance or synergistic effects that may promote human-like disease signatures.

APOE, the strongest genetic determinant of LOAD risk, has been the focus of extensive investigation for many years (Bu, 2009; Arnold et al., 2020; Foley et al., 2020), including the development of multiple mouse models expressing transgenes or targeted mutations (Xu et al., 1996; Raber et al., 1998; Sun et al., 1998; Knouff et al., 1999; Huber et al., 2000; Tesseur et al., 2000; Lesuisse et al., 2001; Bien-Ly et al., 2012). *APOE* is important in lipoprotein metabolism and immunoregulation strongly associated with cardiovascular and Alzheimer's disease (Karch and Goate, 2015; Allen et al., 2016; Cacace et al., 2016; Yamazaki et al., 2016; Wang et al., 2018; Logsdon et al., 2019; Andrews et al., 2020; Bellenguez et al., 2020). Three isoforms of

APOE are expressed in the human population: *APOE*ε2, *APOE*ε3, and *APOE*ε4 which confer increasing risk of LOAD, respectively. Compared to *APOE*ε3 carriers, the ε4 isoform of *APOE* increases AD risk and decreases the age of diagnoses (Saunders et al., 1993; Strittmatter et al., 1993). The three isoforms differ by one amino acid each at positions 112 and 158 that has profound effects on their functions: *APOE*ε2 (Cys112, Cys158); *APOE*ε3 (Cys112, Arg158); and *APOE*ε4 (Arg112, Arg158). The APOE protein has been shown to stimulate binding, transport, and metabolism of lipoproteins, major cholesterol transporters in the central nervous system (CNS) resulting in hypocholesteremia, tight junction failure, and vascular dysregulation (Maezawa et al., 2006c; Jeong et al., 2019). Additionally, reports of mice carrying human *APOEε4*-targeted replacement allele show evidence of blood-brain barrier (BBB) leakiness (Methia et al., 2001; Bell et al., 2012), immune alterations (Laskowitz et al., 2000; Maezawa et al., 2006a,b; Chung et al., 2016), synaptic disfunction (Safieh et al., 2019), and behavior deficits (Wang et al., 2005). Most importantly, APOE is also implicated in beta-amyloid and tau clearance (Verghese et al., 2013; Shi et al., 2017). However, many of the aspects of LOAD are not recapitulated upon expression of *APOE*ε4 alone, including the formation of beta-amyloid plaques and neurofibrillary tangles (Wang et al., 2005).

TREM2 encodes a member of a receptor signaling complex with TYRO protein tyrosine kinase binding (TYROBP) protein, which activates microglia, macrophages, and dendritic cells during damage and immune responses (Ma et al., 2015; Keren-Shaul et al., 2017; Krasemann et al., 2017) functioning in processes like debris clearance (Kleinberger et al., 2017) and amyloid plaque response (Jay et al., 2015; Wang et al., 2015; Yuan et al., 2016). Single nucleotide polymorphisms (SNP) found in *TREM2* have been shown to regulate microglial function (Painter et al., 2015; Krasemann et al., 2017; Mazaheri et al., 2017), the most widely studied being the R47H missense mutation in exon 2. The *TREM2***R47*H mutation triples the carrier's likelihood of Alzheimer's disease (Allen et al., 2016; Cacace et al., 2016; Wang et al., 2018; Logsdon et al., 2019; Andrews et al., 2020; Bellenguez et al., 2020). The increased risk is suggested to be, in part, the result of decreases in the microglial receptor's interactions with ligands (phospholipids, APOE, and beta-amyloid) yielding chronic dysfunction in microglial phagocytosis and inflammatory pathways (Karch and Goate, 2015; Ma et al., 2015; Painter et al., 2015).

Here we describe the application of a multi-faceted, cross-sectional phenotyping approach developed by MODEL-AD that included biometrics, behavioral assays, transcriptomics, neuroimaging, and immunohistochemistry to assess AD-relevant phenotypes in mice expressing combinations of humanized *APOE*ε4 and *Trem2***R47*H alleles.

MATERIALS AND METHODS

Model Backgrounds

All animals were obtained from The Jackson Laboratory. Mouse models of Late-onset Alzheimer's disease (LOAD) developed by MODEL-AD (Model Organism Development and Evaluation for Late-onset Alzheimer's Disease) are congenic to the C57BL/6J (JAX# 000664; B6) strain. Genetic variants, identified from human data compiled by the AMP-AD (Accelerating Medicines Partnership-Alzheimer's Disease) project, expressed in MODEL-AD-generated strains are listed on the MODEL-AD strain table at https://www.model-ad.org/strain-table/, along with relevant links for allele descriptions, data, distribution, and legal disclaimers.

B6J.APOE4.Trem2*R47H (LOAD1) Mice

The B6.*APOE4.Trem2***R47*H (LOAD1) double mutant strain created at The Jackson Laboratory in Bar Harbor, Maine carries two primary risk alleles found in Alzheimer's disease patients. The humanized ApoE knock-in allele, in which a portion of the mouse *Apoe* gene (exons 2, 3, a majority of exon 4, and some 3' UTR sequence) of the mouse *Apoe* gene was replaced by the corresponding sequence of the human APOE4 gene (available as B6(SJL)-Apoe$^{tm1.1(APOE*4)Adiuj}$/J[1], Foley et al., 2020). The second allele, *Trem2*, contains the R47H point mutation and two additional silent mutations (available as C57BL/6J-Trem2^{em1Adiuj}/J[2]). The human R47H variant, when expressed in mouse brains, also confers a novel splice variant due to a cryptic slice acceptor site in exon 2 (Xiang et al., 2018). See additional information in the Jackson Laboratory APOE4.Trem2R47H mouse (JAX strain #028709) strain data sheet. APOE4.Trem2R47H mouse strain data sheet at https://www.jax.org/strain/028709.

Experimental Cohorts

To decipher how these two strong risk factors drive AD-relevant phenotypes, we created a double homozygous B6.*APOE4.Trem2***R47H* model, accompanied by single genotype controls, on a C57BL/6J (B6) background (**Table 1**). In appreciation of sexual dimorphism observed in human aging and disease, cohorts of males and females were established for phenotyping at 4-, 8-, 12- and 24-months using a cross-sectional design. To determine whether the LOAD risk variants *APOE*ε4, *Trem2***R47H*, or the combination produced *in vivo* phenotypes independent from normal healthy aging, a comprehensive cross-sectional phenotyping battery was conducted and included *in vivo* frailty assessments, metabolic screening, microbiome sampling, biomarker evaluation, behavioral phenotyping, and *in vivo* imaging. Postmortem brain tissue was further examined for transcriptomic and neuropathological indications of disease. All accumulated data sets and observations are disseminated for public availability (Kotredes, 2020).

Animal Housing Conditions

All experiments were approved by the Animal Care and Use Committee at The Jackson Laboratory and the Institutional Animal Care and Use Committee at Indiana University. To minimize gene expression variation between mice, animal housing conditions were replicated between both Bar Harbor and Indianapolis campuses. Mice were bred in the mouse facility at Indiana University or The Jackson Laboratory and maintained

[1]https://www.jax.org/strain/027894
[2]https://www.jax.org/strain/027918

TABLE 1 | Description of novel mouse strains expressing human LOAD risk alleles.

Common name	JAX stock #	Strain	Background	Gene location	Allele name	Allele type	Additional considerations
B6	000664	C57BL/6J	-	-	-	-	-
Trem2*R47H	027918	C57BL/6J-Trem2$^{em1\,Adiuj}$/J	C57BL/6J	Chr17:4834 6401-48352276	Trem2 R47H KI	Cas9 endonuclease-mediated (humanized sequence)	- Two silent mutations (lysine AAG>AAA and alanine GCC>GCA) into *Trem2* - R47H mutation also introduces a cryptic splice acceptor site in exon 2, creating a novel splice variant with a deletion of 119bp at the 5' end of exon 2.
APOE4	027894	B6(SJL)-*Apoe*$^{tm1.1(APOE*4)\,Adiuj}$/J	C57BL/6J	Chr7:19696 109-19699188	APOE4 KI	FRT site flanked PGK- neo cassette targeted mutation (gene replacement)	- Exons 2, 3, and a majority of exon 4 of the mouse *Apoe* gene were replaced by exons 2, 3, and 4 of the human *APOE* gene sequence (including a portion of the 3' UTR sequence) - Expression of FLP recombinase was used to remove the FRT site flanked PGK-neo cassette and subsequently backcrossed to remove FLP recombinase
APOE4.Trem2*R47H	028709	B6(SJL)-*Apoe*$^{tm1.1(APOE*4)Adiuj}$ Trem2^{em1Adiuj}/J	C57BL/6J	(see above)	(see above)	(see above)	(see above)

*Mouse strains expressing Trem2*R47H and APOEε4 human late-onset Alzheimer Disease risk factors, alone or in combination, developed on the C57BL/6J background and distributed by The Jackson Laboratory (https://www.jax.org/mouse-search).*

in a 12/12-h light/dark cycle, consisting of 12 h-ON 7 am-7 pm, followed by 12 h-OFF. Room temperatures are maintained at 18–24°C (65–75°F) with 40–60% humidity. All mice were housed in positive, individually ventilated cages (PIV). Standard autoclaved 6% fat diet (Purina Lab Diet 5K52) was available to the mice *ad-lib*, as was water with acidity regulated from pH 2.5–3.0. All breeder and experimental mice were housed in the same mouse room and were aged together. All behavioral characterization was conducted in the Mouse Neurobehavioral Core Facility (MNBF) at The Jackson Laboratory. Briefly, mice were relocated from the housing room in which they were reared to the MNBF in an adjacent building on the Bar Harbor campus. Mice were individually housed at minimum 5 days prior to behavioral testing. The dedicated MNBF housing room consists of PIV caging with temperature controlled at a setting of 22 ± 1°C (72 ± 2°F) and hsumidity at 50 ± 20%. The testing facility was on a 12:12 L:D schedule (lights on at 6:00 am) with all testing performed during the light cycle (typically between 7:00 am and 5:00 pm, with the exception of wheel running which was continuous 24-h testing for up to 5 days). All subjects were randomized and counterbalanced for testing order across multiples of instrumentation and time of day for each test day, with a simplified testing ID number (e.g., #1-100), with all technicians blinded to genotype (e.g., coded as A, B, C, etc.). The blind was maintained throughout testing and until after the data were analyzed with no subjects or data excluded based on any mathematical outliers.

Behavioral Testing

Behavioral tests were conducted as previously reported (Sukoff Rizzo et al., 2018) in the following order with at minimum a 1–2-day rest period between tests: Frailty assessment with core body temperature recording, open field test, spontaneous alternation, rotarod, and wheel-running activity. On each test day, subjects were transported from the adjacent housing room into the procedure room, tails were labeled with a non-toxic permanent marker with the assigned subject ID number, and subjects were left to acclimate undisturbed to the testing environment for a minimum 60 min prior to testing. Between subjects, all testing arenas were sanitized with 70% ethanol solution and dried prior to introducing the next subject. Lighting in the testing rooms were consistent with the housing room (∼500 lux) unless where specifically noted. At minimum 5 days post the conclusion of behavioral testing, mice were sent for tissue harvesting.

Frailty Assessment

Similar to as previously described (53), subjects were individually evaluated for the absence or presence of 26 aging-related characteristic traits and scored a 0, 0.5, or 1 (based on presence/absence, and severity) for each assessment by a trained observer, blind to genotype/age, and included the following assessments: alopecia; loss of fur color; dermatitis/skin lesions; loss of whiskers; coat condition; piloerection; cataracts; eye discharge/swelling; microphthalmia; nasal discharge; rectal prolapse; vaginal/uterine/penile; diarrhea; vestibular disturbance; vision loss assessed by visual placing upon the subject being lowered to a grid; menace reflex; tail stiffening;

impaired gait during free walking; tremor; tumors; distended abdomen; kyphosis; body condition; breathing rate/depth; malocclusions; righting reflex. The frailty index score was calculated as the cumulative score of all measures with a maximum score of 26.

Core Body Temperature

Core body temperature was recorded just prior to the conclusion of the frailty assessment *via* a glycerol lubricated thermistor rectal probe (Braintree Scientific product# RET 3; measuring 3/4" L 0.028 dia. 0.065 tip) inserted ∼2 cm into the rectum of a manually restrained mouse for approximately 10 s. The temperature was recorded to the nearest 0.1°C (Braintree Scientific product#TH5 Thermalert digital thermometer).

Open Field Activity

Versamax Open Field Arenas (40 cm × 40 cm × 40 cm; Omnitech Electronics, OH, USA) were used for this test. Arenas were housed within sound-attenuated chambers with lighting in the testing room and arenas consistent with the housing room (∼500 lux). Mice were placed individually into the center of the arena and infrared beams recorded distance traveled (cm), vertical activity, and perimeter/center time. Data were collected in 5-min time-bins for a duration of 60 min.

Spontaneous Alternation

Mice were acclimated to the testing room under ambient lighting conditions (∼50 lux). A clear polycarbonate y-maze (in-house fabricated; arm dimensions 33.65 cm length, 6 cm width, 15 cm height) placed on top of an infrared reflecting background (Noldus, The Netherlands), surrounded by a black floor-to-ceiling curtain to minimize extramaze visual cues was used for this test. Mice were placed midway of the start arm (A), facing the center of the y for an 8-min test period and the sequence of entries into each arm is recorded *via* a ceiling-mounted infrared camera integrated with behavioral tracking software (Noldus Ethovision XT). Percent spontaneous alternation is calculated as the number of triads (entries into each of the three different arms of the maze in a sequence of three without returning to a previously visited arm) relative to the number of alteration opportunities.

Rotarod Test for Motor Coordination

An accelerating Rotarod (Ugo-Basile; model 47600) is used for this test. Lighting in the testing room is consistent with the housing room (∼500 lux). The trial began with mice being placed on the rotating rod (4 rpm), which accelerates up to 40 rpm over the course of 300 s. Each mouse is subjected to three consecutive trials with an ∼1 min inter-trial interval to allow cleaning of the rod between trials. Latency to fall (sec) is measured. Subjects that fall upon initial placement on the rod, before acceleration begins, are scored as 0 s for that trial.

Wheel Running Activity

Subjects were individually housed in a clean cage with a running wheel (Med-Associates, Vermont, USA) and with food and water ad libitum. The light cycle was identical to the housing room with 12:12 L:D (lights on at 6:00 am). Running wheels were equipped with a wireless transponder that recorded activity on the running wheels (revolutions) in sync with a computer that time stamps events. Mice were left undisturbed throughout the testing period with the exception of daily welfare checks. Data were evaluated for time spent running (min), total distance traveled (meters), and speed (revolutions per min) over the course of three 24-h periods.

Behavioral Data Analysis

Prior to data analysis and while still blinded, results were adjusted to exclude data only from mice which could not be tested or which data was not available inclusive of any equipment failures, escape episodes, etc. Subjects were not excluded by any mathematical determination. Data were analyzed under coded genotypes (A, B, C, etc.) within sex, as one-way or two-way ANOVA as appropriate vs. sex- and age- matched WT control. The blind was revealed at the conclusion of the data analysis for interpretation.

Fasting Blood Glucose Collection and Measurement

Fasted mice were placed into a fresh cage, free of food but with fresh water, at 6 am—the beginning of the light-ON cycle. Mice were made to fast for 6 h, until 12 pm, at which time blood glucose levels were analyzed. Prior to mouse restraint, a Contour Next EZ blood glucose monitor (Ascensia, Parsippany, NJ) was calibrated with Contour glucose control solution and Contour Next test strips. While restraining the animal, with a 5.0 mm lancet a stab incision was made into and perpendicular to the cheek, located dorsal to the cheek skin gland at a distance equal to the height of the eye and caudal distance equal to the length of the eye. One drop of blood, approximately 10 μl, was applied to a blood glucose test strip and readings were recorded.

Fecal Collection

Parallel with the measurement of animal weight, animals were placed in a clean container on a scale. Mouse weight was recorded and upon production, a fecal sample was collected with forceps to prevent contamination. The sample was placed in a pre-marked 1.5 ml tube and snap-frozen immediately on dry ice. Container and forceps were cleaned with 70% ethanol before collecting from subsequent mice. Fecal samples were stored long term at −80°C until analyzed.

Animal Anesthesia

Upon arrival at the terminal endpoint for each aged mouse cohort, individual animals were weighed prior to intraperitoneal administration of either: (A) ketamine (100 mg/kg) and xylazine (10 mg/kg); or (B) tribromoethanol (1 mg/kg). Routine confirmation of deep anesthesia was performed every 5 min by toe pinch. First confirming deep anesthetization *via* toe pinch, an incision along the ventral midline to expose the thorax and abdomen, followed by removal of the lateral borders of the diaphragm and ribcage revealed the heart. If desired, prior to perfusion blood and CSF samples must be collected. To perfuse the animal, a small cut was placed in the right atrium to relieve pressure from the vascular system before perfusing the animal

transcardially with 1× PBS *via* injection into the left ventricle. Completion of perfusion and clearance of the vascular system was indicated by blanching of the liver.

Whole Animal Perfusion

First confirming deep anesthetization *via* toe pinch, animals are secured to a surgical board or tray using needles or pins and abdomen wetted with 70% ethanol followed by an incision along the ventral midline along the entire ventral surface, exposing the underlying muscle of the thorax and abdomen. An additional incision is made into this underlying muscle and cut to puncture the diaphragm, taking care not to cut any major blood vessels or the lungs. To expose the heart the ribcage can be cut along the lateral borders and removed. A small incision is made in the right atrium of the heart to relieve diastolic pressure and begin the removal of blood from the vascular system. To clear the vascular system of all blood a butterfly catheter needle is inserted into the left ventricle attached to a perfusion pump. Approximately 10 ml of 1× PBS solution will clear the system of a 20 g animal. Once the system has been cleared of blood the liver will appear very pale and PBS will be noticed exiting the right atrium. At this time organs of interest were collected as indicated.

Non-fasting Blood Collection and Analysis

Blood was collected by cardiac puncture from non-fasted, anesthetized animals (see Perfusion method) at harvest prior to incision of the right atrium and subsequent perfusion. A 25-gauge EDTA-coated needle, attached to a 1 ml syringe, is inserted into the right atrium of the exposed heart and the plunger gently pulled to slowly aspirate approximately 500 ml of blood, avoiding entrapping air in the syringe to prevent hemolysis. After removal of the needle from the syringe, the blood was slowly injected into a 1.5 ml EDTA coated MAP-K2 blood microtainer (363706, BD, San Jose, CA) on ice. Blood tubes were spun at 4°C and 4,388× *g* for 15 min. Blood serum is then removed and aliquoted equally into three replicate 1.5 ml tubes on ice. Tubes were then snap-frozen on dry ice and stored long-term at −80°C. Thawed blood plasma collected from non-fasted mice was then analyzed by Beckman Coulter AU680 chemistry analyzer (Beckman Coulter, Brea, CA) and Siemens Advia 120 (Germany) for levels of non-fasted glucose, total cholesterol, LDL (low-density lipoproteins), HDL (high-density lipoproteins), triglycerides, and NEFA (non-essential fatty acids).

Brain Harvest

Anesthetized and subsequently perfused animals were decapitated, and heads submerged quickly in cold 1× PBS. The brain was carefully removed from the skull, weighed, and divided midsagitally, into left and right hemispheres, using a brain matrix. The right hemisphere was quickly homogenized on ice and equally aliquoted into three cryotubes for metabolomic, proteomic, and transcriptomic analysis. Cryotubes were immediately snap-frozen on dry ice and stored long-term at −80°C. The left hemisphere was immediately placed in 5 ml 4% PFA at 4°C for no less than 24 h, but no longer than 30 h. The left hemisphere was then moved from PFA solution to 10 ml 15% sucrose at 4°C for 24 h, or until it sinks in the sucrose, when it was then transferred to a 30% sucrose for 24 h at 4°C, or until it sinks in the solution. The left hemisphere was then removed from 30% sucrose solution, snap-frozen on a flat mold, cut-side down, floating in 2-methyl butane solution cooled by dry ice. Once frozen the left hemisphere is then placed into a cryotube and stored at −80°C until used for microtome sectioning and immunohistochemistry analysis.

Immunohistochemistry and Microscopy Imaging

During harvest, whole mouse brains were removed and weighed. Using a brain matrix, left and right hemispheres were separated along the midsagittal plane. The left hemisphere was placed in 5 ml of 4% PFA at 4°C overnight, then moved to 10 ml of 15% sucrose at 4°C overnight, before finally being incubated in 10 ml of 30% sucrose at 4°C overnight or until the brain sinks to the bottom of the tube. The left hemisphere was then snap-frozen and stored at −80°C until sectioned. Left hemispheres (see preparation in Brain harvest method) were cut *via* Thermo Scientific HM430 sliding microtome at 25 μm thickness. Coronal brain tissue sections were oriented to capture the cortex and hippocampus at approximately Bregma: −2.75 mm and Interaural 1.05 mm. Each section was placed into cryoprotectant buffer (37.5% 1× PBS, 31.25% glycerol, 31.25% ethylene glycol) for immediate use or long-term storage at −20°C. Each section was tracked so as to store 100 sections equally distributed over 10 groups, so each of the 10 groups had equal representation of the 10 sections from the forebrain to the hindbrain and the hippocampus. Of these 10 groups of 10 25-micron sections, seven will be used for standardized staining combinations highlighting cell types and markers of interest: (1) Vascular [CD31/Iba1/Fibrin/DAPI]; (2) Neuritic plaques [Lamp1/Iba1/X34]; (3) Astrocytes and microglia [GFAP/Iba1/S100b/DAPI]; (4) Neurons [NeuN/Ctip2/DAPI]; (5) Plaques [ThioS]; (6) Luxol Fast Blue/Cresyl Violet; (7) Haematoxylin and eosin; and (8) Prussian blue (Iron stain). Floating sections were then blocked prior to immunohistochemical staining and mounting. After blocking slides with 10% normal donkey serum or normal goat serum diluted in 1× PBS+0.5%Triton wash buffer all antibodies were washed floating in 1× PBT (1× PBS with 0.5% Triton) wash buffer after blocking for 1 h at room temperature on a shaker in 10% NGS (normal goat serum) or 10% NDS (normal donkey serum) in 1× PBT. Secondary antibodies were incubated in 10% NGS or NDS in 1× PBT for 1 h at room temperature, followed by washes in 1× PBT before mounting onto the slides. Each staining combination of 10 sections was placed onto one slide. DAPI, X34, and ThioS stains were performed on the slide following immunostaining. Slides were then imaged on a Leica Versa slide scanner, automated fluorescent microscope system (Leica, Allendale, NJ). For further analysis, regions of the cortex and hippocampus were processed using CellProfiler (Cambridge, MA) or Imaris (Bitplane, Concord, MA) software to quantify cell counts, fluorescence intensity, and surface area ratios. [CD31 (R&D Systems, MAB3628, 1:500), Iba1 (Wako, 019-19741, 1:300), Fibrin (abcam, ab118533, 1:500), DAPI (1:1,000), Lamp1 (abcam, ab25245, 1:500), X34 (0.04% in 40% ethanol), GFAP

(Origene, AP31806PU-N, 1:1,000), S100b (Thermo Fisher, PA175395, 1:1,000), NeuN (abcam, ab104225, 1:500), Ctip2 (abcam, ab18465, 1:1,000), and ThioS (1% in 50% ethanol)].

In vivo Imaging Radiopharmaceuticals and Study Population

Regional brain glycolytic metabolism was monitored using 2-[18F]-fluoro-2-deoxy-D-glucose (18F-FDG) and was synthesized, purified, and prepared according to established methods (Yu et al., 2006), where clinical unit doses ranging from 185–370 MBq (5–10 mCi) were purchased from PETNet Indiana (PETNET Solutions Inc). To evaluate region brain perfusion, Copper(II) pyruvaldehyde bis(N4-methylthiosemicarbazone) labeled with 64Cu (64Cu-PTSM) was synthesized, purified, and unit doses (i.e., 370–740 MBq (10–25 mCi)) dispensed by the PET Radiochemistry Core Facility at Indiana University according to methods described previously (Green, 1987; Mathias et al., 1990).

Magnetic Resonance Imaging (MRI)

To provide high contrast gray matter images, at least 2 days prior to PET imaging, mice were induced with 5% isoflurane (balance medical oxygen), placed on the head coil, and anesthesia maintained with 1–3% isoflurane for scan duration. High-resolution T2-weighted (T2W) MRI images were acquired using a 3T Siemens Prisma clinical MRI scanner outfitted with a dedicated 4 channel mouse head coil and bed system (RapidMR, Columbus OH). Images were acquired using a SPACE3D sequence (Algin and Ozmen, 2012) using the following acquisition parameters: TA: 5.5 min; TR: 2,080 ms; TE: 162 ms; ETL: 57; FS: On; Ave: 2; Excitation Flip Angle: 150; Norm Filter: On; Restore Magnetization: On; Slice Thickness 0.2 mm: Matrix: 171 × 192; FOV: 35 × 35 mm, yielding 0.18 × 0.18 × 0.2 mm resolution images. At the completion of the imaging period, mice we returned to their warmed home cages and were allowed to recover.

Positron Emission Tomography (PET) Imaging

To evaluate changes in cerebral glycolysis (18F-FDG) and cerebral perfusion (64Cu-PTSM) mice were placed in a restrainer and consciously injected into the peritoneal or tail vein, respectively, with 3.7–11.1 MBq (0.1–0.3 mCi) of purified, sterile radiotracer, where the final volume did not exceed 10% of the animal's body weight. Each animal was returned to its warmed home cage and allowed 30 min (18F-FDG) or 5 min (64Cu-PTSM) to allow for uptake and cellular trapping (Sokoloff, 1977; Mathias et al., 1991a). Post-uptake, mice were induced with 5% isoflurane gas, placed on the scanner imaging bed, and anesthesia maintained at 1–3% isoflurane (balance medical oxygen) during acquisition. In all cases, calibrated PET acquisition was performed in list mode for 15 (18F-FDG) or 30 (64Cu-PTSM) min on an IndyPET3 scanner (Frese et al., 2003), where random prompts did not exceed 10% of the total prompt rate. Post-acquisition, the images were reconstructed into a single-static image with a minimum field of view of 60 mm using filtered-back-projection (FBP), and were corrected for decay, random coincidence events, and dead-time loss (Soon et al., 2007).

In vivo PET/CT Imaging

To assess regional glycolysis and tissue perfusion, mice will be non-invasively imaged *via* PET/CT (n = 10 mice/sex/genotype/age). To measure regional blood flow, copper-pyruvaldehyde-bis (N4-methylthiosemicarbazone; 64Cu-PTSM; Green, 1987), which has a very high first pass (>75%) extraction (Mathias et al., 1991b), and glutathione reductase redox trapping of copper (Mathias et al., 1991b), will be administered *via* tail vein in awake subjects and will be given a 2 min uptake period prior to imaging. To measure regional glycolytic metabolism, 2-fluoro-2-deoxyglucose (18F-FDG) will be administered *via* tail vein in awake subjects and mice will be given a 30 min uptake period prior to imaging. Post uptake, mice will be induced with 5% isoflurane (95% medical oxygen) and maintained during acquisition with 1–2% isoflurane at 37°C. To provide both anatomical structure and function, PET/CT imaging will be performed with a Molecubes β-X-CUBE system (Molecubes NV, Gent Belgium). For PET determination of blood flow and metabolism, calibrated listmode PET images will be acquired on the β-CUBE and reconstructed into a single-static image using ordered subset expectation maximization (OSEM) with 30 iterations and three subsets (Krishnamoorthy et al., 2018). To provide anatomical reference, and attenuation maps necessary to obtain fully corrected quantitative PET images, helical CT images were acquired with tube voltage of 50 kV, 100 mA, 100 μm slice thickness, 75 ms exposure, and 100 μm resolution. In all cases, images will be corrected for radionuclide decay, tissue attenuation, detector dead-time loss, and photon scatter according to the manufacturer's methods (Krishnamoorthy et al., 2018). Post-acquisition, all PET and CT images will be co-registered using a mutual information-based normalized entropy algorithm (Studholme et al., 1998) with 12 degrees of freedom and mapped to stereotactic mouse brain coordinates (Paxinos and Franklin, 2012). Finally, to quantify regional changes, voxels of interest (VOI) for 27 brain (54 bilateral) regions will be extracted and analyzed for SUVR according to published methods (Dandekar et al., 2007).

Autoradiography

To provide secondary confirmation of the *in vivo* PET images, and to quantify tracer uptake regionally, brains were extracted post rapid decapitation, gross sectioned along the midline, slowly frozen on dry ice, then embedded in cryomolds with Optimal Cutting Temperature (OCT) compound (Tissue-Tek). Thin frozen sections (20 um) were obtained *via* cryotomy at prescribed bregma targets (n = 6 bregma/mouse, 6 replicates/bregma) according to stereotactic mouse brain coordinates (Franklin and Paxinos, 2013). Sections were mounted on glass slides, air dried, and exposed on BAS Storage Phosphor Screens (SR 2040 E, Cytiva Inc.) for up to 12 h. Post-exposure, screens were imaged *via* Typhoon FL 7000IP (GE Medical Systems) phosphor-imager at 25 um resolution along with custom 18F or 64Cu standards described previously (Territo et al., 2017).

Image Analysis

All PET and MRI images were co-registered using a ridged-body mutual information-based normalized entropy algorithm (Studholme et al., 1997) with 9 degrees of freedom, and mapped to stereotactic mouse brain coordinates (Franklin and Paxinos, 2013) using Analyze 12 (AnalyzeDirect, Stilwell KS). Post-registration, 56 regions bilateral regions were extracted *via* brain atlas and averaged to yield 27 unique volumes of interest that map to key cognitive and motor centers that include: Agranular Insular Cortex; Auditory Cortex; Caudate Putamen, Cerebellum; Cingulate Cortex; Corpus Callosum; Dorsolateral Orbital Cortex; Dorsintermed Entorhinal Cortex; Dysgranular Insular Cortex; Ectorhinal Cortex; Fornix; Frontal Association Cortex; Hippocampus; Lateral Orbital Cortex; Medial Orbital Cortex; Parietal Cortex; Parietal Association Cortex; Perirhinal Cortex; Prelimbic Cortex; Primary Motor Cortex; Primary Somatosensory Cortex; Retrosplenial Dysgranular Cortex; Secondary Motor Cortex; Secondary Somatosensory Cortex; Temporal Association Cortex, Thalamus; Ventral Orbital Cortex; Visual Cortex. For autoradiographic analysis, tracer uptake was quantified on hemi-coronal sections by manually drawing regions of interest for 17 regions of interest (i.e., Auditory Cortex, Caudate Putamen, Cerebellum, Cingulate Cortex, Corpus Callosum, Dorso-intermed Entorhinal Cortex, Dysgranular Insular Cortex, Ectorhinal Cortex, Hippocampus, Hypothalamus, Medial Septum, Primary Motor Cortex, Primary Somatosensory Cortex, Retrosplenial Dysgranular Cortex, Temporal Association Cortex, Thalamus, Visual Cortex) on calibrated phosphor screen at bregma 0.38, −1.94, and −3.8 mm using MCID (InterFocus Ltd). To permit dose and brain uptake normalization, Standardized Uptake Value Ratios (SUVR) relative to the cerebellum were computed for PET and autoradiograms for each subject, genotype, and age as follows:

$$SUVR(s, R, g, a) = \frac{R(s, g, a)}{C(s, g, a)}$$

where, s, g, a, R, and C are the subject, genotype, age, region/volume of interest, cerebellum region/volume of interest. In all cases, region/volumes of interest were analyzed for differences with time and genotype using a Two-Way ANOVA (Prism, GraphPad Inc.), where significance was taken at $p < 0.05$.

Immunoprecipitation

Tissue samples were homogenized in tissue protein extraction reagent (T-PER ThermoScientific) supplemented with protease and phosphatase inhibitors cocktail (Sigma-Aldrich). Protein concentration was measured using bicinchoninic acid (BCA; Pierce). Immunoprecipitation was performed by incubating a total of 1,500 μg of brain protein extract with 1 μg of biotinylated sheep anti-Trem2 antibody (RnD systems BAF1729) overnight at 4°C, followed by incubation with streptavidin sepharose beads (CST 3419) for 6 h at 4°C, washed three times with ice cold PBS with 0.1% Tween 20. Protein was eluted in sample loading buffer with 1 mM DTT followed by separation *via* Western blot (see below).

Western Immunoblot

Snap-frozen right hemispheres were homogenized by hard tissue homogenizer (USA Scientific, Ocala, FL) and lysed in 1 ml RIPA buffer (R0278, Sigma, St. Louis, MO) supplemented with protease and phosphatase inhibitor reagents (1861281, Thermo Fisher Scientific, Waltham, MA). Lysates were incubated for 1 h at 4°C before pelleting insoluble proteins by spinning at 4°C, 11,000× *g* for 15 min. Protein concentration was determined by Bradford protein assay (Biorad, Hercules, CA), according to the manufacturer's instructions. Samples were mixed with 10× Laemlli buffer (42556.01, Amsbio, Cambridge, MA), boiled for 10 min, and run on 12% SDS PAGE gels (456-1044, BioRad) with a colorimetric ladder (RPN800E, GE, Boston, MA). Gels were transferred to PVDF membranes for immunoblotting and imaging using an iBlot2 dry blotting system (Thermo Fisher). Membranes were blocked in 5% non-fat dry milk in 1× PBS+0.1% Tween20 for 1 h prior to incubating with primary antibodies diluted in 5% non-fat dry milk in 1× PBS+0.1% Tween20 for 1 h at room temperature. Membranes were washed in 1× PBS+0.1% Tween20 before incubating with secondary antibodies diluted in 5% non-fat dry milk in 1× PBS+0.1% Tween20. HRP-conjugated secondary antibodies targeting primary antibody host IgG were incubated at 1 h at room temperature. Membranes were washed in 1× PBS+0.1% Tween20 before digital imaging with SuperSignal West Pico PLUS chemiluminescent substrate (34579, Thermo Fisher). Images for immunoblot were quantified using ImageJ 1.8.0 version. Proteins of interest were visualized with the following primary antibodies against: ACTIN (Abcam, ab179467), GAPDH (abcam, ab9483), APOE4 (Novus, NBP1-49529), TREM2 (R&D Systems, MAB1729), and Alpha-tubulin (Sigma-Aldrich, T9026-100UL).

Cytokine Panel Assay

Hemibrains were homogenized in tissue homogenization buffer containing fresh protease inhibitor cocktail and aliquoted. The supernatant was utilized for the cytokine analysis. Mouse hemibrain samples were assayed in duplicate using the MSD mouse proinflammatory Panel I, a highly sensitive multiplex enzyme-linked immunosorbent assay (ELISA). The panel quantifies 10 cytokines: interferon gamma (IFN-γ), interleukin (IL)-1β, IL-2, IL-4, IL-6, IL-8, IL-10, IL-12p70, IL-13, and tumor necrosis factor α (TNFα) from a single small sample volume (25 μl) using an electrochemiluminescent detection method (MesoScale Discovery, Gaithersburg, MD, USA). The mean intra-assay coefficient for each cytokine was <8.5%, based on cytokine standards. Any value that was below the lowest limit of detection (LLOD) for the cytokine assay was replaced with $\frac{1}{2}$ LLOD of the assay for statistical analysis.

RNA-Sequencing Experimental Design

RNA-Seq data were obtained from whole left hemisphere brain samples from APOE4 KI mouse, carrying a humanized version of the prominent *APOEε4* genetic risk factor for LOAD, and the Trem2*R47H mouse, carrying a rare deleterious variant R47H allele of *Trem2* gene. In addition, a mouse model expressing both human *APOEε4* and the Trem2*R47H mutation was used

to compare the transcriptional changes in mice carrying both variants to mice carrying only a single risk allele and B6 controls. Whole-brain left hemispheres were collected at 4, 8, 12, and 24 months of age from both sexes.

RNA Sample Extraction

Total RNA was extracted from snap-frozen right brain hemispheres using Trizol (Invitrogen, Carlsbad, CA). mRNA was purified from total RNA using biotin-tagged poly dT oligonucleotides and streptavidin-coated magnetic beads and quality was assessed using an Agilent Technologies 2100 Bioanalyzer (Agilent, Santa Clara, CA).

RNA-Sequencing Assay Library Preparation

Sequencing libraries were constructed using TruSeq DNA V2 (Illumina, San Diego, CA) sample prep kits and quantified using qPCR (Kapa Biosystems, Wilmington, MA). The mRNA was fragmented, and double-stranded cDNA was generated by random priming. The ends of the fragmented DNA were converted into phosphorylated blunt ends. An "A" base was added to the 3' ends. Illumina®-specific adaptors were ligated to the DNA fragments. Using magnetic bead technology, the ligated fragments were size-selected and then a final PCR was performed to enrich the adapter-modified DNA fragments since only the DNA fragments with adaptors at both ends will amplify.

RNA-Sequencing

Libraries were pooled and sequenced by the Genome Technologies core facility at The Jackson Laboratory. All samples were sequenced on Illumina HiSeq 4000 using HiSeq 3000/4000 SBS Kit reagents (Illumina), targeting 30 million read pairs per sample. Samples were split across multiple lanes when being run on the Illumina HiSeq, once the data was received the samples were concatenated to have a single file for paired-end analysis.

RNA-Sequencing Data Processing

Sequence quality of reads was assessed using FastQC (v0.11.3, Babraham). Low-quality bases were trimmed from sequencing reads using Trimmomatic (v0.33; Bolger et al., 2014). After trimming, reads of length longer than 36 bases were retained. The average quality score was greater than 30 at each base position and sequencing depth was in range of 60–80 million reads. RNA-Seq sequencing reads from all samples were mapped to the mouse genome (version GRCm38.p6) using ultrafast RNA-Seq aligner STAR (v2.5.3; Dobin et al., 2013). To measure human *APOE* gene expression, we created a chimeric mouse genome by concatenating the human *APOE* gene sequence (human chromosome 19:44905754-44909393) into the mouse genome (GRCm38.p6) as a separate chromosome (referred to as chromosome 21 in chimeric mouse genome). Subsequently, we added gene annotation of the human *APOE* gene into the mouse gene annotation file. Additionally, we have also introduced annotation for novel *Trem2* isoform in mouse gene annotation file (GTF file), that is identical to primary transcript but truncated exon2 by 119 bp from its start position. Afterward, a STAR index was built for this chimeric mouse genome sequence for alignment, then STAR aligner output coordinate-sorted BAM files for each sample mapped to the chimeric mouse genome using this index. Gene expression was quantified in two ways, to enable multiple analytical methods: transcripts per million (TPM) using RSEM (v1.2.31; Li and Dewey, 2011), and raw read counts using HTSeq-count (v0.8.0; Anders et al., 2015).

Differential Expression Analysis

Differential expression in mouse models was assessed using the R Bioconductor package DESeq2 (v1.16.1; Love et al., 2014). DESeq2 takes raw read counts obtained from HTSeq-count as input. Genes with the Benjamini-Hochberg corrected p-values < 0.05 were considered as significantly differentially expressed genes.

Principal Component Analysis

We analyzed a total of 234 RNA-Seq samples originating from different mouse models of different ages and sex. First, the dispersion parameter for each gene was estimated using DESeq2 R package (Love et al., 2014). Afterward, we applied the variance stabilizing transformation (vst) function of DESeq2 (Love et al., 2014) to the read count data in order to produce a data matrix in which expression levels are homoscedastic. Finally, we extracted the principal components using the plot PCA function of DESeq2 in R.

Functional Enrichment Analysis

Functional annotations and enrichment analyses were performed using the R Bioconductor package clusterProfiler (Yu et al., 2012), with Gene Ontology terms and KEGG pathways enrichment analyses performed using functions enrichGO and enrichKEGG, respectively. The function compareCluster was used to compare enriched functional categories of each gene module. The significance threshold for all enrichment analyses was set to 0.05 using Benjamini-Hochberg adjusted p-values.

Human Post-mortem Brain Cohorts and Co-expression Module Identification

Whole-transcriptome data for human post-mortem brain tissue was obtained from the Accelerating Medicines Partnership for Alzheimer Disease-(AMP-AD) consortium, which is a multi-cohort effort to harmonize genomics data from human LOAD patients. Harmonized co-expression modules from the AMP-AD data sets were obtained from the AD Knowledge Portal (DOI: 10.7303/syn11932957.1). The human co-expression modules derive from three independent LOAD cohorts, including 700 samples from the ROS/MAP cohort, 300 samples from the Mount Sinai Brain bank, and 270 samples from the Mayo cohort. A detailed description of post-mortem brain sample collection, tissue and RNA preparation, sequencing, and sample QC has been provided elsewhere (Allen et al., 2016; De Jager et al., 2018; Wang et al., 2018). As part of a transcriptome-wide meta-analysis to decipher the molecular architecture of LOAD, 30 co-expression modules from seven different brain regions across the three cohorts have been recently identified (Logsdon et al., 2019). Briefly, Logsdon et al. (2019) identified 2,978 co-expression modules using multiple techniques across the different regions after adjusting for co-variables and accounting

for batch effects (10.7303/syn10309369.1). A total of 660 co-expression modules were selected based on a specific enrichment in LOAD cases when compared to controls (10.7303/syn11914606). Finally, multiple co-expression module algorithms were used to identify a set of 30 aggregate modules that were replicated by the independent methods (Logsdon et al., 2019).

Mouse-Human Correlation Analysis

First, we performed differential gene expression analysis for each mouse model compared to age and sex-matched B6 control mice using the limma (Ritchie et al., 2015) package in R. Afterward, we computed the correlation between changes in expression (log fold change) for all DE genes in a given module with the fold changes for each mouse model (specified by genotype, sex, diet, and age). Correlation coefficients were computed using cor.test function in R as:

$$\text{cor.test}(\text{LogFC(h)}, \text{LogFC(m)}) \quad (1)$$

where LogFC(h) is the log fold change in transcript expression of human AD patients compared to control patients and LogFC(m) is the log fold change in expression of mouse transcripts compared to control mouse models. LogFC values for human transcripts were obtained *via* the AD Knowledge Portal[3].

Statistical Analysis

Statistical analyses were constrained to comparisons between littermate-controlled subjects only (*B6.APOE4 v.B6.APOE4.Trem2*R47H*). The student's t-test was employed on data sets differing by a single variable (e.g., age, sex, genotype). ANOVA was used in data sets where multiple factors are considered and combined for possible synergistic effects.

Availability of Data and Materials

The LOAD1 data sets are available *via* the AD Knowledge Portal[4]. The AD Knowledge Portal is a platform for accessing data, analyses, and tools generated by the Accelerating Medicines Partnership (AMP-AD) Target Discovery Program and other National Institute on Aging (NIA)-supported programs to enable open-science practices and accelerate translational learning. The data, analyses, and tools are shared early in the research cycle without a publication embargo on a secondary use. Data is available for general research use according to the following requirements for data access and data attribution[5].

For access to content described in this manuscript see: https://doi.org/10.7303/syn23631984.

RESULTS

Biometric Profiles of APOE4.Trem2*R47H Mice Change With Age

Comparison of biometric data from young (4 months) and aged mice (24 months), comprised of both sexes from four genotypes (**Table 2**), revealed the expected age-related accumulation in physical frailty characteristics (**Figures 1A,B**) with inverse correlations in body temperature (**Supplementary Figure 1**) and age-related increases in body weights (**Figures 1C,D**). However, effects due to genotype were not observed overall (see also **Supplementary Table 1**). Statistical analyses were constrained to contrasting only cohorts sharing littermates. Effects of age and genotype on variability were observed in datasets, as well as effective interaction, determined by ANOVA. These results confirm a strong aging effect in all assays. To determine the effects of *APOEε4* and *Trem2*R47H* on mouse metabolome, terminal non-fasted blood plasma levels of metabolites were measured. Homozygous expression of humanized *APOEε4* resulted in a significant decrease of non-fasted serum low-density lipoproteins (LDL) in the absence of corresponding decreases in total cholesterol (**Figures 1E–H**). Expected aging-specific-effects included decreases in glucose and triglyceride levels in both sexes independent of genotypes (**Figures 1I–L**). Other measurements and metabolic analytes included in our panel were unchanged between sex, age, and genotype cohorts (**Supplementary Figures 1C–F** and **Supplementary Table 2**). Additional cohorts, investigating *APOEε4* allele alone compared with littermate B6 controls, were aged to 12 months. Consistent with initial aging-related phenotypes in the 4- and 24-month cohorts, there was an expected increase in cumulative frailty scores, reductions in core body temperature, and increase in body weight in both sexes with no genotype-driven differences observed (**Supplementary Figures 1G–I**).

Age Is the Strongest Determinant of Performance by APOE4.Trem2*R47H Mice in Behavioral Assays

As part of the comprehensive phenotypic characterization, all mice were evaluated through a behavioral testing pipeline consisting of open field, spontaneous alternation (y-maze), rotarod motor coordination, and running wheel activity assessments (**Table 2**; **Supplementary Tables 2–5**). Age-dependent impairments were observed across all genotypes from 4–24 months of age in locomotor activity as measured by open field and entries in the y-maze, motor coordination as measured by rotarod, and wheel- running activity (**Figure 2**; **Supplementary Figures 2, 4**). Spatial working memory was preserved up to 24 months of age with no deficits observed across genotype relative to 4 months of age. Interestingly, in the rotarod motor coordination assay, there was a greater impairment observed in B6.*Trem2*R47H* males relative to B6.*APOE4.Trem2*R47H* or B6.*APOE4* alone at 24 months (**Figures 2A,B**). Compared to 4-month-old animals, we observed a decrease in activity during the active period (dark phase) by 24 months (**Supplementary Figure 4**). At 24 months of age, home cage running wheel activity suggested a correlation between increased activity during the active period and expression of the *APOEε4* allele (both B6.*APOE4* and B6J.*APOE4/Trem2*R47H* mice) by way of total distance traveled and day-time activity in B6.*Trem2*R47H* mice (**Supplementary**

[3]https://www.synapse.org/#!Synapse:syn11180450
[4]https://adknowledgeportal.org
[5]https://adknowledgeportal.org/DataAccess/Instructions

TABLE 2 | Frailty assay and behavioral assays study population.

Mouse models	4M		8M		12M		24M	
	Male	Female	Male	Female	Male	Female	Male	Female
C57BL/6J	16	16	18	18	23	21	12	9
APOE4 KI	12	12	12	12	11	10	11	11
TREM2* R47H	12	11	12	12	13	11	13	14
APOE4.TREM2* R47H	11	10	12	11	12	10	8	6

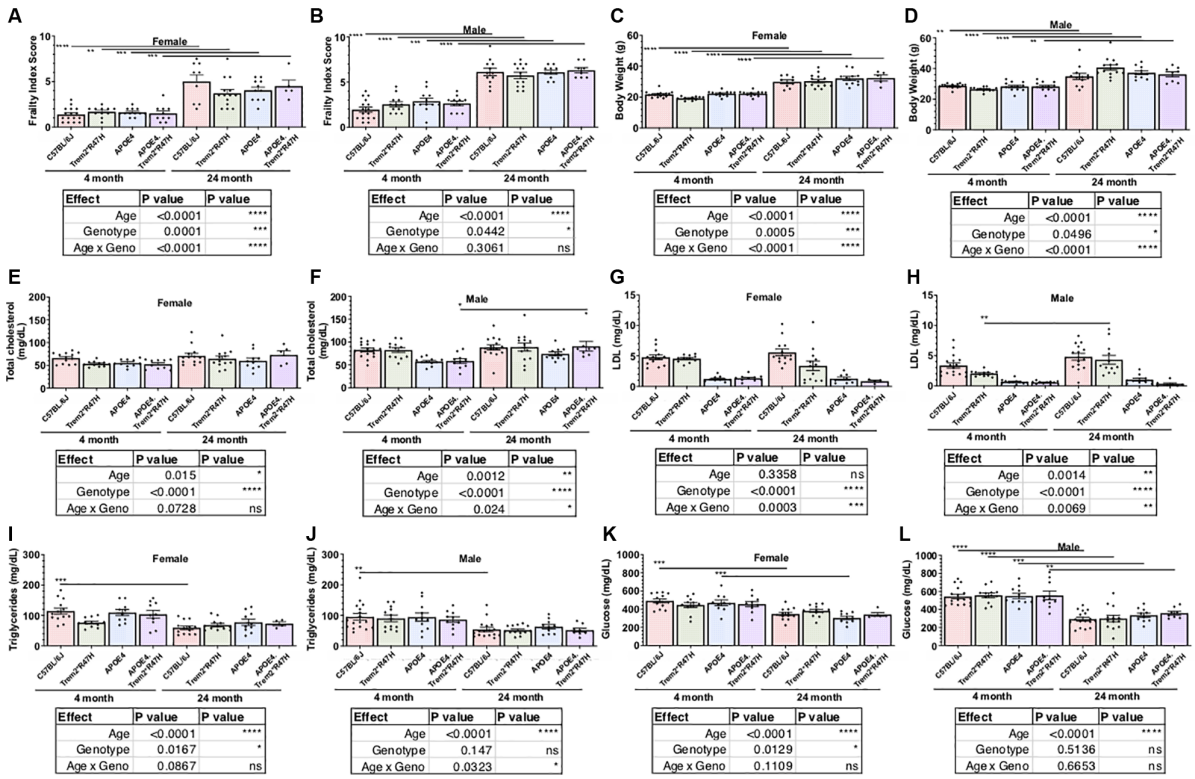

FIGURE 1 | Age is primary factor driving increases in measures of frailty. Cross-sectional cohorts of young and old mice inspected for measures of physical well-being, or frailty **(A,B)**, including body weight **(C,D)**. Post-mortem, non-fasted, blood biochemistry analysis provided serum levels of cholesterol, lipoproteins, lipids, and glucose **(E–L)**. Age-dependent differences within genotype and sex determined by two-way ANOVA. Factor effects and effect interaction displayed in tables. $*p < 0.05$; $**p < 0.01$; $***p < 0.001$. All alleles expressed were homozygous.

Figures 4E,F). In addition to monitoring the physical wellness and behavior of otherwise healthy mice, we also wanted to track the effects of sex and genotype on animal longevity, in the absence of amyloid-associated AD. For this analysis, mortality was defined as subjects that were found dead with no obvious signs of infection, trauma, or intervention during daily monitoring. Mortality risk for each allele was determined by comparing survival scores of cohorts aged upto 24 months. Overall, females had a greater risk than males, and survival probabilities were lowest in both sexes for animals expressing both LOAD risk alleles (**Supplementary Figure 5**).

PET Identified Age- and Genotype-Dependent Differences in Glycolysis and Tissue Perfusion

In an effort to understand the role of risk alleles on regional glycolysis and tissue perfusion, translationally relevant regional measures were acquired *via* 18F-FDG and 64Cu-PTSM PET and autoradiography, respectively (**Figure 3**). By 12 months glycolysis was altered in key brain regions associated with sensory integration, cognition, vision, and motor function in B6.*APOE4* and B6.*APOE4.Trem2*R47H* mice, when compared with controls (**Table 3**; **Supplementary Figure 6**), and were confirmed *via* post-mortem autoradiography, which has a 40-fold greater resolution than PET. As expected, these changes were greater in number of regions and magnitude of change in female mice when compared to males (**Supplementary Figures 6B,C**). These changes were similarly observed through time, where female mice showed significantly altered glycolysis at 4, 8, and 12 months, while male mice largely showed a hypoglycolytic phenotype at 8 months, that was virtually mitigated by 12 months (**Supplementary Figure 6**). Since these risk alleles can alter metabolic functionality and neuroinflammatory-driven tissue perfusion in an independent manner, we quantitatively measured

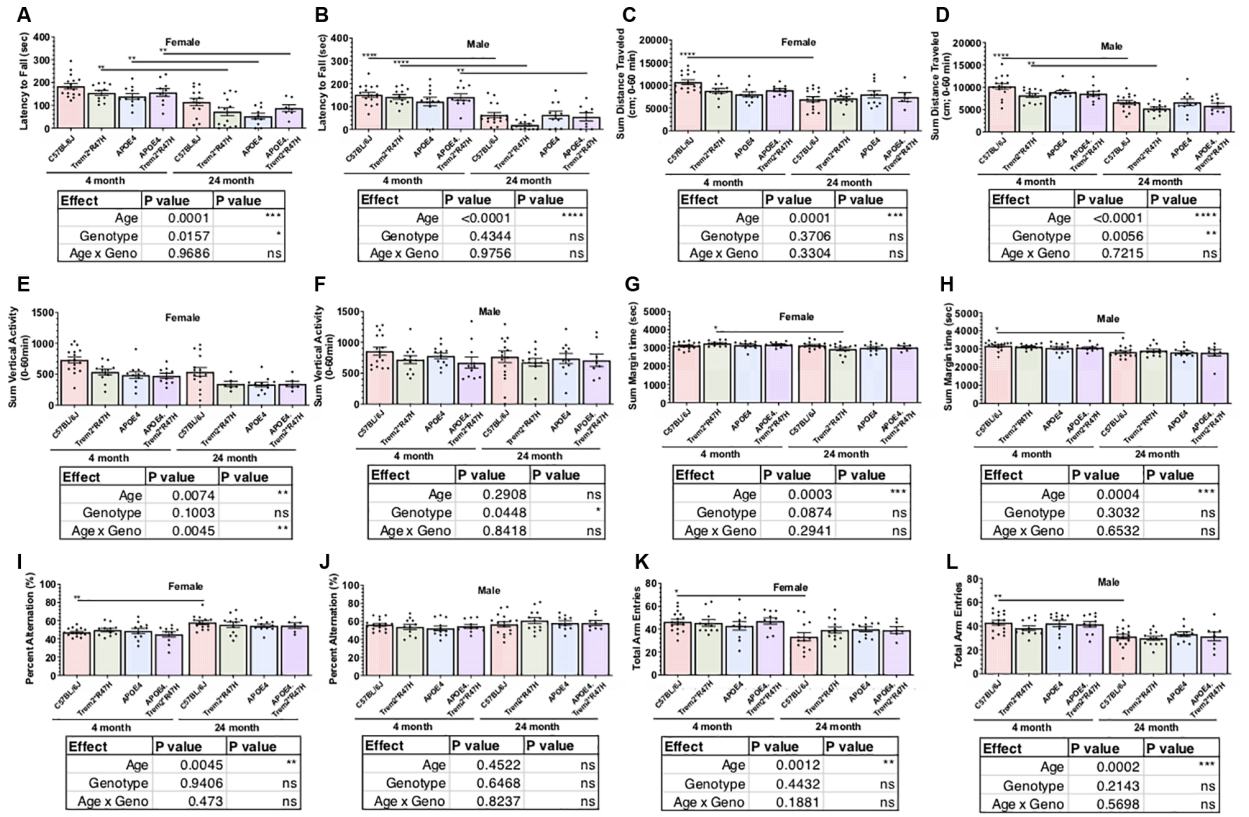

FIGURE 2 | Behavioral testing of LOAD mice to identify functional neurophenotype. Performance of young and aged mice carrying combinations of APOE4 and *Trem2*R47H* alleles incorporated assays to measure neuromuscular coordination (rotarod; **A,B**), locomotor activity (open field; **C–F**), exploratory drive (open field; **G,H**), and spatial working memory (spontaneous alternation in Y-maze; **I–L**). Age-dependent differences within genotype determined by two-way ANOVA. Factor effects and effect interaction are displayed in tables. $*p < 0.05$; $**p < 0.01$; $****p < 0.001$. All alleles expressed were homozygous.

changes in regional tissue perfusion *via* 64Cu-PTSM PET/MRI and confirmed this *via* autoradiography. Brain perfusion was significantly lower in regions associated with sensory integration, cognition, vision, and motor function in both sexes by 12 months and confirmed *via* post-mortem autoradiography (**Supplementary Figure 7**). Interestingly, these changes were manifested temporally, with the greatest reductions occurring across genotypes and regions in both sexes at 4 months (**Supplementary Figure 7**). Unlike glycolysis, these changes were largely resolved by 8 months in female mice, while males continued to show a regional reduction in perfusion at this same age. In 24-month-old animals, APOE4.Trem2*R47H had increased glycolysis compared to C57BL/6J in most brain regions, a trend that was also evident in young cohorts and in both sexes (**Figure 3A**). Age-related increases in brain perfusion were further confirmed in 24 months B6.*APOE4.Trem2*R47H* mice (**Figure 3B**).

Biochemical and Neuropathological Effects of APOEε4 and Trem2*R47H Alleles

Confirmation of protein expression levels in brain tissue was confirmed for alleles encoding human APOE4 and mouse TREM2 carrying the R47H mutation (**Supplementary Figure 8**). Similar to reports of R47H variant-mediated reduction in *Trem2* transcript levels (Logsdon et al., 2019), TREM2 protein levels in the brains of these animals were also decreased. However, instead of a near knock-out of all TREM2 that has been reported previously (Logsdon et al., 2019), levels fell by approximately 50% in *Trem2*R47H* animals compared to C57BL/6J (**Supplementary Figures 8A,B**). We have previously shown APOE4 protein levels are similar to endogenous mouse APOE (Foley et al., 2020) and expression of APOE4 appeared similar between male and female *APOE4.Trem2*R47H* mice (**Supplementary Figure 8C**). Additional molecular characterization of these animals showed both age- and genotype-driven differences in levels of cytokines present in the blood (**Figure 4**) and brain (**Supplementary Figure 9**; **Table 4**). Compared to similarly aged C57BL/6J and younger APOE4.Trem2*R47H cohorts, 18 month B6.*APOE4.Trem2*R47H* mice showed strong differences in circulating concentrations of immunomodulatory cytokines (**Figure 4**). IL-6 and KC/GRO concentrations were highest in B6.*APOE4.Trem2*R47H* brain tissue at 8 months, while blood plasma concentrations continued to increase with age in those mice (**Supplementary Figures 9B,D,E**). On multiple occasions, a trend appeared to suggest increased cytokine concentrations in mice expressing mutated allele *Trem2*.

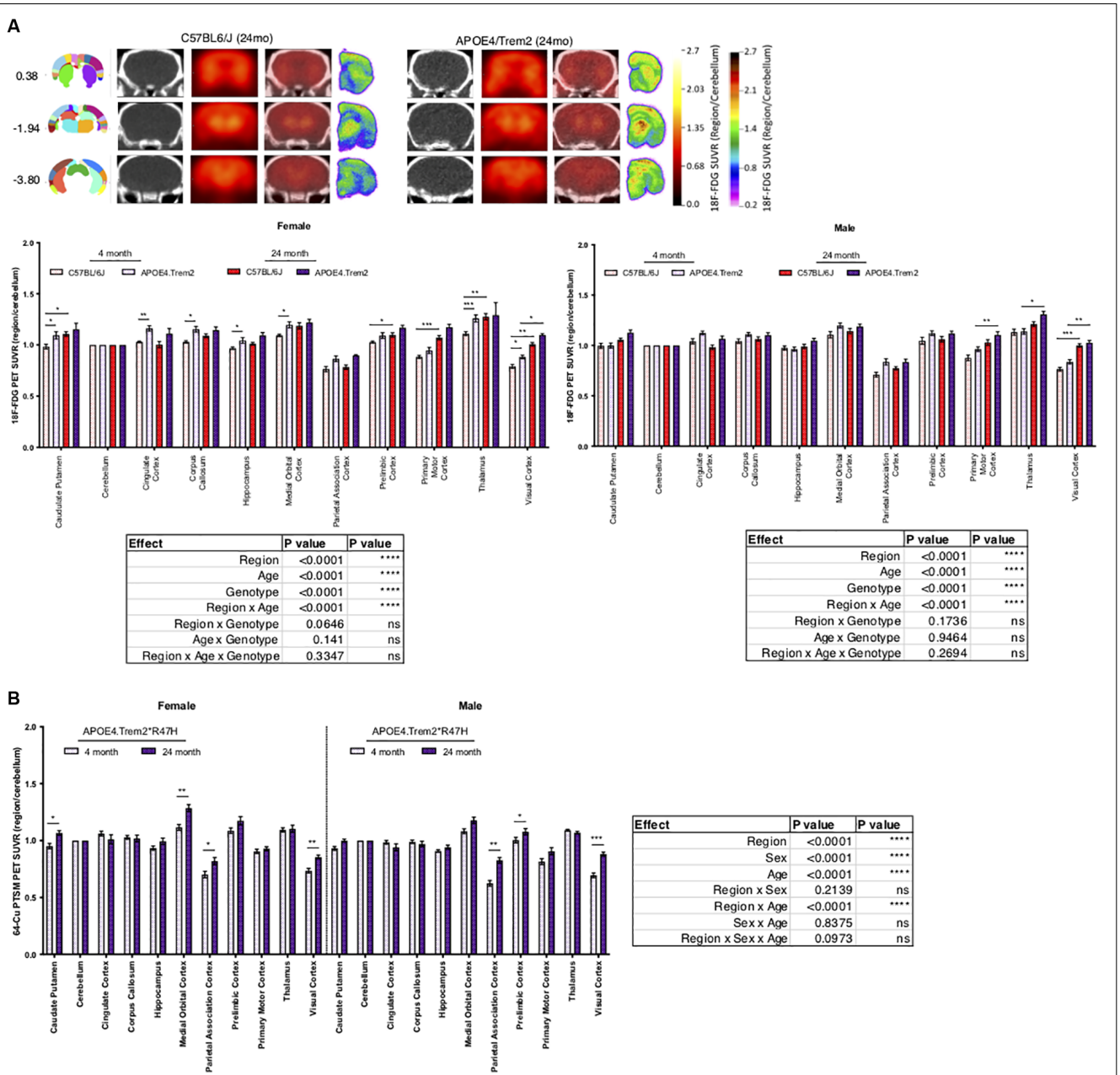

Effect	P value	P value
Region	<0.0001	****
Age	<0.0001	****
Genotype	<0.0001	****
Region x Age	<0.0001	****
Region x Genotype	0.0646	ns
Age x Genotype	0.141	ns
Region x Age x Genotype	0.3347	ns

Effect	P value	P value
Region	<0.0001	****
Age	<0.0001	****
Genotype	<0.0001	****
Region x Age	<0.0001	****
Region x Genotype	0.1736	ns
Age x Genotype	0.9464	ns
Region x Age x Genotype	0.2694	ns

Effect	P value	P value
Region	<0.0001	****
Sex	<0.0001	****
Age	<0.0001	****
Region x Sex	0.2139	ns
Region x Age	<0.0001	****
Sex x Age	0.8375	ns
Region x Sex x Age	0.0973	ns

FIGURE 3 | Increases in regional glucose metabolism due to expression of APOE4 and *Trem2*R47H*. Positron emission tomography (PET; red scale) of radioactive 18F-FDG marker was used to measure tissue glucose uptake, guided by computed tomography (CT; black and white) mapping to brain regions of interest, indicated by bregma coordinates (far left) **(A)**. PET-CT of 64-Cu PTSM of female and male B6.*APOE4.Trem2*R47H* mice revealed age-driven increases in brain perfusion **(B)**. Post-mortem autoradiography of coronal brain tissue is represented in **(A)** (rainbow; far right). Genotype- and age-dependent differences determined by three-way ANOVA. Factor effects and effect interaction are displayed in tables. $^{*}p < 0.05$; $^{**}p < 0.01$; $^{***}p < 0.001$. All alleles expressed were homozygous.

Neuropathological features of AD were then investigated by hematoxylin and eosin (H&E, structure) and luxol fast blue/cresyl violet (LFB/CV, myelin) staining but did not reveal any gross anatomical changes to tissue architecture or myelin (**Figure 5A**). Brain sections were also imaged *via* immunofluorescence and included neuritic plaque-reactive-microglia (X34/Lamp1/Iba1), vascular leakage (CD31/Iba1/Fibrin), and ThioflavinS (amyloid plaques and neurofibrillary tau tangles; **Figure 5B**). No gross abnormalities in cell counts (**Figure 5C**), nor additional neuropathological features were observed in 24-month B6.*APOE4.Trem2*R47H* mice. We focused particularly on the cortex and hippocampus where episodic memory (hippocampus) and memory behavior (cortex) are regulated. Amyloid plaques and hyperphosphorylated Tau were not observed in mice of any genotype at any age.

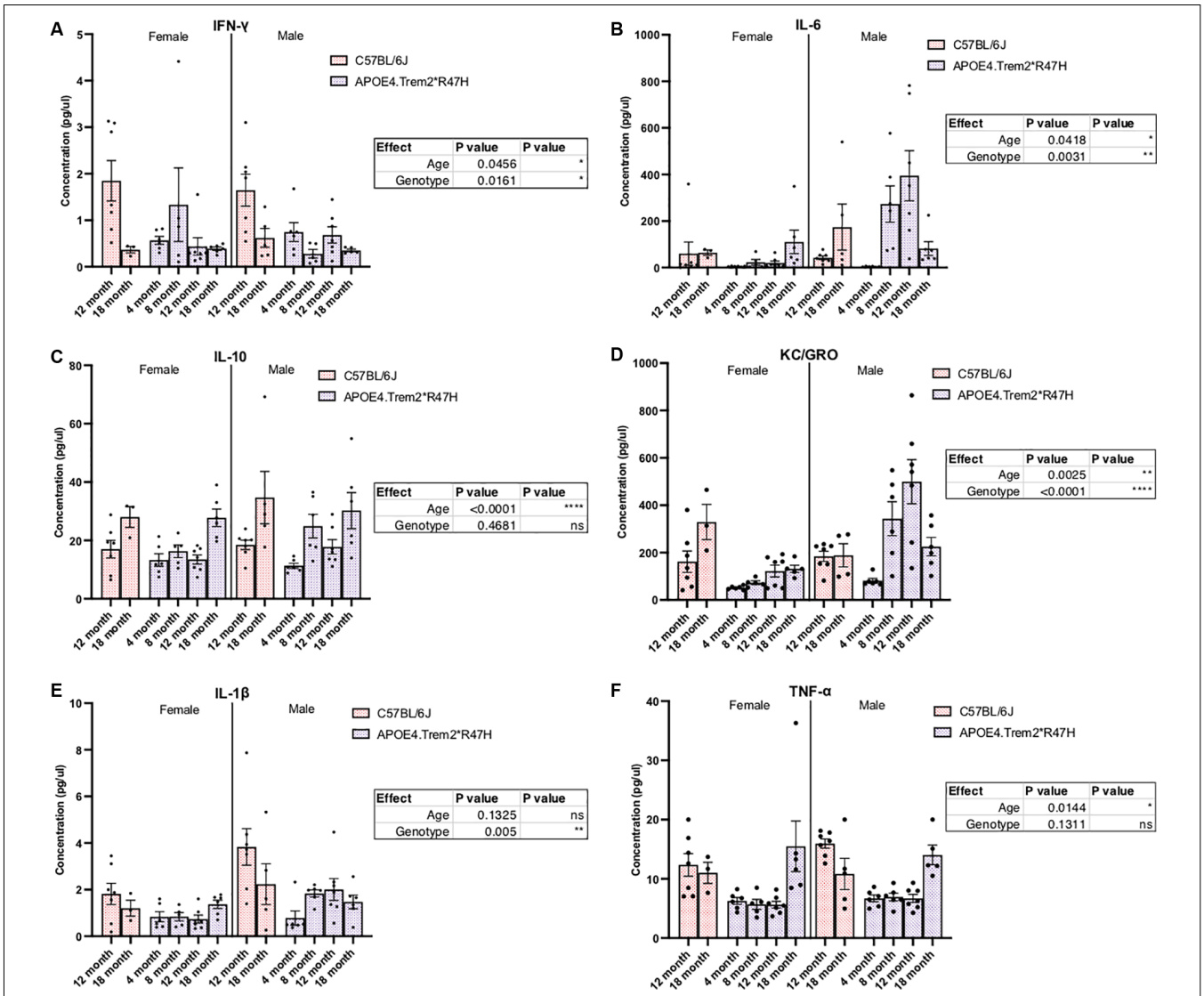

FIGURE 4 | Levels of immunomodulatory cytokines in plasma are significantly different due to increased age and combined expression of APOE4 and *Trem2*R47H* alleles. IFN-gamma (IFN-γ), IL-1beta, IL-10, IL-6, and KC/GRO (CXCL1) levels were measured by multiplex immunoassays of blood plasma from C57BL/6J and B6.APOE4.Trem2R47H mice **(A–F)**. Genotype- and age-dependent differences determined by two-way ANOVA. Factor effects displayed in tables. $^{*}p < 0.05$; $^{**}p < 0.01$; $^{***}p < 0.001$. All alleles expressed were homozygous.

TABLE 3 | *In vivo* imaging study population.

Mouse models	4M		8M		12M	
	Male	Female	Male	Female	Male	Female
C57BL/6J	8	9	12	11	9	10
APOE4 KI	10	10	10	12	12	10
TREM2*R47H	10	12	12	8	12	11
APOE4.TREM2* R47H	12	10	10	12	10	10

Transcriptional Profiling Revealed Individual and Synergistic Effects of APOEε4, Trem2*R47H, and Age

Brain hemispheres from 4 and 24-month male and female B6.*APOE4.Trem2*R47H* mice and single genotype and C57BL/6J controls were assessed using RNA-seq (see "Materials and Methods" section; **Table 5**). The transcriptomic analysis measured the expression levels (log-transformed TPM counts) of mouse *Apoe*, *Trem2*, and human *APOE* genes across all mouse models (**Figures 6A–C**). We observed higher

TABLE 4 | Blood and brain tissue cytokine and metabolomic study population.

Mouse models	4M		8M		12M		24M	
	Male	Female	Male	Female	Male	Female	Male	Female
C57BL/6J	17	13	12	6	10	11	15	13
APOE4 KI	11	10	11	12	13	14	10	10
TREM2*R47H	12	11	11	11	12	10	13	13
APOE4.TREM2*R47H	10	10	11	11	8	5	8	5

expression of human APOE gene in mice carrying humanized *APOEε4* (*B6.APOE4* and B6.*APOE4.Trem2*R47H* mice), whereas mouse *Apoe* gene was highly expressed in B6 and *Trem2*R47H* mice (**Figures 6A,B**). As expected based on protein levels (**Supplementary Figures 7A,B**), expression of *Trem2* was significantly reduced ($p < 0.05$) in B6.*Trem2*R47H* and B6.*APOE4.Trem2*R47H* compared to age-matched B6 (**Figure 6C**), an effect likely caused by a novel effector splice site and truncation introduced by the R47H mutation. Furthermore, the expression level of *Trem2* increased with age across all mouse models, but no such patterns were observed in the expression levels of mouse *Apoe* and human *APOE* genes (**Figures 6A,B**). In addition, there was a lower expression of *Trem2* in B6.*APOE4.Trem2*R47H* compared to B6.*Trem2*R47H* mice at an advanced age (24 months), suggesting expression of *Trem2* might be suppressed by *APOEε4*. Next, principal component analysis (PCA) identified two distinct clusters corresponding to male and female samples separated along with the first principal component (26% of total variance), suggesting sex-specific differences are profound in mice (**Figure 6D**). Analysis of samples from different age groups revealed a gradient of discrimination along with the second principal component (14% of total variance; **Figure 6D**), implying the presence of age-dependent molecular changes in the brain transcriptomes.

To identify molecular effects of the LOAD risk genes, we performed pairwise differential analysis between each genotype (B6.*APOE4*, B6.*Trem2*R47H* or B6.*APOE4.Trem2*R47H*) and age- and sex-matched B6 controls. At an early age (4 months), only a few genes were differentially expressed (DEG; $p < 0.05$) for all genotypes for both sexes (**Supplementary Figure 10A**), and no KEGG pathways were enriched. At 8 months of age, there were 32 DEGs (3 upregulated, 29 downregulated; $p < 0.05$) in male B6.*Trem2*R47H* mice, and 11 DEGs (2 upregulated, 9 downregulated; $p < 0.05$) in female B6.*Trem2*R47H* mice (**Supplementary Figure 10A**). KEGG Pathway analysis identified enrichment of genes involved in immune-related pathways such as "complement and coagulation cascades" and "staphylococcus aureus infection" in the downregulated DEGs in female B6.*Trem2*R47H* mice (**Figure 7**). In 8 months old B6.*APOE4* mice, a total of 145 genes were significantly differentially expressed (42 upregulated, 103 downregulated; $p < 0.05$) in male mice, whereas a total of 25 genes were differentially expressed (11 upregulated, 14 downregulated; $p < 0.05$) in female mice (**Supplementary Figure 10A**). Pathway enrichment analysis of upregulated genes in male B6.*APOE4* mice identified enrichment of "platelet activation" pathway, whereas downregulated genes in female B6.*APOE4* mice were enriched for "protein processing in endoplasmic reticulum" pathway (**Figure 7**). No KEGG pathways were enriched for downregulated DEGs in male *B6.APOE4* mice and upregulated DEGs in female *B6.APOE4* mice. DEGs in male B6.*APOE4.Trem2*R47H* (7 upregulated, 32 downregulated), and female B6.*APOE4.Trem2*R47H* mice (2 upregulated, 1 downregulated; $p < 0.05$; **Supplementary Figure 10**, **Figure 7**) were not enriched in any KEGG pathway.

At 12 months of age, there were a total of 206 DEGs (118 upregulated, 88 downregulated) in male B6.*Trem2*R47H* mice and 285 DEGs (113 upregulated, 172 downregulated; $p < 0.05$) in female B6.*Trem2*R47H* mice. The upregulated DEGs in male *Trem2*R47H* mice were enriched in "RNA transport" and "spliceosome" pathways (**Figure 7**, **Supplementary Figure 10**), while genes in the "oxidative phosphorylation" pathway were downregulated in male B6.*Trem2*R47H* mice (**Figure 7**, **Supplementary Figure 10**). Upregulated and downregulated DEGs in female B6.*Trem2*R47H* mice were enriched for "RNA transport" and "lysosome" pathways respectively (**Figure 7**, **Supplementary Figure 10**). There were very few DEGs in *B6.APOE4* (1 in male, 3 in female) and B6.*APOE4.Trem2*R47H* mice (2 in male, 5 in female; **Supplementary Figure 10**) at this age and therefore no enrichment of KEGG Pathways.

At 24 months old, there were a total of 144 DEGs (15 upregulated, 129 downregulated) in the male B6.*Trem2*R47H* mice and 748 DEGs (359 upregulated, 389 downregulated; $p < 0.05$) in the female B6.*Trem2*R47H* mice. At this age, B6.*APOE4.Trem2*R47H* mice showed a greater number of DEGs ($p < 0.05$) in both male (24 upregulated, 197 downregulated) and female mice (83 upregulated, 400 downregulated) compared to at younger ages (4–12 months; **Supplementary Figure 10**), suggesting that the most dramatic transcriptional changes arise between 12 and 24 months. We also found substantial overlap in downregulated DEGs between B6.*Trem2*R47H* and B6.*APOE4.Trem2*R47H* mice for both sexes (**Supplementary Figure 10**). This suggests that the *Trem2*R47H* allele is the major driving force in age-dependent transcriptional changes in B6.*APOE4.Trem2*R47H* mice. Downregulated DEGs were enriched in multiple AD-related pathways such as "lysosome", "osteoclast differentiation", "phagosome", "antigen processing and presentation", cytokine-cytokine receptor interaction', and "complement and coagulation cascades" in both 24 months old B6.*Trem2*R47H* and B6.*APOE4.Trem2*R47H* mice (**Figure 7**, **Supplementary Figure 10**). In B6.*APOE4* mice, we observed only two DEGs (1 upregulated, 1 downregulated) in male and

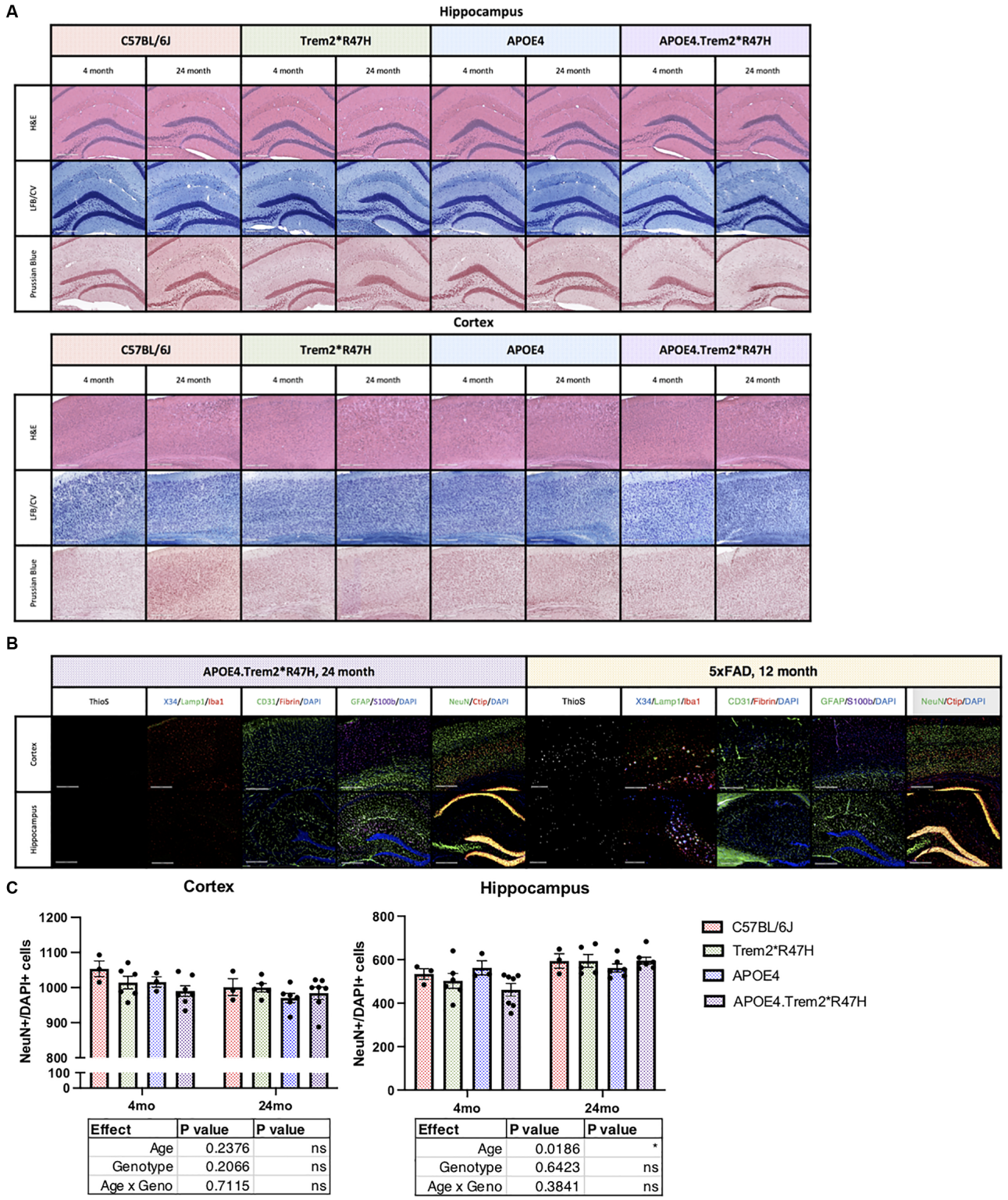

Effect	P value	P value
Age	0.2376	ns
Genotype	0.2066	ns
Age x Geno	0.7115	ns

Effect	P value	P value
Age	0.0186	*
Genotype	0.6423	ns
Age x Geno	0.3841	ns

FIGURE 5 | Neuropathological analysis of cortex and hippocampus. Hematoxylin and eosin (H&E), luxol fast blue/cresyl violet (LFB/CV), and Prussian blue staining tissue staining protocols **(A)** to identify anatomical changes in the cortex and hippocampus of young and aged mice. Thioflavin S (Thios) and four combinations of known neuropathological markers of LOAD in aged mice, 5xFAD included as amyloidogenic positive control **(B)**. Neuropathological analysis of cortex and hippocampus. Neuron (NeuN) cell populations were quantified in panel **(C)**. Age- and genotype-dependent differences determined by two-way ANOVA. Factor effects and effect interaction displayed in tables. $^{*}p < 0.05$; $^{**}p < 0.01$; $^{***}p < 0.001$. All alleles expressed were homozygous.

TABLE 5 | RNA-seq study population.

Mouse models	4M		8M		12M		24M	
	Male	Female	Male	Female	Male	Female	Male	Female
C57BL/6J	12	12	6	6	6	6	7	6
APOE4 KI	13	12	6	6	4	5	5	6
TREM2*R47H	12	12	6	6	6	6	6	3
APOE4.TREM2*R47H	10	12	5	6	8	5	7	6

24 DEGs (1 upregulated, 23 downregulated) in female mice. Downregulated genes in the B6.*APOE4* female mice were enriched in "NOD-like receptor signaling" pathway (**Figure 7**, **Supplementary Figure 10**). We did not observe any enriched KEGG pathways in the upregulated list of genes across all genotypes at 24 months.

Home Cage Voluntary Wheel Running Increased Oxidative Phosphorylation Pathway in APOE4.Trem2*R47H Mouse Brains

In the human population, a sedentary lifestyle is correlated with an increased risk of LOAD (de Rezende et al., 2014; Fenesi et al., 2017; Yan et al., 2020). Therefore, to determine if physical activity influenced transcriptional changes in B6.*APOE4.Trem2*R47H* mice, a running wheel was provided in the home cage of 22-month-old male mice for 2 months. Brain tissue from these animals was profiled by RNA-seq. A total of 292 DEGs (108 upregulated, 184 downregulated) were identified in the running B6.*APOE4.Trem2*R47H* mice compared to 24 months old B6 male mice. Enrichment analysis identified multiple enriched KEGG pathways such as "oxidative phosphorylation", "thermogenesis", and "retrograde endocannabinoid signaling" in the upregulated list of genes, whereas immune system associated pathways were enriched in the downregulated list of genes (**Supplementary Figure 11A**). To identify the effect of exercise, running B6.*APOE4.Trem2*R47H* male mice were compared with sedentary 24-month-old B6.*APOE4.Trem2*R47H* male mice and there was a total of 600 DEGs (312 upregulated, and 288 downregulated). Upregulated DEGs were enriched in pathways such as "oxidative phosphorylation" and "Ribosome" (**Supplementary Figure 11A**). The expression of these upregulated DEGs enriched for oxidative phosphorylation showed reduced expression in age- and sex-matched *B6.APOE4* and B6.*Trem2*R47H* compared to running B6.*APOE4.Trem2*R47H* mice (**Supplementary Figure 11B**). Finally, the expression of the upregulated DEGs associated with the oxidative phosphorylation pathway was assessed in transcriptional data from AMP-AD. Reduced expression of these running signature genes was observed in AD cases compared to controls across multiple brain regions such as parahippocampal gyrus (PHG) and frontal pole brain regions (FP; **Supplementary Figure 11C**). This suggests that exercise induces beneficial effects on health by increasing the expression of oxidative phosphorylation pathway genes that are down regulated across multiple brain regions in AD patients.

DISCUSSION

MODEL-AD was established in response to the many shortcomings of existing mouse models of AD. Aspects of human pathology have been replicated in mouse strains, most prominently the formation of beta-amyloid plaques *via* transgenic over-expression of brain-specific mutant human amyloid-beta precursor protein (APP), presenilin-1 (PS1), and/or microtubule-associated protein tau (MAPT) bearing familial Alzheimer's disease (FAD) mutations (Bilkei-Gorzo, 2014). Legacy preclinical models rely heavily on alleles that overexpress transgenes, resulting in the removal or masking of important human-relevant biological interactions. These mouse strains have been invaluable for understanding the molecular and behavioral phenotypes of early-onset Alzheimer's disease (EOAD) driven by the rapid and robust formation of plaques and tangles in the brain and correlating hyperactivity which is a confound of many cognitive behaviors. However, LOAD is ∼20× more prevalent than EOAD and further implicates aging, inflammation, environmental, and many more genetic risk factors in disease development. *APOE4.Trem2*R47H* mice did not produce any severe phenotypes, even late into life, allowing a better understanding of the effect of AD risk factors in the context of aging (**Supplementary Figure 5**). As the heterogeneity of this disease becomes more appreciated, so is the importance of appropriate disease staging. Molecular targets of interest may only be available during particular evolving disease stages: debris (cell fragments, plaques, tangles, etc.) accumulates over time, and inflammation, interruption/loss of neuronal function all also change with disease progression. In light of the repeated shortcomings of "fit-for-all" therapies, efforts may be better directed at targeted therapies (Cummings et al., 2014, 2020; Safieh et al., 2019). Faithfully modeling a complex, polygenic disease will be aided by the creation of platform strains that carry multiple genetic risk factors to motivate with a scientific rationale rather than a grant-focused one. Of the candidate risk variants identified, expression of the ε4 allele of *APOE* and the R47H mutation in *TREM2* were identified as the strongest candidates for the initial development of a novel LOAD mouse strain. Introduction of the R47H mutation into *Trem2* resulted in the creation of a novel murine splice site yielding a decrease in approximately 50% of TREM2 protein (**Supplementary Figures 8A,B**), and a 20% decrease in *Trem2* transcript (**Figure 6C**). In the absence of amyloid plaque insult, the effects on microglia response due to the mutation and decreased expression are difficult to decipher. Similar models have shown similar decreases in R47H-mediated *Trem2* expression

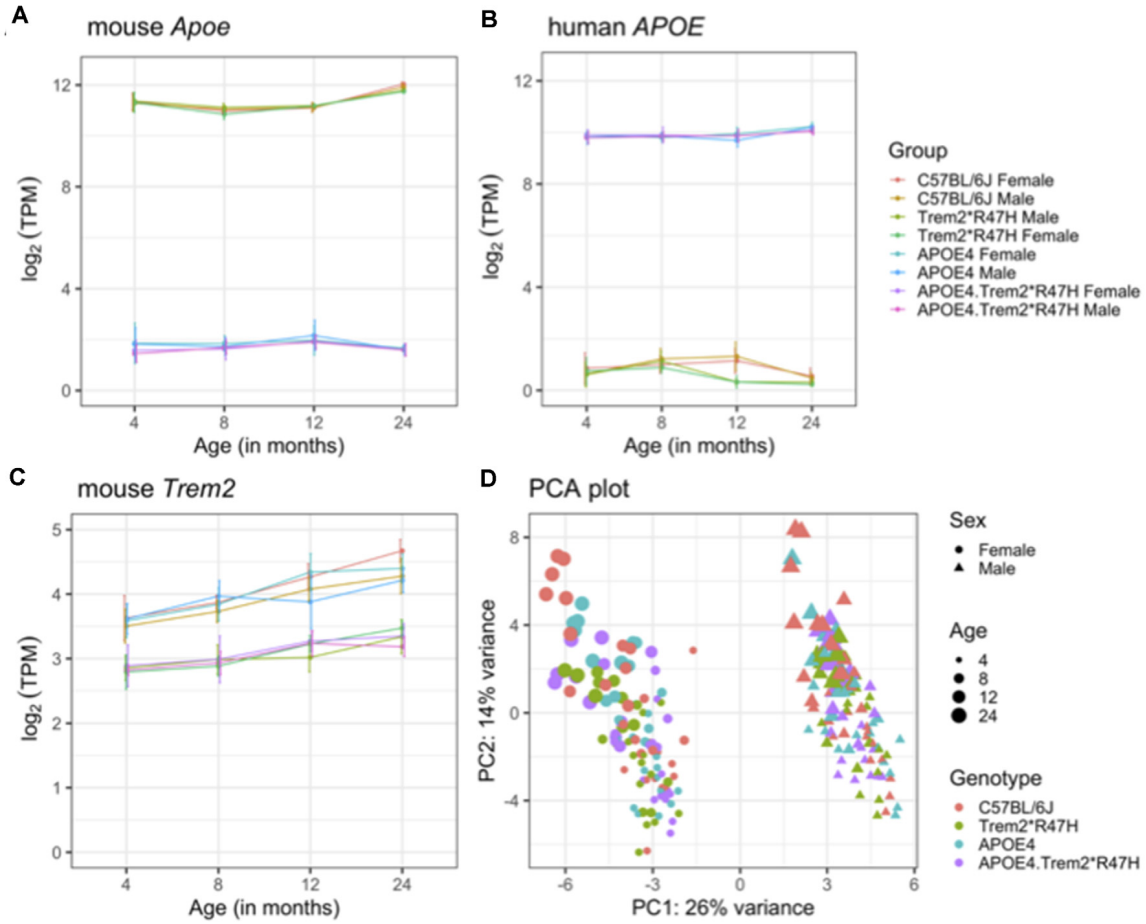

FIGURE 6 | Overview of brain transcriptome. Expression levels of mouse *Apoe* **(A)**, human *APOE* **(B)**, and mouse *Trem2* **(C)** genes in the B6.*APOE4*, B6.*Trem2***R47H*, B6.*APOE4.Trem2***R47H* and C57BL/6J mice at 4, 8, 12, and 24 months in both sexes. Principal component analysis (PCA) of RNA-Seq transcriptomics data from all 234 samples **(D)**. The percent of variation explained by each principal component is displayed on the corresponding axis. Female and male samples are represented as circles and triangles, respectively. Genotypes are shown by different colors and the increasing size of points correspond to the increasing age of mice (4, 8, 12, and 24 months respectively). All alleles expressed were homozygous.

and function (Cheng et al., 2018; Cheng-Hathaway et al., 2018; Xiang et al., 2018). Efforts are ongoing to develop a *Trem2* allele expressing the full-length R47H risk factor at levels similar to wild-type *Trem2*. *APOEε4* is strongly associated with disease development and severity (Bu, 2009; Yamazaki et al., 2019) and at least one allele is present in approximately 65% of AD patients (Mayeux et al., 1998). Unfortunately, endogenous *Apoe* in mice does not express the isoform diversity seen from the *APOE* allele in humans. Insertion of humanized *APOE* alleles into mouse genomes has been a successful strategy to dissect the biology of APOE isoforms in mice (Knouff et al., 1999; Esquerda-Canals et al., 2017; Balu et al., 2019; Safieh et al., 2019; Lewandowski et al., 2020). The MODEL-AD *APOEε3* and *APOEε4* allelic series on a C57BL/6J background has subsequently be shown to consistently reproduce the biology presented in other *APOE* mouse models and most importantly, human patients (Knouff et al., 1999; Foley et al., 2020). Therefore, *APOE4* formed the basis for multiple platform strains that include: B6.*APOE4.Trem2***R47H* (for which we have provided the identifier "LOAD1").

APOE binds to high-density lipoproteins to facilitate cholesterol and phospholipid transport to LDL receptors. As expected (Knouff et al., 1999; Maria Fe Lanfranco et al., 2020), lipoprotein levels differed compared to endogenous *Apoe*, mice expressing the humanized *APOEε4* allele showed decreased plasma lipoprotein levels across all time points (**Supplementary Table 2**). We observed an age-dependent decrease in glucose levels across both sexes and all genotypes (**Figure 1L**), an indication of increased frailty and aging that is common in aging-related-disease studies (Abdelhafiz et al., 2015). The contributions of metabolic and vascular factors are strongly implicated in disease progression, and how APOE or any other metabolic trait, *via* systemic pathways, can influence CNS function should be a continued focus for intervention (Zhao et al., 2020). The brain has one of the richest networks of

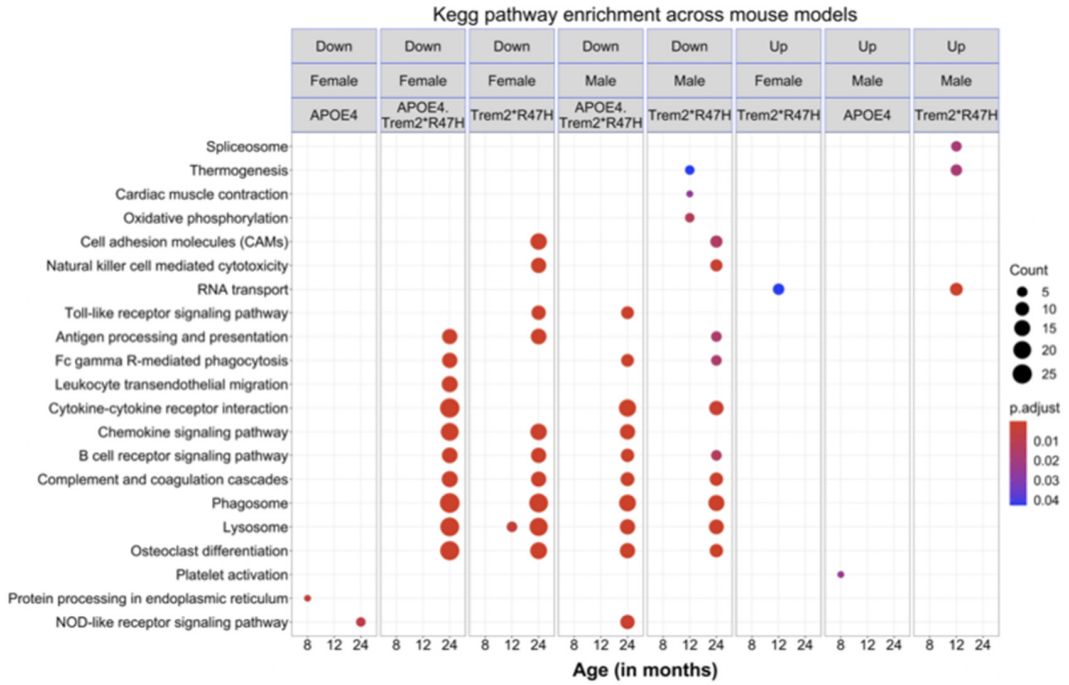

FIGURE 7 | KEGG pathways enrichment analysis. Significantly enriched KEGG pathways ($p < 0.05$) in the downregulated and upregulated list of genes across mouse models at different ages for both sexes. All alleles expressed were homozygous.

blood vessels and is especially vulnerable (block or reduce blood flow, oxygen, and nutrients). For example, the respective influence of *APOEε4*, with and without *Trem2*R47H* expression, in regional changes in brain glycolytic metabolism (Murray et al., 2014; **Figure 3**, **Supplementary Figure 6**), tissue perfusion (Thambisetty et al., 2010; Roher et al., 2012; **Figure 4**, **Supplementary Figure 7**) observed in human AD remain under further study. Additional analyses of this *APOE4* allele have also revealed changes in cholesterol metabolism and transcriptional signatures in the brain compared to carriers of the *APOE3* allele (Foley et al., 2020).

Despite the heterogeneity of AD, age is the strongest risk factor in the human population. As an aging disease, monitoring and evaluating mouse models in relation to age is crucial for understanding the onset and progression of the disease over time. We selected timepoints that reflected different life stages of an adult mouse: Mature, by 3–6 months (beyond development but not yet affected by senescence); Middle-aged, 10–14 months (some senescent changes detected in some, not all, biomarkers of aging); and Aged, 18–24 months (senescent markers can be observed in all animals; Fox et al., 2007). Non-invasive testing of motor activity, behavior, and cognition have been shown to be reliable phenotypes for staging disease onset and trajectory (Sukoff Rizzo et al., 2018; Bogue et al., 2020). Aged mice equally displayed the expected trial-dependent increases in consecutive rotarod trials and decrease in total distance traveled over time in the open field assay, regardless of genotype (**Supplementary Figure 3**). Animal activity, measured by total distance traveled during open field assays (**Figure 2**, **Supplementary Figure 2**), also decreased equally with age. Similarly, home cage wheel running assays, which provide a more comprehensive activity phenotype than the 1-h open field test, also showed a decrease in activity levels during the active (dark phase; Sukoff Rizzo et al., 2018; **Supplementary Figure 4**). Interestingly, at 24 months some indications of increased activity during the active phase in animals carrying the *APOEε4* allele (both B6.*APOE4* and B6J.*APOE4/Trem2*R47H*) and day-time activity in only B6.*Trem2*R47H* mice suggesting a dominant phenotype produced by expression of APOEε4 (**Supplementary Figures 4C,D, 10**). Further consideration of genotype influences in behavioral, biometric, and molecular testing by statistical analysis was restricted by breeding strategy. Only littermate animals are considered for statistical comparisons, preventing C57BL6/J and B6.*Trem2*R47H* animal genotypes from inclusion within timepoints.

In the absence of additional environmental or genetic risk factors, B6.*APOE4/Trem2*R47H* mice did not display penetrant behavioral phenotypes beyond the expected aging-related changes but did exhibit decreased survival probabilities by 24 months (**Supplementary Figure 5**). Very few C57BL/6J mice succumbed during the 24-month aging process (<5%), whereas mortality was higher in mice expressing both LOAD alleles in both males (∼20%) and females (∼35%). Male mice expressing either allele alone had survival probabilities similar to C57BL/6J, whereas females with *APOEε4* or *Trem2*R47H* showed a mortality rate of ∼20%. Therefore, it would seem that these two LOAD risk alleles show an equal and additive risk

when expressed together, but in females, their interaction appears synergistic.

We investigated the molecular signatures in the brain transcriptomes of LOAD mouse models at different ages in both sexes. We identified age-dependent molecular changes associated with LOAD pathologies in mouse models. Introduction of the R47H mutation revealed a novel *Trem2* isoform identical to the primary transcript, but truncated by 119 bp from its start position in exon 2 (see "Materials and Methods" section; Kotredes, 2020). Expression of this novel isoform resulted in a decrease in both transcript and protein compared to wild-type *Trem2* carriers (**Figure 6C**, **Supplementary Figures 8A,B**). Despite the decrease in *Trem2* expression, mouse models carrying R47H mutation in the *Trem2* gene did not exhibit any significant transcriptional changes at a young age, in contrast, APOE4 mice exhibited significant changes only at 8 months of age. We further identified significant downregulation of genes associated with oxidative phosphorylation pathway in the 12 months old B6.*Trem2*R47H* mice, suggesting that oxidative phosphorylation could be prominent early feature for the onset of neurodegeneration/inflammation process. Subsequently, multiple immune-related processes were disrupted in 24 months old B6.*Trem2*R47H* and B6.*APOE4.Trem2*R47H* mice, supporting the profound relationship between aging, *Trem2*, and AD. Interestingly, at 12 months of age, we did not observe any significant transcriptional changes in B6.*APOE4.Trem2*R47H* mice compared to control mice, suggesting that the effect of *Trem2* gene is suppressed due to the presence of *APOEε4*. Similarly, when mouse models were compared with human co-expression modules, we observed a strong negative correlation between the B6.*Trem2*R47H* mice and immune-related human co-expression modules from multiple brain regions and this inflammatory response is dampened in the presence of *APOEε4* in the B6.*APOE4.Trem2*R47H* mice. Distinct mouse models showed concordance with distinct human co-expression modules reflecting a different transcriptional response driven by the human *APOEε4* and *Trem2*R47H* risk variants. We also observed age-dependent shift in co-expression patterns associated with LOAD pathologies. A strong negative correlation between co-expression modules associated with cell cycle and DNA repair was observed in the early-aged mouse B6.*APOE4* model, whereas advanced-aged B6.*APOE4* female mice showed a strong positive correlation with these co-expression modules. This overlap with human late-onset co-expression signatures early in life was observed for a number of different brain regions and was absent in Trem2*R47H knock-in mice. Furthermore, aged B6.*Trem2*R47H* mice showed a moderate overlap with several human neuronal co-expression modules enriched for genes that play an important role in synaptic signaling and myelination. At an advanced age, a strong correlation between the mouse models and immune-related human co-expression modules highlights the important role of the LOAD-associated *APOEε4* and *TREM2* R47H variant in Alzheimer's related immune processes. Our experiments predict that *APOEε4* functions through the suppression of effects brought out by expression of the *Trem2*R47H* allele, displayed by the 455 genes that are upregulated by $TREM2^{R47H}$ but suppressed by *APOEε4* (**Supplementary Figure 10**). Our results mirror some emerging evidence that *APOEε4* suppresses *Trem2*R47H* in AD risk, that there are some suggestions that *APOEε4* carriers do not have increased AD risk with *Trem2*R47H* and *Trem2*R47H* only increases the risk on *APOEε3* carriers (Jendresen et al., 2017; Fitz et al., 2020). Additionally, we observe more differentially expressed genes at middle age than at a later age supporting evidence of an earlier aging phenotype than C57BL/6J mice, with a realignment of transcriptomes at later timepoints (McGeer et al., 1997; Zhao et al., 2020). We employed a weighted gene co-expression network analysis (WGCNA) used to identify modules of correlated genes. Each module was tested for differential expression by strain, then compared with human postmortem brain modules from the Accelerating Medicine's Partnership for AD (AMP-AD) to determine the LOAD-related processes affected by each genetic risk factor (Logsdon et al., 2019; Pandey et al., 2019; Wan et al., 2020). This will be a useful tool in identifying differentially expressed genes correlated with molecular pathways tied to inflammation and identifying a mouse strain that exhibits a similar transcriptional signature to human patients with true neuroinflammation.

Amyloid plaque formation is a primary diagnostic measure of Alzheimer's disease with both APOE and TREM2 linked to amyloid deposition (McGeer et al., 1997; Blennow et al., 2006; Bilkei-Gorzo, 2014; Kanekiyo et al., 2014; Jay et al., 2015; Cacace et al., 2016; Dourlen et al., 2019; Parhizkar et al., 2019). For example, TREM2 can bind amyloid, altering microglial function, linking the TREM2-APOE pathway directly to amyloid-driven disease progression (Zhao et al., 2018; Kober et al., 2020). Loss of functional *Trem2* in mice resulted in plaques that contained reduced amounts of APOE and promoted amyloidogenesis in mice by reducing microglial function (Parhizkar et al., 2019; McQuade et al., 2020) indicating that microglia, through TREM2 mediated signaling, can regulate APOE co-deposition around amyloid deposits. Further, TREM2 KO prevented infiltration of blood-derived myeloid cells and ameliorated plaque burden in *APP/PS1* mice (Jay et al., 2015) and disease-related mutations impair many of its functions (Kober et al., 2016). However, current amyloidogenic mouse models develop amyloid plaques at very young ages, within a few months (**Supplementary Figure 7B**), whereas in human patients the average age of AD onset is at older ages, ∼80 years, potentially causing the disparity in therapeutic outcomes between mouse models and human patients. In the absence of amyloid deposition, many hallmarks of LOAD can be investigated for *APOEε4*- and *Trem2*-influenced effects that precede and may contribute to the onset of AD. However, current work is evaluating the effects of APOE and TREM2 risk alleles in the context of humanized Abeta. For instance, we are currently evaluating a novel B6.*APOE4.Trem2*R47H.hAbeta* (LOAD2) strain and in the process of incorporating humanized Tau (MAPT) alleles into forthcoming strains. These novel platforms or AD-sensitized strains (e.g., LOAD1, LOAD2, etc.) are being used to assess the contribution of additional genetic risk factors identified through genetic and genome-wide association approaches using LOAD1 as a platform strain. These include variations in genes commonly associated with

AD including *ABCA7, PLCG2, CR1, BIN1*, and *SORL1*. The new strains are prioritized for extensive phenotyping using a primary screening approach centered on transcriptional profiling of nearly 800 genes known to be differentially expressed in human AD brains compared to unaffected controls (Preuss et al., 2020). Platform strains are also ideal for studying age-dependent effects of environmental risk factors, such as diet, as well as genetic context. Deeper analysis of *APOE4.Trem2*R47H* transcriptional data, *in vivo* imaging, and neuropathology samples are continuing and will be detailed in future publications. Amendments to the current phenotyping strategy are also in consideration to expand characterizations of the metabolome, proteome, and electrophysiology of LOAD animals. In subsequent studies utilizing new mouse strains, the utility of the APOE4.Trem2*R47H datasets will grow. Ultimately, strains carrying combinations of risk factors that more closely align with the human disease will be incorporated into the pre-clinical testing core of MODEL-AD to assess the potential of prioritized compounds to treat AD.

ARRIVE GUIDELINES STATEMENT

In accordance with ARRIVE (Animal Research: Reporting of *In Vivo* Experiments) guidelines, design and description of experimental animal cohorts are provided to ensure scientific rigor and reproducibility (Percie du Sert et al., 2020; https://arriveguidelines.org/).

DATA AVAILABILITY STATEMENT

The datasets presented in this study can be found in online repositories. The names of the repository/repositories and accession number(s) can be found in the article/**Supplementary Material**.

ETHICS STATEMENT

The animal study was reviewed and approved by Animal Care and Use Committee at The Jackson Laboratory and Indiana University in accordance with guidelines set out in The Eighth Edition of the Guide for the Care and Use of Laboratory Animals. All euthanasia used methods were approved by the American Veterinary Medical Association.

AUTHOR CONTRIBUTIONS

KK and RP: data curation, formal analysis, investigation, methodology, and writing. AO: conceptualization, data curation, formal analysis, investigation, methodology, and writing. PL: formal analysis and investigation. DG, BL, and LM: investigation and methodology. HW: data curation, formal analysis, investigation, and methodology. AU: data curation, formal analysis, and investigation. RO'R, SO'R, CI, DB, MB, ZC, and KF: Investigation. SS and PT: conceptualization, data curation, investigation, methodology, and writing. GC: conceptualization, data curation, methodology, and writing. MS and BL: conceptualization, methodology, and writing. GH: conceptualization, investigation, methodology, and writing.

FUNDING

This work was supported primarily by The Jackson Laboratory startup funds to GH, National Institute on Aging RF1AG055104 (GH) and National Institute on Aging U54AG054345 (MODEL-AD). The funders had no role in study design, data collection and analysis, decision to publish, or preparation of the manuscript.

ACKNOWLEDGMENTS

We would like to acknowledge the members of the Jackson Laboratory Center for Biometrics Analysis for their efforts toward the behavioral phenotyping of these animals, the Jackson Laboratory's Genetic Engineering Technologies Scientific Service for strain development, the Jackson Laboratory's Clinical Assessment Services for tissue and blood chemistry analysis, and the Jackson Laboratory's Genome Technologies group for RNA-sequencing and Nanostring assays.

SUPPLEMENTARY MATERIALS

The Supplementary Material for this article can be found online at: https://www.frontiersin.org/articles/10.3389/fnagi.2021.735524/full#supplementary-material.

REFERENCES

Abdelhafiz, A. H., Rodríguez-Manas, L., Morley, J. E., and Sinclair, A. J. (2015). Hypoglycemia in older people—a less well recognized risk factor for frailty. *Aging Dis.* 6, 156–167. doi: 10.14336/AD.2014.0330

Algin, O., and Ozmen, E. (2012). Heavily T2W 3D-SPACE images for evaluation of cerebrospinal fluid containing spaces. *Indian J. Radiol. Imaging* 22, 74–75. doi: 10.4103/0971-3026.95410

Allen, M., Carrasquillo, M. M., Funk, C., Heavner, B. D., Zou, F., Younkin, C. S., et al. (2016). Human whole genome genotype and transcriptome data for Alzheimer's and other neurodegenerative diseases. *Sci. Data* 3:160089. doi: 10.1038/sdata.2016.89

Alzheimer's Association (2020). 2020 Alzheimer's disease facts and figures. *Alzheimers Dement.* doi: 10.1002/alz.12068. [Epub ahead of print].

Anders, S., Pyl, P. T., and Huber, W. (2015). HTSeq—a Python framework to work with high-throughput sequencing data. *Bioinformatics* 31, 166–169. doi: 10.1093/bioinformatics/btu638

Andrews, S. J., Fulton-Howard, B., and Goate, A. (2020). Interpretation of risk loci from genome-wide association studies of Alzheimer's disease. *Lancet Neurol.* 19, 326–335. doi: 10.1016/S1474-4422(19)30435-1

Arnold, M., Nho, K., Kueider-Paisley, A., Massaro, T., Huynh, K., Brauner, B., et al. (2020). Sex and APOE epsilon4 genotype modify the Alzheimer's disease serum metabolome. *Nat. Commun.* 11:1148. doi: 10.1038/s41467-020-14959-w

Balu, D., Karstens, A. J., Loukenas, E., Maldonado Weng, J., York, J. M., Valencia-Olvera, A. C., et al. (2019). The role of APOE in transgenic mouse models of AD. *Neurosci. Lett.* 707:134285. doi: 10.1016/j.neulet.2019.134285

Bell, R. D., Winkler, E. A., Singh, I., Sagare, A. P., Deane, R., Wu, Z., et al. (2012). Apolipoprotein E controls cerebrovascular integrity *via* cyclophilin A. *Nature* 485, 512–516. doi: 10.1038/nature11087

Bellenguez, C., Grenier-Boley, B., and Lambert, J. C. (2020). Genetics of Alzheimer's disease: where we are and where we are going. *Curr. Opin. Neurobiol.* 61, 40–48. doi: 10.1016/j.conb.2019.11.024

Bien-Ly, N., Gillespie, A. K., Walker, D., Yoon, S. Y., and Huang, Y. (2012). Reducing human apolipoprotein E levels attenuates age-dependent Aβ accumulation in mutant human amyloid precursor protein transgenic mice. *J. Neurosci.* 32, 4803–4811. doi: 10.1523/JNEUROSCI.0033-12.2012

Bilkei-Gorzo, A. (2014). Genetic mouse models of brain ageing and Alzheimer's disease. *Pharmacol. Ther.* 142, 244–257. doi: 10.1016/j.pharmthera.2013.12.009

Blennow, K., de Leon, M. J., and Zetterberg, H. (2006). Alzheimer's disease. *Lancet* 368, 387–403. doi: 10.1016/S0140-6736(06)69113-7

Bogue, M. A., Philip, V. M., Walton, D. O., Grubb, S. C., Dunn, M. H., Kolishovski, G., et al. (2020). Mouse Phenome Database: a data repository and analysis suite for curated primary mouse phenotype data. *Nucleic Acids Res.* 48, D716–D723. doi: 10.1093/nar/gkz1032

Bolger, A. M., Lohse, M., and Usadel, B. (2014). Trimmomatic: a flexible trimmer for Illumina sequence data. *Bioinformatics* 30, 2114–2120. doi: 10.1093/bioinformatics/btu170

Bu, G. (2009). Apolipoprotein E and its receptors in Alzheimer's disease: pathways, pathogenesis and therapy. *Nat. Rev. Neurosci.* 10, 333–344. doi: 10.1038/nrn2620

Cacace, R., Sleegers, K., and Van Broeckhoven, C. (2016). Molecular genetics of early-onset alzheimer's disease revisited. *Alzheimers Dement.* 12, 733–748. doi: 10.1016/j.jalz.2016.01.012

Cheng, Q., Danao, J., Talreja, S., Wen, P., Yin, J., Sun, N., et al. (2018). TREM2-activating antibodies abrogate the negative pleiotropic effects of the Alzheimer's disease variant *Trem2*^{R47H} on murine myeloid cell function. *J. Biol. Chem.* 293, 12620–12633. doi: 10.1074/jbc.RA118.001848

Cheng-Hathaway, P. J., Reed-Geaghan, E. G., Jay, T. R., Casali, B. T., Bemiller, S. M., Puntambekar, S. S., et al. (2018). The Trem2 R47H variant confers loss-of-function-like phenotypes in Alzheimer's disease. *Mol. Neurodegener.* 13:29. doi: 10.1186/s13024-018-0262-8

Chung, W.-S., Verghese, P. B., Chakraborty, C., Joung, J., Hyman, B. T., Ulrich, J. D., et al. (2016). Novel allele-dependent role for APOE in controlling the rate of synapse pruning by astrocytes. *Proc. Natl. Acad. Sci. U S A* 113, 10186–10191. doi: 10.1073/pnas.1609896113

Cummings, J., Lee, G., Ritter, A., Sabbagh, M., and Zhong, K. (2020). Alzheimer's disease drug development pipeline: 2020. *Alzheimers Dement.* 6:e12050. doi: 10.1002/trc2.12050

Cummings, J. L., Morstorf, T., and Zhong, K. (2014). Alzheimer's disease drug-development pipeline: few candidates, frequent failures. *Alzheimers Res. Ther.* 6:37. doi: 10.1186/alzrt269

Dandekar, M., Tseng, J. R., and Gambhir, S. S. (2007). Reproducibility of 18F-FDG microPET studies in mouse tumor xenografts. *J. Nucl. Med.* 48, 602–607. doi: 10.2967/jnumed.106.036608

De Jager, P. L., Ma, Y., McCabe, C., Xu, J., Vardarajan, B. N., Felsky, D., et al. (2018). A multi-omic atlas of the human frontal cortex for aging and Alzheimer's disease research. *Sci. Data* 5:180142. doi: 10.1038/sdata.2018.142

de Rezende, L. F., Rodrigues Lopes, M., Rey-López, J. P., Matsudo, V. K., and Luiz, O. (2014). Sedentary behavior and health outcomes: an overview of systematic reviews. *PLoS One* 9:e105620. doi: 10.1371/journal.pone.0105620

Dobin, A., Davis, C. A., Schlesinger, F., Drenkow, J., Zaleski, C., Jha, S., et al. (2013). STAR: ultrafast universal RNA-seq aligner. *Bioinformatics* 29, 15–21. doi: 10.1093/bioinformatics/bts635

Dourlen, P., Kilinc, D., Malmanche, N., Chapuis, J., and Lambert, J. C. (2019). The new genetic landscape of Alzheimer's disease: from amyloid cascade to genetically driven synaptic failure hypothesis? *Acta Neuropathol.* 138, 221–236. doi: 10.1007/s00401-019-02004-0

Esquerda-Canals, G., Montoliu-Gaya, L., Guell-Bosch, J., and Villegas, S. (2017). Mouse models of Alzheimer's disease. *J. Alzheimers Dis.* 57, 1171–1183. doi: 10.3233/JAD-170045

Fenesi, B., Fang, H., Kovacevic, A., Oremus, M., Raina, P., and Heisz, J. J. (2017). Physical exercise moderates the relationship of apolipoprotein E (APOE) genotype and dementia risk: a population-based study. *J. Alzheimers Dis.* 56, 297–303. doi: 10.3233/JAD-160424

Fitz, N. F., Wolfe, C. M., Playso, B. E., Biedrzycki, R. J., Lu, Y., Nam, K. N., et al. (2020). Trem2 deficiency differentially affects phenotype and transcriptome of human APOE3 and APOE4 mice. *Mol. Neurodegener.* 15:41. doi: 10.1186/s13024-020-00394-4

Foley, K. E., Garceau, D. T., Kotredes, K. P., Carter, G. W., Sasner, M., and Howell, G. R. (2020). APOEε3/ε4 and APOEε4/ε4 genotypes drive unique gene signatures in the cortex of young mice. *bioRxiv* [Preprint]. doi: 10.1101/2020.10.28.359422

Fox, J. G., Barthold, S. W., Davisson, M. T., Newcomer, C. E., Quimby, F. W., and Smith, A. L. (2007). " Spontaneous diseases in commonly used mouse strains," in *The Mouse in Biomedical Research (Second Edition)*, eds J. G. Fox, M. T. Davisson, F. W. Quimby, S. W. Barthold, C. E. Newcomer and A. L. Smith (Burlington: Academic Press), xv–xvi.

Franklin, K. B. J., and Paxinos, G. (2013). *Paxinos and Franklin's The Mouse Brain in Stereotaxic Coordinates.* Amsterdam: Academic Press, an imprint of Elsevier.

Frese, T., Rouze, N. C., Bouman, C. A., Sauer, K., and Hutchins, G. D. (2003). Quantitative comparison of FBP, EM and Bayesian reconstruction algorithms for the IndyPET scanner. *IEEE Trans. Med. Imaging* 22, 258–276. doi: 10.1109/TMI.2002.808353

Green, M. A. (1987). A potential copper radiopharmaceutical for imaging the heart and brain: copper-labeled pyruvaldehyde bis(N4-methylthiosemicarbazone). *Int. J. Rad. Appl. Instrum. B* 14, 59–61. doi: 10.1016/0883-2897(87)90162-0

Huber, G., März, W., Martin, J. R., Malherbe, P., Richards, J. G., Sueoka, N., et al. (2000). Characterization of transgenic mice expressing apolipoprotein E4(C112R) and apolipoprotein E4(L28P; C112R). *Neuroscience* 101, 211–218. doi: 10.1016/s0306-4522(00)00341-9

Jay, T. R., Miller, C. M., Cheng, P. J., Graham, L. C., Bemiller, S., Broihier, M. L., et al. (2015). TREM2 deficiency eliminates TREM2+ inflammatory macrophages and ameliorates pathology in Alzheimer's disease mouse models. *J. Exp. Med.* 212, 287–295. doi: 10.1084/jem.20142322

Jendresen, C., Årskog, V., Daws, M. R., and Nilsson, L. N. (2017). The Alzheimer's disease risk factors apolipoprotein E and TREM2 are linked in a receptor signaling pathway. *J Neuroinflammation* 14:59. doi: 10.1186/s12974-017-0835-4

Jeong, W., Lee, H., Cho, S., and Seo, J. (2019). ApoE4-induced cholesterol dysregulation and its brain cell type-specific implications in the pathogenesis of Alzheimer's disease. *Mol. Cells* 42, 739–746. doi: 10.14348/molcells.2019.0200

Kanekiyo, T., Xu, H., and Bu, G. (2014). ApoE and Aβ in Alzheimer's disease: accidental encounters or partners? *Neuron* 81, 740–754. doi: 10.1016/j.neuron.2014.01.045

Karch, C. M., and Goate, A. M. (2015). Alzheimer's disease risk genes and mechanisms of disease pathogenesis. *Biol. Psychiatry* 77, 43–51. doi: 10.1016/j.biopsych.2014.05.006

Keren-Shaul, H., Spinrad, A., Weiner, A., Matcovitch-Natan, O., Dvir-Szternfeld, R., Ulland, T. K., et al. (2017). A unique microglia type associated with restricting development of Alzheimer's disease. *Cell* 169, 1276–1290.e7. doi: 10.1016/j.cell.2017.05.018

Kleinberger, G., Brendel, M., Mracsko, E., Wefers, B., Groeneweg, L., Xiang, X., et al. (2017). The FTD-like syndrome causing TREM2 T66M mutation impairs microglia function, brain perfusion, and glucose metabolism. *EMBO J.* 36, 1837–1853. doi: 10.15252/embj.201796516

Knouff, C., Hinsdale, M. E., Mezdour, H., Altenburg, M. K., Watanabe, M., Quarfordt, S. H., et al. (1999). Apo E structure determines VLDL clearance and atherosclerosis risk in mice. *J. Clin. Invest.* 103, 1579–1586. doi: 10.1172/JCI6172

Kober, D. L., Alexander-Brett, J. M., Karch, C. M., Cruchaga, C., Colonna, M., Holtzman, M. J., et al. (2016). Neurodegenerative disease mutations in TREM2 reveal a functional surface and distinct loss-of-function mechanisms. *eLife* 5:e20391. doi: 10.7554/eLife.20391

Kober, D. L., Stuchell-Brereton, M. D., Kluender, C. E., Dean, H. B., Strickland, M. R., Steinberg, D. F., et al. (2020). Functional insights from biophysical study of TREM2 interactions with apoE and Aβ1–42. *Alzheimers Dement.* doi: 10.1002/alz.12194. [Epub ahead of print].

Kotredes, K. (2020). *Data Resource for Manuscript—A Multi-Discipline Phenotyping Platform for Late-Onset Alzheimer's Disease Employed*

*on A Novel, Humanized APOEe4Trem2*R47H Mouse Model [Internet]* [Online]. Synapse. Available online at: https://repo-prod.prod.sagebase.org/repo/v1/doi/locate?id=syn23631984&type=ENTITY.

Krasemann, S., Madore, C., Cialic, R., Baufeld, C., Calcagno, N., El Fatimy, R., et al. (2017). The TREM2-APOE pathway drives the transcriptional phenotype of dysfunctional microglia in neurodegenerative diseases. *Immunity* 47, 566–581.e9. doi: 10.1016/j.immuni.2017.08.008

Krishnamoorthy, S., Blankemeyer, E., Mollet, P., Surti, S., Van Holen, R., and Karp, J. S. (2018). Performance evaluation of the MOLECUBES β-CUBE-a high spatial resolution and high sensitivity small animal PET scanner utilizing monolithic LYSO scintillation detectors. *Phys. Med. Biol.* 63:155013. doi: 10.1088/1361-6560/aacec3

Laskowitz, D. T., Lee, D. M., Schmechel, D., and Staats, H. F. (2000). Altered immune responses in apolipoprotein E-deficient mice. *J. Lipid Res.* 41, 613–620. doi: 10.1016/s0022-2275(20)32409-3

Lesuisse, C., Xu, G., Anderson, J., Wong, M., Jankowsky, J., Holtz, G., et al. (2001). Hyper-expression of human apolipoprotein E4 in astroglia and neurons does not enhance amyloid deposition in transgenic mice. *Hum. Mol. Genet.* 10, 2525–2537. doi: 10.1093/hmg/10.22.2525

Lewandowski, C. T., Maldonado Weng, J., and LaDu, M. J. (2020). Alzheimer's disease pathology in APOE transgenic mouse models: the Who, What, When, Where, Why, and How. *Neurobiol. Dis.* 139:104811. doi: 10.1016/j.nbd.2020.104811

Li, B., and Dewey, C. N. (2011). RSEM: accurate transcript quantification from RNA-Seq data with or without a reference genome. *BMC Bioinformatics* 12:323. doi: 10.1016/j.lungcan.2021.08.003

Logsdon, B., Perumal, T. M., Swarup, V., Wang, M., Funk, C., Gaiteri, C., et al. (2019). Meta-analysis of the human brain transcriptome identifies heterogeneity across human AD coexpression modules robust to sample collection and methodological approach. *bioRxiv* [Preprint]. doi: 10.3390/ijms21010207

Love, M. I., Huber, W., and Anders, S. (2014). Moderated estimation of fold change and dispersion for RNA-seq data with DESeq2. *Genome Biol.* 15:550. doi: 10.1186/s13059-014-0550-8

Ma, J., Jiang, T., Tan, L., and Yu, J.-T. (2015). TYROBP in Alzheimer's disease. *Mol. Neurobiol.* 51, 820–826. doi: 10.1007/s12035-014-8811-9

Maezawa, I., Maeda, N., Montine, T. J., and Montine, K. S. (2006a). Apolipoprotein E-specific innate immune response in astrocytes from targeted replacement mice. *J. Neuroinflammation* 3:10. doi: 10.1186/1742-2094-3-10

Maezawa, I., Nivison, M., Montine, K. S., Maeda, N., and Montine, T. J. (2006b). Neurotoxicity from innate immune response is greatest with targeted replacement of E4 allele of apolipoprotein E gene and is mediated by microglial p38MAPK. *FASEB J.* 20, 797–799. doi: 10.1096/fj.05-5423fje

Maezawa, I., Zaja-Milatovic, S., Milatovic, D., Stephen, C., Sokal, I., Maeda, N., et al. (2006c). Apolipoprotein E isoform-dependent dendritic recovery of hippocampal neurons following activation of innate immunity. *J. Neuroinflammation* 3:21. doi: 10.1186/1742-2094-3-21

Maria Fe Lanfranco, M., Anne Ng, C., and William Rebeck, G. (2020). ApoE lipidation as a therapeutic target in Alzheimer's disease. *Int. J. Mol. Sci.* 21:6336. doi: 10.3390/ijms21176336

Mathias, C. J., Welch, M. J., Green, M. A., Diril, H., Meares, C. F., Gropler, R. J., et al. (1991a). *in vivo* comparison of copper blood-pool agents: potential radiopharmaceuticals for use with copper-62. *J. Nucl. Med.* 32, 475–480.

Mathias, C. J., Welch, M. J., Perry, D. J., Mcguire, A. H., Zhu, X., Connett, J. M., et al. (1991b). Investigation of copper-ptsm as a pet tracer for tumor blood-flow. *Int. J. Rad. Appl. Instrum. B* 18, 807–811. doi: 10.1016/0883-2897(91)90022-d

Mathias, C. J., Welch, M. J., Raichle, M. E., Mintun, M. A., Lich, L. L., McGuire, A. H., et al. (1990). Evaluation of a potential generator-produced PET tracer for cerebral perfusion imaging: single-pass cerebral extraction measurements and imaging with radiolabeled Cu-PTSM. *J. Nucl. Med.* 31, 351–359.

Mayeux, R., Saunders, A. M., Shea, S., Mirra, S., Evans, D., Roses, A. D., et al. (1998). Utility of the apolipoprotein E genotype in the diagnosis of Alzheimer's disease. Alzheimer's disease centers consortium on apolipoprotein E and Alzheimer's disease. *N. Engl. J. Med.* 338, 506–511. doi: 10.1056/NEJM199802193380804

Mazaheri, F., Snaidero, N., Kleinberger, G., Madore, C., Daria, A., Werner, G., et al. (2017). TREM2 deficiency impairs chemotaxis and microglial responses to neuronal injury. *EMBO Rep.* 18, 1186–1198. doi: 10.15252/embr.201743922

McGeer, P. L., Walker, D. G., Pitas, R. E., Mahley, R. W., and McGeer, E. G. (1997). Apolipoprotein E4 (ApoE4) but not ApoE3 or ApoE2 potentiates β-amyloid protein activation of complement *in vitro*. *Brain Res.* 749, 135–138. doi: 10.1016/s0006-8993(96)01324-8

McQuade, A., Kang, Y. J., Hasselmann, J., Jairaman, A., Sotelo, A., Coburn, M., et al. (2020). Gene expression and functional deficits underlie TREM2-knockout microglia responses in human models of Alzheimer's disease. *Nat. Commun.* 11:5370. doi: 10.1038/s41467-020-19227-5

Methia, N., Andre, P., Hafezi-Moghadam, A., Economopoulos, M., Thomas, K. L., and Wagner, D. D. (2001). ApoE deficiency compromises the blood brain barrier especially after injury. *Mol. Med.* 7, 810–815. doi: 10.1007/BF03401973

Murray, J., Tsui, W. H., Li, Y., McHugh, P., Williams, S., Cummings, M., et al. (2014). FDG and amyloid PET in cognitively normal individuals at risk for late-onset Alzheimer's disease. *Adv. J. Mol. Imaging* 4, 15–26. doi: 10.4236/ami.2014.42003

Oblak, A. L., Forner, S., Territo, P. R., Sasner, M., Carter, G. W., Howell, G. R., et al. (2020). Model organism development and evaluation for late-onset Alzheimer's disease: MODEL-AD. *Alzheimers Dement.* 6:e12110. doi: 10.1002/trc2.12110

Painter, M. M., Atagi, Y., Liu, C. C., Rademakers, R., Xu, H., Fryer, J. D., et al. (2015). TREM2 in CNS homeostasis and neurodegenerative disease. *Mol. Neurodegener.* 10:43. doi: 10.1186/s13024-015-0040-9

Pandey, R. S., Graham, L., Uyar, A., Preuss, C., Howell, G. R., and Carter, G. W. (2019). Genetic perturbations of disease risk genes in mice capture transcriptomic signatures of late-onset Alzheimer's disease. *Mol. Neurodegener.* 14:50. doi: 10.1186/s13024-019-0351-3

Parhizkar, S., Arzberger, T., Brendel, M., Kleinberger, G., Deussing, M., Focke, C., et al. (2019). Loss of TREM2 function increases amyloid seeding but reduces plaque-associated ApoE. *Nat. Neurosci.* 22, 191–204. doi: 10.1038/s41593-018-0296-9

Paxinos, G., and Franklin, K. (2012). *Paxinos and Franklin's The Mouse Brain in Stereotaxic Coordinates.* New York, NY: Academic Press.

Percie du Sert, N., Hurst, V., Ahluwalia, A., Alam, S., Avey, M. T., Baker, M., et al. (2020). The ARRIVE guidelines 2.0: updated guidelines for reporting animal research. *PLoS Biol.* 18:e3000410. doi: 10.1371/journal.pbio.3000410

Preuss, C., Pandey, R., Piazza, E., Fine, A., Uyar, A., Perumal, T., et al. (2020). A novel systems biology approach to evaluate mouse models of late-onset Alzheimer's disease. *Mol. Neurodegener.* 15:67. doi: 10.1186/s13024-020-00412-5

Raber, J., Wong, D., Buttini, M., Orth, M., Bellosta, S., Pitas, R. E., et al. (1998). Isoform-specific effects of human apolipoprotein E on brain function revealed in ApoE knockout mice: increased susceptibility of females. *Proc. Natl. Acad. Sci. U S A* 95, 10914–10919. doi: 10.1073/pnas.95.18.10914

Ritchie, M. E., Phipson, B., Wu, D., Hu, Y., Law, C. W., Shi, W., et al. (2015). limma powers differential expression analyses for RNA-sequencing and microarray studies. *Nucleic Acids Res.* 43:e47. doi: 10.1093/nar/gkv007

Roher, A. E., Debbins, J. P., Malek-Ahmadi, M., Chen, K., Pipe, J. G., Maze, S., et al. (2012). Cerebral blood flow in Alzheimer's disease. *Vasc. Health Risk Manag.* 8, 599–611. doi: 10.2147/VHRM.S34874

Safieh, M., Korczyn, A. D., and Michaelson, D. M. (2019). ApoE4: an emerging therapeutic target for Alzheimer's disease. *BMC Med.* 17:64. doi: 10.1186/s12916-019-1299-4

Sasaguri, H., Nilsson, P., Hashimoto, S., Nagata, K., Saito, T., De Strooper, B., et al. (2017). APP mouse models for Alzheimer's disease preclinical studies. *EMBO J.* 36, 2473–2487. doi: 10.15252/embj.201797397

Saunders, A. M., Strittmatter, W. J., Schmechel, D., George-Hyslop, P. H., Pericak-Vance, M. A., Joo, S. H., et al. (1993). Association of apolipoprotein E allele epsilon 4 with late-onset familial and sporadic Alzheimer's disease. *Neurology* 43, 1467–1472. doi: 10.1212/wnl.43.8.1467

Shi, Y., Yamada, K., Liddelow, S. A., Smith, S. T., Zhao, L., Luo, W., et al. (2017). ApoE4 markedly exacerbates tau-mediated neurodegeneration in a mouse model of tauopathy. *Nature* 549, 523–527. doi: 10.1038/nature24016

Sokoloff, L. (1977). Relation between physiological function and energy metabolism in the central nervous system. *J. Neurochem.* 29, 13–26. doi: 10.1111/j.1471-4159.1977.tb03919.x

Soon, K. H., Farouque, H. M., Chaitowitz, I., Cox, N., Selvanayagam, J. B., Zakhem, B., et al. (2007). Discrepancy between computed tomography coronary angiography and selective coronary angiography in the pre-stenting assessment of coronary lesion length. *Australas. Radiol.* 51, 440–445. doi: 10.1111/j.1440-1673.2007.01868.x

Strittmatter, W. J., Saunders, A. M., Schmechel, D., Pericak-Vance, M., Enghild, J., Salvesen, G. S., et al. (1993). Apolipoprotein E: high-avidity binding to β-amyloid and increased frequency of type 4 allele in late-onset familial Alzheimer disease. *Proc. Natl. Acad. Sci. U S A* 90, 1977–1981. doi: 10.1073/pnas.90.5.1977

Studholme, C., Hawkes, D. J., and Hill, D. L. G. (1998). A normalized entropy measure for multimodality image alignment. *Proc. SPIE Med. Imaging* 3338, 132–143. doi: 10.1117/12.310835

Studholme, C., Hill, D. L., and Hawkes, D. J. (1997). Automated three-dimensional registration of magnetic resonance and positron emission tomography brain images by multiresolution optimization of voxel similarity measures. *Med. Phys.* 24, 25–35. doi: 10.1118/1.598130

Sukoff Rizzo, S. J., Anderson, L. C., Green, T. L., McGarr, T., Wells, G., and Winter, S. S. (2018). Assessing healthspan and lifespan measures in aging mice: optimization of testing protocols, replicability, and rater reliability. *Curr. Protoc. Mouse Biol.* 8:e45. doi: 10.1002/cpmo.45

Sun, Y., Wu, S., Bu, G., Onifade, M. K., Patel, S. N., LaDu, M. J., et al. (1998). Glial fibrillary acidic protein-apolipoprotein E (apoE) transgenic mice: astrocyte-specific expression and differing biological effects of astrocyte-secreted apoE3 and apoE4 lipoproteins. *J. Neurosci.* 18, 3261–3272. doi: 10.1523/JNEUROSCI.18-09-03261.1998

Territo, P. R., Meyer, J. A., Peters, J. S., Riley, A. A., McCarthy, B. P., Gao, M., et al. (2017). Characterization of (11)C-GSK1482160 for targeting the P2X7 receptor as a biomarker for neuroinflammation. *J. Nucl. Med.* 58, 458–465. doi: 10.2967/jnumed.116.181354

Tesseur, I., Van Dorpe, J., Spittaels, K., Van den Haute, C., Moechars, D., and Van Leuven, F. (2000). Expression of human apolipoprotein E4 in neurons causes hyperphosphorylation of protein tau in the brains of transgenic mice. *Am. J. Pathol.* 156, 951–964. doi: 10.1016/S0002-9440(10)64963-2

Thambisetty, M., Beason-Held, L., An, Y., Kraut, M. A., and Resnick, S. M. (2010). APOE epsilon4 genotype and longitudinal changes in cerebral blood flow in normal aging. *Arch. Neurol.* 67, 93–98. doi: 10.1001/archneurol.2009.913

U.S. Department of Health and Human Services. (2021). *NIA and the National Plan to Address Alzheimer's Disease.* [Online]. USA.gov. Available online at: https://www.nia.nih.gov/about/nia-and-national-plan-address-alzheimers-disease. Accessed 2021.

U.S. Food and Drug Administration. (2021). *FDA Grants Accelerated Approval for Alzheimer's Drug. 6/7/2021 ed.*

Verghese, P. B., Castellano, J. M., Garai, K., Wang, Y., Jiang, H., Shah, A., et al. (2013). ApoE influences amyloid-β (Aβ) clearance despite minimal apoE/Aβ association in physiological conditions. *Proc. Natl. Acad. Sci. U S A* 110, E1807–E1816. doi: 10.1073/pnas.1220484110

Wan, Y.-W., Al-Ouran, R., Mangleburg, C. G., Perumal, T. M., Lee, T. V., Allison, K., et al. (2020). Meta-analysis of the Alzheimer's disease human brain transcriptome and functional dissection in mouse models. *Cell Rep.* 32:107908. doi: 10.1016/j.celrep.2020.107908

Wang, M., Beckmann, N. D., Roussos, P., Wang, E., Zhou, X., Wang, Q., et al. (2018). The Mount Sinai cohort of large-scale genomic, transcriptomic and proteomic data in Alzheimer's disease. *Sci. Data* 5:180185. doi: 10.1038/sdata.2018.185

Wang, Y., Cella, M., Mallinson, K., Ulrich, J. D., Young, K. L., Robinette, M. L., et al. (2015). TREM2 lipid sensing sustains the microglial response in an Alzheimer's disease model. *Cell* 160, 1061–1071. doi: 10.1016/j.cell.2015.01.049

Wang, C., Wilson, W. A., Moore, S. D., Mace, B. E., Maeda, N., Schmechel, D. E., et al. (2005). Human apoE4-targeted replacement mice display synaptic deficits in the absence of neuropathology. *Neurobiol. Dis.* 18, 390–398. doi: 10.1016/j.nbd.2004.10.013

Xiang, X., Piers, T. M., Wefers, B., Zhu, K., Mallach, A., Brunner, B., et al. (2018). The Trem2 R47H Alzheimer's risk variant impairs splicing and reduces Trem2 mRNA and protein in mice but not in humans. *Mol. Neurodegener.* 13:49. doi: 10.1186/s13024-018-0280-6

Xu, P. T., Schmechel, D., Rothrock-Christian, T., Burkhart, D. S., Qiu, H. L., Popko, B., et al. (1996). Human apolipoprotein E2, E3, and E4 isoform-specific transgenic mice: human-like pattern of glial and neuronal immunoreactivity in central nervous system not observed in wild-type mice. *Neurobiol. Dis.* 3, 229–245. doi: 10.1006/nbdi.1996.0023

Yamazaki, Y., Painter, M. M., Bu, G., and Kanekiyo, T. (2016). Apolipoprotein E as a therapeutic target in Alzheimer's disease: a review of basic research and clinical evidence. *CNS Drugs* 30, 773–789. doi: 10.1007/s40263-016-0361-4

Yamazaki, Y., Zhao, N., Caulfield, T. R., Liu, C. C., and Bu, G. (2019). Apolipoprotein E and Alzheimer disease: pathobiology and targeting strategies. *Nat. Rev. Neurol.* 15, 501–518. doi: 10.1038/s41582-019-0228-7

Yan, S., Fu, W., Wang, C., Mao, J., Liu, B., Zou, L., et al. (2020). Association between sedentary behavior and the risk of dementia: a systematic review and meta-analysis. *Transl. Psychiatry* 10:12. doi: 10.1038/s41398-020-0799-5

Yu, G., Wang, L.-G., Han, Y., and He, Q.-Y. (2012). clusterProfiler: an R package for comparing biological themes among gene clusters. *OMICS* 16, 284–287. doi: 10.1089/omi.2011.0118

Yu, C.-H., Wang, T., Sun, Y.-E., Yao, S. L., Tian, J.-H., and Yin, D.-Y. (2006). [Fluorine-18 fluorodeoxyglucose uptake in patients with benign pulmonary nodules]. *Zhonghua Wai Ke Za Zhi* 44, 90–92.

Yuan, P., Condello, C., Keene, C. D., Wang, Y., Bird, T. D., Paul, S. M., et al. (2016). TREM2 haplodeficiency in mice and humans impairs the microglia barrier function leading to decreased amyloid compaction and severe axonal dystrophy. *Neuron* 90, 724–739. doi: 10.1016/j.neuron.2016.05.003

Zhao, N., Ren, Y., Yamazaki, Y., Qiao, W., Li, F., Felton, L. M., et al. (2020). Alzheimer's risk factors age, APOE genotype, and sex drive distinct molecular pathways. *Neuron* 106, 727–742.e6. doi: 10.1016/j.neuron.2020.02.034

Zhao, Y., Wu, X., Li, X., Jiang, L. L., Gui, X., Liu, Y., et al. (2018). TREM2 is a receptor for β-amyloid that mediates microglial function. *Neuron* 97, 1023–1031.e7. doi: 10.1016/j.neuron.2018.01.031

Conflict of Interest: The authors declare that the research was conducted in the absence of any commercial or financial relationships that could be construed as a potential conflict of interest.

Publisher's Note: All claims expressed in this article are solely those of the authors and do not necessarily represent those of their affiliated organizations, or those of the publisher, the editors and the reviewers. Any product that may be evaluated in this article, or claim that may be made by its manufacturer, is not guaranteed or endorsed by the publisher.

frontiers in Aging Neuroscience

REVIEW
published: 29 October 2021
doi: 10.3389/fnagi.2021.730107

Tubulin and Tubulin Posttranslational Modifications in Alzheimer's Disease and Vascular Dementia

*Estibaliz Santiago-Mujika[1], Ruth Luthi-Carter[1], Flaviano Giorgini[2], Raj N. Kalaria[3] and Elizabeta B. Mukaetova-Ladinska[1,4]**

[1] Department of Neuroscience, Behavior and Psychology, University of Leicester, Leicester, United Kingdom, [2] Department of Genetics and Genome Biology, University of Leicester, Leicester, United Kingdom, [3] Translational and Clinical Research Institute, Newcastle University, Newcastle upon Tyne, United Kingdom, [4] Evington Centre, Leicester General Hospital, Leicester, United Kingdom

Alzheimer's disease (AD) and vascular dementia (VaD) are the two most common forms of dementia in older people. Although these two dementia types differ in their etiology, they share many pathophysiological and morphological features, including neuronal loss, which is associated with the microtubule (MT) destabilization. Stabilization of MTs is achieved in different ways: through interactions with MT binding proteins (MTBP) or by posttranslational modifications (PTMs) of tubulin. Polyglutamylation and tyrosination are two foremost PTMs that regulate the interaction between MTs and MTBPs, and play, therefore, a role in neurodegeneration. In this review, we summarize key information on tubulin PTMs in relation to AD and VaD and address the importance of studying further the tubulin code to reveal sites of potential intervention in development of novel and effective dementia therapy.

Keywords: vascular dementia, Alzheimer's disease, tubulin, posttranslational modification, tubulin code

OPEN ACCESS

Edited by:
Natalia Salvadores, Universidad Mayor, Chile

Reviewed by:
Cathryn Louise Haigh, Rocky Mountain Laboratories (NIAID), United States
Roland Brandt, University of Osnabrück, Germany

***Correspondence:**
Elizabeta B. Mukaetova-Ladinska
eml12@le.ac.uk

Received: *24 June 2021*
Accepted: *04 October 2021*
Published: *29 October 2021*

Citation:
Santiago-Mujika E, Luthi-Carter R, Giorgini F, Kalaria RN and Mukaetova-Ladinska EB (2021) Tubulin and Tubulin Posttranslational Modifications in Alzheimer's Disease and Vascular Dementia. Front. Aging Neurosci. 13:730107. doi: 10.3389/fnagi.2021.730107

ALZHEIMER'S DISEASE AND VASCULAR DEMENTIA

Alzheimer's disease (AD) and vascular dementia (VaD) are two of the most common types of dementia, representing ∼85% of all dementia cases (Qiu et al., 2009; Iadecola, 2013). In some cases, patients show mixed dementia, where they combine features of AD with ischemic lesions (Iadecola, 2013). Although they have been thoroughly studied, there is no effective treatment to halt or reverse these diseases.

AD is the most common form of dementia and it accounts for more than 70% of all clinically diagnosed dementias (Qiu et al., 2009). Although memory is the main impaired feature, language difficulties, emotional and behavioral changes are also present (Steinberg et al., 2008). The neuropathological hallmarks are amyloid plaques and neurofibrillary tangles (NFTs) (Šimić et al., 2016). Additional neuropathological AD features include dystrophic neurites, astrogliosis, neuronal loss, and cortical atrophy (McKhann et al., 2011; Serrano-Pozo et al., 2011).

Amyloid plaques are extracellular aggregates of insoluble 40 and 42 amyloid-β (Aβ) peptide, that although present in healthy people, are significantly increased in AD patients. On the other hand, NFTs are intraneuronal aggregates of hyperphosphorylated and/or truncated and misfolded tau. Contrary to amyloid plaques, there is a correlation between the burden of NFTs and disease progression, as well as AD clinical symptoms (Giannakopoulos et al., 2009; Suemoto et al., 2017).

VaD is the second most common form of dementia, accounting for ∼15% of all cases. In spite of the number of patients diagnosed and the annual costs for this syndrome being highly significant, VaD has not been as thoroughly studied as AD (Iadecola, 2013).

There are four types of VaD: post-stroke dementia, subcortical ischemic vascular dementia, multi-infarct dementia and mixed dementia (Kalaria, 2018; Skrobot et al., 2018). VaD is considered a heterogeneous group of brain disorders since it can be caused by several cerebrovascular pathologies (Iadecola, 2013), such as atherosclerosis, small vessel disease or cerebral amyloid angiopathy (CAA), which is the accumulation of Aβ in vessel walls (Serrano-Pozo et al., 2011). These diseases, in turn, can lead to different cerebrovascular lesions, i.e., ischemic or hemorrhagic infarct, white matter lesions or hemorrhages (McAleese et al., 2016; Smith, 2017; Kalaria, 2018). Although in different ways, these lesions ultimately reduce the blood flow to the brain, and consequently the oxygen supply. The lack of oxygen in the brain is what ultimately leads to vascular dementia (**Figure 1**).

Although AD and VaD differ in their etiology, they share risk factors, such as age, obesity, the apolipoprotein E4 allele (ApoE ε4 allele) and hypercholesterolemia (Akinyemi et al., 2013). Furthermore, they also share similarities in their pathophysiology (**Table 1**; Kalaria and Ballard, 1999), i.e., a tendency of $A\beta_{42}$ to be significantly higher in the temporal lobe (Lewis et al., 2006), or a neuronal cell volume loss (Gemmell et al., 2012). In fact, neuronal and synaptic loss are the best predictors of cognitive decline in neurodegenerative diseases (Coleman et al., 2004; Andrade-Moraes et al., 2013; Theofilas et al., 2018). In one study on 14 brains from 80-year-old women, a novel technique called isotropic fractionator was used to determine the absolute cellular composition of brain regions. The study showed there was ∼50% reduction of total neuronal cell numbers in the hippocampus of AD subjects (Andrade-Moraes et al., 2013).

Not only is neuronal cell death a hallmark of neurodegenerative diseases, but in AD it is also correlated with the severity of the disease (Bussière et al., 2003; Arendt et al., 2015; Martínez-Pinilla et al., 2016; Chi et al., 2018). The same has been found in VaD, where both reduced neuronal volume (Gemmell et al., 2012) and cell counts (Jellinger, 2013) are associated with the severity of cognitive impairment in VaD (Kril et al., 2002; Gemmell et al., 2012).

Although there are several descriptions of mechanisms of cell death (Galluzzi et al., 2018), the major ones linked to neurodegenerative diseases are apoptosis and necrosis (Chi et al., 2018). Apoptosis is a controlled process where there are no spillages of the cell contents to the surrounding, whereas necrosis consists of an uncontrolled cell death, induced by external injury, such as hypoxia or inflammation. Ultimately, the cell membrane breaks and the cellular contents are spilled (D'Arcy, 2019). A new type of controlled necrosis has been recently described, called necroptosis (Degterev et al., 2005). Although similar to necrosis, necroptosis can be activated by death receptors such as TNFR1, which leads to the activation of RIPK1 (Yuan et al., 2019). Furthermore, RIPK1 promotes neuroinflammation, another feature of neurodegenerative diseases (Yuan et al., 2019). Necroptosis has been reported to be activated in AD human brains and positively correlated with Braak stages (Caccamo et al., 2017), with changes in the pathways of apoptosis, autophagy and necrosis depending on the stage of AD (Telegina et al., 2019). Necroptosis has also been reported in the hippocampus of one case of VaD due to ischemic injury. In this case, the necroptosis was related to inflammation and increased cytokines, such as TNF-α and IL-1β (Belkhelfa et al., 2018).

In apoptosis, the cytoskeleton undergoes significant morphological changes (Bonfoco et al., 1995) due to a disruption of MTs (Liepins and Bustamante, 1994; **Figure 2A**). Colchicine, an alkaloid plant extract with a therapeutic use in coronary artery diseases, inflammatory and fibrotic conditions, is a drug that disrupts the MTs by fragmenting the tubulin heterodimers and, consequently, leading to apoptosis. Induced apoptosis could be, thus, prevented by the addition of taxol, a drug that stabilizes the MTs (Bonfoco et al., 1995). Although many of the MT-stabilizing drugs, including taxol, do not cross the blood-brain barrier, recent advances of their nanosuspension delivery (Fan et al., 2021) or nasal administration of paclitaxel (Cross et al., 2021) appear to effectively overcome the brain blood barrier and accomplish neuronal cell-targeted drug delivery, thus, offering a potential for novel dementia therapeutic opportunities.

Protein aggregates in neurodegenerative diseases also contribute to neuronal loss (Chi et al., 2018). The localization as well as the composition of the aggregates differ from disease to disease [i.e., intraneuronal aggregates of tau protein in AD (Šimić et al., 2016) or aggregations of α-synuclein in Parkinson's disease (Peng et al., 2018)]. In AD, tau protein undergoes posttranslational modifications (i.e., hyperphosphorylation) and/or truncation (Wischik et al., 1995), which is observed in NFTs. It is not clear, however, whether the phosphorylation occurs before the aggregation or after the formation of NFTs. Similarly, the debate whether tau aggregates or soluble tau oligomers are the toxic species is ongoing. Nonetheless, the NFTs may contribute to the activation of neuronal apoptotic mechanisms in AD (Nixon and Yang, 2011; Chi et al., 2018; Liu et al., 2020). Even though there are many papers in the literature that describe tau as a MT stabilizer which detaches from MTs when hyperphosphorylated (Chi et al., 2018), recent studies might call this statement into question (Baas and Qiang, 2019). Nonetheless, the fact that phosphorylation of tau hinders tubulin and MT assembly remains (Savastano et al., 2021). Furthermore, a study showed that tau protein is only bound to MTs for a very short time of 40 ms. The authors described that tau protein presented a "kiss and hop" interaction with tubulin molecules (Janning et al., 2014).

Not only have the NFTs been related to MT destabilization, but also Aβ. In fact, Fifre et al. (2006) described the possible role of Aβ in the degradation of different MAPs. Gevorkian et al. (2008) detected MT disruption in primary neurons exposed to Aβ as a result of the binding of Aβ with MAP1. In addition, modifications of MTs can also influence the ability of neurons to cope with Aβ neurotoxicity. Namely, MTs disruption leads to increased levels of cytotoxicity caused by the $A\beta_{1-42}$ exposure, and *vice versa*, the stabilized MTs delay the toxicity caused by $A\beta_{1-42}$ (Shamitko-Klingensmith et al., 2016). Similarly, in isolated neuronal cultures, Aβ oligomers cause tau-dependent

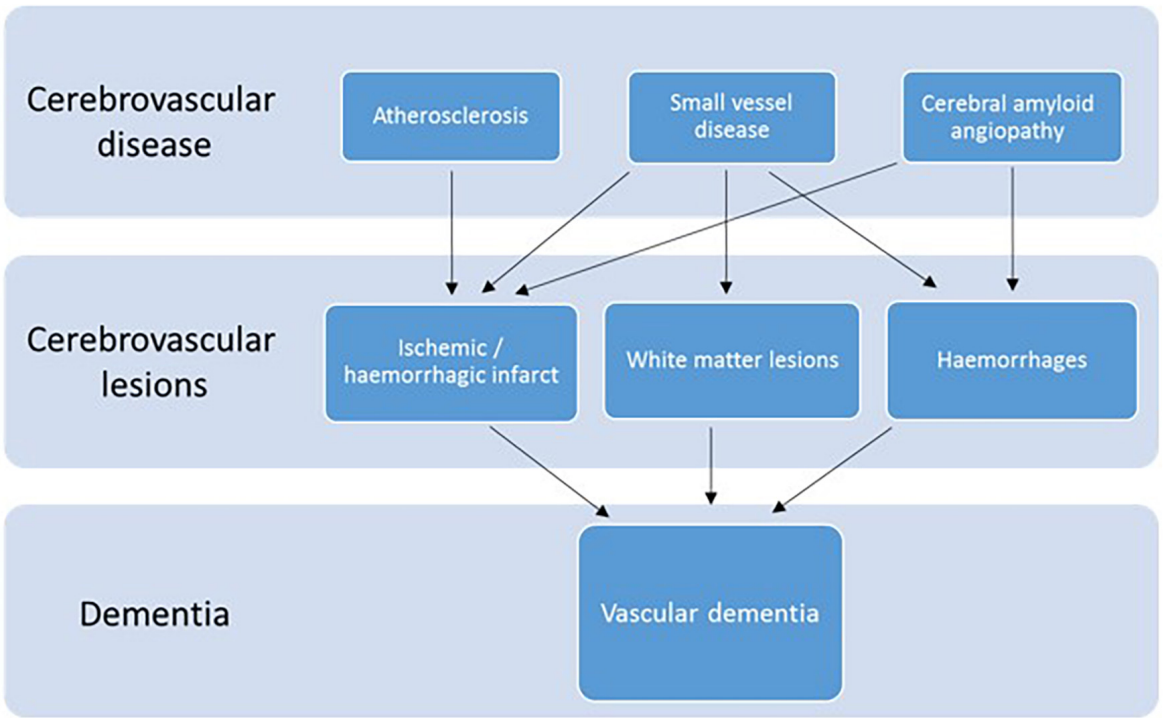

FIGURE 1 | Diagram of the cerebrovascular diseases and lesions that lead to VaD. Modified after (McAleese et al., 2016).

TABLE 1 | Pathophysiological similarities between AD and VaD.

	Alzheimer's disease	**Vascular dementia**
APOE genotype	Higher prevalence of ApoE ε4 allele (Govindpani et al., 2019)	
Altered hemodynamic	Altered vessel hemodynamics, angiogenesis, vascular cell function, vascular coverage, blood-brain barrier permeability. In AD these are attributed to amyloid toxicity (Govindpani et al., 2019)	
Aβ	Significantly higher amounts of $A\beta_{42}$ in the temporal and frontal lobes (Lewis et al., 2006)	Tendency of $A\beta_{42}$ to be higher in the temporal lobe (Lewis et al., 2006)
Tau protein	Significant loss of soluble tau in neocortical areas, hippocampus, and entorhinal cortex (Mukaetova-Ladinska et al., 1993)	Loss of total tau protein in temporal lobe (Mukaetova-Ladinska et al., 2015)
	Widespread significant increase in phosphorylated tau protein (Mukaetova-Ladinska et al., 2015)	No overt change in phosphorylated tau protein (Ser202/Thr205 and Ser262 phosphorylated sites) in temporal and frontal lobes (Mukaetova-Ladinska et al., 2015)
Morphological and cellular changes	Loss of neuronal cell volume (Gemmell et al., 2012)	
	Hippocampal and medial temporal lobe atrophy and CA1 pyramidal neuronal loss (Kril et al., 2002)	
Changes in synaptic proteins	Loss of synaptophysin and SNAP-25 (Mukaetova-Ladinska et al., 2009)	

MT breakdown mediated by spastin, an MT-severing enzyme (Zempel et al., 2013).

When analyzing VaD, it has been found that there is a loss neuronal cell volume in the dorsolateral prefrontal cortex (DLPFC) of patients with VaD when compared to controls (Mukaetova-Ladinska et al., 2009). Another study reported a selective loss of total tau protein in the temporal lobe of subjects with VaD that did not correlate with NFT, senile plaques or amyloid beta (Mukaetova-Ladinska et al., 2015). In a study by Gallart-Palau et al. (2015) where the levels of α1-tubulin and βII-tubulin isotypes were measured in VaD subjects and controls, no differences were observed in the temporal lobe. It is worth mentioning that the same study showed the tubulin proteins were significantly deamidated in VaD patients when compared to controls. Furthermore, these changes were not due to neurofibrillary pathology or any other lesion in VaD, i.e., visible infarcts (Gallart-Palau et al., 2015). Similarly, in a work done with human brain homogenates from VaD and AD patients, Mukaetova-Ladinska's lab found a tendency for reduced levels of tubulin in the temporal lobe of VaD patients

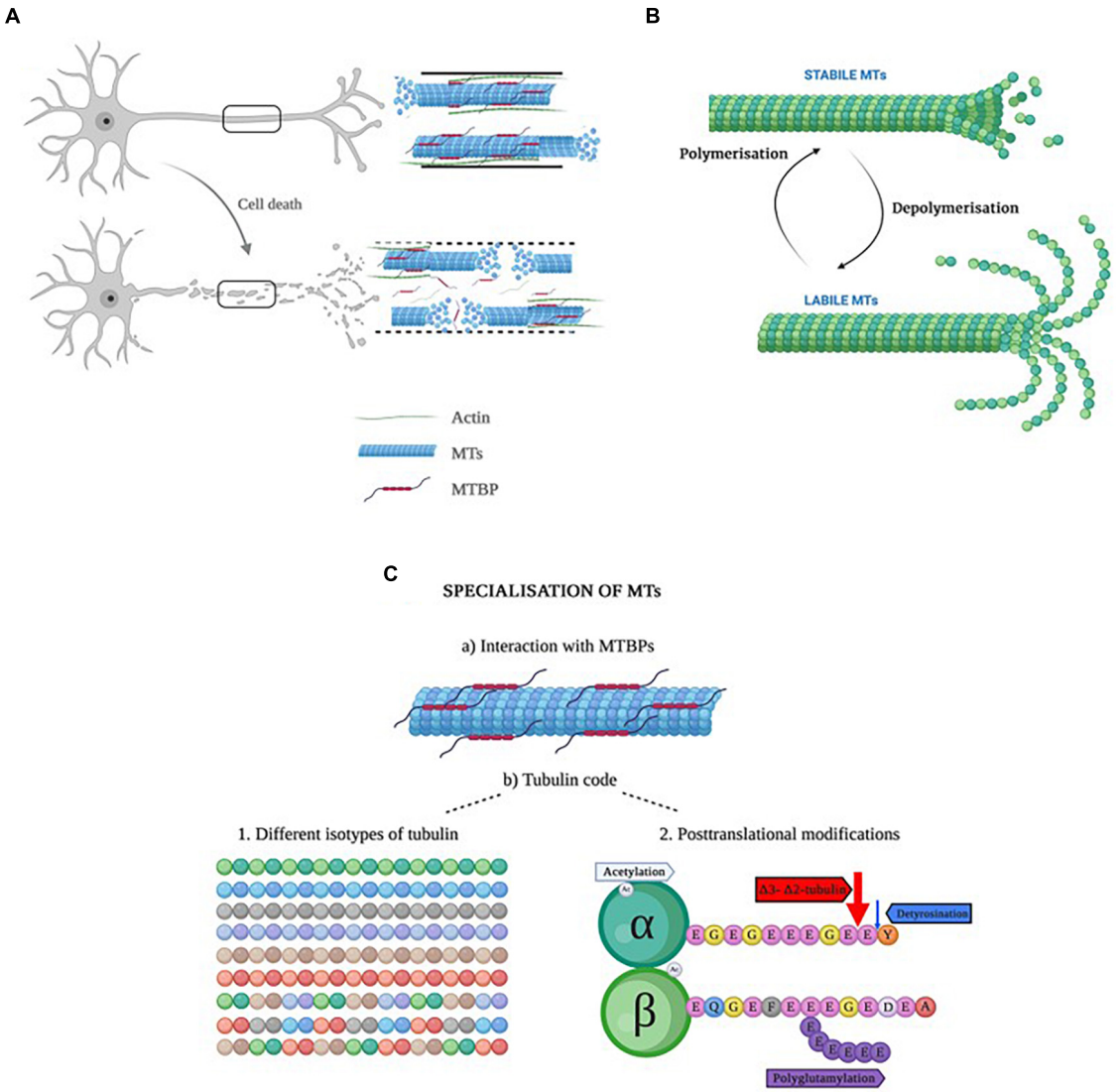

FIGURE 2 | (A) Representation of a healthy neuron with a healthy cytoskeleton (top), and a neuron in apoptosis with increased ratio of labile to stabile MTs. **(B)** Representation of the dynamic instability process in microtubules. When MTs are highly dynamic, they are called labile, whereas when the dynamics are slow, they are named stable MTs (Li and Black, 1996). The important aspect of dynamic instability is the presence of stochastic changes between a growth and a shrinkage phase and vice versa. These two phases can occur in parallel in the cells. The dynamic instability is energy-dependent and driven by GTP hydrolysis. **(C)** Schematic representation of the specialization of MTs. Created with BioRender.com.

(Li et al., 2014), raising the question of whether changes in tubulin, i.e., posttranslational modifications, could be related to the observed loss of tau and neuronal volume.

Although there is no accumulation of NFTs in VaD, the temporal lobe appears to have a significant loss of soluble tau protein (Mukaetova-Ladinska et al., 2015), and this may result in the decreased neuronal cell volume followed by neuronal cell loss and apoptosis (Gemmell et al., 2012). The tubulin loss additionally may be result of: (1) neuronal death secondary to ischemic injury, (2) the process of diaschisis, (3) axonal injury in white matter and reduction of white matter volume, and (4) reduced dendritic arborization due to cell atrophy. Furthermore, these early changes in the interaction between microtubule associated proteins and tubulin may denote the neurobiological crossroad of further clinical and neurobiological progression to either AD or VaD. Having a better understanding of MTs and tubulin changes in the brain might lead to the development of an effective form of therapy.

MICROTUBULES

The cytoskeleton is a complex network of filaments that gives the cell its shape and mechanical resistance. In neurons, the cytoskeleton is formed by MTs, microfilaments and neurofilaments (Penazzi et al., 2016). Out of the three, MTs

are the main protein filaments of the cytoskeleton and they are abundant in the cells (Horio and Murata, 2014; Burbaeva et al., 2020). They constitute approximately 10% of the total protein concentration in the brain (Cleveland et al., 1980).

MTs are involved in a variety of functions, such as cell motility, transport, cell shape and polarity, and mitosis (Mandelkow and Mandelkow, 1995). They are also necessary for synaptic plasticity, and their stability is essential for the physiological functioning of neurons (Carnwath et al., 2018). Cytoskeletal defects and altered MT-mediated processes are indeed linked to neurodevelopmental disorders, such as severe lissencephaly due to a mutation in the tubulin α1A gene (Kumar et al., 2010), or autosomal dominant disorders of axon guidance due to mutations in the TUBB3 gene (Tischfield et al., 2010).

A fundamental characteristic of MTs is that they are dynamic structures, which means they are able to alter their organization in order to adapt to changes in cellular shape (Goodson and Jonasson, 2018). This process, named "dynamic instability" (Horio and Murata, 2014), is considered an intrinsic property consisting on two opposed processes: polymerization or growth, and depolymerization or shrinkage, as seen in **Figure 2B**. The dynamic instability derives from the tubulin's GTPase activity (Hyman et al., 1995; Nogales and Wang, 2006). Both polymerization and depolymerization can happen at the same time in the cell: whereas polymerization occurs in a temperature and concentration-dependent manner, depolymerization occurs randomly (Horio and Murata, 2014). Interestingly, this process occurs stochastically within the same filament, depending on whether MTs are bound to GTP or GDP, and both growing and shrinking MTs can be present in the same cell at any one given time. Thanks to this dynamic instability, fibroblasts are able to migrate and neurons extend their axon and dendrites (Mitchison and Kirschner, 1984; Brouhard, 2015).

MTs are hollow cylinders formed by heterodimers of α- and β-tubulin (Bryan and Wilson, 1971), with an approximate ratio of 1:1 (Alvarez et al., 1998). Both α- and β-tubulin monomers are very similar; they are ∼40% identical and 63% homologous (Nogales, 2013). Each tubulin monomer is composed of 450 amino acid residues which differ slightly from one another (Ludueña et al., 1977; Sullivan and Cleveland, 1986), and a molecular mass of ∼50 kDa (Alvarez et al., 1998; Nogales et al., 1998). The monomers present some structural differences (**Table 2**). Due to the different functions MTs perform, they need to be specialized, and this specialization is achieved in two different ways (Gadadhar et al., 2017): **(a)** by interacting with microtubule binding proteins (MTBPs), or **(b)** by the tubulin code (**Figure 2C**), a highly important event in that it not only controls specific cellular functions, but it also has a role in human pathologies (Gadadhar et al., 2017). Moreover, the tubulin code is a mechanism by which MTs regulate themselves in yet another two different ways (Gadadhar et al., 2017):

1- **Expression of different isotypes of α- and β-tubulin**: both α- and β-tubulin have different isotypes that are encoded by different genes. In humans, there are 7α- and 8β-tubulin isotypes which differ in their C-terminal sequence and present tissue specificity (Ludueña, 1998; Fukushima et al., 2009; Ludueña, 2013). For example, α-tubulin Class II is mostly found in the testis, whereas α-tubulin III is found in brain and muscle (Ludueña, 2013). On the other hand, β-tubulin III is present only in neurons (Katsetos et al., 2003) whereas β tubulin Class VI is present mainly in hematopoietic cells (Murphy et al., 1987). Brains express α 1A-, α 1B-, α 1C-, α 4A-, and α8-tubulin, and β 2A-, β 3-, β 4-, and β5-tubulin (Fukushima et al., 2009). β-tubulin isotypes are evolutionary very well conserved and significantly better understood than α-tubulin isotypes (Ludueña, 2013). The level of expression of the isotypes in each specific tissue is very important since high βI-tubulin and low βII-tubulin levels have been described in breast cancer (Hasegawa et al., 2003; Ohishi et al., 2007). Furthermore, each isotype presents a specific function. Whereas βII is involved in neurite formation, βIII protects the MTs from reactive oxygen species (ROS) (Ludueña, 2013).

2- **Posttranslational modifications (PTMs) of tubulin (Table 3):** there are more than ten modifications that can occur at any given time (Fukushima et al., 2009; Janke, 2014; Gadadhar et al., 2017). More often than not, PTMs are found on stable long-lived MTs, such as neuronal, axonemal, and centriolar MTs (Janke, 2014). In modifying the tubulin, PTMs also modify the binding affinity of tubulin to MTBPs, such as tau, as it is observed by an increase in polyglutamylated tubulin (Eddé et al., 1990).

TABLE 2 | Structural differences between α- and β-tubulin (modified after Nogales et al., 1998; Nogales, 2013).

α-tubulin	β-tubulin
13% of alpha helices	13% of alpha helices
39% of beta sheets	42% of beta sheets
48% of random coils	45% of random coils
Asp -254 site at the E site, an ideal residue for the nucleotide hydrolysis	Lys-254 at the N site that strengthens the monomer-monomer interaction by interacting with the GTP phosphate group
GTP molecule always attached	GTP and GDP molecules are exchangeable for the polymerization of microtubules
Almost completely detyrosinated	Approximately 10% phosphorylated

Interaction With Microtubule Binding Proteins

Any protein that binds to the MTs in a specified manner is considered a MTBP, and they are functionally categorized as stabilizers, destabilizers, capping proteins or bundler/cross-linkers (Goodson and Jonasson, 2018). Probably the most well-known MTBPs are the ones that comprise the MT associated protein (MAP) family, which includes tau protein and MAP2, the major MAPs in the brain (Melková et al., 2019), as well as MAP6, previously known as STOP.

1. **Tau:** this protein is enriched in axonal MTs, although it is also present in dendrites (Melková et al., 2019). Due to alternative splicing, there are six different tau isoforms,

TABLE 3 | Summary of main PTMs, the catalytic enzymes taking part in the reaction and the effects of PTMs on MTs/cells.

PTM	α-tubulin	β-tubulin	Catalytic enzymes	Effect on MTs
Acetylation	Yes	Yes	α-Tat1 and San acetyl transferase	Marker of stable MTs (Li and Yang, 2015) and recruitment of motor MTBPs (Dompierre et al., 2007)
Deacetylation	Yes	Yes	HDAC6 and Sirt2	Increases cell motility (Hubbert et al., 2002)
Tyrosination	Yes	No	TTL family	Marker of stable MTs
Detyrosination	Yes	No	VASH1/SVBP complex	Important for alignment of chromosomes during mitosis (Barisic et al., 2015)
Δ2-tubulin	Yes	No	CCP family	Marker of long-lived MTs (Paturle-Lafanechère et al., 1994)
Δ3-tubulin	Yes	No	CCP family	Marker of long-lived MTs (Paturle-Lafanechère et al., 1994)
Polyglutamylation	Yes	Yes	TTLL family	Regulation of MT-MAP interactions
Deglutamylation	Yes	Yes	CCP family	Regulation of MT-MAP interactions
Polyglycylation	Yes	Yes	TTLL family	Unknown in mammals
Deglycylation	Yes	Yes	Not found	Unknown in mammals
Polyamination	Yes	Yes	Transglutaminases	Stabilization of MTs in neurons
Phosphorylation			CDK1, Syk	Regulate MT behavior during cell division (Janke and Magiera, 2020)

which differ in the number of MT-binding domain repeats (Fischer and Baas, 2020). Five of those isoforms weight around 40 kDa, and present multiple phosphorylation sites. When hyperphosphorylated, these form the characteristic NFTs observed in AD (Himmler et al., 1989), which hinder tubulin assembly (Savastano et al., 2021). On the other hand, the sixth isoform termed "Big Tau," mainly expressed in the peripheral nervous system, weighs 100 kDa and does not present many phosphorylation sites; protecting it from aggregation into tangles (Fischer and Baas, 2020). In addition, the speculated function of big tau is the stabilization of mature axonal cytoskeleton (Oblinger et al., 1991).

2. **MAP2**: present in cell bodies and dendrites, MAP2 is considered a MT stabilizer (Goodson and Jonasson, 2018) as it increases MT rigidity (Felgner et al., 1997). Similar to tau protein, MAP2 is accumulated into granules, which leads to neurotoxicity and neuronal loss (Xie and Miyasaka, 2016). Loss of MAP2 has been widely linked to AD in human samples, as well as in cellular and animal models (Mukaetova-Ladinska et al., 2009; Baazaoui et al., 2017; Kandimalla et al., 2018; Manczak et al., 2018; Reddy et al., 2018; Beggiato et al., 2020; Liang et al., 2020).
3. **MAP6**: formerly known as STOP (stable tubule only polypeptide), it is a genuine MT stabilizer found predominantly in the axon, along with detyrosinated and acetylated tubulin; two PTMs present in stable MTs (Slaughter and Black, 2003).

Posttranslational Modifications of Tubulin

Tubulin can undergo more than 10 different PTMs, some of them occurring solely on the tubulin, such as polyglutamylation. The major modifications that have been linked to neurodegeneration are acetylation, detyrosination, and polyglutamylation. In the following pages, we will discuss the tubulin PTMs and what it is known thus far about their role in neurodegenerative diseases.

1. ***Acetylation and Deacetylation:*** this modification is different from the others in that it happens in the lumen of MTs (Gadadhar et al., 2017). Acetylation can take place either on lysine 40 (K40) on α-tubulin (L'Hernault and Rosenbaum, 1985), where it is linked to stable MTs (Westermann and Weber, 2003; Wloga and Gaertig, 2010; Janke and Bulinski, 2011), or on K252 on β-tubulin (Janke, 2014), where it might slow down the incorporation of tubulin into MTs (Chu et al., 2011). The enzymes that catalyze the reactions are α-Tat1 (specific acetylation of tubulin) and San acetyl transferase (Akella et al., 2010; Janke, 2014), and HDAC6 and Sirt2 (involved in the deacetylation of tubulin and other substrates).
   In a functional level, acetylated tubulin is implicated in intracellular trafficking, endoplasmic reticulum (ER) localization and ER-mitochondria interactions, as well as the regulation of MT dynamics (Daire et al., 2009). It has been observed that in most NFT bearing neurons there is a decrease in acetylated α-tubulin (Brion et al., 2001), a marker of stable MTs (Janke and Bulinski, 2011). Similarly, deacetylation is associated with dysfunctional MT-mediated axonal transport in neurodegenerative diseases, such as AD, Parkinson's disease (PD) and Huntington's disease (HD) (Li and Yang, 2015; Fernández-Barrera et al., 2018). In fact, HDAC6 (histone deacetylase 6, a multidomain cytosolic enzyme with α-tubulin deacetylase activity) is increased in AD (Zhang et al., 2013) and HD (Ferrante et al., 2003), and dysregulation of HDACs also take part in ischemic strokes (Fang et al., 2020).
2. ***Detyrosination and tyrosination:*** α-tubulin isotypes present a tyrosine residue at the end of the C-terminal sequence that β-tubulin isotypes lack; thus, rendering this modification specific to α-tubulin (Prota et al., 2013; Janke and Magiera, 2020). The tyrosine residue can be reversibly removed by the VASH1/SVBP complex (Aillaud et al., 2017) generating detyrosinated tubulin. Retyrosination of the tubulin, however, happens thanks

to the tubulin tyrosine ligase (TTL) (Janke, 2014). These two modifications are spatially and temporally regulated. Whereas tyrosination is mostly found in the growing end of the axons in developing neurons (Ahmad et al., 1993; Sferra et al., 2020), detyrosination is mainly found in the dendrites of mature neurons, and it is considered a marker of stable MTs (Sferra et al., 2020).

Detyrosination regulates MT-MAP interactions whereas tyrosination has a role in spindle orientation and growth cone guidance in neuronal pathfinding (Magiera and Janke, 2014). In the context of AD, one study has suggested that the levels of tyrosinated levels are increased (Zhang et al., 2015).

3. **Δ *2-tubulin and* Δ *3-tubulin:*** these terms are used when after detyrosination, additional C-terminal glutamate residues are eliminated from the tubulin sequence, which means that retyrosination is not possible (Janke, 2014; Gadadhar et al., 2017). Because of the lack of retyrosination, it is believed that one of the functions of Δ2-tubulin is to lock the tubulin in the non-tyrosinatable status or to reduce sites for polyglutamylation or polyglycylation (Magiera and Janke, 2014). It is estimated that 35% of α-tubulin in the brain corresponds to Δ2-tubulin (Paturle-Lafanechère et al., 1994). The enzymes that catalyze these reactions belong to the cytosolic carboxypeptidases (CCPs) family (Janke, 2014; Gadadhar et al., 2017). A study showed that there were increased levels of glutamylated Δ2-tubulin in the hippocampi of post-mortem patients of AD (Vu et al., 2017).
4. ***Polyglutamylation:*** first reported in 1990, it involves the addition of 1–12 glutamate units into a glutamic acid residue in the C-terminal region of either α- or β-tubulin (Eddé et al., 1990). In the brain tissue, there is an average of 3–6 glutamate residues on each tail, with as many as 11 and 7 residues detected on the α- and β-tubulin tails, respectively (Redeker, 2010). The polyglutamylation catalyzing enzymes belong to the TTL like (TTLL) family (Rogowski et al., 2010; Wloga and Gaertig, 2010) whereas the deglutamylases belong to the CCP family (Kimura et al., 2010). There are 8 members in the TTLL family that present different affinities for α- and β-tubulin, and different preferences for either initiating or elongating the glutamylation reaction, as shown in **Table 4** (Yu et al., 2015). As for the CCP family, there are six members. CCP1, -2, -3, -4, and -6 shorten polyglutamylated chains, whereas CCP5 is the only monodeglutamylase found until date (Rogowski et al., 2010; Berezniuk et al., 2013).

   Polyglutamylation is abundant in neurons, centrioles, basal bodies, axonemes of cilia and flagella, as well as in the mitotic spindle (Redeker, 2010), and it is implicated in the regulation of MT and MAP electrostatic interactions, since polyglutamylation affects the charges of the tubulin tails (Janke, 2014).

   Maintaining the correct levels of polyglutamylation is essential. Several defects have been associated with either depletion or overexpression of the enzymes catalyzing glutamylation: TTLL1 knockout mice show respiratory problems (Ikegami et al., 2010), and TTLL6 knock out zebrafish show defective assembly of olfactory cilia (Pathak et al., 2007), whereas overexpression of TTLL6 causes ciliary defects in *Tetrahymena* (Suryavanshi et al., 2010). Another example comes from the Purkinje cell degeneration (*pcd*) mouse model, which lacks the CCP1 enzyme (Rogowski et al., 2010). These mice show overexpression of polyglutamylated tubulin and degeneration of Purkinje cells in the cerebellum (Magiera et al., 2018). Thus, balanced tubulin glutamylation levels are important for neuronal function and survival.

   The excess of TTLL1-mediated polyglutamylation is the cause of cerebellar neurodegeneration in the *pcd* mouse model, and this neurodegeneration could be rescued upon depletion of TTLL1 (Magiera et al., 2018). The excessive polyglutamylation also impairs neuronal transport (Magiera and Janke, 2014), with the mutations of CCP1 in humans leading to childhood-onset neurodegeneration (Shashi et al., 2018). Of interest, in people with Alzheimer's disease (AD), there is a reduction of α-tubulin and a tendency for increased polyglutamylation in the hippocampus when compared to age-matched controls (Zhang et al., 2015). It has already been shown that if tubulin is polyglutamylated with four or more glutamyl residues, the affinity to bind tau decreases (Eddé et al., 1990). However, little is known about MT-MAP interaction in neurodegenerative diseases and the implications this lower affinity has.
5. ***Polyglycylation:*** it refers to the generation of side chains of glycine residues within the C-terminal tails of α- and β-tubulin (Redeker et al., 1994). It happens at the same site as glutamylation and it is also catalyzed by TTLL enzymes (Rogowski et al., 2010). This PTM is restricted to cilia and flagella and the extent of the modification correlates with the length of the axonemes (Rogowski et al., 2010; Wloga and Gaertig, 2010). To date, there is very little known about the function of this modification in mammals. However, a link between the downregulation of TTLL3 and colon cancer has been described in humans (Rocha et al., 2014). Furthermore, it has been observed that polyglycylation in humans is not possible since the enzyme responsible for the elongation, TTLL10, is inactivated (Janke, 2014). There is little to no knowledge about the role of polyglycylation in neurodegeneration.
6. ***Polyamination***: for this modification, glutamine 15 (Q15) is considered to be the primary modification site, and the reaction is catalyzed by transglutaminases (Song et al., 2013). The reaction consists on the addition of amines to either α- or β-tubulin, adding positive charges to the acidic tubulin (Janke and Magiera, 2020). This PTM is irreversible and it most likely stabilizes microtubule subpopulations in neurons (Janke, 2014).
7. ***Phopshorylation:*** the Cdk1 enzyme catalyzes the phosphorylation on Serine 172 (S172) of β-tubulin (Fourest-Lieuvin et al., 2006), and it seems that this modification might be implicated in microtubule dynamics during cell division (Janke, 2014). Another tyrosine kinase

TABLE 4 | Family members of the TTLL family and their specific role in glutamylation.

	α-tubulin	β-tubulin
Initiates reaction	TTLL 1, 5, 6	TTLL 1, 4
Elongates chain	TTLL 6, 9, 11, 13	TTLL 7

known as Syk has been shown to phosphorylate an unidentified residue of α-tubulin (Peters et al., 1996).

8. ***Others:*** tubulin can also undergo palmitoylation (Caron, 1997), ubiquitination (Ren et al., 2003), glycosylation (Walgren et al., 2003), arginylation (Wong et al., 2007), methylation (Xiao et al., 2010), and sumoylation (Rosas-Acosta et al., 2005). However, there is not much information on these processes and how they affect disease pathogenesis.

Therapeutic Drugs Targeting Microtubule Stability

Microtubule Stabilizers

Several studies with MT stabilizers have been carried out as possible treatment for AD and other tauopathies:

1. **Epothilone D (BM2-241027):** this is a brain penetrant microtubule stabilizing agent able to polymerize tubulin and inhibit its depolymerization (Cheng and Huang, 2018). In a study following treatment with this drug, MT dynamicity decreased, whilst cognition improved, as shown in the Morris Water Maze task (Barten et al., 2012). Another study in cortical neurons put in display the importance of the dose, since it can affect the mitochondrial transport (Clark et al., 2020). Studies have also shown that BM2-241027 reduces axonal dysfunction, neurotoxicity, cognitive deficits, and AD-like pathology in PS19 aged tau transgenic mice (Zhang et al., 2012). Although in animal studies Epothilone D rescued working and spatial memory deficits in aged tau transgenic mice (reviewed in Yu et al., 2021), this drug was discontinued following a Phase 1 clinical study in 2013, with no information regarding drug's effectiveness and side effects in humans (Bristol-Myers Squibb, 2013).
2. **TPI-287:** this CNS penetrating taxane was used in another clinical study to assess its efficiency as an AD treatment, progressive supranuclear palsy and corticobasal syndrome. Unfortunately, it was discontinued due to safety, i.e., severe anaphylactoid reactions (Tsai et al., 2020).
3. **Paclitaxel:** it is the generic name of taxol, a very common MT stabilizing drug approved by the Food and Drug Administration for the treatment of several types of cancer (Weaver, 2014). However, they evoke axonal degeneration (Gornstein and Schwarz, 2014). This neurotoxicity prevents it from being used in neurodegenerative diseases. However, its' newer nasal formulation has been successfully used in transgenic animals. Cross et al. (2019) showed that intranasal paclitaxel administered once daily, prevented injury-induced memory deficits in mice. Furthermore, there was reduced evidence of axonal injury and synaptic loss (Cross et al., 2019). The same group has also shown that a transgenic mouse model of AD presented less tau-containing neurons in the CA1 and had improved memory after paclitaxel treatment (Cross et al., 2021). On the other hand, Lehrer and Rheinstein recently proposed that transdermal patches over the cervical spine could revolutionize drug therapy for AD, and may avoid the systemic side effects of the paclitaxel, such as anemia, leukopenia or peripheral neuropathy (Lehrer and Rheinstein, 2019).
4. **NAP (Davunetide):** this agent protects MTs against degradation induced by numerous MT disrupting agents, rendering it a possible potent drug against neurodegenerative diseases. The clinical trials performed in humans with tauopathies had no positive outcome (Ivashko-Pachima and Gozes, 2021). In a phase II double-blind randomized controlled trial, NAP showed cognitive and functional improvement in mild cognitive impairment (MCI) patients, after a 12-week intranasal NAP administration (reviewed by Yu et al. (2021). By the time this review is being written, clinical trials on MCI, progressive supranuclear palsy and schizophrenia have all been discontinued, and the one for frontotemporal dementia is inactive (as per alzforum webpage 20.09.2021).

As observed in these three examples, MT stabilizers have severe side effects (Chiorazzi et al., 2009; Brandt and Bakota, 2017), and although they might help in neurodegenerative diseases, they require very fine-tuning to avoid toxicity.

Drugs Targeting Tubulin Posttranslational Modifications

The only tubulin PTM that has been targeted thus far has been acetylation. There are several histone deacetylases (HDACs) which deacetylase α-tubulin, such as HDAC6 and SIRT2 (Hubbert et al., 2002; North et al., 2003). There are studied that show prevention of cognitive decline upon inhibition of SIRT2 (Diaz-Perdigon et al., 2020). Positive effects were also observed with HDAC6 inhibitors (Selenica et al., 2014). Vorinostat is an HDAC inhibitor which tolerable doses is being studied in patients with mild AD (clinical trial identifier: NCT03056495).

For a more detailed review on cytoskeleton-targeted drugs, refer to Eira et al. (2016).

Drugs Targeting Necroptosis May Stabilize Microtubule

Necrostatin-1 (Nec-1) is an anti-necroptotic molecule that directly targets Aβ and tau proteins, alleviates brain cell death and ameliorates cognitive impairment in AD models (Yang et al., 2017). Via targeting and reducing both Aβ oligomers and hyperphosphorylation of tau protein, it may also improve the MT stabilization and may serve an important role in the development of preventive approach for AD. These findings come from an animal APP/PS1 model (Yang et al., 2017), and

have been recently extended to a vascular animal model with bilateral common carotid artery stenosis. Namely, in the latter vascular animal model, Nec-1 improved animal behavior and enhanced the inhibitory effect of environment enrichment on inflammation response (Zhang et al., 2019).

Another necroptosis inhibitor, necrosulfonamide (NSA), has also been investigated in a rat model of AD. Administration of NSA intraperitoneally for 6 weeks alleviated phosphorylated tau protein and Aβ accumulation, and regulated the high hippocampal expression of tumor necrosis factor-alpha (TNF-α), β-site amyloid precursor protein cleaving enzyme 1 (BACE1), glycogen synthase kinase-3β (GSK-3β), and acetylcholinesterase (Motawi et al., 2020). NSA has been identified as a novel promising anti-AD treatment via targeting necroptosis, and possibly indirectly contributing to MT stabilization in AD.

All the evidence for the necroptotic agents in AD treatment comes from animal studies, and no human clinical trials are being conducted Similarly, the evidence of these agents upon the MT network, as a result of their effect upon hyperphosphorylated tau protein and Aβ, is still missing.

CONCLUSION

AD and VaD represent almost 85% of all clinically diagnosed dementia cases, percentage that raises if we take mixed dementia into account, and neuronal loss is a hallmark in all of them. The neuronal loss is not only the best predictor for cognitive decline, but in AD and VaD it also correlates with the severity of the disease, as well as with Braak stages (Buchanan et al., 2020). On a morphological level, neuronal loss results in significant changes in the cytoskeleton of the cells, and consequently, in the MTs. Stability of MTs is, thus, essential for the physiological functioning of neurons.

Tau and MAP2 are MTBP involved in regulating the dynamics and assembly of MTs. In AD, tau is hyperphosphorylated and leads to neuronal loss. Polyglutamylation also regulates the interaction between tau and tubulin, where the more polyglutamylated the tubulin is, the less affinity it has to binding tau, ultimately leading to destabilization of MTs (Eddé et al., 1990). Although this was shown already in 1990, we still don't know what exactly happens to MT-MTBP interactions in neurodegenerative diseases. Understanding the interplay between tubulin, its PTMs and the binding affinity to MTBPs may help determine if there is a specific event that can prevent or stop neurodegeneration.

Maintaining the levels of tubulin polyglutamylation has proven to be essential for neuronal survival. In fact, it has been shown that there is a tendency for increased α-tubulin polyglutamylation in AD brains when compared to controls (Zhang et al., 2015). However, the number of subjects in this study was relatively low, and a larger number of brain samples should be studied. In addition, tyrosinated levels of tubulin were also measured, with the same outcome. Increasing the number of subjects in these studies is very important. Determining whether polyglutamylation and tyrosination play a role in AD and VaD could have clinical relevance that might lead to the development of new and efficient dementia treatments. It may be possible that tubulin plays a more important role than we know in these diseases, and that its stabilization and PTMs could have a big impact on the severity and progression of the diseases.

Even though there is no increase of phosphorylated tau protein in VaD patients, there is a decrease in the levels of total tau protein (Mukaetova-Ladinska et al., 2015). It is possible that changes in tubulin, such as an increase in polyglutamylation, may lead to a decreased affinity for tau, changes in MT dynamics and increasing the ratio of shrinkage to growth. This could be one plausible explanation for the observed neuronal loss in VaD (Gemmell et al., 2012). It is worth mentioning that some authors state tau works through a "gain of toxicity" mechanism, and that tau-lowering levels might be beneficial in AD and other tauopathies (Goedert, 2016). However, we do not speculate that a decrease in tau could lead to MT destabilization, but that the opposite might happen: tubulin PTMs could lead to molecular changes in tau that, ultimately, could take part in the destabilization of MTs. Even though there is no much literature linking VaD with axonal transport disruption, there are a couple of studies that do. One of them suggests that compromised axonal transport might play an important role in a type of VaD (Binswanger's disease) (Akiguchi et al., 1997). The other one states that since white matter is often affected in VaD, likely both demyelination and focal axonal injury occurs in VaD (Ihara et al., 2010). Therefore, it is fundamental for in-depth studying of VaD to understand the molecular mechanisms as well as the MT-MTBP interactions to aid the pharmacological treatment of VaD.

It is unclear whether MT abnormalities have a causal and early role in the disease process or represent a common end point downstream of the neurodegenerative cascade. Their presence in absence of overt Aβ and tau pathology, as it is the case in VaD, would argue that they may be an early change, though the MT destabilization as seen in AD argues for the opposite. Understanding the chronology of this triad of tightly woven molecular events will provide a new window of opportunity to arrest the dementia process in early, preclinical stages. It is intriguing to speculate that the chronology of events may differ among different dementia syndromes, and thus drive the design of novel dementia-specific therapies.

Restoring the MT network and the balance between labile and stable MTs might be fundamental to stop the progression of cell death and neurodegeneration. We believe that regulation of MTs by the different PTMs might be key on determining if and with how much affinity does tubulin bind to MTBPs. These changes might not affect the cells immediately, but they might accumulate over time and have a progressively negative impact on the brain. What if tubulin is the key link that is missing? What if the accumulation of proteins and gradual synaptic loss comes from a previous gradual accumulation of tubulin PTMs? What if these accumulations or sudden increase in some of the PTMs lead to a strong enough cell destabilization that produces the neuronal loss in neurodegenerative diseases? These are only some of the questions that may help guide the development of the new generation anti-dementia treatments.

AUTHOR CONTRIBUTIONS

ES-M wrote the article. RL-C, FG, RK, and EM-L contributed to the discussion, reviewed, and edited the manuscript. All authors contributed to the article and approved the submitted version.

FUNDING

This financial support for this research has been provided by a Ph.D. grant by the University of Leicester (ES-M/EBM-L).

REFERENCES

Ahmad, F. J., Pienkowski, T. P., and Baas, P. W. (1993). Regional differences in microtubule dynamics in the axon. *J. Neurosci.* 13, 856–866. doi: 10.1523/jneurosci.13-02-00856.1993

Aillaud, C., Bosc, C., Peris, L., Bosson, A., Heemeryck, P., Van Dijk, J., et al. (2017). Vasohibins/SVBP are tubulin carboxypeptidases (TCPs) that regulate neuron differentiation. *Science* 358, 1448–1453. doi: 10.1126/science.aao4165

Akella, J. S., Wloga, D., Kim, J., Starostina, N. G., Lyons-Abbott, S., Morrissette, N. S., et al. (2010). MEC-17 is an alpha-tubulin acetyltransferase. *Nature* 467, 218–222. doi: 10.1038/nature09324

Akiguchi, I., Tomimoto, H., Suenaga, T., Wakita, H., and Budka, H. (1997). Alterations in glia and axons in the brains of Binswanger's disease patients. *Stroke* 28, 1423–1429. doi: 10.1161/01.str.28.7.1423

Akinyemi, R. O., Mukaetova-Ladinska, E. B., Attems, J., Ihara, M., and Kalaria, R. N. (2013). Vascular risk factors and neurodegeneration in ageing related dementias: Alzheimer's disease and vascular dementia. *Curr. Alzheimer Res.* 10, 642–653. doi: 10.2174/15672050113109990037

Alvarez, P., Smith, A., Fleming, J., and Solomon, F. (1998). Modulation of tubulin polypeptide ratios by the yeast protein Pac10p. *Genetics* 149, 857–864.

Andrade-Moraes, C. H., Oliveira-Pinto, A. V., Castro-Fonseca, E., da Silva, C. G., Guimarães, D. M., Szczupak, D., et al. (2013). Cell number changes in Alzheimer's disease relate to dementia, not to plaques and tangles. *Brain* 136(Pt. 12), 3738–3752. doi: 10.1093/brain/awt273

Arendt, T., Brückner, M. K., Morawski, M., Jäger, C., and Gertz, H. J. (2015). Early neurone loss in Alzheimer's disease: cortical or subcortical? *Acta Neuropathol. Commun.* 3:10. doi: 10.1186/s40478-015-0187-1

Baas, P. W., and Qiang, L. (2019). Tau: it's not what you think. *Trends Cell Biol.* 29, 452–461. doi: 10.1016/j.tcb.2019.02.007

Baazaoui, N., Flory, M., and Iqbal, K. (2017). Synaptic compensation as a probable cause of prolonged mild cognitive impairment in Alzheimer's disease: implications from a transgenic mouse model of the disease. *J. Alzheimers Dis.* 56, 1385–1401. doi: 10.3233/jad-160845

Barisic, M., Silva e Sousa, R., Tripathy, S. K., Magiera, M. M., Zaytsev, A. V., Pereira, A. L., et al. (2015). Mitosis. Microtubule detyrosination guides chromosomes during mitosis. *Science* 348, 799–803. doi: 10.1126/science.aaa5175

Barten, D. M., Fanara, P., Andorfer, C., Hoque, N., Wong, P. Y., Husted, K. H., et al. (2012). Hyperdynamic microtubules, cognitive deficits, and pathology are improved in tau transgenic mice with low doses of the microtubule-stabilizing agent BMS-241027. *J. Neurosci.* 32, 7137–7145. doi: 10.1523/jneurosci.0188-12.2012

Beggiato, S., Cassano, T., Ferraro, L., and Tomasini, M. C. (2020). Astrocytic palmitoylethanolamide pre-exposure exerts neuroprotective effects in astrocyte-neuron co-cultures from a triple transgenic mouse model of Alzheimer's disease. *Life Sci.* 257:118037. doi: 10.1016/j.lfs.2020.118037

Belkhelfa, M., Beder, N., Mouhoub, D., Amri, M., Hayet, R., Tighilt, N., et al. (2018). The involvement of neuroinflammation and necroptosis in the hippocampus during vascular dementia. *J. Neuroimmunol.* 320, 48–57. doi: 10.1016/j.jneuroim.2018.04.004

Berezniuk, I., Lyons, P. J., Sironi, J. J., Xiao, H., Setou, M., Angeletti, R. H., et al. (2013). Cytosolic carboxypeptidase 5 removes α- and γ-linked glutamates from tubulin. *J. Biol. Chem.* 288, 30445–30453. doi: 10.1074/jbc.M113.497917

Bonfoco, E., Ceccatelli, S., Manzo, L., and Nicotera, P. (1995). Colchicine induces apoptosis in cerebellar granule cells. *Exp. Cell Res.* 218, 189–200. doi: 10.1006/excr.1995.1147

Brandt, R., and Bakota, L. (2017). Microtubule dynamics and the neurodegenerative triad of Alzheimer's disease: the hidden connection. *J. Neurochem.* 143, 409–417. doi: 10.1111/jnc.14011

Brion, J. P., Anderton, B. H., Authelet, M., Dayanandan, R., Leroy, K., Lovestone, S., et al. (2001). Neurofibrillary tangles and tau phosphorylation. *Biochem. Soc. Symp.* 67, 81–88. doi: 10.1042/bss0670081

Bristol-Myers Squibb (2013). *Therapeutics: Epothilone D*. Available online at: https://www.alzforum.org/therapeutics/epothilone-d

Brouhard, G. J. (2015). Dynamic instability 30 years later: complexities in microtubule growth and catastrophe. *Mol. Biol. Cell* 26, 1207–1210. doi: 10.1091/mbc.E13-10-0594

Bryan, J., and Wilson, L. (1971). Are cytoplasmic microtubules heteropolymers? *Proc. Natl. Acad. Sci. U.S.A.* 68, 1762–1766. doi: 10.1073/pnas.68.8.1762

Buchanan, H., Mackay, M., Palmer, K., Tothová, K., Katsur, M., Platt, B., et al. (2020). Synaptic loss, ER stress and neuro-inflammation emerge late in the lateral temporal cortex and associate with progressive tau pathology in Alzheimer's disease. *Mol. Neurobiol.* 57, 3258–3272. doi: 10.1007/s12035-020-01950-1

Burbaeva, G. S., Androsova, L. V., and Savushkina, O. K. (2020). Binding of colchicine to tubulin in the brain structures in normal conditions and in schizophrenia. *Neurochem. J.* 14, 235–238. doi: 10.1134/S1819712420010067

Bussière, T., Giannakopoulos, P., Bouras, C., Perl, D. P., Morrison, J. H., and Hof, P. R. (2003). Progressive degeneration of nonphosphorylated neurofilament protein-enriched pyramidal neurons predicts cognitive impairment in Alzheimer's disease: stereologic analysis of prefrontal cortex area 9. *J. Comp. Neurol.* 463, 281–302. doi: 10.1002/cne.10760

Caccamo, A., Branca, C., Piras, I. S., Ferreira, E., Huentelman, M. J., Liang, W. S., et al. (2017). Necroptosis activation in Alzheimer's disease. *Nat. Neurosci.* 20, 1236–1246. doi: 10.1038/nn.4608

Carnwath, T., Mohammed, R., and Tsiang, D. (2018). The direct and indirect effects of α-synuclein on microtubule stability in the pathogenesis of Parkinson's disease. *Neuropsychiatr. Dis. Treat.* 14, 1685–1695. doi: 10.2147/ndt.S166322

Caron, J. M. (1997). Posttranslational modification of tubulin by palmitoylation: I. in vivo and cell-free studies. *Mol. Biol. Cell* 8, 621–636. doi: 10.1091/mbc.8.4.621

Cheng, H., and Huang, G. (2018). Synthesis and activity of epothilone D. *Curr. Drug Targets* 19, 1866–1870. doi: 10.2174/1389450119666180803122118

Chi, H., Chang, H. Y., and Sang, T. K. (2018). Neuronal cell death mechanisms in major neurodegenerative diseases. *Int. J. Mol. Sci.* 19:3082. doi: 10.3390/ijms19103082

Chiorazzi, A., Nicolini, G., Canta, A., Oggioni, N., Rigolio, R., Cossa, G., et al. (2009). Experimental epothilone B neurotoxicity: results of in vitro and in vivo studies. *Neurobiol. Dis.* 35, 270–277. doi: 10.1016/j.nbd.2009.05.006

Chu, C. W., Hou, F., Zhang, J., Phu, L., Loktev, A. V., Kirkpatrick, D. S., et al. (2011). A novel acetylation of β-tubulin by san modulates microtubule polymerization via down-regulating tubulin incorporation. *Mol. Biol. Cell* 22, 448–456. doi: 10.1091/mbc.E10-03-0203

Clark, J. A., Chuckowree, J. A., Dyer, M. S., Dickson, T. C., and Blizzard, C. A. (2020). Epothilone D alters normal growth, viability and microtubule dependent intracellular functions of cortical neurons in vitro. *Sci. Rep.* 10:918. doi: 10.1038/s41598-020-57718-z

Cleveland, D. W., Lopata, M. A., MacDonald, R. J., Cowan, N. J., Rutter, W. J., and Kirschner, M. W. (1980). Number and evolutionary conservation of alpha- and beta-tubulin and cytoplasmic beta- and gamma-actin genes using specific cloned cDNA probes. *Cell* 20, 95–105. doi: 10.1016/0092-8674(80)90238-x

Coleman, P., Federoff, H., and Kurlan, R. (2004). A focus on the synapse for neuroprotection in Alzheimer disease and other dementias. *Neurology* 63, 1155–1162. doi: 10.1212/01.wnl.0000140626.48118.0a

Cross, D. J., Huber, B. R., Silverman, M. A., Cline, M. M., Gill, T. B., Cross, C. G., et al. (2021). Intranasal paclitaxel alters Alzheimer's disease phenotypic features in 3xTg-AD mice. *J. Alzheimers Dis.* 83, 379–394. doi: 10.3233/jad-210109

Cross, D. J., Meabon, J. S., Cline, M. M., Richards, T. L., Stump, A. J., Cross, C. G., et al. (2019). Paclitaxel reduces brain injury from repeated head trauma in mice. *J. Alzheimers Dis.* 67, 859–874. doi: 10.3233/jad-180871

Daire, V., Giustiniani, J., Leroy-Gori, I., Quesnoit, M., Drevensek, S., Dimitrov, A., et al. (2009). Kinesin-1 regulates microtubule dynamics via a c-Jun N-terminal kinase-dependent mechanism. *J. Biol. Chem.* 284, 31992–32001. doi: 10.1074/jbc.M109.007906

D'Arcy, M. S. (2019). Cell death: a review of the major forms of apoptosis, necrosis and autophagy. *Cell Biol. Int.* 43, 582–592. doi: 10.1002/cbin.11137

Degterev, A., Huang, Z., Boyce, M., Li, Y., Jagtap, P., Mizushima, N., et al. (2005). Chemical inhibitor of nonapoptotic cell death with therapeutic potential for ischemic brain injury. *Nat. Chem. Biol.* 1, 112–119. doi: 10.1038/nchembio711

Diaz-Perdigon, T., Belloch, F. B., Ricobaraza, A., Elboray, E. E., Suzuki, T., Tordera, R. M., et al. (2020). Early sirtuin 2 inhibition prevents age-related cognitive decline in a senescence-accelerated mouse model. *Neuropsychopharmacology* 45, 347–357. doi: 10.1038/s41386-019-0503-8

Dompierre, J. P., Godin, J. D., Charrin, B. C., Cordelières, F. P., King, S. J., Humbert, S., et al. (2007). Histone deacetylase 6 inhibition compensates for the transport deficit in Huntington's disease by increasing tubulin acetylation. *J. Neurosci.* 27, 3571–3583. doi: 10.1523/jneurosci.0037-07.2007

Eddé, B., Rossier, J., Le Caer, J. P., Desbruyères, E., Gros, F., and Denoulet, P. (1990). Posttranslational glutamylation of alpha-tubulin. *Science* 247, 83–85. doi: 10.1126/science.1967194

Eira, J., Silva, C. S., Sousa, M. M., and Liz, M. A. (2016). The cytoskeleton as a novel therapeutic target for old neurodegenerative disorders. *Prog. Neurobiol.* 141, 61–82. doi: 10.1016/j.pneurobio.2016.04.007

Fan, Y., Cui, Y., Hao, W., Chen, M., Liu, Q., Wang, Y., et al. (2021). Carrier-free highly drug-loaded biomimetic nanosuspensions encapsulated by cancer cell membrane based on homology and active targeting for the treatment of glioma. *Bioact. Mater.* 6, 4402–4414. doi: 10.1016/j.bioactmat.2021.04.027

Fang, Y. C., Chan, L., Liou, J. P., Tu, Y. K., Lai, M. J., Chen, C. I., et al. (2020). HDAC inhibitor protects chronic cerebral hypoperfusion and oxygen-glucose deprivation injuries via H3K14 and H4K5 acetylation-mediated BDNF expression. *J. Cell Mol. Med.* 24, 6966–6977. doi: 10.1111/jcmm.15358

Felgner, H., Frank, R., Biernat, J., Mandelkow, E. M., Mandelkow, E., Ludin, B., et al. (1997). Domains of neuronal microtubule-associated proteins and flexural rigidity of microtubules. *J. Cell Biol.* 138, 1067–1075. doi: 10.1083/jcb.138.5.1067

Fernández-Barrera, J., Correas, I., and Alonso, M. A. (2018). Age-related neuropathies and tubulin acetylation. *Aging* 10, 524–525. doi: 10.18632/aging.101432

Ferrante, R. J., Kubilus, J. K., Lee, J., Ryu, H., Beesen, A., Zucker, B., et al. (2003). Histone deacetylase inhibition by sodium butyrate chemotherapy ameliorates the neurodegenerative phenotype in Huntington's disease mice. *J. Neurosci.* 23, 9418–9427. doi: 10.1523/jneurosci.23-28-09418.2003

Fifre, A., Sponne, I., Koziel, V., Kriem, B., Yen Potin, F. T., Bihain, B. E., et al. (2006). Microtubule-associated protein MAP1A, MAP1B, and MAP2 proteolysis during soluble amyloid beta-peptide-induced neuronal apoptosis. Synergistic involvement of calpain and caspase-3. *J. Biol. Chem.* 281, 229–240. doi: 10.1074/jbc.M507378200

Fischer, I., and Baas, P. W. (2020). Resurrecting the mysteries of big tau. *Trends Neurosci.* 43, 493–504. doi: 10.1016/j.tins.2020.04.007

Fourest-Lieuvin, A., Peris, L., Gache, V., Garcia-Saez, I., Juillan-Binard, C., Lantez, V., et al. (2006). Microtubule regulation in mitosis: tubulin phosphorylation by the cyclin-dependent kinase Cdk1. *Mol. Biol. Cell* 17, 1041–1050. doi: 10.1091/mbc.e05-07-0621

Fukushima, N., Furuta, D., Hidaka, Y., Moriyama, R., and Tsujiuchi, T. (2009). Post-translational modifications of tubulin in the nervous system. *J. Neurochem.* 109, 683–693. doi: 10.1111/j.1471-4159.2009.06013.x

Gadadhar, S., Bodakuntla, S., Natarajan, K., and Janke, C. (2017). The tubulin code at a glance. *J. Cell Sci.* 130, 1347–1353. doi: 10.1242/jcs.199471

Gallart-Palau, X., Serra, A., Qian, J., Chen, C. P., Kalaria, R. N., and Sze, S. K. (2015). Temporal lobe proteins implicated in synaptic failure exhibit differential expression and deamidation in vascular dementia. *Neurochem Int* 80, 87–98. doi: 10.1016/j.neuint.2014.12.002

Galluzzi, L., Vitale, I., Aaronson, S. A., Abrams, J. M., Adam, D., Agostinis, P., et al. (2018). Molecular mechanisms of cell death: recommendations of the nomenclature committee on cell death 2018. *Cell Death Differ.* 25, 486–541. doi: 10.1038/s41418-017-0012-4

Gemmell, E., Bosomworth, H., Allan, L., Hall, R., Khundakar, A., Oakley, A. E., et al. (2012). Hippocampal neuronal atrophy and cognitive function in delayed poststroke and aging-related dementias. *Stroke* 43, 808–814. doi: 10.1161/strokeaha.111.636498

Gevorkian, G., Gonzalez-Noriega, A., Acero, G., Ordoñez, J., Michalak, C., Munguia, M. E., et al. (2008). Amyloid-beta peptide binds to microtubule-associated protein 1B (MAP1B). *Neurochem. Int.* 52, 1030–1036. doi: 10.1016/j.neuint.2007.10.020

Giannakopoulos, P., Gold, G., von Gunten, A., Hof, P. R., and Bouras, C. (2009). Pathological substrates of cognitive decline in Alzheimer's disease. *Front. Neurol. Neurosci.* 24:20–29. doi: 10.1159/000197881

Goedert, M. (2016). The ordered assembly of tau is the gain-of-toxic function that causes human tauopathies. *Alzheimers Dement.* 12, 1040–1050. doi: 10.1016/j.jalz.2016.09.001

Goodson, H. V., and Jonasson, E. M. (2018). Microtubules and microtubule-associated proteins. *Cold Spring Harb. Perspect. Biol.* 10:a022608. doi: 10.1101/cshperspect.a022608

Gornstein, E., and Schwarz, T. L. (2014). The paradox of paclitaxel neurotoxicity: mechanisms and unanswered questions. *Neuropharmacology* 76(Pt. A), 175–183. doi: 10.1016/j.neuropharm.2013.08.016

Govindpani, K., McNamara, L. G., Smith, N. R., Vinnakota, C., Waldvogel, H. J., Faull, R. L., et al. (2019). Vascular Dysfunction in Alzheimer's disease: a prelude to the pathological process or a consequence of it? *J. Clin. Med.* 8:651. doi: 10.3390/jcm8050651

Hasegawa, S., Miyoshi, Y., Egawa, C., Ishitobi, M., Taguchi, T., Tamaki, Y., et al. (2003). Prediction of response to docetaxel by quantitative analysis of class I and III beta-tubulin isotype mRNA expression in human breast cancers. *Clin. Cancer Res.* 9, 2992–2997.

Himmler, A., Drechsel, D., Kirschner, M. W., and Martin, D. W. Jr. (1989). Tau consists of a set of proteins with repeated C-terminal microtubule-binding domains and variable N-terminal domains. *Mol. Cell Biol.* 9, 1381–1388. doi: 10.1128/mcb.9.4.1381

Horio, T., and Murata, T. (2014). The role of dynamic instability in microtubule organization. *Front. Plant Sci.* 5:511. doi: 10.3389/fpls.2014.00511

Hubbert, C., Guardiola, A., Shao, R., Kawaguchi, Y., Ito, A., Nixon, A., et al. (2002). HDAC6 is a microtubule-associated deacetylase. *Nature* 417, 455–458. doi: 10.1038/417455a

Hyman, A. A., Chrétien, D., Arnal, I., and Wade, R. H. (1995). Structural changes accompanying GTP hydrolysis in microtubules: information from a slowly hydrolyzable analogue guanylyl-(alpha,beta)-methylene-diphosphonate. *J. Cell Biol.* 128, 117–125. doi: 10.1083/jcb.128.1.117

Iadecola, C. (2013). The pathobiology of vascular dementia. *Neuron* 80, 844–866. doi: 10.1016/j.neuron.2013.10.008

Ihara, M., Polvikoski, T. M., Hall, R., Slade, J. Y., Perry, R. H., Oakley, A. E., et al. (2010). Quantification of myelin loss in frontal lobe white matter in vascular dementia, Alzheimer's disease, and dementia with Lewy bodies. *Acta Neuropathol.* 119, 579–589. doi: 10.1007/s00401-009-0635-8

Ikegami, K., Sato, S., Nakamura, K., Ostrowski, L. E., and Setou, M. (2010). Tubulin polyglutamylation is essential for airway ciliary function through the regulation of beating asymmetry. *Proc. Natl. Acad. Sci. U.S.A.* 107, 10490–10495. doi: 10.1073/pnas.1002128107

Ivashko-Pachima, Y., and Gozes, I. (2021). Activity-dependent neuroprotective protein (ADNP)-end-binding protein (EB) interactions regulate microtubule dynamics toward protection against tauopathy. *Prog. Mol. Biol. Transl. Sci.* 177, 65–90. doi: 10.1016/bs.pmbts.2020.07.008

Janke, C. (2014). The tubulin code: molecular components, readout mechanisms, and functions. *J. Cell Biol.* 206, 461–472. doi: 10.1083/jcb.201406055

Janke, C., and Bulinski, J. C. (2011). Post-translational regulation of the microtubule cytoskeleton: mechanisms and functions. *Nat. Rev. Mol. Cell Biol.* 12, 773–786. doi: 10.1038/nrm3227

Janke, C., and Magiera, M. M. (2020). The tubulin code and its role in controlling microtubule properties and functions. *Nat. Rev. Mol. Cell Biol.* 21, 307–326. doi: 10.1038/s41580-020-0214-3

Janning, D., Igaev, M., Sündermann, F., Brühmann, J., Beutel, O., Heinisch, J. J., et al. (2014). Single-molecule tracking of tau reveals fast kiss-and-hop

interaction with microtubules in living neurons. *Mol. Biol. Cell* 25, 3541–3551. doi: 10.1091/mbc.E14-06-1099

Jellinger, K. A. (2013). Pathology and pathogenesis of vascular cognitive impairment-a critical update. *Front. Aging Neurosci.* 5:17. doi: 10.3389/fnagi.2013.00017

Kalaria, R. N. (2018). The pathology and pathophysiology of vascular dementia. *Neuropharmacology* 134(Pt. B), 226–239. doi: 10.1016/j.neuropharm.2017.12.030

Kalaria, R. N., and Ballard, C. (1999). Overlap between pathology of Alzheimer disease and vascular dementia. *Alzheimer Dis. Assoc. Disord.* 13(Suppl. 3), S115–S123. doi: 10.1097/00002093-199912003-00017

Kandimalla, R., Manczak, M., Yin, X., Wang, R., and Reddy, P. H. (2018). Hippocampal phosphorylated tau induced cognitive decline, dendritic spine loss and mitochondrial abnormalities in a mouse model of Alzheimer's disease. *Hum. Mol. Genet.* 27, 30–40. doi: 10.1093/hmg/ddx381

Katsetos, C. D., Legido, A., Perentes, E., and Mörk, S. J. (2003). Class III beta-tubulin isotype: a key cytoskeletal protein at the crossroads of developmental neurobiology and tumor neuropathology. *J. Child Neurol.* 18, 851–866;discussion 867. doi: 10.1177/088307380301801205

Kimura, Y., Kurabe, N., Ikegami, K., Tsutsumi, K., Konishi, Y., Kaplan, O. I., et al. (2010). Identification of tubulin deglutamylase among *Caenorhabditis elegans* and mammalian cytosolic carboxypeptidases (CCPs). *J. Biol. Chem.* 285, 22936–22941. doi: 10.1074/jbc.C110.128280

Kril, J. J., Patel, S., Harding, A. J., and Halliday, G. M. (2002). Patients with vascular dementia due to microvascular pathology have significant hippocampal neuronal loss. *J. Neurol. Neurosurg. Psychiatry* 72, 747–751. doi: 10.1136/jnnp.72.6.747

Kumar, R. A., Pilz, D. T., Babatz, T. D., Cushion, T. D., Harvey, K., Topf, M., et al. (2010). TUBA1A mutations cause wide spectrum lissencephaly (smooth brain) and suggest that multiple neuronal migration pathways converge on alpha tubulins. *Hum. Mol. Genet.* 19, 2817–2827. doi: 10.1093/hmg/ddq182

Lehrer, S., and Rheinstein, P. H. (2019). Transspinal delivery of drugs by transdermal patch back-of-neck for Alzheimer's disease: a new route of administration. *Discov. Med.* 27, 37–43.

Lewis, H., Beher, D., Cookson, N., Oakley, A., Piggott, M., Morris, C. M., et al. (2006). Quantification of Alzheimer pathology in ageing and dementia: age-related accumulation of amyloid-beta(42) peptide in vascular dementia. *Neuropathol. Appl. Neurobiol.* 32, 103–118. doi: 10.1111/j.1365-2990.2006.00696.x

L'Hernault, S. W., and Rosenbaum, J. L. (1985). Chlamydomonas alpha-tubulin is posttranslationally modified by acetylation on the epsilon-amino group of a lysine. *Biochemistry* 24, 473–478. doi: 10.1021/bi00323a034

Li, Y., and Black, M. M. (1996). Microtubule assembly and turnover in growing axons. *J. Neurosci.* 16, 531–544. doi: 10.1523/JNEUROSCI.16-02-00531.1996

Li, L., and Yang, X. J. (2015). Tubulin acetylation: responsible enzymes, biological functions and human diseases. *Cell Mol. Life Sci.* 72, 4237–4255. doi: 10.1007/s00018-015-2000-5

Li, M., Mukaetova-Ladinska, E. B., and Kalaria, R. N. (2014). *Tau Protein Changes in Vascular Dementia*. Master thesis.

Liang, S., Zheng, Y., Lei, L., Deng, X., Ai, J., Li, Y., et al. (2020). Corydalis edulis total alkaloids (CETA) ameliorates cognitive dysfunction in rat model of Alzheimer disease through regulation of the antioxidant stress and MAP2/NF-κB. *J. Ethnopharmacol.* 251:112540. doi: 10.1016/j.jep.2019.112540

Liepins, A., and Bustamante, J. O. (1994). Cell injury and apoptosis. *Scanning Microsc.* 8, 631–641;discussion 641–633.

Liu, M., Sui, D., Dexheimer, T., Hovde, S., Deng, X., Wang, K. W., et al. (2020). Hyperphosphorylation renders tau prone to aggregate and to cause cell death. *Mol. Neurobiol.* 57, 4704–4719. doi: 10.1007/s12035-020-02034-w

Ludueña, R. F. (1998). Multiple forms of tubulin: different gene products and covalent modifications. *Int. Rev. Cytol.* 178, 207–275. doi: 10.1016/s0074-7696(08)62138-5

Ludueña, R. F. (2013). A hypothesis on the origin and evolution of tubulin. *Int. Rev. Cell Mol. Biol.* 302, 41–185. doi: 10.1016/b978-0-12-407699-0.00002-9

Ludueña, R. F., Shooter, E. M., and Wilson, L. (1977). Structure of the tubulin dimer. *J. Biol. Chem.* 252, 7006–7014.

Magiera, M. M., and Janke, C. (2014). Post-translational modifications of tubulin. *Curr. Biol.* 24, R351–R354. doi: 10.1016/j.cub.2014.03.032

Magiera, M. M., Bodakuntla, S., Žiak, J., Lacomme, S., Marques Sousa, P., Leboucher, S., et al. (2018). Excessive tubulin polyglutamylation causes neurodegeneration and perturbs neuronal transport. *EMBO J.* 37:e100440. doi: 10.15252/embj.2018100440

Manczak, M., Kandimalla, R., Yin, X., and Reddy, P. H. (2018). Hippocampal mutant APP and amyloid beta-induced cognitive decline, dendritic spine loss, defective autophagy, mitophagy and mitochondrial abnormalities in a mouse model of Alzheimer's disease. *Hum. Mol. Genet.* 27, 1332–1342. doi: 10.1093/hmg/ddy042

Mandelkow, E., and Mandelkow, E. M. (1995). Microtubules and microtubule-associated proteins. *Curr. Opin. Cell Biol.* 7, 72–81. doi: 10.1016/0955-0674(95)80047-6

Martínez-Pinilla, E., Ordóñez, C., Del Valle, E., Navarro, A., and Tolivia, J. (2016). Regional and gender study of neuronal density in brain during aging and in Alzheimer's disease. *Front. Aging Neurosci.* 8:213. doi: 10.3389/fnagi.2016.00213

McAleese, K. E., Alafuzoff, I., Charidimou, A., De Reuck, J., Grinberg, L. T., Hainsworth, A. H., et al. (2016). Post-mortem assessment in vascular dementia: advances and aspirations. *BMC Med.* 14:129. doi: 10.1186/s12916-016-0676-5

McKhann, G. M., Knopman, D. S., Chertkow, H., Hyman, B. T., Jack, C. R. Jr., Kawas, C. H., et al. (2011). The diagnosis of dementia due to Alzheimer's disease: recommendations from the national institute on aging-Alzheimer's association workgroups on diagnostic guidelines for Alzheimer's disease. *Alzheimers Dement.* 7, 263–269. doi: 10.1016/j.jalz.2011.03.005

Melková, K., Zapletal, V., Narasimhan, S., Jansen, S., Hritz, J., Škrabana, R., et al. (2019). Structure and functions of microtubule associated proteins tau and MAP2c: similarities and differences. *Biomolecules* 9:105. doi: 10.3390/biom9030105

Mitchison, T., and Kirschner, M. (1984). Dynamic instability of microtubule growth. *Nature* 312, 237–242. doi: 10.1038/312237a0

Motawi, T. M. K., Abdel-Nasser, Z. M., and Shahin, N. N. (2020). Ameliorative effect of necrosulfonamide in a rat model of Alzheimer's disease: targeting mixed lineage kinase domain-like protein-mediated necroptosis. *ACS Chem. Neurosci.* 11, 3386–3397. doi: 10.1021/acschemneuro.0c00516

Mukaetova-Ladinska, E. B., Abdel-All, Z., Mugica, E. S., Li, M., Craggs, L. J., Oakley, A. E., et al. (2015). Tau proteins in the temporal and frontal cortices in patients with vascular dementia. *J. Neuropathol. Exp. Neurol.* 74, 148–157. doi: 10.1097/nen.0000000000000157

Mukaetova-Ladinska, E. B., Harrington, C. R., Roth, M., and Wischik, C. M. (1993). Biochemical and anatomical redistribution of tau protein in Alzheimer's disease. *Am. J. Pathol.* 143, 565–578.

Mukaetova-Ladinska, E. B., Xuereb, J. H., Garcia-Sierra, F., Hurt, J., Gertz, H. J., Hills, R., et al. (2009). Lewy body variant of Alzheimer's disease: selective neocortical loss of t-SNARE proteins and loss of MAP2 and alpha-synuclein in medial temporal lobe. *ScientificWorldJournal* 9, 1463–1475. doi: 10.1100/tsw.2009.151

Murphy, D. B., Wallis, K. T., Machlin, P. S., Ratrie, H. III, and Cleveland, D. W. (1987). The sequence and expression of the divergent beta-tubulin in chicken erythrocytes. *J. Biol. Chem.* 262, 14305–14312.

Nixon, R. A., and Yang, D. S. (2011). Autophagy failure in Alzheimer's disease–locating the primary defect. *Neurobiol. Dis.* 43, 38–45. doi: 10.1016/j.nbd.2011.01.021

Nogales, E. (2013). "Tubulin and Its Isoforms," in *Encyclopedia of Biological Chemistry*, 2nd Edn, eds W. J. Lennarz and M. D. Lane (Waltham, MA: Academic Press), 450–453.

Nogales, E., and Wang, H. W. (2006). Structural intermediates in microtubule assembly and disassembly: how and why? *Curr. Opin. Cell Biol.* 18, 179–184. doi: 10.1016/j.ceb.2006.02.009

Nogales, E., Wolf, S. G., and Downing, K. H. (1998). Structure of the alpha beta tubulin dimer by electron crystallography. *Nature* 391, 199–203. doi: 10.1038/34465

North, B. J., Marshall, B. L., Borra, M. T., Denu, J. M., and Verdin, E. (2003). The human Sir2 ortholog, SIRT2, is an NAD+-dependent tubulin deacetylase. *Mol. Cell* 11, 437–444. doi: 10.1016/s1097-2765(03)00038-8

Oblinger, M. M., Argasinski, A., Wong, J., and Kosik, K. S. (1991). Tau gene expression in rat sensory neurons during development and regeneration. *J. Neurosci.* 11, 2453–2459. doi: 10.1523/jneurosci.11-08-02453.1991

Ohishi, Y., Oda, Y., Basaki, Y., Kobayashi, H., Wake, N., Kuwano, M., et al. (2007). Expression of beta-tubulin isotypes in human primary ovarian carcinoma. *Gynecol. Oncol.* 105, 586–592. doi: 10.1016/j.ygyno.2007.01.044

Pathak, N., Obara, T., Mangos, S., Liu, Y., and Drummond, I. A. (2007). The zebrafish fleer gene encodes an essential regulator of cilia tubulin polyglutamylation. *Mol. Biol. Cell* 18, 4353–4364. doi: 10.1091/mbc.e07-06-0537

Paturle-Lafanechère, L., Manier, M., Trigault, N., Pirollet, F., Mazarguil, H., and Job, D. (1994). Accumulation of delta 2-tubulin, a major tubulin variant that cannot be tyrosinated, in neuronal tissues and in stable microtubule assemblies. *J. Cell Sci.* 107(Pt. 6), 1529–1543.

Penazzi, L., Bakota, L., and Brandt, R. (2016). Microtubule dynamics in neuronal development, plasticity, and neurodegeneration. *Int. Rev. Cell Mol. Biol.* 321, 89–169. doi: 10.1016/bs.ircmb.2015.09.004

Peng, C., Gathagan, R. J., and Lee, V. M. (2018). Distinct α-Synuclein strains and implications for heterogeneity among α-Synucleinopathies. *Neurobiol. Dis.* 109(Pt. B), 209–218. doi: 10.1016/j.nbd.2017.07.018

Peters, J. D., Furlong, M. T., Asai, D. J., Harrison, M. L., and Geahlen, R. L. (1996). Syk, activated by cross-linking the B-cell antigen receptor, localizes to the cytosol where it interacts with and phosphorylates alpha-tubulin on tyrosine. *J. Biol. Chem.* 271, 4755–4762. doi: 10.1074/jbc.271.9.4755

Prota, A. E., Magiera, M. M., Kuijpers, M., Bargsten, K., Frey, D., Wieser, M., et al. (2013). Structural basis of tubulin tyrosination by tubulin tyrosine ligase. *J. Cell Biol.* 200, 259–270. doi: 10.1083/jcb.201211017

Qiu, C., Kivipelto, M., and von Strauss, E. (2009). Epidemiology of Alzheimer's disease: occurrence, determinants, and strategies toward intervention. *Dialogues Clin. Neurosci.* 11, 111–128.

Reddy, P. H., Yin, X., Manczak, M., Kumar, S., Pradeepkiran, J. A., Vijayan, M., et al. (2018). Mutant APP and amyloid beta-induced defective autophagy, mitophagy, mitochondrial structural and functional changes and synaptic damage in hippocampal neurons from Alzheimer's disease. *Hum. Mol. Genet.* 27, 2502–2516. doi: 10.1093/hmg/ddy154

Redeker, V. (2010). Mass spectrometry analysis of C-terminal posttranslational modifications of tubulins. *Methods Cell Biol.* 95, 77–103. doi: 10.1016/s0091-679x(10)95006-1

Redeker, V., Levilliers, N., Schmitter, J. M., Le Caer, J. P., Rossier, J., Adoutte, A., et al. (1994). Polyglycylation of tubulin: a posttranslational modification in axonemal microtubules. *Science* 266, 1688–1691. doi: 10.1126/science.7992051

Ren, Y., Zhao, J., and Feng, J. (2003). Parkin binds to alpha/beta tubulin and increases their ubiquitination and degradation. *J Neurosci* 23, 3316–3324. doi: 10.1523/jneurosci.23-08-03316.2003

Rocha, C., Papon, L., Cacheux, W., Marques Sousa, P., Lascano, V., Tort, O., et al. (2014). Tubulin glycylases are required for primary cilia, control of cell proliferation and tumor development in colon. *EMBO J.* 33, 2247–2260. doi: 10.15252/embj.201488466

Rogowski, K., van Dijk, J., Magiera, M. M., Bosc, C., Deloulme, J. C., Bosson, A., et al. (2010). A family of protein-deglutamylating enzymes associated with neurodegeneration. *Cell* 143, 564–578. doi: 10.1016/j.cell.2010.10.014

Rosas-Acosta, G., Russell, W. K., Deyrieux, A., Russell, D. H., and Wilson, V. G. (2005). A universal strategy for proteomic studies of SUMO and other ubiquitin-like modifiers. *Mol. Cell Proteom.* 4, 56–72. doi: 10.1074/mcp.M400149-MCP200

Savastano, A., Flores, D., Kadavath, H., Biernat, J., Mandelkow, E., and Zweckstetter, M. (2021). Disease-associated tau phosphorylation hinders tubulin assembly within tau condensates. *Angew. Chem. Int. Edn. Engl.* 60, 726–730. doi: 10.1002/anie.202011157

Selenica, M. L., Benner, L., Housley, S. B., Manchec, B., Lee, D. C., Nash, K. R., et al. (2014). Histone deacetylase 6 inhibition improves memory and reduces total tau levels in a mouse model of tau deposition. *Alzheimers Res. Ther.* 6:12. doi: 10.1186/alzrt241

Serrano-Pozo, A., Frosch, M. P., Masliah, E., and Hyman, B. T. (2011). Neuropathological alterations in Alzheimer disease. *Cold Spring Harb Perspect. Med.* 1:a006189. doi: 10.1101/cshperspect.a006189

Sferra, A., Nicita, F., and Bertini, E. (2020). Microtubule dysfunction: a common feature of neurodegenerative diseases. *Int. J. Mol. Sci.* 21:7354. doi: 10.3390/ijms21197354

Shamitko-Klingensmith, N., Boyd, J. W., and Legleiter, J. (2016). Microtubule modification influences cellular response to amyloid-β exposure. *AIMS Biophys.* 3, 261–285. doi: 10.3934/biophy.2016.2.261

Shashi, V., Magiera, M. M., Klein, D., Zaki, M., Schoch, K., Rudnik-Schöneborn, S., et al. (2018). Loss of tubulin deglutamylase CCP1 causes infantile-onset neurodegeneration. *EMBO J.* 37:e100540. doi: 10.15252/embj.2018100540

Šimić, G., Babić Leko, M., Wray, S., Harrington, C., Delalle, I., Jovanov-Milošević, N., et al. (2016). Tau protein hyperphosphorylation and aggregation in Alzheimer's disease and other tauopathies, and possible neuroprotective strategies. *Biomolecules* 6:6. doi: 10.3390/biom6010006

Skrobot, O. A., Black, S. E., Chen, C., DeCarli, C., Erkinjuntti, T., Ford, G. A., et al. (2018). Progress toward standardized diagnosis of vascular cognitive impairment: guidelines from the vascular impairment of cognition classification consensus study. *Alzheimers Dement.* 14, 280–292. doi: 10.1016/j.jalz.2017.09.007

Slaughter, T., and Black, M. M. (2003). STOP (stable-tubule-only-polypeptide) is preferentially associated with the stable domain of axonal microtubules. *J. Neurocytol.* 32, 399–413. doi: 10.1023/b:Neur.0000011334.70648.87

Smith, E. E. (2017). Clinical presentations and epidemiology of vascular dementia. *Clin. Sci.* 131, 1059–1068. doi: 10.1042/cs20160607

Song, Y., Kirkpatrick, L. L., Schilling, A. B., Helseth, D. L., Chabot, N., Keillor, J. W., et al. (2013). Transglutaminase and polyamination of tubulin: posttranslational modification for stabilizing axonal microtubules. *Neuron* 78, 109–123. doi: 10.1016/j.neuron.2013.01.036

Steinberg, M., Shao, H., Zandi, P., Lyketsos, C. G., Welsh-Bohmer, K. A., Norton, M. C., et al. (2008). Point and 5-year period prevalence of neuropsychiatric symptoms in dementia: the cache county study. *Int. J. Geriatr. Psychiatry* 23, 170–177. doi: 10.1002/gps.1858

Suemoto, C. K., Ferretti-Rebustini, R. E., Rodriguez, R. D., Leite, R. E., Soterio, L., Brucki, S. M., et al. (2017). Neuropathological diagnoses and clinical correlates in older adults in Brazil: a cross-sectional study. *PLoS Med.* 14:e1002267. doi: 10.1371/journal.pmed.1002267

Sullivan, K. F., and Cleveland, D. W. (1986). Identification of conserved isotype-defining variable region sequences for four vertebrate beta tubulin polypeptide classes. *Proc. Natl. Acad. Sci. U.S.A.* 83, 4327–4331. doi: 10.1073/pnas.83.12.4327

Suryavanshi, S., Eddé, B., Fox, L. A., Guerrero, S., Hard, R., Hennessey, T., et al. (2010). Tubulin glutamylation regulates ciliary motility by altering inner dynein arm activity. *Curr. Biol.* 20, 435–440. doi: 10.1016/j.cub.2009.12.062

Telegina, D. V., Suvorov, G. K., Kozhevnikova, O. S., and Kolosova, N. G. (2019). Mechanisms of neuronal death in the cerebral cortex during aging and development of Alzheimer's disease-like pathology in rats. *Int. J. Mol. Sci.* 20:5632. doi: 10.3390/ijms20225632

Theofilas, P., Ehrenberg, A. J., Nguy, A., Thackrey, J. M., Dunlop, S., Mejia, M. B., et al. (2018). Probing the correlation of neuronal loss, neurofibrillary tangles, and cell death markers across the Alzheimer's disease Braak stages: a quantitative study in humans. *Neurobiol. Aging* 61, 1–12. doi: 10.1016/j.neurobiolaging.2017.09.007

Tischfield, M. A., Baris, H. N., Wu, C., Rudolph, G., Van Maldergem, L., He, W., et al. (2010). Human TUBB3 mutations perturb microtubule dynamics, kinesin interactions, and axon guidance. *Cell* 140, 74–87. doi: 10.1016/j.cell.2009.12.011

Tsai, R. M., Miller, Z., Koestler, M., Rojas, J. C., Ljubenkov, P. A., Rosen, H. J., et al. (2020). Reactions to multiple ascending doses of the microtubule stabilizer TPI-287 in patients with alzheimer disease, progressive supranuclear palsy, and corticobasal syndrome: a randomized clinical trial. *JAMA Neurol.* 77, 215–224. doi: 10.1001/jamaneurol.2019.3812

Vu, H. T., Akatsu, H., Hashizume, Y., Setou, M., and Ikegami, K. (2017). Increase in α-tubulin modifications in the neuronal processes of hippocampal neurons in both kainic acid-induced epileptic seizure and Alzheimer's disease. *Sci. Rep.* 7:40205. doi: 10.1038/srep40205

Walgren, J. L., Vincent, T. S., Schey, K. L., and Buse, M. G. (2003). High glucose and insulin promote O-GlcNAc modification of proteins, including alpha-tubulin. *Am. J. Physiol. Endocrinol. Metab.* 284, E424–E434. doi: 10.1152/ajpendo.00382.2002

Weaver, B. A. (2014). How Taxol/paclitaxel kills cancer cells. *Mol. Biol. Cell* 25, 2677–2681. doi: 10.1091/mbc.E14-04-0916

Westermann, S., and Weber, K. (2003). Post-translational modifications regulate microtubule function. *Nat. Rev. Mol. Cell Biol.* 4, 938–947. doi: 10.1038/nrm1260

Wischik, C. M., Edwards, P. C., Lai, R. Y., Gertz, H. N., Xuereb, J. H., Paykel, E. S., et al. (1995). Quantitative analysis of tau protein in paired helical filament preparations: implications for the role of tau protein phosphorylation in PHF assembly in Alzheimer's disease. *Neurobiol. Aging* 16, 409–417;discussion 418–431. doi: 10.1016/0197-4580(95)97327-d

Wloga, D., and Gaertig, J. (2010). Post-translational modifications of microtubules. *J. Cell Sci.* 123(Pt. 20), 3447–3455. doi: 10.1242/jcs.063727

Wong, C. C., Xu, T., Rai, R., Bailey, A. O., Yates, J. R. III, Wolf, Y. I., et al. (2007). Global analysis of posttranslational protein arginylation. *PLoS Biol.* 5:e258. doi: 10.1371/journal.pbio.0050258

Xiao, H., El Bissati, K., Verdier-Pinard, P., Burd, B., Zhang, H., Kim, K., et al. (2010). Post-translational modifications to *Toxoplasma gondii* alpha- and beta-tubulins include novel C-terminal methylation. *J. Proteome Res.* 9, 359–372. doi: 10.1021/pr900699a

Xie, C., and Miyasaka, T. (2016). The role of the carboxyl-terminal sequence of tau and MAP2 in the pathogenesis of dementia. *Front. Mol. Neurosci.* 9:158. doi: 10.3389/fnmol.2016.00158

Yang, S. H., Lee, D. K., Shin, J., Lee, S., Baek, S., Kim, J., et al. (2017). Nec-1 alleviates cognitive impairment with reduction of Aβ and tau abnormalities in APP/PS1 mice. *EMBO Mol. Med.* 9, 61–77. doi: 10.15252/emmm.201606566

Yu, I., Garnham, C. P., and Roll-Mecak, A. (2015). Writing and reading the tubulin code. *J. Biol. Chem.* 290, 17163–17172. doi: 10.1074/jbc.R115.637447

Yu, T. W., Lane, H. Y., and Lin, C. H. (2021). Novel therapeutic approaches for Alzheimer's disease: an updated review. *Int. J. Mol. Sci.* 22:8208. doi: 10.3390/ijms22158208

Yuan, J., Amin, P., and Ofengeim, D. (2019). Necroptosis and RIPK1-mediated neuroinflammation in CNS diseases. *Nat. Rev. Neurosci.* 20, 19–33. doi: 10.1038/s41583-018-0093-1

Zempel, H., Luedtke, J., Kumar, Y., Biernat, J., Dawson, H., Mandelkow, E., et al. (2013). Amyloid-beta oligomers induce synaptic damage via Tau-dependent microtubule severing by TTLL6 and spastin. *EMBO J.* 32, 2920–2937. doi: 10.1038/emboj.2013.207

Zhang, B., Carroll, J., Trojanowski, J. Q., Yao, Y., Iba, M., Potuzak, J. S., et al. (2012). The microtubule-stabilizing agent, epothilone D, reduces axonal dysfunction, neurotoxicity, cognitive deficits, and Alzheimer-like pathology in an interventional study with aged tau transgenic mice. *J. Neurosci.* 32, 3601–3611. doi: 10.1523/jneurosci.4922-11.2012

Zhang, F., Su, B., Wang, C., Siedlak, S. L., Mondragon-Rodriguez, S., Lee, H. G., et al. (2015). Posttranslational modifications of α-tubulin in alzheimer disease. *Transl. Neurodegener.* 4:9. doi: 10.1186/s40035-015-0030-4

Zhang, L., Sheng, S., and Qin, C. (2013). The role of HDAC6 in Alzheimer's disease. *J. Alzheimers Dis.* 33, 283–295. doi: 10.3233/jad-2012-120727

Zhang, S., Si, W., Yu, Q., Wang, Y., and Wu, Y. (2019). Therapeutic effects of combination environmental enrichment with necrostatin-1 on cognition following vascular cognitive impairment in mice. *Eur. J. Inflamm.* 17:2058739219834832. doi: 10.1177/2058739219834832

Conflict of Interest: The authors declare that the research was conducted in the absence of any commercial or financial relationships that could be construed as a potential conflict of interest.

Publisher's Note: All claims expressed in this article are solely those of the authors and do not necessarily represent those of their affiliated organizations, or those of the publisher, the editors and the reviewers. Any product that may be evaluated in this article, or claim that may be made by its manufacturer, is not guaranteed or endorsed by the publisher.

frontiers in Aging Neuroscience

REVIEW
published: 15 November 2021
doi: 10.3389/fnagi.2021.755392

Brain Pathogenesis and Potential Therapeutic Strategies in Myotonic Dystrophy Type 1

Jie Liu[1,2,3], *Zhen-Ni Guo*[1,2,3], *Xiu-Li Yan*[1], *Yi Yang*[1,2,3†] *and Shuo Huang*[1,2,3*]

[1] Department of Neurology, Stroke Center & Clinical Trial and Research Center for Stroke, The First Hospital of Jilin University, Changchun, China, [2] China National Comprehensive Stroke Center, Changchun, China, [3] Jilin Provincial Key Laboratory of Cerebrovascular Disease, Changchun, China

Myotonic dystrophy type 1 (DM1) is the most common muscular dystrophy that affects multiple systems including the muscle and heart. The mutant CTG expansion at the 3′-UTR of the *DMPK* gene causes the expression of toxic RNA that aggregate as nuclear foci. The foci then interfere with RNA-binding proteins, affecting hundreds of mis-spliced effector genes, leading to aberrant alternative splicing and loss of effector gene product functions, ultimately resulting in systemic disorders. In recent years, increasing clinical, imaging, and pathological evidence have indicated that DM1, though to a lesser extent, could also be recognized as true brain diseases, with more and more researchers dedicating to develop novel therapeutic tools dealing with it. In this review, we summarize the current advances in the pathogenesis and pathology of central nervous system (CNS) deficits in DM1, intervention measures currently being investigated are also highlighted, aiming to promote novel and cutting-edge therapeutic investigations.

Keywords: myotonic dystrophy type 1, central nervous system, pathology, mechanism, treatment

OPEN ACCESS

Edited by:
Natalia Salvadores, Universidad Mayor, Chile

Reviewed by:
Stojan Z. Peric, University of Belgrade, Serbia
Bulmaro Cisneros, Instituto Politécnico Nacional de México (CINVESTAV), Mexico
Corrado Italo Angelini, University of Padua, Italy

***Correspondence:**
Shuo Huang
boreas0729@ jlu.edu.cn

†***ORCID:***
Yi Yang
orcid.org/0000-0002-9729-8522

Received: *08 August 2021*
Accepted: *20 October 2021*
Published: *15 November 2021*

Citation:
Liu J, Guo Z-N, Yan X-L, Yang Y and Huang S (2021) Brain Pathogenesis and Potential Therapeutic Strategies in Myotonic Dystrophy Type 1. Front. Aging Neurosci. 13:755392. doi: 10.3389/fnagi.2021.755392

INTRODUCTION

Myotonic dystrophies (DM1 and DM2) are inherited autosomal dominant skeletal muscle diseases that are characterized by progressive muscle weakness and myotonia, and involves multisystem engagement. DM1, also known as Steinert disease, is caused by the abnormal expansion of a CTG-trinucleotide repeat in the 3′-UTR of the dystrophia myotonic protein kinase (*DMPK*) gene (Brook et al., 1992; Fu et al., 1992; Mahadevan et al., 1992). In healthy individuals, there are approximately 5–38 CTG repeats in the *DMPK* gene, while DM1 patients harbor 50 to several thousands of repeats. CTG repeats tend to increase throughout aging. And as the number of repeats increase, disease severity escalates and age of onset decreases (Bird, 1993). As a progressively debilitating disease, DM1 tends to have an earlier onset and more severe phenotype from one generation to the next, while symptoms could be highly variable among patients (Udd and Krahe, 2012).

Conventionally, DM1 can be divided into five types: congenital, childhood-onset, juvenile-onset, adult-onset, and late-onset, with the adult-onset form being the most prevalent (De Antonio et al., 2016). In the past few years, several neurological symptoms, including cognitive impairment, behavioral impairment, and sensory-motor neural integration have attracted more

and more attention, indicating cerebral involvement (Meola and Sansone, 2007; Meola and Cardani, 2015). These central nervous system (CNS) deficits among DM1 individuals significantly increase the disease burden, not only affecting neuropsychological domains but also decreasing the whole quality of life. A large clinical longitudinal study of DM1 patients by Miller et al. (2021) demonstrated that cognitive deficits, hypersomnolence, and apathy are critical brain symptoms of adult-onset DM1 caused by the underlying molecular mechanisms. In contrast, depression and anxiety are secondary coping symptoms with chronic physical and emotional stress (Miller et al., 2021). In addition, Simoncini et al. (2020) proved that the severity and progression rate of neurological impairments are highly variable over time, possibly attributed to underlying neuropathology (Mazzoli et al., 2020). The cognitive impairment in DM1 patients can be severe. This varies significantly with the phenotype, including the typical intellectual disability and lower intelligence quotient (IQ) levels in the congenital phenotype (Angeard et al., 2007, 2011; Echenne et al., 2008; Ekström et al., 2008; Douniol et al., 2012), the reading and spelling impairment, autistic behavior, attention deficits, deficiency in the speed of processing and severe difficulties in social interactions in childhood-onset phenotype (Steyaert et al., 1997), and dysfunctional personality, visuospatial deficits, unawareness of disease symptoms and signs, impaired facial expression and emotion recognition, and later apathy in the adult-onset phenotype (Meola et al., 2003; Winblad et al., 2006; Sansone et al., 2007; Takeda et al., 2009; Kobayakawa et al., 2010, 2012; Sistiaga et al., 2010; Jean et al., 2014; Gallais et al., 2015). Compared with the congenital groups, the childhood group shown greater cognitive and adaptive development (Lindeblad et al., 2019). Fatigue and sleep disorders including excessive daytime sleepiness (EDS) are also prominent complaints in DM1 patients (Steyaert et al., 1997; Quera Salva et al., 2006). Since fatigue involves both central and peripheral performances, the sense of tiredness is primarily caused by CNS dysfunction (Angelini and Tasca, 2012). Till now, a variety of neuropsychological tests have been developed to evaluate the CNS involvement in DM1 (Okkersen et al., 2017a; Simoncini et al., 2020). **Tables 1**, **2** briefly summarizes the critical CNS symptoms in DM1 and the recent findings about CNS involvement measured by neuropsychological tests in DM1, respectively (Meola and Sansone, 2007; Subramony et al., 2020). In addition, multiple neuroimaging studies relying on structural and functional explorations suggest a wide range of brain abnormalities in DM1 (Okkersen et al., 2017b; Minnerop et al., 2018; Angelini and Pinzan, 2019), mainly involving white matter (WM) abnormalities, widespread gray matter (GM) atrophy and hypometabolism in the frontal lobes. The primary studies focused on neuroimaging abnormalities in DM1 have been shown in **Tables 3**, **4**. Furthermore, specific patterns of neuroimaging alterations and their correlations with other clinical parameters, such as clinical performances and neuropsychological test results have also been discovered, such as sleepiness might be associated with WM status in the superior longitudinal fasciculus and cingulum (Wozniak et al., 2014), and visuospatial impairment might be correlated with WM abnormalities and cortical atrophy (Cabada et al., 2017). Although the single structural or functional alterations seems to be critical for specific CNS dysfunctions, recent advance further revealed the abnormal functional connectivity patterns in DM1 brain and their effects on different personality traits (Serra et al., 2014, 2016a,b, 2020b). Besides, the main executive dysfunction and memory and visuo-spatial impairment were associated with the whole brain volume loss, but cannot be attributed to focal atrophy in any specific regions (Baldanzi et al., 2016b). Small but extensive WM damages in DM1 patients with normal-appearing WM beyond the signal changes detected with conventional MR imaging might be associated with the neuropsychological deficit (Anderson, 2013; Baldanzi et al., 2016b). This implying the critical effects of disrupted complex neuronal networks on cognitive impairments in DM1. Explorations on the complex neuronal networks and undetected lesions and their complex mechanisms contributing to clinical impairments might provide effective outcome measurements as well as effective therapeutic targets for DM1 CNS deficits. Despite a large amount of imaging and neuropsychological evidence of CNS involvement in DM1, the molecular mechanisms driving these deficits are largely unidentified, and targeted therapies aimed at ameliorating neurological deficits are scarce. This review summarizes the recent advances in the pathology and pathogenesis of CNS disorders in DM1 and the promising therapeutic strategies, hoping to provide new proposals for future investigations.

TABLE 1 | CNS symptom in DM1.

CNS symptom	Related symptoms
Cognitive change	Mental retardation Reduced IQ values MMSE scores decrease Memory deficits Visual-Spatial deficits Attentional deficits Speech and language delay and verbal memory deficits Impaired facial expression and emotion recognition Difficulty in social communication Brain fog
Behavioral abnormality	Executive dysfunction/aphasia Avoidance behavior Impulsivity Personality changes Apathy Anxiety Depression Anosognosia
Sleep disorder	EDS SDB Restless legs syndrome and PLMS REM sleep dysregulation Long nighttime sleep
Fatigue	

DM1, myotonic dystrophy type 1; CNS, central nervous system; IQ, intelligence quotient; MMSE, Mini Mental State Examination; EDS, excessive daytime sleepiness; SDB, sleep disorder breathing; PLMS, periodic limb movements of sleep; REM, rapid eye movement.

TABLE 2 | Neuropsychological tests in DM1.

References	Neuropsychological tests (alterations)	Participants	Main results
Tremblay et al., 2021	WASI-II (Intellectual abilities); FAB (Executive functioning); LARS (Apathy)	11 patients with DM1	Adults with childhood-onset DM1 present relative dependence in regard to IADLs, the level of which is, at least partially, associated with cognitive impairments
Cabada et al., 2021	Digit Span from TBR, Spatial Span from the WMS-III scale, and Letter-Number Sequencing from the WAIS-IV scale (Working memory); BVRT-Part C, Cubes from TBR (Visuospatial constructional ability); TMT-B (Alternating attention); TAVEC (Verbal memory); Word Accentuation Test-30 (Verbal IQ)	33 patients with DM1	DM1 patients have a significant deterioration in test performance that measures working memory and visuospatial skills, which are significantly associated with white matter lesion load
Lopez-Titla et al., 2021	MMSE and MOCA (Cognitive impairment); 19 CANTAB tests (Cognitive domains of attention, global memory, visual memory, and executive functions)	22 patients with DM1 vs. 22 healthy controls	Patients with DM1 have significant deficits in memory and problem-solving tasks WM integrity degradation at frontal, temporomedial, and parietal lobes could be associated with specific memory impairments in DM1
Woo et al., 2019	Wechsler Adult Intelligence Scale (Intelligence); Rey-Kim memory test (Memory); Executive Intelligence Test (Executive function)	19 patients with DM1	Verbal memory impairment significantly deteriorated in the juvenile-onset DM1 as compared to the adult-onset DM1
Breton et al., 2020	The digit symbol coding subscale of the WAIS-R (Processing speed); CVLT (Learning ability and verbal memory); Ruff 2 & 7 (Sustained and selective attention)	115 patients with adult-onset DM1	DNA methylation at the DMPK gene locus might be a predictor of DM1-related cognitive dysfunction
Romeo et al., 2010a	Raven's progressive Matrices (Non-verbal intelligence); Stroop and Fluency tests (Frontal executive functions); Wechsler Memory Scale and Corsi's Block tests (Memory and learning functions); Rey-Osterrieth Complex Figure (Visuo-spatial abilities)	50 patients with DM1 vs. 14 patients with DM2	There is a specific temporo-insular diffuse lesional pattern in DM1 There might be a possible correlation between cognitive impairment and diffuse frontal lesions Brain involvement might be different in DM1 and DM2, and severer CNS changes are observed in DM1
Meola et al., 2003	SCID-II personality scale (Personality); TMT (Serial ordering and alternation); WCST (Concept formation and set shifting); Stroop Test (Attentional control and response inhibition); TLT (Planning and problem solving)	21 patients with moderately severe DM1	Executive dysfunction and avoidant personality trait are associated with hypoperfusion in frontal and parieto-occipital regions of the brain
Sistiaga et al., 2010	WAIS-III (IQ, attention and working memory); WCST (Categorization and cognitive flexibility); Stroop Color and Word Test (Automatic response inhibition); Raven's Progressive Matrices (Visual deduction, semantic and phonetic verbal fluency); BJLOT (Visuospatial ability); RCF (Visual-motor organization and planning strategies); CalCAP (Maintained attention and simple and complex reaction time); RAVLT (Immediate and delayed memory); MCMI-II (Personality traits and psychopathology)	121 adult patients with DM1 vs. 54 healthy controls	CTG expansion size in DM1 is negatively related to many cognitive and personality deficits The cognitive impairment predominantly affects the frontoparietal lobe
Serra et al., 2014	Clinical interview and Minnesota Multiphasic Personality Inventory-2 (Personality assessment)	27 patients with DM1 vs. 16 matched healthy controls	A continuum of atypical personality profiles ranging from schizotypal personality traits to paranoid personality disorder is discovered in DM1 patients Alterations of functional connectivity of the brain may explain the atypical personality traits observed in DM1 patients
Bertrand et al., 2015	SCL-90-R (Psychological symptoms); NEO-FFI (Personality dimensions); Rosenberg Self-Esteem Scale (Self-esteem); ASIQ (Suicidal ideation); WAIS-R Full Scale IQ (Global intellectual functioning); WAIS-R Information score, WAIS-R Verbal IQ, and Boston Naming Test total score (Language abilities); WAIS-R Picture Completion, WAIS-R Block Design, WAIS-R Performance IQ, Hooper's test, TVPS subtests, and copy of the Rey-Osterrieth Complex Figure (Non-verbal abilities); WAIS-R Digit Span, Ruff 2 & 7 Speed and Accuracy, Stroop subtests, WAIS-R Similarities, Category and Letter verbal fluency, and Raven's progressive matrices (Attention/executive functions); CVLT and Rey-Osterrieth Complex Figure immediate recall, delayed recall, and recognition total scores (Memory)	200 patients with DM1	Psychological traits differ across DM1 phenotypes The presence of higher phobic anxiety and lower self-esteem are associated with lower education, a higher number of CTG repeats, more severe muscular impairment, and lower cognitive functioning
Kobayakawa et al., 2012	RMET and faux pas recognition (ToM)	9 patients with adult-onset DM1	Social cognitive impairment in patients with adult-onset DM1 is associated with ToM dysfunction
Baldanzi et al., 2016b	RAVLT-IR, RAVLT-DR, ROCF, Digit Span, and CBT (Immediate memory); TMT-A and TMT-B (Selective attention and cognitive flexibility); Stroop Test (Automatic response inhibition); FAS, FAB, Modified WCST (Frontal and executive functions); ROCF-copy (Spatial organization and visuo-constructional skills)	30 patients with DM1	Disrupted complex neuronal networks can underlie cognitive-behavioral dysfunctions in DM1

(Continued)

TABLE 2 | (Continued)

References	Neuropsychological tests (alterations)	Participants	Main results
Gallais et al., 2015	LARS (Apathy); Mini International Neuropsychiatric Interview (MDE); MMSE (Cognitive impairment); Stroop Test (Processing speed, attentional control, response inhibition); FAB (Executive abilities); KFSS (Fatigue)	38 patients with adult-onset DM1 vs. 19 patients with FSHD vs. 20 matched healthy controls	Apathy is more prevalent in DM1 than in FSHD, which is independent of the psychopathological domain, fatigue, age, and motor disability, but is associated with general cognitive status
Labayru et al., 2018	K-BIT (Overall cognitive functioning); Digit span subtest from the WAIS-III (Attention performance); POFA (Emotion recognition); The Faux Pas test (ToM); TECA (Empathy)	38 patients with DM1 vs. matched healthy controls	DM1 patients don't manifest specific impairments in ToM, while emotion recognition appears as a core deficit
Serra et al., 2020a	Emotion attribution test, social situations test, moral/conventional distinction test (Social cognition)	30 patients with DM1 vs. 25 healthy controls	Cortical thickness changes in DM1 patients are significantly associated with deficits in social cognition performances
Serra et al., 2016a	RMET and ToM-story test (ToM); WAIS-R (Global cognitive efficiency)	20 patients with DM1 vs. 18 healthy controls	Deficits in ToM are associated with specific patterns of abnormal connectivity between the left inferior temporal and frontocerebellar nodes in DM1 brains
Minnerop et al., 2011	c.I.T.S (Focused attention); c.I.T.I (Interference); TMT A (Psychomotoric speed); TMT B (Attention shift, mental flexibility); DSS (Daytime sleepiness); NeurocogFX (Choice reaction time, interference, verbal memory-recognition, figural memory-recognition); KFSS (Fatigue); PSQI (Sleep quality); Ullanlinna-Narcolepsy Scale (Narcolepsy)	22 patients with DM1 vs. 22 patients with DM2 vs. matched healthy controls	Depression in DM might be a reactive adjustment disorder rather than a direct consequence of structural brain damage DM1 presents with more prominent WM lesions than DM2, with prominent callosal body and limbic system affection. WM changes might dominated the extent of gray matter changes.
Rakocevic-Stojanovic et al., 2014	Hamilton rating scale (Depressive and anxiety); KFSS (Fatigue); DSS (EDS); ACE-R (Global cognitive status); RSPM and the Serbian version of WAIS-R (General intellectual level); RAVLT (Verbal memory); ROCF (Visuoconstructive abilities and visual memory); TMT-A (Speed and attention); WCST and TMT-B (Executive functions); BNT (Phonetic and semantic verbal fluency); CANTAB (Attention, visual memory, executive functions)	22 patients with juvenile-onset DM1 vs. 44 patients with adult-onset DM1	Patients with juvenile-onset DM1 scored lower than adult-onset DM1 patients regarding total INQoL score and all INQoL subdomains, except for myotonia. Different central manifestations strongly influence QoL in patients with both adult-onset DM1 and juvenile-onset DM1
Heatwole et al., 2018	MDHI, INQoL (QoL); SF-36v2 (Health impairment)	52 patients with DM1	The MDHI correlates well with objective metrics that reflect disease severity in DM1 Participants in DM1 clinical studies favored the MDHI over the INQoL and the SF-36v2 in multiple areas of perceived relevance, usability, and responsiveness
Peric et al., 2016	SF-36 (QoL)	84 patients with DM1	QoL improved in DM1 patients during a 5-year period despite the disease progression SF-36 should be used with caution as a patient-reported outcome measure in DM1 clinical trials
Peric et al., 2017b	INQoL (QoL)	67 patients with DM1	INQoL questionnaire scores improved in DM1 patients during a 6-year period INQoL score did not correlate with progression of muscle weakness
Symonds et al., 2017	MDHI (Health status); DM1-Activ, DM1 Activc, LIFE-H (Activities of daily living); INQoL (Health-related quality of life); ESS, DSS, CFS, FSS, FDSS (Sleep and fatigue)	/	Several patient-reported outcome assessments are suited to make valid measurements in DM1 populations
Heatwole et al., 2016	MDHI	70 patients with DM1	MDHI is a valid tool to measure disease burden in DM1 patients
Baldanzi et al., 2016a	TIB (Intellectual functioning); BDI-II, STAI-Y2 (Depressive and anxiety); AES (Apathy); RAVLT-IR, RAVLT-DR, ROCF-DR, ROCF-IR, CBT (Immediate memory); TMT-A and TMT-B (Selective attention and cognitive flexibility); Stroop Test (Automatic response inhibition); FAS, FAB, Modified WCST (Frontal and executive functions); ROCF (Spatial organization and visuo-constructional skills); Raven's progressive matrices (PM47) (Culture-free abstract reasoning); INQoL (Disease awareness)	65 patients with adult-onset DM1	Several cognitive functions, including executive and mnesic domains with visuo-spatial involvement, were affected in DM1 patients The reduced illness awareness occurs across different physical and life domains, and it appears more prominent in Activities and Independence domains The unawareness significantly related to the cognitive performance deficits, specifically in the domains of visuo-spatial memory, cognitive flexibility and conceptualization

ACE-R, Addenbrooke's Cognitive Examination-Revised; AES, Apathy Evaluation Scale; ASIQ, Adult Suicidal Ideation Questionnaire; BDI-II, Beck Depression Inventory-II; BJLOT, Benton Judgment of Line Orientation Test; BNT, Boston naming test; BVRT, Benton Visual Retention Test; CBT, Corsi Block-Tapping test; CFS, Chalder Fatigue Scale; c.I.T.S, subtest (symbol counting) of the Cerebraler Insuffizienztest; c.I.T.I, subtest (response inhibition) of the Cerebraler Insuffizienztest; CVLT, California Verbal Learning Test; CalCAP, California Computerized Assessment Package; CANTAB, Cambridge Neuropsychological Test Automated; DM, myotonic dystrophy; DSS, Daytime Sleepiness Scale; EDS, excessive daytime sleepiness; FDSS, the Fatigue and Daytime Sleepiness Scale; FSHD, facioscapulohumeral dystrophy; FAB, Frontal Assessment Battery; FAS, phonemic verbal fluency test; FSS, the Krupp Fatigue Severity Scale; IADLs, instrumental activities of daily living; INQoL, Individualized Neuromuscular Quality of Life questionnaire; IQ, Intellectual Quotient; KFSS, Krupp's Fatigue Severity Scale; K-BIT, Kaufman Brief Intelligence Test; LARS, Lille Apathy Rating Scale; LIFE-H, Assessment of Life Habits; MCMI, Millon Multiaxial Clinical Inventory; MDE, major depressive episodes; MDHI, Myotonic Dystrophy Health Index; MMSE, Mini Mental State Evaluation; MOCA, Montreal Cognitive Assessment; NEO-FFI, NEO Five-Factor Inventory; NeurocogFX, computerized neuropsychological screening test battery; POFA, Pictures of Facial Affect; PSQI, Pittsburgh Sleep Quality Index; RCF, Rey's Complex Figure; QoL, Quality of life; RMET, Reading the Mind in the Eyes Test; RAVLT-IR, Immediate Recall of the Rey Auditory Verbal Learning Test; RAVLT-DR, Delayed Recall of the Rey Auditory Verbal Learning Test; ROCF-IR, Immediate Recall of the Rey-Osterrieth Complex Figure test; ROCF-DR, Delayed Recall of the Rey-Osterrieth Complex Figure test; RSPM, Raven standard progressive matrices; STAI-Y2, State-Trait Anxiety Inventory-2; SCL-90-R, Symptom Checklist-90-Revised; TAVEC, Test de Aprendizaje Verbal España-Complutense; TBR, Test de Barcelona Revised; TECA, Test of Cognitive and Affective Empathy; TIB, Brief Intelligence Test; TLT, Tower of London Test; TMT, Trail-Making Test; ToM, theory of mind; TVPS, Test of Visual-Perceptual Skills; WAIS, Wechsler Adult Intelligence Scale; WAIS-R, Wechsler Adult Intelligence Scale-Revised; WCST, Wisconsin Card Sorting Test.

TABLE 3 | Structural brain imaging in DM1.

References	Imaging tools	Participants	Imaging abnormalities	Possible correlations between imaging abnormalities and clinical symptoms
Walker et al., 1984	CT	22 adults with DM vs. 45 healthy controls	Increased ventricular surface areas Focal cerebral atrophy	
Glantz et al., 1988	0.5T MRI	14 patients with DM vs. 12 controls	Periventricular hyperintensities Ventricular enlargement	
Hashimoto et al., 1995	MRI	7 patients with adult-onset DM vs. 6 patients with CDM	The incidence of a small corpus callosum or ventricular enlargement is higher in CDM than in adult-onset DM	
Baldanzi et al., 2016b	3T MRI BPF VBM LL% and Fazekas scale	30 patients with DM1 vs. healthy controls	Widespread GM reduction Decreased FA and increased RD, MD and AD	Negative relationships are discovered between left temporal atrophy and verbal memory, between RD and mnesic and visuo-spatial cognitive domains, and between AD and verbal memory The involvement of normal appearance WM, beyond the signal changes detected with conventional MR imaging, is associated with neuropsychological deficit
Romeo et al., 2010a	MRI SPECT	50 patients with DM1 vs. 14 patients with DM2 vs. 44 healthy controls	Scattered supratentorial, bilateral, symmetrical focal or diffuse WMHLs A typical temporo-insular diffuse subcortical pattern Minimal hypoperfusion in the posterior cortex planes	
Weber et al., 2010	BPF VBM FDG-PET	20 patients with DM1 vs. 9 patients with DM2 vs. healthy controls	Global GM volume reduction A bilateral hippocampal volume reduction Frontal and parietal lobes volume reduction A frontotemporal hypometabolism	Hippocampal volume reduction is correlated to episodic memory deficits
Kobayakawa et al., 2010	MRI	9 patients with DM1 vs. 13 healthy controls	More severe lesions in the frontal, temporal, and insular white matters	Sensitivity to the emotion of disgust is negatively correlated with temporal lesions Sensitivity to anger is negatively correlated with frontal, temporal, and insular lesions
Minnerop et al., 2011	3T MRI VBM DTI	22 patients with DM1 vs. 22 patients with DM2 vs. 22 healthy controls	Extensive WM changes involved all cerebral lobes, brainstem, corpus callosum and limbic system, especially in frontal WM	Sleepiness is linked with FA values in the brainstem
Wozniak et al., 2013	DTI	16 patients with DM1 vs. 15 healthy controls	Diffusive WM abnormalities	WM abnormalities are associated with the degree of working memory impairment
Wozniak et al., 2011	DTI	8 patients with DM1 vs. 8 healthy controls	Abnormal WM integrity indices: FA, RD, MD, and AD	Whole cerebrum fractional anisotropy is correlated with full-scale intelligence and a measure of executive functioning
Franc et al., 2012	MRI	5 adults with CDM1 vs. 5 adults with adult onset DM1 vs. 5 adults with DM2 vs. 5 healthy controls	WM integrity reduction GM volumes reduction only in adult-onset DM1 patients	
Wozniak et al., 2014	3T MRI DTI	45 patients with DM1 vs. 44 healthy controls	Bilateral disturbances in WM integrity	DTI metrics are correlated with cognitive functioning, particularly working memory and processing speed WM integrity is correlated with the muscular impairment Sleepiness is associated with WM status in the superior longitudinal fasciculus and cingulum
Caso et al., 2014	MRI VBM	51 patients with DM1 vs. 34 healthy controls	WM hyperintensities Regional GM atrophy WM tract microstructural damage	WMHs and microstructural damage are correlated with cognitive deficits
Schneider-Gold et al., 2015	3T MRI VBM	12 patients with juvenile or classical DM1 vs. 16 adults with DM2 vs. 33 healthy controls	Ventricular enlargement Supratentorial GM and WM atrophy WM reduction in the splenium of the corpus callosum and in left-hemispheric WM adjacent to the pre- and post-central gyrus	Morphological changes is related to reduced flexibility of thinking and atrophy of the left secondary visual cortex
Serra et al., 2015	3T-MRI BPF VBM	10 patients with DM1 vs. 16 healthy controls	Widespread GM atrophy and WM integrity	Extent of GM and WM damage is correlated with CTG triplet expansion and cognition

(Continued)

TABLE 3 | (Continued)

References	Imaging tools	Participants	Imaging abnormalities	Possible correlations between imaging abnormalities and clinical symptoms
Baldanzi et al., 2016b	3T-MRI BPF VBM	30 patients with DM1 vs. 30 healthy controls	Widespread GM atrophy Decreased FA and increased RD, MD, and AD	BPF value is correlated with visuo-spatial and executive impairment Negative relationship between left temporal atrophy and verbal memory, between RD and amnesic and visuo-spatial cognitive domains, and between AD and verbal memory
Zanigni et al., 2016	DTI MRI VBM	24 adults with DM1 vs. 25 healthy controls	Widespread WM DTI abnormalities GM volume reduction	
Cabada et al., 2017	MRI DTI	42 patients with DM1 vs. 42 healthy controls	WML load Cortical and corpus callosum atrophy Diffuse WM DTI abnormalities	Visuospatial impairment is correlated with WM abnormalities and cortical atrophy Daytime sleepiness is associated with WML and ventral diencephalon and pallidum volume loss
Sugiyama et al., 2017	VBM	28 patients with DM1 vs. 28 healthy controls	Extensive GM atrophy, including cortical and subcortical structures Increased connectivity in the left fusiform gyrus and decreased connectivity in the right striatum	Increased connectivity in the left fusiform gyrus and decreased connectivity in the right striatum are associated with impairment in face perception and theory of mind, and schizotypal-paranoid personality traits
Labayru et al., 2019	MRI DTI VBM	31 patients with DM1 vs. 57 healthy controls	Global GM and WM volume reduction FA reduction	Higher ratings on muscular impairment and longer CTG expansion sizes predict a greater volume decrease in GM and lower FA values
van der Plas et al., 2019	3T MRI	79 patients with DM1 vs. 58 healthy controls	Smaller ICV Smaller volume in frontal GM and WM, parietal GM, corpus callosum, thalamus, putamen, and accumbens Larger volumes of the hippocampus and amygdala	Some morphological differences are associated with cognitive deficits and EDS
Serra et al., 2020a	3T MRI	31 patients with DM1 vs. 25 healthy controls	Thickness reduction in the right premotor cortex, angular gyrus, precuneus, and inferior parietal lobule	Cortical thickness are associated with social cognition performances
Cabada et al., 2020	MRI VBM DTI	33 patients with DM1	Increased WML Ventricular enlargement Decreased volume of the left thalamus, caudates, putamen, and hippocampus Global cortical volume decrease Mean diffusivity increase and fractional anisotropy decrease in WM	Working memory and visuospatial skills deterioration are significantly associated with WML load and mean diffusivity increase Progressive WM and GM involvement
Langbehn et al., 2021	3T MRI	59 patients with adult-onset DM1 vs. 68 healthy controls	Pathological increased volume of the hippocampus	Enlarged hippocampal volume is inversely associated with cognitive dysfunction
Leddy et al., 2021	Conventional and qMT MRI	28 patients with DM1 vs. 29 patients with MS vs. 15 healthy controls	Higher prevalence of anterior temporal lobe lesions, but none in the cerebellum and brainstem Characteristic demyelination (significantly reduced F values) A similar WM lesion distribution compare with that typical of relapsing remitting MS	

DM, myotonic dystrophy; MRI, magnetic resonance imaging; CDM, congenital DM; SPECT, single photon emission computed tomography; GM, gray matter; WM, white matter; WMHL, WM hyperintense lesions; BPF, brain parenchymal fraction; VBM, voxel-based morphometry; FDG-PET, fluorodeoxyglucose positron emission tomography; DTI, diffusion tensor imaging; FA, fractional anisotropy; RD, radial diffusivity; MD, mean diffusivity; AD, axial diffusivity; WMH, WM hyperintensities; WML, WM lesion; ICV, intracranial volume; EDS, excessive daytime somnolence; qMT, quantitative magnetization transfer; MS, multiple sclerosis.

MOLECULAR MECHANISMS

The pathogenesis of DM1 has been mainly attributed to the gain-of-function of toxic RNA (Pettersson et al., 2015). Specifically, the mutant CTG repeat at the 3′-UTR of the *DMPK* gene causes toxic RNA expression that accumulate in the nucleus called "nuclear foci," which interferes with RNA-binding proteins (Miller et al., 2000; Fardaei et al., 2002), leading to the sequestration of muscleblind-like (MBNL) proteins and upregulation of CUGBP/Elav-like family (CELF) proteins. These

TABLE 4 | Functional brain imaging in DM1.

References	Imaging tools	Participants	Imaging abnormalities	Possible correlations between imaging abnormalities and clinical symptoms
Toth et al., 2015	fMRI	8 DM1 patients with grip myotonia vs. 8 DM1 patients without grip myotonia		Myotonia is related to cortical function in high-order motor control areas
Serra et al., 2014	RS-fMRI	27 patients with DM1 vs. 16 health controls		DMN functional connectivity in the bilateral posterior cingulate and left parietal nodes are associated with schizotypal-paranoid traits
Serra et al., 2016a	RS-fMRI	20 patients with DM1 vs. 18 healthy controls	Specific patterns of abnormal connectivity between the left inferior temporal and fronto-cerebellar nodes	Specific patterns of abnormal connectivity are associated with atypical personality profiles and ToM deficits
Serra et al., 2016b	RS-fMRI	31 patients with DM1 vs. 26 healthy controls	Reduced connectivity in a large frontoparietal network Peculiar patterns of frontal disconnection Increased parietal-cerebellar connectivity	Reduced connectivity in a large frontoparietal network is correlated with isolated impairment in visuospatial reasoning The balance between loss of connectivity and compensatory mechanisms is correlated with the paradoxical mismatch between structural brain damage and minimal cognitive deficits
Serra et al., 2020b	RS-fMRI	32 patients with DM1 vs. 26 healthy controls	Increased functional connectivity between VTA and the left supramarginal and superior temporal gyri	Deficit of decision-making is related to increased connectivity between VTA and brain areas critically involved in the reward/punishment system and social cognition
Renard et al., 2016	FDG-PET	24 patients with DM1 vs. 24 healthy controls	Reduced FDG-uptake especially in Brodmann area 8	Reduced FDG-uptake in Brodmann area 8 is correlated to CTG-repeat numbers
Peric et al., 2017a	FDG-PET	16 patients with DM1 vs. 13 patients with DM2	Prominent glucose hypometabolism in prefrontal, temporal, and pericentral regions	Right frontotemporal hypometabolism is associated with executive dysfunction
Romeo et al., 2010b	PET/SPECT	58 patients with DM1 subjected to SPECT and 17 patients with DM1 subjected to PET	Reduced CBF and perfusion and abnormal glucose metabolism, more pronounced in the left hemisphere, the frontal lobe and the cortex	
Meola et al., 2003	SPECT	21 patients with moderately severe DM1	Frontal and parieto-occipital hypoperfusion	Specific cognitive and behavioral profile (avoidant trait personality disorder) is associated with hypoperfusion in frontal and parieto-occipital regions of the brain
Chang et al., 1998	MRS	14 patients with DM vs. 24 healthy controls	Elevated levels of myoinositol, total creatine, and choline-containing compounds	Creatine and myoinositol levels are proportional to the number of trinucleotide (CTG)n repeats
Akiguchi et al., 1999	MRS	21 patients with DM vs. 16 healthy controls	Lower ratio of N-acetylaspartate to creatine and phosphocreatine Lower ratio of N-acetylaspartate to choline-containing compounds	
Krogias et al., 2015	TCS	17 patients with DM1 vs. 14 patients with DM2 vs. 31 healthy controls	Third ventricle enlargement	Mesencephalic raphe echogenicity is related with EDS
Peric et al., 2014b	TCS	66 patients with DM1 vs. 55 health controls	Increased third ventricle width Brainstem raphe hypoechogenicity Substantia nigra both hypoechogenicity and hyperechogenicity	

DM, myotonic dystrophy; fMRI, functional MRI; RS-fMRI, resting-state fMRI; ToM, theory of mind; VTA, ventral tegmental area; FDG-PET, fluorodeoxyglucose positron emission tomography; MRS, magnetic resonance spectroscopy; TCS, transcranial sonography.

alterations subsequently affected hundreds of mis-spliced effector genes, resulting in aberrant expression of embryonic splice isoforms and loss of these gene product functions, accounting for the multisystemic phenotype (Udd and Krahe, 2012; Chau and Kalsotra, 2015). In recent years, other factors, such as repeat-associated non-AUG (RAN) translation, which can contribute to the formation of toxic homopolymeric (e.g., polyQ) polypeptides, aberrant polyadenylation, activation of protein kinase C (PKC)-dependent signaling pathway, and microRNA deregulation have also been reported to play important roles in DM1 (Chau and Kalsotra, 2015). Regarding CNS, alternative splicing dysregulation has been frequently reported (Caillet-Boudin et al., 2014). Meanwhile, the widespread distributions of mutant *DMPK* mRNA accumulated in nuclear foci in neurons, astrocytes, oligodendrocytes, as well as in human DM1 induced pluripotent stem cell (iPSC)-derived neural stem cells (NSCs) have been reported (Jiang et al., 2004; Hernández-Hernández et al., 2013a; Xia et al., 2013; Sicot et al., 2017). In animal models, different splicing defects and their associated CNS symptoms were also studied (**Figure 1**). Except for these, emerging pathogenic events independent of splicing defects have also been discovered in the brain of DM1 patients (Marteyn et al., 2011; Hernández-Hernández et al., 2013b). Some CNS symptoms are non-linearly dependent on patient age and CTG repeat length, suggesting the complex and multifactorial mechanisms driving neurological deficits (Heatwole et al., 2012).

This section concludes the current advance about CNS pathogenesis, hoping to better understand the complex nature of the DM1 CNS disorders.

Loss Function of Muscleblind-Like Proteins

Three MBNL paralogs are expressed in mammals, MBNL1, MBNL2, and MBNL3, which can be involved in regulating alternative splicing, mRNA stability, translation and so on (Charizanis et al., 2012; Wang et al., 2012). A large amount of previous studies have revealed the critical role of MBNL proteins in muscle or heart-related disorders, while in recent years, a close relationship between the loss-of-function of MBNL and DM1 brain-related phenotypes were also detected (Matynia et al., 2010; Charizanis et al., 2012; Goodwin et al., 2015), especially MBNL2. Nowadays, hundreds of dysregulated splicing factors, including in *Cacna1d* (McKinney et al., 2009), *Tanc2* (Han et al., 2010), *Ndrg4* (Yamamoto et al., 2011), and *GRIN1* (Shimizu et al., 2000) have been detected in the brain of *Mbnl* 2–/– mice, most of which were similarly dysregulated in DM1 patients, indicating a critical role of the *Mbnl2* loss in DM1 brain pathology (Charizanis et al., 2012). Further, *Mbnl2*–/– mice which are exposed to sleep deprivation also developed several CNS features including impaired long-term potentiation (LTP), deficits in spatial memory, reduced synaptic NMDAR response and impaired hippocampal synaptic plasticity (Charizanis et al., 2012), which were similar to the DM1 phenotype. In 2018, one study described prolonged and enhanced responsiveness to intracortical train stimulation in *Mbnl2*–/– mice, partially attributed to abnormal glutamate neurotransmission (Chen et al., 2018). Particularly, these abnormalities have also been observed in DM1 patients (Meola and Sansone, 2007; Takado et al., 2015).

Several studies also reported a potential role of MBNL1 protein in CNS disorders. For example, cognitive and behavioral abnormalities have been discovered in *Mbnl1*–/– mice (Matynia et al., 2010). In cultured primary hippocampal neurons and EpA960/CaMKII-Cre mice (a brain-specific DM1 model carrying 960 *DMPK* CTG repeats in the postnatal brain), expanded CUG repeats led to deubiquitination of cytoplasmic MBNL1, subsequent nuclear translocation, and morphological defects. These effects can be ameliorated by inhibiting the degradation of lysine 63-linked polyubiquitin chains or by promoting MBNL1 ubiquitination (Wang P. Y. et al., 2018). In 2020, cell studies shown that gain-of-function of MBNL1 could reverse the proliferation defect of skeletal muscle satellite cells in DM1 by inhibiting autophagy *via* the mTOR pathway (Song et al., 2020). Moreover, functional characterization of neuronal cells derived from human embryonic stem (ES) cells reported a reduced proliferative capacity and increased autophagy associated with alterations of the mTOR signaling pathway, while gain-of-function of MBNL1 rescued the phenotype (Denis et al., 2013), suggesting that MBNL1 loss might influence brain pathology by regulating the mTOR signaling pathway. Some important splicing defects have also been detected in the brain of *Mbnl1*–/– mice, in genes such as *Sorbs1*, *Dclk1*, and *Camk2d* (Suenaga et al., 2012). However, the extent of alternative splicing defects in the brain of *Mbnl1*–/– mice was much less than that observed in DM1. A number of alternative exons, such as *GRIN1* exon 4, *APP* exon 7, and *Tau* exons 3 and 9, which have already been reported to be mis-spliced in the brains of DM1 patients, were unaltered in *Mbnl1*–/– mice, thus indicating a limited contribution of MBNL1 to DM1 CNS defects (Suenaga et al., 2012).

In addition, it's worth noting that the combined loss of MBNL1 and MBNL2 has shown infant/immature structural phenotypes in mutant brains, similar to that of DM1 patients (Goodwin et al., 2015). Besides, single gene knockout may also contribute to the compensatory upregulation of the remaining *Mbnl* genes (Lee et al., 2013). In *Mbnl1*–/– mice, the expression of MBNL2 could be upregulated, which subsequently targets transcripts that are normally regulated by MBNL1 (Lee et al., 2013). These findings indicate a collaborative role of MBNL1 and MBNL2 involved in DM1 CNS.

Gain of CUGBP/Elav-Like Family Activities

The human CELF family has six members, all of which are involved in alternative splicing regulation (Ladd et al., 2001, 2004). Among these, the upregulations of CELF1 and CELF2 have been observed in the brain of DM1 patients (Dhaenens et al., 2011).

CELF1 has been identified as a (CUG)n repeat-binding protein (Timchenko et al., 1996). Unlike MBNL1, it is increased in DM1 patients mainly through PKC-mediated phosphorylation to stabilize the protein (Kuyumcu-Martinez et al., 2007), or through decreased levels of miR-23a/b (Kalsotra et al., 2014). In opposite, the increasing expression of CELF2 is not related to protein hyperphosphorylation, indicating other potential regulatory mechanisms. CELF1 and CELF2 can influence various transcripts (Ladd, 2013) in the DM1 brain, such as different exons of *Tau* and *NMDAR1* exon 5 (Leroy et al., 2006a,b). Tau proteins can promote neurite outgrowth, organize axonal microtubules, and participate in kinesin-dependent axonal transport (Andreadis, 2012). NMDARs are key components of glutamate-mediated excitatory signaling, which can contribute to excitatory synaptic transmission and synaptic plasticity, thought to be the basis of learning and memory (Zorumski and Izumi, 2012). It has been discovered that four exons (2, 3, 6, and 10) of *Tau* isoforms could respond to one or more CELF proteins in DM1 (Leroy et al., 2006a,b; Dhaenens et al., 2011). CELF2 can regulate alternative exon 5 transcripts of *NMDAR1* to change neuronal excitation in rat brain (Zhang et al., 2002), while CELF1 is inefficient. Aside from alternative splicing regulation, CELF proteins can also participate in regulating mRNA adenylation status, stability, and translation in various cell types (Dasgupta and Ladd, 2012), indicating its potential cytoplasmic functions in the brain.

A Novel Splicing Regulator—RBFOX Proteins

RBFOX proteins are sequence-specific RNA binding proteins which can regulate alternative splicing in multiple tissues, such as skeletal muscle, heart, and brain (Gehman et al., 2011;

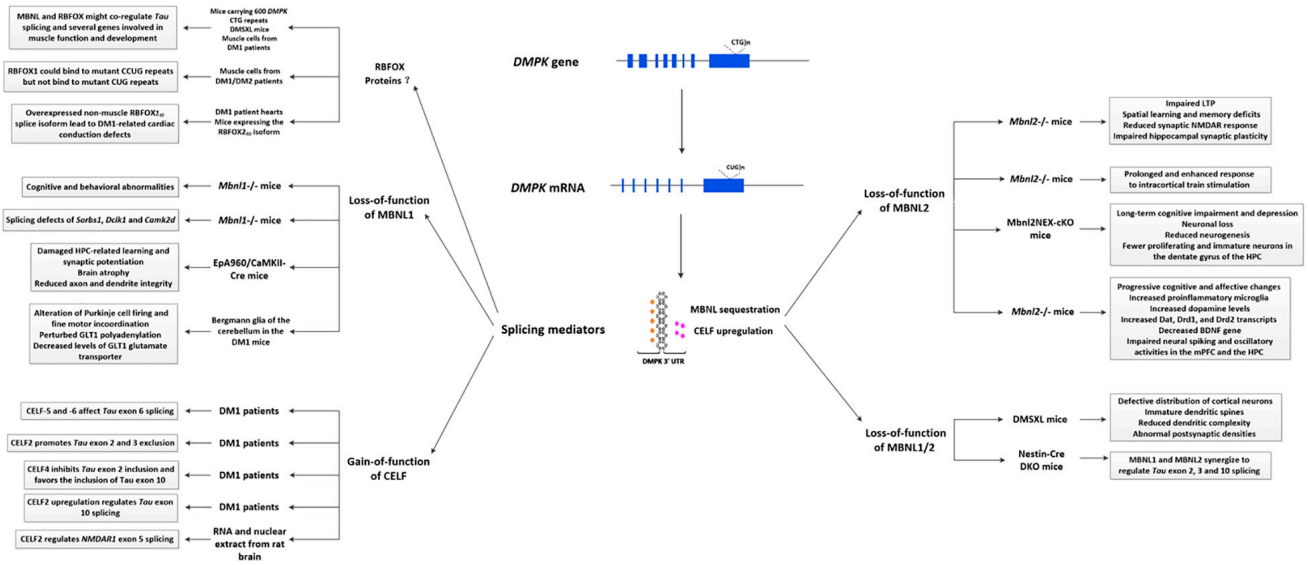

FIGURE 1 | Primary splicing defects described in the DM1 brain. Splicing defects are generally considered the primary cause of DM1 pathology, similar to those in the brain. Specifically, the mutant *DMPK* gene transcripts into expanded CUG RNA, which folds into a hairpin-like structure in the nucleus called "nuclear foci." These nuclear foci then bind and regulate RNA-binding proteins, affecting alternative splicing, eventually causing a wide range of pathogenic changes. Most splicing defects involved in brain pathology are mediated by the sequestration of MBNL proteins and upregulation of CELF proteins. In animal studies, it has been shown that loss-of-function of MBNL1 might be related to cognitive and behavioral abnormalities, learning abnormalities, alteration of Purkinje cell firing and fine motor incoordination, and perturbed GLT1 levels. Besides, it also contributes to alternative splicing alterations of several genes, such as *Sorbs1*, *Dclk1*, and *Camk2d*. Loss-of-function of MBNL2 could be associated with sleep alterations, spatial learning and memory deficits, impaired synaptic NMDAR response and hippocampal synaptic plasticity, neuronal loss, reduced neurogenesis, cognitive and affective changes and so on. Meanwhile, synergistic effects of MBNL1 and MBNL2 can regulate *Tau* exon 2, 3, and 10 splicing, while a combination loss of MBNL1/2 might be related to abnormal sleepiness, defective distribution of cortical neurons, immature dendritic spines, reduced dendritic complexity, and abnormal PSDs. In DM1 patients, it has been shown that gain-of-function of several CELF proteins can regulate *Tau* exon 2, 3, 6, and 10 splicing, and CELF2 can regulate *NMDAR1* exon 5 splicing. A novel splicing regulator, RBFOX protein has recently been considered a new player in DM1 pathogenesis, *via* a competitive or cooperative interaction with MBNL1. Additionally, the non-muscle RBFOX2$_{40}$ splice isoform in DM1 heart may also contribute to cardiac conduction defects. DM1, myotonic dystrophy type 1; CELF, CUGBP/Elav-like family; MBNL, muscleblind-like; GLT1, glutamate transporter 1; LTP, long-term potentiation; mPFC, medial prefrontal cortex; HPC, hippocampus; BNDF, brain derived-neurotrophic factor.

Singh et al., 2014; Conboy, 2017; Jacko et al., 2018). Nowadays, it has been discovered that RBFOX1 is involved in the regulation of synapses and autism-related genes in the cytoplasm of neurons (Wang et al., 2016). Klinck et al. (2014) reported that MBNL1 and RBFOX1 protein could co-regulate the splicing of a series genes involved in muscle function and development, some of which are also mis-spliced in DM1 tissues. And the decreased RBFOX1 may amplify the mis-splicing changes caused by the loss-of-function of MBNL1. At the same time, they found that the ectopic expression of RBFOX1 partially rescued the mis-splicing of *Tau* exon 2 in glioblastoma cells. Since the MBNL proteins have been shown to regulate the splicing of *Tau* exon 2 in DM1 brains, it is therefore interesting to postulate that cooperation of MBNL and RBFOX1 might regulate *Tau* splicing in DM1 brains. Nevertheless, Sellier's researches proposed different results, that RBFOX1 could bind to expanded CUG RNA repeats, competing with MBNL1 and reducing the sequestration of MBNL1 in DM2 muscle cells, which suggest a partly competitive relationship between RBFOX1 and MBNL1 (Sellier et al., 2018). Misra et al. (2020) found a new non-muscle RBFOX2$_{40}$ splice isoform which is overexpressed in DM1 patient hearts. Particularly, mice expressing the RBFOX2$_{40}$ isoform in hearts also performed DM1-related cardiac conduction dysfunctions (Misra et al., 2020), which may due to its promotion of the production of pathogenic ion channel splice variants. All of these results provide a novel idea explaining the splicing dysregulation in DM1, though their possible roles in CNS dysfunctions still need further exploration.

Effector Genes Alterations Due to Splicing Defects

Nowadays, hundreds of spliced effector genes changes have been discovered in the DM1 brain (Jiang et al., 2004; de León and Cisneros, 2008; Suenaga et al., 2012; Hernández-Hernández et al., 2013a; Otero et al., 2021). Jiang et al. (2004) screened 45 exons (in 31 genes) spliced in the brain of DM1 patients, wherein four of them changed in the ratio of exon inclusion/exclusion splice products, including decreased inclusion of *APP* exon 7, *Tau* exons 2 and 10, and increased inclusion of *NMDAR1* receptor exon 5. Interestingly, the sequences encoding *APP* exons 7 and 8 are excluded in neurons, but are included in astrocytes, indicating the splicing defects in astrocytes. In 2021, *via* detecting transcriptome alterations in frontal cortex of DM autopsy samples, Otero et al. (2021) reported 130 high-confidence splicing changes, which occur in ion channels, neurotransmitter receptors, and synaptic scaffolds, while mis-splicing of *GRIP1* might change

kinesin association. In frontal cortex samples, downregulated genes tend to express in neurons, while upregulated genes tended to express preferentially in endothelial and microglial, which suggest neuroinflammatory responses. In DMSXL mice (carrying ∼1,000–1,800 *DMPK* CTG repeats with multisystemic transgene expression), the mis-splicing patterns of *GRIN1* exon 21, *Ldb3* exon 11, and *Mbnl2* exon 7 in frontal cortex, as well as *GRIN1* exon 5, *Ldb3* exon 11, *APP* exon 8, and *Frx1* exons 15/16 in brainstem have been detected (Hernández-Hernández et al., 2013a), and *GRIN1* and *Tau* mis-splicing appear to be involved in synaptic dysfunction. In the brain of *Mbnl1*–/– mice, 14 mis-spliced events have been observed using splicing-sensitive microarray, including *Sorbs1* exons 6 and 25, *Spag9* exon 31, *Dclk1* exon 19, *APP* exon 7 and 8, *GRIN1* exon 4, and so on (Suenaga et al., 2012).

Heterogeneity in Splicing Defects in Different Brain Regions

Recently, the heterogeneity of splicing defects in the DM1 brain also attracted increasing attention. In *Mbnl* knockdown mice, it has been identified that abnormal alternative splicing in the cerebellum are fewer than in other brain regions (Charizanis et al., 2012; Suenaga et al., 2012). The inclusion of *Mbnl1* exon 5 and *Mbnl2* exons 5 and 8 were higher in most brain areas, except in the cerebellum for *Mbnl2* exons 5 and 8. Besides, RNA foci preferentially accumulate in the frontal cortex and certain areas of the brainstem of DM1 transgenic mice (Huguet et al., 2012; Hernández-Hernández et al., 2013a), and seem to be more abundant in cortical astrocytes than in neurons (Hernández-Hernández et al., 2013a). Using autopsied brain tissues of DM1 patients, researchers further observed varying degrees of mis-splicing among the cerebellar cell layers (Furuta et al., 2018). LASER capture microdissection revealed splicing defects in the molecular layer of the cerebellum, but not in the granular layer (Furuta et al., 2018). Similarly, one study reported that mis-splicing in WM is less apparent than in GM of the DM1 brain, which may be attributed to the inability to transfer the abnormal/fetal splicing isoform to the axon (Nishi et al., 2020). Future analysis of the mis-splicing diversity in the DM1 brain may favor a precise therapy targeting specific sites.

Translational RNA Differences

Though sharing with a common pathogenetic mechanism, alternative splicing defects, further findings suggested a new perspective influencing the performances of DM patients. According to the results of Salvatori et al. (2009) the molecular and biochemical differences of troponin T and the insulin receptor between DM1 and DM2 due to different translational patterns and distribution patterns might partially explain the apparent differences on their clinical phenotypes. This phenomenon promotes the exploration of DM1 pathogenesis at the translation level.

Somatic Expansion

Recently, an important aspect of the pathogenesis of DM1 regarding to somatic expansion has attracted increasing attention. It has been demonstrated that the length of modal allele in blood DNA samples of DM1 patients increased over time, driven primarily by the inherited progenitor allele length (ePAL), age-at-sampling, and age-at-onset (Morales et al., 2020). Since the DNA mismatch repair proteins MSH2, MSH3, and MSH6, are considered critical players in CTG repeat expansion, and their decreased expressions inhibit the expansion (Dragileva et al., 2009; Tomé et al., 2009), they provide a new insight into the mechanism of CTG repeat instability in DM1. Tomé et al. (2009) reported that MSH2 ATPase domain mutation could influence somatic instability in DM1 transgenic mice. Compared with fibroblasts, MSH2, MSH3, and MSH6, were highly expressed in DM1 patient-derived iPSC, accompanied with longer CTG repeat, while MSH2 silencing inhibited CTG repeat expansion (Du et al., 2013). Flower et al. (2019) reported that the altered MSH3 levels caused by MSH3 3a repeat allele decreased somatic expansion and changed the DM1 phenotype. Thus, regulation of MSH3 might represent a new roadmap for potential target therapy of DM1.

CELLULAR PROCESSES ALTERATIONS

Synaptic Dysfunction

Synaptic protein dysfunction is an important feature demonstrated in the DM1 brain. RAB3A is an abundant synaptic vesicle protein that regulates neurotransmission by interacting with other synaptic proteins. The upregulation of RAB3A causes spontaneous exocytosis, and plays important roles in spatial learning, sleep control, and synaptic plasticity (Sudhof, 2004). Synapsin I (SYN1) can regulate synaptic vesicle release in a phosphorylation-dependent manner, and its hyperphosphorylation determines short-term synaptic plasticity alterations (Rosahl et al., 1993). Hernández-Hernández et al. (2013a) reported RAB3A upregulation and SYN1 hyperphosphorylation in DMSXL mice, transfected cells, and DM1 patient samples, which were related to altered spontaneous neurosecretion in cell culture, electrophysiological and behavioral deficits in mice, and possibly contributed to the neuropsychological manifestations in DM1 patients. Then, Jimenez-Marin et al. (2021) demonstrated that transcriptional signatures of synaptic vesicle genes at least partially explain the mechanisms of DM1 neurodegeneration. Nowadays, a close relationship between splicing regulator alterations and synaptic protein dysfunctions has been found, possibly contributing to DM1 neurological phenotypes (Hernández-Hernández et al., 2013b). For example, loss-of-function of MBNL1 in DMSXL mice brain mediated the upregulation of RAB3A levels and determined the length of neuronal dendrites and axons (Hernández-Hernández et al., 2013b). The overexpression of CELF1 or CELF2 in neuronal-like PC12 cells containing expanded CUG transcripts mediated SYN1 hyperphosphorylation (Hernández-Hernández et al., 2013b). And other splicing alterations, such as *GRIN1* and *Tau* splicing defects, might also contribute to synaptic dysfunction in DM1 (Hernández-Hernández et al., 2013b). However, although influenced by different splicing regulators, these synaptic protein

alterations seem to be independent of mis-splicing of their coding transcripts, suggesting that DM1 neuropathogenesis have far-reaching implications beyond the disruption of splicing programs.

In addition, other synaptic-related abnormalities have also been identified in the DM1 brain. Lee et al. (2019) found distribution defects of cortical neurons, abnormal dendritic morphology and complexity and postsynaptic densities in the *Mbnl1/2*–/– mice. A time-course study using EpA960/CaMKII-Cre mice revealed that hippocampus (HPC)-related learning and synaptic potentiation were damaged before structural alterations occurred in the brain, followed by brain atrophy associated with progressively reduced axon and dendrite integrity. Notably, cytoplasmic MBNL1 level on dendrites decreased before dendrite degeneration, whereas MBNL2 expression reduction and MBNL-mediated alternative splicing defects were evident after degeneration (Wang et al., 2017), suggesting that MBNL1 reduction might contribute to synaptic transmission dysfunction in the DM1 brain.

The Defective Neuroglial Interactions

A recent study shows that compared to neurons, cortical astrocytes contain more ribonuclear foci in DM1 transgenic mice (carrying 45 kb of human genomic DNA cloned from a DM1 patient) (Hernández-Hernández et al., 2013a). Meanwhile, RNA sequencing discovered more frequent splicing deficits in glia of DMSXL mice (Oude Ophuis et al., 2009; González-Barriga et al., 2021), suggesting a non-negligible presence of neuroglial damage in DM1. Glutamate transporter 1 (GLT1) is a glial-specific glutamate transporter that can recapture excitatory glutamate from the synaptic cleft and protect it from neurotoxicity caused by glutamate overstimulation (Bellamy, 2006). In the Bergmann glia of the cerebellum in DMSXL mice, scientists found glutamate excitotoxicity associated with decreased GLT1 (Sicot et al., 2017). In astrocytes of DMSXL mice, downregulation of GLT1 increased glutamate neurotoxicity and caused neuronal damage, while the upregulation of GLT1 corrected Purkinje cell firing and motor incoordination (Sicot et al., 2017). These studies indicated that the loss-of-function of GLT1 and defective neuroglial interactions might play critical roles in inducing DM1 brain disorders.

Nowadays, studies have identified that the expression of GLT1 is regulated by RNA transcription, splicing and stability, post-translational modifications, and protein activity (Kim et al., 2011). Specifically, loss-of-function of MBNL1 can perturb GLT1 polyadenylation, thus decreasing the levels of GLT1 glutamate transporter, while MBNL2 inactivation did not affect GLT1 levels, but contributed to the compensating increase in MBNL1 protein (Batra et al., 2014; Mohan et al., 2014). In the future, restoring GLT1 protein and glutamate neurotransmission by regulating MBNL proteins might be promising approaches to reverse the defective neuroglial interactions in DM1. Besides, in an inducible glial cell model of DM1 derived from human retinal Müller glial cells (MIO-M1) expressing 648 CUG repeats [MIO-M1 CTG(648)], scientists identified that the activation of inflammatory pathways and immune responses could partially explain DM1 CNS defects associated with defective glia (Azotla-Vilchis et al., 2021; González-Barriga et al., 2021). In glial cells of DMSXL mice, expanded CUG RNA affected preferentially differentiation-associated molecular events, which open new avenues in studying DM1 brain pathology with cell type resolution (González-Barriga et al., 2021).

Altered Brain Insulin Signaling

Previous studies have observed the insulin resistance (IR) phenotype in DM1 patients (Moxley et al., 1978), which could be attributed to the mis-splicing of the insulin receptor gene. While recently, altered insulin signaling in the brain has also been proposed, thus provides potential alternative explanations for the DM1 neuropathogenesis (Nieuwenhuis et al., 2019). For example, animals with impaired insulin receptor signaling have shown reduced motivation, which could translate to apathy in humans (Dagenhardt et al., 2017), a critical symptom in adult DM1 patients (Gallais et al., 2015). In patients with obsessive-compulsive disorder, altered brain insulin signaling has been observed (van de Vondervoort et al., 2016). Besides, cognitive deficits, especially visuospatial and verbal memory deficits (Kullmann et al., 2016), depressive symptoms (Minier et al., 2018; van der Velden et al., 2019) and decreased behavioral flexibility (van de Vondervoort et al., 2019), have also been shown to be associated with brain IR. Moreover, a recent review pointed out the effects of insulin signaling on tauopathy and Aβ metabolism (Gonçalves et al., 2019). And several neuroimaging studies have discovered a decrease in glucose uptake in the brain of DM1 patients (Fiorelli et al., 1992; Peric et al., 2017a), however, it remains unclear whether altered insulin signaling is involved.

Neurochemical Changes

A series of neurochemical changes were also found in DM1, which may account for specific symptoms. For example, the loss of serotonin (5-HT)-containing neurons in the dorsal raphe nucleus (DRN) and the superior central nucleus (SCN) of DM1 patients is associated with hypersomnia (Ono et al., 1998). And the alteration of serotonergic raphe structures might be involved in the pathogenesis of hypersomnia (Peric et al., 2014b; Krogias et al., 2015; Krogias and Walter, 2016). The hypoechogenicity of nucleus raphe might be correlated with EDS and depression in DM patients (Peric et al., 2014b). The extent of WM hyperintensities might be correlated with fatigue (Minnerop et al., 2011). Using conditional *Mbnl2*NEX-cKO mice (a tissue-specific knockout mouse model lacking the *Mbnl2* gene in forebrain glutamatergic neurons), long-term cognitive impairment and depression were found (Ramon-Duaso et al., 2020). This might be associated with significant neuronal loss, reduced neurogenesis, and fewer proliferating and immature neurons in the dentate gyrus of the HPC. Additionally, in *Mbnl2*–/– mice, increased proinflammatory microglia, dopamine levels as well as Dat, Drd1, and Drd2 transcripts levels, decreased expression of the brain derived-neurotrophic factor (BDNF) gene, and impaired neural spiking and oscillatory activities in the medial prefrontal cortex (mPFC) and the HPC have been found, accompanied with progressive cognitive and affective changes (Ramon-Duaso et al., 2019). Similar abnormalities have also been observed in the mPFC and HPC of DM1 patients with severe depression and cognitive impairment (Romeo et al., 2010b).

Currently, chronic treatment with methylphenidate (MPH) has been shown to reverse the behavioral abnormalities, reduce proinflammatory microglia and Dat level, and increase BDNF and Nrf2 mRNA expressions in *Mbnl2–/–* mice. This makes it a promising drug candidate to treat CNS dysfunctions in DM1 patients (Ramon-Duaso et al., 2019). However, this intervention also impaired glutamate uptake and increased glutamate levels in juvenile rats (Schmitz et al., 2016, 2017), querying whether MPH therapy would increase glutamate neurotoxicity and induce the defective neuroglial interactions.

In addition, dysregulation of cerebrospinal fluid (CSF) homeostasis was observed in early onset DM1. A study introducing *DMPK* CTG expansions into the mouse found that mis-splicing significantly affected brain choroid plexus epithelial cells (Nutter et al., 2019). Besides, increased levels of total-Tau, IgG, γ-globulin, and myelin basic protein (MBP), as well as decreased levels of Aß1-42 and orexin-A were found in the CSF of DM1 patients (Hirase and Araki, 1984; Martínez-Rodríguez et al., 2003; Winblad et al., 2008; Peric et al., 2014a). Orexins are hypothalamic peptides that play critical roles in sleep/wake regulation (Sakurai, 2014). A possible correlation between an altered CSF orexin-A levels and EDS in systemic lupus erythematosus (SLE) patients with hypothalamic lesions and patients with frontotemporal dementia (FTD) have been reported (Çoban et al., 2013; Suzuki et al., 2018). Notably, significantly lower orexin-A levels were also detected in the CSF of 6 DM1 patients affected by EDS (Martínez-Rodríguez et al., 2003), thus providing potential explanations for DM1 sleep disorders. Furthermore, in 2015, a decreased level of BDNF, a neurotrophin participate in learning and memory, was detected in the serum of DM1 patients. Since it can cross the brain-blood barrier (BBB), it might be considered a promising biomarker of CNS defects (Comim et al., 2015).

Neuropathological Defects in Early Developmental Processes

To determine the expression patterns of DMPK with age, Langbehn et al. (2021) analyzed the brain from 99 donors with DM1 ranging from 5 postconceptional weeks to 80 years old. They found that peak expression of wildtype *DMPK* coincides with a time of dynamic brain development, thus indicating that the abnormalities in DM1 brain *DMPK* expression may affect early brain development. Besides, direct injection of $(CUG)_{91}$ repeat-containing mRNA into single-cell embryos of zebrafish induced CNS toxicity during early development, resulting in morphological abnormalities, behavioral abnormalities, and extensive transcriptional alterations, while co-injection of zebrafish *Mbnl2* RNA suppressed this toxicity and reversed the associated behavioral and transcriptional abnormalities (Todd et al., 2014). In addition, defects in the genes involved in dysfunctional neurite outgrowth and synaptogenesis at the neuromuscular junction were also observed in neuronal progeny derived from DM1 mutant human ES cells, which are associated with the decreased expression of two genes that belong to the *SLITRK* family, *SLITRK2* and *SLITRK4* (Marteyn et al., 2011). Transfection of *SLITRK2* and *SLITRK4* into cultured DM1 cells restored neurite length to control levels. However, it is interesting that *DMPK* mutation and dysregulation of splicing by MBNL1 do not appear to be involved in SLITRK misexpression or neurite outgrowth, suggesting other new molecular mechanisms involved in DM1 abnormal neurodevelopment (Marteyn et al., 2011).

PATHOLOGICAL FEATURES

Tau Pathology

In the DM1 brain, dysregulation of alternative splicing could lead to pathologic Tau proteins accumulations and the formation of neurofibrillary tangles (NFTs) (Caillet-Boudin et al., 2014), which are mainly located in the HPC, entorhinal cortex, and most of the temporal areas, called Tau pathology. Nowadays, Tau pathology has been confirmed a critical histopathological characteristic in the brain of DM1 patients (Caillet-Boudin et al., 2014), and could interfere with axonal transport and neurosecretion (Caillet-Boudin et al., 2014). Although there is no direct evidence, current research suggests that this pathology may be related to cognitive dysfunctions in DM1.

In the adult brain, *Tau* gene could encode six *Tau* isoforms through alternative splicing of exons 2, 3, and 10, whereas in DM1, all of these exons are absent, thus promoting fetal expression of the 3-repeat *Tau* isoform (Sergeant et al., 2001; Jiang et al., 2004). Interestingly, a recent study in a congenital DM1 patient with intellectual disability also suggested the existence of a 4-repeat tau dominant pathology (Mizuno et al., 2018). Originally, cell studies identified that long CUG repeats-mediated loss-of-function of MBNL1 could be responsible for the changes in *Tau* splicing (Dhaenens et al., 2008). While in 2014, researchers discovered that both MBNL1 and MBNL2 have an enhancer activity of *Tau* exon 2 inclusion, and only the interaction of MBNL1 and MBNL2 can fully reverse the splicing defect of *Tau* exon 2 induced by the mutant CUG repeats, similar to that observed in DM1 (Carpentier et al., 2014). Then in 2015, a further study examining the *Tau* splicing using Nestin-Cre DKO mice (a *Mbnl1/2–/–* mouse model) suggested that both MBNL1 and MBNL2 synergize to regulate *Tau* exon 2, 3, and 10 splicing (Goodwin et al., 2015). These findings proved that the regulation of MBNL1/2 and their interactions are highly essential in DM1 Tau pathology. Except MBNL proteins, CELF proteins also serve as potential regulators of *Tau* splicing. Four exons (2, 3, 6, and 10) of *Tau* isoforms have been discovered to respond to one or more CELF proteins (Leroy et al., 2006a,b). Among them, *Tau* exon 10 responds specifically to CELF2 upregulation (Dhaenens et al., 2011). *Tau* exon 6 splicing is regulated by CELF5 and CELF6 (Leroy et al., 2006b). Notably, the heterogeneous distribution of Tau protein in the DM1 brain has also been reported, which may affect its splicing regulation patterns.

Other than Tau pathology, several kinds of protein and nucleotide deposits have also been observed in the brain of DM1 patients (Weijs et al., 2021), including Lewy bodies (LBs), neuronal intranuclear eosinophilic inclusion bodies, intracytoplasmic inclusion bodies, increased Marinesco bodies,

gliosis (Itoh et al., 2010; Jinnai et al., 2013), skein-like ubiquitin-positive inclusions and granulovacuolar degeneration (GVD), which suggest neurodegeneration in the DM1 brain (Itoh et al., 2010; Yamazaki et al., 2011; Nakamori et al., 2012).

RNAopathy and Spliceopathy

In the DM1 brain, the mutant *DMPK* RNA accumulates as nuclear foci in extensive areas, which contributes to abnormal alternative splicing (Miller et al., 2000; Fardaei et al., 2002). The nuclear foci are widely distributed throughout the brain of DM1 patients, including cortex, WM in subcortical and callosal areas, HPC, thalamus, brainstem, and cerebellum, and presented in various cell types, such as neurons, astrocytes, oligodendrocytes, Purkinje cells and human DM1 iPSC or ES-cell-derived NSCs (Jiang et al., 2004; Denis et al., 2013; Hernández-Hernández et al., 2013a). Their distributions varied from different genetic features, histological features and clinical features in each person (Jiang et al., 2004). Abnormal alternative splicing has been considered the critical pathogenesis of DM1. Changes in RNA-binding proteins, such as MBNL and CELF proteins, can lead to splicing defects of a variety of pre-mRNAs and misexpressions of different protein isoforms. Nowadays, the interaction between RNAopathy, spliceopathy, and Tau pathology have accounted for essential parts of DM1 neuropathology (Caillet-Boudin et al., 2014).

Other Pathological Features

Other neuropathological features of DM1 include neuronal loss in different areas, such as the superficial layer of the frontal and parietal cortices, the occipital cortex, the medullary arcuate nuclei, the anterior and dorsomedial thalamic nuclei, the midbrain, and pontine reticular formation, which may be related to cortical atrophy (Culebras et al., 1973; Ono et al., 1995, 1998; Mizukami et al., 1999). The cell loss of specific areas might also contribute to the cognitive and behavioral abnormalities in DM1 patients (Rosman and Kakulas, 1966; Ono et al., 1996; Mizukami et al., 1999). In the post mortem brain and spinal cord of DM1 patients with congenital or childhood onset with intellectual deficiency, heterotopic neurons have been found, suggesting abnormal neurodevelopment (Ogata et al., 1998). Degenerative WM changes were also reported in DM1 patients, including myelin and axonal loss, expansion of perivascular spaces, gliosis, and hyalinization of capillaries in deep and subcortical WM (Itoh et al., 2010). However, most studies exploring the microscopic brain pathology in DM1 patients, as well as their relationships with neuroimaging features and splicing changes are case reports or small-scale researches. Clearly, larger follow-up studies are eagerly needed to improve the understandings of pathological alterations in DM1.

DEVELOPMENTAL OR NEURODEGENERATIVE?

Multiple studies have identified a wide range of CNS alterations in DM1 patients. However, the varied characteristics between DM1 patients, such as CTG triplet expansion size, duration time, and age, significantly influence the cerebral performances. In several studies based on cross-sectional analyses, progressive GM loss and increased rate of cortex volume loss correlated with age have been reported (Weber et al., 2010; Minnerop et al., 2011; Caso et al., 2014; Serra et al., 2015; Zanigni et al., 2016; Cabada et al., 2017). A longitudinal study evaluating MRI in DM1 patients also revealed that the WM degeneration and ventricular enlargement progressed over time, though it varied between different individuals (Conforti et al., 2016). However, other studies did not find significant associations between WMHL and age or a significant increase of WML during disease progression (Meola and Sansone, 2007; Itoh et al., 2010; Bajrami et al., 2017; Cabada et al., 2017). Moreover, studies by Antonini et al. (2004) demonstrated a significantly reduced GM volume which was negatively correlated with age in DM1 patients, whereas WM volume was shown not to be correlated with cortical atrophy or age. Thus, further longitudinal evaluations are still need to assess spatiotemporal imaging changes. Regarding clinical features, Sansone et al. (2007) noted a progression in frontal cognitive impairment (attentional) in both DM1 and DM2 patients. Studies by Winblad and Gallais reported a cognitive decline in adult-onset DM1 is positively related to the earlier onset and longer duration of the disease (Winblad et al., 2016; Gallais et al., 2017). Moreover, a close relationship between CNS defects and CTG expansion size has also been discovered. For example, the impaired facial emotion recognition is significantly related to CTG repeat size (Winblad et al., 2006). The extent of GM and WM damage could be correlated with CTG expansion (Serra et al., 2015). And longer CTG expansion sizes could indicate a larger decrease in GM volume (Labayru et al., 2019). Further studies are needed to determine the progressive pattern of CNS dysfunctions.

Whether the progressive cerebral involvement in DM1 patients is due to a developmental or a neurodegenerative process is still an open question (Axford and Pearson, 2013). A variety of neurodegenerative pathological features, including NFTs, LBs and WM abnormalities, as well as a progressive cognitive decline reported by a limited number of longitudinal studies have been found in DM1 patients, which support that DM1 is in part a neurodegenerative process. However, another view supports that the progressive CNS dysfunction may be responsible for cognitive impairment, rather than neurodegenerative changes, since the distinct brain alteration patterns different from neurodegenerative features might also be associated with cognitive impairments in DM1 (Axford and Pearson, 2013; van der Plas et al., 2019; Labayru et al., 2020; Langbehn et al., 2021). A newly emerged opinion proposes that DM1 could be considered a progeroid disease (an early and accelerated aging process) (Sansone et al., 2007; Modoni et al., 2008; Caso et al., 2014; Winblad et al., 2016; Gallais et al., 2017; Solovyeva et al., 2021), as typical symptoms related to aging, such as cognitive decline, occur in the early years. However, a recent study shown an interesting contrast, that the presentation of simple tasks is hugely decreased while that of complex tasks are mostly retained in DM1, which is different from normal aging (Gallais et al., 2017). Further, it's worth noting that in the

congenital/childhood-onset DM1 patients, typical molecular and clinical deficits are observed during early developmental processes, which indicate an influence of DM1 on early brain development.

By the way, there are also some limited studies comparing the different characteristics between different phenotypes of DM1 (based on age-onset). In the congenital/childhood-onset DM1 patients, typical clinical deficits including intellectual disability and behavioral abnormalities are frequently reported, without further decline over these ages (Dhaenens et al., 2011; Caillet-Boudin et al., 2014; Fernandez-Gomez et al., 2019; Lindeblad et al., 2019). In addition, compared with adult-onset DM1 patients, verbal intelligence and memory was significantly deteriorated in juvenile-onset DM1 patients, reflecting a more pronounced developmental process in the juvenile type (Woo et al., 2019). However, in contrast, other studies demonstrated that adult-onset DM1 patients presented with more pronounced decrease of quality of life than juvenile-onset DM1 patients in almost all domains (Rakocevic-Stojanovic et al., 2014). A cross sectional study identified a significant cognitive impairment progression by aging in the majority of the cognitive domains in adult-onset DM1 patients (Baldanzi et al., 2016a), suggesting the existence of progressive degeneration. However, verbal memory abilities were relatively preserved, suggesting different changing patterns involved in memory and cognitive deficits (Baldanzi et al., 2016a). Regarding to neuroimaging observations, Caso et al. (2014) observed a more severe damage of GM in adult-onset DM1 patients than in juvenile-onset DM1 patients, supporting a degenerative origin of GM abnormalities. Conversely, the severe and distributed WM microstructural damage detected in both types might support a developmental change of microstructural WM damage. In 2020, the first longitudinal study of structural brain involvement in pediatric and adult/late-onset DM1 shown that the brain volume loss over time in both groups was not significant compared with their healthy controls, thus supporting the probable occurrence of the neurodevelopmental process. However, these findings cannot completely rule out the existence of the neurodegenerative process, since patients were not yet in their 60's at follow-up (Labayru et al., 2020). In the future, additional studies with larger-sample and longitudinal observations are still needed to further clarify the feature of DM1 brain damages.

THERAPEUTIC STRATEGIES OF DM1

Management of Neurological Defects

To date, there are no specific therapeutic agents available to reverse neurological defects in DM1. Modalities for management mainly rely on supportive care, including sleep hygiene improvement, cognitive−behavioral therapy, aerobic exercise training, and careful use of stimulant drugs. Sleep−related disorders have been recognized as primary symptoms of CNS involvement in DM1. Early recognition and treatment of sleep disorder breathing with nocturnal non-invasive mechanical ventilation have served as important countermeasures to deal with these problems (Pincherle et al., 2012). In a large clinical cohort study, scientists found that patients who insist on home mechanical ventilation for $\geq$5 h/24 h shown significantly higher survival rates than those who use it less (Seijger et al., 2021), and their tolerance and adherence were remarkably high. Besides, the biggest multicenter, randomized clinical trial in DM1 named the Observational Prolonged Trial in Myotonic Dystrophy Type 1 to Improve Quality of Life-Standards, a Target Identification Collaboration (OPTIMISTIC) revealed that cognitive behavioral therapy significantly improved the ability for activity and social participation at 10 months in severely fatigued patients with DM1 (NCT02118779) (Okkersen et al., 2018). Compared with usual care, cognitive behavioral therapy plus aerobic exercise training also increased the physical activity in DM1 patients (OPTIMISTIC) (van Engelen, 2015), indicating this therapy as a promising interventions for severe fatigue in DM1. Stimulant drugs also shown the potential to treat EDS. In 2007, the American Academy of Sleep Medicine (AASM) declared that MPH might be an effective tool for treating DM1-related EDS (Morgenthaler et al., 2007). However, a Cochrane review on well-designed psychostimulant trials in patients with DM1 and EDS pointed out the lack of evidence to support its routine use (Annane et al., 2002). Some clinical studies reported that modafinil might improve hypersomnia and fatigue without significantly increasing activity levels in DM1 (Hilton-Jones et al., 2012; Laberge et al., 2013). However, respiratory insufficiency (due to abnormal central drive and respiratory muscle weakness) and sleep fragmentation related to central or obstructive apnea must be excluded (Harper et al., 2002). Except for treating sleep-related disorders, in *Mbnl2*–/– mice, mirtazapine, a kind of antidepressant, has been discovered to reverse cognitive impairments and depression, as well as reduce microglia and neuronal loss (Ramon-Duaso et al., 2020). Moreover, metformin treatment reversed the metabolic and mitochondrial dysfunction and the accelerated aging process, such as impaired proliferation, in fibroblasts derived from DM1 patients (García-Puga et al., 2020). And its beneficial effects on muscle function have been confirmed in several clinical trials (Bassez et al., 2018). Since basic science reports have proposed the important role of abnormal insulin signaling in the brain (Nieuwenhuis et al., 2019), it indicates another possible therapeutic mechanism for metformin in DM1 brain. Furthermore, therapies *via* modulating glutamate levels and dopaminergic function have also emerged to attract more and more attention (Sicot et al., 2017; Serra et al., 2020b), which provide new insights for future DM1 CNS treatment.

Great progress of molecular therapies has been made in DM1, however, before we can move these treatments into clinical trials, there is also a great need to identify feasible outcome measures to evaluate the effectiveness of these therapies by characterizing the component of CNS deficits in DM1. Currently, the main outcome measures actually used to study CNS involvements in DM1 patients are represented by a variety of patient questionnaires and clinical neuropsychological tests which can assess cognitive and behavioral dysfunctions, and computerized neuroimaging techniques which can assess neuroimaging alterations (summarized in **Tables 2**–**4**). Besides, given the high heterogeneity of symptoms in DM1 patients,

several patient-reported outcome measures are also developed, such as DM1 activity and participation scale for clinical use (DM1-ActivC), and the fatigue and daytime sleepiness scale (FDSS) (Hermans et al., 2013, 2015), which have shown valid measurements in DM1 populations (Angelini and Siciliano, 2020). Notably, due to the increasing risk and higher severity of COVID-19 in DM1 patients, and the difficulty in contacting a doctor during the COVID-19 epidemic, the Italian Association for Glycogenosis (AIG) developed telemedicine equipment, the AIGkit application (AIGkit app), which allows patients to receive constant remote monitoring by using dedicated questionnaires and getting personalized treatment (Symonds et al., 2017). A review by Simoncini et al. (2020) comprehensively summarized the clinical instruments available for cognitive and behavioral measures and neuroimaging assessment in DM1 brain. In the future, additional investigations are warranted to improve the reliability of these available measures, as well as to discover the new outcome markers.

Potential Therapeutic Strategies

With significant advances in understanding the molecular pathogenesis of DM1, several approaches targeting disease mechanisms have been developed, such as antisense oligonucleotide (ASO)-based therapy, small-molecule therapy, genome editing, non-coding RNAs (ncRNAs)-based therapy, and iPSC technique, which target different steps in the pathological process of DM1 (Mulders et al., 2010; Magaña and Cisneros, 2011). Focusing on the most upstream target should block the initiation of the toxic cascade and correct more defects in tissues. Since most therapeutic efforts of DM1 mainly focused on the myocardium and skeletal muscle, and only few studies described their effects on the neurological defects, we briefly introduce their roles in the treatment of DM1 and their therapeutic potential in CNS deficits, hoping to provide references for DM1 CNS treatment. **Figure 2** specifically introduced the current management measures as well as promising therapeutic strategies expected to be applied to DM1 CNS disorders.

Antisense Oligonucleotides

Antisense oligonucleotide is one of the important approaches which can target toxic RNA. It consists of a strand of nucleotides that can bind to a specific pre-mRNA/mRNA sequence and then alters protein synthesis through several mechanisms. In DM1, ASOs can interfere with the interaction between MBNL1 protein and toxic RNA, mainly by targeting the CUG repeat to reduce mutant transcripts, or by RNase-H-mediated degradation of expanded transcription (Klein et al., 2015). Other alterative mechanisms including inhibiting mRNA translation or altering RNA stability (Bennett and Swayze, 2010; Schoch and Miller, 2017).

Till now, various kinds of ASOs have shown efficacy *in vitro* and *in vivo* DM1 treatments. In 2003, scientists produced a retrovirus that expressed a 149-base pair (bp) antisense RNA, complementary to the $(CUG)_{13}$ repeats and the proceeding 110-bp region (Furling et al., 2003). Injection of this ASO into human DM1 myoblasts significantly decreased toxic RNA and normalized CELF1 levels, eventually ameliorating the delay of muscle fusion and IR (Furling et al., 2003). However, this approach also reduced the level of normal *DMPK* transcripts and proteins. Since the unmodified ASOs are unstable and could easily be degraded, several chemical modifications to ASOs were developed to increase their stability and affinity for the target mRNA (Bennett et al., 2017; Khorkova and Wahlestedt, 2017). The first and the most widely used generation of modification was the phosphorothioate (PS) backbone modification (Bennett et al., 2017; Schoch and Miller, 2017), usually together with sugar modifications such as 2′-O-methyl (2′-O-Me) and 2′-O-methoxyethyl (2′-MOE). In 2009, a fully 2′-O-Me-PS-modified ASO, complementary to CUG repeats, called CAG7, was developed for DM1. Administration of this ASO in muscle tissue of DM500 mice (a DM1 model carrying > 300 *DMPK* CTG repeats) and HSA^{LR}20b mice (a DM1 model expressing human skeletal actin transcripts containing ∼250 *DMPK* CTG repeats) silenced the expression of mutant RNA and decreased the formation of nuclear foci in a selective and (CUG)n-length-dependent manner (Mulders et al., 2009). Subsequently, morpholino ASO was discovered, which can bind to the toxic RNA and inhibit its interactions with proteins as well as disrupt CUG-exp-MBNL1 complexes. CAG25 was the first morpholino ASO to be used in DM1. Injection of CAG25 into muscle fibers of HSA^{LR} mice by intramuscular injection followed by *in vivo* electroporation significantly reversed myotonia within 4–5 weeks, accompanied with the increased translation of the mutant RNA (Wheeler et al., 2009). Since morpholino ASO does not induce cleavage of target mRNA, they do not affect normal *DMPK* transcripts and proteins (Summerton, 1999).

To date, it is still a question whether *DMPK* knout-out will indeed cause DM1 phenotype. Some studies reported that both *DMPK*± and *DMPK*-/- mice shown abnormal cardiac conduction (Berul et al., 1999, 2000), and homozygous deletion also exhibited skeletal myopathy and muscle weakness (Reddy et al., 1996), while other findings countered that the administration of *DMPK*-targeting ASOs with heterozygous deletion did not influence the normal cardiac or muscle function in mice, thereby supporting the feasibility and safety of ASOs usage in DM1 (Carrell et al., 2016). In the future, more relevant experiments are needed to reach a conclusion.

Since nuclear-retained CUG repeats are sensitive to antisense silencing, and RNase H are essentially ubiquitous expressed in nuclear (Suzuki et al., 2010), the recruitment of diverse gapmer-based ASOs shown promising futures *via* mediating RNase H cleavage and decay of the target RNA (Walder and Walder, 1988; Wheeler et al., 2012; Nguyen and Yokota, 2020). In HSA^{LR} mice, subcutaneous injection of gapmer ASOs significantly degraded expanded CUG transcripts as well as lncRNAs in skeletal muscle, reversing MBNL1 sequestration, myotonia, and mis-splicing without apparent off-target effects (Schoch and Miller, 2017). This strategy is also more attractive since it's highly specific to expanded CUG repeats compared with normal-size repeats, and could maintain effects for 1 year after the treatment. Besides, BNANC gapmers targeting the DMPK 3′ UTR specifically knockdown the expanded CUG RNA and reversed the mis-splicing and RNA foci accumulation without inducing caspase activation (Manning et al., 2017). Moreover,

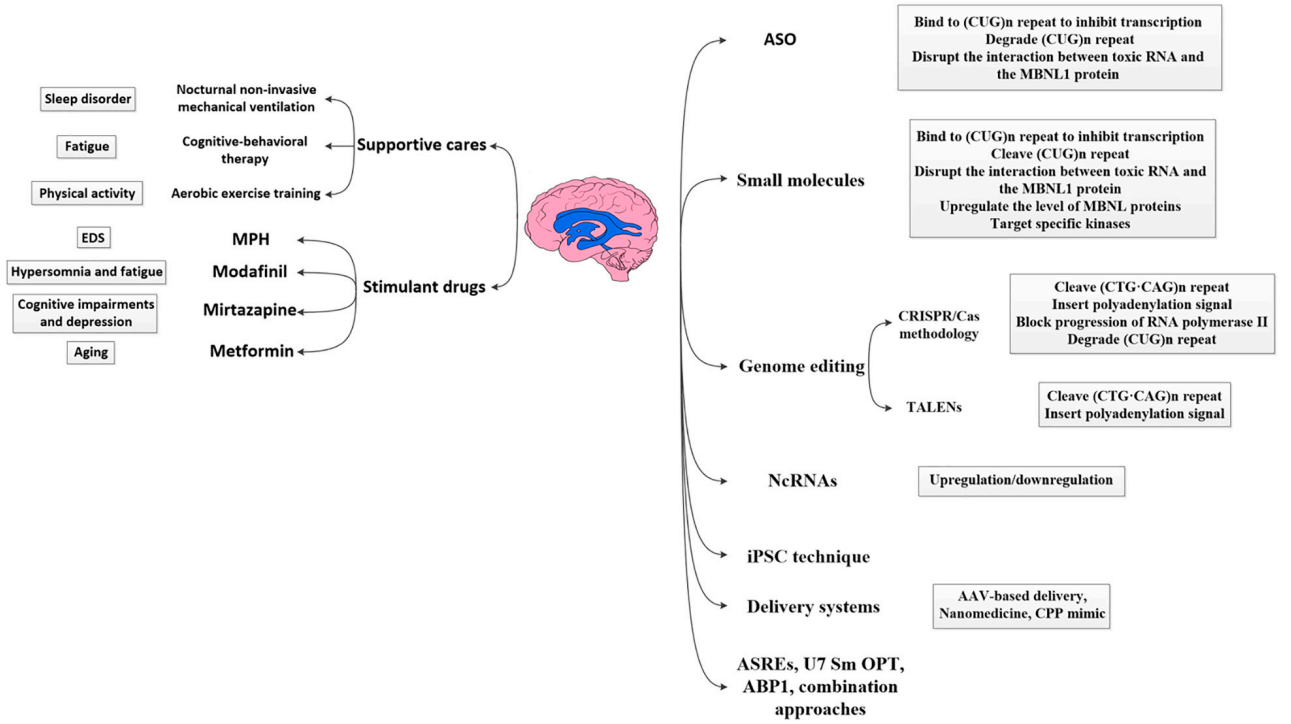

FIGURE 2 | Current and future therapeutic strategies applied to DM1 CNS disorders. The therapeutic strategies for DM1 CNS disorders can be divided into available management measures and future promising strategies. Available modalities for management mainly rely on supportive care, including nocturnal non-invasive mechanical ventilation, cognitive–behavioral therapy, aerobic exercise training, and careful use of stimulant drugs such as MPH, modafinil, mirtazapine, and metformin. Future potential therapeutic strategies currently investigated include ASO-based therapy, small-molecule therapy, genome editing, ncRNAs-based therapy, iPSC technique and so on, which target different levels in the pathological process of DM1 (i.e., DNA level, RNA level, and protein level). Besides, the application of various effective delivery systems also improved the transportation efficiency and promoted the wide distribution of drugs. DM1, myotonic dystrophy type 1; MPH, methylphenidate; EDS, excessive daytime sleepiness; NcRNA, non-coding RNAs; iPSC, induced pluripotent stem cell; AAV, adeno-associated viral vector; ASREs, artificial site-specific RNA endonucleases; CPP, cell-penetrating peptide; ABP1, D-amino acid hexapeptide; ASO, antisense oligonucleotide; CRISPR-Cas9, clustered regularly interspaced short palindromic repeats (CRISPR)/CRISPR-associated system 9; TALEN, transcription activator-like effector nucleases; MBNL, muscleblind-like.

the combinative application of gapmer and CAG25 morpholino produced synergistic effects to reduce expanded CUG repeats by 80% and almost eliminate RNA foci in DM1 cell culture, and get a smaller CUG repeats reduction in skeletal muscle of DM1 mice by half (Lee et al., 2012). However, the competition between gapmer and CAG25 in targeting the CUG repeats might limit their effects.

Other chemical modifications of ASOs also significantly optimized its characteristics. For example, the establishment of modified human U7 small nuclear RNAs (hU7-snRNAs), which contain a poly-CAG antisense sequence targeting the mutant CUG repeats, specifically degraded toxic RNA transcripts without influencing the products of wild-type DMPK alleles (Francois et al., 2011). Since the instability of expanded CTG repeats is a critical characteristic of DM1, which could be enhanced by RNA repeats, recent work shown that early intervention with CAG-repeat ASOs can not only reduce RNA toxicity but also stabilize CTG:CAG repeats at subpathogenic lengths in both DM1 human cells and transgenic mice model (Nakamori et al., 2011). One study using a 2′-4′-constrained ethyl-modified (cEt) ASO (ISIS 486178) effectively decreased *DMPK* mRNA levels in multiple organs of DMSXL mice or cynomolgus monkeys (Pandey et al., 2015). This ASO also exhibits a high level of RNA binding affinity and *in vivo* potency, without any association with muscle or cardiac toxicity. Furthermore, the systemic treatment with ASO (ISIS 486178) targeted to the non-CUG sequence within the 3′-UTR of *DMPK* also specifically rescued DM1 phenotypes of myotonia and cardiac conduction defects in DM200 mice [a DM1 model carrying a GFP-DMPK 3′-UTR (CTG) 200 transgene] (Jauvin et al., 2017; Yadava et al., 2020). In order to overcome the low efficiency of ASOs due to its wide distribution, Klein et al. (2019) developed an arginine-rich 466 cell-penetrating peptide (CPP). Compared with previous ASO strategies, this Pip6a-conjugated morpholino phosphorodiamidate oligomer (PMO) significantly increased ASO delivery into striated muscles after systemic administration in HSA^{LR} mice. Only low-dose treatment with Pip6a-PMO-CAG

sufficiently rescued splicing defects and myotonia in mice (Klein et al., 2019). Hsieh et al. (2018) designed a short miniPEG-γ peptide with terminal pyrenees, which also exhibited high affinity and sequence specificity to toxic RNA repeats and successfully disrupted the CUG-exp–MBNL1 complex. With the new discovery of the imbalance in the splice isoform profile of *DMPK* in DM1 (Groenen et al., 2000; Wansink et al., 2003), two chemically modified ASOs were developed to prompt exon skipping from mRNA and degrade the CUG repeat from pre-mRNA in fibroblasts of DM1 patients. Disappointingly, neither strategy was as successful as predicted, but they did improve the DM1-related molecular phenotypes (Stepniak-Konieczna et al., 2020). It's worth noting that a newly selected ASO called ISIS-DMPKRx (ISIS 598769) gapmer-type candidate has been evaluated in a Phase 1/2a clinical trial for the treatment of DM1 (Lim et al., 2017), for it can bind to a specific 3′-UTR gene sequence outside the CUG repeat and degrade toxic RNA (NCT023412011). Though it presented great safety and tolerance, IONIS proposed an inefficient effect on the functional and biological endpoints set in the trial since no sufficient drug could reach the muscles.

Though a variety of modifications have improved pharmacokinetic and pharmacodynamic properties of ASOs, the systemic and tissue-targeted implementation of ASOs are still challenging due to their poor intracellular uptake in some tissues (particularly skeletal muscle, heart and brain) (Muntoni and Wood, 2011). To overcome this disadvantages, different administration routes were developed to increase the tissue specificity. Nowadays, the delivery of ASOs to a single muscle by intramuscular injection have been frequently used in DM1 pre-clinical trials. Given the multi-organ or systemic features of DM1, systemic delivery *via* intraperitoneal, subcutaneous, or intravenous administration results in a rapid and widespread absorption of ASOs to various peripheral tissues (Yin et al., 2008; Hua et al., 2011). Since the highly charged ASOs cannot cross the BBB (Smith et al., 2006), intraventricular or intrathecal injections were invented to directly introduce ASOs into the CSF or parenchyma, which highly increased the delivery efficiency and ensured adequate distribution of drugs in the CNS (Miller et al., 2013; Chiriboga et al., 2016). However, though intrathecal delivery is currently shown safe and well-tolerated, it's relatively invasive compared with other administrations. Identification of easier ASO delivery routes to the CNS such as intranasal administration may be an important step to promote their translation to human clinical trials. In addition, assisted delivery systems such as CPPs (Lebleu et al., 2008; Lehto et al., 2012; Boisguérin et al., 2015), nanoparticles (Wang et al., 2015) and adeno-associated virus (AAV) vectors (Danos, 2008), also increase the efficacy of ASOs, which would be introduced below.

Small Molecules

Recently, small-molecule-related strategies have received increasing attention in the treatment of DM1. Compared to other strategies, small molecules have many benefits, including low manufacturing cost, better oral delivery with shorter half-lives, longer shelf lives than other biologics, and sufficient biodistribution to affect multiple systems. Since a number of small molecules are existing drugs that explored for new applications, it also reduces the development time and potential risks of toxicity. However, despite the multiple advantages, most small molecules currently established can only target downstream processes to reduce toxic RNA or alter protein levels but cannot correct gene mutations. Meanwhile, their instability *in vivo* also limit their uses.

The mechanisms of molecular therapies can be divided into four aspects: inhibiting transcription of mutant RNA, cleaving CUG repeats, disrupting the interaction between toxic RNA and the MBNL1 protein, or targeting downstream pathways (Mulders et al., 2010; López-Morató et al., 2018; Reddy et al., 2019a). Cell and animal studies have indicated that pentamidine and a series of methylene linker analogs could exert beneficial effects by binding the CTG repeat DNA to inhibit transcription (Coonrod et al., 2013). One study using a DM1 HeLa cell model screened out that multiple microtubule inhibitors can target the toxic CUG RNA to reduce $r(CUG)_{480}$ levels and then rescue mis-splicing to some extent, wherein the clinical microtubule inhibitor colchicine could even make positive effects in HSA^{LR} mice and primary DM1 patient-derived cells (Reddy et al., 2019b). This strategy provides a new avenue for DM1 research and suggests an alternative method of repeat-selective screening. A new molecule, JM642, was reported to have the capacity to bind to the expanded r(CUG) repeat and disrupt ribonuclear foci in the C2C12 DM1 cells and HSA^{LR} mice, finally rescuing mis-splicing (Nakatani et al., 2020). Moreover, several potential therapeutic molecules focus on cleaving the aberrant CUG repeats from disease-affected cells. For example, cugamycin is a small molecule that has been confirmed to selectively bind expanded CUG repeat conjugated to a bleomycin A5-cleaving module to cleave expanded CUG repeat. And deglycobleomycin, an analog in which the carbohydrate domain of bleomycin A5 is removed, significantly improves its selectivity by reducing DNA damage as well as maintaining the cleave ability (Angelbello et al., 2020). The major small-molecule compounds identified in DM1 therapy have been summarized in **Table 5**.

Some promising small molecules have even been tested in clinical trials. For example, AMO-02/tideglusib, a GSK-3β enzyme inhibitor, has been investigated for congenital DM by restoring the expression of CELF1 (Jones et al., 2012; Wang et al., 2019), which improved postnatal survival, weight, and neuromotor activity. Till now, a Phase II clinical trial of tideglusib on patients with congenital and juvenile-onset DM1 has already finished, and most participants presented with improved CNS and clinical neuromuscular performances (Horrigan et al., 2020). And a Phase II/III clinical trial on patients with congenital-onset DM1 is ongoing. In addition, MYD-0124 (erythromycin) and ERX-963 have been shown to bind to the CUG hairpin with high selectivity, reduce nuclear foci and reverse mis-splicing in DM1 vitro and vivo models. A Phase II clinical trial on adult patients with DM1 is currently underway to investigate the clinical effects of erythromycin after oral administration (Jenquin et al., 2019). Other molecules evaluated in clinical trials for specific disease symptoms (e.g., insulin resistance phenotype, myotonia, myalgia, or daytime sleepiness) include metformin, mexiletine, ranolazine, cannabinoids,

TABLE 5 | Small molecules in DM1 treatments.

References	Small molecules	Mechanisms	DM1 models	Effects
Inhibit transcription				
Coonrod et al., 2013	Heptamidine	Interact with the CTG DNA	DM1 HSA^{LR} mice	Reduce CUG repeats Rescue mis-splicing
	Pentamidine and its analogs	Interact with the CTG DNA	DM1 HeLa cells	Rescue mis-splicing Rescue myotonia
Siboni et al., 2015b	Actinomycin D	Interact with the CTG DNA Block progression of the RNA polymerase	DM1 HeLa cells DM1 patient-derived fibroblasts DM1 HSA^{LR} mice	Reduce CUG repeats Reduce ribonuclear foci Rescue mis-splicing
Siboni et al., 2015a	Pentamidine and heptamidine	Inhibit transcription or reduce the stability of the transcript or bind to CUG RNA to displace MBNL proteins	DM1 HeLa cells DM1 HSA^{LR} mice	Reduce CUG RNA levels Reduce ribonuclear foci Rescue mis-splicing
Reddy et al., 2019b	Microtubule inhibitors	Transcriptional interference during failed repair of the expanded CTG repeat	DM1 HeLa cells	Reduce CUG repeats Rescue mis-splicing
	Colchicine	Transcriptional interference during failed repair of the expanded CTG repeat	DM1 HSA^{LR} mice DM1 patient-derived myotubes	Reduce CUG repeats Reduce ribonuclear foci Rescue mis-splicing
Degrade the CUG repeat RNA				
Angelbello et al., 2019	Cugamycin	Cleave the CUG repeat RNA	DM1 patient-derived myotubes DM1 HSA^{LR} mice	Rescue mis-splicing
Angelbello et al., 2020	A small-molecule-deglycobleomycin conjugate	Cleave the CUG repeat RNA	DM1 patient-derived myotubes DM1 C2C12 cells	Reduce CUG repeats with reduced DNA damage Reduce ribonuclear foci Rescue mis-splicing
Disrupt the MBNL–CUG RNA interaction				
Chakraborty et al., 2018	Daunorubicin	Bind to the CUG repeat RNA to displace MBNL1 protein	DM1 patient-derived myoblast cells DM1 patient-derived skin fibroblasts DM1 drosophila-derived cardiomyocytes	Rescue cardiac dysfunction Increase survival Reduce ribonuclear foci Rescue mis-splicing
Hoskins et al., 2014	Dilomofungin	Bind to the CUG repeat RNA to displace MBNL1 protein	C2C12 cells transfected with pLC16	Rescue mis-splicing Increase CUG repeats in nuclear foci
Nakamori et al., 2016	Erythromycin	Bind to the CUG repeat RNA to displace MBNL1 protein	DM1 C2C12 cells DM1 patient-derived fibroblasts DM1 HSA^{LR} mice	Reduce ribonuclear foci Rescue mis-splicing Rescue myotonia
Nakatani et al., 2020	JM642	Bind to the CUG repeat RNA to displace MBNL1 protein	DM1 C2C12 cells DM1 HSA^{LR} mice	Reduce ribonuclear foci Rescue mis-splicing
Warf et al., 2009	Pentamidine	Bind to the CUG repeat RNA to displace MBNL1 protein	DM1 HeLa cells DM1 HEK293 cells DM1 HSA^{LR} mice	Reduce ribonuclear foci Rescue mis-splicing Release MBNL1 from foci
	Neomycin B	Bind to the CUG repeat RNA to displace MBNL2 protein	DM1 HeLa cells	Disrupt the MBNL1–CUG RNA interaction without rescue mis-splicing of any of the tested targets
Childs-Disney et al., 2013	A thiophene-containing compound 1	Bind to MBNL1 protein to inhibits its interaction with RNA	DM1 HeLa cells DM1 C2C12 cells DM1 HEK 293T cells DM1 patient-derived fibroblasts	Improve DM1-associated translational defects Induce splicing defect
	A substituted naphthyridine compound 2	Bind to the CUG repeat RNA to displace MBNL1 protein	DM1 HeLa cells DM1 C2C12 cell DM1 HEK 293T cells	Improve DM1-associated translational defects Improve splicing defects
Luu et al., 2016	Two bisamidinium ligands-linked heterodimer	Bind to the CUG repeat RNA to displace MBNL1 protein	DM1 HeLa cells DM1 drosophila	Reduce ribonuclear foci Rescue mis-splicing Improve eye degeneration and larval crawling defect in drosophila
Ofori et al., 2012	Molecules with benzo[g]quinoline substructure	Bind to the CUG repeat RNA to displace MBNL1 protein	DM1 C2C12 cells DM1 HSA^{LR} mice	Release nuclear CUG-RNA retention Rescue mis-splicing
García-López et al., 2011	D-amino acid hexapeptide	Bind to the CUG repeat RNA to shift duplex it to a single-stranded form	DM1 HSA^{LR} mice DM1 drosophila	Reduce ribonuclear foci Rescue mis-splicing Reverse muscle histopathology

(Continued)

TABLE 5 | (Continued)

References	Small molecules	Mechanisms	DM1 models	Effects
Target downstream proteins				
Wang et al., 2019	Tideglusib	Inhibit GSK3β activity	DM1 HSA^{LR} mice DM1 DMSXL mice CDM1 and DM1 patient-derived myoblasts	Normalize CELF1 activity Reduce CUG repeats Normalize CELF1- and MBNL1-regulated mRNA targets Improve postnatal survival and growth and neuromotor activity
Wojciechowska et al., 2014	C16 and C51	Inhibit ATP-binding site-specific kinase	DM1 patient-derived fibroblasts and myoblasts	Normalize CELF1 activity Reduce the size and number of ribonuclear foci Displace MBNL1 from foci Rescue mis-splicing
Zhang et al., 2017	ISOX and vorinostat	Upregulate MBNL1 protein levels	HeLa cell DM1 patient-derived fibroblasts	Increase MBNL1 protein levels Rescue mis-splicing
Wei et al., 2013	Lithium and TDZD-8	Inhibit GSK3β activity	DM1 HSA^{LR} mice	Normalize CELF1 and cyclin D3 activity Improve DM1 muscle function and histology
Chen et al., 2016	Phenylbutazone	Enhance MBNL1 transcription Attenuate binding of MBNL1 to expanded CUG RNA	DM1 C2C12 cells DM1 HSA^{LR} mice	Increase MBNL1 protein levels Rescue mis-splicing Disrupt MBNL1-CUG RNA interaction Improve DM1 wheel-running activity and muscle histopathology in mice
Wang et al., 2009	Ro-31-8220	Inhibit PKC activity	Tamoxifen-inducible heart-specific DM1 mice	Inhibit PKC-mediated elevation of CELF1 Increase survival Ameliorate the cardiac conduction defects and contraction abnormalities Rescue mis-splicing
Ketley et al., 2014	Ro 31-8220	Target unknown kinase	DM1 patient-derived myoblasts Embryos of zebrafish model	Eliminate nuclear foci Reduce MBNL1 protein in the nucleus Normalize CELF1 activity independent of PKC activity Rescue mis-splicing Rescue the mutant phenotype in zebrafish
Bargiela et al., 2019	Chloroquine	Upregulate MBNL1 and 2 protein levels	DM1 drosophila DM1 HSA^{LR} mice DM1 patient-derived myoblasts	Increase MBNL1 and 2 protein levels Rescue mis-splicing Restore locomotion in drosophila Restore muscle function and histopathology in mice
Yadava et al., 2015	P2D10	Anti-TWEAK activity	Transgenic DM1 mice	Block TWEAK/Fn14 signaling Improve muscle histopathology and functional outcomes
Brockhoff et al., 2017	AICAR	Activate AMPK activity	DM1 HSA^{LR} mice DM1 patient-derived myoblasts	Reduce ribonuclear foci Rescue mis-splicing Reduce myotonia in mice
	Rapamycin	Inhibit mTORC1 activity	DM1 HSA^{LR} mice DM1 patient-derived myoblasts	Improve muscle function *via* splicing-independent mechanisms
Oana et al., 2013	Manumycin A	Inhibit H-Ras farnesyltransferase activity	DM1 C2C12 cells DM1 HSA^{LR} mice	Rescue mis-splicing in mice
Mixed mechanisms				
Jenquin et al., 2018	Furamidine	Inhibit transcription Upregulate MBNL protein levels	DM1 HeLa cells DM1 patient-derived myotubes DM1 HSA^{LR} mice	Reduce CUG repeats Rescue mis-splicing Rescue gene expression Increase MBNL1 and MBNL2 proteins Disrupt the MBNL–CUG complex
Jenquin et al., 2019	A combination of erythromycin and furamidine	Inhibit transcription Disrupt the MBNL–CUG RNA interaction Upregulate MBNL protein levels	DM1 patient-derived myotubes DM1 HSA^{LR} mice	Reduce CUG repeats Rescue mis-splicing Rescue gene expression Increase MBNL1 and MBNL2 proteins Rescue myotonia in mice

DM1, myotonic dystrophy type 1; CDM1, congenital DM1; MBNL, muscleblind-like; CELF, CUGBP/Elav-like family; GSK3β, Glycogen synthase kinase-3β; PKC, Protein kinase C; mTORC1, mTOR complex 1; Fn14, fibroblast growth factor-inducible 14.

pitolisant, Caffeine, and theobromine formulation MYODM™ (Kouki et al., 2005; Logigian et al., 2010; Laustriat et al., 2015; Bassez et al., 2018; Vita et al., 2019; Heatwole et al., 2021; reviewed in Pascual-Gilabert et al., 2021).

Genome Editing

Compared with ASO therapy, the development of genome editing provides an opportunity for permanent corrections of gene mutation, which mainly includes clustered regularly interspaced short palindromic repeats (CRISPR)/CRISPR-associated system (Cas) methodology and transcription activator-like effector nucleases (TALENs) (Richard, 2015; Lee et al., 2016; Long et al., 2016; Nelson et al., 2017; Raaijmakers et al., 2019).

The CRISPR/Cas methodology can be used to target a specific genomic locus in the genome of eukaryotes (Knott and Doudna, 2018). Specifically, the Cas endonuclease is complexed with a small guide RNA (sgRNA) to target a specific genomic locus. Upon binding, the Cas protein generates a double-strand DNA (ds DNA) break by cleaving the DNA in both strands, thereby correcting the genetic defect (Raaijmakers et al., 2019). The main advantage of this strategy is to eliminate the disease defect at the DNA level, so the mutant transcripts and downstream dysregulations are not produced.

So far, the effects of CRISPR/Cas methodology have been validated. In 2017, one study reported that dual cleavage at either side of the CTG expansion can lead to complete and precise excision of the repeat tract from *DMPK* alleles in DM500 cells (myoblasts carrying 500 *DMPK* CTG repeats), myoblasts of DM1 patients, and unaffected individuals. And it also prevented damage to genes in the DM1 locus (van Agtmaal et al., 2017). Then, a CRISPR-Cas9 system from Staphylococcus aureus (Sa) was developed to cleave the CTG repeats in the human *DMPK* locus. A single intramuscular injection of recombinant AAV (rAAV) vectors expressing CRISPR-SaCas9 and selected sgRNAs has been shown to successfully delete the mutant CTG repeats in muscle fibers and reduce the RNA foci in myonuclei of DMSXL mice (Lo Scrudato et al., 2019).

Except for targeting the mutant DNA, RNA-targeting Cas9 (RCas9) systems which can bind to single-stranded RNA were also investigated (Strutt et al., 2018). Batra et al. (2017) found that through delivering a truncated RCas9 system in human DM1 cells, the toxic mRNAs were highly eliminated and aberrant splicing was corrected. This approach also has fewer side effects, since it does not affect normal transcripts. However, the delivery of RCas9 would gradually decay in the genome, which means the requirement of repeat treatments. Other scientists also proposed methods to prevent expanded transcription by inserting a homology-directed polyadenylation signal into the *DMPK* gene (Wang Y. et al., 2018), or recruiting catalytically deficient Cas9 (dCas9) to the repeat effectively to block progression of RNA polymerase II (Pinto et al., 2017). A recent review by Raaijmakers et al. (2019) carefully elaborated CRISPR/Cas-mediated approaches that target the causative mutation in the DNA and the RNA that cause DM1.

In recent years, some novel Cas-associated strategies have gradually emerged. For example, CRISPR-Cas13a is an RNA guided RNase. Zhang et al. (2020) using Leptotrichia shahii (Lsh) Cas13a in DM1 patient-derived myoblasts successfully degraded the expanded CUG RNA and reversed several important mis-splicing events. CRISPR/Cas9-associated base editing (BE) technology is a new therapy that do not rely on a dsDNA break at target sites but directly mediate the conversion of base pairs, and thus reduce the deletions or insertions (Komor et al., 2016; Gaudelli et al., 2017). However, the disability to generate precise edits beyond the allowed mutations might be a huge challenge.

Transcription activator-like effector nucleases is a newly discovered genome editing tool. It relies on modular transcription factors called transcription activator-like effectors, which enables the targeting of any specific DNA sequence (Sun and Zhao, 2013). Previous studies have reported that a dedicated TALEN can induce a dsDNA break into a CAG/CTG tri-nucleotide repeat in heterozygous yeast diploid cells, which shortened the repeat tract with nearly 100% efficacy and very high specificity (Richard et al., 2014). Currently, TALENs has shown great potential in the treatment of DM1. For example, TALENs application corrected the genetic defect of iPSCs, which contribute to the development of autologous stem cell therapy (Xia et al., 2015; Gao et al., 2016). By the way, TALENs seem to be the safest way to shorten trinucleotide repeats to non-pathological lengths, though more research is needed to combat possible off-target effects, immunogenicity to either the genome editing components or delivery particles and unpredictable DNA repair upon cleavage near the unstable repeat.

Non-coding RNAs

NcRNAs are RNA molecules that cannot be translated into proteins but are responsible for important regulatory events in cells (Fabbri et al., 2019). There are several types of ncRNAs, including microRNAs (miRNAs), long ncRNAs (lncRNAs), and circular RNAs (circRNAs). To date, global changes in ncRNA expression patterns in DM1 (Czubak et al., 2019a; López Castel et al., 2019; Voellenkle et al., 2019), as well as their key roles in contributing to DM pathogenesis have been presented (Perbellini et al., 2011; Wheeler et al., 2012; Gudde et al., 2016, 2017; Koutsoulidou et al., 2017; Czubak et al., 2019a,b; López Castel et al., 2019; Koehorst et al., 2020), which make them attractive biomarkers (Gambardella et al., 2010; Perbellini et al., 2011; Rau et al., 2011; Fernandez-Costa et al., 2013; Kalsotra et al., 2014; Perfetti et al., 2014, 2016; Koutsoulidou et al., 2015, 2017; Fritegotto et al., 2017; Koehorst et al., 2020; Pegoraro et al., 2020) and therapeutic targets in DM1 (Rau et al., 2011; Koutalianos et al., 2015; Zhang et al., 2016; Cerro-Herreros et al., 2018, 2020; López Castel et al., 2019; Sabater-Arcis et al., 2020). For example, muscle-specific miRNAs (myomiRNAs) like miR-1, miR-133a, miR-133b, and miR-206 as well as myostatin have been considered as attractive biomarkers of DM1 rehabilitation (Pegoraro et al., 2020). Besides, the therapeutic potential of miRNAs have been detected. Koutalianos et al. (2015) shown that in muscle cells from patients with congenital DM1, upregulation of the miR-206 expression by transfection with a miR-206 mimic into cells overexpressing CEFL1 induced myogenesis by inhibiting the expression of CELF1 and Twist-1. Replenishing of miR-7 with agomiR-7 reversed DM1 myoblast fusion defects and myotube growth, while blocking of miR-7 mediated by oligonucleotide worsen the outcomes (Sabater-Arcis et al., 2020). Silencing the regulatory

dme-miR-277 and dme-miR-304 by miRNA sponge constructs successfully upregulated MBNL expression at the RNA and protein levels in a DM1 drosophila model, which then rescued mis-splicing and reduced muscle atrophy (Cerro-Herreros et al., 2016). This attempt evaluated miRNA sponge constructs as a powerful and attractive strategy to treat DM1 by blocking specific miRNAs. In recent years, RNA interference (RNAi) technology has attracted increased attention in DM1 (Bisset et al., 2015). Bisset et al. (2015) reported that miRNA-based RNAi hairpins delivered by rAAV vectors significantly downregulated mutant transcripts and reduced muscle pathology in HSA^{LR} mice. Besides, the intramuscular injection and electroporation of synthetic short interfering RNAs (siRNAs) significantly reduced toxic RNA transcripts and nuclear foci in HSA^{LR} mice (Sobczak et al., 2013). Antisense technology (antagomiRs) is a newly developed approach to block specific miRNA. Cerro-Herreros et al. (2020) reported that subcutaneous administration of antagomiR-23b in HSA^{LR} mice strongly increased the level of MBNL1 protein and reversed mis-splicing, grip strength, and myotonia in a dose-dependent manner. However, despite the huge potential of miRNA-based interventions, most of these attempts are still in preclinical phases because of their instability and delivery deficits.

Induced Pluripotent Stem Cell Technique

Nowadays, different differentiated cell models, such as neurons or muscle cells, have been used to investigate pathological mechanisms and to evaluate therapeutic strategies of DM1 before clinical validation (Larsen et al., 2011). However, these cell models are strongly limited due to the low *DMPK* transcript levels in affected cells and genetic background variation. Thus, there is a great need to generate alternative myogenic models that can be reliably used for *in vitro* disease modeling and/or drug screening purposes. It's well-known that iPSCs are self-renewal and can differentiate into any cell type, including neurons and muscles cells. Since genome editing methodology could correct the genetic defect of iPSCs as mentioned before, the various phenotypes observed in DM1 can be subsequently reversed by correcting the lengths of CUG repeats in iPSCs and iPSC-derived cells, thereby offering a great translational platform for therapeutic development. Combining human iPSC lines and genome editing technology to create isogenic cell lines can also eliminate background genetic variation that might affect the expected results. In addition, reprogramming of somatic cells to iPSCs has been reported a valuable tool for disease modeling and drug discovery. Mondragon-Gonzalez and Perlingeiro (2018) established two DM1 iPSC lines from patient-derived fibroblasts, which then be differentiated into myotubes. The iPSC-derived myotubes highly recapitulate the molecular features of DM1 while ASO treatment successfully abolished RNA foci and rescued BIN1 mis-splicing. These results indeed confirmed DM1 iPSCs a kind of valuable alternative myogenic model to study DM1 pathogenesis and screen candidate drugs.

Assisted Delivery Systems

The inefficacy of conventional drug delivery and low bioavailability of drugs led to the rapid progress of assisted delivery systems in recent years. Currently, a number of delivery strategies have shown great potential in enhancing the efficacy of therapeutic molecules while minimizing their off-target effects, which can be broadly divided into four types: polymeric, peptide, lipid, and viral delivery systems, wherein AAV-based gene therapy has emerged to be a potent and promising therapeutic tool for DM1. Compared with other strategies, AAV vectors permanently change genetic defects and avoid repeated administrations. Given the multisystemic symptoms of DM1, they can also achieve systemic delivery (Gregorevic et al., 2004; Arruda et al., 2005). Kanadia et al. (2006) reported that upregulation of MBNL1 by AAV-mediated transfection to skeletal muscle effectively reversed mis-splicing and myotonia in HSA^{LR} mice. Besides, systemic AAV-delivered RNAi significantly improved disease phenotype in HSA^{LR} mice (Bisset et al., 2015). Currently, a possible AAV-delivered ASO, AT466 is being established to reduce the toxic RNA levels in cells derived from DM1 patients by RNA degradation, exon skipping or both (Audentes).[1] Recent efforts on viral delivery to the CNS have also taken an exciting leap forward (Miller et al., 2012). The delivery of AAV9 *via* intravenous administration could traverse the BBB in both neonate and adult animals (van der Bent et al., 2018), which provides a promising tool to treat CNS disorders.

The hydrophilic nature as well as large size and high charge of peptides and proteins prevents their penetration across biological membranes. In order to achieve delivery of therapeutic peptide and protein into cells as well as across epithelial barriers and the BBB, a family of delivery vectors called CPPs has been developed, which shown the potential to traverse cellular membranes and promote the uptake of therapeutic peptides with lower toxicity. To date, CPPs have been applied for intracellular, transepithelial, and transendothelial delivery of various therapeutic cargos. Regarding DM1, one study using the CPP mimic as a scaffold to assemble the multivalent ligand construct significantly increased their binding affinity, which then contributed to phenotypic improvement in a DM1 drosophila model (Bai et al., 2016). Compared to unconjugated PMO, systemic administration of Pip6a-conjugated morpholino PMO remarkably enhanced ASO delivery into DM1 mice muscles. Besides, several CPPs have also been identified to mediate cargo delivery across the BBB and exerted protection in the brain (Kilic et al., 2003, 2004; Dietz et al., 2006). And the combination of CPPs and intranasal administration may further enhance CNS delivery (Kamei and Takeda-Morishita, 2015; McGowan et al., 2016; Khafagy et al., 2020; Akita et al., 2021). However, the BBB-specific CPPs remain not to be found and the mechanisms driving the transportation of CPPs are still unknown.

In order to overcome the instability, limited distribution, rapid degradation and toxicity of therapeutic molecules, nanomedicine has been rapidly developed as an effective drug delivery system in recent years, which greatly improved the efficiency and tissue compatibility of gene therapy, increased safety, and ensured systemic distribution (Koebis et al., 2013; Hermans et al., 2015; Lee et al., 2017; Amini et al., 2019), relying on their adjustable physicochemical properties to prevent toxicity and to carry

[1] www.audentestx.com/innovative-therapies

specific biological molecules to target sites (Andreana et al., 2021). In HSA^{LR} mice, using bubble liposomes as delivery tools significantly improved the delivery efficiency of PMO into muscles, which then increased the expression of chloride channel 1 (Clcn1) protein in skeletal muscle and ameliorated the myotonia (Koebis et al., 2013). Besides, given the inefficiency of macromolecules to cross the BBB, the small nanocarriers-mediated transport, including active transport (e.g., receptor-mediated endocytosis) and facilitated diffusion, also provided a promising pathway for smooth BBB passage of large cargos and targeting various cells with intracellular localization specificity (Hernando et al., 2018; Di Filippo et al., 2021; Nehra et al., 2021; Song et al., 2021). Toward future directions, the combinative applications of these delivery vectors and administration routes would attracted more and more attentions since they provide numerous chances for the discovery of both safe and effective delivery strategies to avoid the side effects of any signal technique.

Other Potential Strategies

Artificial site-specific RNA endonucleases (ASREs) are newly discovered molecules specifically targeting mutant RNA accumulated in the nucleus. The results of Zhang et al. (2014) shown that ASRE treatment significantly decreased nuclear foci formation and reversed the mis-splicing of DM1-related genes with few side effects on wild-type alleles. U7 small nuclear ribonucleoproteins (snRNPs) are a specific type of snRNPs that do not participate in splicing mediation but is a key factor in the unique 3′ end processing of replication-dependent histone (RDH) pre-mRNAs. The modified U7 snRNP (U7 Sm OPT) has been used as a promising tool for gene therapy in splicing defects-associated diseases by targeting splicing to induce efficient skipping or inclusion of selected exons. It has multiple advantages, such as small size, good stability, ability to accumulate in the nucleus without toxicity and immunoreactivity, and low risk of transgene dysregulation. In addition, using U7 Sm OPT as a tool in gene therapy also ensures lifelong treatment. Gadgil and Raczyńska et al. (2021) demonstrated that incorporating ASO into the U7 Sm OPT successfully avoided repeated administration. Injection of U7 Sm OPT containing ASO with 15 CAG repeats in skeletal muscle cells isolated from DM1 patients resulted in long-time improvement in splicing and differentiation defects in a dose-dependent manner, without affecting the wild-type *DMPK* transcripts (Le Hir et al., 2013). The critical properties of U7 snRNP might deploy it as a new tool in gene therapy in the future. In a DM1 drosophila model, researchers screened a D-amino acid hexapeptide (ABP1) which can induce the CUG hairpin into a single-stranded conformation and bind the CUG RNA without displacing MBNL1. Compared to ASOs, this method avoids affecting endogenous transcripts. In fly eyes and muscles, overexpression of natural, L-amino acid ABP1 analogs reduced RNA toxicity. And in HSA^{LR} mice, ABP1 reversed muscle histopathology and partially rescued mis-splicing of MBNL1 targets (García-López et al., 2011). Notably, combination approaches such as different small molecules or gene therapies targeting different processes have also attracted increasing attention. This may produce greater benefits in disease modulation than simply additional effects. Importantly, this combination treatment might also reduce off-target effects.

Therapeutic Strategies Targeting Central Nervous System

The current advances in therapeutic strategies should also be applicable in principle to CNS since the pathogenesis of CNS deficits is similar to that of other organs, such as RNA toxicity and splicing defects. However, the existence of BBB hinders the delivery and distribution of drugs in the brain. Therefore, the ideal therapeutic agents need to be able to cross the BBB readily. Some improvements have been made, such as intracellular delivery of the therapeutic molecules to promote uptake, administering molecules intracerebroventricularly or intrathecally (Baughan et al., 2009; Geary et al., 2015), or regulating the molecule size and charge to achieve an efficient delivery to the brain. Recent advances also found that intranasal delivery efficiently bypasses the BBB and highly increases the CNS concentrations of drugs and is non-invasive. Besides, the combination of U7 methodology with highly efficient AAV-mediated delivery, receptor-mediated endocytosis of ASOs, and nanoparticles-, exosomes- or CPP-based delivery of large cargos also favor the BBB passage and the higher distributions of drugs in the CNS (Foust and Kaspar, 2009; Krupa et al., 2014; McGowan et al., 2015, 2016; Bai et al., 2016; Kristensen et al., 2016). In conclusion, all of these therapeutic agents, administration routes, and assisted delivery systems create numerous chances for the discovery of effective therapies for CNS disorders.

Several molecules applied for CNS treatment have shown positive effects in preclinical trials, which may provide new thoughts for DM1 CNS treatment. For example, in mice overexpressing *APP*, intracerebroventricular injections of PS-modified ASOs significantly reduced the expression of APP protein and improved learning and memory deficits (Kumar et al., 2000). In the Alzheimer's disease (AD) mouse model, a designed 2′-O-Me-PS-modified ASO sustainly increased exon 19 splicing of apolipoprotein E receptor 2 (ApoER2) as well as restored synaptic function and learning and memory (Hinrich et al., 2016). Besides, an 2′MOE-modified ASO called IONIS MAPTRx (ISIS 814907) has been evaluated in a phase I/II study in patients with mild AD (NCT03186989), as it highly reduced the expression of tau protein through targeting MAPT mRNA. Hu et al. (2021) using a 20-mer RNase H-active gapmer ASO combined with a 3-month exercise training program in old HSA^{LR} mice reversed all measures of fatigue, though they did not detect the index of fatigue due to CNS dysfunctions. These findings may provide new thoughts for DM1 CNS treatment. Murlidharan et al. (2016) discovered a lab-derived AAV chimeric (AAV2g9), which has favorable CNS properties derived from both parental counterparts, AAV2 and AAV9. Administration of CRISPR/Cas9 with this synthetic AAV vector into the CSF minimized systemic leakage and reduced the sequestration and gene transfer in off-target organs.

The modification of stem cells also offers a new chance for CNS treatment. Previous studies have shown that NSC derived from ES cells or iPSCs could present critical features

of DM1 (Marteyn et al., 2011; Denis et al., 2013; Xia and Ashizawa, 2015; Xia et al., 2015). In DM1 NSCs, insertion of poly A signals upstream of *DMPK* CTG repeats by TALEN-mediated homologous recombination significantly eliminated mutant transcripts and nuclear RNA foci, corrected mis-splicing, and ultimately reversed phenotypes (Xia et al., 2015; Gao et al., 2016). Despite the broad prospects of strategies in CNS treatment, there are still many challenges, such as lower efficiency and distribution to CNS and safety regarding immune response and gene therapy specificity. In addition, no studies have discussed the targeted brain cell types of different strategies and the corresponding alterations of brain cells after treatment. The resolution of these issues may provide a deeper understanding of the therapeutic mechanisms of drugs.

LIMITATIONS AND FUTURE DIRECTIONS

Though great progresses have been made, there are still many limitations in current studies that hinder the understanding of the complex nature of CNS defects and the development of new treatments. Firstly, despite the current knowledge of the molecular basis underlying CNS defects, it is still unclear how these molecular alterations could be translated into specific pathological changes and clinical symptoms, nor do we know how these deficits progress over time. In the future, more longitudinal studies with large sample size are needed to fully understand the DM1 neuropathology and its progression. Secondly, although several cell and animal models have been developed to reproduce the DM1 gene mutation and pathogenesis similar to the human phenotype, such as MBNL-loss or CELF-overexpressing phenotypes, or *in vitro* and *ex vivo* alternatives which can assist animal experimentation, none of them completely recreate the multisystemic phenotypes of DM1, which block the in-depth assessment of DM1 defects and effective evaluations of feasible interventions. Thirdly, more applicable patient questionnaires and clinical neurocognitive evaluation protocols should be investigated to better identify the disease component and serve as potential markers to evaluate the effectiveness of therapeutic strategies. Fourthly, at the pharmacotherapeutic level, more efforts are needed to improve drug delivery efficiency, biodistribution and availability, and reduce toxicity. Meanwhile, the design of drugs for CNS treatment must be able to readily cross the BBB.

CONCLUSION

In this review, we primarily focus on CNS involvement in DM1, outlining the primary pathological alterations and pathogenesis underlying CNS. Then, we highlight promising therapeutic strategies for DM1. Excepting for some available drugs targeting for specific neurological impairments, the promising results of some biological molecules (i.e., ASO, small molecules, CRISPR/Cas9, ncRNA.) *via* targeting mutant DNA, RNA, or downstream proteins in preclinical models or even clinical trials have also provided relevant candidates for DM1 treatment. Particularly, a variety of re-purposed small molecules drugs have been evaluated in DM1, which present with low manufacturing cost, greater safety and stability *in vivo* treatment. Meanwhile, the development of screening and rational design technologies also promote the production of newly potent small molecules, which increases the availability of small molecule therapy in DM1 in the near future. In principle, these interventions should be applicable to the CNS, since strategies such as eliminating toxic RNAs, reducing the formation of nuclear foci, or restoring the levels of splicing-related factors are also effective in brain cells, however, additional researches are still needed to improve the understanding of DM1 progression and to transfer available therapeutic strategies and knowledge into actionable clinical applications.

AUTHOR CONTRIBUTIONS

JL wrote the first draft of the manuscript. X-LY and Z-NG prepared the figures. SH and YY reviewed and edited the manuscript. All authors contributed to critical revision of the manuscript and approved the final manuscript for submission.

FUNDING

This work was supported by the National Natural Science Foundation of China (81971105) to Z-NG, the Program for JLU Science and Technology Innovative Research Team (2017TD-12), and the Jilin Provincial Key Laboratory (20190901005JC) to YY.

REFERENCES

Akiguchi, I., Nakano, S., Shiino, A., Kimura, R., Inubushi, T., Handa, J., et al. (1999). Brain proton magnetic resonance spectroscopy and brain atrophy in myotonic dystrophy. *Arch. Neurol.* 56, 325–330. doi: 10.1001/archneur.56.3.325

Akita, T., Kimura, R., Akaguma, S., Nagai, M., Nakao, Y., Tsugane, M., et al. (2021). Usefulness of cell-penetrating peptides and penetration accelerating sequence for nose-to-brain delivery of glucagon-like peptide-2. *J. Control. Release* 335, 575–583. doi: 10.1016/j.jconrel.2021.06.007

Amini, M. A., Abbasi, A. Z., Cai, P., Lip, H., Gordijo, C. R., Li, J., et al. (2019). Combining tumor microenvironment modulating nanoparticles with doxorubicin to enhance chemotherapeutic efficacy and boost antitumor immunity. *J. Natl. Cancer Institute* 111, 399–408. doi: 10.1093/jnci/djy131

Anderson, P. J. (2013). Leader of the pack - neuropsychological assessment, 5th Edition, Muriel Lezak, Diane B. Howieson, Erin D. Bigler, & Daniel Tranel. *J. Int. Neuropsychol. Soc.* 19, 488–489. doi: 10.1017/S1355617713000337

Andreadis, A. (2012). Tau splicing and the intricacies of dementia. *J. Cell. Physiol.* 227, 1220–1225. doi: 10.1002/jcp.22842

Andreana, I., Repellin, M., Carton, F., Kryza, D., Briançon, S., Chazaud, B., et al. (2021). Nanomedicine for gene delivery and drug repurposing in the treatment of muscular dystrophies. *Pharmaceutics* 13:278. doi: 10.3390/pharmaceutics13020278

Angeard, N., Gargiulo, M., Jacquette, A., Radvanyi, H., Eymard, B., and Héron, D. (2007). Cognitive profile in childhood myotonic dystrophy type 1: is there a global impairment? *Neuromusc. Disord.* 17, 451–458. doi: 10.1016/j.nmd.2007.02.012

Angeard, N., Jacquette, A., Gargiulo, M., Radvanyi, H., Moutier, S., Eymard, B., et al. (2011). A new window on neurocognitive dysfunction in the childhood form of myotonic dystrophy type 1 (DM1). *Neuromusc. Disord.* 21, 468–476. doi: 10.1016/j.nmd.2011.04.009

Angelbello, A. J., DeFeo, M. E., Glinkerman, C. M., Boger, D. L., and Disney, M. D. (2020). Precise targeted cleavage of a r(CUG) repeat expansion in cells by using a small-molecule-deglycobleomycin conjugate. *ACS Chem. Biol.* 15, 849–855. doi: 10.1021/acschembio.0c00036

Angelbello, A. J., Rzuczek, S. G., McKee, K. K., Chen, J. L., Olafson, H., Cameron, M. D., et al. (2019). Precise small-molecule cleavage of an r(CUG) repeat expansion in a myotonic dystrophy mouse model. *Proc. Natl. Acad. Sci. U.S.A.* 116, 7799–7804. doi: 10.1073/pnas.1901484116

Angelini, C., and Pinzan, E. (2019). Advances in imaging of brain abnormalities in neuromuscular disease. *Ther. Adv. Neurol. Disord.* 12:1756286419845567. doi: 10.1177/1756286419845567

Angelini, C., and Siciliano, G. (2020). Neuromuscular diseases and Covid-19: advices from scientific societies and early observations in Italy. *Eur. J. Transl. Myol.* 30:9032. doi: 10.4081/ejtm.2019.9032

Angelini, C., and Tasca, E. (2012). Fatigue in muscular dystrophies. *Neuromusc. Disord.* 22(Suppl. 3), S214–S220. doi: 10.1016/j.nmd.2012.10.010

Annane, D., Miller, R., and Barnes, P. (2002). Psychostimulants for hypersomnia (excessive daytime sleepiness) in myotonic dystrophy. *Cochrane Database Syst. Rev.* 4:Cd003218. doi: 10.1002/14651858.cd003218

Antonini, G., Mainero, C., Romano, A., Giubilei, F., Ceschin, V., Gragnani, F., et al. (2004). Cerebral atrophy in myotonic dystrophy: a voxel based morphometric study. *J. Neurol. Neurosurg. Psychiatry* 75, 1611–1613. doi: 10.1136/jnnp.2003.032417

Arruda, V. R., Stedman, H. H., Nichols, T. C., Haskins, M. E., Nicholson, M., Herzog, R. W., et al. (2005). Regional intravascular delivery of AAV-2-F.IX to skeletal muscle achieves long-term correction of hemophilia B in a large animal model. *Blood* 105, 3458–3464. doi: 10.1182/blood-2004-07-2908

Axford, M. M., and Pearson, C. E. (2013). Illuminating CNS and cognitive issues in myotonic dystrophy: workshop report. *Neuromusc. Disord.* 23, 370–374. doi: 10.1016/j.nmd.2013.01.003

Azotla-Vilchis, C. N., Sanchez-Celis, D., Agonizantes-Juárez, L. E., Suárez-Sánchez, R., Hernández-Hernández, J. M., Peña, J., et al. (2021). Transcriptome analysis reveals altered inflammatory pathway in an inducible glial cell model of myotonic dystrophy type 1. *Biomolecules* 11:159. doi: 10.3390/biom11020159

Bai, Y., Nguyen, L., Song, Z., Peng, S., Lee, J., Zheng, N., et al. (2016). Integrating display and delivery functionality with a cell penetrating peptide mimic as a scaffold for intracellular multivalent multitargeting. *J. Am. Chem. Soc.* 138, 9498–9507. doi: 10.1021/jacs.6b03697

Bajrami, A., Azman, F., Yayla, V., Cagirici, S., Keskinkiliç, C., and Sozer, N. (2017). MRI findings and cognitive functions in a small cohort of myotonic dystrophy type 1: retrospective analyses. *Neuroradiol. J.* 30, 23–27. doi: 10.1177/1971400916678223

Baldanzi, S., Cecchi, P., Fabbri, S., Pesaresi, I., Simoncini, C., Angelini, C., et al. (2016b). Relationship between neuropsychological impairment and grey and white matter changes in adult-onset myotonic dystrophy type 1. *Neuroimage Clin.* 12, 190–197. doi: 10.1016/j.nicl.2016.06.011

Baldanzi, S., Bevilacqua, F., Lorio, R., Volpi, L., Simoncini, C., Petrucci, A., et al. (2016a). Disease awareness in myotonic dystrophy type 1: an observational cross-sectional study. *Orphanet J. Rare Dis.* 11:34. doi: 10.1186/s13023-016-0417-z

Bargiela, A., Sabater-Arcis, M., Espinosa-Espinosa, J., Zulaica, M., Lopez de Munain, A., and Artero, R. (2019). Increased Muscleblind levels by chloroquine treatment improve myotonic dystrophy type 1 phenotypes in in vitro and in vivo models. *Proc. Natl. Acad. Sci. U.S.A.* 116, 25203–25213. doi: 10.1073/pnas.1820297116

Bassez, G., Audureau, E., Hogrel, J. Y., Arrouasse, R., Baghdoyan, S., Bhugaloo, H., et al. (2018). Improved mobility with metformin in patients with myotonic dystrophy type 1: a randomized controlled trial. *Brain* 141, 2855–2865. doi: 10.1093/brain/awy231

Batra, R., Charizanis, K., Manchanda, M., Mohan, A., Li, M., Finn, D. J., et al. (2014). Loss of MBNL leads to disruption of developmentally regulated alternative polyadenylation in RNA-mediated disease. *Mol. Cell* 56, 311–322. doi: 10.1016/j.molcel.2014.08.027

Batra, R., Nelles, D. A., Pirie, E., Blue, S. M., Marina, R. J., Wang, H., et al. (2017). Elimination of toxic microsatellite repeat expansion RNA by RNA-targeting Cas9. *Cell* 170, 899.e10–912.e10. doi: 10.1016/j.cell.2017.07.010

Baughan, T. D., Dickson, A., Osman, E. Y., and Lorson, C. L. (2009). Delivery of bifunctional RNAs that target an intronic repressor and increase SMN levels in an animal model of spinal muscular atrophy. *Hum. Mol. Genet.* 18, 1600–1611. doi: 10.1093/hmg/ddp076

Bellamy, T. C. (2006). Interactions between *Purkinje neurones* and *Bergmann glia*. *Cerebellum* 5, 116–126. doi: 10.1080/14734220600724569

Bennett, C. F., Baker, B. F., Pham, N., Swayze, E., and Geary, R. S. (2017). Pharmacology of antisense drugs. *Annu. Rev. Pharmacol. Toxicol.* 57, 81–105. doi: 10.1146/annurev-pharmtox-010716-104846

Bennett, C. F., and Swayze, E. E. (2010). RNA targeting therapeutics: molecular mechanisms of antisense oligonucleotides as a therapeutic platform. *Annu. Rev. Pharmacol. Toxicol.* 50, 259–293. doi: 10.1146/annurev.pharmtox.010909.105654

Bertrand, J. A., Jean, S., Laberge, L., Gagnon, C., Mathieu, J., Gagnon, J. F., et al. (2015). Psychological characteristics of patients with myotonic dystrophy type 1. *Acta Neurol. Scand.* 132, 49–58. doi: 10.1111/ane.12356

Berul, C. I., Maguire, C. T., Aronovitz, M. J., Greenwood, J., Miller, C., Gehrmann, J., et al. (1999). DMPK dosage alterations result in atrioventricular conduction abnormalities in a mouse myotonic dystrophy model. *J. Clin. Investig.* 103, R1–R7. doi: 10.1172/jci5346

Berul, C. I., Maguire, C. T., Gehrmann, J., and Reddy, S. (2000). Progressive atrioventricular conduction block in a mouse myotonic dystrophy model. *J. Intervent. Cardiac Electrophysiol.* 4, 351–358. doi: 10.1023/a:1009842114968

Bird, T. D. (1993). "Myotonic dystrophy type 1," in *Genereviews((r))*, eds M. P. Adam, H. H. Ardinger, R. A. Pagon, S. E. Wallace, L. J. H. Bean, K. Stephens, et al. (Seattle, WA: University of Washington).

Bisset, D. R., Stepniak-Konieczna, E. A., Zavaljevski, M., Wei, J., Carter, G. T., Weiss, M. D., et al. (2015). Therapeutic impact of systemic AAV-mediated RNA interference in a mouse model of myotonic dystrophy. *Hum. Mol. Genet.* 24, 4971–4983. doi: 10.1093/hmg/ddv219

Boisguérin, P., Deshayes, S., Gait, M. J., O'Donovan, L., Godfrey, C., Betts, C. A., et al. (2015). Delivery of therapeutic oligonucleotides with cell penetrating peptides. *Adv. Drug Deliv. Rev.* 87, 52–67. doi: 10.1016/j.addr.2015.02.008

Breton, É, Légaré, C., Overend, G., Guay, S. P., Monckton, D., Mathieu, J., et al. (2020). DNA methylation at the DMPK gene locus is associated with cognitive functions in myotonic dystrophy type 1. *Epigenomics* 12, 2051–2064. doi: 10.2217/epi-2020-0328

Brockhoff, M., Rion, N., Chojnowska, K., Wiktorowicz, T., Eickhorst, C., Erne, B., et al. (2017). Targeting deregulated AMPK/mTORC1 pathways improves muscle function in myotonic dystrophy type I. *J. Clin. Investig.* 127, 549–563. doi: 10.1172/jci89616

Brook, J. D., McCurrach, M. E., Harley, H. G., Buckler, A. J., Church, D., Aburatani, H., et al. (1992). Molecular basis of myotonic dystrophy: expansion of a trinucleotide (CTG) repeat at the 3′ end of a transcript encoding a protein kinase family member. *Cell* 68, 799–808. doi: 10.1016/0092-8674(92)90154-5

Cabada, T., Díaz, J., Iridoy, M., López, P., Jericó, I., Lecumberri, P., et al. (2020). Longitudinal study in patients with myotonic dystrophy type 1: correlation of brain MRI abnormalities with cognitive performances. *Neuroradiology* 63, 1019–1029. doi: 10.1007/s00234-020-02611-9

Cabada, T., Díaz, J., Iridoy, M., López, P., Jericó, I., Lecumberri, P., et al. (2021). Longitudinal study in patients with myotonic dystrophy type 1: correlation of brain MRI abnormalities with cognitive performances. *Neuroradiology* 63, 1019–1029.

Cabada, T., Iridoy, M., Jericó, I., Lecumberri, P., Seijas, R., Gargallo, A., et al. (2017). Brain involvement in myotonic dystrophy type 1: a morphometric and diffusion tensor imaging study with neuropsychological correlation. *Arch. Clin. Neuropsychol.* 32, 401–412. doi: 10.1093/arclin/acx008

Caillet-Boudin, M. L., Fernandez-Gomez, F. J., Tran, H., Dhaenens, C. M., Buee, L., and Sergeant, N. (2014). Brain pathology in myotonic dystrophy: when tauopathy meets spliceopathy and RNAopathy. *Front. Mol. Neurosci.* 6:57. doi: 10.3389/fnmol.2013.00057

Carpentier, C., Ghanem, D., Fernandez-Gomez, F. J., Jumeau, F., Philippe, J. V., Freyermuth, F., et al. (2014). Tau exon 2 responsive elements deregulated in myotonic dystrophy type I are proximal to exon 2 and synergistically regulated

by MBNL1 and MBNL2. *Biochim. Biophys. Acta* 1842, 654–664. doi: 10.1016/j.bbadis.2014.01.004

Carrell, S. T., Carrell, E. M., Auerbach, D., Pandey, S. K., Bennett, C. F., Dirksen, R. T., et al. (2016). Dmpk gene deletion or antisense knockdown does not compromise cardiac or skeletal muscle function in mice. *Hum. Mol. Genet.* 25, 4328–4338. doi: 10.1093/hmg/ddw266

Caso, F., Agosta, F., Peric, S., Rakočevid-Stojanovid, V., Copetti, M., Kostic, V. S., et al. (2014). Cognitive impairment in myotonic dystrophy type 1 is associated with white matter damage. *PLoS One* 9:e104697. doi: 10.1371/journal.pone.0104697

Cerro-Herreros, E., Fernandez-Costa, J. M., Sabater-Arcis, M., Llamusi, B., and Artero, R. (2016). Derepressing muscleblind expression by miRNA sponges ameliorates myotonic dystrophy-like phenotypes in *Drosophila*. *Sci. Rep.* 6:36230. doi: 10.1038/srep36230

Cerro-Herreros, E., González-Martínez, I., Moreno-Cervera, N., Overby, S., Pérez-Alonso, M., Llamusí, B., et al. (2020). Therapeutic potential of AntagomiR-23b for treating myotonic dystrophy. *Mol. Ther. Nucleic Acids* 21, 837–849. doi: 10.1016/j.omtn.2020.07.021

Cerro-Herreros, E., Sabater-Arcis, M., Fernandez-Costa, J. M., Moreno, N., Perez-Alonso, M., Llamusi, B., et al. (2018). miR-23b and miR-218 silencing increase Muscleblind-like expression and alleviate myotonic dystrophy phenotypes in mammalian models. *Nat. Commun.* 9:2482. doi: 10.1038/s41467-018-04892-4

Chakraborty, M., Sellier, C., Ney, M., Pascal, V., Charlet-Berguerand, N., Artero, R., et al. (2018). Daunorubicin reduces MBNL1 sequestration caused by CUG-repeat expansion and rescues cardiac dysfunctions in a *Drosophila* model of myotonic dystrophy. *Dis. Models Mech.* 11:dmm032557. doi: 10.1242/dmm.032557

Chang, L., Ernst, T., Osborn, D., Seltzer, W., Leonido-Yee, M., and Poland, R. E. (1998). Proton spectroscopy in myotonic dystrophy: correlations with CTG repeats. *Arch. Neurol.* 55, 305–311. doi: 10.1001/archneur.55.3.305

Charizanis, K., Lee, K. Y., Batra, R., Goodwin, M., Zhang, C., Yuan, Y., et al. (2012). Muscleblind-like 2-mediated alternative splicing in the developing brain and dysregulation in myotonic dystrophy. *Neuron* 75, 437–450. doi: 10.1016/j.neuron.2012.05.029

Chau, A., and Kalsotra, A. (2015). Developmental insights into the pathology of and therapeutic strategies for DM1: back to the basics. *Dev. Dyn.* 244, 377–390. doi: 10.1002/dvdy.24240

Chen, G., Carter, R. E., Cleary, J. D., Reid, T. S., Ranum, L. P., Swanson, M. S., et al. (2018). Altered levels of the splicing factor muscleblind modifies cerebral cortical function in mouse models of myotonic dystrophy. *Neurobiol. Dis.* 112, 35–48. doi: 10.1016/j.nbd.2018.01.003

Chen, G., Masuda, A., Konishi, H., Ohkawara, B., Ito, M., Kinoshita, M., et al. (2016). Phenylbutazone induces expression of MBNL1 and suppresses formation of MBNL1-CUG RNA foci in a mouse model of myotonic dystrophy. *Sci. Rep.* 6:25317. doi: 10.1038/srep25317

Childs-Disney, J. L., Stepniak-Konieczna, E., Tran, T., Yildirim, I., Park, H., Chen, C. Z., et al. (2013). Induction and reversal of myotonic dystrophy type 1 pre-mRNA splicing defects by small molecules. *Nat. Commun.* 4:2044. doi: 10.1038/ncomms3044

Chiriboga, C. A., Swoboda, K. J., Darras, B. T., Iannaccone, S. T., Montes, J., De Vivo, D. C., et al. (2016). Results from a phase 1 study of nusinersen (ISIS-SMN(Rx)) in children with spinal muscular atrophy. *Neurology* 86, 890–897. doi: 10.1212/wnl.0000000000002445

Çoban, A., Bilgiç, B., Lohmann, E., Küçükali, C., Benbir, G., Karadeniz, D., et al. (2013). Reduced orexin-A levels in frontotemporal dementia: possible association with sleep disturbance. *Am. J. Alzheimers Dis. Dement.* 28, 606–611. doi: 10.1177/1533317513494453

Comim, C. M., Mathia, G. B., Hoepers, A., Tuon, L., Kapczinski, F., Dal-Pizzol, F., et al. (2015). Neurotrophins, cytokines, oxidative parameters and funcionality in progressive muscular dystrophies. *Anais Acad. Bras. Ciencias* 87, 1809–1818. doi: 10.1590/0001-3765201520140508

Conboy, J. G. (2017). Developmental regulation of RNA processing by Rbfox proteins. *Wiley Interdiscip. Rev. RNA* 8:1398. doi: 10.1002/wrna.1398

Conforti, R., de Cristofaro, M., Cristofano, A., Brogna, B., Sardaro, A., Tedeschi, G., et al. (2016). Brain MRI abnormalities in the adult form of myotonic dystrophy type 1: a longitudinal case series study. *Neuroradiol. J.* 29, 36–45. doi: 10.1177/1971400915621325

Coonrod, L. A., Nakamori, M., Wang, W., Carrell, S., Hilton, C. L., Bodner, M. J., et al. (2013). Reducing levels of toxic RNA with small molecules. *ACS Chem. Biol.* 8, 2528–2537. doi: 10.1021/cb400431f

Culebras, A., Feldman, R. G., and Merk, F. B. (1973). Cytoplasmic inclusion bodies within neurons of the thalamus in myotonic dystrophy. A light and electron microscope study. *J. Neurol. Sci.* 19, 319–329. doi: 10.1016/0022-510x(73)90095-6

Czubak, K., Sedehizadeh, S., Kozlowski, P., and Wojciechowska, M. (2019a). An overview of circular RNAs and their implications in myotonic dystrophy. *Int. J. Mol. Sci.* 20:4385. doi: 10.3390/ijms20184385

Czubak, K., Taylor, K., Piasecka, A., Sobczak, K., Kozlowska, K., Philips, A., et al. (2019b). Global increase in circular RNA levels in myotonic dystrophy. *Front. Genet.* 10:649. doi: 10.3389/fgene.2019.00649

Dagenhardt, J., Trinh, A., Sumner, H., Scott, J., Aamodt, E., and Dwyer, D. S. (2017). Insulin signaling deficiency produces immobility in caenorhabditis elegans that models diminished motivation states in man and responds to antidepressants. *Mol. Neuropsychiatry* 3, 97–107. doi: 10.1159/000478049

Danos, O. (2008). AAV vectors for RNA-based modulation of gene expression. *Gene Ther.* 15, 864–869. doi: 10.1038/gt.2008.69

Dasgupta, T., and Ladd, A. N. (2012). The importance of CELF control: molecular and biological roles of the CUG-BP, Elav-like family of RNA-binding proteins. *Wiley Interdiscip. Rev. RNA* 3, 104–121. doi: 10.1002/wrna.107

De Antonio, M., Dogan, C., Hamroun, D., Mati, M., Zerrouki, S., Eymard, B., et al. (2016). Unravelling the myotonic dystrophy type 1 clinical spectrum: a systematic registry-based study with implications for disease classification. *Revue Neurol.* 172, 572–580. doi: 10.1016/j.neurol.2016.08.003

de León, M. B., and Cisneros, B. (2008). Myotonic dystrophy 1 in the nervous system: from the clinic to molecular mechanisms. *J. Neurosci. Res.* 86, 18–26. doi: 10.1002/jnr.21377

Denis, J. A., Gauthier, M., Rachdi, L., Aubert, S., Giraud-Triboult, K., Poydenot, P., et al. (2013). mTOR-dependent proliferation defect in human ES-derived neural stem cells affected by myotonic dystrophy type 1. *J. Cell Sci.* 126(Pt 8), 1763–1772. doi: 10.1242/jcs.116285

Dhaenens, C. M., Schraen-Maschke, S., Tran, H., Vingtdeux, V., Ghanem, D., Leroy, O., et al. (2008). Overexpression of MBNL1 fetal isoforms and modified splicing of Tau in the DM1 brain: two individual consequences of CUG trinucleotide repeats. *Exp. Neurol.* 210, 467–478. doi: 10.1016/j.expneurol.2007.11.020

Dhaenens, C. M., Tran, H., Frandemiche, M. L., Carpentier, C., Schraen-Maschke, S., Sistiaga, A., et al. (2011). Mis-splicing of Tau exon 10 in myotonic dystrophy type 1 is reproduced by overexpression of CELF2 but not by MBNL1 silencing. *Biochim. Biophys. Acta* 1812, 732–742. doi: 10.1016/j.bbadis.2011.03.010

Di Filippo, L. D., Duarte, J., Fonseca-Santos, B., Tavares Júnior, A. G., Araújo, V., Roque Borda, C. A., et al. (2021). Mucoadhesive nanosystems for nose-to-brain drug delivery in the treatment of central nervous system diseases. *Curr. Med. Chem.* doi: 10.2174/0929867328666210813154019 [Epub ahead of print].

Dietz, G. P., Valbuena, P. C., Dietz, B., Meuer, K., Müeller, P., Weishaupt, J. H., et al. (2006). Application of a blood-brain-barrier-penetrating form of GDNF in a mouse model for Parkinson's disease. *Brain Res.* 1082, 61–66. doi: 10.1016/j.brainres.2006.01.083

Douniol, M., Jacquette, A., Cohen, D., Bodeau, N., Rachidi, L., Angeard, N., et al. (2012). Psychiatric and cognitive phenotype of childhood myotonic dystrophy type 1. *Dev. Med. Child Neurol.* 54, 905–911. doi: 10.1111/j.1469-8749.2012.04379.x

Dragileva, E., Hendricks, A., Teed, A., Gillis, T., Lopez, E. T., Friedberg, E. C., et al. (2009). Intergenerational and striatal CAG repeat instability in Huntington's disease knock-in mice involve different DNA repair genes. *Neurobiol. Dis.* 33, 37–47. doi: 10.1016/j.nbd.2008.09.014

Du, J., Campau, E., Soragni, E., Jespersen, C., and Gottesfeld, J. M. (2013). Length-dependent CTG·CAG triplet-repeat expansion in myotonic dystrophy patient-derived induced pluripotent stem cells. *Hum. Mol. Genet.* 22, 5276–5287. doi: 10.1093/hmg/ddt386

Echenne, B., Rideau, A., Roubertie, A., Sébire, G., Rivier, F., and Lemieux, B. (2008). Myotonic dystrophy type I in childhood Long-term evolution in patients surviving the neonatal period. *Eur. J. Paediatr. Neurol.* 12, 210–223. doi: 10.1016/j.ejpn.2007.07.014

Ekström, A. B., Hakenäs-Plate, L., Samuelsson, L., Tulinius, M., and Wentz, E. (2008). Autism spectrum conditions in myotonic dystrophy type 1: a study

on 57 individuals with congenital and childhood forms. *Am. J. Med. Genet. B Neuropsychiatr. Genet.* 147b, 918–926. doi: 10.1002/ajmg.b.30698

Fabbri, M., Girnita, L., Varani, G., and Calin, G. A. (2019). Decrypting noncoding RNA interactions, structures, and functional networks. *Genome Res.* 29, 1377–1388. doi: 10.1101/gr.247239.118

Fardaei, M., Rogers, M. T., Thorpe, H. M., Larkin, K., Hamshere, M. G., Harper, P. S., et al. (2002). Three proteins, MBNL, MBLL and MBXL, co-localize in vivo with nuclear foci of expanded-repeat transcripts in DM1 and DM2 cells. *Hum. Mol. Genet.* 11, 805–814. doi: 10.1093/hmg/11.7.805

Fernandez-Costa, J. M., Garcia-Lopez, A., Zuñiga, S., Fernandez-Pedrosa, V., Felipo-Benavent, A., Mata, M., et al. (2013). Expanded CTG repeats trigger miRNA alterations in Drosophila that are conserved in myotonic dystrophy type 1 patients. *Hum. Mol. Genet.* 22, 704–716. doi: 10.1093/hmg/dds478

Fernandez-Gomez, F., Tran, H., Dhaenens, C. M., Caillet-Boudin, M. L., Schraen-Maschke, S., Blum, D., et al. (2019). Myotonic dystrophy: an RNA toxic gain of function tauopathy? *Adv. Exp. Med. Biol.* 1184, 207–216. doi: 10.1007/978-981-32-9358-8_17

Fiorelli, M., Duboc, D., Mazoyer, B. M., Blin, J., Eymard, B., Fardeau, M., et al. (1992). Decreased cerebral glucose utilization in myotonic dystrophy. *Neurology* 42, 91–94. doi: 10.1212/wnl.42.1.91

Flower, M., Lomeikaite, V., Ciosi, M., Cumming, S., Morales, F., Lo, K., et al. (2019). MSH3 modifies somatic instability and disease severity in Huntington's and myotonic dystrophy type 1. *Brain* 142, 1876–1886. doi: 10.1093/brain/awz115

Foust, K. D., and Kaspar, B. K. (2009). Over the barrier and through the blood: to CNS delivery we go. *Cell Cycle* 8, 4017–4018. doi: 10.4161/cc.8.24.10245

Franc, D. T., Muetzel, R. L., Robinson, P. R., Rodriguez, C. P., Dalton, J. C., Naughton, C. E., et al. (2012). Cerebral and muscle MRI abnormalities in myotonic dystrophy. *Neuromusc. Disord.* 22, 483–491. doi: 10.1016/j.nmd.2012.01.003

Francois, V., Klein, A. F., Beley, C., Jollet, A., Lemercier, C., Garcia, L., et al. (2011). Selective silencing of mutated mRNAs in DM1 by using modified hU7-snRNAs. *Nat. Struct. Mol. Biol.* 18, 85–87. doi: 10.1038/nsmb.1958

Fritegotto, C., Ferrati, C., Pegoraro, V., and Angelini, C. (2017). Micro-RNA expression in muscle and fiber morphometry in myotonic dystrophy type 1. *Neurol. Sci.* 38, 619–625. doi: 10.1007/s10072-017-2811-2

Fu, Y. H., Pizzuti, A., Fenwick, R. G. Jr., King, J., Rajnarayan, S., Dunne, P. W., et al. (1992). An unstable triplet repeat in a gene related to myotonic muscular dystrophy. *Science* 255, 1256–1258. doi: 10.1126/science.1546326

Furling, D., Doucet, G., Langlois, M. A., Timchenko, L., Belanger, E., Cossette, L., et al. (2003). Viral vector producing antisense RNA restores myotonic dystrophy myoblast functions. *Gene Ther.* 10, 795–802. doi: 10.1038/sj.gt.3301955

Furuta, M., Kimura, T., Nakamori, M., Matsumura, T., Fujimura, H., Jinnai, K., et al. (2018). Macroscopic and microscopic diversity of missplicing in the central nervous system of patients with myotonic dystrophy type 1. *Neuroreport* 29, 235–240. doi: 10.1097/wnr.0000000000000968

Gadgil, A., and Raczyńska, K. D. (2021). U7 snRNA: a tool for gene therapy. *J. Gene Med.* 23:e3321. doi: 10.1002/jgm.3321

Gallais, B., Gagnon, C., Mathieu, J., and Richer, L. (2017). Cognitive decline over time in adults with myotonic dystrophy type 1: a 9-year longitudinal study. *Neuromusc. Disord.* 27, 61–72. doi: 10.1016/j.nmd.2016.10.003

Gallais, B., Montreuil, M., Gargiulo, M., Eymard, B., Gagnon, C., and Laberge, L. (2015). Prevalence and correlates of apathy in myotonic dystrophy type 1. *BMC Neurol.* 15:148. doi: 10.1186/s12883-015-0401-6

Gambardella, S., Rinaldi, F., Lepore, S. M., Viola, A., Loro, E., Angelini, C., et al. (2010). Overexpression of microRNA-206 in the skeletal muscle from myotonic dystrophy type 1 patients. *J. Transl. Med.* 8:48. doi: 10.1186/1479-5876-8-48

Gao, Y., Guo, X., Santostefano, K., Wang, Y., Reid, T., Zeng, D., et al. (2016). Genome therapy of myotonic dystrophy type 1 ips cells for development of autologous stem cell therapy. *Mol. Ther.* 24, 1378–1387. doi: 10.1038/mt.2016.97

García-López, A., Llamusí, B., Orzáez, M., Pérez-Payá, E., and Artero, R. D. (2011). In vivo discovery of a peptide that prevents CUG-RNA hairpin formation and reverses RNA toxicity in myotonic dystrophy models. *Proc. Natl. Acad. Sci. U.S.A.* 108, 11866–11871. doi: 10.1073/pnas.1018213108

García-Puga, M., Saenz-Antoñanzas, A., Fernández-Torrón, R., Munain, A. L., and Matheu, A. (2020). Myotonic Dystrophy type 1 cells display impaired metabolism and mitochondrial dysfunction that are reversed by metformin. *Aging* 12, 6260–6275. doi: 10.18632/aging.103022

Gaudelli, N. M., Komor, A. C., Rees, H. A., Packer, M. S., Badran, A. H., Bryson, D. I., et al. (2017). Programmable base editing of A●T to G●C in genomic DNA without DNA cleavage. *Nature* 551, 464–471. doi: 10.1038/nature24644

Geary, R. S., Norris, D., Yu, R., and Bennett, C. F. (2015). Pharmacokinetics, biodistribution and cell uptake of antisense oligonucleotides. *Adv. Drug Deliv. Rev.* 87, 46–51. doi: 10.1016/j.addr.2015.01.008

Gehman, L. T., Stoilov, P., Maguire, J., Damianov, A., Lin, C. H., Shiue, L., et al. (2011). The splicing regulator Rbfox1 (A2BP1) controls neuronal excitation in the mammalian brain. *Nat. Genet.* 43, 706–711. doi: 10.1038/ng.841

Glantz, R. H., Wright, R. B., Huckman, M. S., Garron, D. C., and Siegel, I. M. (1988). Central nervous system magnetic resonance imaging findings in myotonic dystrophy. *Arch. Neurol.* 45, 36–37. doi: 10.1001/archneur.1988.00520250042017

Gonçalves, R. A., Wijesekara, N., Fraser, P. E., and De Felice, F. G. (2019). The link between tau and insulin signaling: implications for Alzheimer's disease and other tauopathies. *Front. Cell. Neurosci.* 13:17. doi: 10.3389/fncel.2019.00017

González-Barriga, A., Lallemant, L., Dincã, D. M., Braz, S. O., Polvèche, H., Magneron, P., et al. (2021). Integrative cell type-specific multi-omics approaches reveal impaired programs of glial cell differentiation in mouse culture models of DM1. *Front. Cell. Neurosci.* 15:662035. doi: 10.3389/fncel.2021.662035

Goodwin, M., Mohan, A., Batra, R., Lee, K. Y., Charizanis, K., Fernández Gómez, F. J., et al. (2015). MBNL sequestration by toxic RNAs and RNA misprocessing in the myotonic dystrophy brain. *Cell Rep.* 12, 1159–1168. doi: 10.1016/j.celrep.2015.07.029

Gregorevic, P., Blankinship, M. J., Allen, J. M., Crawford, R. W., Meuse, L., Miller, D. G., et al. (2004). Systemic delivery of genes to striated muscles using adeno-associated viral vectors. *Nat. Med.* 10, 828–834. doi: 10.1038/nm1085

Groenen, P. J., Wansink, D. G., Coerwinkel, M., van den Broek, W., Jansen, G., and Wieringa, B. (2000). Constitutive and regulated modes of splicing produce six major myotonic dystrophy protein kinase (DMPK) isoforms with distinct properties. *Hum. Mol. Genet.* 9, 605–616. doi: 10.1093/hmg/9.4.605

Gudde, A., van Heeringen, S. J., de Oude, A. I., van Kessel, I. D. G., Estabrook, J., Wang, E. T., et al. (2017). Antisense transcription of the myotonic dystrophy locus yields low-abundant RNAs with and without (CAG)n repeat. *RNA Biol.* 14, 1374–1388. doi: 10.1080/15476286.2017.1279787

Gudde, A. E., González-Barriga, A., van den Broek, W. J., Wieringa, B., and Wansink, D. G. (2016). A low absolute number of expanded transcripts is involved in myotonic dystrophy type 1 manifestation in muscle. *Hum. Mol. Genet.* 25, 1648–1662. doi: 10.1093/hmg/ddw042

Han, S., Nam, J., Li, Y., Kim, S., Cho, S. H., Cho, Y. S., et al. (2010). Regulation of dendritic spines, spatial memory, and embryonic development by the TANC family of PSD-95-interacting proteins. *J. Neurosci.* 30, 15102–15112. doi: 10.1523/jneurosci.3128-10.2010

Harper, P. S., van Engelen, B. G., Eymard, B., Rogers, M., and Wilcox, D. (2002). 99th ENMC international workshop: myotonic dystrophy: present management, future therapy. 9-11 November 2001, Naarden, The Netherlands. *Neuromusc. Disord.* 12, 596–599. doi: 10.1016/s0960-8966(02)00020-2

Hashimoto, T., Tayama, M., Miyazaki, M., Murakawa, K., Kawai, H., Nishitani, H., et al. (1995). Neuroimaging study of myotonic dystrophy. II. MRI measurements of the brain. *Brain Dev.* 17, 28–32. doi: 10.1016/0387-7604(94)00097-h

Heatwole, C., Bode, R., Johnson, N., Quinn, C., Martens, W., McDermott, M. P., et al. (2012). Patient-reported impact of symptoms in myotonic dystrophy type 1 (PRISM-1). *Neurology* 79, 348–357. doi: 10.1212/WNL.0b013e318260cbe6

Heatwole, C., Bode, R., Johnson, N. E., Dekdebrun, J., Dilek, N., Eichinger, K., et al. (2016). Myotonic dystrophy health index: correlations with clinical tests and patient function. *Muscle Nerve* 53, 183–190. doi: 10.1002/mus.24725

Heatwole, C., Johnson, N., Dekdebrun, J., Dilek, N., Eichinger, K., Hilbert, J., et al. (2018). Myotonic dystrophy patient preferences in patient-reported outcome measures. *Muscle Nerve* doi: 10.1002/mus.26066 [Epub ahead of print].

Heatwole, C., Luebbe, E., Rosero, S., Eichinger, K., Martens, W., Hilbert, J., et al. (2021). Mexiletine in myotonic dystrophy type 1: a randomized, double-blind, placebo-controlled trial. *Neurology* 96, e228–e240. doi: 10.1212/wnl.0000000000011002

Hermans, M. C., Hoeijmakers, J. G., Faber, C. G., and Merkies, I. S. (2015). Reconstructing the rasch-built myotonic dystrophy type 1 activity and participation scale. *PLoS One* 10:e0139944. doi: 10.1371/journal.pone.0139944

Hermans, M. C., Merkies, I. S., Laberge, L., Blom, E. W., Tennant, A., and Faber, C. G. (2013). Fatigue and daytime sleepiness scale in myotonic dystrophy type 1. *Muscle Nerve* 47, 89–95. doi: 10.1002/mus.23478

Hernández-Hernández, O., Guiraud-Dogan, C., Sicot, G., Huguet, A., Luilier, S., Steidl, E., et al. (2013a). Myotonic dystrophy CTG expansion affects synaptic vesicle proteins, neurotransmission and mouse behaviour. *Brain* 136(Pt 3), 957–970. doi: 10.1093/brain/aws367

Hernández-Hernández, O., Sicot, G., Dinca, D. M., Huguet, A., Nicole, A., Buée, L., et al. (2013b). Synaptic protein dysregulation in myotonic dystrophy type 1: disease neuropathogenesis beyond missplicing. *Rare Dis.* 1:e25553. doi: 10.4161/rdis.25553

Hernando, S., Herran, E., Figueiro-Silva, J., Pedraz, J. L., Igartua, M., Carro, E., et al. (2018). Intranasal administration of TAT-conjugated lipid nanocarriers loading GDNF for Parkinson's disease. *Mol. Neurobiol.* 55, 145–155. doi: 10.1007/s12035-017-0728-7

Hilton-Jones, D., Bowler, M., Lochmueller, H., Longman, C., Petty, R., Roberts, M., et al. (2012). Modafinil for excessive daytime sleepiness in myotonic dystrophy type 1–the patients' perspective. *Neuromusc. Disord.* 22, 597–603. doi: 10.1016/j.nmd.2012.02.005

Hinrich, A. J., Jodelka, F. M., Chang, J. L., Brutman, D., Bruno, A. M., Briggs, C. A., et al. (2016). Therapeutic correction of ApoER2 splicing in Alzheimer's disease mice using antisense oligonucleotides. *EMBO Mol. Med.* 8, 328–345. doi: 10.15252/emmm.201505846

Hirase, T., and Araki, S. (1984). Cerebrospinal fluid proteins in muscular dystrophy patients. *Brain Dev.* 6, 10–16. doi: 10.1016/s0387-7604(84)80003-0

Horrigan, J., Gomes, T. B., Snape, M., Nikolenko, N., McMorn, A., Evans, S., et al. (2020). A phase 2 study of AMO-02 (Tideglusib) in congenital and childhood-onset myotonic dystrophy type 1 (DM1). *Pediatr. Neurol.* 112, 84–93. doi: 10.1016/j.pediatrneurol.2020.08.001

Hoskins, J. W., Ofori, L. O., Chen, C. Z., Kumar, A., Sobczak, K., Nakamori, M., et al. (2014). Lomofungin and dilomofungin: inhibitors of MBNL1-CUG RNA binding with distinct cellular effects. *Nucleic Acids Res.* 42, 6591–6602. doi: 10.1093/nar/gku275

Hsieh, W. C., Bahal, R., Thadke, S. A., Bhatt, K., Sobczak, K., Thornton, C., et al. (2018). Design of a "mini" nucleic acid probe for cooperative binding of an RNA-repeated transcript associated with myotonic dystrophy type 1. *Biochemistry* 57, 907–911. doi: 10.1021/acs.biochem.7b01239

Hu, N., Kim, E., Antoury, L., Li, J., González-Pérez, P., Rutkove, S. B., et al. (2021). Antisense oligonucleotide and adjuvant exercise therapy reverse fatigue in old mice with myotonic dystrophy. *Mol. Ther. Nucleic Acids* 23, 393–405. doi: 10.1016/j.omtn.2020.11.014

Hua, Y., Sahashi, K., Rigo, F., Hung, G., Horev, G., Bennett, C. F., et al. (2011). Peripheral SMN restoration is essential for long-term rescue of a severe spinal muscular atrophy mouse model. *Nature* 478, 123–126. doi: 10.1038/nature10485

Huguet, A., Medja, F., Nicole, A., Vignaud, A., Guiraud-Dogan, C., Ferry, A., et al. (2012). Molecular, physiological, and motor performance defects in DMSXL mice carrying >1,000 CTG repeats from the human DM1 locus. *PLoS Genet.* 8:e1003043. doi: 10.1371/journal.pgen.1003043

Itoh, K., Mitani, M., Kawamoto, K., Futamura, N., Funakawa, I., Jinnai, K., et al. (2010). Neuropathology does not correlate with regional differences in the extent of expansion of CTG repeats in the brain with myotonic dystrophy type 1. *Acta Histochem. Cytochem.* 43, 149–156. doi: 10.1267/ahc.10019

Jacko, M., Weyn-Vanhentenryck, S. M., Smerdon, J. W., Yan, R., Feng, H., Williams, D. J., et al. (2018). Rbfox splicing factors promote neuronal maturation and axon initial segment assembly. *Neuron* 97, 853.e6–868.e6. doi: 10.1016/j.neuron.2018.01.020

Jauvin, D., Chretien, J., Pandey, S. K., Martineau, L., Revillod, L., Bassez, G., et al. (2017). Targeting DMPK with Antisense Oligonucleotide Improves Muscle Strength in Myotonic Dystrophy Type 1 Mice. *Mol. Ther. Nucleic Acids* 7, 465–474. doi: 10.1016/j.omtn.2017.05.007

Jean, S., Richer, L., Laberge, L., and Mathieu, J. (2014). Comparisons of intellectual capacities between mild and classic adult-onset phenotypes of myotonic dystrophy type 1 (DM1). *Orphanet J. Rare Dis.* 9:186. doi: 10.1186/s13023-014-0186-5

Jenquin, J. R., Coonrod, L. A., Silverglate, Q. A., Pellitier, N. A., Hale, M. A., Xia, G., et al. (2018). Furamidine rescues myotonic dystrophy type I associated mis-splicing through multiple mechanisms. *ACS Chem. Biol.* 13, 2708–2718. doi: 10.1021/acschembio.8b00646

Jenquin, J. R., Yang, H., Huigens, R. W. III, Nakamori, M., and Berglund, J. A. (2019). Combination treatment of erythromycin and furamidine provides additive and synergistic rescue of mis-splicing in myotonic dystrophy type 1 models. *ACS Pharmacol. Transl. Sci.* 2, 247–263. doi: 10.1021/acsptsci.9b00020

Jiang, H., Mankodi, A., Swanson, M. S., Moxley, R. T., and Thornton, C. A. (2004). Myotonic dystrophy type 1 is associated with nuclear foci of mutant RNA, sequestration of muscleblind proteins and deregulated alternative splicing in neurons. *Hum. Mol. Genet.* 13, 3079–3088. doi: 10.1093/hmg/ddh327

Jimenez-Marin, A., Diez, I., Labayru, G., Sistiaga, A., Caballero, M. C., Andres-Benito, P., et al. (2021). Transcriptional signatures of synaptic vesicle genes define myotonic dystrophy type I neurodegeneration. *Neuropathol. Appl. Neurobiol.* doi: 10.1111/nan.12725 [Epub ahead of print].

Jinnai, K., Mitani, M., Futamura, N., Kawamoto, K., Funakawa, I., and Itoh, K. (2013). Somatic instability of CTG repeats in the cerebellum of myotonic dystrophy type 1. *Muscle Nerve* 48, 105–108. doi: 10.1002/mus.23717

Jones, K., Wei, C., Iakova, P., Bugiardini, E., Schneider-Gold, C., Meola, G., et al. (2012). GSK3β mediates muscle pathology in myotonic dystrophy. *J. Clin. Investig.* 122, 4461–4472. doi: 10.1172/jci64081

Kalsotra, A., Singh, R. K., Gurha, P., Ward, A. J., Creighton, C. J., and Cooper, T. A. (2014). The Mef2 transcription network is disrupted in myotonic dystrophy heart tissue, dramatically altering miRNA and mRNA expression. *Cell Rep.* 6, 336–345. doi: 10.1016/j.celrep.2013.12.025

Kamei, N., and Takeda-Morishita, M. (2015). Brain delivery of insulin boosted by intranasal coadministration with cell-penetrating peptides. *J. Control. Release* 197, 105–110. doi: 10.1016/j.jconrel.2014.11.004

Kanadia, R. N., Shin, J., Yuan, Y., Beattie, S. G., Wheeler, T. M., Thornton, C. A., et al. (2006). Reversal of RNA missplicing and myotonia after muscleblind overexpression in a mouse poly(CUG) model for myotonic dystrophy. *Proc. Natl. Acad. Sci. U.S.A.* 103, 11748–11753. doi: 10.1073/pnas.0604970103

Ketley, A., Chen, C. Z., Li, X., Arya, S., Robinson, T. E., Granados-Riveron, J., et al. (2014). High-content screening identifies small molecules that remove nuclear foci, affect MBNL distribution and CELF1 protein levels via a PKC-independent pathway in myotonic dystrophy cell lines. *Hum. Mol. Genet.* 23, 1551–1562. doi: 10.1093/hmg/ddt542

Khafagy, E. S., Kamei, N., Fujiwara, Y., Okumura, H., Yuasa, T., Kato, M., et al. (2020). Systemic and brain delivery of leptin via intranasal coadministration with cell-penetrating peptides and its therapeutic potential for obesity. *J. Control. Release* 319, 397–406. doi: 10.1016/j.jconrel.2020.01.016

Khorkova, O., and Wahlestedt, C. (2017). Oligonucleotide therapies for disorders of the nervous system. *Nat. Biotechnol.* 35, 249–263. doi: 10.1038/nbt.3784

Kilic, U., Kilic, E., Dietz, G. P., and Bähr, M. (2003). Intravenous TAT-GDNF is protective after focal cerebral ischemia in mice. *Stroke* 34, 1304–1310. doi: 10.1161/01.str.0000066869.45310.50

Kilic, U., Kilic, E., Dietz, G. P., and Bähr, M. (2004). The TAT protein transduction domain enhances the neuroprotective effect of glial-cell-line-derived neurotrophic factor after optic nerve transection. *Neuro Degener. Dis.* 1, 44–49. doi: 10.1159/000076669

Kim, K., Lee, S. G., Kegelman, T. P., Su, Z. Z., Das, S. K., Dash, R., et al. (2011). Role of excitatory amino acid transporter-2 (EAAT2) and glutamate in neurodegeneration: opportunities for developing novel therapeutics. *J. Cell. Physiol.* 226, 2484–2493. doi: 10.1002/jcp.22609

Klein, A. F., Dastidar, S., Furling, D., and Chuah, M. K. (2015). Therapeutic approaches for dominant muscle diseases: highlight on myotonic dystrophy. *Curr. Gene Ther.* 15, 329–337. doi: 10.2174/1566523215666150630120537

Klein, A. F., Varela, M. A., Arandel, L., Holland, A., Naouar, N., Arzumanov, A., et al. (2019). Peptide-conjugated oligonucleotides evoke long-lasting myotonic dystrophy correction in patient-derived cells and mice. *J. Clin. Investig.* 129, 4739–4744. doi: 10.1172/jci128205

Klinck, R., Fourrier, A., Thibault, P., Toutant, J., Durand, M., Lapointe, E., et al. (2014). RBFOX1 cooperates with MBNL1 to control splicing in muscle, including events altered in myotonic dystrophy type 1. *PLoS One* 9:e107324. doi: 10.1371/journal.pone.0107324

Knott, G. J., and Doudna, J. A. C. R. I. S. P. R. - (2018). Cas guides the future of genetic engineering. *Science* 361, 866–869. doi: 10.1126/science.aat5011

Kobayakawa, M., Tsuruya, N., and Kawamura, M. (2012). Theory of mind impairment in adult-onset myotonic dystrophy type 1. *Neurosci. Res.* 72, 341–346. doi: 10.1016/j.neures.2012.01.005

Kobayakawa, M., Tsuruya, N., Takeda, A., Suzuki, A., and Kawamura, M. (2010). Facial emotion recognition and cerebral white matter lesions in myotonic dystrophy type 1. *J. Neurol. Sci.* 290, 48–51. doi: 10.1016/j.jns.2009.11.011

Koebis, M., Kiyatake, T., Yamaura, H., Nagano, K., Higashihara, M., Sonoo, M., et al. (2013). Ultrasound-enhanced delivery of morpholino with Bubble liposomes ameliorates the myotonia of myotonic dystrophy model mice. *Sci. Rep.* 3:2242. doi: 10.1038/srep02242

Koehorst, E., Ballester-Lopez, A., Arechavala-Gomeza, V., Martínez-Piñeiro, A., and Nogales-Gadea, G. (2020). The biomarker potential of miRNAs in myotonic dystrophy type I. *J. Clin. Med.* 9:3939. doi: 10.3390/jcm9123939

Komor, A. C., Kim, Y. B., Packer, M. S., Zuris, J. A., and Liu, D. R. (2016). Programmable editing of a target base in genomic DNA without double-stranded DNA cleavage. *Nature* 533, 420–424. doi: 10.1038/nature17946

Kouki, T., Takasu, N., Nakachi, A., Tamanaha, T., Komiya, I., and Tawata, M. (2005). Low-dose metformin improves hyperglycaemia related to myotonic dystrophy. *Diabetic Med.* 22, 346–347. doi: 10.1111/j.1464-5491.2005.01432.x

Koutalianos, D., Koutsoulidou, A., Mastroyiannopoulos, N. P., Furling, D., and Phylactou, L. A. (2015). MyoD transcription factor induces myogenesis by inhibiting Twist-1 through miR-206. *J. Cell Sci.* 128, 3631–3645. doi: 10.1242/jcs.172288

Koutsoulidou, A., Kyriakides, T. C., Papadimas, G. K., Christou, Y., Kararizou, E., Papanicolaou, E. Z., et al. (2015). Elevated muscle-specific miRNAs in serum of myotonic dystrophy patients relate to muscle disease progress. *PLoS One* 10:e0125341. doi: 10.1371/journal.pone.0125341

Koutsoulidou, A., Photiades, M., Kyriakides, T. C., Georgiou, K., Prokopi, M., Kapnisis, K., et al. (2017). Identification of exosomal muscle-specific miRNAs in serum of myotonic dystrophy patients relating to muscle disease progress. *Hum. Mol. Genet.* 26, 3285–3302. doi: 10.1093/hmg/ddx212

Kristensen, M., Birch, D., and Mørck Nielsen, H. (2016). Applications and challenges for use of cell-penetrating peptides as delivery vectors for peptide and protein cargos. *Int. J. Mol. Sci.* 17:185. doi: 10.3390/ijms17020185

Krogias, C., Bellenberg, B., Prehn, C., Schneider, R., Meves, S. H., Gold, R., et al. (2015). Evaluation of CNS involvement in myotonic dystrophy type 1 and type 2 by transcranial sonography. *J. Neurol.* 262, 365–374. doi: 10.1007/s00415-014-7566-6

Krogias, C., and Walter, U. (2016). Transcranial sonography findings in depression in association with psychiatric and neurologic diseases: a review. *J. Neuroimaging* 26, 257–263. doi: 10.1111/jon.12328

Krupa, P., Řehák, S., Diaz-Garcia, D., and Filip, S. (2014). Nanotechnology - new trends in the treatment of brain tumours. *Acta Med.* 57, 142–150. doi: 10.14712/18059694.2015.79

Kullmann, S., Heni, M., Hallschmid, M., Fritsche, A., Preissl, H., and Häring, H. U. (2016). Brain insulin resistance at the crossroads of metabolic and cognitive disorders in humans. *Physiol. Rev.* 96, 1169–1209. doi: 10.1152/physrev.00032.2015

Kumar, V. B., Farr, S. A., Flood, J. F., Kamlesh, V., Franko, M., Banks, W. A., et al. (2000). Site-directed antisense oligonucleotide decreases the expression of amyloid precursor protein and reverses deficits in learning and memory in aged SAMP8 mice. *Peptides* 21, 1769–1775. doi: 10.1016/s0196-9781(00)00339-9

Kuyumcu-Martinez, N. M., Wang, G. S., and Cooper, T. A. (2007). Increased steady-state levels of CUGBP1 in myotonic dystrophy 1 are due to PKC-mediated hyperphosphorylation. *Mol. Cell* 28, 68–78. doi: 10.1016/j.molcel.2007.07.027

Labayru, G., Arenzana, I., Aliri, J., Zulaica, M., López de Munain, A., and Sistiaga, A. A. (2018). Social cognition in myotonic dystrophy type 1: specific or secondary impairment? *PLoS One* 13:e0204227. doi: 10.1371/journal.pone.0204227

Labayru, G., Diez, I., Sepulcre, J., Fernández, E., Zulaica, M., Cortés, J. M., et al. (2019). Regional brain atrophy in gray and white matter is associated with cognitive impairment in Myotonic Dystrophy type 1. *Neuroimage Clin.* 24:102078. doi: 10.1016/j.nicl.2019.102078

Labayru, G., Jimenez-Marin, A., Fernández, E., Villanua, J., Zulaica, M., Cortes, J. M., et al. (2020). Neurodegeneration trajectory in pediatric and adult/late DM1: a follow-up MRI study across a decade. *Ann. Clin. Transl. Neurol.* 7, 1802–1815. doi: 10.1002/acn3.51163

Laberge, L., Gagnon, C., and Dauvilliers, Y. (2013). Daytime sleepiness and myotonic dystrophy. *Curr. Neurol. Neurosci. Rep.* 13:340. doi: 10.1007/s11910-013-0340-9

Ladd, A. N. (2013). CUG-BP, Elav-like family (CELF)-mediated alternative splicing regulation in the brain during health and disease. *Mol. Cell. Neurosci.* 56, 456–464. doi: 10.1016/j.mcn.2012.12.003

Ladd, A. N., Charlet, N., and Cooper, T. A. (2001). The CELF family of RNA binding proteins is implicated in cell-specific and developmentally regulated alternative splicing. *Mol. Cell. Biol.* 21, 1285–1296. doi: 10.1128/mcb.21.4.1285-1296.2001

Ladd, A. N., Nguyen, N. H., Malhotra, K., and Cooper, T. A. (2004). CELF6, a member of the CELF family of RNA-binding proteins, regulates muscle-specific splicing enhancer-dependent alternative splicing. *J. Biol. Chem.* 279, 17756–17764. doi: 10.1074/jbc.M310687200

Langbehn, K. E., van der Plas, E., Moser, D. J., Long, J. D., Gutmann, L., and Nopoulos, P. C. (2021). Cognitive function and its relationship with brain structure in myotonic dystrophy type 1. *J. Neurosci. Res.* 99, 190–199. doi: 10.1002/jnr.24595

Larsen, J., Pettersson, O. J., Jakobsen, M., Thomsen, R., Pedersen, C. B., Hertz, J. M., et al. (2011). Myoblasts generated by lentiviral mediated MyoD transduction of myotonic dystrophy type 1 (DM1) fibroblasts can be used for assays of therapeutic molecules. *BMC Res. Notes* 4:490. doi: 10.1186/1756-0500-4-490

Laustriat, D., Gide, J., Barrault, L., Chautard, E., Benoit, C., Auboeuf, D., et al. (2015). *In vitro* and *In vivo* modulation of alternative splicing by the biguanide metformin. *Mol. Ther. Nucleic Acids* 4:e262. doi: 10.1038/mtna.2015.35

Le Hir, M., Goyenvalle, A., Peccate, C., Précigout, G., Davies, K. E., Voit, T., et al. (2013). AAV genome loss from dystrophic mouse muscles during AAV-U7 snRNA-mediated exon-skipping therapy. *Mol. Ther.* 21, 1551–1558. doi: 10.1038/mt.2013.121

Lebleu, B., Moulton, H. M., Abes, R., Ivanova, G. D., Abes, S., Stein, D. A., et al. (2008). Cell penetrating peptide conjugates of steric block oligonucleotides. *Adv. Drug Deliv. Rev.* 60, 517–529. doi: 10.1016/j.addr.2007.09.002

Leddy, S., Serra, L., Esposito, D., Vizzotto, C., Giulietti, G., Silvestri, G., et al. (2021). Lesion distribution and substrate of white matter damage in myotonic dystrophy type 1: comparison with multiple sclerosis. *Neuroimage Clin.* 29:102562. doi: 10.1016/j.nicl.2021.102562

Lee, H. B., Sundberg, B. N., Sigafoos, A. N., and Clark, K. J. (2016). Genome engineering with TALE and CRISPR systems in neuroscience. *Front. Genet.* 7:47. doi: 10.3389/fgene.2016.00047

Lee, J. E., Bennett, C. F., and Cooper, T. A. (2012). RNase H-mediated degradation of toxic RNA in myotonic dystrophy type 1. *Proc. Natl. Acad. Sci. U.S.A.* 109, 4221–4226. doi: 10.1073/pnas.1117019109

Lee, K., Conboy, M., Park, H. M., Jiang, F., Kim, H. J., Dewitt, M. A., et al. (2017). Nanoparticle delivery of Cas9 ribonucleoprotein and donor DNA in vivo induces homology-directed DNA repair. *Nat. Biomed. Eng.* 1, 889–901. doi: 10.1038/s41551-017-0137-2

Lee, K. Y., Chang, H. C., Seah, C., and Lee, L. J. (2019). Deprivation of muscleblind-like proteins causes deficits in cortical neuron distribution and morphological changes in dendritic spines and postsynaptic densities. *Front. Neuroanat.* 13:75. doi: 10.3389/fnana.2019.00075

Lee, K. Y., Li, M., Manchanda, M., Batra, R., Charizanis, K., Mohan, A., et al. (2013). Compound loss of muscleblind-like function in myotonic dystrophy. *EMBO Mol. Med.* 5, 1887–1900. doi: 10.1002/emmm.201303275

Lehto, T., Kurrikoff, K., and Langel, Ü (2012). Cell-penetrating peptides for the delivery of nucleic acids. *Expert Opin. Drug Deliv.* 9, 823–836. doi: 10.1517/17425247.2012.689285

Leroy, O., Dhaenens, C. M., Schraen-Maschke, S., Belarbi, K., Delacourte, A., Andreadis, A., et al. (2006a). ETR-3 represses Tau exons 2/3 inclusion, a splicing event abnormally enhanced in myotonic dystrophy type I. *J. Neurosci. Res.* 84, 852–859. doi: 10.1002/jnr.20980

Leroy, O., Wang, J., Maurage, C. A., Parent, M., Cooper, T., Buée, L., et al. (2006b). Brain-specific change in alternative splicing of Tau exon 6 in myotonic dystrophy type 1. *Biochim. Biophys. Acta* 1762, 460–467. doi: 10.1016/j.bbadis.2005.12.003

Lim, J. J., Derby, M. A., Zhang, Y., Deng, R., Larouche, R., Anderson, M., et al. (2017). A phase 1, randomized, double-blind, placebo-controlled, single-ascending-dose study to investigate the safety, tolerability, and pharmacokinetics of an anti-influenza B virus monoclonal antibody,

MHAB5553A, in healthy volunteers. *Antimicrob. Agents Chemother.* 61:e00279-17. doi: 10.1128/aac.00279-17

Lindeblad, G., Kroksmark, A. K., and Ekström, A. B. (2019). Cognitive and adaptive functioning in congenital and childhood forms of myotonic dystrophy type 1: a longitudinal study. *Dev. Med. Child Neurol.* 61, 1214–1220. doi: 10.1111/dmcn.14161

Lo Scrudato, M., Poulard, K., Sourd, C., Tomé, S., Klein, A. F., Corre, G., et al. (2019). Genome editing of expanded CTG repeats within the human DMPK gene reduces nuclear RNA foci in the muscle of DM1 mice. *Mol. Ther.* 27, 1372–1388. doi: 10.1016/j.ymthe.2019.05.021

Logigian, E. L., Martens, W. B., Moxley, RTt, McDermott, M. P., Dilek, N., Wiegner, A. W., et al. (2010). Mexiletine is an effective antimyotonia treatment in myotonic dystrophy type 1. *Neurology* 74, 1441–1448. doi: 10.1212/WNL.0b013e3181dc1a3a

Long, C., Amoasii, L., Bassel-Duby, R., and Olson, E. N. (2016). Genome editing of monogenic neuromuscular diseases: a systematic review. *JAMA Neurol.* 73, 1349–1355. doi: 10.1001/jamaneurol.2016.3388

López Castel, A., Overby, S. J., and Artero, R. (2019). MicroRNA-based therapeutic perspectives in myotonic dystrophy. *Int. J. Mol. Sci.* 20:5600. doi: 10.3390/ijms20225600

López-Morató, M., Brook, J. D., and Wojciechowska, M. (2018). Small molecules which improve pathogenesis of myotonic dystrophy type 1. *Front. Neurol.* 9:349. doi: 10.3389/fneur.2018.00349

Lopez-Titla, M. M., Chirino, A., Cruz Solis, S. V., Hernandez-Castillo, C. R., Diaz, R., Márquez-Quiroz, L. D. C., et al. (2021). Cognitive decline and white matter integrity degradation in myotonic dystrophy type I. *J. Neuroimaging* 31, 192–198. doi: 10.1111/jon.12786

Luu, L. M., Nguyen, L., Peng, S., Lee, J., Lee, H. Y., Wong, C. H., et al. (2016). A potent inhibitor of protein sequestration by expanded triplet (CUG) repeats that shows phenotypic improvements in a drosophila model of myotonic dystrophy. *Chem. Med. Chem.* 11, 1428–1435. doi: 10.1002/cmdc.201600081

Magaña, J. J., and Cisneros, B. (2011). Perspectives on gene therapy in myotonic dystrophy type 1. *J. Neurosci. Res.* 89, 275–285. doi: 10.1002/jnr.22551

Mahadevan, M., Tsilfidis, C., Sabourin, L., Shutler, G., Amemiya, C., Jansen, G., et al. (1992). Myotonic dystrophy mutation: an unstable CTG repeat in the 3′ untranslated region of the gene. *Science* 255, 1253–1255. doi: 10.1126/science.1546325

Manning, K. S., Rao, A. N., Castro, M., and Cooper, T. A. (2017). BNA (NC) gapmers revert splicing and reduce RNA foci with low toxicity in myotonic dystrophy cells. *ACS Chem. Biol.* 12, 2503–2509. doi: 10.1021/acschembio.7b00416

Marteyn, A., Maury, Y., Gauthier, M. M., Lecuyer, C., Vernet, R., Denis, J. A., et al. (2011). Mutant human embryonic stem cells reveal neurite and synapse formation defects in type 1 myotonic dystrophy. *Cell Stem Cell* 8, 434–444. doi: 10.1016/j.stem.2011.02.004

Martínez-Rodríguez, J. E., Lin, L., Iranzo, A., Genis, D., Martí, M. J., Santamaria, J., et al. (2003). Decreased hypocretin-1 (Orexin-A) levels in the cerebrospinal fluid of patients with myotonic dystrophy and excessive daytime sleepiness. *Sleep* 26, 287–290. doi: 10.1093/sleep/26.3.287

Matynia, A., Ng, C. H., Dansithong, W., Chiang, A., Silva, A. J., and Reddy, S. (2010). Muscleblind1, but not Dmpk or Six5, contributes to a complex phenotype of muscular and motivational deficits in mouse models of myotonic dystrophy. *PLoS One* 5:e9857. doi: 10.1371/journal.pone.0009857

Mazzoli, M., Ariatti, A., Garuti, G. C., Agnoletto, V., Genovese, M., Gozzi, M., et al. (2020). Predictors of prognosis in type 1 myotonic dystrophy (DM1): longitudinal 18-years experience from a single center. *Acta Myol.* 39, 109–120. doi: 10.36185/2532-1900-015

McGowan, J. W., Bidwell, G. L. III, and Vig, P. J. (2015). Challenges and new strategies for therapeutic peptide delivery to the CNS. *Ther. Deliv.* 6, 841–853. doi: 10.4155/tde.15.30

McGowan, J. W., Shao, Q., Vig, P. J., and Bidwell, G. L. III (2016). Intranasal administration of elastin-like polypeptide for therapeutic delivery to the central nervous system. *Drug Design Dev. Ther.* 10, 2803–2813. doi: 10.2147/dddt.s106216

McKinney, B. C., Sze, W., Lee, B., and Murphy, G. G. (2009). Impaired long-term potentiation and enhanced neuronal excitability in the amygdala of Ca(V)1.3 knockout mice. *Neurobiol. Learn. Mem.* 92, 519–528. doi: 10.1016/j.nlm.2009.06.012

Meola, G., and Cardani, R. (2015). Myotonic dystrophies: an update on clinical aspects, genetic, pathology, and molecular pathomechanisms. *Biochim. Biophys. Acta* 1852, 594–606. doi: 10.1016/j.bbadis.2014.05.019

Meola, G., and Sansone, V. (2007). Cerebral involvement in myotonic dystrophies. *Muscle Nerve* 36, 294–306. doi: 10.1002/mus.20800

Meola, G., Sansone, V., Perani, D., Scarone, S., Cappa, S., Dragoni, C., et al. (2003). Executive dysfunction and avoidant personality trait in myotonic dystrophy type 1 (DM-1) and in proximal myotonic myopathy (PROMM/DM-2). *Neuromusc. Disord.* 13, 813–821. doi: 10.1016/s0960-8966(03)00137-8

Miller, J. N., Kruger, A., Moser, D. J., Gutmann, L., van der Plas, E., Koscik, T. R., et al. (2021). Cognitive deficits, apathy, and hypersomnolence represent the core brain symptoms of adult-onset myotonic dystrophy type 1. *Front. Neurol.* 12:700796. doi: 10.3389/fneur.2021.700796

Miller, J. W., Urbinati, C. R., Teng-Umnuay, P., Stenberg, M. G., Byrne, B. J., Thornton, C. A., et al. (2000). Recruitment of human muscleblind proteins to (CUG)(n) expansions associated with myotonic dystrophy. *Embo J.* 19, 4439–4448. doi: 10.1093/emboj/19.17.4439

Miller, R. G., Mitchell, J. D., and Moore, D. H. (2012). Riluzole for amyotrophic lateral sclerosis (ALS)/motor neuron disease (MND). *Cochrane Database Syst. Rev.* 2012:Cd001447. doi: 10.1002/14651858.CD001447.pub3

Miller, T. M., Pestronk, A., David, W., Rothstein, J., Simpson, E., Appel, S. H., et al. (2013). An antisense oligonucleotide against SOD1 delivered intrathecally for patients with SOD1 familial amyotrophic lateral sclerosis: a phase 1, randomised, first-in-man study. *Lancet Neurol.* 12, 435–442. doi: 10.1016/s1474-4422(13)70061-9

Minier, L., Lignier, B., Bouvet, C., Gallais, B., and Camart, N. (2018). A review of psychopathology features, personality, and coping in myotonic dystrophy type 1. *J. Neuromusc. Dis.* 5, 279–294. doi: 10.3233/jnd-180310

Minnerop, M., Gliem, C., and Kornblum, C. (2018). Current progress in CNS imaging of myotonic dystrophy. *Front. Neurol.* 9:646. doi: 10.3389/fneur.2018.00646

Minnerop, M., Weber, B., Schoene-Bake, J. C., Roeske, S., Mirbach, S., Anspach, C., et al. (2011). The brain in myotonic dystrophy 1 and 2: evidence for a predominant white matter disease. *Brain* 134(Pt 12), 3530–3546. doi: 10.1093/brain/awr299

Misra, C., Bangru, S., Lin, F., Lam, K., Koenig, S. N., Lubbers, E. R., et al. (2020). Aberrant expression of a non-muscle RBFOX2 isoform triggers cardiac conduction defects in myotonic dystrophy. *Dev. Cell* 52, 748.e6–763.e6. doi: 10.1016/j.devcel.2020.01.037

Mizukami, K., Sasaki, M., Baba, A., Suzuki, T., and Shiraishi, H. (1999). An autopsy case of myotonic dystrophy with mental disorders and various neuropathologic features. *Psychiatry Clin. Neurosci.* 53, 51–55. doi: 10.1046/j.1440-1819.1999.00470.x

Mizuno, Y., Maeda, N., Hamasaki, H., Arahata, H., Sasagasako, N., Honda, H., et al. (2018). Four-repeat tau dominant pathology in a congenital myotonic dystrophy type 1 patient with mental retardation. *Brain Pathol.* 28, 431–433. doi: 10.1111/bpa.12603

Modoni, A., Silvestri, G., Vita, M. G., Quaranta, D., Tonali, P. A., and Marra, C. (2008). Cognitive impairment in myotonic dystrophy type 1 (DM1): a longitudinal follow-up study. *J. Neurol.* 255, 1737–1742. doi: 10.1007/s00415-008-0017-5

Mohan, A., Goodwin, M., and Swanson, M. S. (2014). RNA-protein interactions in unstable microsatellite diseases. *Brain Res.* 1584, 3–14. doi: 10.1016/j.brainres.2014.03.039

Mondragon-Gonzalez, R., and Perlingeiro, R. C. R. (2018). Recapitulating muscle disease phenotypes with myotonic dystrophy 1 induced pluripotent stem cells: a tool for disease modeling and drug discovery. *Dis. Models Mech.* 11:dmm034728. doi: 10.1242/dmm.034728

Morales, F., Vásquez, M., Corrales, E., Vindas-Smith, R., Santamaría-Ulloa, C., Zhang, B., et al. (2020). Longitudinal increases in somatic mosaicism of the expanded CTG repeat in myotonic dystrophy type 1 are associated with variation in age-at-onset. *Hum. Mol. Genet.* 29, 2496–2507. doi: 10.1093/hmg/ddaa123

Morgenthaler, T. I., Kapur, V. K., Brown, T., Swick, T. J., Alessi, C., Aurora, R. N., et al. (2007). Practice parameters for the treatment of narcolepsy and other hypersomnias of central origin. *Sleep* 30, 1705–1711. doi: 10.1093/sleep/30.12.1705

Moxley, R. T. III, Griggs, R. C., Goldblatt, D., VanGelder, V., Herr, B. E., and Thiel, R. (1978). Decreased insulin sensitivity of forearm muscle in myotonic dystrophy. *J. Clin. Investig.* 62, 857–867. doi: 10.1172/jci109198

Mulders, S. A., van den Broek, W. J., Wheeler, T. M., Croes, H. J., van Kuik-Romeijn, P., de Kimpe, S. J., et al. (2009). Triplet-repeat oligonucleotide-mediated reversal of RNA toxicity in myotonic dystrophy. *Proc. Natl. Acad. Sci. U.S.A.* 106, 13915–13920. doi: 10.1073/pnas.0905780106

Mulders, S. A., van Engelen, B. G., Wieringa, B., and Wansink, D. G. (2010). Molecular therapy in myotonic dystrophy: focus on RNA gain-of-function. *Hum. Mol. Genet.* 19, R90–R97. doi: 10.1093/hmg/ddq161

Muntoni, F., and Wood, M. J. (2011). Targeting RNA to treat neuromuscular disease. *Nat. Rev. Drug Discov.* 10, 621–637. doi: 10.1038/nrd3459

Murlidharan, G., Sakamoto, K., Rao, L., Corriher, T., Wang, D., Gao, G., et al. (2016). CNS-restricted transduction and CRISPR/Cas9-mediated gene deletion with an engineered AAV vector. *Mol. Ther. Nucleic Acids* 5:e338. doi: 10.1038/mtna.2016.49

Nakamori, M., Gourdon, G., and Thornton, C. A. (2011). Stabilization of expanded (CTG)•(CAG) repeats by antisense oligonucleotides. *Mol. Ther.* 19, 2222–2227. doi: 10.1038/mt.2011.191

Nakamori, M., Takahashi, T., Yamazaki, Y., Kurashige, T., Yamawaki, T., and Matsumoto, M. (2012). Cyclin-dependent kinase 5 immunoreactivity for granulovacuolar degeneration. *Neuroreport* 23, 867–872. doi: 10.1097/WNR.0b013e328358720b

Nakamori, M., Taylor, K., Mochizuki, H., Sobczak, K., and Takahashi, M. P. (2016). Oral administration of erythromycin decreases RNA toxicity in myotonic dystrophy. *Ann. Clin. Transl. Neurol.* 3, 42–54. doi: 10.1002/acn3.271

Nakatani, K., Matsumoto, J., Nakamori, M., Okamoto, T., Murata, A., and Dohno, C. (2020). The dimeric form of 1,3-diaminoisoquinoline derivative rescued the mis-splicing of Atp2a1 and Clcn1 genes in myotonic dystrophy type 1 mouse model. *Chemistry* 26, 14305–14309. doi: 10.1002/chem.202001572

Nehra, M., Uthappa, U. T., Kumar, V., Kumar, R., Dixit, C., Dilbaghi, N., et al. (2021). Nanobiotechnology-assisted therapies to manage brain cancer in personalized manner. *J. Control. Release* 338, 224–243. doi: 10.1016/j.jconrel.2021.08.027

Nelson, C. E., Robinson-Hamm, J. N., and Gersbach, C. A. (2017). Genome engineering: a new approach to gene therapy for neuromuscular disorders. *Nat. Rev. Neurol.* 13, 647–661. doi: 10.1038/nrneurol.2017.126

Nguyen, Q., and Yokota, T. (2020). Degradation of toxic RNA in myotonic dystrophy using gapmer antisense oligonucleotides. *Methods Mol. Biol.* 2176, 99–109. doi: 10.1007/978-1-0716-0771-8_7

Nieuwenhuis, S., Okkersen, K., Widomska, J., Blom, P., t Hoen, P. A. C., van Engelen, B., et al. (2019). Insulin signaling as a key moderator in myotonic dystrophy type 1. *Front. Neurol.* 10:1229. doi: 10.3389/fneur.2019.01229

Nishi, M., Kimura, T., Igeta, M., Furuta, M., Suenaga, K., Matsumura, T., et al. (2020). Differences in splicing defects between the grey and white matter in myotonic dystrophy type 1 patients. *PLoS One* 15:e0224912. doi: 10.1371/journal.pone.0224912

Nutter, C. A., Bubenik, J. L., Oliveira, R., Ivankovic, F., Sznajder, ŁJ., Kidd, B. M., et al. (2019). Cell-type-specific dysregulation of RNA alternative splicing in short tandem repeat mouse knockin models of myotonic dystrophy. *Genes Dev.* 33, 1635–1640. doi: 10.1101/gad.328963.119

Oana, K., Oma, Y., Suo, S., Takahashi, M. P., Nishino, I., Takeda, S., et al. (2013). Manumycin A corrects aberrant splicing of Clcn1 in myotonic dystrophy type 1 (DM1) mice. *Sci. Rep.* 3:2142. doi: 10.1038/srep02142

Ofori, L. O., Hoskins, J., Nakamori, M., Thornton, C. A., and Miller, B. L. (2012). From dynamic combinatorial 'hit' to lead: in vitro and in vivo activity of compounds targeting the pathogenic RNAs that cause myotonic dystrophy. *Nucleic Acids Res.* 40, 6380–6390. doi: 10.1093/nar/gks298

Ogata, A., Terae, S., Fujita, M., and Tashiro, K. (1998). Anterior temporal white matter lesions in myotonic dystrophy with intellectual impairment: an MRI and neuropathological study. *Neuroradiology* 40, 411–415. doi: 10.1007/s002340050613

Okkersen, K., Buskes, M., Groenewoud, J., Kessels, R. P. C., Knoop, H., van Engelen, B., et al. (2017a). The cognitive profile of myotonic dystrophy type 1: a systematic review and meta-analysis. *Cortex* 95, 143–155. doi: 10.1016/j.cortex.2017.08.008

Okkersen, K., Monckton, D. G., Le, N., Tuladhar, A. M., Raaphorst, J., and van Engelen, B. G. M. (2017b). Brain imaging in myotonic dystrophy type 1: a systematic review. *Neurology* 89, 960–969. doi: 10.1212/wnl.0000000000004300

Okkersen, K., Jimenez-Moreno, C., Wenninger, S., Daidj, F., Glennon, J., Cumming, S., et al. (2018). Cognitive behavioural therapy with optional graded exercise therapy in patients with severe fatigue with myotonic dystrophy type 1: a multicentre, single-blind, randomised trial. *Lancet Neurol.* 17, 671–680. doi: 10.1016/s1474-4422(18)30203-5

Ono, S., Kanda, F., Takahashi, K., Fukuoka, Y., Jinnai, K., Kurisaki, H., et al. (1995). Neuronal cell loss in the dorsal raphe nucleus and the superior central nucleus in myotonic dystrophy: a clinicopathological correlation. *Acta Neuropathol.* 89, 122–125. doi: 10.1007/bf00296355

Ono, S., Kanda, F., Takahashi, K., Fukuoka, Y., Jinnai, K., Kurisaki, H., et al. (1996). Neuronal loss in the medullary reticular formation in myotonic dystrophy: a clinicopathological study. *Neurology* 46, 228–231. doi: 10.1212/wnl.46.1.228

Ono, S., Takahashi, K., Jinnai, K., Kanda, F., Fukuoka, Y., Kurisaki, H., et al. (1998). Loss of serotonin-containing neurons in the raphe of patients with myotonic dystrophy: a quantitative immunohistochemical study and relation to hypersomnia. *Neurology* 50, 535–538. doi: 10.1212/wnl.50.2.535

Otero, B. A., Poukalov, K., Hildebrandt, R. P., Thornton, C. A., Jinnai, K., Fujimura, H., et al. (2021). Transcriptome alterations in myotonic dystrophy frontal cortex. *Cell Rep.* 34:108634. doi: 10.1016/j.celrep.2020.108634

Oude Ophuis, R. J., Mulders, S. A., van Herpen, R. E., van de Vorstenbosch, R., Wieringa, B., and Wansink, D. G. (2009). DMPK protein isoforms are differentially expressed in myogenic and neural cell lineages. *Muscle Nerve* 40, 545–555. doi: 10.1002/mus.21352

Pandey, S. K., Wheeler, T. M., Justice, S. L., Kim, A., Younis, H. S., Gattis, D., et al. (2015). Identification and characterization of modified antisense oligonucleotides targeting DMPK in mice and nonhuman primates for the treatment of myotonic dystrophy type 1. *J. Pharmacol. Exp. Ther.* 355, 329–340. doi: 10.1124/jpet.115.226969

Pascual-Gilabert, M., López-Castel, A., and Artero, R. (2021). Myotonic dystrophy type 1 drug development: a pipeline toward the market. *Drug Discov. Today* 26, 1765–1772. doi: 10.1016/j.drudis.2021.03.024

Pegoraro, V., Cudia, P., Baba, A., and Angelini, C. (2020). MyomiRNAs and myostatin as physical rehabilitation biomarkers for myotonic dystrophy. *Neurol. Sci.* 41, 2953–2960. doi: 10.1007/s10072-020-04409-2

Perbellini, R., Greco, S., Sarra-Ferraris, G., Cardani, R., Capogrossi, M. C., Meola, G., et al. (2011). Dysregulation and cellular mislocalization of specific miRNAs in myotonic dystrophy type 1. *Neuromusc. Disord.* 21, 81–88. doi: 10.1016/j.nmd.2010.11.012

Perfetti, A., Greco, S., Bugiardini, E., Cardani, R., Gaia, P., Gaetano, C., et al. (2014). Plasma microRNAs as biomarkers for myotonic dystrophy type 1. *Neuromusc. Disord.* 24, 509–515. doi: 10.1016/j.nmd.2014.02.005

Perfetti, A., Greco, S., Cardani, R., Fossati, B., Cuomo, G., Valaperta, R., et al. (2016). Validation of plasma microRNAs as biomarkers for myotonic dystrophy type 1. *Sci. Rep.* 6:38174. doi: 10.1038/srep38174

Peric, S., Brajkovic, L., Belanovic, B., Ilic, V., Salak-Djokic, B., Basta, I., et al. (2017a). Brain positron emission tomography in patients with myotonic dystrophy type 1 and type 2. *J. Neurol. Sci.* 378, 187–192. doi: 10.1016/j.jns.2017.05.013

Peric, S., Heatwole, C., Durovic, E., Kacar, A., Nikolic, A., Basta, I., et al. (2017b). Prospective measurement of quality of life in myotonic dystrophy type 1. *Acta Neurol. Scand.* 136, 694–697. doi: 10.1111/ane.12788

Peric, S., Pavlovic, A., Ralic, V., Dobricic, V., Basta, I., Lavrnic, D., et al. (2014b). Transcranial sonography in patients with myotonic dystrophy type 1. *Muscle Nerve* 50, 278–282. doi: 10.1002/mus.24162

Peric, S., Mandic-Stojmenovic, G., Markovic, I., Stefanova, E., Ilic, V., Parojcic, A., et al. (2014a). Cerebrospinal fluid biomarkers of neurodegeneration in patients with juvenile and classic myotonic dystrophy type 1. *Eur. J. Neurol.* 21, 231–237. doi: 10.1111/ene.12237

Peric, S., Vujnic, M., Dobricic, V., Marjanovic, A., Basta, I., Novakovic, I., et al. (2016). Five-year study of quality of life in myotonic dystrophy. *Acta Neurol. Scand.* 134, 346–351. doi: 10.1111/ane.12549

Pettersson, O. J., Aagaard, L., Jensen, T. G., and Damgaard, C. K. (2015). Molecular mechanisms in DM1 - a focus on foci. *Nucleic Acids Res.* 43, 2433–2441. doi: 10.1093/nar/gkv029

Pincherle, A., Patruno, V., Raimondi, P., Moretti, S., Dominese, A., Martinelli-Boneschi, F., et al. (2012). Sleep breathing disorders in 40 Italian patients with Myotonic dystrophy type 1. *Neuromusc. Disord.* 22, 219–224. doi: 10.1016/j.nmd.2011.08.010

Pinto, B. S., Saxena, T., Oliveira, R., Méndez-Gómez, H. R., Cleary, J. D., Denes, L. T., et al. (2017). Impeding transcription of expanded microsatellite repeats by deactivated Cas9. *Mol. Cell* 68, 479.e5–490.e5. doi: 10.1016/j.molcel.2017.09.033

Quera Salva, M. A., Blumen, M., Jacquette, A., Durand, M. C., Andre, S., De Villiers, M., et al. (2006). Sleep disorders in childhood-onset myotonic dystrophy type 1. *Neuromusc. Disord.* 16, 564–570. doi: 10.1016/j.nmd.2006.06.007

Raaijmakers, R. H. L., Ripken, L., Ausems, C. R. M., and Wansink, D. G. (2019). CRISPR/Cas applications in myotonic dystrophy: expanding opportunities. *Int. J. Mol. Sci.* 20:3689. doi: 10.3390/ijms20153689

Rakocevic-Stojanovic, V., Peric, S., Madzarevic, R., Dobricic, V., Ralic, V., Ilic, V., et al. (2014). Significant impact of behavioral and cognitive impairment on quality of life in patients with myotonic dystrophy type 1. *Clin. Neurol. Neurosurg.* 126, 76–81. doi: 10.1016/j.clineuro.2014.08.021

Ramon-Duaso, C., Gener, T., Consegal, M., Fernández-Avilés, C., Gallego, J. J., Castarlenas, L., et al. (2019). Methylphenidate attenuates the cognitive and mood alterations observed in Mbnl2 knockout mice and reduces microglia overexpression. *Cerebr. Cortex* 29, 2978–2997. doi: 10.1093/cercor/bhy164

Ramon-Duaso, C., Rodríguez-Morató, J., Selma-Soriano, E., Fernández-Avilés, C., Artero, R., de la Torre, R., et al. (2020). Protective effects of mirtazapine in mice lacking the Mbnl2 gene in forebrain glutamatergic neurons: relevance for myotonic dystrophy 1. *Neuropharmacology* 170:108030. doi: 10.1016/j.neuropharm.2020.108030

Rau, F., Freyermuth, F., Fugier, C., Villemin, J. P., Fischer, M. C., Jost, B., et al. (2011). Misregulation of miR-1 processing is associated with heart defects in myotonic dystrophy. *Nat. Struct. Mol. Biol.* 18, 840–845. doi: 10.1038/nsmb.2067

Reddy, K., Jenquin, J. R., Cleary, J. D., and Berglund, J. A. (2019a). Mitigating RNA toxicity in myotonic dystrophy using small molecules. *Int. J. Mol. Sci.* 20:4017. doi: 10.3390/ijms20164017

Reddy, K., Jenquin, J. R., McConnell, O. L., Cleary, J. D., Richardson, J. I., Pinto, B. S., et al. (2019b). A CTG repeat-selective chemical screen identifies microtubule inhibitors as selective modulators of toxic CUG RNA levels. *Proc. Natl. Acad. Sci. U.S.A.* 116, 20991–21000. doi: 10.1073/pnas.1901893116

Reddy, S., Smith, D. B., Rich, M. M., Leferovich, J. M., Reilly, P., Davis, B. M., et al. (1996). Mice lacking the myotonic dystrophy protein kinase develop a late onset progressive myopathy. *Nat. Genet.* 13, 325–335. doi: 10.1038/ng0796-325

Renard, D., Collombier, L., Castelli, C., Pouget, J. P., Kotzki, P. O., and Boudousq, V. (2016). In myotonic dystrophy type 1 reduced FDG-uptake on FDG-PET is most severe in Brodmann area 8. *BMC Neurol.* 16:100. doi: 10.1186/s12883-016-0630-3

Richard, G. F. (2015). Shortening trinucleotide repeats using highly specific endonucleases: a possible approach to gene therapy? *Trends Genet.* 31, 177–186. doi: 10.1016/j.tig.2015.02.003

Richard, G. F., Viterbo, D., Khanna, V., Mosbach, V., Castelain, L., and Dujon, B. (2014). Highly specific contractions of a single CAG/CTG trinucleotide repeat by TALEN in yeast. *PLoS One* 9:e95611. doi: 10.1371/journal.pone.0095611

Romeo, V., Pegoraro, E., Squarzanti, F., Sorarù, G., Ferrati, C., Ermani, M., et al. (2010b). Retrospective study on PET-SPECT imaging in a large cohort of myotonic dystrophy type 1 patients. *Neurol. Sci.* 31, 757–763. doi: 10.1007/s10072-010-0406-2

Romeo, V., Pegoraro, E., Ferrati, C., Squarzanti, F., Sorarù, G., Palmieri, A., et al. (2010a). Brain involvement in myotonic dystrophies: neuroimaging and neuropsychological comparative study in DM1 and DM2. *J. Neurol.* 257, 1246–1255. doi: 10.1007/s00415-010-5498-3

Rosahl, T. W., Geppert, M., Spillane, D., Herz, J., Hammer, R. E., Malenka, R. C., et al. (1993). Short-term synaptic plasticity is altered in mice lacking synapsin I. *Cell* 75, 661–670. doi: 10.1016/0092-8674(93)90487-b

Rosman, N. P., and Kakulas, B. A. (1966). Mental deficiency associated with muscular dystrophy. A neuropathological study. *Brain* 89, 769–788. doi: 10.1093/brain/89.4.769

Sabater-Arcis, M., Bargiela, A., Furling, D., and Artero, R. (2020). miR-7 restores phenotypes in myotonic dystrophy muscle cells by repressing hyperactivated autophagy. *Mol. Ther. Nucleic Acids* 19, 278–292. doi: 10.1016/j.omtn.2019.11.012

Sakurai, T. (2014). The role of orexin in motivated behaviours. *Nat. Rev. Neurosci.* 15, 719–731. doi: 10.1038/nrn3837

Salvatori, S., Furlan, S., Fanin, M., Picard, A., Pastorello, E., Romeo, V., et al. (2009). Comparative transcriptional and biochemical studies in muscle of myotonic dystrophies (DM1 and DM2). *Neurol. Sci.* 30, 185–192. doi: 10.1007/s10072-009-0048-4

Sansone, V., Gandossini, S., Cotelli, M., Calabria, M., Zanetti, O., and Meola, G. (2007). Cognitive impairment in adult myotonic dystrophies: a longitudinal study. *Neurol. Sci.* 28, 9–15. doi: 10.1007/s10072-007-0742-z

Schmitz, F., Pierozan, P., Rodrigues, A. F., Biasibetti, H., Coelho, D. M., Mussulini, B. H., et al. (2016). Chronic treatment with a clinically relevant dose of methylphenidate increases glutamate levels in cerebrospinal fluid and impairs glutamatergic homeostasis in prefrontal cortex of juvenile rats. *Mol. Neurobiol.* 53, 2384–2396. doi: 10.1007/s12035-015-9219-x

Schmitz, F., Pierozan, P., Rodrigues, A. F., Biasibetti, H., Grings, M., Zanotto, B., et al. (2017). Methylphenidate decreases ATP levels and impairs glutamate uptake and Na(+),K(+)-ATPase activity in juvenile rat hippocampus. *Mol. Neurobiol.* 54, 7796–7807. doi: 10.1007/s12035-016-0289-1

Schneider-Gold, C., Bellenberg, B., Prehn, C., Krogias, C., Schneider, R., Klein, J., et al. (2015). Cortical and subcortical grey and white matter atrophy in myotonic dystrophies type 1 and 2 is associated with cognitive impairment, depression and daytime sleepiness. *PLoS One* 10:e0130352. doi: 10.1371/journal.pone.0130352

Schoch, K. M., and Miller, T. M. (2017). Antisense oligonucleotides: translation from mouse models to human neurodegenerative diseases. *Neuron* 94, 1056–1070. doi: 10.1016/j.neuron.2017.04.010

Seijger, C., Raaphorst, J., Vonk, J., van Engelen, B., Heijerman, H., Stigter, N., et al. (2021). New insights in adherence and survival in myotonic dystrophy patients using home mechanical ventilation. *Respir. Int. Rev. Thor. Dis.* 100, 154–163. doi: 10.1159/000511962

Sellier, C., Cerro-Herreros, E., Blatter, M., Freyermuth, F., Gaucherot, A., Ruffenach, F., et al. (2018). rbFOX1/MBNL1 competition for CCUG RNA repeats binding contributes to myotonic dystrophy type 1/type 2 differences. *Nat. Commun.* 9:2009. doi: 10.1038/s41467-018-04370-x

Sergeant, N., Sablonnière, B., Schraen-Maschke, S., Ghestem, A., Maurage, C. A., Wattez, A., et al. (2001). Dysregulation of human brain microtubule-associated tau mRNA maturation in myotonic dystrophy type 1. *Hum. Mol. Genet.* 10, 2143–2155. doi: 10.1093/hmg/10.19.2143

Serra, L., Scocchia, M., Meola, G., D'Amelio, M., Bruschini, M., Silvestri, G., et al. (2020b). Ventral tegmental area dysfunction affects decision-making in patients with myotonic dystrophy type-1. *Cortex* 128, 192–202. doi: 10.1016/j.cortex.2020.03.022

Serra, L., Bianchi, G., Bruschini, M., Giulietti, G., Domenico, C. D., Bonarota, S., et al. (2020a). Abnormal cortical thickness is associated with deficits in social cognition in patients with myotonic dystrophy type 1. *Front. Neurol.* 11:113. doi: 10.3389/fneur.2020.00113

Serra, L., Cercignani, M., Bruschini, M., Cipolotti, L., Mancini, M., Silvestri, G., et al. (2016a). "I know that you know that i know": neural substrates associated with social cognition deficits in DM1 patients. *PLoS One* 11:e0156901. doi: 10.1371/journal.pone.0156901

Serra, L., Mancini, M., Silvestri, G., Petrucci, A., Masciullo, M., Spanò, B., et al. (2016b). Brain connectomics' modification to clarify motor and nonmotor features of myotonic dystrophy type 1. *Neural Plast.* 2016:2696085. doi: 10.1155/2016/2696085

Serra, L., Petrucci, A., Spanò, B., Torso, M., Olivito, G., Lispi, L., et al. (2015). How genetics affects the brain to produce higher-level dysfunctions in myotonic dystrophy type 1. *Funct. Neurol.* 30, 21–31.

Serra, L., Silvestri, G., Petrucci, A., Basile, B., Masciullo, M., Makovac, E., et al. (2014). Abnormal functional brain connectivity and personality traits in myotonic dystrophy type 1. *JAMA Neurol.* 71, 603–611. doi: 10.1001/jamaneurol.2014.130

Shimizu, E., Tang, Y. P., Rampon, C., and Tsien, J. Z. (2000). NMDA receptor-dependent synaptic reinforcement as a crucial process for memory consolidation. *Science* 290, 1170–1174. doi: 10.1126/science.290.5494.1170

Siboni, R. B., Nakamori, M., Wagner, S. D., Struck, A. J., Coonrod, L. A., Harriott, S. A., et al. (2015b). Actinomycin D specifically reduces expanded CUG repeat

RNA in myotonic dystrophy models. *Cell Rep.* 13, 2386–2394. doi: 10.1016/j.celrep.2015.11.028

Siboni, R. B., Bodner, M. J., Khalifa, M. M., Docter, A. G., Choi, J. Y., Nakamori, M., et al. (2015a). Biological efficacy and toxicity of diamidines in myotonic dystrophy type 1 models. *J. Med. Chem.* 58, 5770–5780. doi: 10.1021/acs.jmedchem.5b00356

Sicot, G., Servais, L., Dinca, D. M., Leroy, A., Prigogine, C., Medja, F., et al. (2017). Downregulation of the glial GLT1 glutamate transporter and purkinje cell dysfunction in a mouse model of myotonic dystrophy. *Cell Rep.* 19, 2718–2729. doi: 10.1016/j.celrep.2017.06.006

Simoncini, C., Spadoni, G., Lai, E., Santoni, L., Angelini, C., Ricci, G., et al. (2020). Central nervous system involvement as outcome measure for clinical trials efficacy in myotonic dystrophy type 1. *Front. Neurol.* 11:624. doi: 10.3389/fneur.2020.00624

Singh, R. K., Xia, Z., Bland, C. S., Kalsotra, A., Scavuzzo, M. A., Curk, T., et al. (2014). Rbfox2-coordinated alternative splicing of Mef2d and Rock2 controls myoblast fusion during myogenesis. *Mol. Cell* 55, 592–603. doi: 10.1016/j.molcel.2014.06.035

Sistiaga, A., Urreta, I., Jodar, M., Cobo, A. M., Emparanza, J., Otaegui, D., et al. (2010). Cognitive/personality pattern and triplet expansion size in adult myotonic dystrophy type 1 (DM1): CTG repeats, cognition and personality in DM1. *Psychol. Med.* 40, 487–495. doi: 10.1017/s0033291709990602

Smith, R. A., Miller, T. M., Yamanaka, K., Monia, B. P., Condon, T. P., Hung, G., et al. (2006). Antisense oligonucleotide therapy for neurodegenerative disease. *J. Clin. Investig.* 116, 2290–2296. doi: 10.1172/jci25424

Sobczak, K., Wheeler, T. M., Wang, W., and Thornton, C. A. (2013). RNA interference targeting CUG repeats in a mouse model of myotonic dystrophy. *Mol. Ther.* 21, 380–387. doi: 10.1038/mt.2012.222

Solovyeva, E. M., Ibebunjo, C., Utzinger, S., Eash, J. K., Dunbar, A., Naumann, U., et al. (2021). New insights into molecular changes in skeletal muscle aging and disease: differential alternative splicing and senescence. *Mech. Age. Dev.* 197:111510. doi: 10.1016/j.mad.2021.111510

Song, J., Lu, C., Leszek, J., and Zhang, J. (2021). Design and development of nanomaterial-based drug carriers to overcome the blood-brain barrier by using different transport mechanisms. *Int. J. Mol. Sci.* 22:10118. doi: 10.3390/ijms221810118

Song, K. Y., Guo, X. M., Wang, H. Q., Zhang, L., Huang, S. Y., Huo, Y. C., et al. (2020). MBNL1 reverses the proliferation defect of skeletal muscle satellite cells in myotonic dystrophy type 1 by inhibiting autophagy via the mTOR pathway. *Cell Death Dis.* 11:545. doi: 10.1038/s41419-020-02756-8

Stepniak-Konieczna, E., Konieczny, P., Cywoniuk, P., Dluzewska, J., and Sobczak, K. (2020). AON-induced splice-switching and DMPK pre-mRNA degradation as potential therapeutic approaches for myotonic dystrophy type 1. *Nucleic Acids Research* 48, 2531–2543. doi: 10.1093/nar/gkaa007

Steyaert, J., Umans, S., Willekens, D., Legius, E., Pijkels, E., de Die-Smulders, C., et al. (1997). A study of the cognitive and psychological profile in 16 children with congenital or juvenile myotonic dystrophy. *Clin. Genet.* 52, 135–141. doi: 10.1111/j.1399-0004.1997.tb02533.x

Strutt, S. C., Torrez, R. M., Kaya, E., Negrete, O. A., and Doudna, J. A. (2018). RNA-dependent RNA targeting by CRISPR-Cas9. *eLife* 7:e32724. doi: 10.7554/eLife.32724

Subramony, S. H., Wymer, J. P., Pinto, B. S., and Wang, E. T. (2020). Sleep disorders in myotonic dystrophies. *Muscle Nerve* 62, 309–320. doi: 10.1002/mus.26866

Sudhof, T. C. (2004). The synaptic vesicle cycle. *Annu. Rev. Neurosci.* 27, 509–547. doi: 10.1146/annurev.neuro.26.041002.131412

Suenaga, K., Lee, K. Y., Nakamori, M., Tatsumi, Y., Takahashi, M. P., Fujimura, H., et al. (2012). Muscleblind-like 1 knockout mice reveal novel splicing defects in the myotonic dystrophy brain. *PLoS One* 7:e33218. doi: 10.1371/journal.pone.0033218

Sugiyama, A., Sone, D., Sato, N., Kimura, Y., Ota, M., Maikusa, N., et al. (2017). Brain gray matter structural network in myotonic dystrophy type 1. *PLoS One* 12:e0187343. doi: 10.1371/journal.pone.0187343

Summerton, J. (1999). Morpholino antisense oligomers: the case for an RNase H-independent structural type. *Biochim. Biophys. Acta* 1489, 141–158. doi: 10.1016/s0167-4781(99)00150-5

Sun, N., and Zhao, H. (2013). Transcription activator-like effector nucleases (TALENs): a highly efficient and versatile tool for genome editing. *Biotechnol. Bioeng.* 110, 1811–1821. doi: 10.1002/bit.24890

Suzuki, K., Miyamoto, M., Miyamoto, T., Matsubara, T., Inoue, Y., Iijima, M., et al. (2018). Cerebrospinal fluid orexin-A levels in systemic lupus erythematosus patients presenting with excessive daytime sleepiness. *Lupus* 27, 1847–1853. doi: 10.1177/0961203318778767

Suzuki, Y., Holmes, J. B., Cerritelli, S. M., Sakhuja, K., Minczuk, M., Holt, I. J., et al. (2010). An upstream open reading frame and the context of the two AUG codons affect the abundance of mitochondrial and nuclear RNase H1. *Mol. Cell. Biol.* 30, 5123–5134. doi: 10.1128/mcb.00619-10

Symonds, T., Randall, J. A., and Campbell, P. (2017). Review of patient-reported outcome measures for use in myotonic dystrophy type 1 patients. *Muscle Nerve* 56, 86–92. doi: 10.1002/mus.25469

Takado, Y., Terajima, K., Ohkubo, M., Okamoto, K., Shimohata, T., Nishizawa, M., et al. (2015). Diffuse brain abnormalities in myotonic dystrophy type 1 detected by 3.0 T proton magnetic resonance spectroscopy. *Eur. Neurol.* 73, 247–256. doi: 10.1159/000371575

Takeda, A., Kobayakawa, M., Suzuki, A., Tsuruya, N., and Kawamura, M. (2009). Lowered sensitivity to facial emotions in myotonic dystrophy type 1. *J. Neurol. Sci.* 280, 35–39. doi: 10.1016/j.jns.2009.01.014

Timchenko, L. T., Miller, J. W., Timchenko, N. A., DeVore, D. R., Datar, K. V., Lin, L., et al. (1996). Identification of a (CUG)n triplet repeat RNA-binding protein and its expression in myotonic dystrophy. *Nucleic Acids Res.* 24, 4407–4414. doi: 10.1093/nar/24.22.4407

Todd, P. K., Ackall, F. Y., Hur, J., Sharma, K., Paulson, H. L., and Dowling, J. J. (2014). Transcriptional changes and developmental abnormalities in a zebrafish model of myotonic dystrophy type 1. *Dis. Models Mech.* 7, 143–155. doi: 10.1242/dmm.012427

Tomé, S., Holt, I., Edelmann, W., Morris, G. E., Munnich, A., Pearson, C. E., et al. (2009). MSH2 ATPase domain mutation affects CTG*CAG repeat instability in transgenic mice. *PLoS Genet.* 5:e1000482. doi: 10.1371/journal.pgen.1000482

Toth, A., Lovadi, E., Komoly, S., Schwarcz, A., Orsi, G., Perlaki, G., et al. (2015). Cortical involvement during myotonia in myotonic dystrophy: an fMRI study. *Acta Neurol. Scand.* 132, 65–72. doi: 10.1111/ane.12360

Tremblay, M., Muslemani, S., Côté, I., Gagnon, C., Fortin, J., and Gallais, B. (2021). Accomplishment of instrumental activities of daily living and its relationship with cognitive functions in adults with myotonic dystrophy type 1 childhood phenotype: an exploratory study. *BMC Psychol.* 9:56. doi: 10.1186/s40359-021-00562-1

Udd, B., and Krahe, R. (2012). The myotonic dystrophies: molecular, clinical, and therapeutic challenges. *Lancet Neurol.* 11, 891–905. doi: 10.1016/s1474-4422(12)70204-1

van Agtmaal, E. L., André, L. M., Willemse, M., Cumming, S. A., van Kessel, I. D. G., van den Broek, W., et al. (2017). CRISPR/Cas9-induced (CTG·CAG)(n) repeat instability in the myotonic dystrophy type 1 locus: implications for therapeutic genome editing. *Mol. Ther.* 25, 24–43. doi: 10.1016/j.ymthe.2016.10.014

van de Vondervoort, I., Amiri, H., Bruchhage, M. M. K., Oomen, C. A., Rustogi, N., Cooper, J. D., et al. (2019). Converging evidence points towards a role of insulin signaling in regulating compulsive behavior. *Transl. Psychiatry* 9:225. doi: 10.1038/s41398-019-0559-6

van de Vondervoort, I., Poelmans, G., Aschrafi, A., Pauls, D. L., Buitelaar, J. K., Glennon, J. C., et al. (2016). An integrated molecular landscape implicates the regulation of dendritic spine formation through insulin-related signalling in obsessive-compulsive disorder. *J. Psychiatry Neurosci.* 41, 280–285. doi: 10.1503/jpn.140327

van der Bent, M. L., Paulino da Silva Filho, O., van Luijk, J., Brock, R., and Wansink, D. G. (2018). Assisted delivery of antisense therapeutics in animal models of heritable neurodegenerative and neuromuscular disorders: a systematic review and meta-analysis. *Sci. Rep.* 8:4181. doi: 10.1038/s41598-018-22316-7

van der Plas, E., Hamilton, M. J., Miller, J. N., Koscik, T. R., Long, J. D., Cumming, S., et al. (2019). Brain structural features of myotonic dystrophy type 1 and their relationship with CTG repeats. *J. Neuromuscul. Dis.* 6, 321–332. doi: 10.3233/jnd-190397

van der Velden, B. G., Okkersen, K., Kessels, R. P., Groenewoud, J., van Engelen, B., Knoop, H., et al. (2019). Affective symptoms and apathy in myotonic dystrophy type 1 a systematic review and meta-analysis. *J. Affect. Disord.* 250, 260–269. doi: 10.1016/j.jad.2019.03.036

van Engelen, B. (2015). Cognitive behaviour therapy plus aerobic exercise training to increase activity in patients with myotonic dystrophy type 1

(DM1) compared to usual care (OPTIMISTIC): study protocol for randomised controlled trial. *Trials* 16:224. doi: 10.1186/s13063-015-0737-7

Vita, G., Vita, G. L., Musumeci, O., Rodolico, C., and Messina, S. (2019). Genetic neuromuscular disorders: living the era of a therapeutic revolution. Part 2: diseases of motor neuron and skeletal muscle. *Neurol. Sci.* 40, 671–681. doi: 10.1007/s10072-019-03764-z

Voellenkle, C., Perfetti, A., Carrara, M., Fuschi, P., Renna, L. V., Longo, M., et al. (2019). Dysregulation of circular RNAs in myotonic dystrophy type 1. *Int. J. Mol. Sci.* 20:1938. doi: 10.3390/ijms20081938

Walder, R. Y., and Walder, J. A. (1988). Role of RNase H in hybrid-arrested translation by antisense oligonucleotides. *Proc. Natl. Acad. Sci. U.S.A.* 85, 5011–5015. doi: 10.1073/pnas.85.14.5011

Walker, G. L., Rosser, R., Mastaglia, F. L., and Walton, J. N. (1984). Psychometric and cranial CT study in myotonic dystrophy. *Clin. Exp. Neurol.* 20, 161–167.

Wang, E. T., Cody, N. A., Jog, S., Biancolella, M., Wang, T. T., Treacy, D. J., et al. (2012). Transcriptome-wide regulation of pre-mRNA splicing and mRNA localization by muscleblind proteins. *Cell* 150, 710–724. doi: 10.1016/j.cell.2012.06.041

Wang, E. T., Taliaferro, J. M., Lee, J. A., Sudhakaran, I. P., Rossoll, W., Gross, C., et al. (2016). Dysregulation of mRNA localization and translation in genetic disease. *J. Neurosci.* 36, 11418–11426. doi: 10.1523/jneurosci.2352-16.2016

Wang, G. S., Kuyumcu-Martinez, M. N., Sarma, S., Mathur, N., Wehrens, X. H., and Cooper, T. A. (2009). PKC inhibition ameliorates the cardiac phenotype in a mouse model of myotonic dystrophy type 1. *J. Clin. Investig.* 119, 3797–3806. doi: 10.1172/jci37976

Wang, M., Weng, W. C., Stock, L., Lindquist, D., Martinez, A., Gourdon, G., et al. (2019). Correction of glycogen synthase kinase 3β in myotonic dystrophy 1 reduces the mutant RNA and improves postnatal survival of DMSXL mice. *Mol. Cell. Biol.* 39:e00155-19. doi: 10.1128/mcb.00155-19

Wang, P. Y., Chang, K. T., Lin, Y. M., Kuo, T. Y., and Wang, G. S. (2018). Ubiquitination of MBNL1 Is required for its cytoplasmic localization and function in promoting neurite outgrowth. *Cell Rep.* 22, 2294–2306. doi: 10.1016/j.celrep.2018.02.025

Wang, P. Y., Lin, Y. M., Wang, L. H., Kuo, T. Y., Cheng, S. J., and Wang, G. S. (2017). Reduced cytoplasmic MBNL1 is an early event in a brain-specific mouse model of myotonic dystrophy. *Hum. Mol. Genet.* 26, 2247–2257. doi: 10.1093/hmg/ddx115

Wang, Y., Hao, L., Wang, H., Santostefano, K., Thapa, A., Cleary, J., et al. (2018). Therapeutic genome editing for myotonic dystrophy type 1 using CRISPR/Cas9. *Mol. Ther.* 26, 2617–2630. doi: 10.1016/j.ymthe.2018.09.003

Wang, Y., Miao, L., Satterlee, A., and Huang, L. (2015). Delivery of oligonucleotides with lipid nanoparticles. *Adv. Drug Deliv. Rev.* 87, 68–80. doi: 10.1016/j.addr.2015.02.007

Wansink, D. G., van Herpen, R. E., Coerwinkel-Driessen, M. M., Groenen, P. J., Hemmings, B. A., and Wieringa, B. (2003). Alternative splicing controls myotonic dystrophy protein kinase structure, enzymatic activity, and subcellular localization. *Mol. Cell. Biol.* 23, 5489–5501. doi: 10.1128/mcb.23.16.5489-5501.2003

Warf, M. B., Nakamori, M., Matthys, C. M., Thornton, C. A., and Berglund, J. A. (2009). Pentamidine reverses the splicing defects associated with myotonic dystrophy. *Proc. Natl. Acad. Sci. U.S.A.* 106, 18551–18556. doi: 10.1073/pnas.0903234106

Weber, Y. G., Roebling, R., Kassubek, J., Hoffmann, S., Rosenbohm, A., Wolf, M., et al. (2010). Comparative analysis of brain structure, metabolism, and cognition in myotonic dystrophy 1 and 2. *Neurology* 74, 1108–1117. doi: 10.1212/WNL.0b013e3181d8c35f

Wei, C., Jones, K., Timchenko, N. A., and Timchenko, L. (2013). GSK3β is a new therapeutic target for myotonic dystrophy type 1. *Rare Dis.* 1:e26555. doi: 10.4161/rdis.26555

Weijs, R., Okkersen, K., van Engelen, B., Küsters, B., Lammens, M., Aronica, E., et al. (2021). Human brain pathology in myotonic dystrophy type 1: a systematic review. *Neuropathology* 41, 3–20. doi: 10.1111/neup.12721

Wheeler, T. M., Leger, A. J., Pandey, S. K., MacLeod, A. R., Nakamori, M., Cheng, S. H., et al. (2012). Targeting nuclear RNA for in vivo correction of myotonic dystrophy. *Nature* 488, 111–115. doi: 10.1038/nature11362

Wheeler, T. M., Sobczak, K., Lueck, J. D., Osborne, R. J., Lin, X., Dirksen, R. T., et al. (2009). Reversal of RNA dominance by displacement of protein sequestered on triplet repeat RNA. *Science* 325, 336–339. doi: 10.1126/science.1173110

Winblad, S., Hellström, P., Lindberg, C., and Hansen, S. (2006). Facial emotion recognition in myotonic dystrophy type 1 correlates with CTG repeat expansion. *J. Neurol. Neurosurg. Psychiatry* 77, 219–223. doi: 10.1136/jnnp.2005.070763

Winblad, S., Månsson, J. E., Blennow, K., Jensen, C., Samuelsson, L., and Lindberg, C. (2008). Cerebrospinal fluid tau and amyloid beta42 protein in patients with myotonic dystrophy type 1. *Eur. J. Neurol.* 15, 947–952. doi: 10.1111/j.1468-1331.2008.02217.x

Winblad, S., Samuelsson, L., Lindberg, C., and Meola, G. (2016). Cognition in myotonic dystrophy type 1: a 5-year follow-up study. *Eur. J. Neurol.* 23, 1471–1476. doi: 10.1111/ene.13062

Wojciechowska, M., Taylor, K., Sobczak, K., Napierala, M., and Krzyzosiak, W. J. (2014). Small molecule kinase inhibitors alleviate different molecular features of myotonic dystrophy type 1. *RNA Biol.* 11, 742–754. doi: 10.4161/rna.28799

Woo, J., Lee, H. W., and Park, J. S. (2019). Differences in the pattern of cognitive impairments between juvenile and adult onset myotonic dystrophy type 1. *J. Clin. Neurosci.* 68, 92–96. doi: 10.1016/j.jocn.2019.07.029

Wozniak, J. R., Mueller, B. A., Bell, C. J., Muetzel, R. L., Lim, K. O., and Day, J. W. (2013). Diffusion tensor imaging reveals widespread white matter abnormalities in children and adolescents with myotonic dystrophy type 1. *J. Neurol.* 260, 1122–1131. doi: 10.1007/s00415-012-6771-4

Wozniak, J. R., Mueller, B. A., Lim, K. O., Hemmy, L. S., and Day, J. W. (2014). Tractography reveals diffuse white matter abnormalities in myotonic dystrophy type 1. *J. Neurol. Sci.* 341, 73–78. doi: 10.1016/j.jns.2014.04.005

Wozniak, J. R., Mueller, B. A., Ward, E. E., Lim, K. O., and Day, J. W. (2011). White matter abnormalities and neurocognitive correlates in children and adolescents with myotonic dystrophy type 1: a diffusion tensor imaging study. *Neuromusc. Disord.* 21, 89–96. doi: 10.1016/j.nmd.2010.11.013

Xia, G., and Ashizawa, T. (2015). Dynamic changes of nuclear RNA foci in proliferating DM1 cells. *Histochem. Cell Biol.* 143, 557–564. doi: 10.1007/s00418-015-1315-5

Xia, G., Gao, Y., Jin, S., Subramony, S. H., Terada, N., Ranum, L. P., et al. (2015). Genome modification leads to phenotype reversal in human myotonic dystrophy type 1 induced pluripotent stem cell-derived neural stem cells. *Stem Cells* 33, 1829–1838. doi: 10.1002/stem.1970

Xia, G., Santostefano, K. E., Goodwin, M., Liu, J., Subramony, S. H., Swanson, M. S., et al. (2013). Generation of neural cells from DM1 induced pluripotent stem cells as cellular model for the study of central nervous system neuropathogenesis. *Cell. Reprogram.* 15, 166–177. doi: 10.1089/cell.2012.0086

Yadava, R. S., Foff, E. P., Yu, Q., Gladman, J. T., Kim, Y. K., Bhatt, K. S., et al. (2015). TWEAK/Fn14, a pathway and novel therapeutic target in myotonic dystrophy. *Hum. Mol. Genet.* 24, 2035–2048. doi: 10.1093/hmg/ddu617

Yadava, R. S., Yu, Q., Mandal, M., Rigo, F., Bennett, C. F., and Mahadevan, M. S. (2020). Systemic therapy in an RNA toxicity mouse model with an antisense oligonucleotide therapy targeting a non-CUG sequence within the DMPK 3′UTR RNA. *Hum. Mol. Genet.* 29, 1440–1453. doi: 10.1093/hmg/ddaa060

Yamamoto, H., Kokame, K., Okuda, T., Nakajo, Y., Yanamoto, H., and Miyata, T. (2011). NDRG4 protein-deficient mice exhibit spatial learning deficits and vulnerabilities to cerebral ischemia. *J. Biol. Chem.* 286, 26158–26165. doi: 10.1074/jbc.M111.256446

Yamazaki, Y., Matsubara, T., Takahashi, T., Kurashige, T., Dohi, E., Hiji, M., et al. (2011). Granulovacuolar degenerations appear in relation to hippocampal phosphorylated tau accumulation in various neurodegenerative disorders. *PLoS One* 6:e26996. doi: 10.1371/journal.pone.0026996

Yin, H., Moulton, H. M., Seow, Y., Boyd, C., Boutilier, J., Iverson, P., et al. (2008). Cell-penetrating peptide-conjugated antisense oligonucleotides restore systemic muscle and cardiac dystrophin expression and function. *Hum. Mol. Genet.* 17, 3909–3918. doi: 10.1093/hmg/ddn293

Zanigni, S., Evangelisti, S., Giannoccaro, M. P., Oppi, F., Poda, R., Giorgio, A., et al. (2016). Relationship of white and gray matter abnormalities to clinical and genetic features in myotonic dystrophy type 1. *Neuroimage Clin.* 11, 678–685. doi: 10.1016/j.nicl.2016.04.012

Zhang, B. W., Cai, H. F., Wei, X. F., Sun, J. J., Lan, X. Y., Lei, C. Z., et al. (2016). miR-30-5p regulates muscle differentiation and alternative splicing of muscle-related genes by targeting MBNL. *Int. J. Mol. Sci.* 17:182. doi: 10.3390/ijms17020182

Zhang, F., Bodycombe, N. E., Haskell, K. M., Sun, Y. L., Wang, E. T., Morris, C. A., et al. (2017). A flow cytometry-based screen identifies MBNL1 modulators that

rescue splicing defects in myotonic dystrophy type I. *Hum. Mol. Genet.* 26, 3056–3068. doi: 10.1093/hmg/ddx190

Zhang, N., Bewick, B., Xia, G., Furling, D., and Ashizawa, T. (2020). A CRISPR-Cas13a based strategy that tracks and degrades toxic RNA in myotonic dystrophy type 1. *Front. Genet.* 11:594576. doi: 10.3389/fgene.2020.594576

Zhang, W., Liu, H., Han, K., and Grabowski, P. J. (2002). Region-specific alternative splicing in the nervous system: implications for regulation by the RNA-binding protein NAPOR. *RNA* 8, 671–685. doi: 10.1017/s1355838202027036

Zhang, W., Wang, Y., Dong, S., Choudhury, R., Jin, Y., and Wang, Z. (2014). Treatment of type 1 myotonic dystrophy by engineering site-specific RNA endonucleases that target (CUG)(n) repeats. *Mol. Ther.* 22, 312–320. doi: 10.1038/mt.2013.251

Zorumski, C. F., and Izumi, Y. (2012). NMDA receptors and metaplasticity: mechanisms and possible roles in neuropsychiatric disorders. *Neurosci. Biobehav. Rev.* 36, 989–1000. doi: 10.1016/j.neubiorev.2011.12.011

Conflict of Interest: The authors declare that the research was conducted in the absence of any commercial or financial relationships that could be construed as a potential conflict of interest.

Publisher's Note: All claims expressed in this article are solely those of the authors and do not necessarily represent those of their affiliated organizations, or those of the publisher, the editors and the reviewers. Any product that may be evaluated in this article, or claim that may be made by its manufacturer, is not guaranteed or endorsed by the publisher.

frontiers in Aging Neuroscience

MINI REVIEW
published: 19 November 2021
doi: 10.3389/fnagi.2021.782617

Recent High-Resolution Structures of Amyloids Involved in Neurodegenerative Diseases

*Rodrigo Diaz-Espinoza**

Departamento de Biología, Facultad de Química y Biología, Universidad de Santiago de Chile, Santiago, Chile

Amyloids are highly ordered aggregates composed of proteins or peptides. They are involved in several pathologies, including hallmark neurodegenerative disorders such as Alzheimer's (AD) and Parkinson's (PD). Individuals affected by these diseases accumulate in their brains amyloids inclusions composed of misfolded forms of a peptide (Aβ) and a protein (Tau) in AD and α-synuclein protein (α-Sn) in PD. Tau and α-Sn aggregates are also present in other neurodegenerative diseases. The insoluble nature and heterogeneity of amyloids have hampered their study at the molecular level. However, the use of solid state NMR and Cryogenic-electron microscopy along with fine-tuned modulation of the aggregation *in vitro* and improved isolation methods of brain-derived amyloids has allowed the elucidation of these elusive conformations at high resolution. In this work, we review the latest progress on the recent amyloid structures reported for Aβ, Tau, and α-Sn. The two-fold symmetry emerges as a convergent feature in the tridimensional arrangement of the protofilaments in the fibrillary structure of these pathological amyloids, with many of them exhibiting a Greek-key topology as part of their overall architecture. These specific features can serve as novel guides to seek potential molecular targets in drug design efforts.

Keywords: neurodegenerative diseases, misfolding, amyloid, structure, Aβ, Tau, α-Sn

OPEN ACCESS

Edited by:
Natalia Salvadores, Universidad Mayor, Chile

Reviewed by:
Victor Banerjee, University of Texas Health Science Center at Houston, United States
Rodrigo Gallardo, University of Leeds, United Kingdom

***Correspondence:**
Rodrigo Diaz-Espinoza
rodrigo.diaz.e@usach.cl

Received: *24 September 2021*
Accepted: *28 October 2021*
Published: *19 November 2021*

Citation:
Diaz-Espinoza R (2021) Recent High-Resolution Structures of Amyloids Involved in Neurodegenerative Diseases. Front. Aging Neurosci. 13:782617. doi: 10.3389/fnagi.2021.782617

INTRODUCTION

The amyloid state of proteins is nowadays recognized as a convergent conformation that is accessible to most proteins and peptides under the appropriate conditions (Hartl and Hayer-Hartl, 2009). However, the proteinaceous nature of amyloids was recognized decades after their original descriptions (Kyle, 2001). Since then, amyloid deposits have been identified in different human pathologies and also in many organisms as functional assemblies (Chiti and Dobson, 2017). These aggregates are relevant pathological agents in neurodegenerative disorders such as AD and PD where they accumulate in the brain as inclusions with disease-dependent morphological features and location (Terry, 1963; Spillantini et al., 1997; Selkoe and Hardy, 2016). In AD, the affected individuals have two types of amyloid deposits that are composed of aggregated Aβ or misfolded Tau, whereas in PD misfolded α-Sn forms intracellular aggregates. Their specific pathological roles constitute active areas of research. However, their peculiar structural features have imposed important challenges to their study at the molecular level. Since these are unique pathological agents, elucidating their structures is crucial to design novel therapeutic approaches. We will review here the three iconic amyloids involved in neurodegenerative diseases along with their recently solved high-resolution structures.

OVERVIEW OF AMYLOID STRUCTURE

Amyloids are highly ordered aggregates stabilized by a beta-sheet core (Greenwald and Riek, 2010). Misfolded proteins or peptides are arranged in the beta-sheet in an intermolecular fashion through a hydrogen-bonded network in which the strands are transversally disposed with respect to the growing axis of the amyloid fibril, creating an overall "cross-beta" pattern (Riek, 2017). Beta-sheets can be arranged in a parallel or anti-parallel manner. Interestingly, regardless of the specific sequence all amyloids exhibit a similar overall architecture. This is indicative of a convergent misfolding pathway (Hartl and Hayer-Hartl, 2009). Moreover, amyloids are formed by the self-assembly of not only proteins but also small peptides and even single aromatic amino acids, indicating that the amyloid fold may be structurally and universally encrypted in the hydrocarbon chain of polypeptides (Balbach et al., 2000; Dobson, 2004; Adler-Abramovich et al., 2012). Still, the type and ordering of the amino acids within a given sequence is recognized to have a significant role in the aggregation propensity, with hydrophobic residues being the main contributors to the stability of the amyloid fold (Gazit, 2002; Hall et al., 2005; Greenwald and Riek, 2010). Despite their structural convergence, amyloids can still exhibit structural diversity at the molecular level (Gallardo et al., 2020). Such variations can be dependent on the specific polypeptide sequence as well as on the size.

Although amyloids are in general very stable, the non-covalent nature of the intermolecular interactions makes amyloid fibrils relatively fragile, which can fragment into smaller fibrils when subjected to mechanical or chemical stresses (Xue et al., 2010). Therefore, amyloids suffer from an inherent heterogeneity with respect to size distribution (Morales et al., 2016; Eisenberg and Sawaya, 2017). Such heterogeneity and their often-low solubility has made their structural characterization extremely challenging using classical structural biology techniques, let alone high-resolution approaches (Diaz-Espinoza and Soto, 2012; Fändrich et al., 2018). The first high-resolution amyloid structures were achieved using small peptides that formed amyloid-like structures when subjected to controlled dehydration (Nelson et al., 2005; Sawaya et al., 2007). The fine-tuning of experimental approaches aimed at increasing the homogeneity of the samples as well as implementing and combining novel and refined techniques such as sold-state NMR (ssNMR) and Cryogenic-Electron Microscopy (Cryo-EM) have allowed to obtain high-resolution structures of several amyloids, including those formed by Aβ, Tau, and α-Sn.

Aβ

Aβ are peptides of varying sizes released upon proteolytic cleavage of a membrane protein (amyloid precursor protein) (Kang et al., 1987). Some of these peptides can aggregate into fibrillary species, which then accumulates as plaques in the brain (Glenner and Wong, 1984; Selkoe and Hardy, 2016). These plaques typically contain Aβ fragments 1–40 ($A\beta_{40}$) and 1–42 ($A\beta_{42}$) among other components (Roher et al., 1993). Cellular toxicity associated to misfolded Aβ proceeds through diverse mechanisms including microglia-mediated localized inflammation around the plaques, impaired synapsis, membrane disruptions induced by Aβ oligomeric species, metals imbalance, etc (Cavallucci et al., 2012). Moreover, Aβ fibrils and oligomers ($A\beta_{40}$ and $A\beta_{42}$) prepared *in vitro* using chemically synthesized or recombinant Aβ peptide display dose-dependent cytotoxicity in cell cultures of diverse neuronal lines (Zagorski et al., 1999; Finder et al., 2010). The *in vitro* assembly of synthetic Aβ into amyloids has been characterized extensively in the literature and has enabled access to molecular details of Aβ aggregation, which may partially resemble the *in vivo* mechanisms during plaque formation (Caughey and Lansbury, 2003). $A\beta_{42}$ is more abundant in the plaques than $A\beta_{40}$ and hence it has been studied in greater detailed (Roher et al., 1993). The assembly into amyloids *in vitro* from monomeric $A\beta_{42}$ is a sequential nucleation-polymerization (NP) process that involves the emergence of nucleating oligomers followed by the formation of small fibrillary species or proto-fibrils, which then associate to form mature fibrils (Hardy and Higgins, 1992; Chen et al., 2017). The plaques in AD contain mature-like $A\beta_{42}$ fibrils and hence these fibrils can serve as an *in vitro* model for their study. $A\beta_{42}$ fibrils subjected to mechanical disruption can give rise to small fragments that can act as seeds of $A\beta_{42}$ polymerization, accelerating the formation of mature fibrils. This seeding mechanism along with the NP process is a general trait of amyloids (Jarrett and Lansbury, 1993; Ke et al., 2020).

Two recent works have produced the first structures of full length $A\beta_{42}$ in the amyloid state and at atomic resolution using ssNMR combined with molecular dynamics (MD; Colvin et al., 2016; Wälti et al., 2016). Wälti et al. (2016) showed that serially seeding the *in vitro* aggregation of synthetic $A\beta_{42}$ along with fine-tuning the solution conditions can produce highly homogenous $A\beta_{42}$ fibrils, with the resulting fibrils being recognized by plaque-specific antibodies. Colvin et al. (2016) grew $A\beta_{42}$ fibrils overnight at cooler temperatures without agitation to produce the homogenous fibrils. Interestingly, both approaches yielded very similar structures (**Figure 1**, pdb codes 2NAO and 5KK3). The amyloids are arranged by a two-fold symmetry, in which two protofilaments are stabilized mainly by lateral contacts. Each $A\beta_{42}$ monomer is stacked in a parallel, in-register fashion along the fibril axis. In both models the $A\beta_{42}$ N-terminal region (1–14) does not make specific contacts with the amyloid core probably due to its flexible and less hydrophobic nature. In a later work, Gremer et al. (2017) combined data from ssNMR with Cryo-EM to provide a novel structure for $A\beta_{42}$ in a fibrillary state. Homogenous fibrils were obtained by growing $A\beta_{42}$ at low pH in a solution containing a small fraction of acetonitrile and trifluoroacetic acid. The resulting fibrils were similarly toxic to PC12 rat brain cells as fibrils grown at neutral pH. Considering the fibrillary nature of this structure, the resulting model exhibited several significant differences with the previous models (**Figure 1**, pdb code 5OQV). First, the N-terminal region (1–15) appeared as part of the amyloid arrangement and engaged in specific contacts including intermolecular (^{1}Asp-^{28}Lys) and intramolecular salt bridges (^{5}Arg-^{7}Asp, ^{6}His-^{13}His-^{11}Glu). Secondly, the C-terminal region (38–42) makes direct intermolecular, inter-subunit hydrophobic

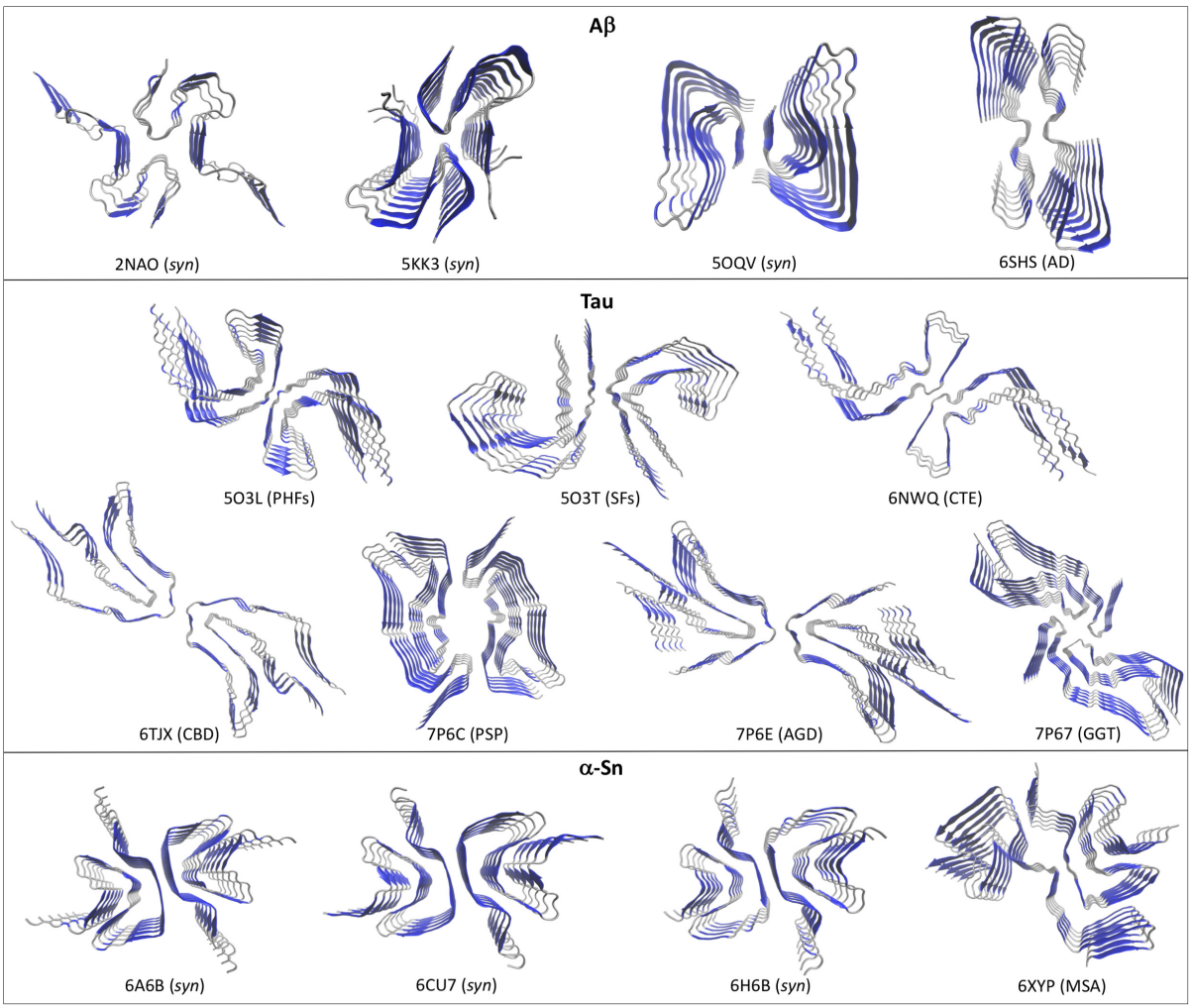

FIGURE 1 | Different high-resolution structures of Aβ, Tau, and α-Sn in the amyloid state. Top views are shown to highlight the two-fold symmetry arrangement of the protofilaments. Aβ: 2NAO, 5KK3, and 5OQV are synthetic $A\beta_{42}$ fibrils (*syn*); 6SHS are brain-derived Type II $A\beta_{40}$ fibrils from AD. Tau: 5O3L and 5O3T are respectively, *ex vivo* PHFs and SFs from AD; 6NWQ, 6TJX, 7P6C, 7P6E, and 7P67 are *ex vivo* Type II filaments from CTE, CBD, PSP, AGD, and GGT, respectively. α-Sn: 6A6B, 6CU7, and 6H6B are synthetic fibrils (*syn*); 6XYP are brain-derived Type I fibrils from MSA. Beta-sheets are depicted in blue and coils and α-helices in silver.

contacts that appears as key in stabilizing the two-fold symmetry, whereas in the previous models these residues extend outward the amyloid core. Interestingly, $A\beta_{40}$ lacks the last two of these C-terminal residues and peptides containing the full C-terminal region (sequence GGVVIA) spontaneously self-assembly into amyloids *in vitro*, which may suggest that this fibril model may be capturing a key feature of plaque-like $A\beta_{42}$ fibrils (Sawaya et al., 2007). Despite these differences, all the structures show a left-handed twist with a general two-fold symmetry formed by two interacting protofilaments.

Although high-resolution structures of full length $A\beta_{42}$ fibrils isolated from diseased brains (*ex vivo*) are not yet available, fibrillary structures of brain-derived $A\beta_{40}$ fibrils from an AD-affected patient were recently solved using Cryo-EM (Kollmer et al., 2019). These structures differed significantly from those obtained with synthetic $A\beta_{42}$ fibrils in that they showed a right-handed twist, different stabilizing hydrophobic contacts and different arrangements of the protofilaments. A single protofilament fibrillary arrangement was dominant in the sample (Type I), in which two stacks of $A\beta_{40}$ peptides are stabilized by hydrophobic contacts and arranged symmetrically. Additional fibrils were also observed in which two (Type II) or three (Type III) Type I protofilaments interact through lateral contacts mediated by two salt bridges (^{3}Glu-^{5}Arg), with Type II filaments showing a two-fold symmetry (**Figure 1**, pdb code 6H6S). It remains to be seen whether these structural features are exclusive of *ex vivo* $A\beta_{40}$ fibrils or they rather represent a convergent trait of brain-derived Aβ fibrils.

TAU

In addition to $A\beta_{42}$ plaques, AD-affected brains can also contain intracellular inclusions composed of misfolded Tau protein

(Terry, 1963; Lee et al., 1991). These Tau filaments give rise to neurofibrillary lesions, which can accumulate in different areas of the affected brains, including neocortex and limbic system, among others. In the case of AD, two types of Tau inclusions are commonly: paired helical filaments (PHFs) and straight filaments (SFs; Kidd, 1963; Crowther, 1991). Tau-associated inclusions are not an exclusive feature of AD and similar depositions can be found in other neurodegenerative disorders such as Pick's disease (PiD), chronic traumatic encephalopathy (CTE), corticobasal degeneration (CBD), progressive supranuclear palsy (PSP), argyrophilic grain disease (AGD) and globular glial tauopathy (GGT), among others (Crowther and Goedert, 2000; Ghetti et al., 2015).

Contrary to Aβ, Tau is a constitutively expressed protein involved in cytoskeleton homeostasis through direct stabilizing interactions with microtubules (Desai and Mitchison, 1997). At the structural level, Tau is an intrinsically disorder protein that can be found in six isoforms with sequence lengths varying from 352 to 441 amino acids (Goedert et al., 1989; Schweers et al., 1994). The details of Tau aggregation *in vivo* are intricate and different mechanisms have been proposed to contribute, including post-translational modifications such as hyperphosphorylation, glycosylation and truncation, ligand interactions, dimerization events, etc (Goedert et al., 1992; Alquezar et al., 2020). Such complexity has been very difficult to recreate *in vitro* and hence synthetic Tau fibrils that fully mimic PHFs and SFs is an ongoing challenge. However, alternative approaches that rely on isolating Tau amyloid inclusions at high homogeneity from diseased brains has proven a valuable tool for structural studies. In fact, high resolution structures of Tau PHFs and SFs isolated from an AD-affected brain have been recently solved using Cryo-EM (Fitzpatrick et al., 2017). Fitzpatrick et al. (2017) isolated and purified sarkosyl-insoluble fractions that were enriched in PHFs and SFs, which were then used to obtain high resolution structures of both filaments (**Figure 1**). Both PHFs and SFs showed a two-fold symmetry similar to that observed with *in vitro*-prepared $A\beta_{42}$ fibrils, in which Tau monomers are stacked through parallel beta-sheets with each molecule containing eight beta strands alternated with loop regions, forming two protofilaments running along the fibril axis. Interestingly, each Tau protofilament is arranged in a clear Greek-like key pattern (**Figure 2**). Compared to Aβ, only one of all the solved Aβ fibril structures showed this topology and with a much less organized fashion. Although Tau is not particularly hydrophobic as $A\beta_{42}$, the main intramolecular hydrophobic contacts reside precisely at the end of the end hinge region of the Greek-key fold, which may help stabilize this particular shape. Intermolecular contacts between the two protofilaments in PHFs involve H-bonds among residues ^{332}PGGGQ^{336} in an anti-parallel fashion. SFs intermolecular interactions are more asymmetrical, with contacts between region ^{321}KCGS^{324} and ^{313}VDLSK^{317}, though the specific types of stabilizing interactions are not yet clear. Using a similar approach the same group have elucidated high resolution structures of brain-derived Tau amyloids from patients affected with PiD, CTE, CBD, PSP, GPT, or GGT (Falcon et al., 2018, 2019; Zhang et al., 2020; Shi et al., 2021). As observed with brain-derived $A\beta_{40}$ amyloids, heterogeneous arrangements of the protofilaments were evident in several of the structures, particularly in those from CBD, CTE, PSP, and GGT. Still, the two-fold symmetry emerged again as a common feature in Type I and II filaments in CTE, and Type II filaments from CBD, PSP, AGD, and GGT, whereas single protofilament arrangements included Tau from PiD, PSP and Type I filaments from CBD, PSP, AGD, and GGT (**Figure 1**). Regardless of the disease, most Tau filaments have the Greek-key topology as a general feature, including Type I and II filaments from CTE, CBD, PSP, and AGD and in a less organized fashion the single protofilaments from PSP and Type I and II filaments from GGT (**Figure 2**).

α-Sn

One of the hallmark and specific pathological features of PD is the formation of intracellular depositions called Lewy bodies (LB) and Lewy neurites (LN) in nerve cells (Yves, 1991). These inclusions are mainly composed of an abnormally folded α-Sn protein in a fibrillary state (Spillantini et al., 1998b) and hence the intracellular accumulation of fibrillary α-Sn is recognized as a pathological condition. Fibrils prepared *in vitro* using recombinant α-Sn can seed the formation of LB- and LN-like inclusions in cell culture models, reinforcing the role of α-Sn in PD (Luk et al., 2009; Volpicelli-Daley et al., 2011). Furthermore, intracerebral inoculation of these synthetic fibrils in wild-type mice can not only seed the aggregation of native brain α-Sn but also initiate a PD-like pathology in the mice (Luk et al., 2012). Therefore, these synthetic fibrils have served as important models for molecular studies.

Several high-resolution structures of synthetic α-Sn fibrils have been reported in the last years. Tuttle et al. (2016) prepared *in vitro* recombinant α-Sn fibrils (full length) that seeded in a dose-dependent manner the aggregation of α-Sn in primary hippocampal neuronal cells and also produced toxicity to the same cells at high protein concentrations. A high-resolution structure of a single α-Sn protofilament was then obtained using ssNMR, electron and X-ray fiber diffraction (**Figure 1**, pdb code 2NAO). Based on this structure, the amyloid Greek-key pattern was proposed for the first time (**Figure 2**). Interestingly, for α-Sn this topology exhibits specific intramolecular interactions that appear as poised for its overall stabilization, including a combination of hydrophobic contacts (^{88}Ile-^{90}Ala-^{94}Phe), a salt bridge (^{46}Glu-^{80}Lys), and a H-bond (^{79}Gln-^{90}QAla). In a later work, Guerrero-Ferreira et al. (2018) reported the high-resolution structure of α-Sn in a fibrillary state by using Cryo-EM (**Figure 1**, pdb code 6H6B). They showed that a truncated recombinant α-Sn (residues 1–121) was the only preparation to yield homogenous fibrils upon self-assembly *in vitro*, as confirmed by EM. This truncated α-Sn is known to be highly prone to form amyloids *in vitro* and has been observed to naturally emerge in cells (Crowther et al., 1998; Li et al., 2005). The protofilaments are arranged in a two-fold symmetry (**Figure 1**). As observed with Tau filaments, α-Sn monomers are stacked onto the amyloid fold with eight beta strands alternated with loops in each of the protofilaments. The interface

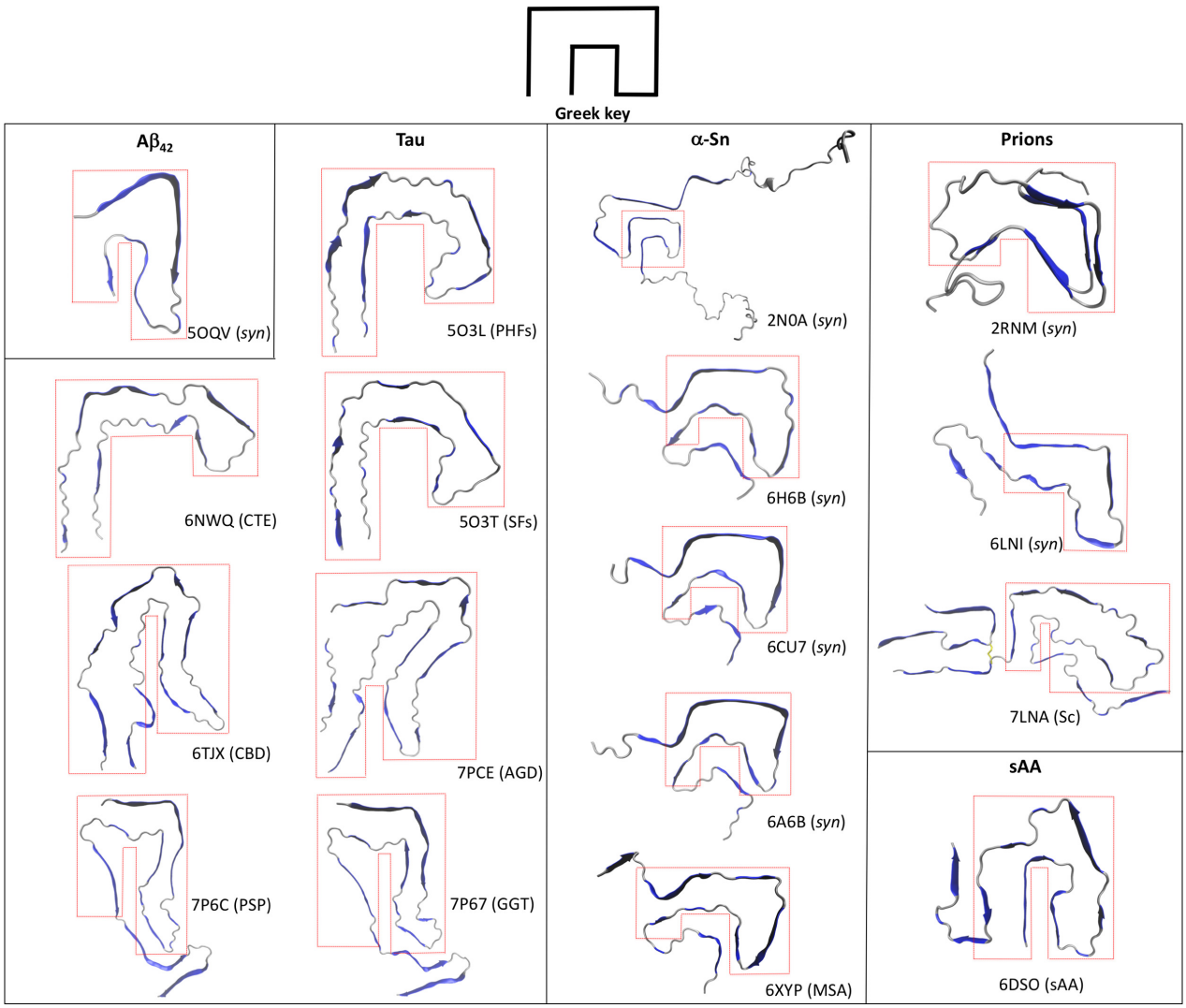

FIGURE 2 | Greek-key topology in the amyloid fold. Top views of the single chains of several amyloid structures of $A\beta_{42}$, Tau, and α-Sn are shown along with their associated disease or synthetic nature (*syn*). Synthetic HET prion (2RNM), human recombinant prion protein in the amyloid state (6LNI), infectious hamster brain-derived prion protein (7LNA), and mouse spleen-derived acute phase protein serum amyloid A1 (6DSO) are depicted for comparison. The enclosing red dotted lines highlight the Greek-key topology in each structure.

between both protofilaments is dominated by intermolecular hydrophobic interactions (^{53}Ala-^{53}Ala and ^{55}Val-^{51}Gly) and salt bridges (^{50}His-^{57}Glu). From the six familial mutations described for α-Sn, four occur directly in this interface, which suggest that the two-fold symmetry may have a key role in pathogenesis. The Greek-key pattern is again evident in the overall structure (**Figure 2**). Although the final Cryo-EM model was built using the structure from Tuttle et al. (2016) major refinements were needed for the protofilaments structure, which is indicative of structural differences. The corresponding interacting strands at the interface are positioned differently in the parent model since only a single protofilament was solved. Moreover, several key residues of the interface such as ^{53}Ala are positioned inward. Two additional Cryo-EM structures for α-Sn fibrils were also reported in the same year (**Figure 1**, pdb codes 6A6B and 6CU7). These structures were obtained using full length recombinant α-Sn that upon *in vitro* aggregation was able to seed the misfolding of endogenous α-Sn in rat primary neurons (Li Y. et al., 2018) or HEK 293T cells (Li B. et al., 2018). Both preparations were toxic to different cell lines in a dose-dependent manner. The solved structures were very similar to that reported by Guerrero-Ferreira et al. (2018) showing again a Greek-key pattern (**Figure 2**). The ^{53}Ala-^{53}Ala interaction appears again as key for the stability of the protofilaments interface. Interestingly, an intramolecular hydrophobic contact (^{70}Val-^{66}Val) within the hinge of the Greek key is present in all of the reported structures, suggesting this interaction may be pivotal for stabilizing the topology. In a later work, Ni et al. (2019) reported several Cryo-EM structures using recombinant α-Sn with different truncations. The Greek-key topology was again evident in all of the structures, showing

that this pattern is still maintained upon α-Sn truncation. The fact that all these synthetic fibrils exhibited similar overall structures is interesting, with a very similar overall two-fold symmetry, Greek-key topology and interface interactions.

Misfolded α-Sn forms are also present in other neurodegenerative diseases such as multiple system atrophy (MSA; Spillantini et al., 1998a). Schweighauser et al. (2020) recently reported the first high-resolution structure of brain-derived α-Sn fibrils using Cryo-EM, from a patient affected by MSA. As observed with *ex vivo* fibrillary structures of $A\beta_{40}$ and Tau, the α-Sn protofilaments are arranged in different fashions that in this case was also patient-dependent. The described filament types (I and II) showed a very similar two-protofilament overall arrangement but organized without full symmetry (**Figure 1**, pdb code 6XYP). Despite the low two-fold symmetry, the Greek-key topology of each protofilament is in general remarkably similar to those observed with synthetic α-Sn fibrils (**Figure 2**).

CONCLUSION

Advances in state-of-the-art experimental techniques such as ssNMR and Cryo-EM have enabled access to the molecular details of different amyloid assemblies. By using these techniques in combination with reducing size and conformational heterogeneity of the aggregates as well as improving isolation methods of brain-derived amyloids, solving high-resolution structures of amyloids formed by synthetic protein or *ex vivo* material of $A\beta_{42}$, Tau, and α-Sn has became feasible. Analysis of the structures shows that at the molecular level, amyloid structures can be heterogeneous, with a single primary sequence yielding different conformations and/or protofilaments arrangements in a disease-, sample- and in some cases patient-dependent manner. Still, the fibrillary states of these proteins show that two interacting protofilaments appear as a common amyloid arrangement emerging beyond the classical cross-beta pattern. In addition, the Greek-key topology can be observed in several of the structures though this is not as a convergent feature as the two-fold symmetry. In most of the structures reviewed, the hinge of this topology appears as the minimal and ubiquitous feature, which is stabilized mainly by hydrophobic interactions. Greek-key motifs are common in proteins that have beta-barrels and beta-sandwiches, which suggests that beta-sheets are a requirement for this fold (Zhang and Kim, 2000). Interestingly, high-resolution structures of amyloids prepared with synthetic prion proteins also exhibit architectures that resemble a Greek key (**Figure 2**; Wasmer et al., 2008; Wang et al., 2020). Furthermore, the same topology is described in a recently reported Cryo-EM structure of a mammalian prion isolated directly from scrapie-infected (Sc) brains and can be also observed in the amyloid fibril structure of acute phase protein serum amyloid A1 involved in systemic amyloidosis (sAA; Liberta et al., 2019; Kraus et al., 2021). Still, the fact that this topology is not observed in all of the samples serves as evidence of the different amyloid conformations that even a single primary sequence can reach. Contrary to the less complex and more homogeneous amyloid structures obtained with small peptides, all these unique structural arrangements may be only accessible for proteins or large peptides, which by combining beta strands with flexible loop-like regions can then reach more intricate amyloid conformations. Rational design of drugs aimed at disrupting the protofilament interface and/or the Greek-key fold may hold promise for novel therapeutic approaches. For a given protein, however, interactions stabilizing these arrangements show great variability depending not only on the specific disease but also on the type of sample utilized (*ex vivo* fibrils, synthetic fibrils, full-length, or different fragments, etc.). Therefore, each of these models can serve as potential targets in drug design efforts for exploring and validating their biological relevance in each pathology.

AUTHOR CONTRIBUTIONS

RD-E conceived, wrote, revised, and approved the manuscript.

FUNDING

This work was funded by research grant ANID FONDECYT 1211821 and Dicyt-Usach program.

REFERENCES

Adler-Abramovich, L., Vaks, L., Carny, O., Trudler, D., Magno, A., Caflisch, A., et al. (2012). Phenylalanine assembly into toxic fibrils suggests amyloid etiology in phenylketonuria. *Nat. Chem. Biol.* 8, 701–706. doi: 10.1038/nchembio.1002

Alquezar, C., Arya, S., and Kao, A. W. (2020). Tau post-translational modifications: dynamic transformers of tau function, degradation, and aggregation. *Front. Neurol.* 11:595532. doi: 10.3389/fneur.2020.595532

Balbach, J. J., Ishii, Y., Antzutkin, O. N., Leapman, R. D., Rizzo, N. W., Dyda, F., et al. (2000). Amyloid fibril formation by Aβ 16–22, a seven-residue fragment of the Alzheimer's β-amyloid peptide, and structural characterization by solid state NMR. *Biochemistry* 39, 13748–13759. doi: 10.1021/bi0011330

Caughey, B., and Lansbury, P. T. (2003). Protofibrils, pores, fibrils, and neurodegeneration: separating the responsible protein aggregates from the innocent bystanders. *Annu. Rev. Neurosci.* 26, 267–298. doi: 10.1146/annurev.neuro.26.010302.081142

Cavallucci, V., D'Amelio, M., and Cecconi, F. (2012). Aβ toxicity in Alzheimer's disease. *Mol. Neurobiol.* 45, 366–378. doi: 10.1007/s12035-012-8251-3

Chen, G. F., Xu, T. H., Yan, Y., Zhou, Y. R., Jiang, Y., Melcher, K., et al. (2017). Amyloid beta: structure, biology and structure-based therapeutic development. *Acta Pharmacol. Sin.* 38, 1205–1235. doi: 10.1038/aps.2017.28

Chiti, F., and Dobson, C. M. (2017). Protein misfolding, amyloid formation, and human disease: a summary of progress over the last decade. *Annu. Rev. Biochem.* 86, 27–68. doi: 10.1146/annurev-biochem-061516-045115

Colvin, M. T., Silvers, R., Ni, Q. Z., Can, T. V., Sergeyev, I., Rosay, M., et al. (2016). Atomic resolution structure of monomorphic Aβ42 amyloid fibrils. *J. Am. Chem. Soc.* 138, 9663–9674. doi: 10.1021/jacs.6b05129

Crowther, R. A. (1991). Straight and paired helical filaments in Alzheimer disease have a common structural unit. *Proc. Natl. Acad. Sci. U.S.A.* 88, 2288–2292. doi: 10.1073/pnas.88.6.2288

Crowther, R. A., and Goedert, M. (2000). Abnormal tau-containing filaments in neurodegenerative diseases. *J. Struct. Biol.* 30, 271–279. doi: 10.1006/jsbi.2000.4270

Crowther, R. A., Jakes, R., Spillantini, M. G., and Goedert, M. (1998). Synthetic filaments assembled from C-terminally truncated alpha-synuclein. *FEBS Lett.* 436, 309–312. doi: 10.1016/S0014-5793(98)01146-6

Desai, A., and Mitchison, T. J. (1997). Microtubule polymerization dynamics. *Annu. Rev. Cell. Dev. Biol.* 13, 83–117. doi: 10.1146/annurev.cellbio.13.1.83

Diaz-Espinoza, R., and Soto, C. (2012). High-resolution structure of infectious prion protein: the final frontier. *Nat. Struct. Mol. Biol.* 19, 370–377. doi: 10.1038/nsmb.2266

Dobson, C. M. (2004). Principles of protein folding, misfolding and aggregation. *Semin. Cell Dev. Biol.* 15, 3–16. doi: 10.1016/j.semcdb.2003.12.008

Eisenberg, D. S., and Sawaya, M. R. (2017). Structural studies of amyloid proteins at the molecular level. *Annu. Rev. Biochem.* 86, 69–95. doi: 10.1146/annurev-biochem-061516-045104

Falcon, B., Zhang, W., Murzin, A. G., Murshudov, G., Garringer, H. J., Vidal, R., et al. (2018). Structures of filaments from Pick's disease reveal a novel tau protein fold. *Nature* 561, 137–140. doi: 10.1038/s41586-018-0454-y

Falcon, B., Zivanov, J., Zhang, W., Murzin, A. G., Garringer, H. J., Vidal, R., et al. (2019). Novel tau filament fold in chronic traumatic encephalopathy encloses hydrophobic molecules. *Nature* 568, 420–423. doi: 10.1038/s41586-019-1026-5

Fändrich, M., Nyström, S., Nilsson, K. P. R., Böckmann, A., LeVine, H., and Hammarström, P. (2018). Amyloid fibril polymorphism: a challenge for molecular imaging and therapy. *J. Intern. Med.* 283, 218–237.

Finder, V. H., Vodopivec, I., Nitsch, R. M., and Glockshuber, R. (2010). The recombinant amyloid-beta peptide Abeta1-42 aggregates faster and is more neurotoxic than synthetic Abeta1-42. *J. Mol. Biol.* 396, 9–18. doi: 10.1016/j.jmb.2009.12.016

Fitzpatrick, A. W. P., Falcon, B., He, S., Murzin, A. G., Murshudov, G., Garringer, H. J., et al. (2017). Cryo-EM structures of tau filaments from Alzheimer's disease. *Nature* 547, 185–190. doi: 10.1038/nature23002

Gallardo, R., Ranson, N. A., and Radford, S. E. (2020). Amyloid structures: much more than just a cross-β fold. *Curr. Opin. Struct. Biol.* 60, 7–16. doi: 10.1016/j.sbi.2019.09.001

Gazit, E. (2002). A possible role for pi-stacking in the self-assembly of amyloid fibrils. *FASEB J.* 16, 77–83. doi: 10.1096/fj.01-0442hyp

Ghetti, B., Oblak, A. L., Boeve, B. F., Johnson, K. A., Dickerson, B. C., and Goedert, M. (2015). Frontotemporal dementia caused by microtubule-associated protein tau gene (MAPT) mutations: a chameleon for neuropathology and neuroimaging. *Neuropathol. Appl. Neurobiol.* 41, 24–46. doi: 10.1111/nan.12213

Glenner, G. G., and Wong, C. W. (1984). Alzheimer's disease and Down's syndrome: sharing of a unique cerebrovascular amyloid fibril protein. *Biochem. Biophys. Res. Commun.* 122, 1131–1135. doi: 10.1016/0006-291x(84)91209-9

Goedert, M., Spillantini, M. G., Cairns, N. J., and Crowther, R. A. (1992). Tauproteinsof Alzheimer paired helical filaments: abnormal phosphorylation of all six brain isoforms. *Neuron* 8, 159–168. doi: 10.1016/0896-6273(92)90117-v

Goedert, M., Spillantini, M. G., Jakes, R., Rutherford, D., and Crowther, R. A. (1989). Multiple isoforms of human microtubule-associated protein tau: sequences and localization in neurofibrillary tangles of Alzheimer's disease. *Neuron* 3, 519–526. doi: 10.1016/0896-6273(89)90210-9

Greenwald, J., and Riek, R. (2010). Biology of amyloid: structure, function, and regulation. *Structure* 18, 1244–1260. doi: 10.1016/j.str.2010.08.009

Gremer, L., Schölzel, D., Schenk, C., Reinartz, E., Labahn, J., Ravelli, R. B. G., et al. (2017). Fibril structure of amyloid-β(1-42) by cryo-electron microscopy. *Science* 358, 116–119. doi: 10.1126/science.aao2825

Guerrero-Ferreira, R., Taylor, N. M., Mona, D., Ringler, P., Lauer, M. E., Riek, R., et al. (2018). Cryo-EM structure of alpha-synuclein fibrils. *Elife* 7:e36402. doi: 10.7554/eLife.36402

Hall, D., Hirota, N., and Dobson, C. M. (2005). A toy model for predicting the rate of amyloid formation from unfolded protein. *J. Mol. Biol.* 351, 195–205. doi: 10.1016/j.jmb.2005.05.013

Hardy, J. A., and Higgins, G. A. (1992). Alzheimer's disease: the amyloid cascade hypothesis. *Science* 256, 184–185. doi: 10.1126/science.1566067

Hartl, F. U., and Hayer-Hartl, M. (2009). Converging concepts of protein folding in vitro and in vivo. *Nat. Struct. Mol. Biol.* 6, 574–581. doi: 10.1038/nsmb.1591

Jarrett, J. T., and Lansbury, P. T. Jr. (1993). Seeding "one-dimensional crystallization" of amyloid: a pathogenic mechanism in Alzheimer's disease and scrapie? *Cell* 73, 1055–1058. doi: 10.1016/0092-8674(93)90635-4

Kang, J., Lemaire, H. G., Unterbeck, A., Salbaum, J. M., Masters, C. L., Grzeschik, K. H., et al. (1987). The precursor of Alzheimer's disease amyloid A4 protein resembles a cell-surface receptor. *Nature* 325, 733–736. doi: 10.1038/325733a0

Ke, P. C., Zhou, R., Serpell, L. C., Riek, R., Knowles, T. P. J., Lashuel, H. A., et al. (2020). Half a century of amyloids: past, present and future. *Chem. Soc. Rev.* 49, 5473–5509. doi: 10.1039/c9cs00199a

Kidd, M. (1963). Paired helical filaments in electron microscopy of Alzheimer's disease. *Nature* 197, 192–193. doi: 10.1038/197192b0

Kollmer, K., Close, W., Funk, L., Rasmussen, J., Bsoul, A., Schierhorn, A., et al. (2019). Cryo-EM structure and polymorphism of Aβ amyloid fibrils purified from Alzheimer's brain tissue. *Nat. Commun.* 10:4760. doi: 10.1038/s41467-019-12683-8

Kraus, A., Hoyt, F., Schwartz, C. L., Hansen, B., Artikis, E., Hughson, A. G., et al. (2021). High-resolution structure and strain comparison of infectious mammalian prions. *Mol. Cell* 81, 4540–4551. doi: 10.1016/j.molcel.2021.08.011

Kyle, R. A. (2001). Amyloidosis: a convoluted story. *Br. J. Haematol.* 3, 529–538. doi: 10.1046/j.1365-2141.2001.02999.x

Lee, V. M., Balin, B. J., Otvos, L. Jr., and Trojanowski, J. Q. (1991). A68: a major subunit of paired helical filaments and derivatized forms of normal Tau. *Science* 251, 675–678. doi: 10.1126/science.1899488

Li, B., Ge, P., Murray, K. A., Sheth, P., Zhang, M., Nair, G., et al. (2018). Cryo-EM of full-length α-synuclein reveals fibril polymorphs with a common structural kernel. *Nat. Commun.* 9:3609. doi: 10.1038/s41467-018-05971-2

Li, W., West, N., Colla, E., Pletnikova, O., Troncoso, J. C., Marsh, L., et al. (2005). Aggregation promoting C-terminal truncation of alpha-synuclein is a normal cellular process and is enhanced by the familial Parkinson's disease-linked mutations. *Proc. Natl. Acad. Sci. U.S.A.* 102, 2162–2167. doi: 10.1073/pnas.0406976102

Li, Y., Zhao, C., Luo, F., Liu, Z., Gui, X., Luo, Z., et al. (2018). Amyloid fibril structure of α-synuclein determined by cryo-electron microscopy. *Cell. Res.* 28, 897–903. doi: 10.1038/s41422-018-0075-x

Liberta, F., Loerch, S., Rennegarbe, M., Schierhorn, A., Westermark, P., Westermark, G. T., et al. (2019). Cryo-EM fibril structures from systemic AA amyloidosis reveal the species complementarity of pathological amyloids. *Nat. Commun.* 10:1104. doi: 10.1038/s41467-019-09033-z

Luk, K. C., Kehm, V., Carroll, J., Zhang, B., O'Brien, P., Trojanowski, J. Q., et al. (2012). Pathological α-synuclein transmission initiates Parkinson-like neurodegeneration in nontransgenic mice. *Science* 338, 949–953. doi: 10.1126/science.1227157

Luk, K. C., Song, C., O'Brien, P., Stieber, A., Branch, J. R., Brunden, K. R., et al. (2009). Exogenous α-synuclein fibrils seed the formation of Lewy body-like intracellular inclusions in cultured cells. *Proc. Natl. Acad. Sci. U.S.A.* 106, 20051–20056. doi: 10.1073/pnas.0908005106

Morales, R., Hu, P., Duran-Aniotz, C., Moda, F., Diaz-Espinoza, R., Chen, B., et al. (2016). Strain-dependent profile of misfolded prion protein aggregates. *Sci. Rep.* 6:20526. doi: 10.1038/srep20526

Nelson, R., Sawaya, M. R., Balbirnie, M., Madsen, A. Ø, Riekel, C., Grothe, R., et al. (2005). Structure of the cross-beta spine of amyloid-like fibrils. *Nature* 435, 773–778. doi: 10.1038/nature03680

Ni, X., McGlinchey, R. P., Jiang, J., and Lee, J. C. (2019). Structural insights into α-synuclein fibril polymorphism: effects of Parkinson's disease-related C-terminal truncations. *J. Mol. Biol.* 431, 3913–3919. doi: 10.1016/j.jmb.2019.07.001

Riek, R. (2017). The three-dimensional structures of amyloids" in Perspectives in Prion Biology. *Cold Spring Harb. Perspect. Biol.* 9:a023572. doi: 10.1101/cshperspect.a023572

Roher, A. E., Lowenson, J. D., Clarke, S., Woods, A. S., Cotter, R. J., Gowing, E., et al. (1993). beta-Amyloid-(1-42) is a major component of cerebrovascular amyloid deposits: implications for the pathology of Alzheimer disease. *Proc. Natl. Acad. Sci. U.S.A.* 90, 10836–10840. doi: 10.1073/pnas.90.22.10836

Sawaya, M. R., Sambashivan, S., Nelson, R., Ivanova, M. I, Sievers, S. A., Apostol, M. I, et al. (2007). Atomic structures of amyloid cross-beta spines reveal varied steric zippers. *Nature* 447, 453–457. doi: 10.1038/nature05695

Schweers, O., Schönbrunn-Hanebeck, E., Marx, A., and Mandelkow, E. (1994). Structural studies of tau protein and Alzheimer paired helical filaments show no evidence for beta-structure. *J. Biol. Chem.* 269, 24290–24297.

Schweighauser, M., Shi, Y., Tarutani, A., Kametani, F., Murzin, A. G., Ghetti, B., et al. (2020). Structures of α-synuclein filaments from multiple system atrophy. *Nature* 585, 464–469. doi: 10.1038/s41586-020-2317-6

Selkoe, D. J., and Hardy, J. (2016). The amyloid hypothesis of Alzheimer's disease at 25 years. *EMBO Mol. Med.* 6, 595–608. doi: 10.15252/emmm.201606210

Shi, Y., Zhang, W., Yang, Y., Murzin, A. G., Falcon, B., Kotecha, A., et al. (2021). Structure-based classification of tauopathies. *Nature* 598, 359–363. doi: 10.1038/s41586-021-03911-7

Spillantini, M. G., Crowther, R. A., Jakes, R., Hasegawa, M., and Goedert, M. (1998b). Alpha-Synuclein in filamentous inclusions of Lewy bodies from Parkinson's disease and dementia with lewy bodies. *Proc. Natl. Acad. Sci. U.S.A.* 95, 6469–6473. doi: 10.1073/pnas.95.11.6469

Spillantini, M. G., Crowther, R. A., Jakes, R., Cairns, N. J., Lantos, P. L., and Goedert, M. (1998a). Filamentous alpha-synuclein inclusions link multiple system atrophy with Parkinson's disease and dementia with Lewy bodies. *Neurosci. Lett.* 251, 205–208. doi: 10.1016/s0304-3940(98)00504-7

Spillantini, M. G., Schmidt, M. L., Lee, V. M., Trojanowski, J. Q., Jakes, R., and Goedert, M. (1997). Alpha-synuclein in Lewy bodies. *Nature* 388, 839–840. doi: 10.1038/42166

Terry, R. D. (1963). The fine structure of neurofibrillary tangles in Alzheimer's disease. *J. Neuropathol. Exp. Neurol.* 22, 629–642. doi: 10.1097/00005072-196310000-00005

Tuttle, M. D., Comellas, G., Nieuwkoop, A. J., Covell, D. J., Berthold, D. A., Kloepper, K. D., et al. (2016). Solid-state NMR structure of a pathogenic fibril of full-length human α-synuclein. *Nat. Struct. Mol. Biol.* 23, 409–415. doi: 10.1038/nsmb.3194

Volpicelli-Daley, L. A., Luk, K. C., Patel, T. P., Tanik, S. A., Riddle, D. M., Stieber, A., et al. (2011). Exogenous α-synuclein fibrils induce Lewy body pathology leading to synaptic dysfunction and neuron death. *Neuron* 72, 57–71. doi: 10.1016/j.neuron.2011.08.033

Wälti, M. A., Ravotti, F., Arai, H., Glabe, C. G., Wall, J. S., Böckmann, A., et al. (2016). Atomic-resolution structure of a disease-relevant Aβ(1-42) amyloid fibril. *Proc. Natl. Acad. Sci. U.S.A.* 113, E4976–E4984. doi: 10.1073/pnas.1600749113

Wang, L. Q., Zhao, K., Yuan, H. Y., Wang, Q., Guan, Z., Tao, T., et al. (2020). Cryo-EM structure of an amyloid fibril formed by full-length human prion protein. *Nat. Struct. Mol. Biol.* 27, 598–602. doi: 10.1038/s41594-020-0441-5

Wasmer, C., Lange, A., Melckebeke, H. V., Siemer, A. B., Riek, R., and Meier, B. H. (2008). Amyloid fibrils of the HET-s(218-289) prion form a beta solenoid with a triangular hydrophobic core. *Science* 319, 1523–1526. doi: 10.1126/science.1151839

Xue, W. F., Hellewell, A. L., Hewitt, E. W., and Radford, S. E. (2010). Fibril fragmentation in amyloid assembly and cytotoxicity. *Prio* 4, 20–25. doi: 10.4161/pri.4.1.11378

Yves, A. (1991). Parkinson's disease: pathophysiology. *Lancet* 337, 1321–1324. doi: 10.1016/0140-6736(91)92989-f

Zagorski, M. G., Yang, J., Shao, H., Ma, K., Zeng, H., and Hong, A. (1999). Methodological and chemical factors affecting amyloid beta peptide amyloidogenicity. *Methods Enzymol.* 309, 189–204. doi: 10.1016/s0076-6879(99)09015-1

Zhang, C., and Kim, S. H. (2000). A comprehensive analysis of the Greek key motifs in protein beta-barrels and beta-sandwiches. *Proteins* 40, 409–419.

Zhang, W., Tarutani, A., Newell, K. L., Murzin, A. G., Matsubara, T., Falcon, B., et al. (2020). Novel tau filament fold in corticobasal degeneration. *Nature* 580, 283–287. doi: 10.1038/s41586-020-2043-0

Conflict of Interest: The author declares that the research was conducted in the absence of any commercial or financial relationships that could be construed as a potential conflict of interest.

frontiers in Aging Neuroscience

ORIGINAL RESEARCH
published: 30 November 2021
doi: 10.3389/fnagi.2021.772980

Deficits in N-Methyl-D-Aspartate Receptor Function and Synaptic Plasticity in Hippocampal CA1 in APP/PS1 Mouse Model of Alzheimer's Disease

Le Xu[1,2], Yiying Zhou[1,3], Linbo Hu[1], Hongde Jiang[1], Yibei Dong[1], Haowei Shen[1,3], Zhongze Lou[2,4], Siyu Yang[1], Yunxin Ji[2], Liemin Ruan[2] and Xiaoqin Zhang[1,3]**

[1] Zhejiang Key Laboratory of Pathophysiology, Department of Pharmacology, School of Medicine, Ningbo University, Ningbo, China, [2] Department of Psychosomatic Medicine, Ningbo First Hospital, Ningbo Hospital of Zhejiang University, Ningbo, China, [3] Key Laboratory of Addiction Research of Zhejiang Province, Ningbo Kangning Hospital, Ningbo, China, [4] Central Laboratory of the Medical Research Center, Ningbo First Hospital, Ningbo Hospital of Zhejiang University, Ningbo, China

The N-methyl-D-aspartate receptor is a critical molecule for synaptic plasticity and cognitive function. Impaired synaptic plasticity is thought to contribute to the cognitive impairment associated with Alzheimer's disease (AD). However, the neuropathophysiological alterations of N-methyl-D-aspartate receptor (NMDAR) function and synaptic plasticity in hippocampal CA1 in transgenic rodent models of AD are still unclear. In the present study, APP/PS1 mice were utilized as a transgenic model of AD, which exhibited progressive cognitive impairment including defective working memory, recognition memory, and spatial memory starting at 6 months of age and more severe by 8 months of age. We found an impaired long-term potentiation (LTP) and reduced NMDAR-mediated spontaneous excitatory postsynaptic currents (sEPSCs) in the hippocampal CA1 of APP/PS1 mice with 8 months of age. Golgi staining revealed that dendrites of pyramidal neurons had shorter length, fewer intersections, and lower spine density in APP/PS1 mice compared to control mice. Further, the reduced expression levels of NMDAR subunits, PSD95 and SNAP25 were observed in the hippocampus of APP/PS1 mice. These results suggest that NMDAR dysfunction, impaired synaptic plasticity, and disrupted neuronal morphology constitute an important part of the neuropathophysiological alterations associated with cognitive impairment in APP/PS1 mice.

Keywords: Alzheimer's disease, NMDAR, synaptic plasticity, cognitive behavior, dendritic morphology

OPEN ACCESS

Edited by:
Yasmina Manso, Center for Biomedical Research on Neurodegenerative Diseases (CIBERNED), Spain

Reviewed by:
Nicola B. Mercuri, University of Rome Tor Vergata, Italy
Daniel John Whitcomb, University of Bristol, United Kingdom

****Correspondence:***
Liemin Ruan
13805869162@163.com
Xiaoqin Zhang
zhangxiaoqin1@nbu.edu.cn

Received: *09 September 2021*
Accepted: *29 October 2021*
Published: *30 November 2021*

Citation:
Xu L, Zhou Y, Hu L, Jiang H, Dong Y, Shen H, Lou Z, Yang S, Ji Y, Ruan L and Zhang X (2021) Deficits in N-Methyl-D-Aspartate Receptor Function and Synaptic Plasticity in Hippocampal CA1 in APP/PS1 Mouse Model of Alzheimer's Disease. Front. Aging Neurosci. 13:772980. doi: 10.3389/fnagi.2021.772980

INTRODUCTION

Alzheimer's disease is a progressive neurologic disorder characterized by cognitive dysfunction, mainly learning and memory. The pathological alterations in the hippocampus have clinical consequences in cognitive impairment in Alzheimer's disease (AD). The volume of the hippocampus was reduced in patients with AD, which can be used as an auxiliary examination

to improve the accuracy of AD diagnosis (Hampel et al., 2002; Ewers et al., 2011). Particularly, the hippocampal CA1 area is one of the most influenced regions in AD (Gómez-Isla et al., 1997; Llorens-Martín et al., 2014; Yang et al., 2018), which is involved in spatial orientation, learning, and different aspects of memory, such as consolidation and retrieval (Bartsch et al., 2011; Fouquet et al., 2012). The impairment of these functions is related to the core clinical symptom in AD patients (Llorens-Martín et al., 2014). In animal models of AD, studies have found that abnormalities of neuronal morphology and expression levels of synapse-associated proteins contribute to the impaired neural plasticity in the hippocampal CA1 in AD models (Le Douce et al., 2020; Wang et al., 2020; Li et al., 2021).

N-methyl-D-aspartate receptors (NMDARs) are the major ligand-gated glutamate receptors and are crucial for neuronal development, synaptic plasticity, and excitotoxicity (Li et al., 2003). Amyloid beta (Aβ), one of the hallmarks of AD, directly disturbed NMDAR function in cultured neurons, whether synthetic or naturally secreted Aβ; in the cultured neurons from APPswe mice, the surface expression of NR1, an NMDAR subunit, was lower than neurons from WT mice (Snyder et al., 2005). Memantine, one of the commonly used drugs for AD, is the NMDAR antagonist and protects the neurons from excitatory toxicity (Parsons et al., 2007; Martinez-Coria et al., 2010). D-serine, as an NMDAR co-agonist, effectively prevents both synaptic and behavioral deficits in AD mice (Le Douce et al., 2020). In clinical researches, the blood level of D-amino acid oxidase was negatively correlated with age-related cognitive decline (Lin et al., 2017); benzoate, a D-amino acid oxidase inhibitor, substantially improved cognitive function in randomized, double-blind, placebo-controlled trials (Lin et al., 2014; Lane et al., 2021). These pieces of evidence imply that the changes of NMDAR function are complicated in AD, which may be attributable to the fact that AD is a heterogeneous disorder with various phenotypes and genotypes (Devi and Scheltens, 2018). The neuropathophysiological alterations of NMDAR function and synaptic plasticity in hippocampal CA1 in transgenic rodent models of AD are still unclear.

The transgenic mouse, APPswe/PS1dE9 (APP/PS1), is one of the most commonly used animal models in pathogenesis studies of AD (Hall and Roberson, 2012). Previous studies have reported that Aβ deposits and cognitive deficits were developed around 6–7 months of age in these mice (Jankowsky et al., 2004). In the present study, we assessed cognitive functions of APP/PS1 mice at 4, 6, and 8 months of age, and then investigated synaptic plasticity and NMDAR function in hippocampal CA1 *via* examining long-term potentiation (LTP) induction and NMDAR-mediated spontaneous excitatory postsynaptic currents (sEPSCs) in 8-month-old APP/PS1 mice. Furthermore, to understand the structural and molecular basis of altered synaptic plasticity, the neuronal morphology and expression levels of synapse-associated proteins, including glutamate receptor subunits, PSD95, and SNAP25, were determined using Golgi staining and western blotting, respectively. These results suggested that NMDAR dysfunction, impaired synaptic plasticity, and disrupted neuronal morphology constitute an important part of the neuropathophysiological alterations associated with cognitive impairment in APP/PS1 mice.

MATERIALS AND METHODS

Animal

All experiments were conducted in line with the National Institutes of Health Guide for the Care and Use of Laboratory Animal, which were approved by the Animal Care and Use Committees of Ningbo University. APP/PS1 mice, purchased from the Hangzhou Ziyuan, Inc. of China, express a chimeric mouse/human APP gene harboring the Swedish double mutation K595N/M596L (APPswe) and a human PS1 gene harboring the exon 9 deletion (PS1dE9). The mice were housed under a 12 h light/dark cycle in groups of three to five per cage with free access to food and water. The breeding room was a temperature (20–22°C) and humidity (45–55%) controlled environment. Both female and male mice were used in the experiment and were equally distributed in each group.

Behavioral Tests

All behavioral experiments were performed in three age stages (4, 6, and 8 months) between 7:00 a.m. and 6:00 p.m. The week before the behavioral test, each mouse was habituated to a room and a single experimenter, who handled subjects in the behavioral room for 5 min per day. The behavioral data were recorded and analyzed by ANY-maze software (Stoelting, United Kingdom).

Open Field Test

Open-field tests (OFTs) were conducted to test locomotor activity by a white box (40 cm long × 40 cm wide × 40 cm high) made of Plexiglas plate. Mice were placed in the center of the bottom of the box to explore freely for 10 min with a video camera recording their movements. The total distance traveled, the time spent in the central area (20 cm × 20 cm), and the immobile time (the timer started when the mouse was stationary for more than 2 s) of each mouse were measured.

Y-Maze

Y-maze tests were performed to assess short-term spatial working memory by spontaneous alternations. The device is a three-arm horizontal maze (40 cm long and 10 cm wide with 25 cm high) in which the angle between each of the two adjacent arms is 120°. Mice were placed at the center of the three arms and allowed to explore freely for 8 min. The total arm entries and sequences of each arm were recorded. The percent alternations, reflecting spatial working memory, were defined as the proportion of arm choices that differed from the last two choices.

Novel Location Recognition and Novel Object Recognition

Novel location recognition (NLR) and novel object recognition (NOR) tests were performed to test the ability of learning and memory in mice. In the NLR test, the device includes a small open field box (25 cm long × 25 cm wide × 25 cm high walls, one of whose walls are specially marked) and two identical objects.

Mice were acclimated to the open field box for 3 days, 10 min a day. During training, 24 h after the last acclimatization, mice were allowed to explore two identical objects for 10 min. Investigation time for each object was measured. Afterward, 1 h after training for the test, one of the objects was picked up and placed to the opposite side of the box, and mice were allowed again to explore two objects for 5 min. The time of investigation for each object was measured again. Object exploration time was measured for each case in which the nose of a mouse touched the object or was oriented toward the object and came within 2 cm of it. The NLR discrimination index, reflecting spatial memory, was defined as (novel location investigation time - familiar location investigation time)/(novel location investigation time + familiar location investigation). NOR tests were performed as previously described, with minor modification. The device is the same as the NLR and two objects of different shapes but of the same material. Also, the acclimating and training phases are the same as the NLR test in the first 4 days. On the fifth day (24 h after the training phases), one of the objects was replaced with a new object, mice were allowed to explore two different objects for 5 min. The data are recorded in the same way as the NLR test. The NOR discrimination index, reflecting long-term recognition memory, was defined as (novel object investigation time – familiar object investigation time)/(novel object investigation time + familiar object investigation time).

Barnes Maze

The Barnes maze was performed to estimate spatial learning and memory. The maze consists of a white circular plate, 90 cm in diameter with 20 evenly distributed circular holes on the edge. The diameter of the holes is 5 cm and it is 4 cm from the plate edge. The maze was elevated above the floor (90 cm), light intensity was set at 200 lx, which was regarded as a mild aversive stimulus and visual cues were on the wall of the test room (within 50 cm of the maze). The test consists of 4 days of training and 1 day of probes. During training, under one of these holes is a dark box made of black Plexiglas with dimensions of 10 cm long × 10 cm wide × 6 cm high (escape box), where animals can stay here to some extent away from light and open spaces. Mice were trained to learn the location of the escape box over 4 days with 4 trials per day. At the beginning of each training session, mice were acclimated to the maze in the metal cylindrical cage at the center of the platform for 30 s. Next, mice were allowed to explore the maze to find and reach the escape box. The maximum duration of each training session was 180 s, and the interval between two adjacent training sessions was 15–25 min. If the mice fail to reach the escape box, the experimenter would gently guide it into the escape box by the end of 180 s. At the end of each training session (mice reached the escape box), every mouse was allowed to remain in the escape box for 30 s before returning to the home cage. On the fifth day, in the probe session, each mouse was allowed to explore the maze only for 90 s with the escape box removed. The maze was cleaned with 70% EtOH and rotated 90° after each session to avoid the effects of odors. The escape latency is the time from leaving the metal cylindrical cage to reaching the escape box. The target quadrant is the quadrant in which the escape hole was on its axis of symmetry. Errors mean visits to incorrect holes before finding the escape hole.

Electrophysiology

The electrophysiology was performed as previously described (Kasanetz and Manzoni, 2009; Zhang et al., 2021). Coronal brain slices containing hippocampal CA1 were prepared for field excitatory postsynaptic potentials (fEPSPs) and whole-cell recording from WT and APP/PS1 mice during PND 250–270. Mice were anesthetized with sodium pentobarbital (80 mg/kg, i.p.) and decapitated, and then brains were dissected quickly and placed in an ice-cold solution containing below substances (in mM): 75 sucrose, 87 NaCl, 3.0 KCl, 1.5 $CaCl_2$, 1.3 $MgCl_2$, 1.0 NaH_2PO_4, 26 $NaHCO_3$, 20 glucose equilibrated with 95% O_2–5% CO_2. Coronal brain slices (220 μm thickness) were prepared with a vibratome (Leica VT1200S, Leica Microsystems, Germany), and then incubated in a chamber with artificial cerebrospinal fluid (aCSF) containing below substances (in mM): 124 NaCl, 3.0 KCl, 1.0 NaH_2PO_4, 1.3 $MgCl_2$, 2.0 $CaCl_2$, 26 $NaHCO_3$, and 20 glucose, 295–305 mOsm, equilibrated at 32°C with 95% O_2–5% CO_2). Slices were incubated for at least 1 h before recording. Following incubation, the slices were transferred to a recording chamber, where the submerged slices were perfused with aCSF (32°C) saturated with mixed gas at a flow rate of 2 ml per min. Standard recordings were made using Multiclamp 700B amplifier and Digidata 1550B (Molecular Devices, Axon Instruments, CA, United States) for data acquisition. Vertical two stages puller (PC-10, NARISHIGE, JAPAN) was used to make glass electrodes (3IN thin-wall GL1.5 OD/1.12 ID, TW150-3, WPI) into pipettes with resistance between 1.5 and 2.0 mOhm when filled with internal. The fEPSPs were recorded with glass electrodes (∼3 MΩ tip resistance) filled with ACSF and evoked with a bipolar tungsten electrode (FHC, Inc., United States). Stimulus strength was adjusted to ∼40% of the maximal fEPSP response. For LTP recording, after a 20 min stable baseline was established, LTP was induced by theta-burst stimulation (TBS) (four theta bursts were applied at 15 s intervals; each theta-burst consisted of five bursts, at 200 ms intervals, of five 100 Hz pulses). For whole-cell recording, to record NMDAR-mediated sEPSCs, patch pipettes were filled with an intracellular solution containing (in mM): 110 cesium methyl sulfate, 15 CsCl, 4.0 Mg-ATP, 0.3 Na2-GTP, 0.5 EGTA, 10 HEPES, 4.0 QX-314, 5.0 Phosphocreatine-Na2, pH 7.2–7.4 (270–280 mOsm). sEPSCs mediated by both AMPAR and NMDAR were detected with digitally designed templates (Molecular Devices). The sEPSC charge was computed by the following formula: sEPSC charge = current (pA) × time (ms). For dual sEPSCs, a template with the rise and decay times of 3 and 150 ms, respectively, was used. A lower-amplitude threshold of 16 pA was applied. AMPAR sEPSCs at +40 mV were isolated in the presence of the NMDAR antagonist D-2-amino-5-phosphonovaleric acid (D-APV, 14539, Cayman, United States; 100 μM) with a template with the rise and decay times of 1.2 and 4 ms, respectively. A lower-amplitude threshold of 9 pA was applied. The NMDAR sEPSCs were obtained by the following formula: NMDAR sEPSCs = dual (AMPAR + NMDAR) sEPSCs – AMPAR sEPSCs. Series resistance was normally <20 MΩ and recordings exceeding

20% change in series resistance were terminated. All holding potentials were corrected for liquid junction potential. Data were low-pass filtered at 1 kHz and digitized at a sampling frequency of 10 kHz. The superfusion medium contained picrotoxin (P1675, Sigma, Germany; 100 μM) to block γ-aminobutyric acid type A receptors. All chemicals used in the patch-clamp were purchased from Sinopharm Chemical Reagent Co., Ltd., China, except as noted.

Golgi-Cox Staining and the Analysis of Dendrites and Spines

Mice brains were immersed in the Golgi-Cox solution for 2 weeks and then transferred to 30% sucrose solution for 3–5 days in the dark at RT (room temperature). Coronal slices (140 μm thickness) containing the hippocampus were cut by a vibratome (Leica VT1200S, Leica Microsystems, Germany). Pyramidal neurons in the hippocampal CA1 region were selected for structural analysis. Total dendritic length and the number of intersections at concentric circles (10 μm apart) were measured by Sholl analysis, and the number of dendritic spines per 10 μm was analyzed using ImageJ software (version 1.52a; National Institutes of Health).

Immunofluorescent Staining and Quantitative Analysis

Brains were isolated and fixed in 4% paraformaldehyde (PFA) for 24 h and then cryoprotected in 30% sucrose solution in PBS 1X for additional 2 days. After fixation and cryoprotection procedures, brains were cut using Leica Cryostat in 30 μm thickness. Sections were transferred into a blocking solution containing 0.1% Triton X-100, 10% goat serum in PBS 1X for 1 h at RT. Then, sections were incubated at 4°C overnight with the primary antibody, rabbit anti-NeuN (26975-1-AP; Proteintech, Wuhan, China; 1:500) diluted in PBS 1X, 0.1% Triton X-100, and 10% goat serum. After washing with PBS 1X for 1 h, the sections were incubated with secondary antibodies (Proteintech, Wuhan, China) diluted in PBS 1X for 2 h at RT. Afterward, sections were washed by PBS 1X thoroughly for 1 h and mounted with an antifading medium (Solarbio, Beijing, China). For quantitative analysis of NeuN staining, the average fluorescence intensity was determined using ImageJ software (version 1.52a; National Institutes of Health).

Western Blot Analysis

The mice were deeply anesthetized with pentobarbital (80 mg/kg, i.p.) and decapitated during PND 250-270. Briefly, the hippocampus tissues were directly lysed in sodium dodecyl sulfate sample buffer and incubated at 95°C for 5 min before being loaded onto a 10% sodium dodecyl sulfate-polyacrylamide gel. The protein concentration was determined before being loaded onto the gel and then 40 μg protein per sample was loaded onto each track. Proteins were separated by electrophoresis and then transferred to a nitrocellulose membrane (BioRad, Hercules, CA, United States). The membrane was blocked in 5% milk-TBST at RT and probed with rabbit anti-NR2A (ab133265, Abcam, United Kingdom; 1:1,000), rabbit anti-NR2B (ab183942, Abcam, United Kingdom; 1:1,000), rabbit anti-NR1 (ab109182, Abcam, United Kingdom; 1:1,000), rabbit anti-GluR1 (04-855, Millipore, Germany; 1:1,000), mouse anti-GluR2 (MAB397, Millipore, Germany; 1:1,000), PSD95 antibody (sc2290, Santa Cruz Biotechnology Inc., United States; 1:500), SNAP25 antibody (A2234, Abclonal, China; 1:500) at 4°C overnight and then reacted with the Alexa Fluor 800 conjugated antibody (1:5,000) for 60 min. Detection and quantification of specific bands were performed using a fluorescence scanner (Odyssey Infrared Imaging System, LI-COR Biotechnology, Lincoln, NE, United States). All samples were analyzed at least in triplicate. β-Actin (AC026, Abclonal, China; 1:5,000) served as an internal protein control.

Statistical Analysis

GraphPad Prism version 7 (GraphPad Software, San Diego, CA, United States) was used to conduct statistical analyses. Unpaired Student's *t*-test was used to compare pairs of means. Two-way ANOVA followed by Bonferroni's *post hoc* test when appropriate was used to analyze the latency to escape in the Barnes maze. The linear relationship between mobility and cognitive performance was analyzed by the Pearson's coefficient after a Shapiro-Wilk normality test. Two-way repeated-measures ANOVA by Bonferroni's *post hoc* test when appropriate was used to analyze the number of dendritic intersections. Data are presented as mean ± SEM. $p < 0.05$ was considered statistically significant for all results.

RESULTS

Impaired Cognitive Function in 6- and 8-Month-Old APP/PS1 Mice

The behavioral tests including Y-maze, NLR, and NOR are easy-to-use to measure different aspects of cognitive function. Four-month-old APP/PS1 mice showed no difference from age-matched WT mice in Y-maze [**Figures 1A,B**; total entries, unpaired *t*-test: $t_{(15)} = 0.6515$; $P = 0.5246$; alternations, unpaired *t*-test: $t_{(15)} = 0.0382$; $P = 0.97$], NLR [**Figure 1C**; unpaired *t*-test: $t_{(15)} = 1.182$; $P = 0.2555$], and NOR tests [**Figure 1D**; unpaired *t*-test: $t_{(14)} = 0.5405$; $P = 0.5973$]. The 6-month-old APP/PS1 mice exhibited the decreased spontaneous alternations in Y-maze [**Figure 1F**; unpaired *t*-test: $t_{(15)} = 2.692$; $P = 0.0167$], the reduced discrimination index in NOR [**Figure 1H**; unpaired *t*-test: $t_{(15)} = 2.402$; $P = 0.0297$] compared with WT mice. No differences were observed in the number of total arm entries in Y-maze [**Figure 1E**; unpaired *t*-test: $t_{(15)} = 1.534$; $P = 0.1458$] and the discrimination index in NLR [**Figure 1G**; unpaired *t*-test: $t_{(15)} = 0.5997$; $P = 0.5577$]. The 8-month-old APP/PS1 mice showed the decreased spontaneous alternations in Y-maze [**Figure 1J**; unpaired *t*-test: $t_{(16)} = 2.585$; $P = 0.0199$], the reduced discrimination index in NOR and NLR tests [**Figures 1K,L**; NLR, unpaired *t*-test: $t_{(15)} = 2.464$; $P = 0.0263$; NOR, unpaired *t*-test: $t_{(14)} = 3.097$; $P = 0.0079$] compared with WT mice, and no difference in the number of total arm entries in Y-maze [**Figure 1I**; unpaired *t*-test: $t_{(16)} = 0.4037$; $P = 0.6918$]. These results suggested that APP/PS1

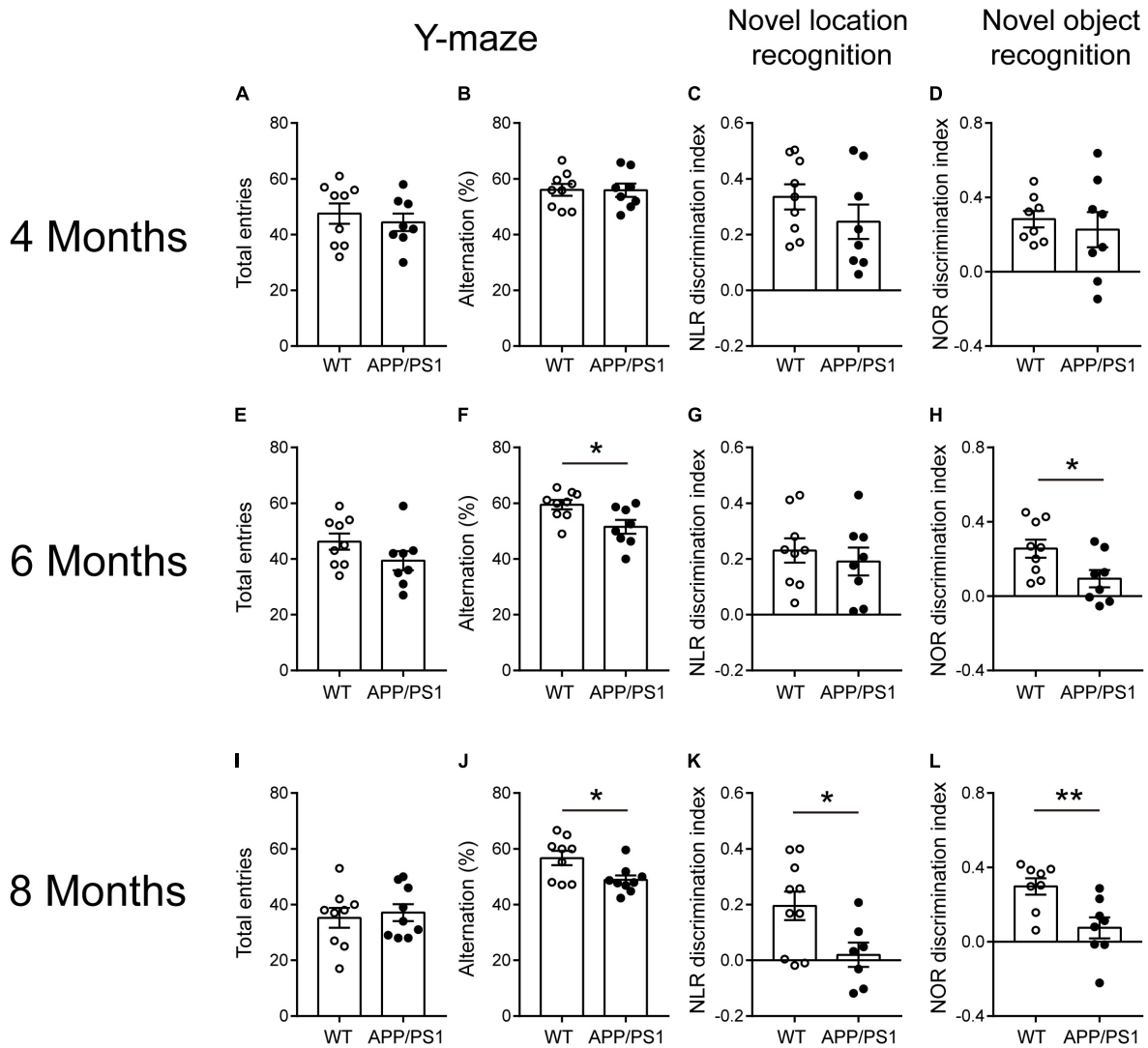

FIGURE 1 | Cognitive-behavioral performance for 4-, 6-, and 8- months-old WT and APP/PS1 mice (n = 8–10/group). **(A–D)** 4-month-old WT and APP/PS1 mice showed no difference in Y-maze, NLR, and NOR tests. **(E–H)** In 6-month-old mice, APP/PS1 mice showed the decreased spontaneous alternations in Y-maze (*$p < 0.05$, unpaired t-test), reduced discrimination index in NOR (*$p < 0.05$, unpaired t-test) compared with WT mice, and no differences were observed in the number of total arm entries in Y-maze and discrimination index in NLR. **(I–L)** In 8-month-old mice, APP/PS1 mice showed the decreased spontaneous alternations in Y-maze (*$p < 0.05$, unpaired t-test), the reduced (*$p < 0.05$, unpaired t-test) discrimination index in NOR and NLR tests (**$p < 0.001$, unpaired t-test) compared with WT mice and there was no difference on the number of total arm entries in Y-maze.

mice manifested impaired working memory and long-term recognition memory at 6 months of age, and the impaired spatial recognition memory at 8 months of age.

Impaired Spatial Learning and Memory in 6- and 8-Month-Old APP/PS1 Mice

We found that APP/PS1 mice showed abnormalities in some aspects of cognitive function at 6 months of age, and more comprehensive cognitive impairment at 8 months of age through some simple behavioral tests. As a more complex behavioral task, the Barnes maze test (**Figure 2A**) was conducted to further verify cognitive dysfunction in APP/PS1 mice. In 4-month-old WT and APP/PS1 mice, no statistically significant differences were observed in the indicators of the Barnes maze (**Figures 2C–E**). In 6-month-old mice, the time APP/PS1 mice spent in the target quadrant is decreased [**Figure 2G**; unpaired t-test: $t_{(11)} = 2.216$; $P = 0.0487$] compared with WT mice, but no differences were observed in the escape latency [**Figure 2F**; two-way ANOVA: factor of day: $F_{(3,\ 44)} = 18.31$, $P < 0.0001$; factor of genotype: $F_{(1,\ 44)} = 1.425$, $P = 0.2389$; interaction of two factors: $F_{(3,\ 44)} = 0.066$, $P = 0.9776$] and the number of errors [**Figure 2H**; Unpaired t-test: $t_{(11)} = 2.071$; $P = 0.0626$]. The **Figure 2B** showed the trajectory diagrams of 8-month-old APP/PS1 mice, the escape latency was decreased in both day 3 and 4 of training phase [**Figure 2I**; two-way ANOVA followed by Bonferroni's *post hoc* test: factor

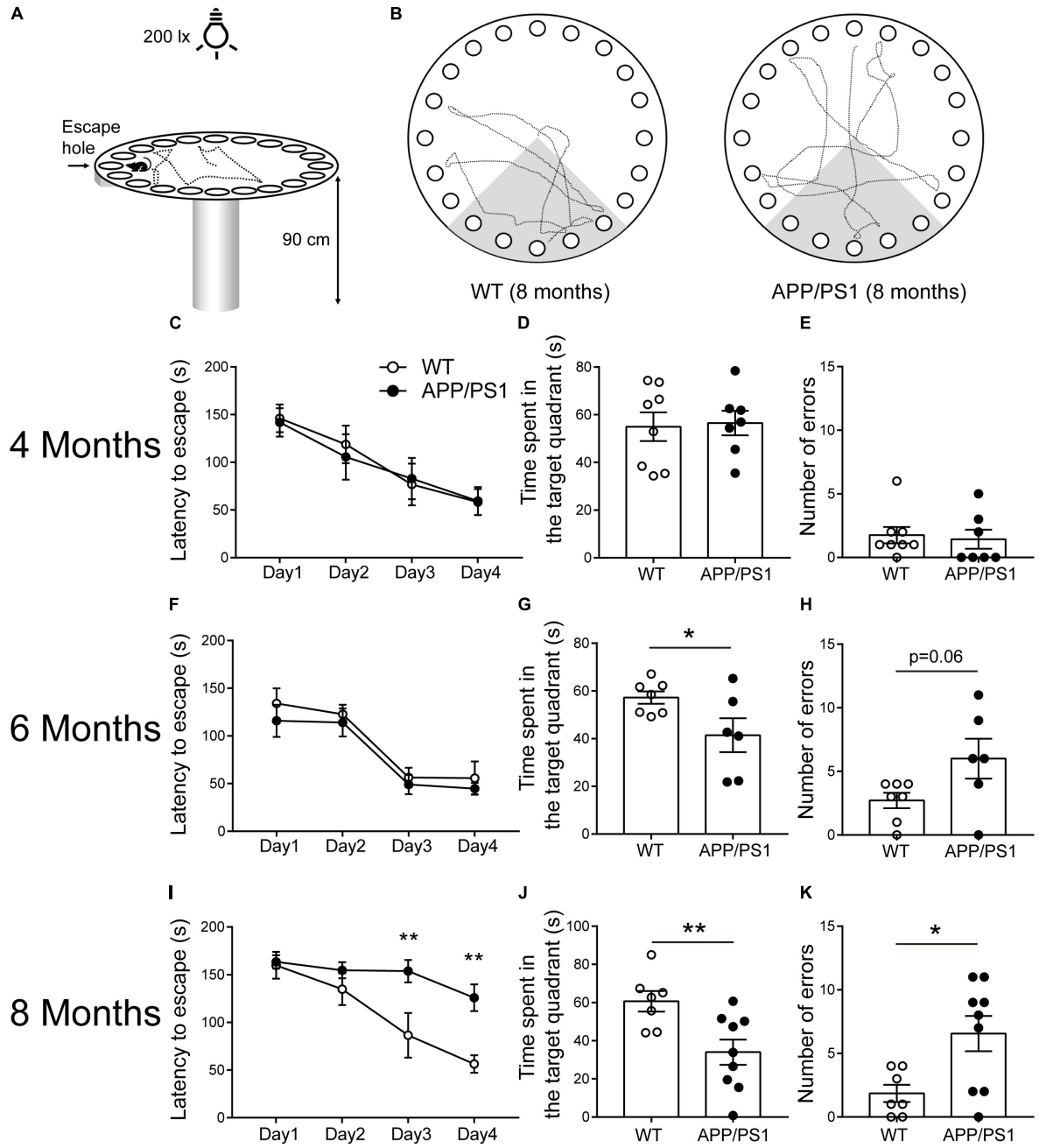

FIGURE 2 | Barnes maze performance for 4-, 6-, and 8-months-old WT and APP/PS1 mice (n = 6–9/group). **(A)** The illustration shows our Barnes maze installation. **(B)** Example of trajectories of 8-month-old WT and APP/PS1 mice during the probe session. **(C–E)** In 4-month-old WT and APP/PS1 mice, no statistically significant differences were observed in the indicators (latency to escape, time spent in the quadrant, and the number of errors) of the Barnes maze. **(F–H)** In 6-month-old mice, the time APP/PS1 mice spent in the target quadrant is decreased compared with WT mice (*$p < 0.05$, unpaired t-test), but no differences were observed in the escape latency and the number of errors. **(I–K)** In 8-month-old APP/PS mice, the latency to escape was decreased in both day 3 and 4 of the training phase (interaction: *$p < 0.05$; at Day 3 or Day 4, **$p < 0.01$, two-way ANOVA followed by Bonferroni's *post hoc* test), the time spent in the target quadrant was reduced (**$p < 0.01$, unpaired t-test), and the number of errors was increased compared with WT mice (*$p < 0.05$, unpaired t-test).

of day: $F_{(3,\ 56)} = 18.31$, $P < 0.0001$; factor of genotype: $F_{(1,\ 56)} = 17.92$, $P < 0.0001$; interaction of two factors: $F_{(3,\ 56)} = 3.114$, $P = 0.0333$], the time spent in the target quadrant was reduced [**Figure 2J**; unpaired t-test: $t_{(14)} = 2.986$; $P = 0.0098$], and the number of errors was increased compared with WT mice [**Figure 2K**; unpaired t-test: $t_{(14)} = 2.783$; $P = 0.0147$]. These results were consistent with the findings in the NLR test, suggesting that APP/PS1 mice have a progressive decline of memory task performance, which is closely related to the hippocampus as well.

Reduced Locomotor Activity in APP/PS1 Mice at the Age of 6 Months

Open field test is a basic measurement of exploratory and locomotor activity in rodents. Our results showed that the total distance was decreased only in the 6-month-old APP/PS1 mice, compared with age-matched WT mice [**Figure 3D**; unpaired *t*-test: $t_{(15)} = 2.166$; $P = 0.0469$]. Accordingly, the 6-month-old APP/PS1 mice showed significantly increased periods of immobility in OFTs [**Figure 3E**; unpaired *t*-test: $t_{(15)} = 3.194$; $P = 0.006$]. However, when 4- and 8-month-old mice were used as experimental subjects, no statistically significant differences were observed in the above two indicators between APP/PS1 mice and WT mice (**Figures 3A,B,G,H**). Concerning the time spent in the center, there were no differences between APP/PS1 mice and WT mice at 4, 6, and 8 months of age, respectively (**Figures 3C,F,I**). These results suggested that 6-month-old APP/PS1 mice showed a decreased locomotor activity in the novel environment. To evaluate whether the magnitude of mobility loss is sufficient to cause impairment in Barnes maze (**Figure 2G**), Y-maze (**Figure 1F**), and NOR (**Figure 1H**) in the 6-month-old APP/PS1 mice, we analyzed the correlation between the total distance of OFTs and performance in Y-maze (**Figure 3J**), NOR (**Figure 3K**), or Barnes maze (**Figure 3L**). However, no significant correlation between the mobility and cognitive performance was found in 6-month-old APP/PS1 mice (**Figure 3J**, $R^2 = 0.13$, $P = 0.38$; **Figure 3K**, $R^2 = 0.059$, $P = 0.562$; **Figure 3L**, $R^2 = 0.027$, $P = 0.753$).

Impaired Long-Term Potentiation in the CA1 of 8-Month-Old APP/PS1 Mice

Our behavioral results found that impaired hippocampal-dependent cognition in 8-month-old APP/PS1 mice. We then examined the LTP at the Schaffer collateral-CA1 pyramidal neuron synapses of APP/PS1 mice at the same age (**Figure 4A**). First, the dependence of the fEPSP on stimulation intensity was analyzed in input/output curves [**Figure 4B**; two-way repeated-measures ANOVA: factor of genotype: $F_{(1,\ 3)} = 0.01896$, $P = 0.8992$; factor of intensity: $F_{(10,\ 30)} = 168.9$, $P < 0.0001$; interaction of two factors: $F_{(10,\ 30)} = 0.2026$]. This result showed that the baseline synaptic transmission was not changed in 8-month-old APP/PS1 mice compared with the age-matched WT mice. Next, LTP was induced by TBS after 20 min of stable baseline recording (**Figure 4C**). Our results revealed that LTP in CA1 area of 8-month-old APP/PS1 mice was significantly depressed in comparison with control mice [**Figure 4D**; WT: 149.1 ± 5.935, APP/PS1: 131.2 ± 2.48, unpaired *t*-test: $t_{(14)} = 2.772$; $P = 0.015$], reflecting the deficits in synaptic plasticity.

Reduced Spontaneous N-Methyl-D-Aspartate Receptor Current of Pyramidal Neurons in the CA1 of 8-Month-Old APP/PS1 Mice

Furthermore, we recorded NMDAR-mediated spontaneous excitatory postsynaptic currents (sEPSCs) *via* whole-cell recording (**Figure 4E**). When presumed pyramidal neurons were held at +40 mV, sEPSCs consisted of both α-amino-3-hydroxy-5-methyl-4-isoxazole propionic acid receptor (AMPAR)- and NMDAR-mediated current (dual sEPSCs). Within 30 ms after dual sEPSCs appeared, a time point at which AMPAR sEPSCs charge already decayed to zero. Next, AMPAR sEPSCs were isolated by the presence of D-APV (**Figure 4F**). The results showed that NMDAR sEPSCs were largely diminished in 8-month-old APP/PS1 mice [**Figure 4G**; unpaired *t*-test: $t_{(20)} = 3.885$; $P = 0.0009$]. In addition, the ratio of the AMPAR sEPSCs to NMDAR sEPSCs was significantly increased in pyramidal neurons from APP/PS1 mice [**Figure 4H**; unpaired *t*-test: $t_{(20)} = 4.192$; $P = 0.0004$]. Taken together, these data suggest the functional decline of NMDAR in APP/PS1 mice.

Reduced Morphological Complexity and Dendritic Spines of Pyramidal Neurons in 8-Month-Old APP/PS1 Mice

The reason behind attenuated LTP may also be abnormal neuronal morphology and changed synaptic density in the CA1 area. Then we performed Golgi-Cox staining to detect the morphology and dendritic spine density of pyramidal neurons in CA1 (**Figure 5A**). Anatomical reconstruction of analyzed pyramidal neurons (**Figure 5B**) showed that the dendritic length [**Figure 5D**; WT: $1{,}321 \pm 69.72$, APP/PS1: 979 ± 105.7, unpaired *t*-test: $t_{(14)} = 2.702$; $P = 0.0172$], and the number of intersections [**Figure 5E**; two-way repeated-measures ANOVA followed by Bonferroni's *post hoc* test: factor of genotype: $F_{(19,\ 133)} = 39.04$, $P < 0.0001$; factor of distance from soma: $F_{(1,\ 7)} = 2.727$, $P = 0.1427$; interaction of two factors: $F_{(19,\ 133)} = 0.001$] were decreased in 8-month-old APP/PS1 mice, suggesting a lower level of complexity of cells. In addition, 8-month-old APP/PS1 mice exhibited a significantly lower spine density compared with WT mice [**Figures 5C,F**; WT: 8.258 ± 0.7125, APP/PS1: 5.617 ± 0.4642, unpaired *t*-test: $t_{(14)} = 3.106$; $P = 0.0077$]. Since the loss of neurons mainly in the hippocampus and cortex is another hallmark at this stage of AD (Niikura et al., 2006; Wirths and Zampar, 2020), we then conducted the fluorescence stainings of the NeuN antibody (**Figure 5G**). And no significant differences were observed between APP/PS1 and WT mice at 8 months of age [**Figure 5H**; unpaired *t*-test: $t_{(8)} = 0.1188$; $P = 0.9084$].

Decreased Expression Levels of N-Methyl-D-Aspartate Receptor Subunits and Synapse-Associated Proteins in the Hippocampus of 8-Month-Old APP/PS1 Mice

Combined with the above results, to determine whether functional alterations of NMDARs are caused by receptor subunits, the expression levels of NMDAR subunits NR1, NR2A, and NR2B and AMPAR subunits GluR1 and GluR2 in the hippocampus of 8-month-old APP/PS1 mice were detected (**Figure 6A**). The results showed that the expression levels of NR2A, NR2B significantly declined in the hippocampus of APP/PS1 mice [**Figures 6B,C**; NR2A, unpaired *t*-test:

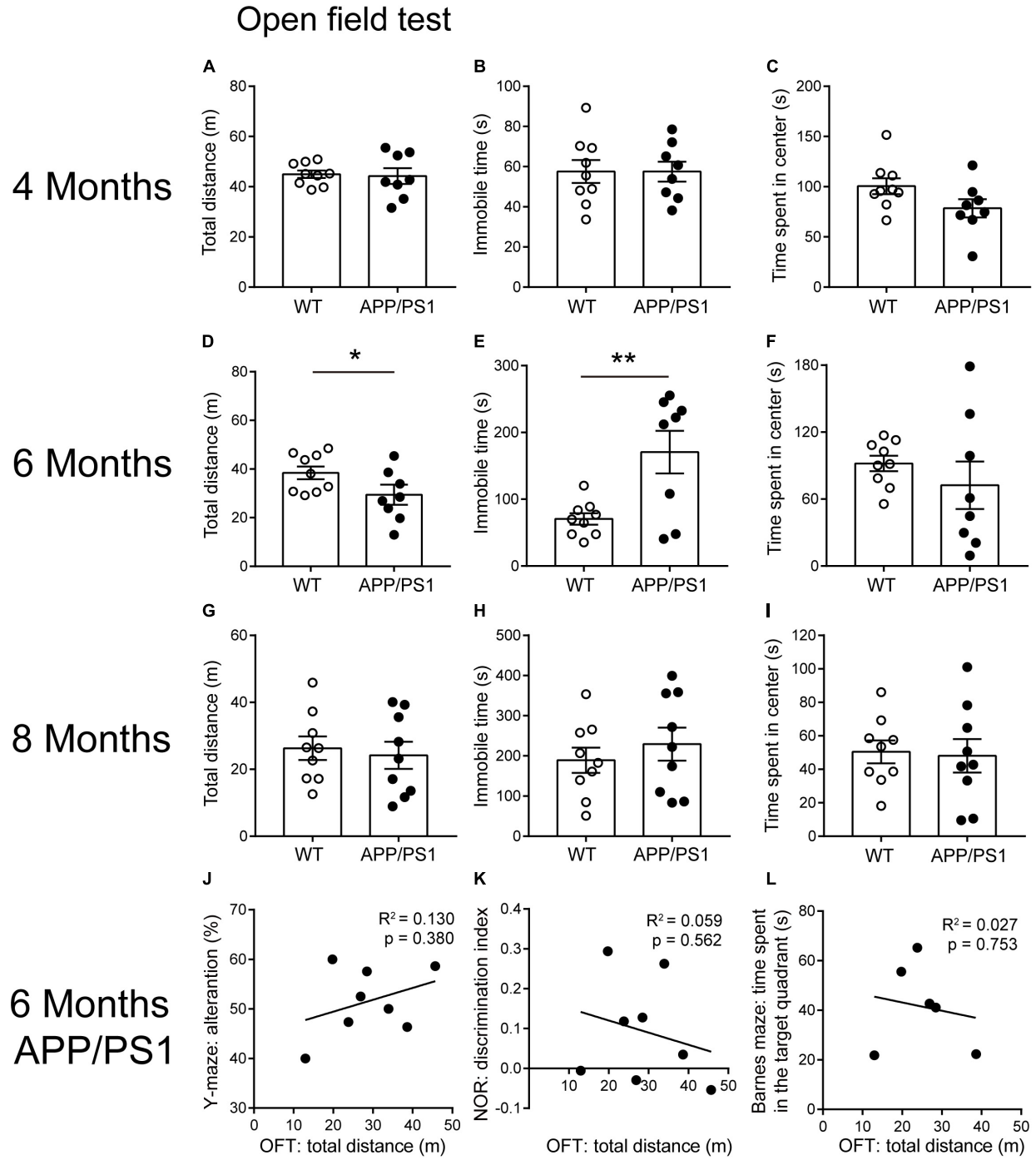

FIGURE 3 | Open field test performance for 4-, 6-, and 8-month-old WT and APP/PS1 mice (n = 8–9/group). **(A–C)** In 4-month-old WT and APP/PS1 mice, no statistically significant differences were observed in the indicators (total distance, time spent in the center, and immobile time) of OFT. **(D–F)** In 6-month-old mice, APP/PS1 mice showed reduced total distance (*$p < 0.05$, unpaired t-test) and increased immobile time (**$p < 0.001$, unpaired t-test) in OFT, compared with WT mice, but there was no difference in the time spent in the center. **(G–I)** In 8-month-old mice, there were no differences in these indicators of OFT. **(J–L)** There was no significant correlation between the total distance in OFTs and the performance in Y-maze, NOR, or Barnes maze in 6-month-old APP/PS1 mice. Each point on these graphs represents an independent mouse.

$t_{(10)}$ = 4.364; P = 0.0014; NR2B, unpaired t-test: $t_{(10)}$ = 2.853; P = 0.0172]. However, no statistically significant differences were observed in the expression levels of NR1, GluR1, and GluR2 between APP/PS1 mice and WT mice (**Figures 6D–F**). In addition, the expression levels of other synaptic function proteins were also detected (**Figure 6G**). The results showed that

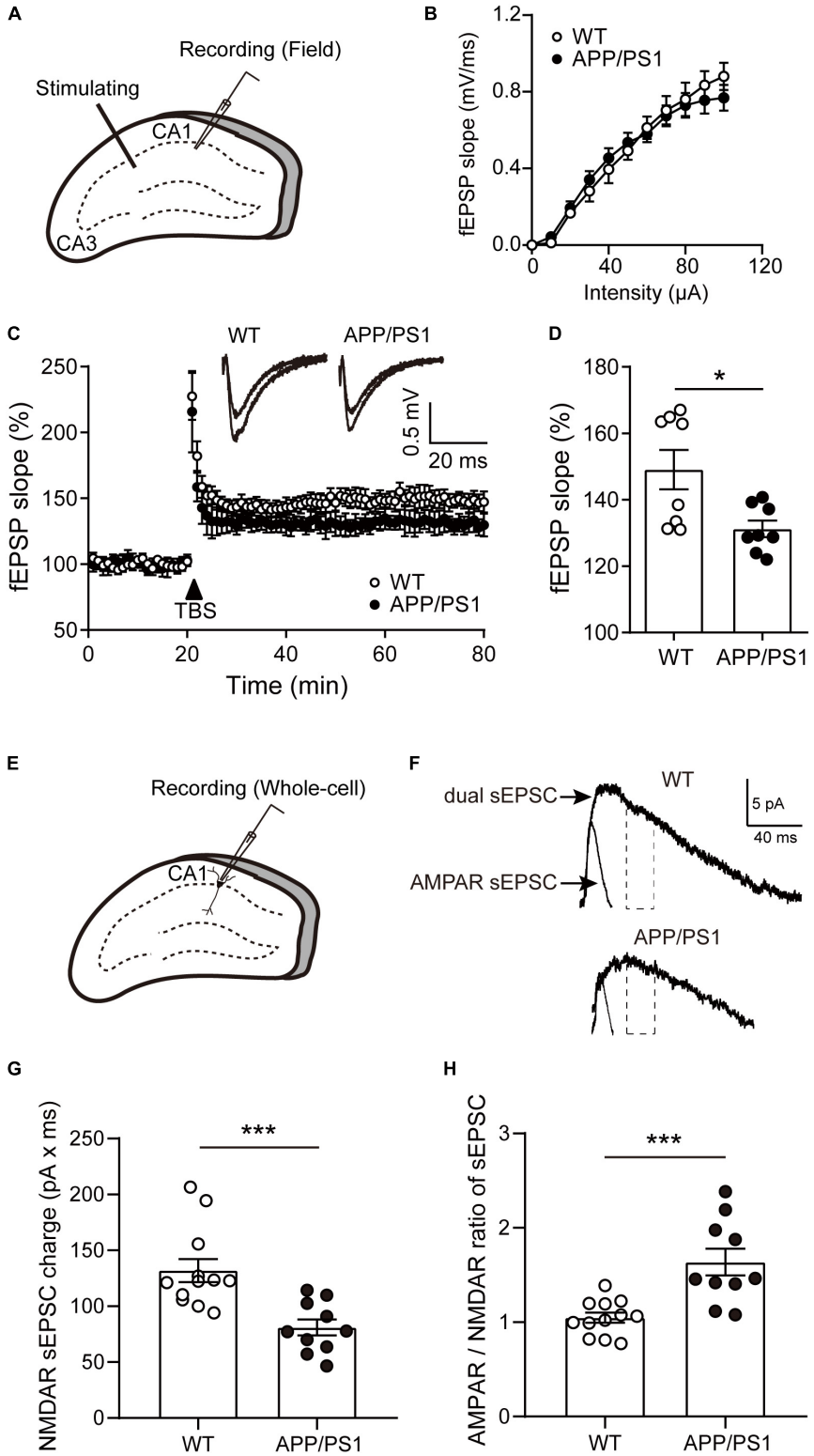

FIGURE 4 | The LTP and NMDAR sEPSCs of pyramidal neurons in the CA1 of 8-month-old APP/PS1 mice. **(A)** Schematic diagram of fEPSP recording. **(B)** The input-output (I/O) curves in response to stimulus in the CA1 of WT and APP/PS1 mice. **(C)** Representative traces showing LTP in CA1 of WT and APP/PS1 mice. **(D)** Quantification of the last 15 min of fEPSP recordings (n = 8 slices from 4 mice/group; *$p < 0.05$, unpaired t-test). **(E)** Schematic diagram of whole-cell recording. **(F)** The diagram showed typical average events from WT and APP/PS1 mice. NMDAR sEPSCs were estimated from the charge of the dual sEPSCs after AMPAR

(Continued)

FIGURE 4 | contribution decayed to zero. Dotted lines represent the time window in which the NMDAR sEPSCs charge was calculated. **(G)** The NMDAR sEPSCs charge was reduced in the cells from APP/PS1 (n = 10–12 cells from 4 to 6 mice/group; ***$p < 0.001$, unpaired t-test). **(H)** The AMPAR/NMDAR ratio of sEPSCs was increased in pyramidal neurons of CA1 from APP/PS1 mice, compared with WT mice (***$p < 0.001$, unpaired t-test).

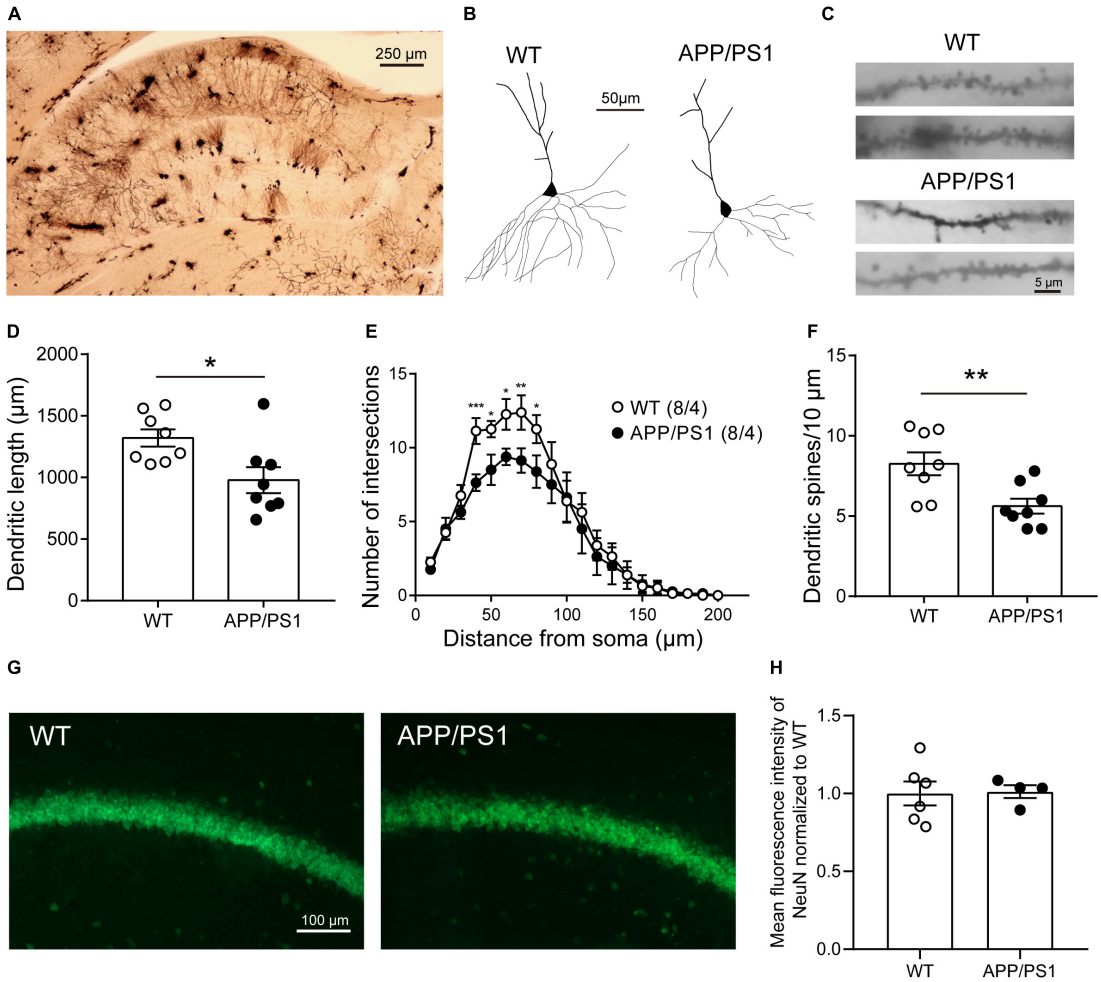

FIGURE 5 | The morphology and number of pyramidal neurons in the CA1 of 8-month-old APP/PS1 mice. **(A)** Golgi-Cox staining of brain tissue samples. Scale bar, 250 μm. **(B)** Representative examples of reconstructed pyramidal neurons in the CA1 of 8-month-old WT and APP/PS1 mice. Scale bar, 50 μm. **(C)** Representative spine morphology of pyramidal neurons in WT and APP/PS1 mice. Scale bar, 5 μm. **(D)** The dendritic length of pyramidal neurons was decreased in APP/PS1 mice compared with WT mice (n = 8 from 4 mice; *$p < 0.05$, unpaired t-test). **(E)** The complexity of dendrites of pyramidal neurons was decreased in APP/PS1 mice compared with WT mice (interaction: ***$p < 0.001$; two-way repeated-measures ANOVA followed by Bonferroni's *post hoc* test, *$p < 0.05$, **$p < 0.01$, ***$p < 0.001$). **(F)** The total dendritic spine density of pyramidal neurons was decreased in APP/PS1 mice compared with WT mice (n = 8 from 4 mice; **$p < 0.01$, unpaired t-test). **(G)** Representative images of NeuN staining of the hippocampal CA1 area of 8-month-old APP/PS1 and WT mice. Scale bar: 100 μm. **(H)** The quantitative results of the mean fluorescence intensity of NeuN were not altered significantly between 8-month-old APP/PS1 and WT mice (n = 4–6 mice/group).

a significant decrease in the levels of postsynaptic density 95 (PSD95) [**Figure 6H**; unpaired t-test: $t_{(6)} = 3.012$; $P = 0.0236$] and synaptosomal-associated protein 25 (SNAP25) [**Figure 6I**; unpaired t-test: $t_{(6)} = 3.41$; $P = 0.0143$] was found in 8-month-old APP/PS1 mice.

DISCUSSION

In the present study, we investigated synaptic plasticity and NMDAR function in hippocampal CA1 in 8-month-old APP/PS1 mice, because the cognitive dysfunction is more severe at this age. The results showed that LTP and NMDAR-mediated sEPSCs were reduced and pyramidal neuron dendrites had shorter length, fewer intersections, and lower spine density in the hippocampal CA1 of APP/PS1 mice. Further, the reduced expression levels of NMDAR subunits, PSD95 and SNAP25 were observed in the hippocampus of APP/PS1 mice. These results suggest that NMDAR dysfunction, impaired synaptic plasticity, and disrupted neuronal morphology constitute an important part of the neuropathophysiological alterations associated with cognitive impairment in APP/PS1 mice (**Figure 7**).

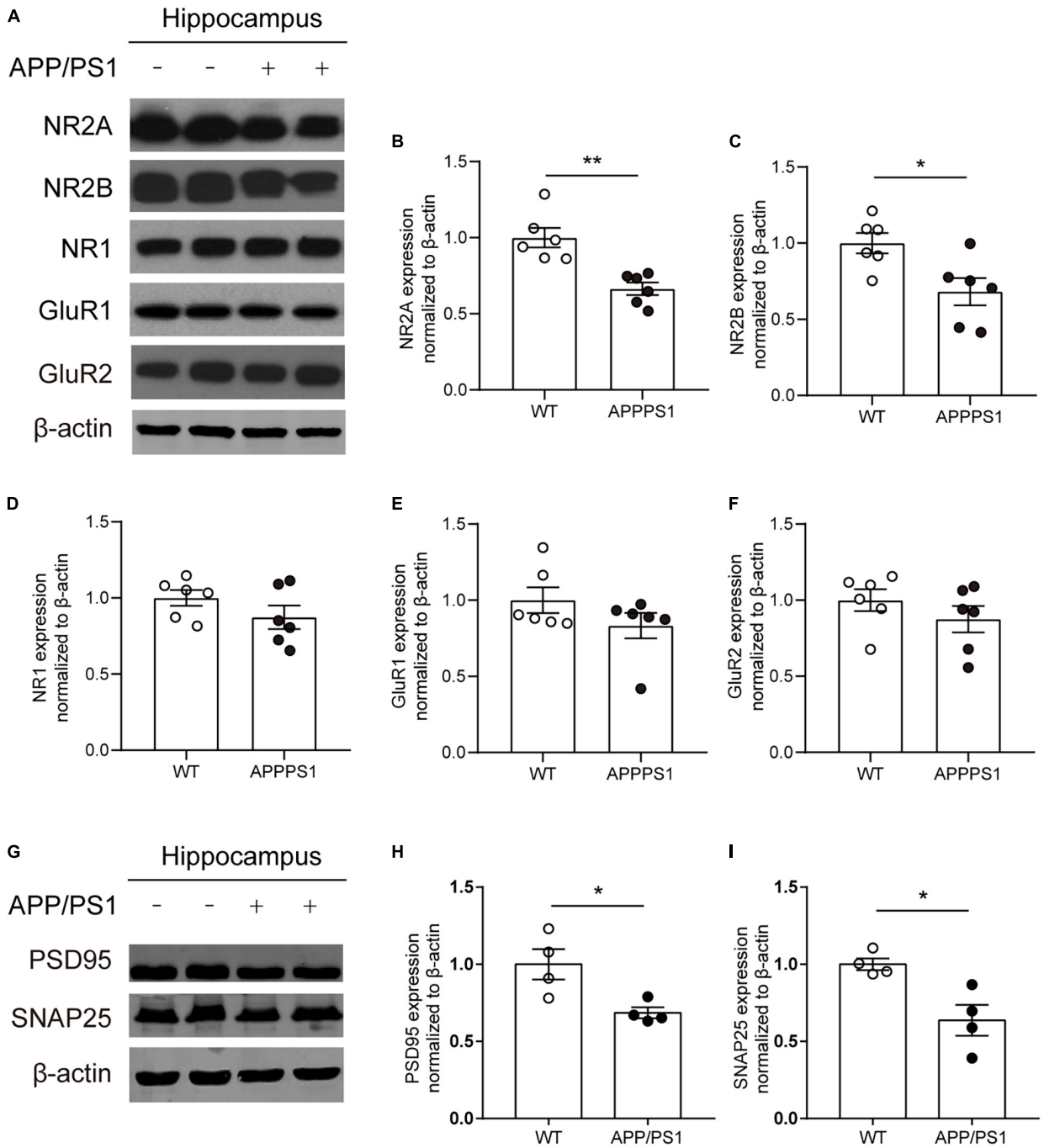

FIGURE 6 | The expression of synapse-associated proteins and glutamate receptor subunit proteins in the CA1 area of 8-month-old WT and APP/PS1 mice. **(A)** Representative western blots of glutamate receptor subunits. **(B–D)** Quantitative of NMDAR subunits expression showed a significant decrease of NR2A and NR2B expression (n = 6 mice/group, $^{*}p < 0.05$, $^{**}p < 0.01$, unpaired t-test) in the hippocampus in 8-month-old APP/PS1 mice compared with WT mice, but there was no difference on the expression of NR1 from two groups. **(E,F)** Quantitative of AMPA receptors subunits (GluR1, GluR2) expression showed no change in hippocampus from 8-month-old APP/PS1 mice and WT mice. **(G)** Representative western blots of PSD95 and SNAP25. **(H,I)** A significant decrease of the levels of PSD95 and SNAP25 in the hippocampus from 8-month-old APP/PS1 mice compared with WT mice (n = 4 mice/group, $^{*}p < 0.05$, unpaired t-test).

Cognitive dysfunction is the most significant symptom of AD, which is often preceded by a period of mild cognitive impairment (MCI). About one-third of all patients with MCI progress to AD in 5 years (Palmer et al., 2007). Consistent with previous reports (Bruce-Keller et al., 2011; Chen et al., 2012), we confirmed the deterioration of cognitive function with the increase of the age of APP/PS1 mice, which included working memory, short-term spatial memory, long-term recognition

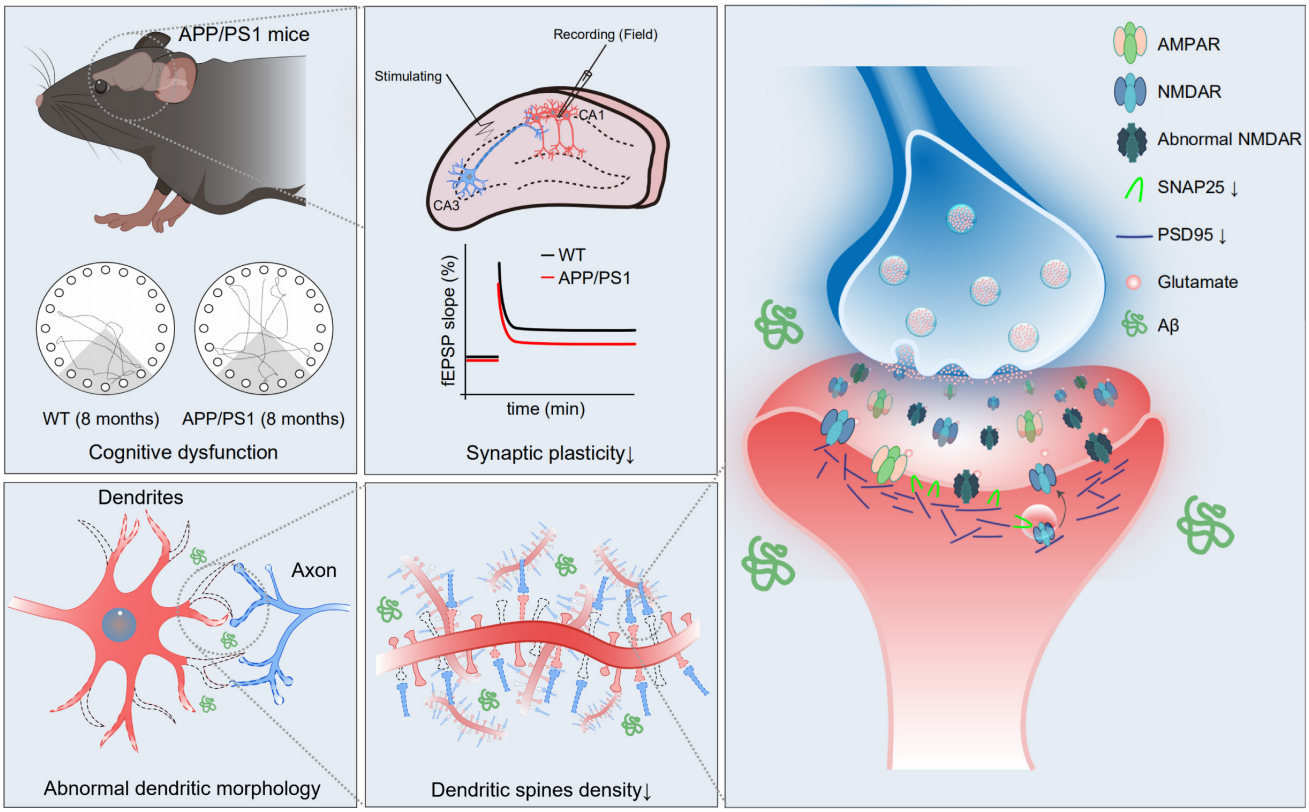

FIGURE 7 | Schematic diagram of the mechanism of cognitive impairment in 8-month-old APP/PS1 mice. In hippocampal CA1 area of APP/PS1 mice, impaired function of NMDAR, reduced expression of synaptic proteins, abnormal neuronal morphology, and decreased dendritic spine density may give rise to weak synaptic plasticity, which mediates age-related cognitive dysfunction.

memory, and spatial learning and memory. These cognitive tasks mainly reflect the ability of hippocampus-dependent learning and memory (Zheng et al., 2009; Gonzalez et al., 2021), and the results hinted at an abnormality of hippocampal function in APP/PS mice at 8 months of age. To exclude the effect of locomotor activity in cognitive tests, we performed OFTs and found that APP/PS1 mice showed decreased locomotor activity in the novel environment at 6 months, but not at 8 months of age. However, correlation analysis showed that mobility loss was not associated with impaired cognitive performance in 6-month-old APP/PS1 mice. Interestingly, a decrease in locomotor activity was also reported in other AD models (Samaey et al., 2019) and aging mice (Shoji et al., 2016; Shoji and Miyakawa, 2019), the latter may suggest that reduced locomotor activity may be an indicator of aging. Taken together, genotype-specific pathogenic effects may accelerate aging and cause reduced mobility in 6-month-old APP/PS1 mice. By contrast, at 8 months of age, since the mobility of WT mice was also reduced due to aging, no significant differences were observed between the APP/PS1 and WT mice.

Long-term potentiation as an indicator of synaptic plasticity in the hippocampal CA1 area is deeply involved in spatial learning and memory (Bartsch et al., 2011; Fouquet et al., 2012). Reduced LTP of the CA1 area is often seen in diseases characterized or accompanied by cognitive dysfunction, such as AD, schizophrenia, and depression (Liu et al., 2019; Le Douce et al., 2020; Percelay et al., 2021). The mechanism of impaired synaptic plasticity in AD has been not fully understood. The elicitation of many forms of LTP requires NMDAR activation and the weakening or strengthening of the plasticity is controlled mainly by the kinetics of CA^{2+} influx through NMDARs (Yashiro and Philpot, 2008). Previous studies have found an impaired NMDAR function might be related to the pathophysiology of AD (Mota et al., 2014; Zhang et al., 2016; Wang and Reddy, 2017). For example, Aβ recruited internalization of synaptic NMDARs and the reduction of NMDAR-mediated currents in the cultured cortical neurons (Snyder et al., 2005). In addition, some novel therapies modulating NMDAR function have been shown to restore cognitive function in clinical trials (Goetghebeur et al., 2019; Lin et al., 2021). Taken together, there is growing evidence of NMDAR-associated synaptic abnormalities in AD, which is consistent with our results that NMDAR-mediated sEPSCs were reduced in hippocampal CA1 with impaired synaptic plasticity in APP/PS1 mice.

The structural adaptation of neurons is also an important form of synaptic plasticity. The loss of neurons, abnormal neuronal morphology like reduced dendritic spine density, and abnormal synaptic structure were all constantly associated with impaired

LTP (Bencsik et al., 2019; Reza-Zaldivar et al., 2020; Meftahi et al., 2021). We found aberrant dendritic length, complexity, and decreased dendritic spine density of pyramidal neurons in the CA1 area of APP/PS1 mice. However, no change was observed in the number of neurons. These results suggested that pyramidal neurons in CA1 in AD mice might have lower efficiency of signal transmission with other neurons, which could be partly responsible for the impaired synaptic plasticity and cognition in APP/PS1 mice (Yuste and Bonhoeffer, 2001; Yang et al., 2015).

Experiments with western blots showed reduced expressing levels of NR2A and NR2B in hippocampal CA1 of APP/PS1 mice. These results support our electrophysiological findings, suggesting that the reduction of NMDAR-mediated sEPSCs may be due to the low expression of specific receptor subunits. In addition, decreased expression levels of PSD95 and SNAP25 were observed in hippocampal CA1 of APP/PS1 mice. PSD95 is a scaffold protein that assembles glutamate receptors, ion channel complexes, and signaling proteins. It is significant for regulating synaptic strength and plasticity when receiving patterns of neural signals (Migaud et al., 1998; Carlisle et al., 2008). PSD95 has also been reported to promote the formation of dendritic spines and maintain their stability (Nikonenko et al., 2008; Cane et al., 2014). Therefore, the downregulated PSD95 expression might count for the reduction of dendritic spine density in APP/PS1 mice. SNAP25 is a member of the SNARE family, which plays a significant role in the trafficking of postsynaptic glutamate receptors. In the hippocampus, it takes part in the incorporation of synaptic NMDARs as the target of protein kinase phosphorylation (Lau et al., 2010). In light of the above reports and our results, we speculate that the reduced expression of SNAP25 may also be associated with the NMDAR dysfunction in APP/PS1 mice.

It should be acknowledged that there are some limitations to our research. First, the decreased NMDAR sEPSCs in APP/PS1 mice may not occur in other AD models that present the Tau mutations or mimic the late-onset progression seen in sporadic human AD. Second, our detection of receptor subunit protein expression and electrophysiological research did not distinguish the location of the NMDARs (inside or outside the synapse). Additional studies are necessary to determine the dynamic change of NMDAR function during disease progression and differentiate the changes in the synaptic and extrasynaptic NMDARs in AD models. Altogether, further studies of the destructive effects of NMDAR dysfunction are needed for the development of more effective, mechanism-targeted treatments for AD.

DATA AVAILABILITY STATEMENT

The original contributions presented in the study are included in the article/supplementary material, further inquiries can be directed to the corresponding authors.

ETHICS STATEMENT

The animal study was reviewed and approved by the Animal Care and Use Committee of the Ningbo University.

AUTHOR CONTRIBUTIONS

XZ and LR initiated and designed this study. XZ, LX, HJ, and SY performed the brain slice electrophysiology recordings and analyzed the data. LX and HJ performed the behavioral test. LH and YD performed the Golgi-Cox staining. YZ performed the western blotting. ZL and YJ performed the immunofluorescent staining. LX, YZ, XZ, and HS wrote the manuscript. All authors contributed to the article and approved the submitted version.

FUNDING

The study was supported by the Natural Science Foundation of Zhejiang Province (Grant No. LQ20C090002), the Major Social Development Special Foundation of Ningbo (Grant No. 2017C510010), and the Medical and Health Science and Technology Plan Project of Zhejiang Province (Grant No. 2019KY564).

REFERENCES

Bartsch, T., Döhring, J., Rohr, A., Jansen, O., and Deuschl, G. (2011). CA1 neurons in the human hippocampus are critical for autobiographical memory, mental time travel, and autonoetic consciousness. *Proc. Natl. Acad. Sci. U.S.A.* 108, 17562–17567. doi: 10.1073/pnas.1110266108

Bencsik, N., Pusztai, S., Borbély, S., Fekete, A., Dülk, M., Kis, V., et al. (2019). Dendritic spine morphology and memory formation depend on postsynaptic Caskin proteins. *Sci. Rep.* 9:16843. doi: 10.1038/s41598-019-53317-9

Bruce-Keller, A., Gupta, S., Knight, A., Beckett, T., Mcmullen, J., Davis, P., et al. (2011). Cognitive impairment in humanized APP×PS1 mice is linked to Aβ(1-42) and NOX activation. *Neurobiol. Dis.* 44, 317–326. doi: 10.1016/j.nbd.2011.07.012

Cane, M., Maco, B., Knott, G., and Holtmaat, A. (2014). The relationship between PSD-95 clustering and spine stability in vivo. *J. Neurosci.* 34, 2075–2086. doi: 10.1523/jneurosci.3353-13.2014

Carlisle, H., Fink, A., Grant, S., and O'dell, T. (2008). Opposing effects of PSD-93 and PSD-95 on long-term potentiation and spike timing-dependent plasticity. *J. Physiol.* 586, 5885–5900. doi: 10.1113/jphysiol.2008.163469

Chen, S., Cai, Q., Shen, Y., Wang, P., Teng, G., Zhang, W., et al. (2012). Age-related changes in brain metabolites and cognitive function in APP/PS1 transgenic mice. *Behav. Brain Res.* 235, 1–6. doi: 10.1016/j.bbr.2012.07.016

Devi, G., and Scheltens, P. (2018). Heterogeneity of Alzheimer's disease: consequence for drug trials? *Alzheimers Res. Ther.* 10:122. doi: 10.1186/s13195-018-0455-y

Ewers, M., Cheng, X., Zhong, Z., Nural, H. F., Walsh, C., Meindl, T., et al. (2011). Increased CSF-BACE1 activity associated with decreased hippocampus volume in Alzheimer's disease. *J. Alzheimers Dis.* 25, 373–381. doi: 10.3233/jad-2011-091153

Fouquet, M., Desgranges, B., La Joie, R., Rivière, D., Mangin, J., Landeau, B., et al. (2012). Role of hippocampal CA1 atrophy in memory encoding deficits

in amnestic Mild Cognitive Impairment. *Neuroimage* 59, 3309–3315. doi: 10.1016/j.neuroimage.2011.11.036

Goetghebeur, P., Wesnes, K., and Targum, S. (2019). D-cycloserine improves difficult discriminations in a pattern separation task in Alzheimer's disease patients with dementia. *J. Alzheimers Dis.* 69, 377–383. doi: 10.3233/jad-181094

Gómez-Isla, T., Hollister, R., West, H., Mui, S., Growdon, J., Petersen, R., et al. (1997). Neuronal loss correlates with but exceeds neurofibrillary tangles in Alzheimer's disease. *Ann. Neurol.* 41, 17–24. doi: 10.1002/ana.410410106

Gonzalez, M., Rossato, J., Radiske, A., Bevilaqua, L., and Cammarota, M. (2021). Dopamine controls whether new declarative information updates reactivated memories through reconsolidation. *Proc. Natl. Acad. Sci. U.S.A* 118:e2025275118. doi: 10.1073/pnas.2025275118

Hall, A. M., and Roberson, E. D. (2012). Mouse models of Alzheimer's disease. *Brain Res. Bull.* 88, 3–12. doi: 10.1016/j.brainresbull.2011.11.017

Hampel, H., Teipel, S. J., Bayer, W., Alexander, G. E., Schwarz, R., Schapiro, M. B., et al. (2002). Age transformation of combined hippocampus and amygdala volume improves diagnostic accuracy in Alzheimer's disease. *J. Neurol. Sci.* 194, 15–19. doi: 10.1016/s0022-510x(01)00669-4

Jankowsky, J., Fadale, D., Anderson, J., Xu, G., Gonzales, V., Jenkins, N., et al. (2004). Mutant presenilins specifically elevate the levels of the 42 residue beta-amyloid peptide in vivo: evidence for augmentation of a 42-specific gamma secretase. *Hum. Mol. Genet.* 13, 159–170. doi: 10.1093/hmg/ddh019

Kasanetz, F., and Manzoni, O. J. (2009). Maturation of excitatory synaptic transmission of the rat nucleus accumbens from juvenile to adult. *J. Neurophysiol.* 101, 2516–2527. doi: 10.1152/jn.91039.2008

Lane, H., Tu, C., Lin, W., and Lin, C. (2021). Brain activity of benzoate, a d-amino acid oxidase inhibitor, in patients with mild cognitive impairment in a randomized, double-blind, placebo controlled clinical trial. *Int. J. Neuropsychopharmacol.* 24, 392–399. doi: 10.1093/ijnp/pyab001

Lau, C., Takayasu, Y., Rodenas-Ruano, A., Paternain, A., Lerma, J., Bennett, M., et al. (2010). SNAP-25 is a target of protein kinase C phosphorylation critical to NMDA receptor trafficking. *J. Neurosci.* 30, 242–254. doi: 10.1523/jneurosci.4933-08.2010

Le Douce, J., Maugard, M., Veran, J., Matos, M., Jégo, P., Vigneron, P., et al. (2020). Impairment of glycolysis-derived L-serine production in astrocytes contributes to cognitive deficits in Alzheimer's disease. *Cell Metab* 31, 503–517.e508. doi: 10.1016/j.cmet.2020.02.004

Li, B., Otsu, Y., Murphy, T. H., and Raymond, L. A. (2003). Developmental decrease in NMDA receptor desensitization associated with shift to synapse and interaction with postsynaptic density-95. *J. Neurosci.* 23, 11244–11254. doi: 10.1523/jneurosci.23-35-11244.2003

Li, P., Xu, J., Gu, H., Peng, H., Yin, Y., and Zhuang, J. (2021). Memantine ameliorates cognitive deficit in AD mice via enhancement of entorhinal-CA1 projection. *BMC Neurosci.* 22:41. doi: 10.1186/s12868-021-00647-y

Lin, C., Chen, P., Chang, Y., Chuo, L., Chen, Y., Tsai, G., et al. (2014). Benzoate, a D-amino acid oxidase inhibitor, for the treatment of early-phase Alzheimer disease: a randomized, double-blind, placebo-controlled trial. *Biol. Psychiatry* 75, 678–685. doi: 10.1016/j.biopsych.2013.08.010

Lin, C., Chen, P., Wang, S., and Lane, H. (2021). Effect of sodium benzoate on cognitive function among patients with behavioral and psychological symptoms of dementia: secondary analysis of a randomized clinical trial. *JAMA Netw. Open* 4:e216156. doi: 10.1001/jamanetworkopen.2021.6156

Lin, C., Yang, H., Chiu, C., and Lane, H. (2017). Blood levels of D-amino acid oxidase vs. D-amino acids in reflecting cognitive aging. *Sci. Rep.* 7:14849. doi: 10.1038/s41598-017-13951-7

Liu, S., Hu, W., Zhang, W., Yang, L., Li, Y., Xiao, Z., et al. (2019). Paeoniflorin attenuates impairment of spatial learning and hippocampal long-term potentiation in mice subjected to chronic unpredictable mild stress. *Psychopharmacology (Berl.)* 236, 2823–2834. doi: 10.1007/s00213-019-05257-5

Llorens-Martín, M., Blazquez-Llorca, L., Benavides-Piccione, R., Rabano, A., Hernandez, F., Avila, J., et al. (2014). Selective alterations of neurons and circuits related to early memory loss in Alzheimer's disease. *Front. Neuroanat.* 8:38. doi: 10.3389/fnana.2014.00038

Martinez-Coria, H., Green, K., Billings, L., Kitazawa, M., Albrecht, M., Rammes, G., et al. (2010). Memantine improves cognition and reduces Alzheimer's-like neuropathology in transgenic mice. *Am. J. Pathol.* 176, 870–880. doi: 10.2353/ajpath.2010.090452

Meftahi, G. H., Bayat, M., Zarifkar, A. H., Akbari, S., Borhani Haghighi, A., Naseh, M., et al. (2021). Treatment with edaravone improves the structure and functional changes in the hippocampus after chronic cerebral hypoperfusion in rat. *Brain Res. Bull.* 174, 122–130. doi: 10.1016/j.brainresbull.2021.06.006

Migaud, M., Charlesworth, P., Dempster, M., Webster, L., Watabe, A., Makhinson, M., et al. (1998). Enhanced long-term potentiation and impaired learning in mice with mutant postsynaptic density-95 protein. *Nature* 396, 433–439. doi: 10.1038/24790

Mota, S., Ferreira, I., and Rego, A. (2014). Dysfunctional synapse in Alzheimer's disease – A focus on NMDA receptors. *Neuropharmacology* 14, 16–26. doi: 10.1016/j.neuropharm.2013.08.013

Niikura, T., Tajima, H., and Kita, Y. (2006). Neuronal cell death in Alzheimer's disease and a neuroprotective factor, humanin. *Curr. Neuropharmacol.* 4, 139–147. doi: 10.2174/157015906776359577

Nikonenko, I., Boda, B., Steen, S., Knott, G., Welker, E., and Muller, D. (2008). PSD-95 promotes synaptogenesis and multiinnervated spine formation through nitric oxide signaling. *J. Cell Biol.* 183, 1115–1127. doi: 10.1083/jcb.200805132

Palmer, K., Berger, A. K., Monastero, R., Winblad, B., Bäckman, L., and Fratiglioni, L. (2007). Predictors of progression from mild cognitive impairment to Alzheimer disease. *Neurology* 68, 1596–1602. doi: 10.1212/01.wnl.0000260968.92345.3f

Parsons, C., Stöffler, A., and Danysz, W. (2007). Memantine: a NMDA receptor antagonist that improves memory by restoration of homeostasis in the glutamatergic system–too little activation is bad, too much is even worse. *Neuropharmacology* 53, 699–723. doi: 10.1016/j.neuropharm.2007.07.013

Percelay, S., Billard, J., Freret, T., Andrieux, A., Boulouard, M., and Bouet, V. (2021). Functional dysregulations in CA1 hippocampal networks of a 3-hit mouse model of schizophrenia. *Int. J. Mol. Sci.* 22:644. doi: 10.3390/ijms22052644

Reza-Zaldivar, E. E., Hernandez-Sapiens, M. A., Minjarez, B., Gomez-Pinedo, U., Sanchez-Gonzalez, V. J., Marquez-Aguirre, A. L., et al. (2020). Dendritic spine and synaptic plasticity in Alzheimer's disease: a focus on MicroRNA. *Front. Cell Dev. Biol.* 8:255. doi: 10.3389/fcell.2020.00255

Samaey, C., Schreurs, A., Stroobants, S., and Balschun, D. (2019). Early cognitive and behavioral deficits in mouse models for tauopathy and Alzheimer's disease. *Front. Aging Neurosci.* 11:335. doi: 10.3389/fnagi.2019.00335

Shoji, H., and Miyakawa, T. (2019). Age-related behavioral changes from young to old age in male mice of a C57BL/6J strain maintained under a genetic stability program. *Neuropsychopharmacol. Rep.* 39, 100–118. doi: 10.1002/npr2.12052

Shoji, H., Takao, K., Hattori, S., and Miyakawa, T. (2016). Age-related changes in behavior in C57BL/6J mice from young adulthood to middle age. *Mol. Brain* 9:11. doi: 10.1186/s13041-016-0191-9

Snyder, E., Nong, Y., Almeida, C., Paul, S., Moran, T., Choi, E., et al. (2005). Regulation of NMDA receptor trafficking by amyloid-beta. *Nat. Neurosci.* 8, 1051–1058. doi: 10.1038/nn1503

Wang, R., and Reddy, P. H. (2017). Role of glutamate and NMDA receptors in Alzheimer's disease. *J. Alzheimers Dis.* 57, 1041–1048. doi: 10.3233/jad-160763

Wang, Y., Zhao, J., Guo, F. L., Gao, X., Xie, X., Liu, S., et al. (2020). Metformin ameliorates synaptic defects in a mouse model of AD by inhibiting Cdk5 activity. *Front. Cell. Neurosci.* 14:170. doi: 10.3389/fncel.2020.00170

Wirths, O., and Zampar, S. (2020). Neuron loss in Alzheimer's disease: translation in transgenic mouse models. *Int. J. Mol. Sci.* 21:144. doi: 10.3390/ijms21218144

Yang, X., Liao, X., Uribe-Mariño, A., Liu, R., Xie, X., Jia, J., et al. (2015). Stress during a critical postnatal period induces region-specific structural abnormalities and dysfunction of the prefrontal cortex via CRF1. *Neuropsychopharmacology* 40, 1203–1215. doi: 10.1038/npp.2014.304

Yang, X., Yao, C., Tian, T., Li, X., Yan, H., Wu, J., et al. (2018). A novel mechanism of memory loss in Alzheimer's disease mice via the degeneration of entorhinal-CA1 synapses. *Mol. Psychiatry* 23, 199–210. doi: 10.1038/mp.2016.151

Yashiro, K., and Philpot, B. (2008). Regulation of NMDA receptor subunit expression and its implications for LTD, LTP, and metaplasticity. *Neuropharmacology* 55, 1081–1094. doi: 10.1016/j.neuropharm.2008.07.046

Yuste, R., and Bonhoeffer, T. (2001). Morphological changes in dendritic spines associated with long-term synaptic plasticity. *Annu. Rev. Neurosci.* 24, 1071–1089. doi: 10.1146/annurev.neuro.24.1.1071

Zhang, X., Mei, Y., He, Y., Wang, D., Wang, J., Wei, X., et al. (2021). Ablating adult neural stem cells improves synaptic and cognitive functions in Alzheimer models. *Stem Cell Rep.* 16, 89–105. doi: 10.1016/j.stemcr.2020.12.003

Zhang, Y., Li, P., Feng, J., and Wu, M. (2016). Dysfunction of NMDA receptors in Alzheimer's disease. *Neurol. Sci.* 37, 1039–1047. doi: 10.1007/s10072-016-2546-5

Zheng, J., Patil, S., Chen, W., An, W., He, J., Höger, H., et al. (2009). Hippocampal protein levels related to spatial memory are different in the Barnes maze and in the multiple T-maze. *J. Proteome Res.* 8, 4479–4486. doi: 10.1021/pr900 2596

Conflict of Interest: The authors declare that the research was conducted in the absence of any commercial or financial relationships that could be construed as a potential conflict of interest.

Publisher's Note: All claims expressed in this article are solely those of the authors and do not necessarily represent those of their affiliated organizations, or those of the publisher, the editors and the reviewers. Any product that may be evaluated in this article, or claim that may be made by its manufacturer, is not guaranteed or endorsed by the publisher.

frontiers in Aging Neuroscience

ORIGINAL RESEARCH
published: 11 January 2022
doi: 10.3389/fnagi.2021.784665

Tau Knockout and α-*Synuclein A53T* Synergy Modulated Parvalbumin-Positive Neurons Degeneration Staging in Substantia Nigra Pars Reticulata of Parkinson's Disease-Liked Model

Meige Zheng[1†], *Yanchang Liu*[1†], *Zhaoming Xiao*[1], *Luyan Jiao*[2*] and *Xian Lin*[3,4*]

[1] Department of Orthopaedics, The Second Hospital of Anhui Medical University, Hefei, China, [2] Nuwacell Biotechnologies Co., Ltd, Hefei, China, [3] Guangdong Province Key Laboratory of Brain Function and Disease, Zhongshan School of Medicine, Sun Yat-sen University, Guangzhou, China, [4] Department of Anatomy, Zhongshan School of Medicine, Sun Yat-sen University, Guangzhou, China

OPEN ACCESS

Edited by:
Mario Sanhueza,
Universidad Mayor, Chile

Reviewed by:
Ichiro Kawahata,
Tohoku University, Japan
Sachchida Nand Rai,
University of Allahabad, India
Roberta Marongiu,
Weill Cornell Medicine, United States

***Correspondence:**
Luyan Jiao
ljiao@nuwacell.com
Xian Lin
linxian3@mail.sysu.edu.cn

[†] These authors have contributed equally to this work

Specialty section:
This article was submitted to Cellular and Molecular Mechanisms of Brain-aging, a section of the journal Frontiers in Aging Neuroscience

Received: 28 September 2021
Accepted: 29 November 2021
Published: 11 January 2022

Citation:
Zheng M, Liu Y, Xiao Z, Jiao L and Lin X (2022) Tau Knockout and α-Synuclein A53T Synergy Modulated Parvalbumin-Positive Neurons Degeneration Staging in Substantia Nigra Pars Reticulata of Parkinson's Disease-Liked Model. Front. Aging Neurosci. 13:784665. doi: 10.3389/fnagi.2021.784665

The loss of parvalbumin-positive (PV^+) neurons in the substantia nigra pars reticulata (SNR) was observed in patients with end-stage Parkinson's disease (PD) and our previously constructed old-aged *Pitx3-A53T*α*-Syn* × *Tau*$^{-/-}$ triple transgenic mice model of PD. The aim of this study was to examine the progress of PV^+ neurons loss. We demonstrated that, as compared with non-transgenic (*nTg*) mice, the accumulation of α-*synuclein* in the SNR of aged *Pitx3-A53T*α*-Syn* × *Tau*$^{-/-}$ mice was increased obviously, which was accompanied by the considerable degeneration of PV^+ neurons and the massive generation of apoptotic $NeuN^+TUNEL^+$ co-staining neurons. Interestingly, PV was not costained with TUNEL, a marker of apoptosis. PV^+ neurons in the SNR may undergo a transitional stage from decreased expression of PV to increased expression of NeuN and then to TUNEL expression. In addition, the degeneration of PV^+ neurons and the expression of NeuN were rarely observed in the SNR of *nTg* and the other triple transgenic mice. Hence, we propose that *Tau* knockout and α-*syn A53T* synergy modulate PV^+ neurons degeneration staging in the SNR of aged PD-liked mice model, and NeuN may be suited for an indicator that suggests degeneration of SNR PV^+ neurons. However, the molecular mechanism needs to be further investigated.

Keywords: *Tau* knockout, α-*synuclein*, parvalbumin, NeuN, degeneration staging

INTRODUCTION

The most predominant pathological feature of Parkinson's disease (PD) is the massive loss of dopaminergic neurons in the substantial nigra pars compacta (SNC) (Poewe et al., 2017). It may be closely related to the massive accumulation of α-*synuclein* (α-syn) and the aberrant expression of the microtubule-associated protein tau (Bassil et al., 2021; Han et al., 2021), both of which have been identified as the first two

genes of the population attributable risk underlying PD in genome-wide association studies (Simon-Sanchez et al., 2009).

The majority of PD research has focused on the SNC, while substantia nigra pars reticulata (SNR), as the other part of the substantia nigra, has received little attention (Dionísio et al., 2021; Pirooznia et al., 2021). Previous studies showed that the activity of parvalbumin-positive (PV^{+}) neurons in the SNR were affected in PD animal models (Wichmann et al., 1999; Mallet et al., 2019; Pamukcu et al., 2020). The loss of parvalbumin (PV) immunoreactivity was detected even in patients with end-stage PD (Hardman et al., 1996). Recently, Lilascharoen et al. (2020) indicated that the frequency of quantal-like inhibitory postsynaptic currents was significantly decreased in SNR neurons, which might indeed contribute to immobility in the 6-hydroxydopamine-lesioned PD mice model, as selective manipulation of the SNR-projecting external globus pallidus PV^{+} neurons alleviated the locomotor deficit. Our previous study found that the *Pitx3-A53T*α*-Syn* × *Tau*$^{-/-}$ triple transgenic mice model of PD showed anxiety-like behavior among 12- to 18-mouth-old, which may be related to the substantial degeneration of PV^{+} neurons in the SNR (Jiao et al., 2020). However, the progress and stage marker of PV^{+} neurons loss are still unclear.

In this study, we demonstrated that, as compared with non-transgenic (*nTg*) mice, the accumulation of α-syn in the SNR of aged *Pitx3-A53T*α*-Syn* × *Tau*$^{-/-}$ mice was increased obviously, which was accompanied by the considerable loss of PV^{+} neurons and the massive generation of apoptotic NeuN^{+}TUNEL^{+} neurons. PV^{+} neurons in the SNR may undergo a transitional stage from decreased PV expression to increased NeuN expression and then to TUNEL expression of apoptosis, whereas no co-localization was observed for PV and TUNEL during the progress.

MATERIALS AND METHODS

Construction of Triple Transgenic Mice

As described previously (Jiao et al., 2020), the line of pituitary homeobox 3 (*Pitx3*) promoter-controlled tetracycline transactivator (*tTA*) (*Pitx3-tTA*) mice, the lines of human α-syn A53T inducible transgenic mice (*tetO-A53T*) and human wild-type Tau inducible transgenic mice (*tetO-hTau*), in which the expression of human α-syn *A53T* and human wild-type Tau were under the transcriptional control of tetracycline operator (*tetO*), and the line of *Tau*$^{-/-}$ mice were used to generate triple transgenic mice and maintained on C57BL/6J background. The mice were reared under specific-pathogen-free (SPF) conditions, with 12-h light/12-h dark cycles and fed a regular diet *ad libitum*. All experimental procedures performed in this study were approved by the Institutional Animal Care and Use Committee of Sun Yat-sen University.

Genotype Identification

The genotype of the mice was determined by PCR analysis of genomic DNA extracted from tail biopsy and had been further validated histologically, as described in the previous study (Jiao et al., 2020).

Immunofluorescence

The mice were perfused transcardially with phosphate-buffered saline (PBS). Brains were separated and soaked in 4% paraformaldehyde for 48 h. Then, 30% sucrose solution was used for dehydration treatment. A cryostat (Leica SM 2010R, Germany) was used to cut the brains into continuous slices with a thickness of 40 μm. The following primary and secondary antibodies were used as recommended by the manufacturers: rabbit anti-human/mouse α-*synuclein* (α-syn; Santa Cruz Biotechnology, United States, sc-7011-R, 1:1000), mouse anti-PV (Sigma-Aldrich, United States, P3088, 1:500), rabbit anti-PV (Abcam, United States, ab11427, 1:1000), rabbit anti-c-fos (Sigma-Aldrich, United States, F7799, 1:1000), mouse anti-neuronal nucleus (NeuN; Chemicon, United States, MAB 377, 1:500), and Alexa 488 or Alexa 555 conjugated secondary antibody (Invitrogen, United States, 1:500). For antibodies produced in mice, the mouse-on-mouse immunodetection kit (Vector Laboratories, United States, BMK-2202) was used following the manufacturer's protocol. A laser scanning confocal microscope (LSM 710; Zeiss, Germany) was used for observing and photographing. The paired images in all the figures were acquired under the same conditions and processed uniformly after collection.

Terminal Deoxynucleotidyl Transferase-Mediated dUTP Nick End Labeling Staining

According to the manufacturer's protocol, apoptotic cells were labeled with an apoptosis detection kit (Roche, United States, 11684795910). The frozen sections were adhered to the slides and air-dried at 50°C for 30 minutes. Slides were rinsed in PBS for 5 min × 4 times, and then immersed in the permeabilization solution (0.1% sodium citrate, containing0.1% TritonX-100) and incubated on ice (2–8°C) for 2 min. Slides were washed in PBS for 5 min × 4 times. Afterward, the terminal deoxynucleotidyl transferase-mediated dUTP nick end labeling (TUNEL) reaction mixture was added to the slides and incubated at 37°C in the dark for 1 h. Slides were then rinsed in PBS for 5 min × 4 times and in ddH2O for 5 min × 3 times. After air-drying for 2 h at 37°C in the dark, the slides were mounted with ProLong® Gold anti-fading reagent (Invitrogen, United States, 1724814) before analysis.

Image Analysis

Cell counting of TUNEL^{+}, NeuN^{+}, and PV^{+} cells was performed in serial coronal sections across the SNR (every fourth from bregma, −3.28 to −4.04 mm). Fluorescence images of TUNEL, NeuN, and PV on each of the coronal sections in the SNR of 2-, 6-, and 12-month-old *Pitx3-A53T*α*-Syn* × *Tau*$^{-/-}$ mice were captured with a laser-scanning confocal microscope (LSM 710; Zeiss, Germany) at 20 × magnification. The numbers of TUNEL^{+}, NeuN^{+}, and PV^{+} cells, PV and NeuN double-positive cells, and TUNEL and NeuN double-positive cells were counted with NIS-Elements BR Imaging software (Nikon Instruments, Japan). The percentage of PV and NeuN double-positive cells to the total number of PV^{+} cells and the percentage of TUNEL and NeuN double-positive cells to the total number of TUNEL^{+} or NeuN^{+} cells in the SNR were determined.

To quantify the relative immunofluorescence intensity of α-syn, c-fos, and PV in the SNR of mice, images were taken using identical settings and then analyzed using ImageJ software (NIH, United States). To measure c-fos and PV fluorescent intensity, only fluorescence within the PV^{+}/c-fos^{+} co-staining neurons in the SNR was analyzed. All the images were converted to an 8-bit color scale and the background was subtracted. Areas of interest were selected by the freehand selection tools and subjected to measurement by mean gray value to determine the average intensity.

Three mice were used per genotype and at each time point. Counters were blinded to the information of the samples.

Statistics

GraphPad Prism 7 (GraphPad Software, United States) was used for statistical analysis. Data were expressed as mean ± SEM. The one-way analysis of variance was used to compare the means of different groups, followed by Tukey's honestly significant difference *post hoc* test, and significance was set at $P < 0.05$.

RESULTS

Tau Knockout Exacerbated the Accumulation of α-Syn in the Substantia Nigra Pars Reticulata of α-*Syn A53T* Conditional Transgenic Mice

As described in our previous study, we continued to use the triple transgenic mice that overexpressed PD-related α-*syn A53T* missense mutation in the midbrain dopaminergic neurons with different tau gene dosage from high to low, which were named as *Pitx3-A53Tα-Syn* × *hTau*, *Pitx3-A53Tα-Syn* × *Tau*$^{+}$/$^{+}$, *Pitx3-A53Tα-Syn* × *Tau*$^{+/-}$, and *Pitx3-A53Tα-Syn* × *Tau*$^{-/-}$ mice, respectively (Jiao et al., 2020).

Considering that *Pitx3-A53Tα-Syn* × *Tau*$^{-/-}$ mice specifically developed severe degeneration of PV^{+} neurons in the SNR at 18-month-old, we presumed that this may be related to the accumulation of α-syn. We stained α-syn in the SNR of 18-month-old mice. The results showed that compared with *nTg* mice, α-syn was significantly overexpressed in the SNC of all triple transgenic mice, as expected (**Figure 1A**). But more prominently, *Pitx3-A53Tα-Syn* × *Tau*$^{-/-}$ mice had the highest level of α-syn (**$P < 0.01$, vs. *nTg*), while other triple transgenic mice had almost the same α-syn content in the SNR with no statistical difference as compared to *nTg* mice (**Figures 1A,B**). These results indicated that tau knockout could modestly exacerbate the accumulation of α-syn in the SNR of α-*syn A53T* conditional transgenic mice at old age.

Pitx3-A53Tα-Syn × *Tau*$^{-/-}$ Mice Showed Actually Decreased Parvalbumin-Positive and c-fos^{+} Neurons in the Substantia Nigra Pars Reticulata at 18-Month-Old

As the expression product of the Fos gene, c-fos is most commonly used to detect the activity of neurons in the central nervous system. The expression level of c-fos is directly proportional to the activity of neurons (Dragunow and Faull, 1989; VanElzakker et al., 2008). To determine whether different tau protein expression levels affect the changes in PV^{+} neuron activity mediated by A53T α-syn, we stained PV and c-fos in the SNR region of 6- and 18-month-old mice. The results indicated PV staining almost costained with c-fos, demonstrating that the remnant PV^{+} neurons were active (**Figures 2A,B**). It was worth noting that, accompanied by the significantly decreased PV^{+} neurons, c-fos expression was reduced accordingly in the SNR of *Pitx3-A53Tα-Syn* × *Tau*$^{-/-}$ mice at 18-month-old (**Figures 2B–D**). These suggested that the number of PV^{+} neurons was proportional to the level of their activities, and *Pitx3-A53Tα-Syn* × *Tau*$^{-/-}$ mice showed practically degeneration of PV^{+} and c-fos^{+} neurons in the SNR at old age.

Tau Knockout Exacerbated Cell Apoptosis and Parvalbumin-Positive Neuron Loss Asynchronously in the Substantia Nigra Pars Reticulata of α-Syn A53T Conditional Transgenic Mice

To determine whether the decrease of PV^{+} neurons was due to cell apoptosis, we stained PV and TUNEL in the SNR of 18-month-old mice. The results revealed that the less PV expressed, the more TUNEL signals were detected, as shown in the *Pitx3-A53Tα-Syn* × *Tau*$^{-/-}$ mice. However, TUNEL did not costain with PV in the SNR of all the triple transgenic mice (**Figure 3**). These suggested that the degenerating PV^{+} neurons could not be labeled by TUNEL, and they might undergo a transitional stage between the expression of PV and TUNEL.

Pitx3-A53Tα-Syn × *Tau*$^{-/-}$ Mice Presented Massive NeuN^{+} Neuronal Apoptosis in the Substantia Nigra Pars Reticulata

NeuN is a neuron-specific marker, but its expression in the SNR is species-specific. For example, the neurons in the gerbil SNR do not express NeuN, whereas the neurons in the rats' SNR strongly express NeuN (Mullen et al., 1992; Kumar and Buckmaster, 2007; Gusel'nikova and Korzhevskiy, 2015). To determine the type of cells which presented massive apoptosis in the SNR but did not co-stain with PV, we examined TUNEL and NeuN staining in the SNR of 18-month-old mice. The results showed that TUNEL was highly costained with NeuN in the SNR of *Pitx3-A53Tα-Syn* × *Tau*$^{-/-}$ mice (**Figure 4A**). The percentage of TUNEL^{+}NeuN^{+} co-staining cells relative to the total number of TUNEL^{+} or NeuN^{+} cells reached 94.47 ± 2.12% or 92.72 ± 1.1%, respectively (**Figure 4B**). However, in the SNR of the other triple transgenic mice and *nTg* mice, the neurons rarely expressed NeuN, which did not co-stain with TUNEL either (**Figure 4A**). Considering the previous experimental results (**Figure 3**), we preliminarily speculated that NeuN may be suited for an indicator of the transitional stage of degenerating neurons in SNR between expression of PV and TUNEL, especially, at the beginning of 6-month-old.

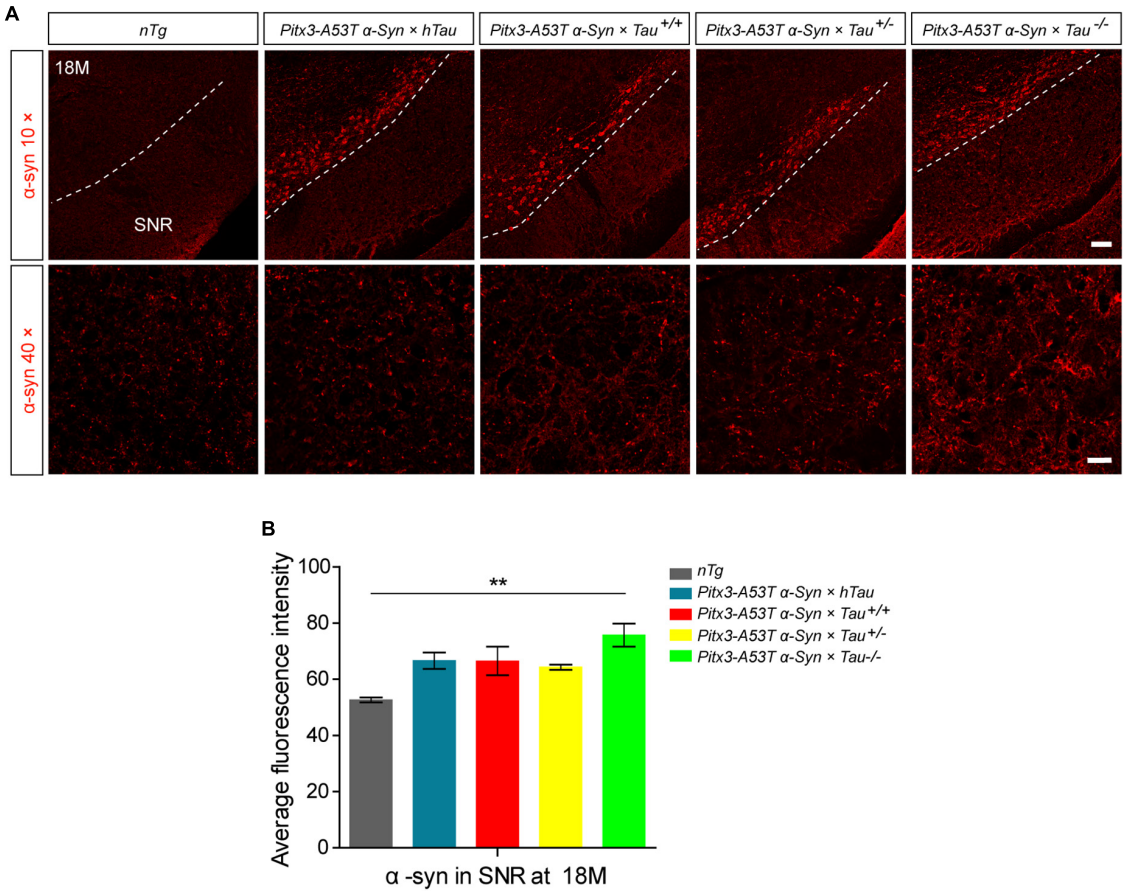

FIGURE 1 | α-syn accumulation was increased in the substantia nigra pars reticulata (SNR) of 18-month-old *Pitx3-A53T*α*-Syn* × *Tau*$^{-/-}$ mice. **(A)** α-syn immunostaining in the SNR of 18-month-old mice. compared to *nTg* mice, α-syn was obviously overexpressed in dopaminergic neurons in SNC of the triple transgenic mice. White dotted lines demarcate the boundary between SNC and SNR. The ventrolateral area was considered as SNR. Scale bars: low magnification (10×), 100 μm; higher magnification (40×) in SNR, 25 μm. **(B)** Quantitative analysis of α-syn fluorescence intensity in SNR of 18-month-old mice. $n = 3$ per genotype. Values are mean ± SEM. $^{**}P < 0.01$ (*Pitx3-A53T*α*-Syn* × *Tau*$^{-/-}$ vs *nTg*).

NeuN Gradually Replaced Parvalbumin to Mark Apoptotic Neurons in the Substantia Nigra Pars Reticulata of *Pitx3-A53T*α*-Syn* × *Tau*$^{-/-}$ Mice

To further explore whether NeuN can specifically label the degenerating PV^{+} neurons, we stained PV and NeuN in the SNR of *Pitx3-A53T*α*-Syn* × *Tau*$^{-/-}$ mice at 2- and 6-months old. The results showed that PV^{+} neurons in the SNR did not begin to degenerate at 2-month-old because the expression level of PV was high while the expression level of NeuN was low (**Figure 5A**). At 6-month-old, NeuN was gradually increased and highly costained with PV (**Figures 5A,C**). Combining the previous results, while the loss of PV^{+} neurons (12- and 18-month-old) becoming significantly (**Figures 2**, **3**), NeuN was highly costained with TUNEL (**Figures 4**, **5B,C**). Therefore, we suspected that in the SNR of *Pitx3-A53T*α*-Syn* × *Tau*$^{-/-}$ mice, the rapidly progressed loss of PV^{+} neurons may undergo a transitional stage, i.e., from decreasing PV expression, to increasing NeuN expression, finally to TUNEL expression (**Figure 6**); NeuN may be a compatible marker labeling the degeneration of PV^{+} neurons at the beginning of 6-month-old.

DISCUSSION

In the present study, we revealed that tau knockout specifically aggravated A53T α-syn-mediated PV^{+} neurons degeneration staging and α-syn accumulation in the SNR of mice at old age (late-stage). We used the most classic TUNEL assay to stain the apoptotic neurons in the SNR and attempted to demonstrate that the neurons lost in SNR were PV^{+} neurons. Contrary to our expectations, TUNEL and PV were not co-stained. Indeed, through continuously observing the co-staining of PV and NeuN, NeuN, and TUNEL, we divided three stages by the different active states in the SNR of *Pitx3-A53T*α*-Syn* × *Tau*$^{-/-}$ mice, as shown in **Figure 6**. At 2–6 months (initial-stage), PV was expressed normally in the SNR, while NeuN was modestly expressed and costained with PV. At 6–12 months (Middle stage), PV expression was

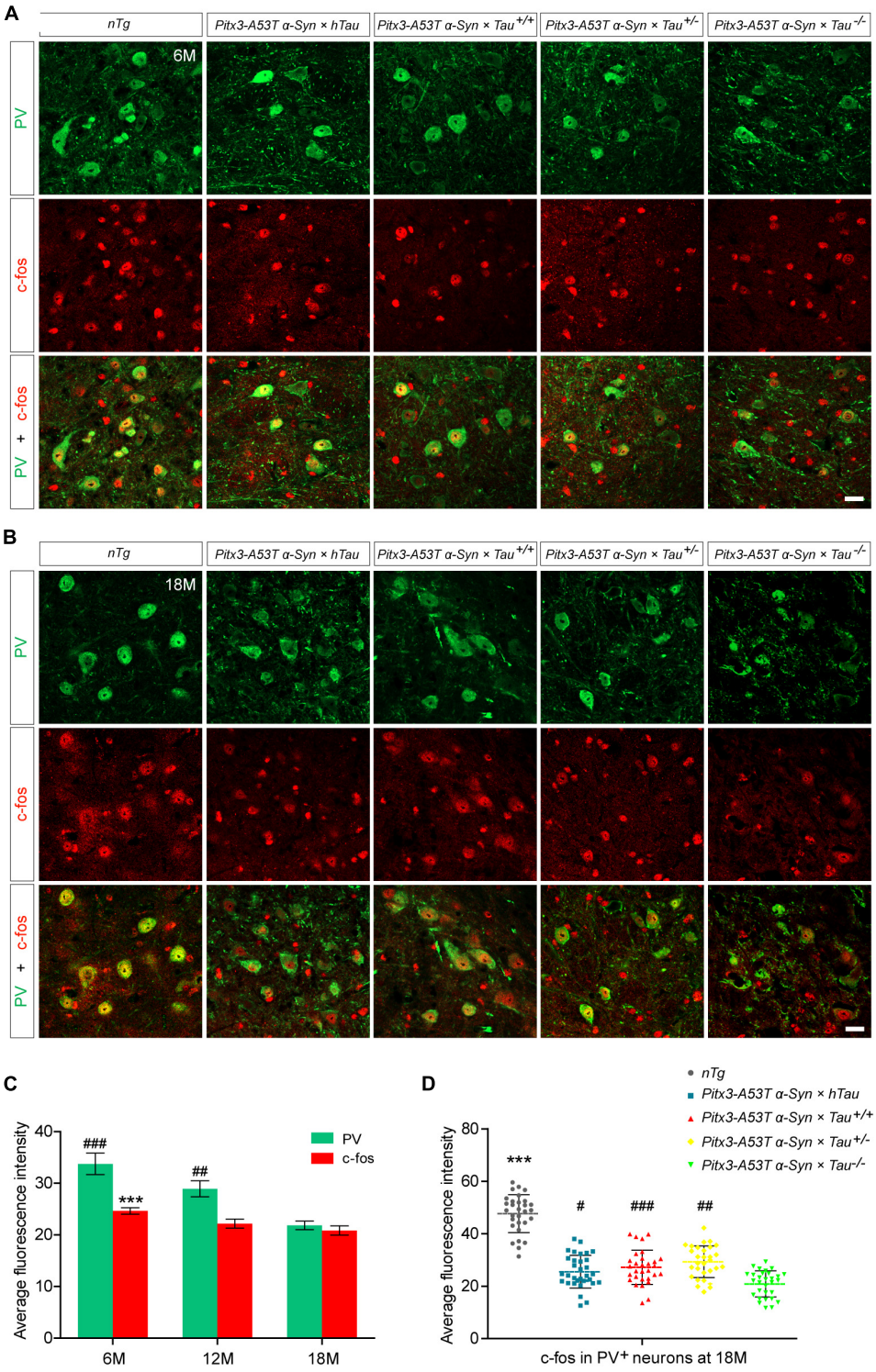

FIGURE 2 | Decreased expression of c-fos in the parvalbumin-positive (PV^{+}) neurons in the SNR of α-*syn A53T* transgenic mice. **(A,B)** PV (green) and c-fos (red) costained in the SNR of 6- **(A)** and 18-month-old **(B)** mice. Scale bars: 25 μm. **(C)** Quantification of c-fos and PV fluorescence mean intensity in PV^{+}/c-fos^{+} co-staining cells in the SNR of 6-, 12- and 18-month-old *Pitx3-A53T*α-*Syn* × *Tau*$^{-/-}$ mice ($n = 30$ cells for each sample, 3 mice for each time point). Values are mean ± SEM. $^{***}P < 0.001$ (c-fos, 6-month-old vs 18-month-old *Pitx3-A53T*α-*Syn* × *Tau*$^{-/-}$); $^{\#\#}P < 0.01$, $^{\#\#\#}P < 0.001$ (PV, 6- and 12-month-old vs 18-month-old *Pitx3-A53T*α-*Syn* × *Tau*$^{-/-}$). **(D)** Representative dot plots of c-fos fluorescence mean intensity in PV^{+} neurons in the SNR of 18-month-old mice ($n \geq 30$ cells for each sample, 3 mice per genotype). $^{***}P < 0.001$ (*nTg* vs triple transgenic); $^{\#}P < 0.05$, $^{\#\#}P < 0.01$, $^{\#\#\#}P < 0.001$ (other triple transgenic vs *Pitx3-A53T*α-*Syn* × *Tau*$^{-/-}$).

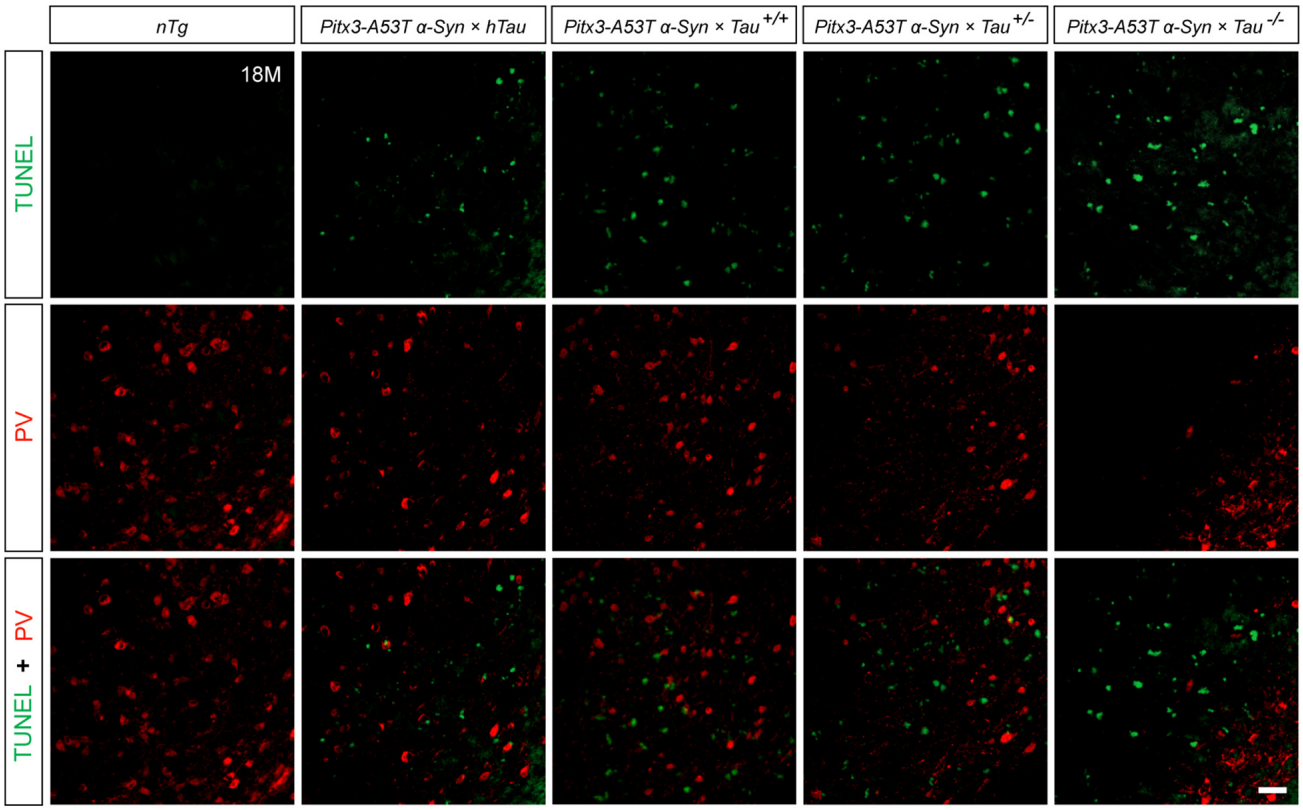

FIGURE 3 | Terminal deoxynucleotidyl transferase (TdT)-mediated dUTP nick end labeling (TUNEL) (green) and PV (red) double-staining in the SNR of 18-month-old mice. Scale bar: 50 μm.

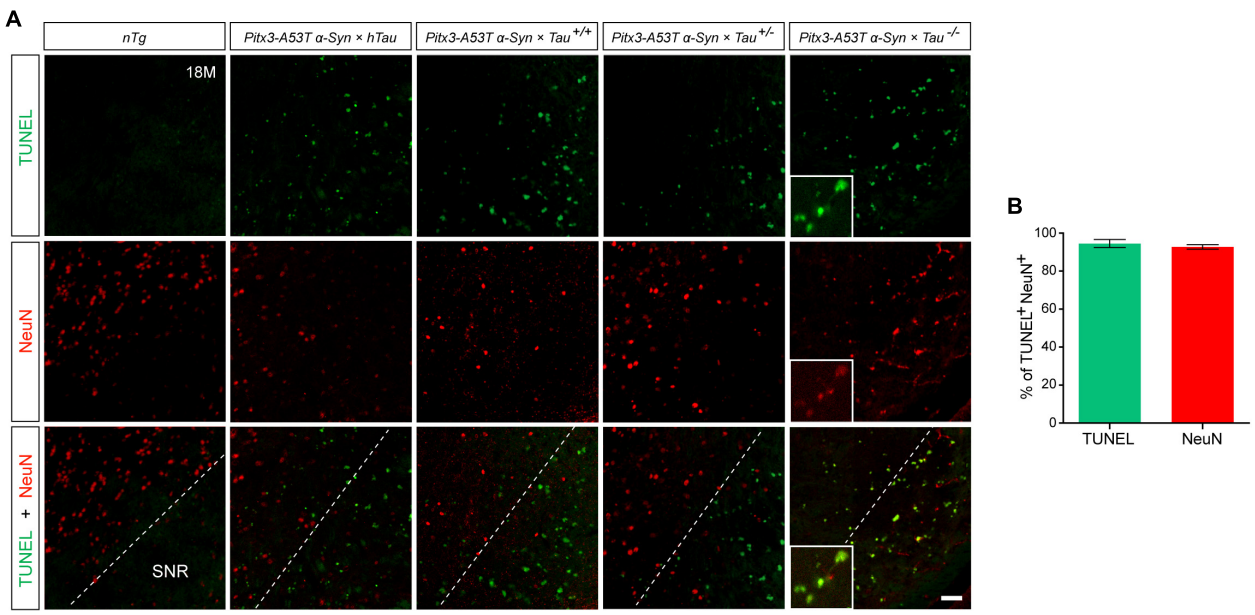

FIGURE 4 | *Pitx3-A53Tα-Syn* × *Tau*$^{-/-}$ mice presented massive NeuN^{+} neuron apoptosis in the SNR at old age. **(A)** TUNEL (green) and NeuN (red) double-staining in the SNR of 18-month-old mice. Scale bar: 50 μm. Figures in the white boxes represent the high-magnification images of TUNEL and NeuN co-staining in the SNR of 18-month-old *Pitx3-A53Tα-Syn* × *Tau*$^{-/-}$ mice. **(B)** The percentage of TUNEL^{+}NeuN^{+} co-staining cells relative to the total number of TUNEL^{+} or NeuN^{+} cells in the SNR of 18-month-old *Pitx3-A53Tα-Syn* × *Tau*$^{-/-}$ mice. $n = 3$, values are mean ± SEM.

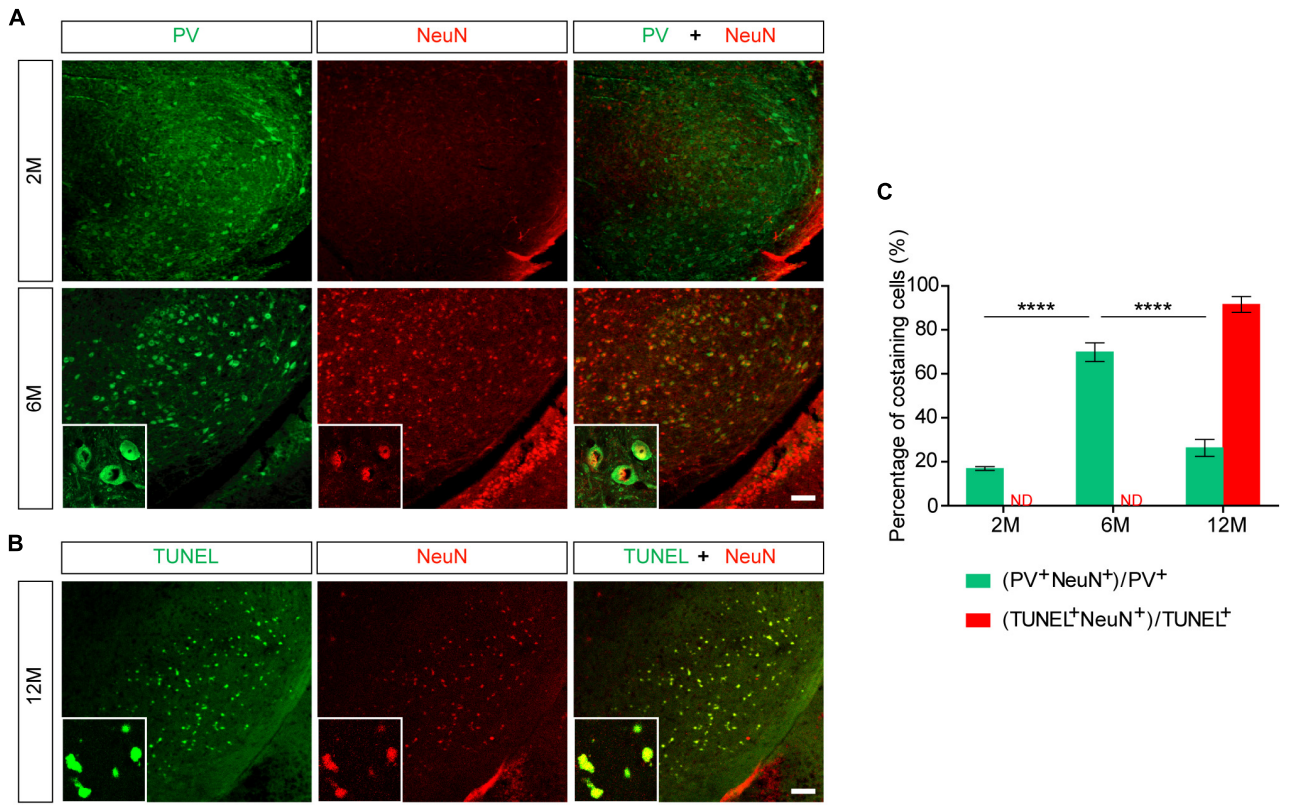

FIGURE 5 | NeuN may be suited for an indicator that suggests degeneration of PV^{+} neurons in the SNR of *Pitx3-A53Tα-Syn* × *Tau*$^{-/-}$ mice at the beginning of 6-month-old. **(A)** PV (green) and NeuN (red) double-staining in the SNR of 2- and 6-month-old *Pitx3-A53Tα-Syn* × *Tau*$^{-/-}$ mice. Scale bar: 100 μm. Figures in the white boxes represented the high-magnification images of PV and NeuN co-staining in the SNR of 6-month-old *Pitx3-A53Tα-Syn* × *Tau*$^{-/-}$ mice. **(B)** TUNEL (green) and NeuN (red) co-staining in the SNR of 12-month-old *Pitx3-A53Tα-Syn* × *Tau*$^{-/-}$ mice. Figures in the white boxes represented the high-magnification images of TUNEL and NeuN co-staining. Scale bar: 100 μm. **(C)** Percentage of PV and NeuN co-staining cells to the total number of PV^{+} cells, and percentage of TUNEL and NeuN co-staining cells to the total number of TUNEL^{+} cells in the SNR of 2-, 6-, and 12-month-old *Pitx3-A53Tα-Syn* × *Tau*$^{-/-}$ mice. $n = 3$ per genotype per time point. Values are mean ± SEM. ****$P < 0.0001$ (2- and 12-month-old vs. 6-month-old *Pitx3-A53Tα-Syn* × *Tau*$^{-/-}$). ND, not determined.

decreased and replaced by NeuN, which was increased obviously. At 12–18 months (late-stage), neurons developed apoptosis as TUNEL was expressed and co-stained with NeuN. So, we propose that the loss of PV^{+} neurons in the SNR of *Pitx3-A53Tα-Syn* × *Tau*$^{-/-}$ mice may undergo a transitional stage, i.e., from decreased expression of PV to increased expression of NeuN to TUNEL expression.

Numerous studies have demonstrated that tau plays an important role in maintaining neuronal integrity and axonal transport (Augustinack et al., 2002; Combs et al., 2019). This might be because the main function of tau is responsible for the dynamic assembly of the cytoskeleton in neurons (Venkatramani and Panda, 2019). Tau depletion caused preferential loss of the labile microtubule fraction in the axon (Qiang et al., 2018). Thus, in the case of stalled growth cones of tau-depleted axons, axonal regeneration was retarded extremely (Biswas and Kalil, 2017). In the present study, we have used *A53Tα-syn* conditionally transgenic mice to construct PD models with different expression levels of tau, all of which had developed selective loss of SNC dopaminergic neurons and severe motor coordination and balance disorders, as described previously (Jiao et al., 2020). Interestingly, we found that different degrees of SNR neuronal death were specifically induced by different tau gene dosages. At 18-mouth-old of the triple transgenic mice, PV^{+} neurons degeneration caused by tau knockout was the most significant. It indicates that tau is important for maintaining the activity of PV^{+} neurons in SNR, and tau knockout could accelerate the progression of PD mediated by A53T α-syn and promote the degeneration of SNR PV^{+} neurons.

Parvalbumin (PV) is a calcium-binding protein, which accounts for an abundant subpopulation of GABAergic neurons (Hu et al., 2014). GABAergic neurons exhibit fast-spiking patterns and form direct inhibitory synapses with the cell bodies, proximal dendrites, and starting segments of cortical pyramidal neurons (Siemian et al., 2020). Numerous studies have suggested that the number of PV^{+} GABAergic neurons in the SNR is absolutely dominant (McRitchie et al., 1996; Galaj et al., 2020). Therefore, PV can specifically mark the SNR and reflect the physiological state of this area. In this study, *Pitx3-A53Tα-Syn* × *Tau*$^{-/-}$ mice showed specific decreased expression of PV and c-fos in the SNR at old age, which may be

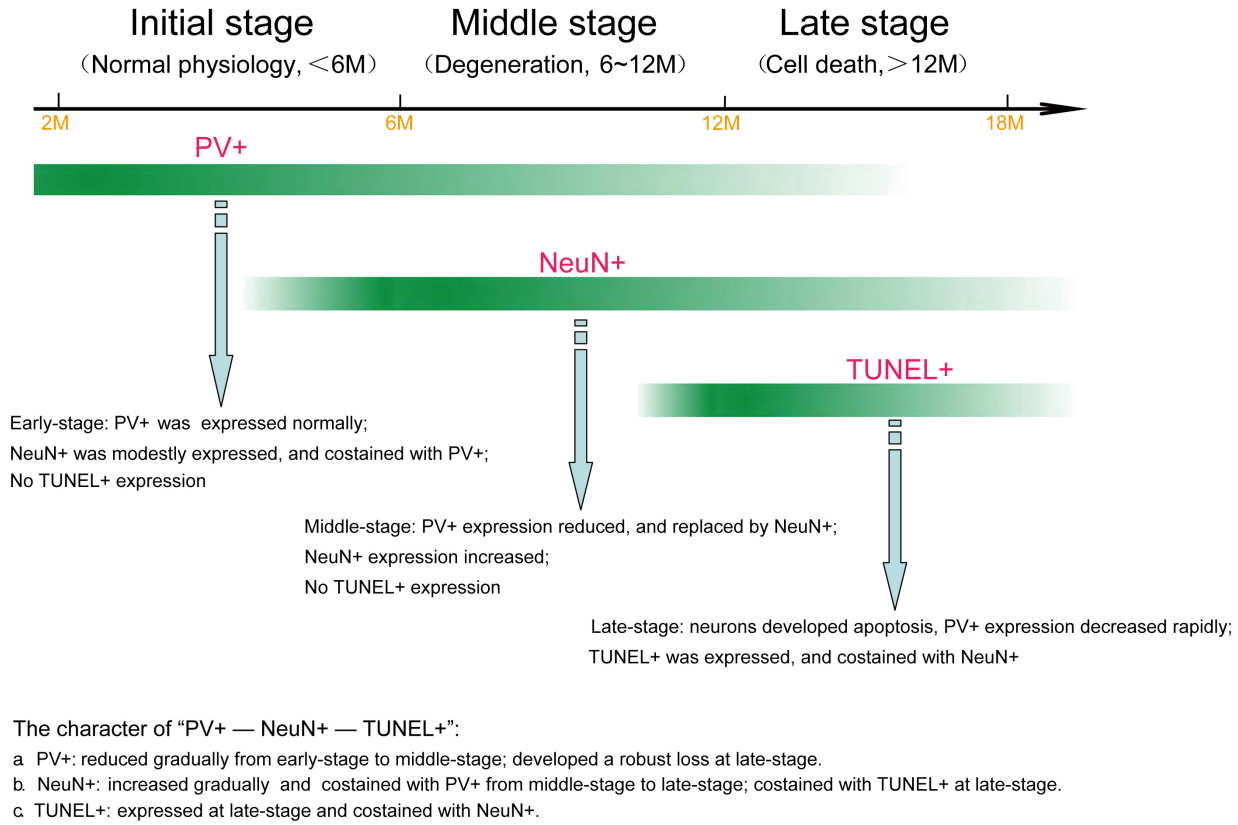

The character of "PV+ — NeuN+ — TUNEL+":

a. PV+: reduced gradually from early-stage to middle-stage; developed a robust loss at late-stage.
b. NeuN+: increased gradually and costained with PV+ from middle-stage to late-stage; costained with TUNEL+ at late-stage.
c. TUNEL+: expressed at late-stage and costained with NeuN+.

We divided the three stages by the different active states in the SNR of *Pitx3-A53T α-Syn* × *Tau*$^{-/-}$ mice, which may be occured simultaneously and overlappingly.

FIGURE 6 | The loss of PV^{+} neurons in the SNR of *Pitx3-A53Tα-Syn* × *Tau*$^{-/-}$ mice may undergo a transitional stage, i.e., from decreased expression of PV to increased expression of NeuN to TUNEL expression.

correlated with their increased α-syn aggregates and anxiety-like behavior. However, the mechanism of this specificity in the tau knockout state remains unclear. Uchida et al. (2014) reported that maternal stress and mutations in glutamate decarboxylase (GAD) 67, both risk factors for psychiatric disorders, can cause selective loss of PV^{+} GABAergic interneurons in the cerebral cortex. This suggests that specific degeneration of PV^{+} neurons can be associated with dysfunction of tau and GAD67, which needs further study.

Unexpectedly, our study found that tau knockout exacerbated TUNEL^{+} cell apoptosis and PV^{+} neuron loss asynchronously in the SNR of α-syn A53T conditional transgenic mice, as TUNEL did not costain with PV. This suggests that the degenerating SNR neurons might undergo a transitional stage between the expression of PV and TUNEL. Although NeuN is usually used as a definitive marker of mature neurons in neurodegenerative diseases, its role has been challenged by recent studies, indicating that NeuN staining is variable and even absent during certain diseases and specific physiological states (Duan et al., 2016). For example, NeuN expression in the SNR is species-specific. While neurons in the rats' SNR strongly express NeuN, neurons in the gerbil SNR do not express it (Kumar and Buckmaster, 2007). Here we propose that NeuN may be an indicator of the transition of PV^{+} neurons from normal to degenerating phase in the SNR of mice. The progressive degeneration of PV^{+} neurons in the SNR of *Pitx3-A53Tα-Syn* × *Tau*$^{-/-}$ mice may undergo a transitional process from decreased PV expression to increased NeuN expression and finally to TUNEL expression (**Figure 6**). Furthermore, from the results of PV, NeuN, and TUNEL staining in the SNR of the triple transgenic mice, we suppose that there may be two different types of the apoptotic neurons existing in the SNR of *Pitx3-A53Tα-Syn* × *Tau*$^{-/-}$ mice and the other triple transgenic mice at 12- and 18-month-old: PV^{+} neurons and PV-negative (PV^{-}) neurons, respectively, as classified in the previous studies (Ren et al., 1992; Fernández-Suárez et al., 2012; Mészár et al., 2012). In the SNR of *Pitx3-A53Tα-Syn* × *Tau*$^{-/-}$ mice, PV^{+} neurons might be more susceptible to A53T α-syn-mediated cytotoxicity and underwent apoptosis.

In conclusion, our results suggested that tau knockout can exacerbate α-syn A53T-mediated PV^{+} neurons degeneration staging, from PV expression reduced to NeuN expression increased to TUNEL expression, in the SNR of mice. The rapid increase of NeuN at the middle stage and co-staining with TUNEL at the late stage made it gradually replace PV as a better

indicator of the degeneration of PV^{+} neurons in the SNR. We hope that this research can provide a reference for long-term observation of the neuron degeneration in the brain of the mouse model of PD.

DATA AVAILABILITY STATEMENT

The raw data supporting the conclusions of this article will be made available by the authors, without undue reservation.

ETHICS STATEMENT

The animal study was reviewed and approved by Institutional Animal Care and Use Committee of Sun Yat-sen University.

AUTHOR CONTRIBUTIONS

XL conceived the project. XL and LJ designed the experimental scheme, revised and edited the manuscript. MZ and YL conducted the major experiments, analyzed the data, and wrote the manuscript. ZX performed some experiments and aided in data analysis. All authors contributed to the article and approved the submitted version.

FUNDING

This research was supported in part by the National Natural Science Foundation of China Grants 82071425 (to XL); the Natural Science Foundation Grants of Guangdong Province #2020A1515010318 (to XL); and Science and Technology Program of Guangzhou 202007030001 (to XL).

REFERENCES

Augustinack, J. C., Schneider, A., Mandelkow, E.-M., and Hyman, B. T. (2002). Specific tau phosphorylation sites correlate with severity of neuronal cytopathology in Alzheimer's disease. *Acta Neuropathol.* 103, 26–35. doi: 10.1007/s004010100423

Bassil, F., Meymand, E. S., Brown, H. J., Xu, H., Cox, T. O., Pattabhiraman, S., et al. (2021). α-Synuclein modulates tau spreading in mouse brains. *J. Exp. Med.* 218, 1156–1172. doi: 10.1084/jem.20192193

Biswas, S., and Kalil, K. (2017). The microtubule associated protein tau mediates the organization of microtubules and their dynamic exploration of actin-rich lamellipodia and filopodia of cortical growth cones. *J. Neurosci.* 22, 2281–2317. doi: 10.1523/JNEUROSCI.2281-17.2017

Combs, B., Mueller, R. L., Morfini, G., Brady, S. T., and Kanaan, N. M. (2019). Tau and axonal transport misregulation in tauopathies. *Adv. Exp. Med. Biol.* 1184, 81–95. doi: 10.1007/978-981-32-9358-8_7

Dionísio, P. A., Amaral, J. D., and Rodrigues, C. M. P. (2021). Oxidative stress and regulated cell death in Parkinson's disease. *Ageing Res. Rev.* 67, 843–861. doi: 10.1016/j.arr.2021.101263

Dragunow, M., and Faull, R. (1989). The use of c-fos as a metabolic marker in neuronal pathway tracing. *J. Neurosci. Methods* 29, 261–265. doi: 10.1016/0165-0270(89)90150-7

Duan, W., Zhang, Y.-P., Hou, Z., Huang, C., Zhu, H., Zhang, C.-Q., et al. (2016). Novel insights into NeuN: from neuronal marker to splicing regulator. *Mol. Neurobiol.* 53, 759–775. doi: 10.1007/s12035-015-9122-5

Fernández-Suárez, D., Celorrio, M., Lanciego, J. L., Franco, R., and Aymerich, M. S. (2012). Loss of parvalbumin-positive neurons from the globus pallidus in animal models of Parkinson disease. *J. Neuropathol. Exp. Neurol.* 24, 973–982. doi: 10.1097/NEN.0b013e3182717cba

Galaj, E., Han, X., Shen, H., Jordan, C. J., He, Y., Humburg, B., et al. (2020). versusDissecting the role of GABA neurons in the VTA SNr in opioid reward. *J. Neurosci.* 40, 3653–3667. doi: 10.1523/JNEUROSCI.0988-20.2020

Gusel'nikova, V. V., and Korzhevskiy, D. E. (2015). NeuN As a neuronal nuclear antigen and neuron differentiation marker. *Acta Nat.* 7, 42–47. doi: 10.32607/20758251-2015-7-2-42-47

Han, J., Fan, Y., Wu, P., Huang, Z., Li, X., Zhao, L., et al. (2021). Parkinson's disease dementia: synergistic effects of alpha-synuclein, tau, beta-amyloid, and iron. *Front. Aging Neurosci.* 13:743754. doi: 10.3389/fnagi.2021.743754

Hardman, C. D., McRitchie, D. A., Halliday, G. M., Cartwright, H. R., and Morris, J. G. (1996). Substantia nigra pars reticulata neurons in Parkinson's disease. *Neurodegeneration* 5, 49–55. doi: 10.1006/neur.1996.0007

Hu, H., Gan, J., and Jonas, P. (2014). Fast-spiking, parvalbumin^{+} GABAergic interneurons: from cellular design to microcircuit function. *Science* 345:1255263. doi: 10.1126/science.1255263

Jiao, L., Zheng, M., Duan, J., Wu, T., Li, Z., Liu, L., et al. (2020). Tau knockout exacerbates degeneration of parvalbumin-positive neurons in substantia nigra pars reticulata in Parkinson's disease-related α-synuclein A53T mice. *FASEB J.* 34, 12239–12254. doi: 10.1096/fj.202000017RR

Kumar, S. S., and Buckmaster, P. S. (2007). Neuron-specific nuclear antigen NeuN is not detectable in gerbil subtantia nigra pars reticulata. *Brain Res.* 1142, 54–60. doi: 10.1016/j.brainres.2007.01.027

Lilascharoen, V., Wang, E. H.-J., Do, N., Pate, S. C., Tran, A. N., Wang, X.-Y., et al. (2020). Divergent pallidal pathways underlying distinct Parkinsonian behavioral deficits. *Nat. Neurosci.* 24, 763–780. doi: 10.1101/2020.11.27.401554

Mallet, N., Delgado, L., Chazalon, M., Miguelez, C., and Baufreton, J. (2019). Cellular and synaptic dysfunctions in Parkinson's disease: stepping out of the striatum. *Cells* 8:1005. doi: 10.3390/cells8091005

McRitchie, D. A., Hardman, C. D., and Halliday, G. M. (1996). Cytoarchitectural distribution of calcium binding proteins in midbrain dopaminergic regions of rats and humans. *J. Comp. Neurol.* 364, 7428–7443. doi: 10.1002/(SICI)1096-9861(19960101)364:1<121::AID-CNE11<3.0.CO;2-1

Mészár, Z., Girard, F., Saper, C. B., and Celio, M. R. (2012). The lateral hypothalamic parvalbumin-immunoreactive (PV1) nucleus in rodents. *J. Comp. Neurol.* 520, 497–512. doi: 10.1002/cne.22789

Mullen, R. J., Buck, C. R., and Smith, A. M. (1992). NeuN, a neuronal specific nuclear protein in vertebrates. *Development* 116, 201–211.

Pamukcu, A., Cui, Q., Xenias, H. S., Berceau, B. L., Augustine, E. C., Fan, I., et al. (2020). Parvalbumin and Npas1 Pallidal neurons have distinct circuit topology and function. *J. Neurosci.* 40, 7855–7876. doi: 10.1523/JNEUROSCI.0361-20.2020

Pirooznia, S. K., Rosenthal, L. S., Dawson, V. L., and Dawson, T. M. (2021). Parkinson disease: translating insights from molecular mechanisms to neuroprotection. *Pharmacol. Rev.* 73, 1715–1732. doi: 10.1124/pharmrev.120.000189

Poewe, W., Seppi, K., Tanner, C. M., Halliday, G. M., Brundin, P., Volkmann, J., et al. (2017). Parkinson disease. *Nat. Rev. Dis. Primers* 23, 6587–6596. doi: 10.1038/nrdp.2017.13

Qiang, L., Sun, X., Austin, T. O., Muralidharan, H., Jean, D. C., Liu, M., et al. (2018). Tau does not stabilize axonal microtubules but rather enables them to have long labile domains. *Curr. Biol.* 28, 2181–2189. doi: 10.1016/j.cub.2018.05.045

Ren, J. Q., Aika, Y., Heizmann, C. W., and Kosaka, T. (1992). Quantitative analysis of neurons and glial cells in the rat somatosensory cortex, with special reference to GABAergic neurons and parvalbumin-containing neurons. *Exp. Brain Res.* 92, 769–784. doi: 10.1007/BF00230378

Siemian, J. N., Sarsfield, S., and Aponte, Y. (2020). Glutamatergic fast-spiking parvalbumin neurons in the lateral hypothalamus: electrophysiological properties to behavior. *Physiol. Behav.* 221, 6247–6268. doi: 10.1016/j.physbeh.2020.112912

Simon-Sanchez, J., Schulte, C., Bras, J. M., Sharma, M., Gibbs, J. R., Berg, D., et al. (2009). Genome-wide association study reveals genetic risk underlying Parkinson's disease. *Nat. Genet.* 41, 1308–1312. doi: 10.1038/ng.487

Uchida, T., Furukawa, T., Iwata, S., Yanagawa, Y., and Fukuda, A. (2014). Selective loss of parvalbumin-positive GABAergic interneurons in the cerebral cortex of maternally stressed Gad1-heterozygous mouse offspring. *Transl. Psychiatry* 11, 539–553. doi: 10.1038/tp.2014.13

VanElzakker, M., Fevurly, R. D., Breindel, T., and Spencer, R. L. (2008). Environmental novelty is associated with a selective increase in Fos expression in the output elements of the hippocampal formation and the perirhinal cortex. *Learn. Mem.* 15, 899–908. doi: 10.1101/lm.1196508

Venkatramani, A., and Panda, D. (2019). Regulation of neuronal microtubule dynamics by tau: Implications for tauopathies. *Int. J. Biol. Macromol.* 133, 473–483. doi: 10.1016/j.ijbiomac.2019.04.120

Wichmann, T., Bergman, H., Starr, P. A., Subramanian, T., Watts, R. L., and DeLong, M. R. (1999). Comparison of MPTP-induced changes in spontaneous neuronal discharge in the internal pallidal segment and in the substantia nigra pars reticulata in primates. *Exp. Brain Res.* 125, 397–409. doi: 10.1007/s002210050696

Conflict of Interest: LJ is employed by Nuwacell Biotechnologies Co.

The remaining authors declare that the research was conducted in the absence of any commercial or financial relationships that could be construed as a potential conflict of interest.

Publisher's Note: All claims expressed in this article are solely those of the authors and do not necessarily represent those of their affiliated organizations, or those of the publisher, the editors and the reviewers. Any product that may be evaluated in this article, or claim that may be made by its manufacturer, is not guaranteed or endorsed by the publisher.

frontiers in Aging Neuroscience

SYSTEMATIC REVIEW
published: 12 January 2022
doi: 10.3389/fnagi.2021.807764

Systematic Review: microRNAs as Potential Biomarkers in Mild Cognitive Impairment Diagnosis

Natalia Ogonowski[1,2], Stefanny Salcidua[1,3], Tomas Leon[4,5], Nayaret Chamorro-Veloso[6], Cristian Valls[6], Constanza Avalos[1], Alejandro Bisquertt[6], Miguel E. Rentería[7], Paulina Orellana[1,8] and Claudia Duran-Aniotz[1,8]**

[1] Latin American Institute for Brain Health (BrainLat), Universidad Adolfo Ibanez, Santiago, Chile, [2] Cognitive Neuroscience Center (CNC), National Scientific and Technical Research Council (CONICET), Universidad de San Andrés, Buenos Aires, Argentina, [3] Faculty of Engineering and Sciences, Universidad Adolfo Ibanez, Santiago, Chile, [4] Global Brain Health Institute, Trinity College, Dublin, Ireland, [5] Memory and Neuropsychiatric Clinic (CMYN) Neurology Department, Hospital del Salvador, Faculty of Medicine, University of Chile, Santiago, Chile, [6] Neurognos Spa, Santiago, Chile, [7] Department of Genetics and Computational Biology, Queensland Institute of Medical Research (QIMR) Berghofer Medical Research Institute, Brisbane, QLD, Australia, [8] Center for Social and Cognitive Neuroscience (CSCN), School of Psychology, Universidad Adolfo Ibanez, Santiago, Chile

The rate of progression from Mild Cognitive Impairment (MCI) to Alzheimer's disease (AD) is estimated at >10% per year, reaching up to 80–90% after 6 years. MCI is considered an indicator of early-stage AD. In this context, the diagnostic screening of MCI is crucial for detecting individuals at high risk of AD before they progress and manifest further severe symptoms. Typically, MCI has been determined using neuropsychological assessment tools such as the Montreal Cognitive Assessment (MoCA) or Mini-Mental Status Examination (MMSE). Unfortunately, other diagnostic methods are not available or are unable to identify MCI in its early stages. Therefore, identifying new biomarkers for MCI diagnosis and prognosis is a significant challenge. In this framework, miRNAs in serum, plasma, and other body fluids have emerged as a promising source of biomarkers for MCI and AD-related cognitive impairments. Interestingly, miRNAs can regulate several signaling pathways *via* multiple and diverse targets in response to pathophysiological stimuli. This systematic review aims to describe the current state of the art regarding AD-related target genes modulated by differentially expressed miRNAs in peripheral fluids samples in MCI subjects to identify potential miRNA biomarkers in the early stages of AD. We found 30 articles that described five miRNA expression profiles from peripheral fluid in MCI subjects, showing possible candidates for miRNA biomarkers that may be followed up as fluid biomarkers or therapeutic targets of early-stage AD. However, additional research is needed to validate these miRNAs and characterize the precise neuropathological mechanisms.

Keywords: systematic review, microRNA, biomarkers, fluid biomarkers, diagnosis, mild cognitive impairment

OPEN ACCESS

Edited by:
Yasmina Manso, Center for Biomedical Research on Neurodegenerative Diseases (CIBERNED), Spain

Reviewed by:
Eva Maria Jimenez-Mateos, Trinity College Dublin, Ireland
Samuil R. Umansky, DiamiR, LLC, United States

***Correspondence:**
Claudia Duran-Aniotz
claudia.duran@uai.cl
Paulina Orellana
paulinaorellana@alumnos.uai.cl

Specialty section:
This article was submitted to Alzheimer's Disease and Related Dementias, a section of the journal Frontiers in Aging Neuroscience

Received: *02 November 2021*
Accepted: *15 December 2021*
Published: *12 January 2022*

Citation:
Ogonowski N, Salcidua S, Leon T, Chamorro-Veloso N, Valls C, Avalos C, Bisquertt A, Rentería ME, Orellana P and Duran-Aniotz C (2022) Systematic Review: microRNAs as Potential Biomarkers in Mild Cognitive Impairment Diagnosis. Front. Aging Neurosci. 13:807764. doi: 10.3389/fnagi.2021.807764

INTRODUCTION

Diagnostic Criteria in MCI

Diagnostic criteria for Mild Cognitive Impairment (MCI) have changed over time (Petersen, 2004; Winblad et al., 2004; Sachdev et al., 2015; Alzheimer's Association, 2018). At present, MCI is defined as a heterogeneous clinical syndrome which presents a significant change in cognitive function and deficits on neuropsychological testing but a relatively intact functionality (Winblad et al., 2004). The diagnosis of MCI depends on which cognitive and functional tests are used (Albert et al., 2011), these include the Mini-Mental Status Examination (MMSE; Arevalo-Rodriguez et al., 2021) or the Montreal Cognitive Assessment (MoCA; Nasreddine et al., 2005; Albert et al., 2011; Ciesielska et al., 2016). The presence or absence of MCI depends on the sensitivity and specificity of those tests and estimates of premorbid cognitive functioning. Appropriate and valid screening tests are crucial in evaluating patients with suspected MCI (Albert et al., 2011).

Currently, the MoCA is the recommended cognitive screening tool for MCI (Pinto et al., 2019). MoCA has a sensitivity between 80 and 100% and a specificity between 75 and 82% (Langa and Levine, 2014). However, the MoCA assessment varies depending on educational level, lifestyle factors, and ethnic diversities (Gagnon et al., 2013; O'Driscoll and Shaikh, 2017), limiting its use as a screening tool. Other cognitive assessments, including the MMSE and the Dementia Rating Scale (DRS), are not recommended as screening tools for MCI because of their specificity and sensitivity (Espino et al., 2001; Matallana et al., 2011). MoCA is currently more sensitive to diagnosing MCI than MMSE (Langa and Levine, 2014; Ciesielska et al., 2016).

The prevalence rate of MCI ranges from 6% (Sachdev et al., 2015) up to 25% for ages 80–84 (Livingston et al., 2017) in the population over 60 years of age. MCI is often considered a prodromal stage of dementia since neurodegenerative changes in the brain develop many years before symptoms are presented and dementia is diagnosed (Hulette et al., 1998). In long follow-up studies, annual rates of progression of MCI to dementia have been estimated at between 8 and 15% (Mitchell and Shiri-Feshki, 2009; Grill et al., 2013), which increases 80–90% after ∼6 years (Petersen et al., 2001; DeCarli, 2003; Bruscoli and Lovestone, 2004; Petersen, 2004; Panza et al., 2005; Pinto and Subramanyam, 2009).

Traditional and New Biomarkers in the Diagnosis of MCI

Since MCI is defined based on clinical criteria, biomarkers are not mentioned in its definition and diagnosis (Blennow and Hampel, 2003; Yin et al., 2013; Blennow and Zetterberg, 2018). However, based on recent research, biomarkers could offer support in identifying if the etiology of the MCI is AD-related or related to other pathologies, predicting the risk of progression to dementia, and helping in deciding the treatments options (Albert et al., 2011).

Biomarkers to Diagnose MCI Due to AD

Biomarkers for the diagnosis of MCI due to AD have not been validated yet. Most of them are based on the study of neuroimaging in AD (Yin et al., 2013) and the analysis of peripheral proteins in cerebrospinal fluid (CSF), including amyloid-beta (Aβ) and total (t-Tau) or phosphorylated (p-Tau) forms of Tau (Blennow and Zetterberg, 2018).

Neuroimaging techniques allow the evaluation of atrophy in medial temporal lobe regions, mainly the hippocampus and entorhinal regions, as well as the posterior cingulate cortex (Fennema-Notestine et al., 2009). In addition, neuroimaging could help to evaluate hypometabolism in the temporoparietal and posterior cingulate cortex (Kim et al., 2010; Habert et al., 2011). The techniques mainly used in neuroimaging are magnetic resonance imaging (MRI; Yin et al., 2013), fluorodeoxyglucose positron emission tomography (FDG-PET; Kim et al., 2010), and hypoperfusion of parietal cortices and the hippocampus as measured by single-photon emission computed tomography (SPECT; Habert et al., 2011). In addition, neuroimaging can assess Aβ accumulation using positron emission tomography using the (11)C-labeled Pittsburgh Compound-B ((11)C-PIB) ligand (Zhang et al., 2014).

On the other hand, lower concentrations of Aβ ($A\beta_{1-40}$, $A\beta_{1-42}$, and $A\beta_{1-42}/A\beta_{1-40}$ ratio) were detected in the CSF of patients with MCI, indicating higher concentrations of cerebral Aβ and progressive cognitive decline (Blennow and Hampel, 2003; Herukka et al., 2005; Okonkwo et al., 2010; Parnetti et al., 2012; Forlenza et al., 2015; Hansson et al., 2018). Similarly, the detection of t-Tau and p-Tau in CSF samples are also used to diagnose MCI and AD with 85% sensitivity and 80% specificity approximately, indicating neuronal damage and predicting the progression from MCI to AD (Trojanowski et al., 2010). The combination of $A\beta_{1-42}$ and Tau biomarkers has demonstrated a high sensitivity of 95% and specificity of 83% (Hansson et al., 2006).

The use of these biomarkers is limited in the case of neuroimaging by the high cost and low availability and access to these technologies (el Kadmiri et al., 2018; Swarbrick et al., 2019). At the same time, the analysis of CSF biomarkers is limited by the difficulty of obtaining the samples, low patient acceptance rates, and high costs (Hampel et al., 2018). For these reasons, it is necessary to find easily accessible and inexpensive biomarkers, such as blood biomarkers (Hampel et al., 2018).

In this line, Aβ and Tau protein levels have been measured in the blood (plasma or serum) of MCI subjects (Thambisetty and Lovestone, 2010; Colijn and Grossberg, 2015; Janelidze et al., 2020). Studies of Aβ plasma have yielded contradictory results in MCI subjects. Some studies have shown increased $A\beta_{1-42}$ levels in MCI and AD compared with controls (Giliberto et al., 2004; Chouraki et al., 2015; Hanon et al., 2018). In contrast, a decrease in plasma $A\beta_{1-42}$ or $A\beta_{1-42}/A\beta_{1-40}$ ratio has been observed in the progression of healthy controls and MCI to AD (Graff-Radford et al., 2007; Seppälä et al., 2010; Fei et al., 2011; Chouraki et al., 2015). Similarly, plasma t-Tau some studies have also shown inconsistent results. Increased levels of t-Tau have been found in AD but not in MCI (Zetterberg et al., 2013; Mattsson-Carlgren et al., 2021). Additionally, in another study, t-Tau increases in

MCI (Dage et al., 2016), or increases in both MCI and early AD (Chiu et al., 2014), or no changes in MCI or AD (Wang et al., 2016). Finally, levels of t-Tau have also been shown to decrease in MCI and AD (Larry Sparks et al., 2012). These discrepancies may be given by differences in the methodology for measuring biomarker levels, clinical factors referred to the characteristics of the subjects under study, and the lack of validation of brain accumulation of Aβ and Tau (Chen et al., 2019; Qu et al., 2021).

Plasma p-Tau has been validated with measurements of p-Tau in CSF and Tau-PET (Herukka et al., 2005; Dage et al., 2016; Barthélemy et al., 2020; Mattsson-Carlgren et al., 2021). Two phosphorylation epitopes, p-Tau181 and p-Tau217, have been extensively studied and described as biomarkers in MCI (Barthélemy et al., 2020; Mattsson-Carlgren et al., 2021). Two studies have shown that plasma p-Tau181 can predict AD and differentiate AD from other neurodegenerative diseases (Janelidze et al., 2020; Karikari et al., 2020). In a longitudinal study in MCI subjects, increased plasma levels of p-Tau217 have been correlated with cognitive impairment and increased brain atrophy (Mattsson et al., 2016; Janelidze et al., 2020), showing the same results which have also been observed in longitudinal studies of p-Tau in CSF (Falcon et al., 2018; Koychev et al., 2020). Additionally, another longitudinal study evaluating the same previously mentioned biomarkers in controls, MCI subjects, and AD patients demonstrated that plasma p-Tau, rather than plasma Aβ, is related to cognitive changes in the MCI stage (Chen et al., 2019).

The presence of biomarkers is a predictive factor for rapid progression to dementia, which includes (van Maurik et al., 2019): significant cerebral white matter hyperintensities (WMH), Apolipoprotein E4 (APOE4) carrier status, abnormal brain $A\beta_{1-42}$ on positron emission tomography (PET) or CSF analysis, abnormal Tau on PET or CSF analysis (Dunne et al., 2021).

Biomarkers and Treatment

Currently, there is no specific pharmacological treatment for MCI (Kasper et al., 2020). However, recent studies have suggested that some MCI subgroups (defined by biomarkers) might benefit from the treatment of acetylcholinesterase inhibitors (AChEIs) or Memantine (Dunne et al., 2021). Notably, despite the lack of specific and FDA-approved treatment, over 60% of patients with MCI are prescribed of AChEIs after positive amyloid PET scans. On the other hand, 24% of MCI patients are recommended to receive counseling about safety and future planning (Makizako et al., 2016; Rabinovici et al., 2019).

Nevertheless, several pharmacological clinical trials have shown little to no cognitive improvement in patients with MCI, both for classical anti-dementia drugs (e.g., acetylcholinesterase inhibitors) and other medications (Russ and Morling, 2012; Kasper et al., 2020) thus the importance of non-pharmacological treatments has increased. Several trials are showing the impact of cognitive training (Hill et al., 2017), physical activity (Rovner et al., 2018) and multimodal interventions (Chandler et al., 2016) on cognitive and functional outcomes. Unfortunately, the impact of these treatments on dementia prevention is still unclear (Livingston et al., 2020; Dunne et al., 2021). In AD-related dementia, several non-pharmacological interventions have been evaluated for both cognitive (Loi et al., 2018) and non-cognitive symptoms (Abraha et al., 2017) however, due to methodological differences, there is still no clear evidence of its effectiveness (Wang et al., 2020).

Currently, several investigations aim to search for biomarkers in peripheral fluids that account for pathological changes in the brain during the development and course of AD (Irizarry, 2004), which also allow detection of the disease at earlier stages. Some peripheral biomarkers that have been studied included molecules such as proteins, peptides, nucleic acids, microRNAs (miRNAs), lipids, and metabolites, which can be detected in serum, plasma, cellular components, and exosomes (Thambisetty and Lovestone, 2010; Lista et al., 2013). Among them, levels of peripheral miRNAs have been found dysregulated in AD (Sheinerman et al., 2013; Roderburg and Luedde, 2014; Schwarzenbach et al., 2014; Mushtaq et al., 2016; Silvestro et al., 2019). Importantly, detection of miRNAs is fast, uncomplicated, and sensitive, with cost-effective methods allowing their early application as a diagnostic tool (Chen et al., 2008; Gilad et al., 2008; Mitchell and Shiri-Feshki, 2009).

miRNA a Potential Biomarker for MCI

miRNAs are integral components of biological networks with fundamental roles in regulating gene expression (Singer et al., 2005; Weiner, 2013; Liu et al., 2014b). miRNAs are short non-coding RNA segments, ∼20–25-nt in length, that suppress target mRNA translation or induce messenger RNA (mRNA) decay *via* binding with seed sequences in one or more 3'untranslated regions (3'UTR) of target mRNA (Cai et al., 2004; Bartel, 2009; McNeill and van Vactor, 2012). One miRNA can affect many genes involved in the regulation of multiple cellular events and pathways. Circulating miRNA levels have been reported to be transported in blood exosomes, extracellular microvesicles (Kosaka et al., 2010), Argonaute2 (Turchinovich et al., 2011), and other proteins that protect them from being degraded (Geekiyanage et al., 2012).

miRNAs are differentially expressed in specific cell types, organs, and tissues in many human pathologies (Hua et al., 2009). Interestingly, some miRNAs are enriched in specific cellular compartments, such as dendrites and synapses (Lugli et al., 2008; Pichardo-Casas et al., 2012), suggesting a specific role in multiple cellular processes, including development, cell proliferation, replicative senescence, and aging (Qiu et al., 2014; Reddy et al., 2017; Saliminejad et al., 2019). Taking into account that over 70% of reported miRNAs are expressed in the human brain (O'Carroll and Schaefer, 2013; Danka Mohammed et al., 2017) and the crucial role in multiple processes, miRNA could be considered a promising blood biomarker for MCI. Here we performed a systematic review that aims to update and identify potential miRNAs as fluid biomarkers in early stages of AD. Furthermore, we will focus on identifying AD-related target genes modulated by differentially expressed miRNAs in peripheral fluids samples in MCI subjects.

METHODS

A systematic PRISMA review was performed to determine the significantly dysregulated miRNAs in MCI reported in the literature (Page et al., 2021). The search using two search engines

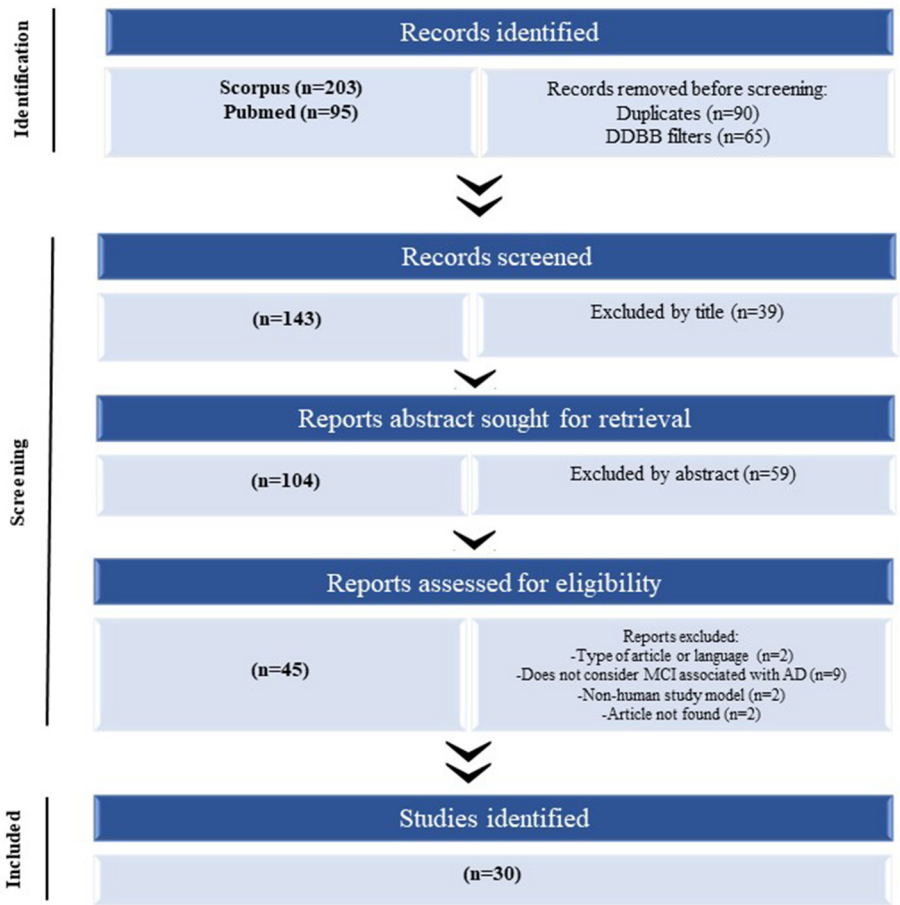

FIGURE 1 | The flow of information of the systematic review according to the PRISMA statement. The search of PubMed and Scopus databases provided a total of 298 citations. Of these, 155 studies were removed after filtering the duplicated and DDBB, and of those, 39 studies were discarded after reviewing the titles. After adjusting for abstracts that did not clearly meet the criteria, 45 articles remained. Finally, the full text of the remaining 45 citations was examined in more detail, and 15 studies did not meet the inclusion criteria as described, achieving a selection of 30 articles for parsing.

(Scopus and PubMed) using the same query was searched on both. For the construction of this query, keywords were defined regarding the source for obtaining the sample ("blood," "serum," "plasma," and "exosome"). The following step was considered in the title, abstract, or author keywords; at least one of the keywords mentioned above, in addition, mentions "miRNA" or "microRNA" and "cognitive impairment." The last searches were carried out on August 2, 2021 (**Figure 1**).

The following criteria were considered for the manuscripts to be included in this review: original articles written in English considering miRNA and cognitive impairment related to AD and human samples. Conversely, review, note, book chapter, or any classification other than original article, and articles that do not include cognitive impairment or that are not related to AD were considered an exclusion criterion.

First, the duplicates and manuscripts categorized other than "article" in the search engine were eliminated from the analysis. The next step was to read all abstract articles, eliminating those determined from those that did not meet the inclusion criteria. Finally, articles were read completely, eliminating those that did not meet the inclusion criteria.

In the process of reading the articles included in this review, the following information was extracted: dysregulated miRNAs, change in expression observed, target gene, type of sample studied, the origin of the population, sample size, diagnostic criteria used in the patients evaluated, neuropsychology, age ranges of the evaluated individuals, whether the study is longitudinal or not, miRNA analysis methodology and bioinformatics methodology used.

The Search Strategy Used in the miRNAs Databases

In order to provide a comprehensive overview of differentially regulated miRNA expression data in MCI, we selected miRNAs associated with MCI and AD in the PhenomiR database (Ruepp et al., 2010) (**Figure 2**). Due to the increasing amount of data in miRNA research, several resources which experimentally validated miRNA targets have been selected, including Tarbase

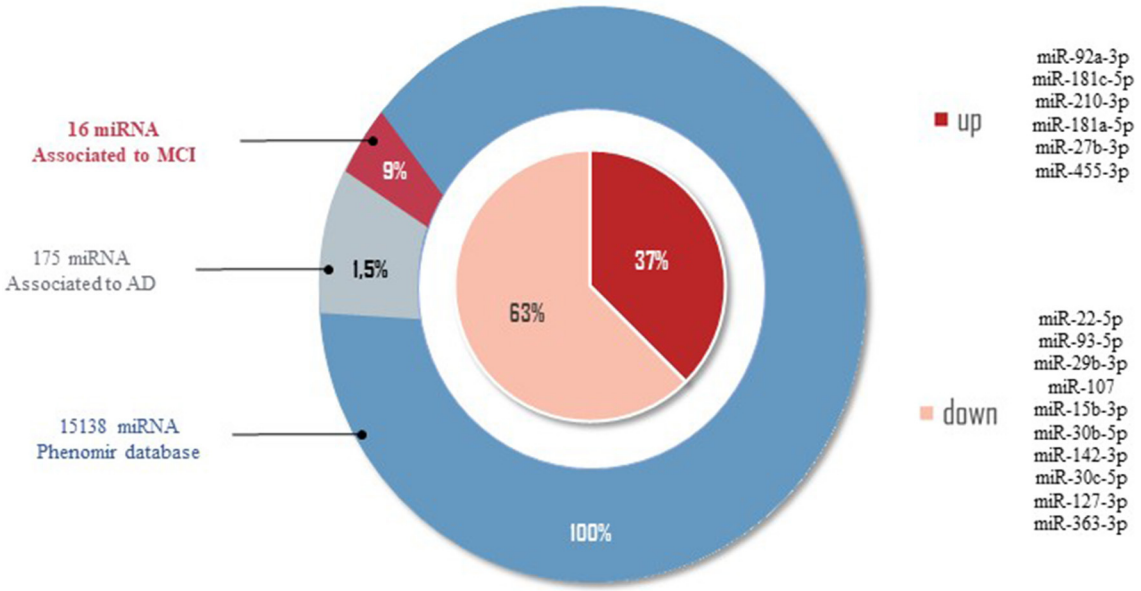

FIGURE 2 | miRNAs related to AD by PhenomiR database. One hundred and seventy-five miRNAs were found after filtering the miRNAs AD-associated. Of those, 10 miRNAs downregulated and six miRNAs upregulated in MCI cases were observed.

(Papadopoulos et al., 2009), myRTarBase (Hsu et al., 2011) and myRecords (Xiao et al., 2009), and the prediction of miRNA targets by Targetscan (Csardi, 2013) and the miRNA repositories by miRBase (Griffiths-Jones et al., 2006). The miRNAs included addressed the MCI stage, regardless of sex and ethnicity. To perform target interaction, MIENTURNET was used (Licursi et al., 2019) to find the target genes of each miRNA reported in the articles included in this review, using myRTarBase (Hsu et al., 2011). In some articles, miRNAs are generally mentioned without specifying whether it is 3p or 5p; for these purposes, the variation with more reeds between 3p and 5p was considered. **Figures 3**, **4** were built with Cytoscape (Shannon et al., 2003), which represent two interactomes, the first one being the interactions found for the miRNAs reported in the articles of this review and the second being the subset of these interactions validated by luciferase reporter assays (standard gold method), highlighting the target genes found related to AD or dementia.

RESULTS

After performing the PRISMA analysis, a total of 30 articles on MCI and miRNAs were identified. The selection process is depicted in the flowchart in **Figure 1**. We excluded 39 articles by title and 59 articles after reading the abstracts and reviewed the remaining 45 full-text articles, after which a further 15 articles were excluded.

Demographic and Clinical Features

In chronological order, we systematized the main features of 30 selected articles in **Table 1**, including the authors and the year of publication of each study, and indicated the study population and sample, clinical criteria, and neuropsychological assessments. Most of the studies came from Asian cohorts (50%), while 33.3% corresponded to European populations, including Italy, Poland, Germany, and others. Only four of them involve cohorts coming from the United States and Canada. **Table 1** summarizes the number and means ages of the different study cohorts comprising the selected articles, 13 (43.37%) of them date patients between 63 and 70 years of age, 14 (46.67%) papers describe populations between 70-79 years of age and 3 articles describe patients over 80 years of age (10%). Within the clinical criteria used in the 30 selected articles, 11 (36.6%) of them used the criteria established by the National Institute of Neurological and Communicative Disorders and Stroke and the Alzheimer's Disease and Related Disorders Association (NINCDS-ADRDA), 9 (30%) papers applied the Petersen's criteria. Some authors opted for the Alberts, Winblad, Grundman, IWG-2, DSM-IV criteria to a lesser extent. Among all reported neuropsychological assessments for MCI subjects, 16 (53.3%) studies used MMSE scores of 24 or higher, while 8 (26.67%) articles used MoCA scores ranging from 17 to 23. **Table 1** notes that 9 (30%) articles have applied a clinical criterion or a neuropsychological tool as inclusion criteria for MCI.

miRNAs Identified in MCI Subjects

The miRNAs reported in the 30 selected articles were analyzed in three different stages. In the first stage, the discovery stage of miRNA families MCI-associated. In the second stage, miRNAs were detected as differentially expressed between MCI and AD in longitudinal studies. Finally, in the third stage, the detected miRNAs and their target genes are based on the information reported in databases.

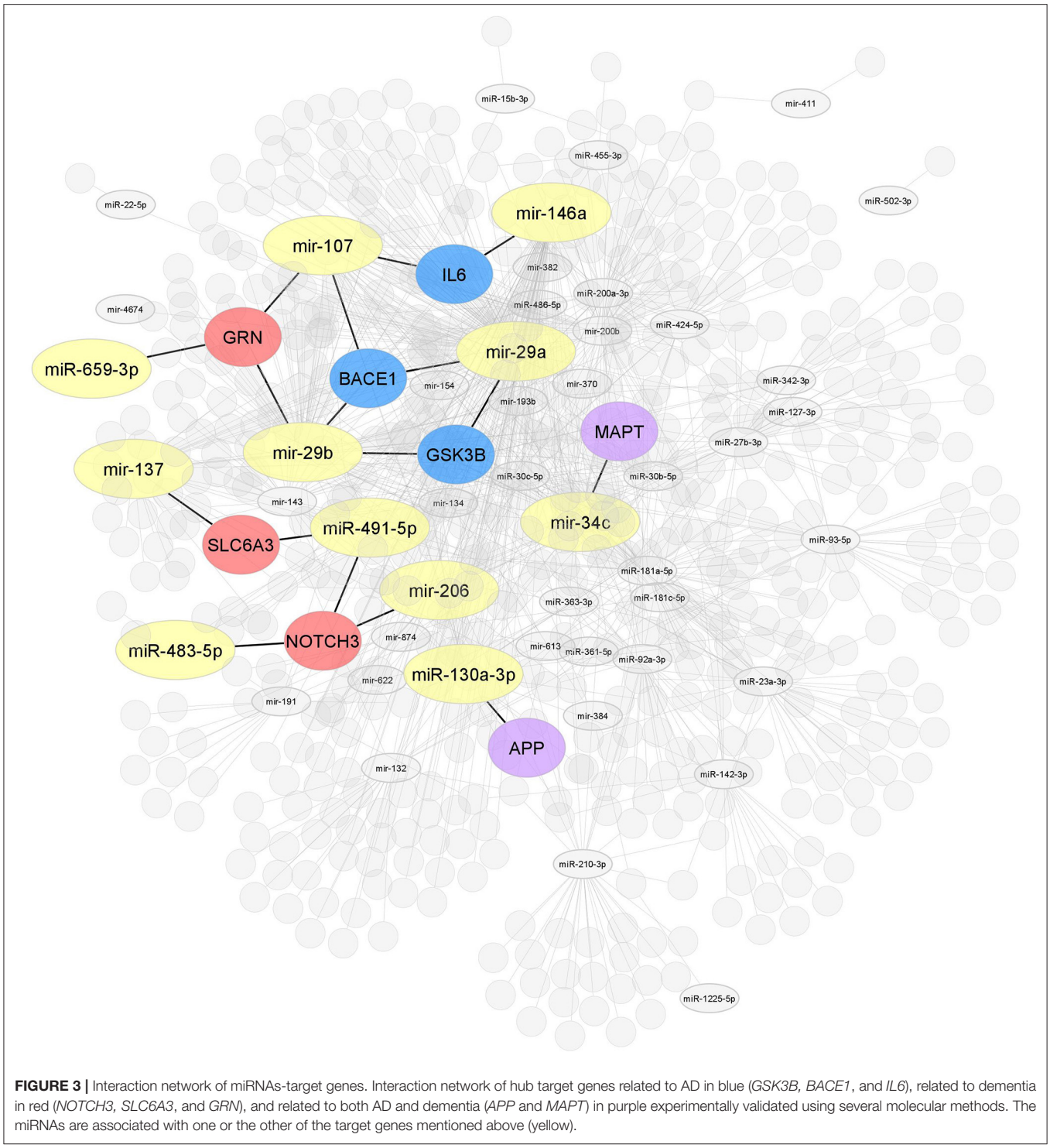

FIGURE 3 | Interaction network of miRNAs-target genes. Interaction network of hub target genes related to AD in blue (*GSK3B, BACE1*, and *IL6*), related to dementia in red (*NOTCH3, SLC6A3*, and *GRN*), and related to both AD and dementia (*APP* and *MAPT*) in purple experimentally validated using several molecular methods. The miRNAs are associated with one or the other of the target genes mentioned above (yellow).

Stage 1: miRNAs Family Reported in MCI Cases

Members from the same miRNA family are important because they have a typical sequence in genes that hints a shared function (Kaczkowski et al., 2009). miRNA genes in a family exhibit full or partial conservation of miRNAs seed sequences (Mathelier and Carbone, 2013). Notably, more evidence suggests that miRNA genes in the same miRNA family are non-randomly co-localized around genes involved in neurodegenerative diseases, cancer, immune system, among others (Kamanu et al., 2013). Of the 86 miRNAs reported in 30 selected articles, we have identified 4 miRNAs' families; 2 downregulated miRNA families (mir-29 and mir-30), 1 upregulated miRNA family

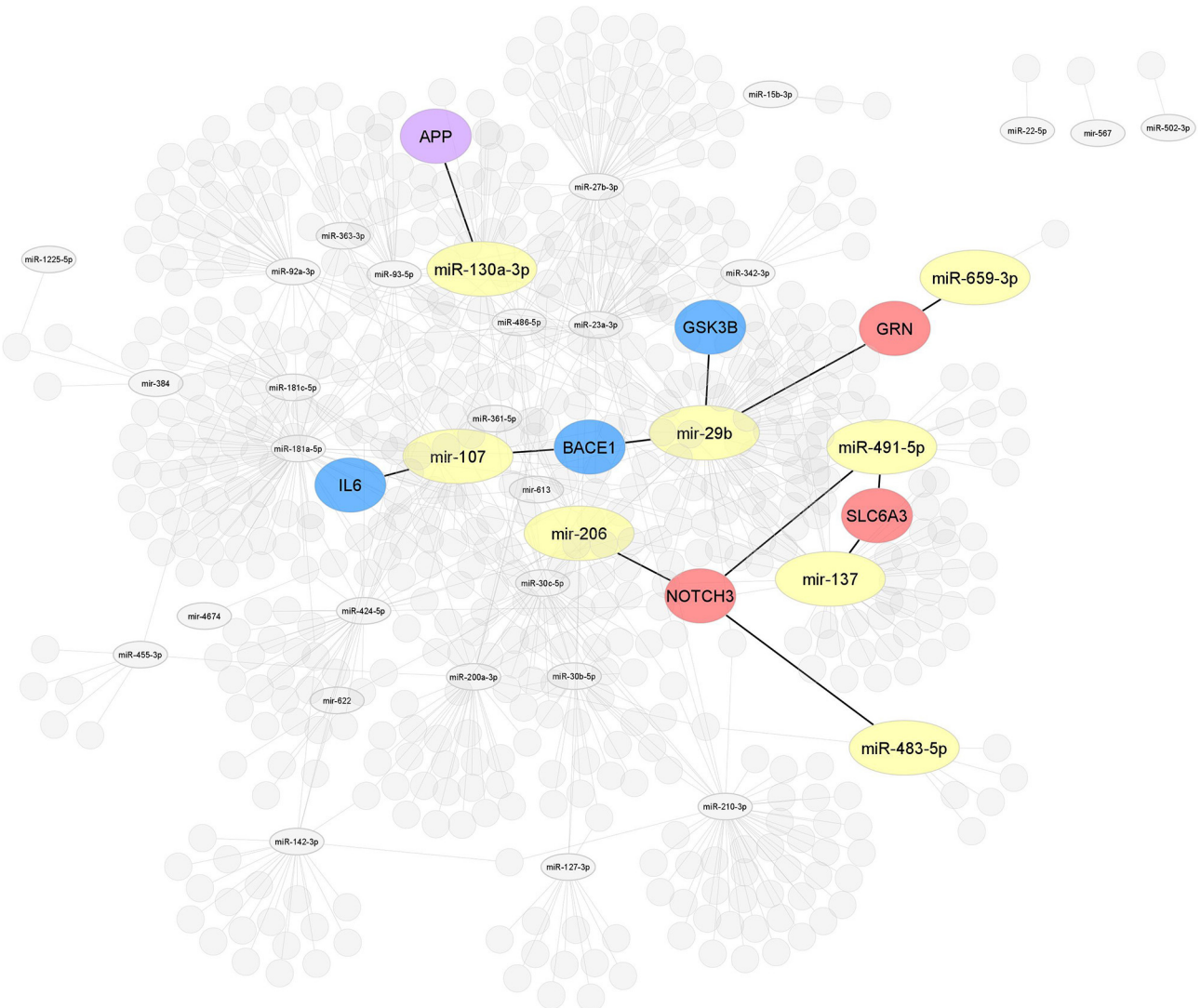

FIGURE 4 | Interaction network of miRNAs-target genes 2. After selecting 86, miRNAs studied in MCI cases were highlighted, all miRNAs (yellow) associated with the modulation of target genes related to AD or other dementias. Interaction network of hub target genes related to AD in blue (*GSK3B, BACE1*, and *IL6*), related to dementia in red (*NOTCH3, SLC6A3*, and *GRN*), and related to both AD and dementia (*APP*) in purple experimentally validated by luciferase reporter assay.

(mir-200), and 1 up-/downregulated miRNA family (mir-181) (see **Table 2A**).

Five miRNAs have been shown to be downregulated in serum and plasma samples from MCI cases in Asian and European cohorts. Three of them belong to 2 isomiR (mir-29a and mir-29b) of the mir-29 family (Geekiyanage et al., 2012). The other two miRNA sequences come from 2 isomiR sequences (mir-30b and mir-30c) belonging to the mir-30 family (Keller et al., 2016; Nagaraj et al., 2017). On the other hand, of the 30 articles, only three of them have reported 1 upregulated miRNA family. miR-200a-3p sequence, a product of mir-200a, showed upregulation in blood samples from MCI subjects in a Polish MCI cohort (Liu et al., 2014a; Guedes et al., 2016; Nagaraj et al., 2017). Six selected articles have reported 4 miRNAs to belong to 1 miRNAs family which shows to be up- or downregulated depending on the type of isomiR, mature sequences, and precursor-miRNA. miR-181a-5p, miR-181c-5p, and mir-181a sequences were upregulated in plasma samples in European MCI populations (Nagaraj et al., 2017; Agostini et al., 2019; Ansari et al., 2019). However, two studies reported that mir-181c isomiR levels in serum and plasma samples in North America MCI subjects were downregulated (Geekiyanage et al., 2012; Zirnheld et al., 2016).

Often genes in the same miRNA family exhibit similar functions due to their structural configuration, suggesting that miRNA genes could be involved in a familiar regulatory role (Kaczkowski et al., 2009). Our results showed that of the 4 miRNA families found, one of them (mir-181) reported several related members in both up- and downregulated.

Stage 2: miRNAs Reported in Longitudinal Studies

Longitudinal studies allow the study of changes that occur in the progression of the disease and aim to make predictions of the development of AD (Sheinerman et al., 2013; Xie et al., 2017; Ansari et al., 2019). Four articles were found that correspond to longitudinal studies where the expression of miRNAs in stages of MCI and its progression to AD was assessed. The average follow-up was between 1 and 5 years (see **Table 2B**).

In a first longitudinal study performed in MCI subjects, two miRNAs, mir-132 and mir-134, were evaluated (Sheinerman et al., 2013). The study was performed in 19 healthy control (HC) subjects with a follow-up of 2–5 years where, after the follow-up, nine subjects continued as HC and 10 subjects progressed to MCI. Regarding the results identified for mir-132, which considers miRNAs mir-128, mir-132, mir-874, and miR-491-5p, significant differences are observed between MCI and HC, with a 79–89% sensitivity and a specificity of 83–100% in discriminating subjects converting from a normal cognitive state to MCI. On the other hand, the mir-134, which considers miRNAs mir-134, miR-323-3p, mir-382, and mir-370, can discriminate subjects converting from a normal state to MCI with a sensitivity of 80–95% and a specificity of 79–84% (Sheinerman et al., 2013).

In 2017, another study evaluated a larger cohort of 458 subjects with MCI, followed up for 5 years, classifying subjects into amnestic mild cognitive impairment (aMCI) stable ($n = 330$) and MCI-converted AD ($n = 128$). Interestingly, the expression level of mir-206 was increased in MCI subjects who progressed to AD compared to subjects who remained stable MCI (Xie et al., 2017). By ROC (Receiver Operating Characteristic) analysis, an AUC (Area Under the ROC Curve) of 0.95 was described, with a sensitivity of 95.3% and a specificity of 77.8% for identifying MCI subjects who progressed to AD, concluding that increased serum mir-206 levels would accelerate the progression of aMCI to AD (Xie et al., 2017).

Additionally, another longitudinal study was performed with a 4-year follow-up of a small cohort classified into three groups, group 1 ($n = 6$) stable MCI, group 2 ($n = 6$) controls converting to AD, and group 3 ($n = 6$) subjects with MCI converting to AD (Kenny et al., 2019). Likewise, Xie et al. showed that the levels mir-206 were increased in MCI and MCI converting to AD (Xie et al., 2017).

Subsequently, subjects were classified depending on the results in two cognitive tests, Free and Cued Selective Reminding Test (FCSRT) and MMSE, where it was identified that higher levels of mir-206 expression correlate with more significant memory deficit (FCSRT) with an AUC of 0.82 and more significant cognitive impairment measured by MMSE with an AUC of 0.83 (Kenny et al., 2019).

Finally, the last longitudinal study identified in this systematic review was conducted with a 2-year follow-up of 44 subjects with MCI, where 25 subjects remained stable MCI while 19 subjects converted to AD (Ansari et al., 2019). Two miRNAs, including mir-146a and mir-181a, were evaluated in this study, showing increased expression in MCI subjects that converted to AD compared to stable MCI (Ansari et al., 2019). In the same study, correlations were found between increased expression of these miRNAs and Aβ CSF levels, hippocampal atrophy, and alterations in l regions (Ansari et al., 2019).

Stage 3: Database of miRNA Related to MCI and AD

Of the 2633 miRNAs structural characterized in the miRBase databases (Griffiths-Jones et al., 2006, 2008), one-third of these miRNAs are found in the coding part of genes, and the remaining are in the intronic regions, meaning that 33% of miRNAs modulate different target genes, being of our interest those miRNAs modulating AD-related target genes. In order to provide an overview of the differentially expressed data of miRNAs in MCI, we selected from the 86 miRNAs those that correlate with AD by the PhenomiR database (Ruepp et al., 2010). Of the 15138 different miRNAs associated with several diseases, 175 miRNAs (1.5%) were associated with AD. Of these 175 miRNAs, only 16 miRNAs (9%) dysregulated in MCI cases were observed (see **Figure 2**). Thirty-seven percent of miRNAs associated in both AD and MCI have shown to be upregulated, including miR-27b-3p, miR-92a-3p, miR-181c-5p, miR-181a-5p, miR-210-3p, miR-455-3p, while 67% of miRNAs were downregulated, including miR-15b-3p, miR-22-5p, miR-29b-3p, miR-30c-5p, miR-30b-5p, miR-93-5p, miR-107, miR-127-3p, miR-142-3p, and miR-363-3p (**Figure 2**). This result suggests that these 16 miRNAs could be potential prognostic biomarkers for MCI.

In order to provide a comprehensive search of the targets of the 86 miRNAs obtained from our systematic review, two approaches were used. First, we noted all putative target genes reported in 30 articles by several methods (see **Table 2**). Over half of those target genes were validated by qRT-PCR, one-third by sequencing, followed by other techniques such as western blotting, miRNA microarrays, and *in situ* hybridization. Second, we highlight the miRNAs associated with target genes validated by the well-known standard gold method luciferase reporter assay (see **Table 3**).

Target Genes Validated by qRT-PCR/Sequencing/Others

Most of the reported miRNAs regulate the expression of AD-related genes, of which 21 miRNAs regulate the β-site amyloid-protein precursor (*APP*) cleaving enzyme 1 (*BACE1*) and 13 miRNAs regulate. Although *APP*- and *BACE1*-associated miRNAs suggest that the regulatory process is complex and extensive, 85% of *BACE1*-associated miRNAs and 62% of APP-associated miRNAs were observed to be downregulated. Among the 30 selected articles, other target genes associated with the 86 miRNAs mentioned were a brain-derived neurotrophic factor (*BDNF*), Sirtuin 1 (*SIRT1*), transforming growth factor-beta receptor 1 (*TGF-β1*), microtubule-associated protein tau (*MAPT*), serine palmitoyltransferase long chain base subunit 1 and subunit 2 (*SPTLC1/2*), synaptosome associated protein 25 (*SNAP-25*), and dipeptidyl peptidase 4 (*DPP4*) genes.

Interactome 1 shows a schematic representation of the target genes of the 86 miRNAs AD-associated, other dementias, and both (AD and other dementias) (**Figure 3**). The mir-107, miR-29b-3p, miR-29a-3p, miR-146a-5p showed a direct interaction with the gene targets *BACE1, IL6*, and *GSK3B*; three target genes highly AD-associated. The mir-107, miR-29b-3p, miR-659-3p, mir-137, miR-491-5p, miR-483-5p, and mir-206 presented a

TABLE 1 | Articles resume table.

References	DOI	Country	Sample	Sample size (*n*)	Age, years	Clinical criteria	Neuropsychological assessments for MCI
Geekiyanage et al. (2012)	10.1016/j.expneurol.2011.11.026	United Kingdom	Serum	MCI (3), early MCI (1), AD (7), early AD (3), HC (7)	MCI (86 ± 1), early MCI (89), AD (88 ± 6.5), early AD (89 ± 2.5), HC (86.8 ± 3.5)	NA	MMSE
Sheinerman et al. (2013)	10.18632/aging.100624	California, United States	Plasma	MCI (50), age-matched controls (50)	MCI (68.2 ± 10.5), age-matched controls (65.1 ± 10.8)	NA	ADAS-Cog, CDRS, MMSE, Wechsler Memory Scale
Liu et al. (2014c)	10.1016/j.brainres.2014.04.026	Xuanwu, China	Blood	MCI (31), AD (38), HC (30)	MCI (72.8 ± 6.1), AD (76.8 ± 6.8), HC (75.2 ± 6.5)	NA	NA
Liu et al. (2014b)	10.3892/ijmm.2014.1780	Beijin, China	Serum	MCI (32), AD (45), HC (50)	MCI (63.2 ± 6.1), AD (64.2 ± 5.8), HC (63.9 ± 5.7)		NA
Liu et al. (2014a)	10.3892/mmr.2014.2484	Beijin, China	Plasma exosome	MCI (43), AD (51)	MCI (63.8 ± 6.1), AD (64.2 ± 6.5)	NA	NA
Dong et al. (2015)	10.1155/2015/625659	Shangai, China	Serum	MCI (30), AD (127), HC (123)	MCI (81.1 ± 6.8), AD (79.3 ± 8.9), HC (79.5 ± 6.8)	NA	MMSE
Zhu et al. (2015)	10.3892/etm.2015.2179	Zaozhuang, China	Serum	MCI (30), AD (26), HC (42)	MCI (71.6 ± 7.8), AD (72.3 ± 8.1), HC (71.9 ± 7.8)	NINCDS-ADRDA	NA
Li et al. (2016)	10.5582/bst.2016.01127	Tianjin, China	Serum	MCI (42), AD (48), HC (40)	MCI (64.8 ± 7.2), AD (65.5 ± 6.8), HC (63.2 ± 6.3)	NINCDS-ADRDA	NA
Guedes et al. (2016)	10.1016/j.dadm.2015.11.004	Portugal	Blood-derived monocytes and monocyte-derived macrophages	MCI (52), AD (36), age-matched HC (36)	MCI (73.6 ± 8.9), AD (74.9 ± 8.8), amHC (70.3 ± 6.6)	NINCDS-ADRDA, Albert's and Petersen's criteria	MMSE, MoCA, the Alzheimer's Disease Assessment Scale-Cognitive (ADAS-Cog), Battery of Lisbon for the Assessment of Dementia and the clinical dementia rating (CDR), and the geriatric depression scale (GDS-30) to exclude depression.
Kayano et al. (2016)	10.1186/s40364-016-0076-1	Japan	Plasma	MCI (23), HC (30)	MCI (72.8 ± 3.1), HC (70.4 ± 4.9)	Petersen criteria	MMSE
Keller et al. (2016)	10.1016/j.jalz.2015.12.012	German/ United States	Blood	MCI (20), AD (103), HC (77)	MCI (67.7 ± 8.2), AD (70.7 ± 8.2), HC (67.3 ± 7.8)	NA	MMSE, MoCA
Wang et al. (2016)	10.3389/fnagi.2016.00112	China	Plasma	aMCI (20), cognitively normal HC (24)	aMCI (70.1 ± 7.2), cnHC (69.9 ± 7.6)	Medical history, physical and neurological examinations, and MRI scans.	MMSE, MoCA
Zirnheld et al. (2016)	10.4172/0975-9042.000117	Montreal, Canada	Plasma	MCI (34), Mild AD (16), Moderate-Severe AD (20), normal elderly controls (NEC, 37)	MCI (75.3 ± 5.4), Mild AD (78.2 ± 3.5), Moderate-Severe AD (77.7 ± 6.8), NEC (75.3 ± 5.4)	Winblad's criteria	Full neuropsychological assessment including Modified WAIS subtests (digit symbol), Wechsler Memory Scale-R subtests (Logical Memory, Digit Span), Raven's Progressive Matrices, Visual perceptual tests, RAVLT, as well as Verbal Fluency, MoCA and MMSE.
Kumar et al. (2017)	10.1093/hmg/ddx267	Texas, United States	serum/plasma	MCI (20), AD (11), HC (18)	MCI (74 ± 11.1), AD (73 ± 13.5), HC(77 ± 17.5)	NINCDS-ADRDA	MMSE
Nagaraj et al. (2017)	10.18632/oncotarget.15109	Poland	Plasma	MCI-AD (15), AD (20), age-matched HC (15)	MCI-AD (65.8 ± 7), AD (67.5 ± 8), age-matched HC (66 ± 3)	DSM-IV, NINCDS-ADRDA and Alzheimer's Association workgroups on diagnostic guidelines for Alzheimer's disease	MMSE
Yang et al. (2018)	10.3967/bes2018.011	China	Serum exosomal	MCI (101), AD (107)	MCI (61.63 ± 7.32), AD (74.15 ± 7.93)	NINCDS-ADRDA	NA

(Continued)

TABLE 1 | Continued

References	DOI	Country	Sample	Sample size (*n*)	Age, years	Clinical criteria	Neuropsychological assessments for MCI
Agostini et al. (2019)	10.3389/fnagi.2019.00052	Italy	Blood	MCI (22), AD (22), HC (22)	MCI (76 ± 4.0), AD (78 ± 4.0), HC (70 ± 9.9)	NINCDS-ADRDA, Petersen and Grundman criteria, MRI, computed tomography scan.	MMSE
Lu et al. (2019)	10.1007/s12264-019-00361-0	Tongji, China	Blood	aMCI (10), AD (7), HC (17)	aMCI (70.20 ± 10.40), AD (70.43 ± 5.08), HC (70.86 ± 4.11)	NINCDS-ADRDA, exclusion of brain tumor, vascular dementia, and cerebrovascular diseases	MMSE
Salama et al. (2019)	10.3889/oamjms.2019.834	Egypt	Plasma	adults (186), MCI was detected among 14	Between 40 and 65 years, mean 51.3 ± 4.1 years	National Institute on Aging–Alzheimer's Association recommendations	ACE III, MoCA, Quick cognitive tests (Quick MCI)
Siedlecki-Wullich et al. (2019)	10.1186/s13195-019-0501-5	Barcelona, Spain	Plasma	MCI (26), AD (56), HC (38)	MCI (72.0 ± 8.49), AD (77.77 ± 6.69), HC (68.29 ± 8.99)	Petersen criteria	Neuropsychological battery used in Fundació ACE (NBACE) and tests
Zhao et al. (2020)	10.1373/jalm.2019.029595	England	Serum	MCI (13), AD (51), HC (32)	MCI (75 ± 11), AD (73 ± 5), HC (80 ± 10)	NINCDS-ADRDA and Petersen criteria.	NA
de Felice et al. (2020)	10.1007/s12035-020-02029-7		Blood/Serum	MCI-AD (18), AD (18)	MCI-AD (69.9 ± 5.04), AD (70.8 ± 10.22)	Petersen and IWG-2 criteria	Full neuropsychological assessment and MMSE
Li et al. (2020)	10.1016/j.neuroscience.2020.02.044	Jinzhou, China	Plasma-derived Extracellular Vesicles	MCI (28), AD (31), HC (28)	MCI (76.6 ± 5.4), AD (74.2 ± 6.1), HC (74.6 ± 5.0)	NINCDS–ADRDA	NA
Al-Rawaf et al. (2021)	10.2147/CIA.S285689	Saudi Arabia	Serum	MCI (70), HC (80)	MCI (64.9 ± 4.1), HC (65.3 ± 3.5)	Petersen criteria	The Clinical Dementia Rating scale, MoCA, MMSE
Liu et al. (2021)	10.1155/2021/5450397	Xuanwu and Beijing, China	Blood, Serum, Plasma exosomes	subjective cognitive decline (SCD, 89), MCI (92), AD (92), HC (60)	SCD (75.7 ± 4.9), MCI (75.2 ± 8.0), AD (78.1 ± 7.2), HC (76.5 ± 6.1)	NA	NA
He et al. (2021)	10.3233/JAD-210307	China	Plasma	MCI (5,20,40), NC (5,10,40)	MCI (68 ± 2.83∼78.25 ± 5.48)/NC(70 ± 2.12∼78.23 ± 5.62)	Petersen criteria	Full neuropsychological assessment including: MMSE, MoCA, Wechsler Memory Scale, Verbal Fluency Test-fruits and idioms, Hopkins Verbal Learning and 30-min Delayed Test, Visual Recognition Function Test.
*Sheinerman et al. (2012)	10.18632/aging.100486	California, United States	Plasma	MCI (30), AD (30), age matched HC (30)	MCI (81.7 ± 3.2), AD (76.9 ± 3.5) age matched HC (77.4 ± 4.9)	NINCDS–ADRDA, Petersen criteria	Consensus team determined cognitive status after completing the Consortium to Establish a Registry for Alzheimer's Disease (CERAD) battery
*Xie et al. (2017)	10.3233/JAD-160468	China	Serum	aMCI-aMCI (330), aMCI-AD (128)	aMCI-aMCI (69.91 ± 4.01), aMCI-AD (76.04 ± 4.82)	Petersen criteria	Wechsler Memory Scale Revised (WMS-R, Chinese version), Clinical Dementia Rating (CDR), MMSE and MoCA
*Ansari et al. (2019)	10.1016/j.neurobiolaging.2019.06.005	European Alzheimer's Disease Neuroimaging Initiative	Blood	progressor MCI (19), stable MCI (26)	pMCI (66.68 ± 5.8), sMCI (66.23 ± 7.1)	NA	MMSE, CDR, logical memory test. They also used the geriatric depression scale (GDS-15) to exclude depression.
*Kenny et al. (2019)	10.3390/biom9110734	Madrid, Spain	Plasma	MCI (30), AD (25), HC (31)	MCI (76.8 ± 4.0), AD (84.6 ± 3.5), HC (75.0 ± 4.7)	NA	Full neuropsychological assessment including: MMSE, Free and Cued Selective Reminding Test (FCSRT), Clinical Dementia Rating (CDR) and Functional Activities Questionnaire (FAQ)

Selected articles used for the data analysis show an organization following an order by authors, year, digital object identifier (DOI), country, sample, sample size (n), age, clinical criteria, and neuropsychological assessment for MCI.
**Longitudinal studies.*

TABLE 2 | Differentially expressed peripheral fluid-associated miRNAs in MCI.

miRNA	Up/down	Sample				Target genes	Publication
		Blood	Plasma	Serum	Plasma/ serum exosome		
(A) miRNA FAMILIES							
mir-29							
mir-29a	Down			X		*SPTLC1/2*	Geekiyanage et al., 2012
mir-29b	Down			X		*SPTLC1/2*	Geekiyanage et al., 2012
miR-29b-3p	Down		X			*BACE 1*	He et al., 2021
mir-30							
miR-30b-5p	Down		X			*PSEN2*	Nagaraj et al., 2017
miR-30c-5p	Down	X				-	Keller et al., 2016
mir-181							
mir-181a	Up	X	X			*Fidgetin, B-cell lymphoma 2, SIRT1*	Sheinerman et al., 2013; Ansari et al., 2019
miR-181a-5p	Up	X				*SNAP-25*	Agostini et al., 2019
mir-181c	Down		X	X		*SPTLC1/2*	Geekiyanage et al., 2012; Zirnheld et al., 2016
miR-181c-5p	Up		X			*NPTX1, NPTXR*	Siedlecki-Wullich et al., 2019
mir-200							
miR-200a-3p	Up		X			*MAPK, BACE1*	Nagaraj et al., 2017
mir-200b	Up	X				*APP, Aβ42, MGAT3*	Liu et al., 2014a; Guedes et al., 2016
(B) miRNA REPORTED IN LONGITUDINAL STUDIES							
mir-9	Down		X	X		*SPTLC1/2*	Geekiyanage et al., 2012; Sheinerman et al., 2013
mir-29a	Down			X		*SPTLC1/2*	Geekiyanage et al., 2012
mir-29b	Down			X		*SPTLC1/2*	Geekiyanage et al., 2012
miR-30b-5p	Down		X			-	Nagaraj et al., 2017
mir-34c	Down		X			*SIRT1, ONECUT2, BCL2*	Zirnheld et al., 2016
mir-137	Down			X		*SPTLC1/2*	Geekiyanage et al., 2012
miR-142-3p	Down		X	X		*BDNF, DPP4, SIRT1, FRS2, PP2A, PI3K*	Nagaraj et al., 2017; Al-Rawaf et al., 2021
mir-146a	Up	X		X		*CFH, TLR2*	Dong et al., 2015; Ansari et al., 2019
mir-181a	Up	X	X			*SIRT1*	Sheinerman et al., 2013; Ansari et al., 2019
mir-181c	Down		X	X		*SPTLC1/2*	Geekiyanage et al., 2012; Zirnheld et al., 2016
miR-200a-3p	Up		X			*MAPK, BACE1*	Nagaraj et al., 2017
mir-206	Up		X	X		*BDNF, SIRT1*	Xie et al., 2017; Kenny et al., 2019
mir-411	Down		X			-	Zirnheld et al., 2016
miR-455-3p	Up		X	X		*TGF-β1, APP*	Kumar et al., 2017
miR-483-5p	Up		X	X		*BDNF, DPP4, SIRT1, BACE1, MAPT*	Nagaraj et al., 2017; Al-Rawaf et al., 2021
miR-486-5p	Up		X			*BACE1, IGFRI, MAPT*	Nagaraj et al., 2017
miR-502-3p	Up		X			*SSTR, SOD2*	Nagaraj et al., 2017
mir-567	Down	X		X		*NEUROD2, NEUROG2, TCF3, TCF4, TBR1*	de Felice et al., 2020
mir-613	Up			X		*BDNF*	Li et al., 2016
mir-3658	Up	X		X		-	de Felice et al., 2020
mir-3908	Up	X		X		-	de Felice et al., 2020
miR-5588-5p	Up	X		X		-	de Felice et al., 2020
(C) OTHERS miRNA MCI-ASSOCIATED							
mir-7	Up/down		X			-	Sheinerman et al., 2013
miR-15b-3p	Down	X			X	*SNAP-25*	Agostini et al., 2019; Li et al., 2020

(Continued)

TABLE 2 | Continued

miRNA	Up/down	Sample				Target genes	Publication
		Blood	Plasma	Serum	Plasma/ serum exosome		
miR-22-5p	Down		X			*BACE 1*	He et al., 2021
mir-23a	Up	X				*CCR2*	Guedes et al., 2016
miR-23a-3p	Up	X				*SNAP-25*	Agostini et al., 2019
miR-27b-3p	Up	X				*SNAP-25*	Agostini et al., 2019
miR-92a-3p	Up		X			*NPTX1, NPTXR*	Siedlecki-Wullich et al., 2019
mir-93	Up			X		*CFH*	Dong et al., 2015
miR-93-5p	Down				X	*MAPT*	Li et al., 2020
mir-107	Down		X			*BACE 1*	Wang et al., 2016
mir-124a	Up/down			X		*BDNF, DPP4, SIRT1*	Al-Rawaf et al., 2021
mir-125b	Up/down		X	X		*BDNF, DPP4, SIRT1, TP53*	Sheinerman et al., 2013; Kayano et al., 2016; Al-Rawaf et al., 2021
miR-127-3p	Down	X				-	Sheinerman et al., 2013
mir-128	Up	X	X			*CCR2*	Sheinerman et al., 2013; Guedes et al., 2016
miR-130a-3p	Up	X				*SNAP-25*	Agostini et al., 2019
mir-132	Up		X			*Rasa1, BDNF, SIRT1*	Sheinerman et al., 2013; Salama et al., 2019
mir-134	Up		X			-	Sheinerman et al., 2013; Salama et al., 2019
miR-134-3p	Down		X			*BACE 1*	He et al., 2021
mir-135	Down or undetectable		X			-	Kenny et al., 2019
miR-135a	Down				X	*BACE1, APP*	Yang et al., 2018
mir-138	Up	X				*APP*	Lu et al., 2019
mir-143	Down			X		*CFH*	Dong et al., 2015
mir-154	Up	X				*CCR2*	Guedes et al., 2016
mir-191	Up		X			*TP53*	Kayano et al., 2016
mir-193b	Up/down	X		X	X	*BACE1, APP*	Liu et al., 2014a; Yang et al., 2018
mir-210	Down			X		*VEGF*	Zhu et al., 2015
miR-210-3p	Up		X			*NPTX1, NPTXR*	Siedlecki-Wullich et al., 2019
miR-323-3p	Up/down		X			-	Sheinerman et al., 2013
miR-342-3p	Down				X	-	Li et al., 2020
miR-361-5p	Down	X				*SNAP-25*	Agostini et al., 2019
miR-363-3p	Down	X				-	Keller et al., 2016
mir-370	Down		X			-	Sheinerman et al., 2013
mir-382	Up/down		X			-	Sheinerman et al., 2013
mir-384	Down			X	X	*BACE 1, APP*	Liu et al., 2014c; Yang et al., 2018
miR-424-5p	Down				X	*MAPT*	Li et al., 2020
miR-491-5p	Down		X			-	Sheinerman et al., 2013
mir-554	Down		X			*BACE 1*	He et al., 2021
mir-604	Down		X			*BACE 1*	He et al., 2021
mir-622	Down		X			*BACE 1*	He et al., 2021
miR-659-3p	Down		X			*BACE 1*	He et al., 2021
mir-874	Up/down		X			-	Sheinerman et al., 2013
miR-1185-2-3p	Down		X			*BACE 1*	He et al., 2021
miR-1225-5p	Down		X			*BACE 1*	He et al., 2021
miR-1306-5p	Up				X	*MAPT*	Li et al., 2020
miR-1909-3p	Down		X			*BACE 1*	He et al., 2021
mir-1972	Down		X	X		*TGF-β1, APP*	Kumar et al., 2017
miR-3065-5p	Down				X	*MAPT*	Li et al., 2020

(Continued)

TABLE 2 | Continued

miRNA	Up/down	Sample				Target genes	Publication
		Blood	Plasma	Serum	Plasma/ serum exosome		
miR-3124-3p	Up		X	X		*TGF-β1, APP*	Kumar et al., 2017
miR-3156-5p	Down		X			*BACE 1*	He et al., 2021
miR-3613-3p	Up		X	X		*TGF-β1, APP*	Kumar et al., 2017
mir-4317	Up		X	X		*TGF-β1, APP*	Kumar et al., 2017
miR-4659b-5p	Down		X			*BACE 1*	He et al., 2021
miR-4668-5p	Up		X	X		*TGF-β1, APP*	Kumar et al., 2017
mir-4674	Up		X	X		*TGF-β1, APP*	Kumar et al., 2017
mir-4698	Down		X			*BACE 1*	He et al., 2021
mir-5691	Down		X			*BACE 1*	He et al., 2021
mir-6722	Down		X	X		*TGF-β1, APP*	Kumar et al., 2017
miR-6856-3p	Up		X	X		*TGF-β1, APP*	Kumar et al., 2017
Let-7b	Up		X			-	Kenny et al., 2019

(A) miRNAs families up/downregulated in MCI cases.
(B) miRNAs up/downregulated revealed in four longitudinal studies.
(C) Other miRNAs mentioned in the 30 articles MCI-associated. miRNAs articles used for the data analysis, showing an organization following an order by type of miRNA, up/down expression level, sample (blood, plasma, serum, plasma/serum exosome), altered gene expression, and publication.

direct association with the targets *GRN, SLC6A3,* and *NOTCH3*; genes related to other dementias. Finally, miR-34c-5p and miR-130a-3p reflected an interaction with the *MAPT* and *APP* gene, both in dementia and AD-associated (**Figure 3**).

Target Genes Validated by Luciferase Reporter Assay

Of the 86 miRNAs evaluated, 55 were further analyzed, 31 miRNAs were discarded from this analysis because they were not recognized in the evaluated databases. **Table 3** shows the total output of validated gene targets for each of the 55 miRNAs. Within this search, mir-554 showed the lowest count of targets with 36 validated ones, while the mir-107 presented the highest count with 4,403 targets (**Table 3**). Due to the large volume of data, we selected only those targets validated by luciferase reported assay. **Figure 4** shows the interaction between the 55 miRNAs and the target genes AD and other dementias associated. The mir-107 and miR-29b-3p showed a direct interaction with the AD-associated gene targets. The miR-29b-3p, miR-659-3p, mir-137, miR-491-5p, miR-483-5p, and mir-206 presented a direct association with the targets related to other dementias, while miR-130a-3p reflected an interaction with *APP* gene, both in dementia and AD-associated (**Figure 4**).

Our results claim that of the total 86 miRNAs MCI-associated, only the mir-107 and miR-29b-3p were reported by the whole database analyzed. In addition, those miRNAs also showed close interaction with AD-related target genes, including *BACE 1, IL6*, and *GSK3B* (**Figures 3**, **4**). An interesting insight derived from our analysis is (i) the first one, the miR-29a-3p, miR-146a-5p, miR-34c-5p, and miR-130a-3p, were related to AD-associated genes, but not characterized in the PhenomiR database as miRNAs AD-associated (**Figure 3**), being the interest as potential prognostic biomarkers for early-stage AD and (ii) although the mir-181 family did not show a direct interaction with AD-related genes, several members were up-and downregulated in cases of MCI, indicating that other biological pathways may be involved in addition to those well-known (**Table 2A** and **Figure 2**).

DISCUSSION

Currently, MCI has become a broad construct defined as a clinical syndrome with multiple clinical profiles due to various etiologies (Hulette et al., 1998; Bruscoli and Lovestone, 2004). MCI is considered an intermediate stage of cognitive impairment that may be a transitional phase before dementia (Petersen et al., 2014). Up to this day, the diagnosis of MCI is based on clinical criteria and evaluation and therefore relies on the evaluator's expertise, the neuropsychological tools applied, and the characteristic of the patient (Dunne et al., 2021).

Some neuropsychological profiles could provide some information about the underlying etiology of the MCI (Petersen et al., 1999) and the risk of progression to dementia (Petersen et al., 2001) or regression to normal cognition (Koepsell and Monsell, 2012). However, the information provided solely by the neuropsychological assessment is not enough to give an adequate risk assessment, and therefore some authors suggest complementing this information with the use of biomarkers (Campbell et al., 2013; Dunne et al., 2021). In this context, peripheral biomarkers could add or provide information on the possible etiology of the MCI, the individual risk of progression and help to decide about potential treatments.

Within the study of biomarkers, it is crucial and necessary to work with (i) an easily accessible sample and (ii) a stable, quickly obtained, sensitive, and reproducible biomarker (Lashley et al., 2018). miRNAs obtained in blood meet perfectly with these conditions and are therefore of great interest for implementation as diagnostic or prognostic biomarkers (Swarbrick et al., 2019).

TABLE 3 | Validate target genes regulated by peripheral fluid-associated miRNAs in MCI cases.

miRNA	Up/down	Targets genes reported in 30 articles	Validated targets by several methods	Validated targets by luciferase reporter assays	Publication
miR-15b-3p	Down	*SNAP-25*	295		Agostini et al., 2019; Li et al., 2020
miR-22-5p	Down	*BACE 1*	1,135		He et al., 2021
miR-23a-3p	Up	*SNAP-25*	2,093		Agostini et al., 2019
miR-27b-3p	Up	*SNAP-25*	2,761		Agostini et al., 2019
miR-29b-3p	Down	*BACE 1*	1,781	*GSK3B, BACE1, GRN*	He et al., 2021
miR-30b-5p	Down	*PSEN2*	2,139		Nagaraj et al., 2017
miR-30c-5p	Down	-	2,377		Keller et al., 2016
miR-92a-3p	Up	*NPTX1, NPTXR*	3,344	*SIRT1*	Siedlecki-Wullich et al., 2019
miR-93-5p	Down	*MAPT*	4,119		Li et al., 2020
mir-107	Down	*BACE 1*	4,403	*IL6, BACE1*	Wang et al., 2016
miR-127-3p	Down	-	108		Sheinerman et al., 2013
miR-130a-3p	Up	*SNAP-25*	2,704	*APP*	Agostini et al., 2019
miR-134-3p	Down	*BACE 1*	89		He et al., 2021
mir-137	Down	*SPTLC1/2*	985	*NOTCH3, SLC6A3*	Geekiyanage et al., 2012
miR-142-3p	Down	*BDNF, DPP4, SIRT1, FRS2, PP2A, PI3K*	1416		Nagaraj et al., 2017; Al-Rawaf et al., 2021
miR-181a-5p	Up	*SNAP-25*	2,933	*SIRT1*	Agostini et al., 2019
miR-181c-5p	Up	*NPTX1, NPTXR*	1,504		Siedlecki-Wullich et al., 2019
miR-200a-3p	Up	*MAPK, BACE1*	900	*TRAPPC8*	Nagaraj et al., 2017
mir-206	Up	*BDNF, SIRT1*	234	*NOTCH3, G9PD, GPD2, PGD, TKT*	Xie et al., 2017; Kenny et al., 2019
miR-210-3p	Up	*NPTX1, NPTXR*	3,624	*BDNF, NPTX1*	Siedlecki-Wullich et al., 2019
miR-342-3p	Down	-	1,019		Li et al., 2020
miR-361-5p	Down	*SNAP-25*	1,154		Agostini et al., 2019
miR-363-3p	Down	-	937		Keller et al., 2016
mir-384	Down	*BACE 1, APP*	131		Liu et al., 2014a; Yang et al., 2018
miR-424-5p	Down	*MAPT*	3,021		Li et al., 2020
miR-455-3p	Up	*TGF-β1, APP*	1,526		Kumar et al., 2017
miR-483-5p	Up	*BDNF, DPP4, SIRT1, BACE1, MAPT*	388		Nagaraj et al., 2017; Al-Rawaf et al., 2021
miR-486-5p	Up	*BACE1, IGFRl, MAPT*	372		Nagaraj et al., 2017
miR-491-5p	Down	-	637	*NOTCH3, SLC6A3*	Sheinerman et al., 2013
miR-502-3p	Up	*dynactin, SSTR, Crk, SOD2*	532		Nagaraj et al., 2017
mir-554	Down	*BACE 1*	36		He et al., 2021
mir-567	Down	*NEUROD2, NEUROG2, TCF3, TCF4, TBR1*	356		de Felice et al., 2020
mir-604	Down	*BACE 1*	109		He et al., 2021
mir-613	Up	*BDNF*	129	*BDNF*	Li et al., 2016
mir-622	Down	*BACE 1*	265		He et al., 2021
miR-659-3p	Down	*BACE 1*	159	*GRN*	He et al., 2021
miR-1185-2-3p	Down	*BACE 1*	194		He et al., 2021
miR-1225-5p	Down	*BACE 1*	179		He et al., 2021
miR-1306-5p	Up	*MAPT*	655		Li et al., 2020
miR-1909-3p	Down	*BACE 1*	260		He et al., 2021
mir-1972	Down	*TGF-β1, APP*	154		Kumar et al., 2017
miR-3065-5p	Down	*MAPT*	443		Li et al., 2020
miR-3124-3p	Up	*TGF-β1, APP*	231		Kumar et al., 2017
miR-3156-5p	Down	*BACE 1*	84		He et al., 2021
miR-3613-3p	Up	*TGF-β1, APP*	914		Kumar et al., 2017
mir-3658	Up	-	222		de Felice et al., 2020

(Continued)

TABLE 3 | Continued

miRNA	Up/down	Targets genes reported in 30 articles	Validated targets by several methods	Validated targets by luciferase reporter assays	Publication
mir-3908	Up	-	124		de Felice et al., 2020
mir-4317	Up	*TGF-β1, APP*	120		Kumar et al., 2017
miR-4659b-5p	Down	*BACE 1*	111		He et al., 2021
miR-4668-5p	Up	*TGF-β1, APP*	548		Kumar et al., 2017
mir-4674	Up	*TGF-β1, APP*	65		Kumar et al., 2017
mir-4698	Down	*BACE 1*	402		He et al., 2021
miR-5588-5p	Up	-	67		de Felice et al., 2020
mir-5691	Down	*BACE 1*	166		He et al., 2021
miR-6856-3p	Up	*TGF-β1, APP*	142		Kumar et al., 2017

Additionally, miRNAs can regulate several signaling pathways *via* multiple and diverse targets in response to pathophysiological stimuli making them also potentially attractive candidates with therapeutic interest. As we described, numerous dysregulated miRNAs have been detected in biofluids from MCI patients. Some of these miRNAs participate in the regulation of Aβ generation, synaptic dysfunction, and Tau phosphorylation (Lu et al., 2019). miRNA profiles are known to be altered in several regions of the brain in AD; however, which miRNAs are associated with early-stage AD remains uncertain. Here, we performed a systematic review of miRNAs reported to date in peripheral fluids in MCI cases. In addition, we specifically focused our analysis on the association between each reported miRNA and modulation of AD-associated target genes since its deregulation may reflect critical pathological changes in the brain.

Prior studies have noted that members of a miRNA family exhibit similar functions due to conserved motifs, such as seed sequences (Gardner et al., 2009; Kamanu et al., 2013). This insight provides an interest in comprehensively understanding the function of family-specific mature miRNA, their co-expression, and finding possible inter-miRNA family relationships between miRNAs and specific-target gene modulation (Kamanu et al., 2013). In line with our observation, of the 86 miRNAs levels reported in the 30 selected articles, 4 miRNAs families (mir-29, mir-30, mir-181, and mir-200) were found. Geekiyanage et al. showed significant correlations between MCI to AD progression status and mir-29a, mir-29b, and mir-181c in the regulation of *SPTLC1/2* gene expression, an enzyme involved in the modulation of ceramide levels, which is increased in the cerebral cortices of patients with sporadic AD (Geekiyanage et al., 2012). Furthermore, the mature sequence miR-29b-3p, product of mir-29b isomiR, was downregulated in plasma samples from aMCI subjects in a small Chinese cohort. Molecular evidence indicated that miR-29b-3p might be closely associated with AD pathology by regulating *BACE1* activity (He et al., 2021).

On the other hand, the mir-181 family has been extensively evaluated by several researchers. Agostini et al. have observed a significant correlation of miR-181a-5p levels and *SNAP-25* gene expression, and activity detected in blood in an Italian AD and MCI cohort (Agostini et al., 2019). The *SNAP-25* gene plays a pivotal role in the functional restoration of brain decline observed in neurodegenerative disease (Agostini et al., 2019). Similar results were found by Cai et al., who suggest that the interaction between miRNA and SNAP-25 expression could contribute to the alterations in synaptic functionality, activity, and neuroplasticity observed in the progression of MCI to AD (Cai et al., 2009). Siedlecki-Wullich et al. have shown an increase in miR-181c-5p plasma levels in both MCI and AD subjects. miR-181c-5p have two synaptic proteins as potential targets: neuronal pentraxin 1 (*NPTX1*) and neuronal pentraxin receptor (*NPTXR*) (Siedlecki-Wullich et al., 2019). These proteins are involved in synaptic homeostatic plasticity. Several authors have reported a transient increase in *NPTX1* and *NPTXR* levels in CSF samples in autosomal dominant AD, MCI, and early-stage AD cases (Ringman et al., 2012; Wildsmith et al., 2014; Llano et al., 2017; Duits et al., 2018). A fourth mir-181 family member was found to be upregulated in MCI before conversion to AD. mir-181 levels correlate with an increased CSF Aβ concentration and hippocampal atrophy, suggesting that mir-181c could be involved in the conversion from MCI to AD by regulating Fidgetin, B-cell lymphoma 2, and *SIRT1* genes expression (Ansari et al., 2019). In our integrated analysis of miRNA datasets, it must be noted that mir-181 family members did not show a direct correlation to AD-associated target genes. However, as several studies refer, its association to other targets involved in AD-associated pathways indicate that other biological process may be modulated in addition to those well-known (Cai et al., 2004, 2009; Agostini et al., 2019; Ansari et al., 2019; Siedlecki-Wullich et al., 2019).

Among all miRNA precursor families associated and reported in MCI, we observed one miRNA family upregulated, the mir-200 family. Guedes et al. have shown that mir-200b isomiR was upregulated in blood-derived monocytes and monocyte-derived macrophages samples from a large Portuguese population MCI (Guedes et al., 2016). mir-200b targets the 3' untranslated region of the *APP,* $A\beta_{42,}$ and *MGAT3* genes. Lu et al. reported that serum mir-200b levels in MCI subjects were significantly higher than in AD cases; however, the mir-200b level in AD subjects was lower concerning controls (Liu et al., 2021). This finding suggests

that miRNA families encode more complex intrinsic features than conserved motifs, inter-miRNA family relationships, or imply shared roles in specific biological pathways and regulatory mechanisms that are not yet fully understood.

Regarding longitudinal studies, we observed a significant disadvantage related to the number of subjects analyzed in each study, with the number of subjects studied being <50 subjects with MCI (Sheinerman et al., 2013; Ansari et al., 2019; Kenny et al., 2019). Only one study stands out for analyzing a larger cohort of about 450 subjects with MCI (Xie et al., 2017). Longitudinal studies allow ROC curve analyses, which provide study accuracy, sensitivity, and specificity values that allow predicting the usefulness of these miRNAs as biomarkers capable of predicting the risk of progression from an altered cognitive state to dementia such as AD (Colijn and Grossberg, 2015). In this line, Xie et al. provided a prognostic role of circulating mir-206 in converting from aMCI to AD. According to the mir-206 predictors had as target genes *BDNF* and *SIRT1* genes, which showed that the expression levels of the genes were reduced while the levels of mir-206 were upregulated (Xie et al., 2017).

Genetic regulation is complex, including transcriptional, translational, and posttranslational processes, which are affected by miRNAs directly or indirectly (Kaczkowski et al., 2009; Kamanu et al., 2013; Mushtaq et al., 2016). miRNA targets can be validated experimentally *via* multiple molecular biology techniques. Here, we found that the most used techniques in the literature include qRT-PCR, sequencing, western blotting, miRNA microarrays, and *in situ* hybridization. In addition, we also found that most of the target genes regulated by the 86 miRNAs were *BACE1* and *APP*, two genes highly related to AD. Our dataset identified eight target genes in the same block that were functionally related to AD and dementia. Therefore, the miRNAs (mir-29a, mir-29b, mir107, mir-146a, mir-34c, and miR-130a-3p) in module highly correlated with AD could be considered interesting biomarkers for clinical screening and treatment of early-stage AD (**Figure 3**). This suggests that these miRNAs could play an essential role in regulating cognitive decline and progression to AD.

In order to further explore the validated target genes in the expression module of miRNAs, we selected four predicted target databases to perform the analysis for the miRNAs with validated target genes related to AD or dementia. Empirical validation of miRNAs target is time-consuming and expensive; hence, computational approaches to predict targets have also been developed, such as Tarbase (Papadopoulos et al., 2009), myRTarBase (Hsu et al., 2011), myRecords (Xiao et al., 2009), and Targetscan (Csardi, 2013). The validation methods used to demonstrate the physical interaction between the miRNAs and the target include luciferase reporter assay, PAR-CLIP, CLASH, and HITS-CLIP (Nicolas, 2011). Due to the large volume of data, we selected only those targets validated by the standard gold method (luciferase reporter assay). Among the blue modules, the miRNAs of the target genes involved in AD were mir-107, mir-29b, and miR-130a-3p, whereas red modules, the mir-135, miR-659-3p, miR-491-5p, miR-483-5p, and mir-206, are associated with targets related to other dementias (**Figure 4**). These results suggest that there may be miRNAs related to the early stages of AD. According to our analysis, the mir-181 family, miR-29a-3p, miR-146a-5p, miR-34c-5p, and miR-130a-3p, could be potential biomarkers; however, more research needs to be done to verify these miRNAs as possible biomarkers as well as the target genes they regulate and the neurobiological pathways involved.

CONCLUDING REMARKS

A promising biomarker is the one that is technically easy to measure, is obtained *via* non-invasive techniques, has an excellent sensibility to represent the progression status of a disease or treatment-associated changes as well as specificity to inform a differential diagnostic (Gupta et al., 2013; el Kadmiri et al., 2018). Biomarkers could also confirm a diagnosis or classify a specific cluster of patients, for example, MCI subjects (Lista et al., 2013; Kayano et al., 2016). In this scenario, miRNAs have become promising alternatives because (i) miRNAs can be detected from plasma, urine, saliva, CSF, extracellular fluid, and tissues, (ii) cell-free miRNA are stable in blood samples (Tribolet et al., 2020), (iii) evidence indicates that miRNA expression patterns reflect some aberrant conditions, and sometimes, it shows a time-progression response (Keller et al., 2014), and (iv) miRNAs can be easily detected with qRT-PCR with no considerable time-consuming protocols and economic considerations.

Despite the advances in the biological role of miRNAs, some technical difficulties complicate the transfer of these small molecules to clinical setups as biomarkers. Some problems arise from the high conservative nature of some miRNA families (Kaczkowski et al., 2009), the low concentration of these molecules in biological fluids (Kayano et al., 2016; Yang et al., 2018; Liu et al., 2021), and that generally there is no single miRNA associated with a tissue-specific condition (Mushtaq et al., 2016; Swarbrick et al., 2019); it is more a pattern expression condition, hence it no feasible to use a single miRNAs as a biomarker (He et al., 2021).

Another important factor is that the plasma concentration of brain-enriched miRNA can originate from different sources. Of the total miRNA known to date, ∼70% are expressed in the brain, spinal cord, or peripheral nerves (Adlakha and Saini, 2014) where they play key roles in processes such as neurogenesis (Stappert et al., 2018), synaptic transmission (McGowan et al., 2018) synaptic plasticity (Ye et al., 2016), regulation of the blood-brain barrier integrity, and disease (Ma et al., 2020). Some miRNAs are highly expressed in specific neuronal compartments, such as axons, dendrites, and synapses (Kye et al., 2007), where they are essential for normal neuronal function and survival (Schratt, 2009). Furthermore, dysregulated miRNA levels have been previously linked to impaired learning, memory, and cognition (Wang et al., 2012). Despite that miRNAs are differentially expressed in certain cell types, organs and tissues in many human pathologies (Hua et al., 2009) it is well-known that miRNAs expressed in the brain can cross the blood-brain barrier and be released into the blood circulatory system. In this

context it is reasonable to think that changes in the expression of these miRNA in the blood? can be used to monitor the neurodegeneration that occurs in the brain.

Additionally, the normalization of circulating miRNA concentration is fundamental to infer the technical variability between samples (i.e., the difference in sample volume, processing time, PCR yield, library composition). The normalization strategy depends on which experimental methodology is used to evaluate miRNAs. For qPCR, which is highly used as a platform for the validation of biomarkers, normalization relies on exogenous and endogenous controls or against the total levels of miRNA (Huggett et al., 2005). Nevertheless, the Minimum Information for Publication of Quantitative Real-Time PCR Experiments (MIQE) guidelines indicate that the preferred way to normalize is by using internal reference genes that have the same nature as the molecule being analyzed, hence it is preferable to use two or more endogenous miRNAs as reference genes rather than exogenous miRNAs or lncRNAs. It is important to note that no one-fits-all miRNA endogenous control can be used for every tissue or sample analyzed, so researchers must validate its reference controls in each setting. There are multiple software available that calculate the stability score of each reference controls that can be used to evaluate which control is more stable and which combination of miRNAs have less inter- and intragroup variability (for more information, see BestKeeper, NormFinder, and GeNorm algorithms). Once reference controls are selected, the geometric average of the quantification cycle (Cq) of the endogenous controls is used to normalize the samples. Afterward, the relative expression of miRNAs can be calculated using the $\Delta\Delta$Cq methodology. For high-throughput methodologies, used principally in the screening phase of biomarker discovery, the normalization is based on mathematical approaches, whereas microarrays can be normalized using the mean expression of all miRNAs detected or a quantile normalization.

In the same line, other controls necessary when using plasma and serum samples are hemolysis controls, as hemolysis has been described to alter the detection of circulating miRNAs. Hemolysis can be assessed by either spectrophotometer reads or ratios of specific miRNAs (Shah et al., 2016). Regarding the compensation of biological differences (e.g., changes in microRNAs explained by the permeability of the blood-brain barrier), these are not compensated and in fact, these differences are used to detect a pattern of expression that is putatively the base of a miRNA diagnosis panel. However, in order to make a correct differential diagnosis we need to take into account that MCI can be a precursor to AD, but not all MCI patients develop AD. Furthermore, some MCI patients remain stable, convert back to normal, or progress to non-AD disease, therefore biomarkers with good prediction capacity have been developed using longitudinal studies to evaluate MCI that convert to AD, from those who do not (Shigemizu et al., 2020).

miRNAs are involved in neural development and differentiation; thus, it appears to have a potential role in the development of neurodegenerative diseases such as AD (Moradifard et al., 2018). Since one miRNA could regulate many genes as targets, and those targets can be regulated by several miRNAs, studying the miRNA profile in multifactorial diseases such as AD appears to be a potential advantage (Iqbal and Grundke-Iqbal, 2010). We are confident that the study of the miRNA expression profile could avoid the condition where genes can be up or downregulated by miRNAs. In addition, relationships have been found between the target genes of the dysregulated miRNAs in patients with AD and the biological pathways related to this disease (Moradifard et al., 2018).

On the other hand, in this review we have shown that there are dysregulated miRNAs in early stages of AD such as MCI. Due to the reported relationship between these miRNAs and genes related to AD, specifically *BACE1, MAPT, SNAP-25, SPTLC1/2, TGF -β1,* and *APP* (Geekiyanage et al., 2012; Kumar et al., 2017; Nagaraj et al., 2017; Agostini et al., 2019), establishing a link between these genes and the differential levels of miRNAs at early stages of AD, would allow us to understand their association with biological pathways related to the disease. This link will provide us with an important insight that could considerably contribute to the early diagnosis of AD and the development of preventive therapies.

In summary, we identified five miRNAs expression profiles from peripheral fluid in MCI cases reported in 30 articles, with target genes related to AD. The relationship between AD modules and miRNAs related to MCI show possible candidate miRNAs that may be exploited as fluid biomarkers or therapeutic targets of early-stage AD. However, additional research needs to be used to verify these miRNAs, the target genes they regulate, and the neurobiological pathways involved.

DATA AVAILABILITY STATEMENT

The original contributions presented in the study are included in the article/supplementary material, further inquiries can be directed to the corresponding author/s.

AUTHOR CONTRIBUTIONS

NO, PO, and CD-A developed the study concept and the study design. NO, SS, and PO performed PRISMA analysis. NO and PO performed data analysis and interpretation under the supervision of CD-A. NO, SS, CA, TL, PO, NC-V, CV, and CD-A drafted the manuscript and discussed contributions from all co-authors. MR, CA, and AB provided critical revisions. All authors have participated sufficiently in work and approved the final version of the manuscript for submission.

FUNDING

This work was funded by the Alzheimer's Disease Association 2018-AARG-591107, ANID/FONDEF ID20I10152, ANID/FONDECYT 1210622, and Anillo ACT210096 to CD-A. PO was fully supported by the fellowship of Social Neuroscience and Cognition Ph.D. program from Universidad Adolfo Ibanez.

REFERENCES

Abraha, I., Rimland, J. M., Trotta, F. M., Dell'Aquila, G., Cruz-Jentoft, A., Petrovic, M., et al. (2017). Systematic review of systematic reviews of non-pharmacological interventions to treat behavioural disturbances in older patients with dementia. the SENATOR-OnTop series. *BMJ Open* 7:e012759. doi: 10.1136/bmjopen-2016-012759

Adlakha, Y. K., and Saini, N. (2014). Brain microRNAs and insights into biological functions and therapeutic potential of brain enriched miRNA-128. *Mol. Cancer* 13:33. doi: 10.1186/1476-4598-13-33

Agostini, S., Mancuso, R., Liuzzo, G., Bolognesi, E., Costa, A. S., Bianchi, A., et al. (2019). Serum miRNAs expression and SNAP-25 genotype in Alzheimer's disease. *Front. Aging Neurosci.* 11:52. doi: 10.3389/fnagi.2019.00052

Albert, M. S., DeKosky, S. T., Dickson, D., Dubois, B., Feldman, H. H., Fox, N. C., et al. (2011). The diagnosis of mild cognitive impairment due to Alzheimer's disease: recommendations from the National Institute on Aging-Alzheimer's Association workgroups on diagnostic guidelines for Alzheimer's disease. *Alzheimer's Dement.* 7, 270–279. doi: 10.1016/j.jalz.2011.03.008

Al-Rawaf, H. A., Alghadir, A. H., and Gabr, S. A. (2021). Molecular changes in circulating microRNAs' expression and oxidative stress in adults with mild cognitive impairment: a biochemical and molecular study. *Clin. Interv. Aging* 16, 57–70. doi: 10.2147/CIA.S285689

Alzheimer's Association (2018). 2018 Alzheimer's disease facts and figures. *Alzheimer's Dement.* 14, 110–133. doi: 10.1016/j.jalz.2018.02.001

Ansari, A., Maffioletti, E., Milanesi, E., Marizzoni, M., Frisoni, G. B., Blin, O., et al. (2019). miR-146a and miR-181a are involved in the progression of mild cognitive impairment to Alzheimer's disease. *Neurobiol. Aging* 82, 102–109. doi: 10.1016/j.neurobiolaging.2019.06.005

Arevalo-Rodriguez, I., Smailagic, N., Roqué-Figuls, M., Ciapponi, A., Sanchez-Perez, E., Giannakou, A., et al. (2021). Mini-Mental State Examination (MMSE) for the early detection of dementia in people with mild cognitive impairment (MCI). *Cochr. Datab. Systemat. Rev.* 2021:CD010783. doi: 10.1002/14651858.CD010783.pub3

Bartel, D. P. (2009). microRNAs: target recognition and regulatory functions. *Cell* 136, 215–233. doi: 10.1016/j.cell.2009.01.002

Barthélemy, N. R., Li, Y., Joseph-Mathurin, N., Gordon, B. A., Hassenstab, J., Benzinger, T. L. S., et al. (2020). A soluble phosphorylated tau signature links tau, amyloid and the evolution of stages of dominantly inherited Alzheimer's disease. *Nat. Med.* 26, 398–407. doi: 10.1038/s41591-020-0781-z

Blennow, K., and Hampel, H. (2003). Review CSF markers for incipient Alzheimer's disease CSF markers for incipient AD. *Lancet* 2, 605–613. doi: 10.1016/S1474-4422(03)00530-1

Blennow, K., and Zetterberg, H. (2018). Biomarkers for Alzheimer's disease: current status and prospects for the future. *J. Intern. Med.* 284, 643–663. doi: 10.1111/joim.12816

Bruscoli, M., and Lovestone, S. (2004). Is MCI really just early dementia? A systematic review of conversion studies. *Int. Psychogeriatr.* 16, 129–140. doi: 10.1017/S1041610204000092

Cai, X., Hagedorn, C. H., and Cullen, B. R. (2004). Human microRNAs are processed from capped, polyadenylated transcripts that can also function as mRNAs. *RNA* 10, 1957–1966. doi: 10.1261/rna.7135204

Cai, Y., Yu, X., Hu, S., and Yu, J. (2009). A brief review on the mechanisms of miRNA regulation. *Genom. Proteom. Bioinformat.* 7, 147–154. doi: 10.1016/S1672-0229(08)60044-3

Campbell, N. L., Unverzagt, F., LaMantia, M. A., Khan, B. A., and Boustani, M. A. (2013). Risk factors for the progression of mild cognitive impairment to dementia. *Clin. Geriatr. Med.* 29, 873–893. doi: 10.1016/j.cger.2013.07.009

Chandler, M. J., Parks, A. C., Marsiske, M., Rotblatt, L. J., and Smith, G. E. (2016). Everyday impact of cognitive interventions in mild cognitive impairment: a systematic review and meta-analysis. *Neuropsychol. Rev.* 26:4. doi: 10.1007/s11065-016-9330-4

Chen, T., bin, Lee, Y. J., Lin, S. Y., Chen, J. P., Hu, C. J., Wang, P. N., et al. (2019). Plasma Aβ42 and total tau predict cognitive decline in amnestic mild cognitive impairment. *Sci. Rep.* 9:13984. doi: 10.1038/s41598-019-50315-9

Chen, X., Ba, Y., Ma, L., Cai, X., Yin, Y., Wang, K., et al. (2008). Characterization of microRNAs in serum: a novel class of biomarkers for diagnosis of cancer and other diseases. *Cell Res.* 18, 997–1006. doi: 10.1038/cr.2008.282

Chiu, M. J., Chen, Y. F., Chen, T. F., Yang, S. Y., Yang, F. P. G., Tseng, T. W., et al. (2014). Plasma tau as a window to the brain-negative associations with brain volume and memory function in mild cognitive impairment and early alzheimer's disease. *Hum. Brain Map.* 35, 3132–3142. doi: 10.1002/hbm.22390

Chouraki, V., Beiser, A., Younkin, L., Preis, S. R., Weinstein, G., Hansson, O., et al. (2015). Plasma amyloid-β and risk of Alzheimer's disease in the Framingham Heart Study. *Alzheimer's Dement.* 11, 249–257.e1. doi: 10.1016/j.jalz.2014.07.001

Ciesielska, N., Sokołowski, R., Mazur, E., Podhorecka, M., Polak-Szabela, A., and Kedziora-Kornatowska, K. (2016). Is the Montreal Cognitive Assessment (MoCA) test better suited than the Mini-Mental State Examination (MMSE) in mild cognitive impairment (MCI) detection among people aged over 60? Meta-analysis. *Psychiatr. Polska* 50:45368. doi: 10.12740/PP/45368

Colijn, M. A., and Grossberg, G. T. (2015). Amyloid and tau biomarkers in subjective cognitive impairment. *J. Alzheimer's Dis.* 47, 1–8. doi: 10.3233/JAD-150180

Csardi, G. (2013). *targetscan.Hs.eg.db: TargetScan miRNA target predictions for human.* R package version 0.6.1. doi: 10.18129/B9.bioc.targetscan.Hs.eg.db

Dage, J. L., Wennberg, A. M. V., Airey, D. C., Hagen, C. E., Knopman, D. S., Machulda, M. M., et al. (2016). Levels of tau protein in plasma are associated with neurodegeneration and cognitive function in a population-based elderly cohort. *Alzheimer's Dement.* 12, 1226–1234. doi: 10.1016/j.jalz.2016.06.001

Danka Mohammed, C. P., Park, J. S., Nam, H. G., and Kim, K. (2017). MicroRNAs in brain aging. *Mech. Ageing Dev.* 168, 3–9. doi: 10.1016/j.mad.2017.01.007

de Felice, B., Montanino, C., Oliva, M., Bonavita, S., di Onofrio, V., and Coppola, C. (2020). MicroRNA expression signature in mild cognitive impairment due to Alzheimer's disease. *Mol. Neurobiol.* 57, 4408–4416. doi: 10.1007/s12035-020-02029-7

DeCarli, C. (2003). Mild cognitive impairment: prevalence, prognosis, aetiology, and treatment. *Lancet Neurol.* 2, 15–21. doi: 10.1016/S1474-4422(03)00262-X

Dong, H., Li, J., Huang, L., Chen, X., Li, D., Wang, T., et al. (2015). Serum MicroRNA profiles serve as novel biomarkers for the diagnosis of alzheimer's disease. *Dis. Markers* 2015:625659. doi: 10.1155/2015/625659

Duits, F. H., Brinkmalm, G., Teunissen, C. E., Brinkmalm, A., Scheltens, P., van der Flier, W. M., et al. (2018). Synaptic proteins in CSF as potential novel biomarkers for prognosis in prodromal Alzheimer's disease. *Alzheimer's Res. Ther.* 10:5. doi: 10.1186/s13195-017-0335-x

Dunne, R. A., Aarsland, D., O'Brien, J. T., Ballard, C., Banerjee, S., Fox, N. C., et al. (2021). Mild cognitive impairment: the manchester consensus. *Age Ageing* 50, 72–80. doi: 10.1093/ageing/afaa228

el Kadmiri, N., Said, N., Slassi, I., el Moutawakil, B., and Nadifi, S. (2018). Biomarkers for Alzheimer disease: classical and novel candidates' review. *Neuroscience* 370, 181–190. doi: 10.1016/j.neuroscience.2017.07.017

Espino, D. v., Lichtenstein, M. J., Palmer, R. F., and Hazuda, H. P. (2001). Ethnic differences in Mini-Mental State Examination (MMSE) scores: where you live makes a difference. *J. Am. Geriatr. Soc.* 49, 538–548. doi: 10.1046/j.1532-5415.2001.49111.x

Falcon, C., Tucholka, A., Monté-Rubio, G. C., Cacciaglia, R., Operto, G., Rami, L., et al. (2018). Longitudinal structural cerebral changes related to core CSF biomarkers in preclinical Alzheimer's disease: a study of two independent datasets. *NeuroImage Clin.* 19, 190–201. doi: 10.1016/j.nicl.2018.04.016

Fei, M., Jianghua, W., Rujuan, M., Wei, Z., and Qian, W. (2011). The relationship of plasma Aβ levels to dementia in aging individuals with mild cognitive impairment. *J. Neurol. Sci.* 305, 92–96. doi: 10.1016/j.jns.2011.03.005

Fennema-Notestine, C., McEvoy, L. K., Hagler, D. J., Jacobson, M. W., and Dale, A. M. (2009). Structural neuroimaging in the detection and prognosis of pre-clinical and early AD. *Behav. Neurol.* 21, 1669–1674. doi: 10.1155/2009/698156

Forlenza, O. v., Radanovic, M., Talib, L. L., Aprahamian, I., Diniz, B. S., Zetterberg, H., et al. (2015). Cerebrospinal fluid biomarkers in Alzheimer's disease: diagnostic accuracy and prediction of dementia. *Alzheimer's Dement.* 1, 455–463. doi: 10.1016/j.dadm.2015.09.003

Gagnon, K., Baril, A., Cary, A., Lafond, C., Gagnon, J., and Gosselin, N. (2013). Mild cognitive impairment in obstructive sleep apnea. *Sleep Med.* 14, 816–817. doi: 10.1016/j.sleep.2013.11.296

Gardner, P. P., Daub, J., Tate, J. G., Nawrocki, E. P., Kolbe, D. L., Lindgreen, S., et al. (2009). Rfam: updates to the RNA families database. *Nucl. Acids Res.* 37, 136–140. doi: 10.1093/nar/gkn766

Geekiyanage, H., Jicha, G. A., Nelson, P. T., and Chan, C. (2012). Blood serum miRNA: non-invasive biomarkers for Alzheimer's disease. *Exp. Neurol.* 235, 491–496. doi: 10.1016/j.expneurol.2011.11.026

Gilad, S., Meiri, E., Yogev, Y., Benjamin, S., Lebanony, D., Yerushalmi, N., et al. (2008). Serum microRNAs are promising novel biomarkers. *PLoS ONE* 3:e3148. doi: 10.1371/journal.pone.0003148

Giliberto, L., Assini, A., Cammarata, S., Colucci, M., Borghi, R., Piccini, A., et al. (2004). P2-261 plasma levels of amyloid beta-protein 42 are increased in women with mild cognitive impairment. *Neurobiol. Aging* 25, 828–831. doi: 10.1016/S0197-4580(04)81007-8

Graff-Radford, N. R., Crook, J. E., Lucas, J., Boeve, B. F., Knopman, D. S., Ivnik, R. J., et al. (2007). Association of low plasma Aβ42/Aβ40 ratios with increased imminent risk for mild cognitive impairment and Alzheimer disease. *Archiv. Neurol.* 64, 354–362. doi: 10.1001/archneur.64.3.354

Griffiths-Jones, S., Grocock, R. J., van Dongen, S., Bateman, A., and Enright, A. J. (2006). miRBase: microRNA sequences, targets and gene nomenclature. *Nucl. Acids Res.* 34, 140–144. doi: 10.1093/nar/gkj112

Griffiths-Jones, S., Saini, H. K., van Dongen, S., and Enright, A. J. (2008). miRBase: tools for microRNA genomics. *Nucl. Acids Res.* 36, 154–158. doi: 10.1093/nar/gkm952

Grill, J. D., Di, L., Lu, P. H., Lee, C., Ringman, J., Apostolova, L. G., et al. (2013). Estimating sample sizes for predementia Alzheimer's trials based on the Alzheimer's disease neuroimaging initiative. *Neurobiol. Aging* 34, 62–72. doi: 10.1016/j.neurobiolaging.2012.03.006

Guedes, J. R., Santana, I., Cunha, C., Duro, D., Almeida, M. R., Cardoso, A. M., et al. (2016). MicroRNA deregulation and chemotaxis and phagocytosis impairment in Alzheimer's disease. *Alzheimer's Dement.* 3, 7–17. doi: 10.1016/j.dadm.2015.11.004

Gupta, V. B., Sundaram, R., and Martins, R. N. (2013). Multiplex biomarkers in blood. *Alzheimer's Res. Ther.* 5:31. doi: 10.1186/alzrt185

Habert, M. O., Horn, J. F., Sarazin, M., Lotterie, J. A., Puel, M., Onen, F., et al. (2011). Brain perfusion SPECT with an automated quantitative tool can identify prodromal Alzheimer's disease among patients with mild cognitive impairment. *Neurobiol. Aging* 32, 15–23. doi: 10.1016/j.neurobiolaging.2009.01.013

Hampel, H., O'Bryant, S. E., Molinuevo, J. L., Zetterberg, H., Masters, C. L., Lista, S., et al. (2018). Blood-based biomarkers for Alzheimer disease: mapping the road to the clinic. *Nat. Rev. Neurol.* 14, 639–652. doi: 10.1038/s41582-018-0079-7

Hanon, O., Vidal, J. S., Lehmann, S., Bombois, S., Allinquant, B., Tréluyer, J. M., et al. (2018). Plasma amyloid levels within the Alzheimer's process and correlations with central biomarkers. *Alzheimer's Dement.* 14, 858–868. doi: 10.1016/j.jalz.2018.01.004

Hansson, O., Seibyl, J., Stomrud, E., Zetterberg, H., Trojanowski, J. Q., Bittner, T., et al. (2018). CSF biomarkers of Alzheimer's disease concord with amyloid-β PET and predict clinical progression: a study of fully automated immunoassays in BioFINDER and ADNI cohorts. *Alzheimer's Dement.* 14, 1470–1481. doi: 10.1016/j.jalz.2018.01.010

Hansson, O., Zetterberg, H., Buchhave, P., Londos, E., Blennow, K., and Minthon, L. (2006). Association between CSF biomarkers and incipient Alzheimer's disease in patients with mild cognitive impairment: a follow-up study. *Lancet Neurol.* 5, 228–234. doi: 10.1016/S1474-4422(06)70355-6

He, H., Liu, A., Zhang, W., Yang, H., Zhang, M., Xu, H., et al. (2021). Novel plasma miRNAs as biomarkers and therapeutic targets of Alzheimer's disease at the prodromal stage. *J. Alzheimer's Dis.* 83, 779–790. doi: 10.3233/JAD-210307

Herukka, S. K., Hallikainen, M., Soininen, H., and Pirttilä, T. (2005). CSF Aβ42 and tau or phosphorylated tau and prediction of progressive mild cognitive impairment. *Neurology* 64, 1294–1297. doi: 10.1212/01.WNL.0000156914.16988.56

Hill, N. T. M., Mowszowski, L., Naismith, S. L., Chadwick, V. L., Valenzuela, M., and Lampit, A. (2017). Computerized cognitive training in older adults with mild cognitive impairment or dementia: a systematic review and meta-analysis. *Am. J. Psychiatr.* 174, 329–340. doi: 10.1176/appi.ajp.2016.16030360

Hsu, S., da, Lin, F. M., Wu, W. Y., Liang, C., Huang, W. C., Chan, W. L., et al. (2011). MiRTarBase: a database curates experimentally validated microRNA-target interactions. *Nucl. Acids Res.* 39, 163–169. doi: 10.1093/nar/gkq1107

Hua, Y. J., Tang, Z. Y., Tu, K., Zhu, L., Li, Y. X., Xie, L., et al. (2009). Identification and target prediction of miRNAs specifically expressed in rat neural tissue. *BMC Genom.* 10:214. doi: 10.1186/1471-2164-10-214

Huggett, J., Dheda, K., Bustin, S., and Zumla, A. (2005). Real-time RT-PCR normalisation; strategies and considerations. *Genes Immun.* 6, 279–284. doi: 10.1038/sj.gene.6364190

Hulette, C. M., Welsh-Bohmer, K. A., Murray, M. G., Saunders, A. M., Mash, D. C., and McIntyre, L. M. (1998). Neuropathological and neurolasychological changes in "normal" aging: evidence for preclinical Alzheimer Disease in cognitively normal individuals. *J. Neuropathol. Exp. Neurol.* 57, 1168–1174. doi: 10.1097/00005072-199812000-00009

Iqbal, K., and Grundke-Iqbal, I. (2010). Alzheimer's disease, a multifactorial disorder seeking multitherapies. *Alzheimer's Dement.* 6, 420–424. doi: 10.1016/j.jalz.2010.04.006

Irizarry, M. C. (2004). Biomarkers of Alzheimer disease in plasma. *NeuroRx* 1, 226–234. doi: 10.1602/neurorx.1.2.226

Janelidze, S., Mattsson, N., Palmqvist, S., Smith, R., Beach, T. G., Serrano, G. E., et al. (2020). Plasma P-tau181 in Alzheimer's disease: relationship to other biomarkers, differential diagnosis, neuropathology and longitudinal progression to Alzheimer's dementia. *Nat. Med.* 26, 379–386. doi: 10.1038/s41591-020-0755-1

Kaczkowski, B., Torarinsson, E., Reiche, K., Havgaard, J. H., Stadler, P. F., and Gorodkin, J. (2009). Structural profiles of human miRNA families from pairwise clustering. *Bioinformatics* 25, 291–294. doi: 10.1093/bioinformatics/btn628

Kamanu, T. K. K., Radovanovic, A., Archer, J. A. C., and Bajic, V. B. (2013). Exploration of miRNA families for hypotheses generation. *Sci. Rep.* 3:2940. doi: 10.1038/srep02940

Karikari, T. K., Pascoal, T. A., Ashton, N. J., Janelidze, S., Benedet, A. L., Rodriguez, J. L., et al. (2020). Blood phosphorylated tau 181 as a biomarker for Alzheimer's disease: a diagnostic performance and prediction modelling study using data from four prospective cohorts. *Lancet Neurol.* 19, 422–433. doi: 10.1016/S1474-4422(20)30071-5

Kasper, S., Bancher, C., Eckert, A., Förstl, H., Frölich, L., Hort, J., et al. (2020). Management of mild cognitive impairment (MCI): the need for national and international guidelines. *World J. Biol. Psychiatr.* 21, 579–594. doi: 10.1080/15622975.2019.1696473

Kayano, M., Higaki, S., Satoh, J. I., Matsumoto, K., Matsubara, E., Takikawa, O., et al. (2016). Plasma microRNA biomarker detection for mild cognitive impairment using differential correlation analysis. *Biomarker Res.* 4:22. doi: 10.1186/s40364-016-0076-1

Keller, A., Backes, C., Haas, J., Leidinger, P., Maetzler, W., Deuschle, C., et al. (2016). Validating Alzheimer's disease micro RNAs using next-generation sequencing. *Alzheimer's Dement.* 12, 565–576. doi: 10.1016/j.jalz.2015.12.012

Keller, A., Leidinger, P., Vogel, B., Backes, C., ElSharawy, A., Galata, V., et al. (2014). miRNAs can be generally associated with human pathologies as exemplified for miR-144. *BMC Med.* 12:224. doi: 10.1186/s12916-014-0224-0

Kenny, A., McArdle, H., Calero, M., Rabano, A., Madden, S. F., Adamson, K., et al. (2019). Elevated plasma microRNA-206 levels predict cognitive decline and progression to dementia from mild cognitive impairment. *Biomolecules* 9:734. doi: 10.3390/biom9110734

Kim, S. H., Seo, S. W., Yoon, D. S., Chin, J., Lee, B. H., Cheong, H. K., et al. (2010). Comparison of neuropsychological and fdg-pet findings between early- versus late-onset mild cognitive impairment: a five-year longitudinal study. *Dement. Geriatr. Cogn. Disord.* 29, 213–223. doi: 10.1159/000278422

Koepsell, T. D., and Monsell, S. E. (2012). Reversion from mild cognitive impairment to normal or near-Normal cognition; risk factors and prognosis. *Neurology* 79, 1591–1598. doi: 10.1212/WNL.0b013e31826e26b7

Kosaka, N., Iguchi, H., Yoshioka, Y., Takeshita, F., Matsuki, Y., and Ochiya, T. (2010). Secretory mechanisms and intercellular transfer of microRNAs in living cells. *J. Biol. Chem.* 285, 17442–17452. doi: 10.1074/jbc.M110.107821

Koychev, I., Vaci, N., Bilgel, M., An, Y., Muniz, G. T., Wong, D. F., et al. (2020). Prediction of rapid amyloid and phosphorylated-Tau accumulation in cognitively healthy individuals. *Alzheimer's Dement.* 12:e12019. doi: 10.1002/dad2.12019

Kumar, S., Vijayan, M., and Reddy, P. H. (2017). MicroRNA-455-3p as a potential peripheral biomarker for Alzheimer's disease. *Hum. Mol. Genet.* 26, 3808–3822. doi: 10.1093/hmg/ddx267

Kye, M. J., Liu, T., Levy, S. F., Nan, L. X., Groves, B. B., Bonneau, R., et al. (2007). Somatodendritic microRNAs identified by laser capture and multiplex RT-PCR. *RNA* 13, 1224–1234. doi: 10.1261/rna.480407

Langa, K. M., and Levine, D. A. (2014). The diagnosis and management of mild cognitive impairment: a clinical review. *J. Am. Med. Assoc.* 312, 2551–2561. doi: 10.1001/jama.2014.13806

Larry Sparks, D., Kryscio, R. J., Sabbagh, M. N., Ziolkowski, C., Lin, Y., Sparks, L. M., et al. (2012). Tau is reduced in AD plasma and validation of employed ELISA methods. *Am. J. Neurodegener. Dis.* 1, 99–106.

Lashley, T., Schott, J. M., Weston, P., Murray, C. E., Wellington, H., Keshavan, A., et al. (2018). Molecular biomarkers of Alzheimer's disease: progress and prospects. *Dis. Models Mechanism.* 11:dmm031781. doi: 10.1242/dmm.031781

Li, F., Xie, X. Y., Sui, X. F., Wang, P., Chen, Z., and Zhang, J. B. (2020). Profile of pathogenic proteins and MicroRNAs in plasma-derived extracellular vesicles in Alzheimer's disease: a pilot study. *Neuroscience* 432, 240–246. doi: 10.1016/j.neuroscience.2020.02.044

Li, W., Li, X., Xin, X., Kan, P. C., and Yan, Y. (2016). MicroRNA-613 regulates the expression of brain-derived neurotrophic factor in Alzheimer's disease. *BioSci. Trends* 10, 372–377. doi: 10.5582/bst.2016.01127

Licursi, V., Conte, F., Fiscon, G., and Paci, P. (2019). MIENTURNET: an interactive web tool for microRNA-target enrichment and network-based analysis. *BMC Bioinformat.* 20:545. doi: 10.1186/s12859-019-3105-x

Lista, S., Faltraco, F., Prvulovic, D., and Hampel, H. (2013). Blood and plasma-based proteomic biomarker research in Alzheimer's disease. *Progr. Neurobiol.* 101–102, 1–17. doi: 10.1016/j.pneurobio.2012.06.007

Liu, C. G., Song, J., Zhang, Y. Q., and Wang, P. C. (2014a). MicroRNA-193b is a regulator of amyloid precursor protein in the blood and cerebrospinal fluid derived exosomal microRNA-193b is a biomarker of Alzheimer's disease. *Mol. Med. Rep.* 10, 2395–2400. doi: 10.3892/mmr.2014.2484

Liu, C. G., Wang, J. L., Li, L., and Wang, P. C. (2014b). MicroRNA-384 regulates both amyloid precursor protein and β-secretase expression and is a potential biomarker for Alzheimer's disease. *Int. J. Mol. Med.* 34, 160–166. doi: 10.3892/ijmm.2014.1780

Liu, C. G., Wang, J. L., Li, L., Xue, L. X., Zhang, Y. Q., and Wang, P. C. (2014c). MicroRNA-135a and−200b, potential biomarkers for Alzheimer's disease, regulate β secretase and amyloid precursor protein. *Brain Res.* 1583, 55–64. doi: 10.1016/j.brainres.2014.04.026

Liu, C. G., Zhao, Y., Lu, Y., and Wang, P. C. (2021). ABCA1-labeled exosomes in serum contain higher MicroRNA-193b levels in Alzheimer's disease. *BioMed Res. Int.* 2021:5450397. doi: 10.1155/2021/5450397

Livingston, G., Huntley, J., Sommerlad, A., Ames, D., Ballard, C., Banerjee, S., et al. (2020). Dementia prevention, intervention, and care: 2020 report of the Lancet Commission. *Lancet* 396, 413–446. doi: 10.1016/S0140-6736(20)30367-6

Livingston, G., Sommerlad, A., Orgeta, V., Costafreda, S. G., Huntley, J., Ames, D., et al. (2017). Dementia prevention, intervention, and care. *Lancet* 390, 2673–2734. doi: 10.1016/S0140-6736(17)31363-6

Llano, D. A., Bundela, S., Mudar, R. A., and Devanarayan, V. (2017). A multivariate predictive modeling approach reveals a novel CSF peptide signature for both Alzheimer's Disease state classification and for predicting future disease progression. *PLoS ONE* 12:e0182098. doi: 10.1371/journal.pone.0182098

Loi, S. M., Eratne, D., Kelso, W., Velakoulis, D., and Looi, J. C. L. (2018). Alzheimer disease: non-pharmacological and pharmacological management of cognition and neuropsychiatric symptoms. *Austral. Psychiatr.* 26, 358–365. doi: 10.1177/1039856218766123

Lu, Y., Tan, L., and Wang, X. (2019). Circular HDAC9/microRNA-138/Sirtuin-1 pathway mediates synaptic and amyloid precursor protein processing deficits in Alzheimer's disease. *Neurosci. Bullet.* 35, 877–888. doi: 10.1007/s12264-019-00361-0

Lugli, G., Torvik, V. I., Larson, J., and Smalheiser, N. R. (2008). Expression of microRNAs and their precursors in synaptic fractions of adult mouse forebrain. *J. Neurochem.* 106, 650–661. doi: 10.1111/j.1471-4159.2008.05413.x

Ma, F., Zhang, X., and Yin, K. J. (2020). MicroRNAs in central nervous system diseases: a prospective role in regulating blood-brain barrier integrity. *Exp. Neurol.* 323:113094. doi: 10.1016/j.expneurol.2019.113094

Makizako, H., Shimada, H., Doi, T., Tsutsumimoto, K., Hotta, R., Nakakubo, S., et al. (2016). Comorbid mild cognitive impairment and depressive symptoms predict future dementia in community older adults: a 24-month follow-up longitudinal study. *J. Alzheimer's Dis.* 54, 1473–1482. doi: 10.3233/JAD-160244

Matallana, D., de Santacruz, C., Cano, C., Reyes, P., Samper-Ternent, R., Markides, K. S., et al. (2011). The relationship between education level and mini-mental state examination domains among older Mexican Americans. *J. Geriatr. Psychiatr. Neurol.* 24, 9–18. doi: 10.1177/0891988710373597

Mathelier, A., and Carbone, A. (2013). Large scale chromosomal mapping of human microRNA structural clusters. *Nucl. Acids Res.* 41, 4392–4408. doi: 10.1093/nar/gkt112

Mattsson, N., Zetterberg, H., Janelidze, S., Insel, P. S., Andreasson, U., Stomrud, E., et al. (2016). Plasma tau in Alzheimer disease. *Neurology* 87, 1827–1835. doi: 10.1212/WNL.0000000000003246

Mattsson-Carlgren, N., Janelidze, S., Palmqvist, S., Cullen, N., Svenningsson, A. L., Strandberg, O., et al. (2021). Longitudinal plasma p-tau217 is increased in early stages of Alzheimer's disease. *Brain* 143, 3234–3241. doi: 10.1093/brain/awaa286

McGowan, H., Mirabella, V. R., Hamod, A., Karakhanyan, A., Mlynaryk, N., Moore, J. C., et al. (2018). hsa-let-7c miRNA regulates synaptic and neuronal function in human neurons. *Front. Synapt. Neurosci.* 10:19. doi: 10.3389/fnsyn.2018.00019

McNeill, E., and van Vactor, D. (2012). MicroRNAs shape the neuronal landscape. *Neuron* 75, 169–175. doi: 10.1016/j.neuron.2012.07.005

Mitchell, A. J., and Shiri-Feshki, M. (2009). Rate of progression of mild cognitive impairment to dementia - meta-analysis of 41 robust inception cohort studies. *Acta Psychiatr. Scand.* 119, 252–265. doi: 10.1111/j.1600-0447.2008.01326.x

Moradifard, S., Hoseinbeyki, M., Ganji, S. M., and Minuchehr, Z. (2018). Analysis of microRNA and gene expression profiles in Alzheimer's disease: a meta-analysis approach. *Sci. Rep.* 8:4767. doi: 10.1038/s41598-018-20959-0

Mushtaq, G. H., Greig, N., Anwar, F., Zamzami, M. A., Choudhry, H., Shaik, M. M., et al. (2016). miRNAs as circulating biomarkers for Alzheimer's disease and Parkinson's disease. *Med. Chem.* 12, 217–225. doi: 10.2174/1573406411666151030112140

Nagaraj, S., Laskowska-Kaszub, K., Debski, K. J., Wojsiat, J., Dabrowski, M., Gabryelewicz, T., et al. (2017). Profile of 6 microRNA in blood plasma distinguish early stage Alzheimer's disease patients from non-demented subjects. *Oncotarget* 8, 16122–16143. doi: 10.18632/oncotarget.15109

Nasreddine, Z. S., Phillips, N. A., Bédirian, V., Charbonneau, S., Whitehead, V., Collin, I., et al. (2005). The Montreal Cognitive Assessment, MoCA: a brief screening tool for mild cognitive impairment. *J. Am. Geriatr. Soc.* 53, 695–699. doi: 10.1111/j.1532-5415.2005.53221.x

Nicolas, F. E. (2011). Experimental validation of microRNA targets using a luciferase reporter system. *Methods Mol. Biol.* 732, 139–152. doi: 10.1007/978-1-61779-083-6_11

O'Carroll, D., and Schaefer, A. (2013). General principals of miRNA biogenesis and regulation in the brain. *Neuropsychopharmacology* 38, 39–54. doi: 10.1038/npp.2012.87

O'Driscoll, C., and Shaikh, M. (2017). Cross-cultural applicability of the Montreal Cognitive Assessment (MoCA): a systematic review. *J. Alzheimer's Dis.* 58, 789–801. doi: 10.3233/JAD-161042

Okonkwo, O. C., Alosco, M. L., Griffith, H. R., Mielke, M. M., Shaw, L. M., Trojanowski, J. Q., et al. (2010). Cerebrospinal fluid abnormalities and rate of decline in everyday function across the dementia spectrum: normal aging, mild cognitive impairment, and Alzheimer disease. *Archiv. Neurol.* 67, 688–696. doi: 10.1001/archneurol.2010.118

Page, M. J., McKenzie, J. E., Bossuyt, P. M., Boutron, I., Hoffmann, T. C., Mulrow, C. D., et al. (2021). The PRISMA 2020 statement: an updated guideline for reporting systematic reviews. *BMJ* 372:n71. doi: 10.1136/bmj.n71

Panza, F., D'Introno, A., Colacicco, A. M., Capurso, C., del Parigi, A., Caselli, R. J., et al. (2005). Current epidemiology of mild cognitive impairment and other predementia syndromes. *Am. J. Geriatr. Psychiatr.* 13, 267–275. doi: 10.1097/00019442-200508000-00002

Papadopoulos, G. L., Reczko, M., Simossis, V. A., Sethupathy, P., and Hatzigeorgiou, A. G. (2009). The database of experimentally supported targets: a functional update of TarBase. *Nucl. Acids Res.* 37, 155–158. doi: 10.1093/nar/gkn809

Parnetti, L., Chiasserini, D., Eusebi, P., Giannandrea, D., Bellomo, G., de Carlo, C., et al. (2012). Performance of Aβ1-40, Aβ1-42, total tau, and phosphorylated tau as predictors of dementia in a cohort of patients with mild cognitive impairment. *J. Alzheimer's Dis.* 29, 229–238. doi: 10.3233/JAD-2011-111349

Petersen, R. C. (2004). Mild cognitive impairment as a diagnostic entity. *J. Internal Med.* 256, 183–194. doi: 10.1111/j.1365-2796.2004.01388.x

Petersen, R. C., Caracciolo, B., Brayne, C., Gauthier, S., Jelic, V., and Fratiglioni, L. (2014). Mild cognitive impairment: a concept in evolution. *J. Internal Med.* 275, 214–228. doi: 10.1111/joim.12190

Petersen, R. C., Doody, R., Kurz, A., Mohs, R. C., Morris, J. C., Rabins, P., et al. (2001). Current concepts in mild cognitive impairment. *Archiv. Neurol.* 58, 1985–1992. doi: 10.1001/archneur.58.12.1985

Petersen, R. C., Smith, G. E., Waring, S. C., Ivnik, R. J., Tangalos, E. G., and Kokmen, E. (1999). Mild cognitive impairment: clinical characterization and outcome. *Archiv. Neurol.* 56, 303–308. doi: 10.1001/archneur.56.3.303

Pichardo-Casas, I., Goff, L. A., Swerdel, M. R., Athie, A., Davila, J., Ramos-Brossier, M., et al. (2012). Expression profiling of synaptic microRNAs from the adult rat brain identifies regional differences and seizure-induced dynamic modulation. *Brain Res.* 1436, 20–33. doi: 10.1016/j.brainres.2011.12.001

Pinto, C., and Subramanyam, A. A. (2009). Mild cognitive impairment: the dilemma. *Indian J. Psychiatr.* 51(Suppl.1), S44–S51.

Pinto, T. C. C., Machado, L., Bulgacov, T. M., Rodrigues-Júnior, A. L., Costa, M. L. G., Ximenes, R. C. C., et al. (2019). Is the Montreal Cognitive Assessment (MoCA) screening superior to the Mini-Mental State Examination (MMSE) in the detection of mild cognitive impairment (MCI) and Alzheimer's Disease (AD) in the elderly? *Int. Psychogeriatr.* 31, 491–504. doi: 10.1017/S1041610218001370

Qiu, L., Zhang, W., Tan, E. K., and Zeng, L. (2014). Deciphering the function and regulation of microRNAs in Alzheimer's disease and Parkinson's disease. *ACS Chem. Neurosci.* 5, 884–894. doi: 10.1021/cn500149w

Qu, Y., Ma, Y. H., Huang, Y. Y., Ou, Y. N., Shen, X. N., Chen, S. D., et al. (2021). Blood biomarkers for the diagnosis of amnestic mild cognitive impairment and Alzheimer's disease: a systematic review and meta-analysis. *Neurosci. Biobehav. Rev.* 128, 479–486. doi: 10.1016/j.neubiorev.2021.07.007

Rabinovici, G. D., Gatsonis, C., Apgar, C., Chaudhary, K., Gareen, I., Hanna, L., et al. (2019). Association of amyloid positron emission tomography with subsequent change in clinical management among medicare beneficiaries with mild cognitive impairment or dementia. *J. Am. Med. Assoc.* 321, 1939–1949. doi: 10.1001/jama.2019.2000

Reddy, P. H., Williams, J., Smith, F., Bhatti, J. S., Kumar, S., Vijayan, M., et al. (2017). MicroRNAs, aging, cellular senescence, and Alzheimer's disease. *Progr. Mol. Biol. Transl. Sci.* 146, 127–171. doi: 10.1016/bs.pmbts.2016.12.009

Ringman, J. M., Schulman, H., Becker, C., Jones, T., Bai, Y., Immermann, F., et al. (2012). Proteomic changes in cerebrospinal fluid of presymptomatic and affected persons carrying familial Alzheimer disease mutations. *Archiv. Neurol.* 69. doi: 10.1001/archneurol.2011.642

Roderburg, C., and Luedde, T. (2014). Circulating microRNAs as markers of liver inflammation, fibrosis and cancer. *J. Hepatol.* 61, 1434–1437. doi: 10.1016/j.jhep.2014.07.017

Rovner, B. W., Casten, R. J., Hegel, M. T., and Leiby, B. (2018). Preventing cognitive decline in black individuals with mild cognitive impairment: a randomized clinical trial. *J Am Med Assoc Neurol.* 75, 1487–1493. doi: 10.1001/jamaneurol.2018.2513

Ruepp, A., Kowarsch, A., Schmidl, D., Buggenthin, F., Brauner, B., Dunger, I., et al. (2010). PhenomiR: a knowledgebase for microRNA expression in diseases and biological processes. *Genome Biol.* 11:R6. doi: 10.1186/gb-2010-11-1-r6

Russ, T. C., and Morling, J. R. (2012). Cholinesterase inhibitors for mild cognitive impairment. *Cochr. Datab. Systemat. Rev.* 2012:CD009132. doi: 10.1002/14651858.CD009132.pub2

Sachdev, P. S., Lipnicki, D. M., Kochan, N. A., Crawford, J. D., Thalamuthu, A., Andrews, G., et al. (2015). The prevalence of mild cognitive impairment in diverse geographical and ethnocultural regions: the COSMIC collaboration. *PLoS ONE* 10:e0142388. doi: 10.1371/journal.pone.0142388

Salama, I. I., Salama, S. I., Elmosalami, D. M., Saleh, R. M., Rasmy, H., Ibrahim, M. H., et al. (2019). Risk factors associated with mild cognitive impairment among apparently healthy people and the role of microRNAs. *Open Access Macedonian J. Med. Sci.* 7, 3253–3261. doi: 10.3889/oamjms.2019.834

Saliminejad, K., Khorram Khorshid, H. R., Soleymani Fard, S., and Ghaffari, S. H. (2019). An overview of microRNAs: biology, functions, therapeutics, and analysis methods. *J. Cell. Physiol.* 234, 1–15. doi: 10.1002/jcp.27486

Schratt, G. (2009). MicroRNAs at the synapse. *Nat. Rev. Neurosci.* 10, 842–849. doi: 10.1038/nrn2763

Schwarzenbach, H., Nishida, N., Calin, G. A., and Pantel, K. (2014). Clinical relevance of circulating cell-free microRNAs in cancer. *Nat. Rev. Clin. Oncol.* 11, 145–156. doi: 10.1038/nrclinonc.2014.5

Seppälä, T. T., Herukka, S. K., Hänninen, T., Tervo, S., Hallikainen, M., Soininen, H., et al. (2010). Plasma Aβ42 and Aβ40 as markers of cognitive change in follow-up: a prospective, longitudinal, population-based cohort study. *J. Neurol. Neurosurg. Psychiatr.* 81, 1123–1127. doi: 10.1136/jnnp.2010.205757

Shah, J. S., Soon, P. S., and Marsh, D. J. (2016). Comparison of methodologies to detect low levels of hemolysis in serum for accurate assessment of serum microRNAs. *PLoS ONE* 11:e0153200. doi: 10.1371/journal.pone.0153200

Shannon, P., Markiel, A., Ozier, O., Baliga, N. S., Wang, J. T., Ramage, D., et al. (2003). Cytoscape: a software Environment for integrated models of biomolecular interaction networks. *Genome Res.* 13, 2498–2504. doi: 10.1101/gr.1239303

Sheinerman, K. S., Tsivinsky, V. G., Abdullah, L., Crawford, F., and Umansky, S. R. (2013). Plasma microRNA biomarkers for detection of mild cognitive impairment: biomarker validation study. *Aging* 5, 925–938. doi: 10.18632/aging.100624

Sheinerman, K. S., Tsivinsky, V. G., Crawford, F., Mullan, M. J., Abdullah, L., and Umansky, S. R. (2012). Plasma microRNA biomarkers for detection of mild cognitive impairment. *Aging.* (2012) 4, 590–605. doi: 10.18632/aging.100486

Shigemizu, D., Akiyama, S., Higaki, S., Sugimoto, T., Sakurai, T., Boroevich, K. A., et al. (2020). Prognosis prediction model for conversion from mild cognitive impairment to Alzheimer's disease created by integrative analysis of multi-omics data. *Alzheimer's Res. Ther.* 12:145. doi: 10.1186/s13195-020-00716-0

Siedlecki-Wullich, D., Català-Solsona, J., Fábregas, C., Hernández, I., Clarimon, J., Lleó, A., et al. (2019). Altered microRNAs related to synaptic function as potential plasma biomarkers for Alzheimer's disease. *Alzheimer's Res. Ther.* 11:46. doi: 10.1186/s13195-019-0501-4

Silvestro, S., Bramanti, P., and Mazzon, E. (2019). Role of miRNAs in alzheimer's disease and possible fields of application. *Int. J. Mol. Sci.* 20:3979. doi: 10.3390/ijms20163979

Singer, O., Marr, R. A., Rockenstein, E., Crews, L., Coufal, N. G., Gage, F. H., et al. (2005). Targeting BACE1 with siRNAs ameliorates Alzheimer disease neuropathology in a transgenic model. *Nat. Neurosci.* 8, 1343–1349. doi: 10.1038/nn1531

Stappert, L., Klaus, F., and Brüstle, O. (2018). MicroRNAs engage in complex circuits regulating adult neurogenesis. *Front. Neurosci.* 12:707. doi: 10.3389/fnins.2018.00707

Swarbrick, S., Wragg, N., Ghosh, S., and Stolzing, A. (2019). Systematic review of miRNA as biomarkers in Alzheimer's disease. *Mol. Neurobiol.* 56, 6156–6167. doi: 10.1007/s12035-019-1500-y

Thambisetty, M., and Lovestone, S. (2010). Blood-based biomarkers of Alzheimers disease: challenging but feasible. *Biomark. Med.* 4, 65–79. doi: 10.2217/bmm.09.84

Tribolet, L., Kerr, E., Cowled, C., Bean, A. G. D., Stewart, C. R., Dearnley, M., et al. (2020). MicroRNA biomarkers for infectious diseases: from basic research to biosensing. *Front. Microbiol.* 11:1197. doi: 10.3389/fmicb.2020.01197

Trojanowski, J. Q., Vandeerstichele, H., Korecka, M., Clark, C. M., Aisen, P. S., Petersen, R. C., et al. (2010). Update on the biomarker core of the Alzheimer's disease neuroimaging initiative subjects. *Alzheimer's Dement.* 6, 230–238. doi: 10.1016/j.jalz.2010.03.008

Turchinovich, A., Weiz, L., Langheinz, A., and Burwinkel, B. (2011). Characterization of extracellular circulating microRNA. *Nucl. Acids Res.* 39, 7223–7233. doi: 10.1093/nar/gkr254

van Maurik, I. S., Slot, R. E. R., Verfaillie, S. C. J., Zwan, M. D., Bouwman, F. H., Prins, N. D., et al. (2019). Personalized risk for clinical progression in cognitively normal subjects - the ABIDE project. *Alzheimer's Res. Ther.* 11:33. doi: 10.1186/s13195-019-0487-y

Wang, L. Y., Pei, J., Zhan, Y. J., and Cai, Y. W. (2020). Overview of meta-analyses of five non-pharmacological interventions for Alzheimer's disease. *Front. Aging Neurosci.* 12:594432. doi: 10.3389/fnagi.2020.594432

Wang, T., Shi, F., Jin, Y., Jiang, W., Shen, D., and Xiao, S. (2016). Abnormal changes of brain cortical anatomy and the association with plasma MicroRNA107 level in amnestic mild cognitive impairment. *Front. Aging Neurosci.* 8:112. doi: 10.3389/fnagi.2016.00112

Wang, W., Kwon, E. J., and Tsai, L. H. (2012). MicroRNAs in learning, memory, and neurological diseases. *Learn. Mem.* 19, 359–368. doi: 10.1101/lm.026492.112

Weiner, M. W. (2013). Further insights into Alzheimer disease pathogenesis. *Nat. Rev. Neurol.* 9, 65–66. doi: 10.1038/nrneurol.2012.275

Wildsmith, K. R., Schauer, S. P., Smith, A. M., Arnott, D., Zhu, Y., Haznedar, J., et al. (2014). Identification of longitudinally dynamic biomarkers in Alzheimer's disease cerebrospinal fluid by targeted proteomics. *Mol. Neurodegener.* 9:22. doi: 10.1186/1750-1326-9-22

Winblad, B., Palmer, K., Kivipelto, M., Jelic, V., Fratiglioni, L., Wahlund, L. O., et al. (2004). Mild cognitive impairment - beyond controversies, towards a consensus: report of the International Working Group on Mild Cognitive Impairment. *J. Internal Med.* 256, 240–246. doi: 10.1111/j.1365-2796.2004.01380.x

Xiao, F., Zuo, Z., Cai, G., Kang, S., Gao, X., and Li, T. (2009). miRecords: an integrated resource for microRNA-target interactions. *Nucl. Acids Res.* 37, 105–110. doi: 10.1093/nar/gkn851

Xie, B., Liu, Z., Jiang, L., Liu, W., Song, M., Zhang, Q., et al. (2017). Increased serum miR-206 level predicts conversion from amnestic mild cognitive impairment to Alzheimer's disease: a 5-year follow-up study. *J. Alzheimer's Dis.* 55, 391–401. doi: 10.3233/JAD-160468

Yang, T. T., Liu, C. G., Gao, S. C., Zhang, Y., and Wang, Y. (2018). The serum exosome derived MicroRNA−135a, −193b, and −384 were potential Alzheimer's disease biomarkers. *Biomed. Environ. Sci.* 31, 87–96. doi: 10.3967/bes2018.011

Ye, Y., Xu, H., Su, X., and He, X. (2016). Role of MicroRNA in governing synaptic plasticity. *Neural Plast.* 2016:4959523. doi: 10.1155/2016/4959523

Yin, C. H., Li, S. O., Zhao, W. N., and Feng, J. C. (2013). Brain imaging of mild cognitive impairment and Alzheimer's disease. *Neural Regener. Res.* 8, 435–444. doi: 10.3969/j.issn.1673-5374.2013.05.007

Zetterberg, H., Wilson, D., Andreasson, U., Minthon, L., Blennow, K., Randall, J., et al. (2013). Plasma tau levels in Alzheimer's disease. *Alzheimer's Res. Ther.* 5:9. doi: 10.1186/alzrt163

Zhang, S., Smailagic, N., Hyde, C., Noel-Storr, A. H., Takwoingi, Y., Mcshane, R., et al. (2014). 11C-PIB-PET for the early diagnosis of Alzheimer's disease dementia and other dementias in people with mild cognitive impairment (MCI). *Cochr. Datab. Systemat. Rev.* 2014:CD010386. doi: 10.1002/14651858.CD010386.pub2

Zhao, X., Kang, J., Svetnik, V., Warden, D., Wilcock, G., Smith, A. D., et al. (2020). A machine learning approach to identify a circulating microrna signature for Alzheimer Disease. *J. Appl. Lab. Med.* 5, 15–28. doi: 10.1373/jalm.2019.029595

Zhu, Y., Li, C., Sun, A., Wang, Y., and Zhou, S. (2015). Quantification of microRNA-210 in the cerebrospinal fluid and serum: Implications for Alzheimer's disease. *Exp. Therapeut. Med.* 9, 1013–1017. doi: 10.3892/etm.2015.2179

Zirnheld, A. L., Shetty, V., Chertkow, H., Schipper, H. M., and Wang, E. (2016). Distinguishing mild cognitive impairment from Alzheimer's disease by increased expression of key circulating microRNAs. *Curr. Neurobiol.* 7:117. doi: 10.4172/0975-9042.000117

Conflict of Interest: NC-V, CV, and AB were employed by company Neurognos Spa.

The remaining authors declare that the research was conducted in the absence of any commercial or financial relationships that could be construed as a potential conflict of interest.

The reviewer EJ-M declared a shared affiliation with one of the authors, TL, to the handling editor at time of review.

Publisher's Note: All claims expressed in this article are solely those of the authors and do not necessarily represent those of their affiliated organizations, or those of the publisher, the editors and the reviewers. Any product that may be evaluated in this article, or claim that may be made by its manufacturer, is not guaranteed or endorsed by the publisher.

frontiers in Aging Neuroscience

ORIGINAL RESEARCH
published: 13 January 2022
doi: 10.3389/fnagi.2021.788519

Impaired Glymphatic Function and Pulsation Alterations in a Mouse Model of Vascular Cognitive Impairment

*Mosi Li[1,2], Akihiro Kitamura[1,3], Joshua Beverley[1], Juraj Koudelka[1], Jessica Duncombe[1], Ross Lennen[4], Maurits A. Jansen[4], Ian Marshall[5], Bettina Platt[6], Ulrich K. Wiegand[1], Roxana O. Carare[7], Rajesh N. Kalaria[8], Jeffrey J. Iliff[9,10,11] and Karen Horsburgh[1]**

[1] Centre for Discovery Brain Sciences, University of Edinburgh, Edinburgh, United Kingdom, [2] Edinburgh Medical School, UK Dementia Research Institute, University of Edinburgh, Edinburgh, United Kingdom, [3] Department of Neurology, Shiga University of Medical Science, Otsu, Japan, [4] Centre for Cardiovascular Science, University of Edinburgh, Edinburgh, United Kingdom, [5] Centre for Clinical Brain Sciences, University of Edinburgh, Edinburgh, United Kingdom, [6] School of Medicine, Medical Sciences and Nutrition, College of Life Sciences and Medicine, University of Aberdeen, Aberdeen, United Kingdom, [7] Faculty of Medicine, University of Southampton, Southampton, United Kingdom, [8] Translational and Clinical Research Institute, Newcastle University, Newcastle upon Tyne, United Kingdom, [9] VISN 20 Mental Illness Research, Education and Clinical Center, VA Puget Sound Health Care System, Seattle, WA, United States, [10] Department of Psychiatry and Behavioral Sciences, University of Washington School of Medicine, Seattle, WA, United States, [11] Department of Neurology, University of Washington School of Medicine, Seattle, WA, United States

OPEN ACCESS

Edited by:
Natalia Salvadores, Universidad Mayor, Chile

Reviewed by:
Masafumi Ihara, National Cerebral and Cardiovascular Center, Japan
Leon Munting, Massachusetts General Hospital and Harvard Medical School, United States

***Correspondence:**
Karen Horsburgh
Karen.Horsburgh@ed.ac.uk

Specialty section:
This article was submitted to Neuroinflammation and Neuropathy, a section of the journal Frontiers in Aging Neuroscience

Received: *02 October 2021*
Accepted: *07 December 2021*
Published: *13 January 2022*

Citation:
Li M, Kitamura A, Beverley J, Koudelka J, Duncombe J, Lennen R, Jansen MA, Marshall I, Platt B, Wiegand UK, Carare RO, Kalaria RN, Iliff JJ and Horsburgh K (2022) Impaired Glymphatic Function and Pulsation Alterations in a Mouse Model of Vascular Cognitive Impairment. Front. Aging Neurosci. 13:788519. doi: 10.3389/fnagi.2021.788519

Large vessel disease and carotid stenosis are key mechanisms contributing to vascular cognitive impairment (VCI) and dementia. Our previous work, and that of others, using rodent models, demonstrated that bilateral common carotid stenosis (BCAS) leads to cognitive impairment via gradual deterioration of the neuro-glial-vascular unit and accumulation of amyloid-β (Aβ) protein. Since brain-wide drainage pathways (glymphatic) for waste clearance, including Aβ removal, have been implicated in the pathophysiology of VCI via glial mechanisms, we hypothesized that glymphatic function would be impaired in a BCAS model and exacerbated in the presence of Aβ. Male wild-type and Tg-SwDI (model of microvascular amyloid) mice were subjected to BCAS or sham surgery which led to a reduction in cerebral perfusion and impaired spatial learning acquisition and cognitive flexibility. After 3 months survival, glymphatic function was evaluated by cerebrospinal fluid (CSF) fluorescent tracer influx. We demonstrated that BCAS caused a marked regional reduction of CSF tracer influx in the dorsolateral cortex and CA1-DG molecular layer. In parallel to these changes increased reactive astrogliosis was observed post-BCAS. To further investigate the mechanisms that may lead to these changes, we measured the pulsation of cortical vessels. BCAS impaired vascular pulsation in pial arteries in WT and Tg-SwDI mice. Our findings show that BCAS influences VCI and that this is paralleled by impaired glymphatic drainage and reduced vascular pulsation. We propose that these additional targets need to be considered when treating VCI.

Keywords: carotid stenosis, vascular pulsation, glymphatic function, vascular cognitive impairment, amyloid-β (Aβ), cerebral amyloid angiopathy (CAA)

INTRODUCTION

Cerebral vascular disease (CVD) is a major contributor to vascular cognitive impairment (VCI) and dementia such as Alzheimer's disease (Gorelick et al., 2011; Montine et al., 2014). Large well-characterized cohort studies have highlighted the co-existence of vascular disease with Alzheimer's disease (De Jong et al., 1997; Hachinski and Munoz, 1997; Snowdon et al., 1997; Esiri et al., 1999; de la Torre, 2000a,b,c). Key neuroimaging features (white matter lesions, microbleeds, lacunes and perivascular spaces) are found in both Alzheimer's disease and VCI sharing a number of vascular risk factors, such as hypertension, diabetes and atherosclerosis (Dichgans and Leys, 2017). Vascular risk factors in midlife are also associated with increased burden of Alzheimer-related pathology, such as amyloid protein, suggesting a direct relationship (Gottesman et al., 2017).

Chronic cerebral hypoperfusion has been proposed as a central common mechanism which contributes to cognitive decline and degenerative processes leading to dementia (Duncombe et al., 2017a). Global reductions in blood flow are associated with increased risk of progression from mild cognitive impairment to dementia suggesting that perfusion plays a key role in disease progression (Alsop et al., 2010; Chao et al., 2010). Reduced cerebral perfusion has been linked to white matter attenuation, a key feature common to both Alzheimer's disease and dementia associated with CVD (Schuff et al., 2009; Barker et al., 2014). Common artery stenosis of varying degrees is invariably associated with cognitive impairment (Johnston et al., 2004; Cheng et al., 2012; Alosco et al., 2013; Balestrini et al., 2013) and carotid stenosis (> 25%) has been linked to a greater burden of white matter hyperintensities (Romero et al., 2009). Large and small vessel disease is also linked to Alzheimer's disease dementia (Arvanitakis et al., 2016). Reduced cerebral perfusion, impaired cerebrovascular reactivity and hemodynamic responses are increasingly recognized in the early stages of Alzheimer's disease (de la Torre, 2012b; Hughes et al., 2014). Our work and others using animal models have shown that chronic cerebral hypoperfusion as a result of bilateral carotid stenosis leads to cognitive decline through mechanisms that involve hypoxia-induced white matter damage and gradual deterioration of the neuro-glial-vascular unit including endothelial dysfunction, microvascular inflammation and BBB leakage (Shibata et al., 2004; Holland et al., 2015; Fowler et al., 2017; Kitamura et al., 2017; Roberts et al., 2018). There is substantial evidence that reduced blood flow contributes to vascular disease. However, a causal relationship remains a matter of controversy largely due to the cross-sectional nature of clinical studies and, in the few longitudinal studies conducted, reduced blood flow occurs subsequent to vascular disease burden (de la Torre, 2012a). Impaired glymphatic function is emerging as a key player in vascular disease and dementia. The glymphatic pathway is a brain wide clearance process that relies on the movement of CSF along the perivascular network facilitated by aquaporin-4 water channels on the astroglial endfeet to promote the elimination of waste out of the brain (Iliff et al., 2012). CSF flow within the perivascular space (PVS) is regulated by cerebrovascular pulsatility and constriction, which is now considered to be a key factor regulating glymphatic function (Iliff et al., 2013b; Mestre et al., 2018, 2020). Enlarged PVS, identified by neuroimaging, are a common feature of CVD and dementia linked to vascular risk factors and inflammation (Doubal et al., 2010; Wardlaw et al., 2013; Aribisala et al., 2014b; Potter et al., 2015; Shi and Wardlaw, 2016; Ding et al., 2017). There is also evidence of impaired glymphatic function in pre-clinical models relevant to CVD. Notably advanced age, acute ischemic stroke and multi-infarct stroke, diabetes and subarachnoid hemorrhage (SAH) have all been shown to have a major impact on glymphatic drainage (Gaberel et al., 2014; Kress et al., 2014; Wang et al., 2017). Disturbances of the glymphatic function are also related to a build-up of Aβ in both human and rodent brain (Xu et al., 2015; Shokri-Kojori et al., 2018).

Recent studies from our group and others have shown that carotid stenosis reduces cerebral perfusion and alters the Aβ peptide pools culminating in cerebral amyloid angiopathy (CAA) and vascular related lesions (Okamoto et al., 2012; Salvadores et al., 2017). In light of the evidence that flow-limiting large-vessel stenosis contributes to vascular and Alzheimer's disease pathophysiology (Gupta and Iadecola, 2015), and that impaired glymphatic function is a key contributor to impaired Aβ clearance we hypothesized that the complex interaction of Alzheimer's disease and carotid stenosis leading to cognitive impairment occurs via impaired glymphatic function in addition to perfusion deficits. We interrogated this by examining glymphatic influx in a well-characterized murine model of VCI induced by bilateral common carotid stenosis (BCAS) (Shibata et al., 2004) and then assessed Aβ accumulation in a model of microvascular amyloid (Tg-SwDI) post-BCAS. We further assessed astrocytes and cerebral vascular pulsation as potential mechanisms since they govern CSF-ISF exchange in murine brain (Iliff et al., 2013b).

Abbreviations: (Aβ), Amyloid-β; ASL, Arterial spin labeling; ACSF, Artificial cerebrospinal fluid; BCAS, Bilateral common carotid stenosis; CAA, Cerebral amyloid angiopathy; CBF, Cerebral blood flow; CVD, Cerebral vascular disease; DG, Dentate gyrus; DL CTX, Dorsolateral cortex; MCA, Middle cerebral artery; PVS, Perivascular space; PBS, Phosphate-buffered saline; ROI, Region of interest; SAH, Subarachnoid hemorrhage; Tg-SwDI, Transgenic mouse containing the Swedish, Dutch and Iowa mutations; VCI, Vascular cognitive impairment; WT, Wild-type.

MATERIALS AND METHODS

Mice

All experiments were conducted in accordance with the United Kingdom Home Office Animals (Scientific Procedures) Act 1986 and additional local ethical and veterinary approval (Biomedical Research Resources, University of Edinburgh) and the ARRIVE guidelines. We used male C57Bl/6J (Charles River Laboratories Inc., United Kingdom) and Tg-SwDI mice (transgenic mice with Swedish, Dutch and Iowa mutations in human amyloid precursor protein (APP), with primarily microvascular amyloidosis) for all experiments. At the outset, mice from cohort 1 (n = 42) (Tg-SwDI and wild-type littermates

at 7–9 months old) were randomly assigned to experiments of MRI and behavioral tests, and tissues were collected for evaluation of microvascular amyloid level. A second cohort of mice (cohort 2) (n = 33) (Tg-SwDI at 5–7 months and imported C57Bl/6J mice at 4–5 months) were used for the investigation of glymphatic influx and astrogliosis. Mice from cohort 3 were used for *in vivo* investigation of vessel pulsation. Investigators were blinded to surgery and genotype throughout the data collection and analysis. Final group size for analysis: cohort 1: n = 8 WT sham, n = 10 WT BCAS, n = 6 Tg-SwDI sham, n = 10 Tg-SwDI BCAS. Cohort 2, n = 10 WT sham, n = 8 WT BCAS, n = 7 Tg-SwDI sham, n = 8 Tg-SwDI BCAS. Cohort 3, n = 7 WT sham, n = 7 WT BCAS, n = 6 Tg-SwDI sham, n = 7 Tg-SwDI BCAS.

Bilateral Common Carotid Stenosis Surgery

BCAS surgery was performed under isoflurane anesthesia by applying microcoils (0.18 mm internal diameter, Sawane Spring Co, Shizuoka, Japan) permanently to both common carotid arteries. Details of surgical methods have been described in previous studies (Shibata et al., 2004; Coltman et al., 2011; Holland et al., 2011; Reimer et al., 2011). A 30-min interval was given between two microcoils application to minimize the acute CBF changes caused by the placement of microcoils. Sham-operated animals underwent the identical procedure except the application of microcoils to both arteries. In cohort 1, one Tg-SwDI mouse was culled during surgery due to severe bleeding; and after 3 days of surgery, two WT and five Tg-SwDI were culled due to poor recovery as their weight loss exceeded 20%. Therefore, these mice were excluded from the study.

Cerebral Blood Flow Measure by Arterial Spin Labeling

A 7.0T (Agilent Technologies, Yarnton, United Kingdom) preclinical MRI system was used to collect T1-weighted and arterial spin labeling (ASL) data as we previously described (Duncombe et al., 2017b). Experimental animals were anesthetized under 5% isoflurane in oxygen for induction then placed in an MRI compatible holder (Rapid Biomedical, Wurzburg, Germany). Isoflurane was maintained at 1.5% in oxygen during scanning. Rectal temperature was monitored and regulated at around 37°C by an airflow heating system. Respiratory rate was regulated at 70–100 breaths per minute. The T1-weighted images were acquired at 1.7 mm posterior to Bregma in stereotactic coordinates of Mouse Brain Atlas (Paxinos and Franklin, 2001). ASL was performed using a Look-Locker FAIR single gradient echo (LLFAIRGE) sequence (Kober et al., 2008) covering a 1.5 mm thick brain slice centered −1.7 mm posterior from Bregma. Forty gradient echoes spaced 200 ms apart were acquired after a slice-selective or global adiabatic inversion pulse for each phase encoding, resulting in a total observation time of approximately 16 min for a 64 × 64 imaging matrix. The flip angle was 20°. The first 20° pulse occurred 3 ms after the inversion pulse. The echo time was 1.42 ms. Maps of cerebral blood flow (CBF) were constructed from ASL data in MATLAB using in-house scripts. CBF maps were analyzed in ImageJ (v1.46, NIH, Bethesda, MD, United States) using unbiased and uniform regions of interest from T1-weighted images acquired with the ASL sequence. The CBF values in each region of interest were reported as % change compared to baseline.

Assessment of Cognitive Function Using Barnes Maze

A Barnes maze was used to assess the differences in spatial learning and memory at 3 months after BCAS or sham surgery (Barnes maze schedule shown in **Figure 1A**). The maze consists of one white circular platform and 20 circular holes around the outside edge of the platform, with 91.5 cm diameter and 115 cm height (San Diego Instruments). The maze was brightly lit with lamps and overhead room lights (450 lux), and an aversive white noise stimulus is played at 85 dB. There is one dark escape chamber attached to one of the holes allocated to each experimental animal. Visual cues were placed on the curtains and walls around the maze. There was one white cylinder with 10.5 cm diameter for retaining animals at the beginning of each trial. All the tests were recorded by a video-based automatic tracking system ANY-maze v 4.99. All the tests were performed in the behavior testing room where the room temperature can be controlled at constant 20°C.

Acclimation and Habituation

Animals were brought into the behavioral testing room and placed in the holding cylinder to acclimate to the testing environment for 10 s for 2 days before habituation. One week prior to the training session, animals were habituated to the maze and escape chamber. Each mouse was placed in the holding cylinder for 10 s then allowed 3 min free exploration under low stress conditions after removal of the cylinder, without aversive white noise stimulation. Then mice were guided to the escape chamber and allowed inside for 2 min. All the animals were allocated one fixed number for the chamber during the behavior test. The maze and the escape chamber were cleaned with ethanol to avoid any olfactory cues between each trial.

Visuo-Spatial Learning and Working Memory Test (Acquisition Training)

During the training session, mice were trained to find the escape chamber over 6 days with 2 trials per day (60-min inter-trial interval). The platform consists of 20 escape holes and the location of escape chamber remained constant to each mouse but was shifted clockwise 90 degree between mice to avoid any olfactory cues. The mouse was placed in the holding cylinder for 10 s. The aversive white noise (85 dB) was given once the test started and switched off once the mouse entered the escape chamber. If the mouse failed to enter the target hole, the experimenter guided the mouse to the escape chamber. The aversive stimulus was stopped as soon as the mouse entered the chamber.

72 h Probe

A probe trial was performed 72 h after the final acquisition training and each mouse was allowed 90 s to explore the maze

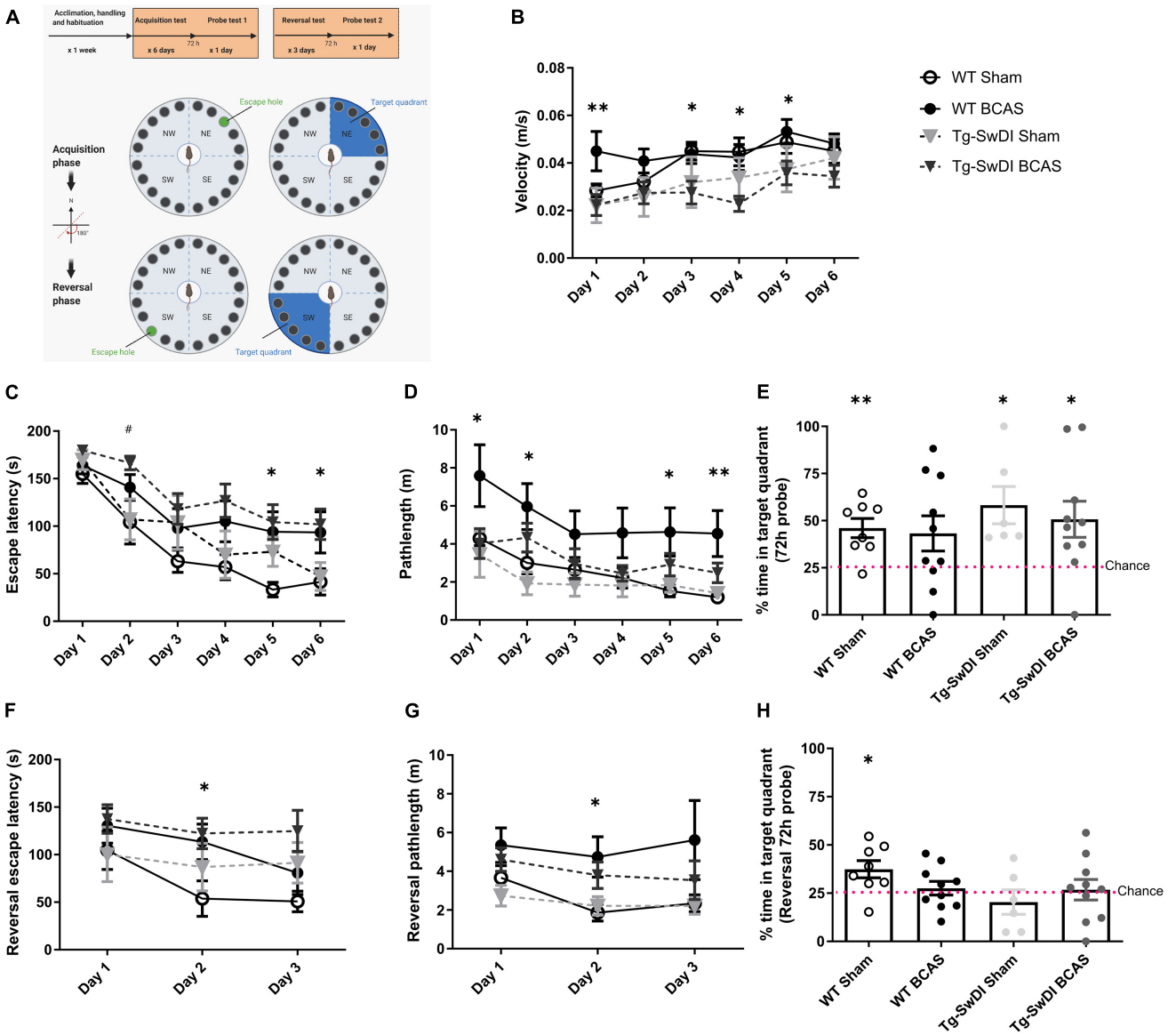

FIGURE 1 | BCAS causes a decline in spatial learning acquisition and cognitive flexibility. Spatial learning and memory and cognitive flexibility were assessed using a Barnes maze at 3 months post-BCAS in WT and Tg-SwDI mice. **(A)** In the acquisition phase one hole (indicated by green) was designated as the target hole with an escape box. A probe test was performed 72 h after the last acquisition training session, in which the escape box was removed. In the reversal phase, the target hole was moved 180 degrees to the original target hole. 1 day after the probe test. A reversal probe test was performed 72 h after the last training session. **(B)** Motor ability assessment in acquisition training. The speed or velocity was measured at the outset to assess whether motor function was affected by the genotype or surgery across different groups. There was a significant effect of genotype between WT and Tg-SwDI mice. *Post hoc* tests showed significant difference between WT BCAS and Tg-SwDI BCAS mice at day 1 (**$p < 0.01$), 3, 4 and 5 (*$p < 0.05$), respectively. **(C)** Spatial learning was assessed by comparing escape latency over 6 days with 2 sessions per day. There was a significant effect of BCAS surgery but not genotype across groups. *Post hoc* tests showed significant effect of BCAS in WT at day 5, 6 (*$p < 0.05$) and in Tg-SwDI at day 2 ($^{\#}p < 0.05$) compared to their sham counterparts. **(D)** Pathlength measure was also used to evaluate spatial learning function. There was a significant effect of BCAS surgery but not genotype across groups. *Post hoc* tests showed significant effect of BCAS in WT mice when compared to their sham counterparts at day 1, 2, 5 (*$p < 0.05$) and 6 (**$p < 0.01$). **(E)** In the acquisition 72 h probe test all mice performed above chance except WT BCAS mice (one sample *t*-test). No significant effect of BCAS and genotype were detected (Two-way ANOVA). To enhance the detection of spatial learning ability, reversal trials were taken to evaluate the ability of mice to learn a new location using Barnes maze **(F–H)**. In the reversal tests, spatial learning was assessed by comparing escape latency and pathlength over 3 days with 2 sessions per day training across all groups. **(F)** There was a significant effect of BCAS surgery but not genotype by comparing escape latency. *Post hoc* tests showed significant effect of BCAS in WT mice when compared to their sham counterparts at day 2 (*$p < 0.05$). **(G)** By comparing the pathlength in the test, there was a significant effect of BCAS surgery but not genotype. *Post hoc* tests showed significant effect of BCAS in WT mice when compared to their sham counterparts at day 2 ($p < 0.05$). **(H)** In the reversal probe test only WT sham mice performed above chance (one sample *t*-test). There was no significant effect of either genotype or surgery on the percentage time spent in the correct quadrant (Two-way ANOVA). Data are mean ± SEM, $n = 6$–10 per group.

with the escape chamber removed and the rest of elements remained same. The 72 h probe trials aimed to test the long-term memory of the mice after a period of training to locate the escape chamber.

Reversal Training

During the reversal training session, mice were trained to find the escape chamber following same procedure as the acquisition training phase, but with the allocated escape chamber shifted 180 degree to the opposite side of the stage. The mice were trained over 3 days with 2 trials per day (60-min inter-trial interval) in reversal training to evaluate the spatial learning ability in increased difficulty of task.

Reversal Probe

The reversal probe trial was performed 72 h after the final reversal training. Animals were given 90 s to explore the maze with the escape chamber removed. All the elements in reversal probe remained same as reversal training test.

Measurements

Trials were recorded by a camera above the maze and measured using tracking software Any-maze version 4.99. Spatial learning was assessed by the total time to enter the escape chamber (escape latency) and the total distance traveled (pathlength) during this period.

Assessment of Glymphatic Function by Intracisternal Injection of Fluorescent Tracers

Mice were initially anesthetized with isoflurane (5% in oxygen), then positioned on a stereotaxic frame and anesthetic maintained at approximately 1.5% (in oxygen). The respiration was regulated using a ventilator. The posterior atlanto-occipital membrane was surgically exposed and a 32GA needle attached to a Hamilton syringe was inserted into cisterna magna. Dextran, fluorescein and biotin labeled 3 kDa soluble lysine fixable (D7156, Invitrogen) and ovalbumin Alexa Fluor® 594 conjugate 45 kDa (O34783, Invitrogen) tracers were mixed at 1:1 ratio and infused at a concentration of 5 μg/μl, at a rate of 0.5 μl/min over 20 min (10 μl total volume) through a syringe pump (Harvard Apparatus). The needle was held in place for 10 min and then removed, and atlanto-occipital membrane was sealed to avoid any reflux of CSF.

Tissue Processing

At the end of the experiments, mice from cohort 1 and 2 were transcardially perfused with 30 ml heparinized saline then whole brains were fixed in 4% paraformaldehyde in PBS for 24 h. For cohort 1, brain tissues were further transferred into 30% sucrose solution in PBS for 72 h. Brains were placed in pre-cool isopentane –42°C for 5 min then stored in –80°C freezer and coronal sections (12 μm) were cut using a cryostat. For cohort 2, the brains were sectioned into coronal planes (100 μm) on a vibratome then stored in cryoprotective medium in a –20°C freezer.

Imaging of Fluorescent Tracer Movement

Tracer movement from the subarachnoid space of the cisterna magna into the brain was imaged using a slide scanner (ZEISS Axio Scan.Z1). Multi-channel whole-slice images of each animal at hippocampal level (–1.82 mm to bregma, Mouse Brain Atlas) was generated at 20 × magnification. This included separate DAPI, Alexa Fluor 488 and Alexa Fluor 594 channels. All images were scanned using constant exposure time for each individual channel by the slide scanner. For the quantification of tracer movement into the brain, scanned images were analyzed in ImageJ software (v1.46, NIH, Bethesda, MD, United States) as described previously (Iliff et al., 2012). Region of interest (ROI) was defined using DAPI channel to identify anatomical regions. Auto-thresholding (triangle method) was used to measure the % area of positive signal that is the glymphatic CSF influx.

Immunohistochemistry

Immunostaining was carried out according to standard protocols. Frozen sections were removed from the freezer and allowed to air dry for 30 min. Slides were washed in phosphate-buffered saline (PBS) followed by a series of ethanol (70, 90, and 100%) for dehydration then placed in xylene for 10 min. Sections were rehydrated through serial ethanol (100, 90, and 70%) then rinsed in water. Antigen retrieval was performed using 10 mM citric buffer (PH 6.0) at 100°C under pressure for 10 min then covered with proteinase K working solution for 10 min at room temperature. Sections were rinsed in PBS and incubated in blocking buffer (10% normal serum, 0.5% BSA) for 1 h at room temperature. Subsequently, sections were incubated in primary antibody solution (amyloid 6E10, 1:1,000, Covance, SIG-39320, mouse monoclonal antibody; COL4, 1:400, Fitzgerald, 70R-CR013X, rabbit polyclonal antibody) overnight at 4°C. Sections were then rinsed in PBS and incubated in secondary antibody (anti-rabbit Alexa Fluor 546, 1:500, Invitrogen A-11010; anti-mouse Alexa Fluor 488 1:500, Invitrogen A-11001) for 1 h at room temperature.

Vibratome sections were rinsed in PBS and mounted on to superfrost plus slides (VWR international) followed by serial ethanol (70, 90, and 100%) and then placed in xylene for 10 min. Sections were rehydrated through serial ethanol (100, 90, and 70%) then rinsed in running water. Antigen retrieval was performed using 10 mM citric buffer (PH 6.0) at 100°C under pressure for 10 min. Then sections were incubated in primary antibody solution (GFAP, 1:1,000, Life technologies, 13-0300, Rat monoclonal antibody) overnight at 4°C. Sections were rinsed in PBS and incubated in non-fluorescent biotinylated secondary antibody (anti-rat, 1:100, Vector Laboratories, YO809) for 1 h at room temperature followed by 1 h incubation with Vector ABC Elite kit (Vector Laboratories). Finally, sections were visualized with DAB peroxidase substrate kit (Vector Laboratories).

Analysis of Immunohistochemistry

Immunostained 12 μm frozen sections were analyzed using a laser scanning confocal microscope (ZEISS LSM 710, Germany). Cortical amyloid load and blood vessel density were determined

by measuring the percentage of areas occupied by 6E10 and COL4 staining, respectively. Vascular amyloid load was determined by colocalization analysis for blood vessels and amyloid by calculating the Mander's coefficient and data shown as % vascular amyloid. Images from the cortex in Tg-SwDI mice were selected, amyloid, blood vessels (COL4) and vascular amyloid images were quantified at the brain regions from the pial surface to approximate the depth of 250 μm. Immunostained 100 μm thick vibratome sections were analyzed using a slide scanner (ZEISS Axio Scan.Z1). Astrogliosis were assessed by measuring the percentage of stained area occupied by GFAP staining, using auto thresholding (triangle method). All measurements were carried out using ImageJ (v1.46, NIH, Bethesda, MD, United States).

Cranial Window Implantation

Animals were initially anesthetized using 4–5% isoflurane, delivered through a face mask via a ventilator and kept on 1.5–2% through the surgery. Subcutaneous injection of Caprofen (5 mg/kg) was administered at the start of the surgery. Body temperature was monitored through the surgery. Skin was removed to expose the skull, dried, and secured using VetBond (3M, #1649). Using a high-speed micro drill, an area of 6 × 3 mm was drilled over until a thin layer of bone was left. A drop of artificial cerebrospinal fluid (ACSF) (ACSF; 125 mM NaCl, 10 mM glucose, 10 mM HEPES, 3.1 mM $CaCl_2$, 1.3 mM $MgCl_2$, pH 7.4), was applied to the skull and left for 10 min. Using angled forceps, the skull was lifted without disrupting the dura. Hemocollagene soaked in ACSF was applied on the exposed brain for 5 min. A sterile coverslip was placed on top of the exposed brain, and secured by a mixture of liquid glue and dental cement. Immediately afterward, a custom made head plate (Protolabs) was applied to the cranial window prep and secured by additional glue/cement mixture. The cranial window was left to dry for 5 min and the animal was placed for recovery. Animals were rested for 4 weeks prior to imaging.

In vivo Vascular Pulsation Assessment

In separate cohorts of 7–8 month old WT and Tg-SwDI mice (cohort 3) cerebral vascular pulsatility was evaluated in WT and Tg-SwDI mice 1 month after sham and BCAS surgery. Cerebral vascular pulsation was assessed through the cortical vascular network with the use of multiphoton microscopy (LaVision Biotech TriMScope with Nikon CFI-Apo 25 × NA1.1 lens and Leica SP8 DIVE with IRAPO L 25 × NA1.0 lens) using a method based on those described previously within the literature (Iliff et al., 2013b; Kress et al., 2014). Mice were anesthetized in 5% isoflurane and maintained at 1.5–2% through imaging. Cortical vascular network was visualized via multiphoton microscopy through the injection of fluorescently conjugated dextran into the blood stream (Rhodamine B, 20 mg/ml, Sigma R9379). The pulsatility of individual vessels was determined by positioning linescans orthogonal to the vessel's axis. Linescans were performed in a repeated loop scans at a frequency of 1086.96 Hz (LaVision Biotech TriMScope) and 8,000 Hz (Leica SP8 DIVE) to equal duration of 3,600 ms. To calculate dynamic vessel width changes over time, the kymograph resulting from line scans was smoothed in FIJI (Smooth 3D) and thresholded (default automatic threshold). Using ROI placement over the whole graph, the distribution of pixel density for each line was calculated using a multi-plot. After conversion of pixels to μms and ms, the vessel width (μm) within each region was plotted against time (ms). Vessel wall pulsatility (μm*ms) was calculated from the resulting graphs as the absolute value of area under the diameter-time plot, integrated to the running average calculated across the entire 3,600 ms sampling time (GraphPad Prism, AUC analysis).

Statistical Analysis

Data were analyzed using a two-way ANOVA with surgery and genotype as two between-subject factors followed by Bonferroni's multiple comparison test to compare CBF levels, CSF glymphatic drainage and astrogliosis. Statistical comparison of spatial learning was carried out by repeated measures ANOVA with surgery and genotype as between subject factors followed by Bonferroni's multiple comparison test, the probe trials were carried out by using two-way ANOVA for comparison between groups. One sample *t*-test was used to compare the performance of each group with the chance. Mann Whitney *U*-test was used to compare the amyloid burden, blood vessel density and pulsation. Statistical analysis was performed using IBM SPSS Statistics 22.

RESULTS

Regional Cerebral Perfusion Is Reduced Post- Bilateral Common Carotid Stenosis in Wild-Type and Tg-SwDI Mice

At the outset of the studies, we determined whether carotid stenosis affected cerebral blood flow (CBF) in Tg-SwDI compared to WT mice using arterial spin labeling (ASL). We used a similar method to that reported previously (Kober et al., 2008; Duncombe et al., 2017b) which overestimates perfusion values and thus determined the % changes in CBF in BCAS compared to baseline (**Figure 2**) (note: absolute values are shown in **Supplementary Figure 1**). The % reductions in regional CBF in the dorsolateral cortex and hippocampal CA1-DG region in BCAS compared to sham mice are shown (**Figure 2A**). In the dorsolateral cortex (DL CTX), there was a significant main effect of surgery [$F(1, 26) = 14.816$, $p < 0.001$] but no effect in Tg-SwDI mice ($p > 0.05$) on resting CBF (**Figure 2B**). *Post hoc* analysis indicated that CBF was significantly reduced in BCAS mice in both wild-type ($p = 0.013$) and Tg-SwDI ($p = 0.010$) groups. Furthermore, in the hippocampal CA1-DG region, there was a main effect of surgery [$F(1, 26) = 17.963$, $p < 0.001$] but not genotype ($p > 0.05$) (**Figure 2C**). *Post hoc* analysis showed significantly reduced CBF in both wild-type ($p = 0.022$) and Tg-SwDI ($p = 0.002$) BCAS groups. Although there was a sustained and prominent reduction in CBF, there were no genotype differences indicating that perfusion was reduced to a similar extent in WT and Tg-SwDI mice.

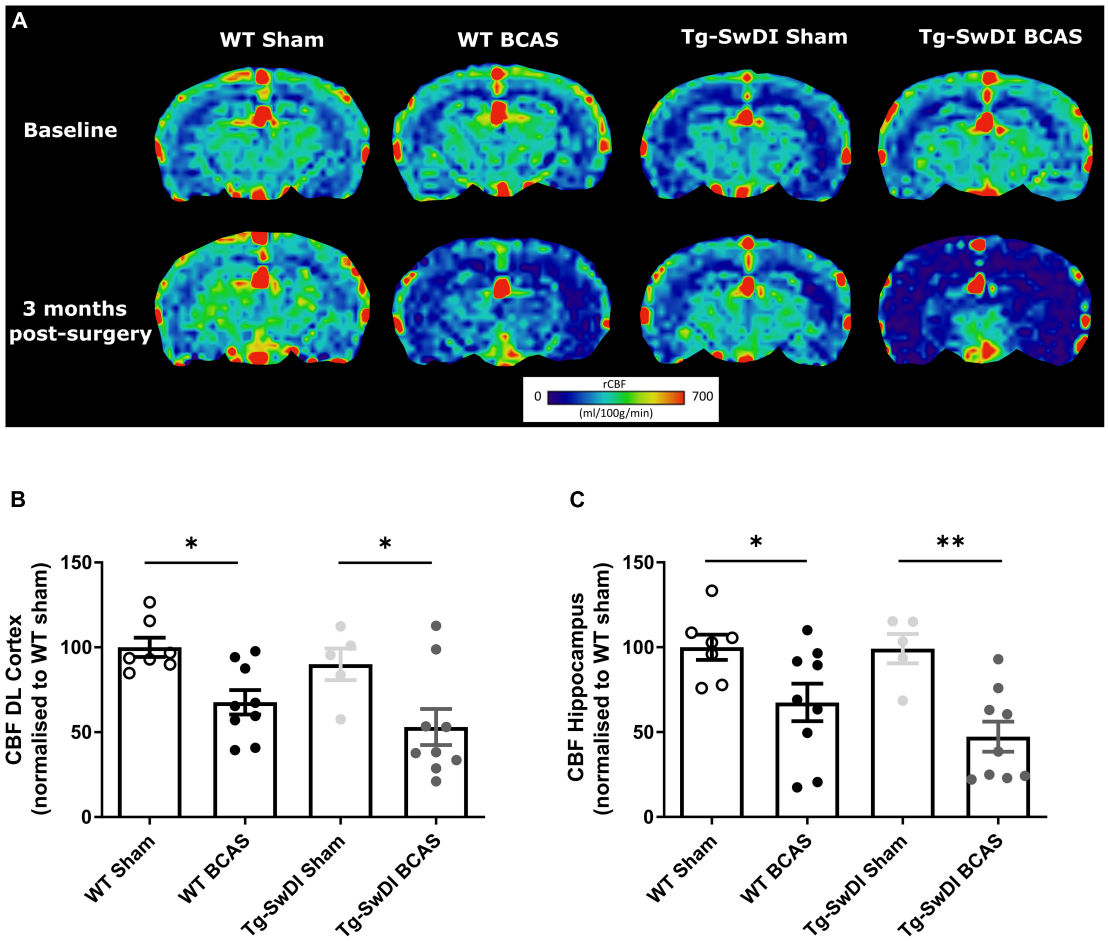

FIGURE 2 | Decreased resting CBF following BCAS. MRI arterial spin labeling (ASL) was used to measure regional alterations in CBF. **(A)** Representative images of arterial spin labeling (ASL) from sham and BCAS WT and Tg-SwDI mice at 3 months following surgery. **(B,C)** A significant reduction of CBF in the brain cortex and hippocampus was determined post-BCAS but there was no genotype effect. * and ** indicate $p < 0.05$ and 0.01, respectively. Data are presented as individual data points, mean ± SEM, $n = 6$–10 per group.

Bilateral Common Carotid Stenosis Causes a Decline in Spatial Learning Acquisition and Cognitive Flexibility in Wild-Type and Tg-SwDI Mice

We and others have previously reported that BCAS caused short-term spatial working memory impairments and spatial learning and memory deficits in WT mice (Shibata et al., 2007; Coltman et al., 2011; Holland et al., 2015; Matin et al., 2016; Kitamura et al., 2017; Patel et al., 2017). In this study spatial learning and memory abilities were assessed in BCAS wild-type mice but additionally it was determined whether BCAS would cause an exacerbated impairment in Tg-SwDI mice. The experimental paradigm is outlined in **Figure 1A**. The speed or velocity was measured at the outset to assess whether motor function was affected by the genotype or surgery across different groups. There was a significant effect of genotype between WT and Tg-SwDI mice [$F(1, 30) = 8.239$, $p < 0.01$] (**Figure 1B**). *Post hoc* tests showed significant difference between WT BCAS and Tg-SwDI BCAS mice at day 1 ($p < 0.01$), 3, 4, and 5 ($p < 0.05$), respectively. The Barnes maze paradigm was used to evaluate visuo-spatial learning whereby mice were trained to locate an escape hole using spatial cues over 6 days with 2 sessions per day and the escape latency measured. There was a significant effect of BCAS [$F(1, 30) = 9.60$, $p < 0.01$] but not genotype ($p > 0.05$) on escape latency (**Figure 1C**). *Post hoc* tests showed a significant effect of BCAS in both WT and Tg-SwDI mice when compared to their sham counterparts at day 5, 6 ($p < 0.05$) and day 2 ($p < 0.05$), respectively. We next analyzed the distance traveled in the tests (pathlength) as an additional measure to evaluate spatial learning. There was a significant effect of BCAS [$F(1, 30) = 5.826$, $p = 0.022$] but no effect of genotype ($p > 0.05$) on the pathlength across groups (**Figure 1D**). *Post hoc* tests showed a significant effect of BCAS in WT mice when compared to their sham counterparts at day 1, 2, 5 ($p < 0.05$) and 6 ($p < 0.01$). To investigate the effect of BCAS on long-term memory, a probe test was taken after 72 h of the final acquisition training to examine whether

experimental animals remember the previous target location after removing the escape chamber. Data was quantified as the percentage of time each mouse spent in the target quadrant where the allocated chamber was previously located. WT sham (p = 0.004), Tg-SwDI sham (p = 0.021) and Tg-SwDI BCAS (p = 0.025) all spent a significantly higher percentage of time than chance (25%) in the target quadrant but wild-type BCAS mice, did not perform above chance level (p = 0.84) (**Figure 1E**). There was no significant effect of BCAS or genotype on the percentage of time spent in the correct quadrant across groups ($p > 0.05$, respectively). To enhance the detection of spatial learning ability, reversal training and probe trials were then undertaken to evaluate the ability of experimental animals to learn a new location and to test cognitive flexibility. The escape hole location was switched 180° to the opposite side of maze. In the reversal tests, spatial learning was assessed by comparing escape latency and pathlength over 3 days with 2 sessions per day training across all groups. There was a significant effect of

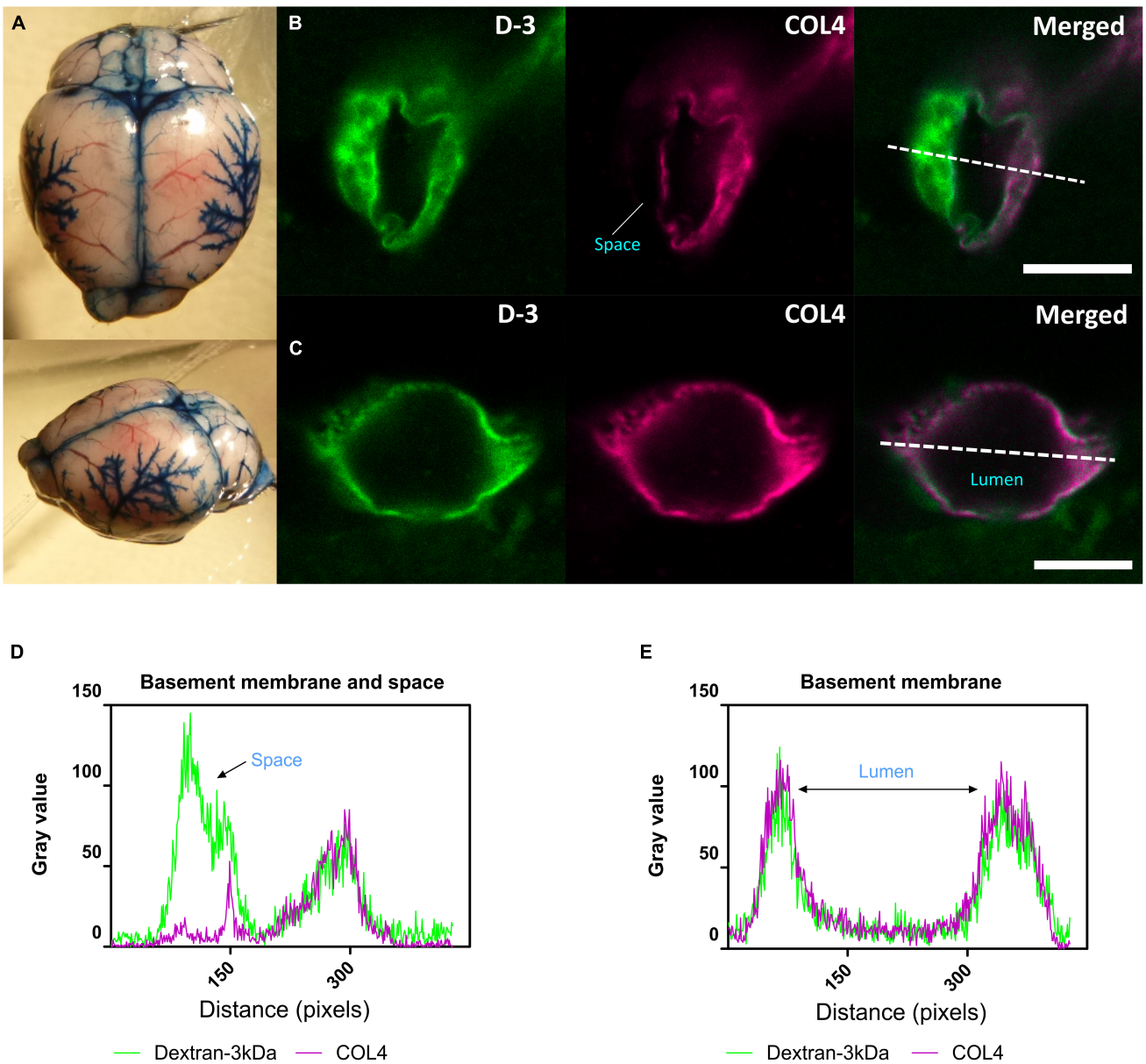

FIGURE 3 | CSF tracer influx in the perivascular space. **(A)** Evans blue dye was injected into cisterna magna of a normal mouse. At the surface of the brain, dyes were found distributed along blood vessels, the middle cerebral artery (MCA) and its branches, along the superior sagittal sinus, inferior cerebral vein, and transverse sinus. **(B) (Arteriole, in cortical area)** and **(D)** Co-labeling of sections with the vascular basement membrane marker COL4 revealed the localization of CSF fluorescent tracer to the adjacent space. **(C) (Capillary, in subcortical area)** and **(E)** Tracer colocalized with the basement membrane. Representative images showing spatial location of tracer soluble lysine fixable dextran 3 kDa (D-3) (green). Scale bar: top (space) = 10 μm, bottom (lumen) = 5 μm.

BCAS surgery [$F(1, 30) = 4.70$, $p = 0.038$] but not genotype by comparing escape latency ($p > 0.05$) (**Figure 1F**). *Post hoc* tests showed a significant effect of BCAS in WT mice when compared to their sham counterparts at day 2 ($p < 0.05$). By comparing the pathlength in the test, there was a significant effect of BCAS surgery [$F(1, 30) = 5.84$, $p = 0.022$] but not genotype ($p > 0.05$) (**Figure 1G**). *Post hoc* tests showed a significant effect of BCAS in WT mice when compared to their sham counterparts at day 2 ($p < 0.05$). The reversal probe was performed following 72 h after the final reversal training trial. Only WT sham mice ($p < 0.05$) spent a significantly higher percentage of time than chance in the target quadrant whereas all other groups did not perform above chance (WT BCAS, Tg-SwDI sham, Tg-SwDI BCAS $p > 0.05$, respectively) (**Figure 1H**). There was no significant effect of surgery ($p > 0.05$) or genotype ($p > 0.05$) on percentage time spent in the correct quadrant. Collectively the data demonstrate that BCAS impairs learning acquisition and cognitive flexibility.

Cerebrospinal Fluid Glymphatic Influx in the Brain Cortex

We next determined whether glymphatic function would be impaired post-stenosis at a time when both cerebral perfusion and cognitive abilities are impaired. To address this, we first examined the distribution of Evans blue following cisterna magna injection as a method to visualize glymphatic entry/influx and found that the dye distributed along the surface brain vessels (e.g., middle cerebral artery), along the superior sagittal sinus, inferior cerebral vein, and transverse sinus (**Figure 3A**). Following this CSF influx was then investigated by injection of fluorescently labeled CSF tracer (Dextran 3 kDa, D-3) into the cisterna magna and tracer distribution evaluated by imaging *ex vivo* fixed brain slices labeled with a marker of the basement membrane (COL4). CSF tracer influx was observed colocalized with the basement membrane and in the adjacent space (**Figure 3B**), colocalized with basement membrane (**Figure 3C**). Intensity profile graphs show strong colocalization between

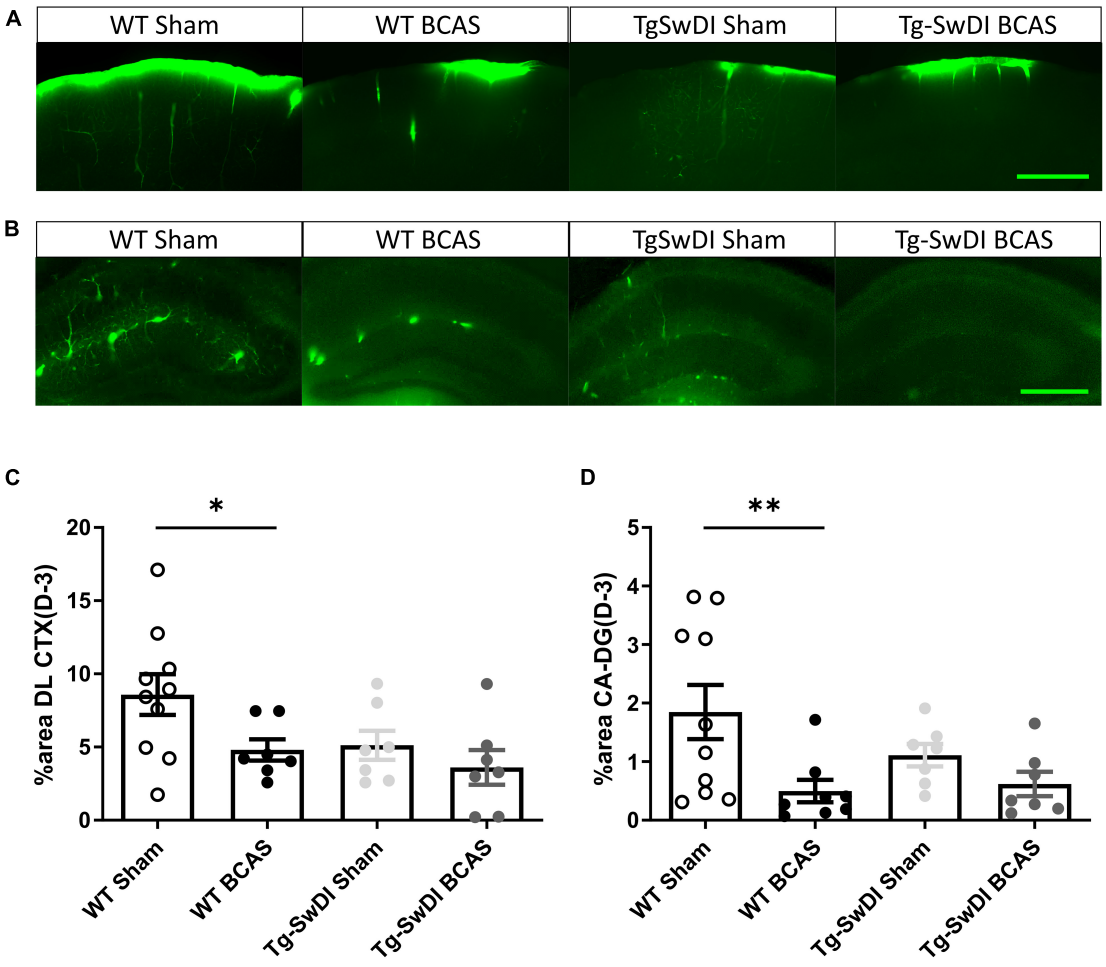

FIGURE 4 | Regional CSF tracer influx is altered in BCAS and Tg-SwDI mice. Representative images of fluorescent tracer influx (D-3) (green) in the **(A)** DL CTX and **(B)** hippocampus (CA1-DG molecular layer) of WT and Tg-SwDI mice sham and post-BCAS. **(C,D)** Quantification of D-3 tracer distribution in the DL CTX and CA1-DG molecular layer. * and ** indicate $p < 0.05$ and 0.01, respectively. Data are shown as individual data points, mean ± SEM, $n = 6$–10 per group. Scale bar = 500 μm.

CSF tracer (D-3) and vascular basement membrane (COL4) (**Figures 3D,E**) with partial tracer occupancy in the perivascular compartment (**Figure 3D**).

Regional Cerebrospinal Fluid Tracer Influx Is Altered Post-bilateral Common Carotid Stenosis in Wild-Type and Tg-SwDI Mice

The distribution of CSF tracer influx was then measured post-BCAS in both wild-type and Tg-SwDI mice. It was noted that the tracer distribution was quite heterogeneous between the different cohorts particularly in different brain regions, notably the dorsolateral cortex (DL CTX) and hippocampus (CA1-DG molecular layer). CSF tracer influx in the region of dorsolateral cortex was distributed along the middle cerebral artery (MCA) and its branches (**Figure 3A**) but this was less prominent post-BCAS compared to sham (**Figure 4A**). Quantification of tracer indicated a significant reduction in the dorsolateral cortex post-BCAS [$F(1, 27) = 4.81$, $p = 0.037$] and a trend toward an effect of genotype albeit this did not reach statistical significance ($p = 0.064$). *Post hoc* analysis showed a significant reduction in WT BCAS compared to sham animals ($p < 0.05$) (**Figure 4C**). It was also noted that CSF tracer was prominently distributed along the vascular network within the hippocampus but was markedly restricted post-BCAS in the hippocampal subregion: CA1-DG molecular layer (**Figure 4B**). It was determined that there was a reduction in tracer post-BCAS with a significant main effect

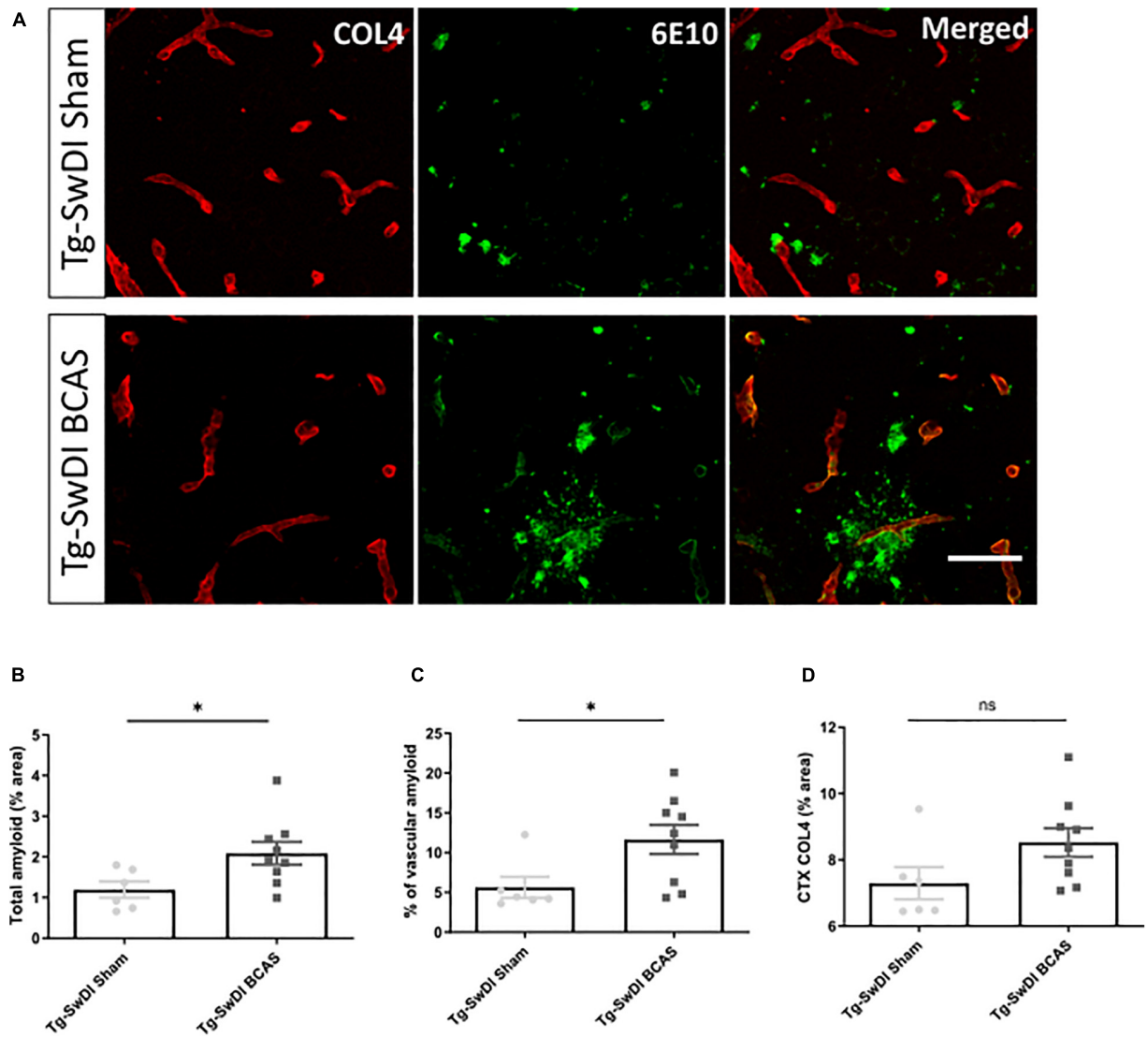

FIGURE 5 | BCAS exacerbates amyloid deposition in Tg-SwDI mice. **(A)** Representative images of amyloid (green) and COL4 as a marker of vascular basement membranes (red) in the superficial brain cortex in Tg-SwDI sham and BCAS mice. **(B)** Total amyloid and **(C)** vascular amyloid were increased post-BCAS. **(D)** No significant changes of basement membrane were found. * indicates $p < 0.05$. Data are shown as individual data points, mean ± SEM, $n = 6$–9 per group. Scale bar = 50 μm.

of surgery [$F(1, 28) = 7.5$, $p = 0.011$], but no effect of genotype ($p > 0.05$). *Post hoc* tests showed a significant reduction between WT sham and BCAS mice ($p = 0.005$) (**Figure 4D**). Collectively, the results demonstrate that carotid stenosis has a major impact on cortical and hippocampal glymphatic function.

Bilateral Common Carotid Stenosis Exacerbates Vascular Amyloid Accumulation

The vascular basement membranes have been proposed as pathways for the movement of fluid in the brain and involved in the build-up of amyloid causing CAA (Morris et al., 2016). To investigate the potential changes of amyloid burden post-BCAS, we evaluated Aβ (6E10) load in the cortex and co-labeled with COL4 (a marker of basement membrane of blood vessels) to enable the assessment of microvascular amyloid in our Tg-SwDI mouse model with vascular amyloidosis (**Figure 5A**). A significant increase in the total amount of amyloid ($p < 0.05$) and vascular amyloid was determined post-stenosis ($p < 0.05$) in the cortex (∼250 μm from the pial surface) (**Figures 5B,C**, respectively). Since basement membranes have been shown as pathways for the clearance of Aβ we further determined COL4 levels but did not find significant changes post-BCAS ($p > 0.05$) (**Figure 5D**).

Increased Astrogliosis Following Bilateral Common Carotid Stenosis in Cortex

To discern the mechanisms by which BCAS may impact on glymphatic function we next studied the extent of astrogliosis. Astrocytes and their end-feet have been shown to alter glymphatic function (Iliff et al., 2012). GFAP immunostaining was undertaken to investigate the extent of reactive gliosis post-BCAS and in Tg-SwDI mice. BCAS surgery had a significant effect [$F(1, 27) = 0.309$, $p = 0.01$] but there was no effect of genotype ($p > 0.05$) on the extent of astrogliosis in the dorsolateral cortex. *Post hoc* tests showed a significant increase of astrogliosis between WT sham and BCAS mice ($p = 0.021$) (**Figures 6A,C**). We further analyzed the hippocampal CA1-DG molecular layer. There was a significant effect of genotype [$F(1,$

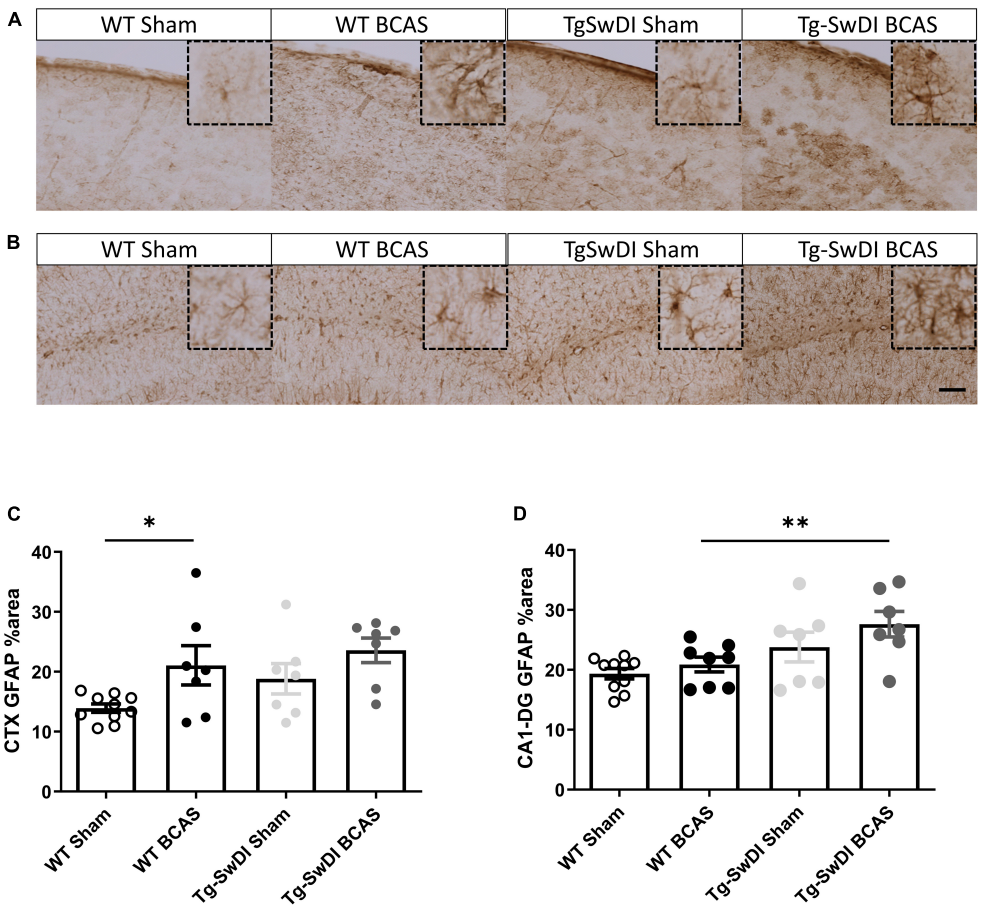

FIGURE 6 | Increased astrogliosis post-BCAS in cortex. Representative images of GFAP immunostaining to assess the degree of astrogliosis in the superficial brain cortex of WT and Tg-SwDI, sham and BCAS mice. **(A,C)** In the superficial cortex, BCAS caused increased astrogliosis but was unaffected in Tg-SwDI mice. **(B,D)** In the hippocampus, there was increased astrogliosis in Tg-SwDI mice but not post-BCAS. * and ** indicate $p < 0.05$ and 0.01, respectively. Data are shown as individual data points, mean ± SEM, $n = 6$–10 per group. Scale bar = 100 μm.

28) = 0.457, p = 0.002] but no effect of BCAS ($p > 0.05$) on astrogliosis. *Post hoc* tests showed a significant increase of astrogliosis in Tg-SwDI BCAS mice compared to WT BCAS group (p = 0.009) and a trend of increased astrogliosis between the WT sham and Tg-SwDI mice (p = 0.061) (**Figures 6B,D**). Thus, alterations in astrogliosis did not always parallel the impairment in glymphatic function observed post-BCAS.

Cerebral Arterial Pulsation Is Impaired in Tg-SwDI and Post-bilateral Common Carotid Stenosis in Subset of Vessels

Cerebral arterial pulsation is thought to drive the glymphatic influx into and through the brain and is essential for the clearance of Aβ (Iliff et al., 2013b; Kress et al., 2014). Most recent evidence using two-photon imaging has supported the role of arterial pulsations in CSF movement in the perivascular spaces and basement membranes (Mestre et al., 2018). To investigate whether vascular pulsation is affected in Tg-SwDI animals and post-BCAS, we used *in vivo* two-photon microscopy which provides high temporal resolution of individual blood vessels. We measured multiple levels of the cerebral vascular network including pial veins and arteries, penetrating arteries and ascending veins (**Figure 7A**). There was a significant effect of genotype on vascular pulsatility of vessel diameter in all types of vessels measured (**Figure 7B**): pial veins [F(1, 22) = 53.841, p = 0.000], pial arteries [F(1, 23) = 4.744, p = 0.04], penetrating arteries [F(1, 22) = 46.398, p = 0.000] and ascending veins [F(1, 22) = 40.658, p = 0.000]. *Post hoc* tests revealed a significant decrease in vascular pulsation between wild type and Tg-SwDI sham animals in pial veins (p = 0.000), pial arteries (p = 0.041), penetrating arteries (p = 0.001) as well as ascending veins (p = 0.002). Vascular pulsation was also reduced in Tg-SwDI when compared to wild type BCAS mice in pial veins (p = 0.000), penetrating arteries (p = 0.000), ascending veins (p = 0.000), but not in pial arteries ($p > 0.05$). Interestingly, we found a significant effect of surgery in pial arteries only [F(1, 23) = 9.536, p = 0.005], but not in any other type of vessel. *Post hoc* analysis showed a significant decrease in vascular pulsation in wild type BCAS animals when compared to shams (p = 0.008), but no effect in Tg-SwDI animals (**Figure 7B**). In addition, heart rate was measured during imaging in all animals and was found to be similar across all groups (**Supplementary Figure 2**). Thus the decreased pulsatility is likely not driven by changes in frequency but rather by decreases in amplitude.

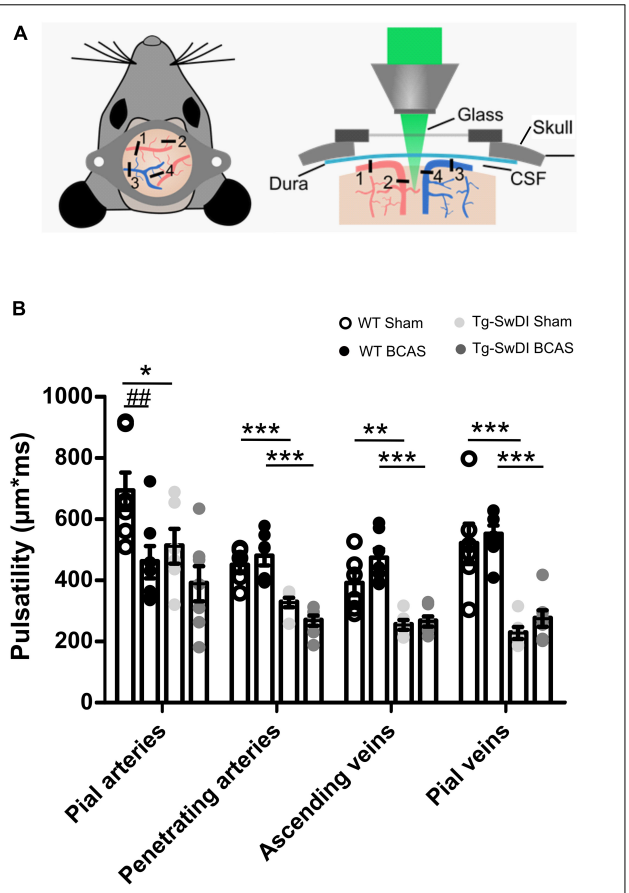

FIGURE 7 | Vascular pulsatility is reduced in Tg-SwDI animals **(A)** Two-photon microscopy was used to assess vessel pulsation in sham and post-BCAS WT and Tg-SwDI mice. Four categories of blood vessels were investigated: 1. Pial arteries; 2. Penetrating arteries; 3. Ascending veins; 4. Pial veins. **(B)** There was a significant effect of genotype on vascular pulsatility in all types of vessels measured, and significant effect of surgery on pial arteries. *Post hoc* test revealed a significant decrease in vascular pulsation between wild type and Tg-SwDI sham animals in pial veins (p = 0.000), pial arteries (p = 0.041), penetrating arteries (p = 0.001) as well as ascending veins (p = 0.002) Vascular pulsation was also reduced in Tg-SwDI when compared to wild type BCAS mice in pial veins (p = 0.000), penetrating arteries (p = 0.000), ascending veins (p = 0.000) but not in pial arteries ($p > 0.05$). Finally, vascular pulsation was decreased in wild type BCAS animals when compared to shams (p = 0.008). Data are presented as mean ± SEM, n = 6–7 per group. $^{\#}$ indicates significant difference between sham and BCAS; * indicates significant difference between WT and Tg-SwDI. $^{*}p < 0.05$, **, $^{\#\#}p < 0.01$; $^{***}p < 0.001$.

DISCUSSION

Our findings provide experimental evidence that long-term BCAS, whilst reducing cerebral perfusion, may also affect glymphatic function (summarized in **Figure 8**). This new data adds credence to a growing body of human studies that have challenged the view that reduced blood flow post-stenosis is the major contributor to VCI. Instead, alternative or additional mechanisms should be considered (Aribisala et al., 2014a; Wardlaw et al., 2017; Alhusaini et al., 2018; Shi et al., 2018a).

A substantial number of studies have shown that BCAS, using microcoils applied to both common carotid arteries in mice, leads to cognitive impairment (Shibata et al., 2007; Matin et al., 2016; Patel et al., 2017). Consistent with these studies, we show that at 3 months after BCAS, impaired spatial learning acquisition and cognitive flexibility are evident. The mechanistic link between BCAS and VCI has largely been attributed to the post-BCAS cerebral perfusion deficits initiating hypoxia–induced white matter pathology and degenerative changes to the glial-vascular unit (Holland et al., 2015).

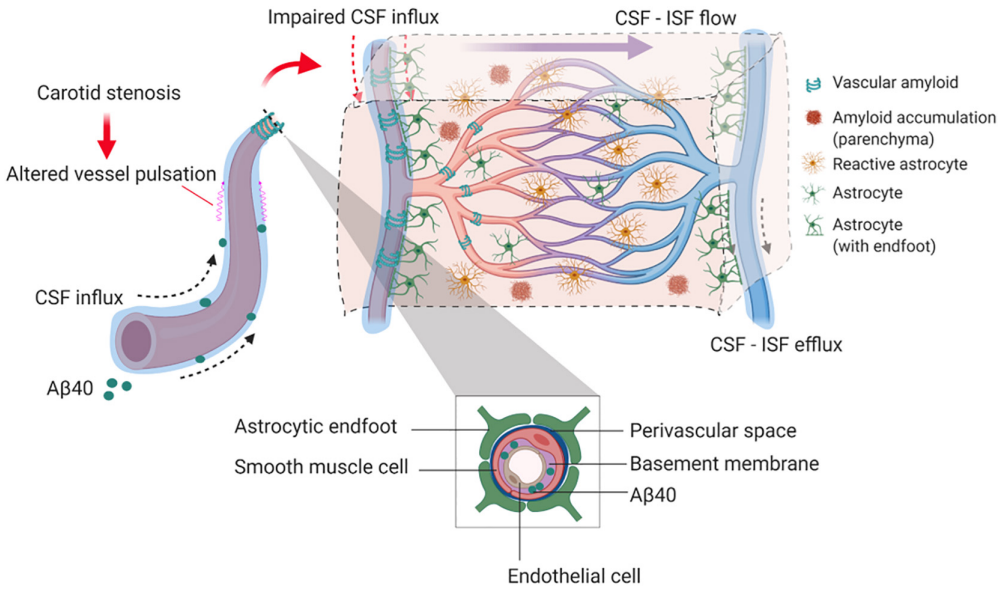

FIGURE 8 | Proposed model by which BCAS and amyloid may impact on glymphatic function and predispose to VCI. In the long-term response to BCAS, reduced arterial pulsatility may impede CSF influx along the periarterial space and contribute in part to amyloid accumulation within the parenchyma and vasculature. Independently amyloid (Aβ40) has a profound impact on arterial pulsatility and impedes CSF influx. Downstream these events may influence glial cell responses including reactive astrogliosis and inflammation that can contribute to VCI.

Our novel data suggest that BCAS can also lead to impaired CSF influx along the glymphatic pathway. In the first instance, we injected fluorescent tracer into the cisterna magna and were able to observe the tracers surrounding cerebral arteries e.g., middle cerebral artery (MCA) within the perivascular compartment (**Figure 3**) consistent with previous observations showing that CSF influx moves along the periarterial components into deeper brain regions (Iliff et al., 2012). It has been shown by *in vivo* two-photon imaging that intracisternal CSF tracer travels along the perivascular component surrounding pial surface (Iliff et al., 2012; Xie et al., 2013). Using confocal microscopy, we were able to measure the regional distribution of tracer post-BCAS. Following 3 months of carotid stenosis impaired glymphatic function was determined in cortical and deep hippocampal regions suggesting that prolonged disruption to the vascular system may lead to enduring suppression of CSF influx to the brain.

CSF influx along the glymphatic drainage pathway has also shown to be impaired in other models relevant to cerebral vascular disease. In a rodent model of multiple infarcts, caused by intra-arterial injection of cholesterol crystals via the internal carotid artery, a transient suppression of CSF influx was determined (Wang et al., 2017). However, in this study glymphatic function was restored within 2 weeks. In other models a sustained or progressive impairment of glymphatic function has been shown such as with aging (Wang et al., 2017), hypertension (Mestre et al., 2018) and in models relevant to AD (Peng et al., 2016). Interestingly, in another study of APP/PS1 mice, a model relevant to AD, glymphatic function is severely compromised before amyloid accumulation (Peng et al., 2016) and it is likely that there are different pathophysiological mechanisms that can contribute to VCI.

To examine potential mechanisms underlying the impaired CSF influx, we assessed the extent of astrogliosis as astrocytes have an important function in CSF influx and clearance (Iliff et al., 2012), and deletion of the astrocytic end feet reduces the CSF influx into the parenchyma following ischemia (Mestre et al., 2020). In this study there was a tendency for astrogliosis post-BCAS. In the cortex there was pronounced astrogliosis most notable in WT mice post-BCAS and in the hippocampus astrogliosis was increased in Tg-SwDI post-BCAS mice. We further explored additional mechanisms that may account for the impaired CSF influx post-BCAS. Cerebrovascular pulsatility is a key driving force facilitating CSF flow into and through brain parenchyma (Iliff et al., 2013b; Mestre et al., 2018) and vasoconstriction was shown previously to play an important role in CSF flow following ischemia (Mestre et al., 2020). Using intravital imaging we found that arterial pulsation in pial vessels was affected in transgenic animals and was further exacerbated by BCAS surgery. Our results are in accordance with previous data showing that 30 min of unilateral ligation of internal carotid artery leads to significantly reduced pulsatility in the penetrating arteries with impaired glymphatic influx (Iliff et al., 2013b). Our data shows that venous pulsation, on the other hand, as well as pulsation of penetrating and ascending vessels was impaired in transgenic animals, but not affected by BCAS surgery. Together, these data suggest that BCAS has a differential effect on vascular pulsation within the vascular bed with arterial pulsation predominantly exacerbated by BCAS. Since cerebral pulsation may govern CSF-ISF exchange in murine brain leading to accumulation of solutes/proteins in the brain, this impairment may partly explain the accumulation of Aβ that we determined in Tg-SwDI animals post-BCAS. Altered carotid function has

been associated with impaired cognitive function, greater Aβ deposition and several features of vascular disease in both human and animal studies (Huang et al., 2012; Poels et al., 2012; Ding et al., 2015; Holland et al., 2015; Hughes et al., 2018). It has been also shown that the impaired glymphatic function can result in increased Aβ burden in the brain (Kress et al., 2014; Peng et al., 2016; Shokri-Kojori et al., 2018). In the current study arterial pulsation was impaired by BCAS and independently by Aβ in Tg-SwDI in the absence of BCAS. It has been suggested that arterial vessel stiffening and reduced pulsatility may cause decreased CSF fluid influx (Benveniste and Nedergaard, 2021) and thus BCAS/Aβ accumulation may impact on vascular hemodynamics resulting in altered glymphatic function. In keeping with this, in studies of human SVD, pulsatility index as a measure of vascular stiffness is increased (Shi et al., 2018b). However of note in this study is, that although BCAS led to an increase in Aβ accumulation, this was not associated with a more prominent impairment in glymphatic function. One explanation may be that glymphatic function is already markedly reduced in Tg-SwDI mice. Alternatively there may be other mechanisms that contribute to amyloid accumulation post-BCAS (e.g., oxidative stress), which we have previously shown (Salvadores et al., 2017). A prospective population-based study has also shown alterations of pulsation in the carotid artery may contribute to the pathophysiology of cerebral microbleeds in deep brain region secondary to hypertension (Ding et al., 2015). Interestingly we have also shown that sustained carotid stenosis leads to the development of vascular lesions (both microbleeds and microinfarcts) in deep subcortical structures several months post-stenosis (Holland et al., 2015).

The present study was restricted to evaluation of CSF influx at 3 months post-BCAS and future longitudinal approaches to evaluate potential progression of changes could be interrogated using contrast-enhanced MRI (Iliff et al., 2013a). One of the limitations of the present study was the inability to intervene and modify glymphatic function. Thus in future it will be important to discern whether glymphatic failure can be reversed and whether this may impact on the onset and progression of VCI.

DATA AVAILABILITY STATEMENT

The original contributions presented in the study are included in the article/**Supplementary Material**, further inquiries can be directed to the corresponding author: (Karen.Horsburgh@ed.ac.uk).

ETHICS STATEMENT

The animal study was reviewed and approved by the UK Home Office Animals (Scientific Procedures) Act 1986 and additional local ethical and veterinary approval (Biomedical Research Resources, University of Edinburgh).

AUTHOR CONTRIBUTIONS

ML carried out, designed, analyzed most of the experiments, and wrote the manuscript. AK carried out and designed the CSF tracer experiment. JB carried out multiphoton experiments, data analysis, and some behavioral work. JK carried out multiphoton experiment and CSF tracer experiment analysis. JD carried out MR imaging and behavioral and IHC experiment. RL, MJ, and IM overseen the MR/ASL imaging and analysis. BP assisted with the behavioral study design. UW assisted with the multiphoton work. RC assisted the CSF tracer experiment design, data interpretation, and editing manuscript. RK assisted the data interpretation, and editing manuscript. JI assisted the study design, data interpretation, and editing manuscript. KH conducted the surgeries, supervised the project and assisted in study design, data interpretation, and writing of the manuscript. All authors assisted with editing of the manuscript.

FUNDING

We gratefully acknowledge the grant support from the Alzheimer's Society (152 (PG-157); 290 (AS-PG-15b-018); 228 (AS-DTC-2014-017), 314 (AS –PhD-16-006), and Alzheimer's Research United Kingdom (ART-PG2010-3; ARUK-PG2013-22; ARUK-PG2016B-6), and The University of Edinburgh Centre for Cognitive Ageing and Cognitive Epidemiology, part of the cross council Lifelong Health and Wellbeing Initiative (G0700704/84698). ML and JB are funded by an Alzheimer's Society Scotland Doctoral Training Programme and RS Macdonald Trust. ML was also funded by a China Scholarship Council (CSC)/University of Edinburgh scholarship.

ACKNOWLEDGMENTS

Schematic diagrams in **Figures 2**, **8** are created with Biorender.com.

SUPPLEMENTARY MATERIAL

The Supplementary Material for this article can be found online at: https://www.frontiersin.org/articles/10.3389/fnagi.2021.788519/full#supplementary-material

REFERENCES

Alhusaini, S., Karama, S., Nguyen, T. V., Thiel, A., Bernhardt, B. C., Cox, S. R., et al. (2018). Association between carotid atheroma and cerebral cortex structure at age 73 years. *Ann. Neurol.* 84, 576–587. doi: 10.1002/ana.25324

Alosco, M. L., Brickman, A. M., Spitznagel, M. B., Garcia, S. L., Narkhede, A., Griffith, E. Y., et al. (2013). Cerebral perfusion is associated with white matter hyperintensities in older adults with heart failure. *Congest. Heart Fail* 19, E29–E34. doi: 10.1111/chf.12025

Alsop, D. C., Dai, W., Grossman, M., and Detre, J. A. (2010). Arterial spin labeling blood flow MRI: its role in the early characterization of Alzheimer's disease. *J. Alzheimers Dis.* 20, 871–880. doi: 10.3233/JAD-2010-091699

Aribisala, B. S., Wiseman, S., Morris, Z., Valdes-Hernandez, M. C., Royle, N. A., Maniega, S. M., et al. (2014b). Circulating inflammatory markers are associated with magnetic resonance imaging-visible perivascular spaces but not directly with white matter hyperintensities. *Stroke* 45, 605–607. doi: 10.1161/STROKEAHA.113.004059

Aribisala, B. S., Morris, Z., Eadie, E., Thomas, A., Gow, A., Valdes Hernandez, M. C., et al. (2014a). Blood pressure, internal carotid artery flow parameters, and age-related white matter hyperintensities. *Hypertension* 63, 1011–1018. doi: 10.1161/HYPERTENSIONAHA.113.02735

Arvanitakis, Z., Capuano, A. W., Leurgans, S. E., Bennett, D. A., and Schneider, J. A. (2016). Relation of cerebral vessel disease to Alzheimer's disease dementia and cognitive function in elderly people: a cross-sectional study. *Lancet Neurol.* 15, 934–943. doi: 10.1016/S1474-4422(16)30029-1

Balestrini, S., Perozzi, C., Altamura, C., Vernieri, F., Luzzi, S., Bartolini, M., et al. (2013). Severe carotid stenosis and impaired cerebral hemodynamics can influence cognitive deterioration. *Neurology* 80, 2145–2150. doi: 10.1212/WNL.0b013e318295d71a

Barker, R., Ashby, E. L., Wellington, D., Barrow, V. M., Palmer, J. C., Kehoe, P. G., et al. (2014). Pathophysiology of white matter perfusion in Alzheimer's disease and vascular dementia. *Brain* 137, 1524–1532. doi: 10.1093/brain/awu040

Benveniste, H., and Nedergaard, M. (2021). Cerebral small vessel disease: a glymphopathy? *Curr. Opin. Neurobiol.* 72, 15–21. doi: 10.1016/j.conb.2021.07.006

Chao, L. L., Buckley, S. T., Kornak, J., Schuff, N., Madison, C., Yaffe, K., et al. (2010). ASL perfusion MRI predicts cognitive decline and conversion from MCI to dementia. *Alzheimer Dis. Assoc. Disord.* 24, 19–27. doi: 10.1097/WAD.0b013e3181b4f736

Cheng, H. L., Lin, C. J., Soong, B. W., Wang, P. N., Chang, F. C., Wu, Y. T., et al. (2012). Impairments in cognitive function and brain connectivity in severe asymptomatic carotid stenosis. *Stroke* 43, 2567–2573. doi: 10.1161/STROKEAHA.111.645614

Coltman, R., Spain, A., Tsenkina, Y., Fowler, J. H., Smith, J., Scullion, G., et al. (2011). Selective white matter pathology induces a specific impairment in spatial working memory. *Neurobiol. Aging* 32, 2323.e7–e12. doi: 10.1016/j.neurobiolaging.2010.09.005

De Jong, G. I., De Vos, R. A., Steur, E. N., and Luiten, P. G. (1997). Cerebrovascular hypoperfusion: a risk factor for Alzheimer's disease? Animal model and postmortem human studies. *Ann. N. Y. Acad. Sci.* 826, 56–74. doi: 10.1111/j.1749-6632.1997.tb48461.x

de la Torre, J. C. (2000a). Cerebral hypoperfusion, capillary degeneration, and development of Alzheimer disease. *Alzheimer Dis. Assoc. Disord.* 14(Suppl. 1), S72–S81. doi: 10.1097/00002093-200000001-00012

de la Torre, J. C. (2000b). Critically attained threshold of cerebral hypoperfusion: can it cause Alzheimer's disease? *Ann. N. Y Acad. Sci.* 903, 424–436. doi: 10.1111/j.1749-6632.2000.tb06394.x

de la Torre, J. C. (2000c). Impaired cerebromicrovascular perfusion. Summary of evidence in support of its causality in Alzheimer's disease. *Ann. N. Y. Acad. Sci.* 924, 136–152. doi: 10.1111/j.1749-6632.2000.tb05572.x

de la Torre, J. C. (2012b). Cerebral Hemodynamics and Vascular Risk Factors: setting the stage for Alzheimer's disease. *J. Alzheimers Dis.* 32, 553–567. doi: 10.3233/JAD-2012-120793

de la Torre, J. C. (2012a). Cardiovascular risk factors promote brain hypoperfusion leading to cognitive decline and dementia. *Cardiovasc. Psychiatry Neurol.* 2012:367516. doi: 10.1155/2012/367516

Dichgans, M., and Leys, D. (2017). Vascular cognitive impairment. *Circ. Res.* 120, 573–591.

Ding, J., Mitchell, G. F., Bots, M. L., Sigurdsson, S., Harris, T. B., Garcia, M., et al. (2015). Carotid arterial stiffness and risk of incident cerebral microbleeds in older people: the Age, Gene/Environment Susceptibility (AGES)-Reykjavik study. *Arterioscler. Thromb. Vasc. Biol.* 35, 1889–1895. doi: 10.1161/ATVBAHA.115.305451

Ding, J., Sigurethsson, S., Jonsson, P. V., Eiriksdottir, G., Charidimou, A., Lopez, O. L., et al. (2017). Large perivascular spaces visible on magnetic resonance imaging, cerebral small vessel disease progression, and risk of dementia: the age, gene/environment susceptibility-reykjavik study. *JAMA Neurol.* 74, 1105–1112. doi: 10.1001/jamaneurol.2017.1397

Doubal, F. N., Maclullich, A. M., Ferguson, K. J., Dennis, M. S., and Wardlaw, J. M. (2010). Enlarged perivascular spaces on MRI are a feature of cerebral small vessel disease. *Stroke* 41, 450–454. doi: 10.1161/STROKEAHA.109.564914

Duncombe, J., Kitamura, A., Hase, Y., Ihara, M., Kalaria, R. N., and Horsburgh, K. (2017a). Chronic cerebral hypoperfusion: a key mechanism leading to vascular cognitive impairment and dementia. Closing the translational gap between rodent models and human vascular cognitive impairment and dementia. *Clin. Sci. (Lond.)* 131, 2451–2468. doi: 10.1042/CS20160727

Duncombe, J., Lennen, R. J., Jansen, M. A., Marshall, I., Wardlaw, J. M., and Horsburgh, K. (2017b). Ageing causes prominent neurovascular dysfunction associated with loss of astrocytic contacts and gliosis. *Neuropathol. Appl. Neurobiol.* 43, 477–491. doi: 10.1111/nan.12375

Esiri, M. M., Nagy, Z., Smith, M. Z., Barnetson, L., and Smith, A. D. (1999). Cerebrovascular disease and threshold for dementia in the early stages of Alzheimer's disease. *Lancet* 354, 919–920. doi: 10.1016/S0140-6736(99)02355-7

Fowler, J. H., Mcqueen, J., Holland, P. R., Manso, Y., Marangoni, M., Scott, F., et al. (2017). Dimethyl fumarate improves white matter function following severe hypoperfusion: involvement of microglia/macrophages and inflammatory mediators. *J. Cereb. Blood Flow Metab.* 38, 1354–1370. doi: 10.1177/0271678X17713105

Gaberel, T., Gakuba, C., Goulay, R., Martinez De Lizarrondo, S., Hanouz, J. L., Emery, E., et al. (2014). Impaired glymphatic perfusion after strokes revealed by contrast-enhanced MRI: a new target for fibrinolysis? *Stroke* 45, 3092–3096. doi: 10.1161/STROKEAHA.114.006617

Gorelick, P. B., Scuteri, A., Black, S. E., Decarli, C., Greenberg, S. M., Iadecola, C., et al. (2011). Vascular contributions to cognitive impairment and dementia: a statement for healthcare professionals from the american heart association/american stroke association. *Stroke* 42, 2672–2713. doi: 10.1161/str.0b013e3182299496

Gottesman, R. F., Schneider, A. L., Zhou, Y., Coresh, J., Green, E., Gupta, N., et al. (2017). Association between midlife vascular risk factors and estimated brain amyloid deposition. *JAMA* 317, 1443–1450. doi: 10.1001/jama.2017.3090

Gupta, A., and Iadecola, C. (2015). Impaired Abeta clearance: a potential link between atherosclerosis and Alzheimer's disease. *Front. Aging Neurosci.* 7:115. doi: 10.3389/fnagi.2015.00115

Hachinski, V., and Munoz, D. G. (1997). Cerebrovascular pathology in Alzheimer's disease: cause, effect or epiphenomenon? *Ann. N. Y. Acad. Sci.* 826, 1–6. doi: 10.1111/j.1749-6632.1997.tb48456.x

Holland, P. R., Bastin, M. E., Jansen, M. A., Merrifield, G. D., Coltman, R. B., Scott, F., et al. (2011). MRI is a sensitive marker of subtle white matter pathology in hypoperfused mice. *Neurobiol. Aging* 32:2325.e1–6. doi: 10.1016/j.neurobiolaging.2010.11.009

Holland, P. R., Searcy, J. L., Salvadores, N., Scullion, G., Chen, G., Lawson, G., et al. (2015). Gliovascular disruption and cognitive deficits in a mouse model with features of small vessel disease. *J. Cereb. Blood Flow Metab.* 35, 1005–1014. doi: 10.1038/jcbfm.2015.12

Huang, K. L., Lin, K. J., Ho, M. Y., Chang, Y. J., Chang, C. H., Wey, S. P., et al. (2012). Amyloid deposition after cerebral hypoperfusion: evidenced on [F-18]AV-45 positron emission tomography. *J. Neurol. Sci.* 319, 124–129. doi: 10.1016/j.jns.2012.04.014

Hughes, T. M., Kuller, L. H., Barinas-Mitchell, E. J., Mcdade, E. M., Klunk, W. E., Cohen, A. D., et al. (2014). Arterial stiffness and beta-amyloid progression in nondemented elderly adults. *JAMA Neurol.* 71, 562–568. doi: 10.1001/jamaneurol.2014.186

Hughes, T. M., Wagenknecht, L. E., Craft, S., Mintz, A., Heiss, G., Palta, P., et al. (2018). Arterial stiffness and dementia pathology: atherosclerosis risk in communities (ARIC)-PET study. *Neurology* 90, e1248–e1256. doi: 10.1212/WNL.0000000000005259

Iliff, J. J., Wang, M., Zeppenfeld, D. M., Venkataraman, A., Plog, B. A., Liao, Y., et al. (2013b). Cerebral arterial pulsation drives paravascular CSF-interstitial fluid exchange in the murine brain. *J. Neurosci.* 33, 18190–18199. doi: 10.1523/JNEUROSCI.1592-13.2013

Iliff, J. J., Lee, H., Yu, M., Feng, T., Logan, J., Nedergaard, M., et al. (2013a). Brain-wide pathway for waste clearance captured by contrast-enhanced MRI. *J. Clin. Invest.* 123, 1299–1309. doi: 10.1172/JCI67677

Iliff, J. J., Wang, M., Liao, Y., Plogg, B. A., Peng, W., Gundersen, G. A., et al. (2012). A paravascular pathway facilitates CSF flow through the brain parenchyma and the clearance of interstitial solutes, including amyloid beta. *Sci. Transl. Med.* 4:147ra111. doi: 10.1126/scitranslmed.3003748

Johnston, S. C., O'meara, E. S., Manolio, T. A., Lefkowitz, D., O'leary, D. H., Goldstein, S., et al. (2004). Cognitive impairment and decline are associated with carotid artery disease in patients without clinically evident cerebrovascular disease. *Ann. Intern. Med.* 140, 237–247. doi: 10.7326/0003-4819-140-4-200402170-00005

Kitamura, A., Manso, Y., Duncombe, J., Searcy, J., Koudelka, J., Binnie, M., et al. (2017). Long-term cilostazol treatment reduces gliovascular damage and memory impairment in a mouse model of chronic cerebral hypoperfusion. *Sci. Rep.* 7:4299. doi: 10.1038/s41598-017-04082-0

Kober, F., Duhamel, G., and Cozzone, P. J. (2008). Experimental comparison of four FAIR arterial spin labeling techniques for quantification of mouse cerebral blood flow at 4.7 T. *NMR Biomed.* 21, 781–792. doi: 10.1002/nbm.1253

Kress, B. T., Iliff, J. J., Xia, M., Wang, M., Wei, H. S., Zeppenfeld, D., et al. (2014). Impairment of paravascular clearance pathways in the aging brain. *Ann. Neurol.* 76, 845–861. doi: 10.1002/ana.24271

Matin, N., Fisher, C., Jackson, W. F., and Dorrance, A. M. (2016). Bilateral common carotid artery stenosis in normotensive rats impairs endothelium-dependent dilation of parenchymal arterioles. *Am. J. Physiol. Heart Circ. Physiol.* 310, H1321–H1329. doi: 10.1152/ajpheart.00890.2015

Mestre, H., Du, T., Sweeney, A. M., Liu, G., Samson, A. J., Peng, W., et al. (2020). Cerebrospinal fluid influx drives acute ischemic tissue swelling. *Science* 367:eaax7171. doi: 10.1126/science.aax7171

Mestre, H., Tithof, J., Du, T., Song, W., Peng, W. G., Sweeney, A. M., et al. (2018). Flow of cerebrospinal fluid is driven by arterial pulsations and is reduced in hypertension. *Nat. Commun.* 9:4878. doi: 10.1038/s41467-018-07318-3

Montine, T. J., Koroshetz, W. J., Babcock, D., Dickson, D. W., Galpern, W. R., Glymour, M. M., et al. (2014). Recommendations of the Alzheimer's disease-related dementias conference. *Neurology* 83, 851–860. doi: 10.1212/WNL.0000000000000733

Morris, A. W., Sharp, M. M., Albargothy, N. J., Fernandes, R., Hawkes, C. A., Verma, A., et al. (2016). Vascular basement membranes as pathways for the passage of fluid into and out of the brain. *Acta Neuropathol.* 131, 725–736. doi: 10.1007/s00401-016-1555-z

Okamoto, Y., Yamamoto, T., Kalaria, R. N., Senzaki, H., Maki, T., Hase, Y., et al. (2012). Cerebral hypoperfusion accelerates cerebral amyloid angiopathy and promotes cortical microinfarcts. *Acta Neuropathol.* 123, 381–394. doi: 10.1007/s00401-011-0925-9

Patel, A., Moalem, A., Cheng, H., Babadjouni, R. M., Patel, K., Hodis, D. M., et al. (2017). Chronic cerebral hypoperfusion induced by bilateral carotid artery stenosis causes selective recognition impairment in adult mice. *Neurol. Res.* 39, 910–917. doi: 10.1080/01616412.2017.1355423

Paxinos, G., and Franklin, K. B. J. (2001). *The Mouse Brain in Stereotaxic Coordinates*, 2nd Edn. San Diego: Academic Press.

Peng, W., Achariyar, T. M., Li, B., Liao, Y., Mestre, H., Hitomi, E., et al. (2016). Suppression of glymphatic fluid transport in a mouse model of Alzheimer's disease. *Neurobiol. Dis.* 93, 215–225. doi: 10.1016/j.nbd.2016.05.015

Poels, M. M., Zaccai, K., Verwoert, G. C., Vernooij, M. W., Hofman, A., Van Der Lugt, A., et al. (2012). Arterial stiffness and cerebral small vessel disease: the Rotterdam Scan Study. *Stroke* 43, 2637–2642. doi: 10.1161/strokeaha.111.642264

Potter, G. M., Chappell, F. M., Morris, Z., and Wardlaw, J. M. (2015). Cerebral perivascular spaces visible on magnetic resonance imaging: development of a qualitative rating scale and its observer reliability. *Cerebrovasc. Dis.* 39, 224–231. doi: 10.1159/000375153

Reimer, M. M., Mcqueen, J., Searcy, L., Scullion, G., Zonta, B., Desmazieres, A., et al. (2011). Rapid disruption of axon-glial integrity in response to mild cerebral hypoperfusion. *J. Neurosci.* 31, 18185–18194. doi: 10.1523/JNEUROSCI.4936-11.2011

Roberts, J. M., Maniskas, M. E., and Bix, G. J. (2018). Bilateral carotid artery stenosis causes unexpected early changes in brain extracellular matrix and blood-brain barrier integrity in mice. *PLoS One* 13:e0195765. doi: 10.1371/journal.pone.0195765

Romero, J. R., Beiser, A., Seshadri, S., Benjamin, E. J., Polak, J. F., Vasan, R. S., et al. (2009). Carotid artery atherosclerosis, MRI indices of brain ischemia, aging, and cognitive impairment: the Framingham study. *Stroke* 40, 1590–1596. doi: 10.1161/STROKEAHA.108.535245

Salvadores, N., Searcy, J. L., Holland, P. R., and Horsburgh, K. (2017). Chronic cerebral hypoperfusion alters amyloid-beta peptide pools leading to cerebral amyloid angiopathy, microinfarcts and haemorrhages in Tg-SwDI mice. *Clin. Sci. (Lond.)* 131, 2109–2123. doi: 10.1042/CS20170962

Schuff, N., Matsumoto, S., Kmiecik, J., Studholme, C., Du, A., Ezekiel, F., et al. (2009). Cerebral blood flow in ischemic vascular dementia and Alzheimer's disease, measured by arterial spin-labeling magnetic resonance imaging. *Alzheimers Dement.* 5, 454–462. doi: 10.1016/j.jalz.2009.04.1233

Shi, Y., and Wardlaw, J. M. (2016). Update on cerebral small vessel disease: a dynamic whole-brain disease. *Stroke Vasc. Neurol.* 1, 83–92. doi: 10.1136/svn-2016-000035

Shi, Y., Thrippleton, M. J., Blair, G. W., Dickie, D. A., Marshall, I., Hamilton, I., et al. (2018a). Small vessel disease is associated with altered cerebrovascular pulsatility but not resting cerebral blood flow. *J. Cereb. Blood Flow Metab.* 40, 85–99. doi: 10.1177/0271678X18803956

Shi, Y., Thrippleton, M. J., Marshall, I., and Wardlaw, J. M. (2018b). Intracranial pulsatility in patients with cerebral small vessel disease: a systematic review. *Clin. Sci. (Lond.)* 132, 157–171. doi: 10.1042/CS20171280

Shibata, M., Ohtani, R., Ihara, M., and Tomimoto, H. (2004). White matter lesions and glial activation in a novel mouse model of chronic cerebral hypoperfusion. *Stroke* 35, 2598–2603. doi: 10.1161/01.STR.0000143725.19053.60

Shibata, M., Yamasaki, N., Miyakawa, T., Kalaria, R. N., Fujita, Y., Ohtani, R., et al. (2007). Selective impairment of working memory in a mouse model of chronic cerebral hypoperfusion. *Stroke* 38, 2826–2832. doi: 10.1161/STROKEAHA.107.490151

Shokri-Kojori, E., Wang, G. J., Wiers, C. E., Demiral, S. B., Guo, M., Kim, S. W., et al. (2018). beta-Amyloid accumulation in the human brain after one night of sleep deprivation. *Proc. Natl. Acad. Sci. U.S.A.* 115, 4483–4488. doi: 10.1073/pnas.1721694115

Snowdon, D. A., Greiner, L. H., Mortimer, J. A., Riley, K. P., Greiner, P. A., and Markesbery, W. R. (1997). Brain infarction and the clinical expression of Alzheimer disease. The Nun Study. *JAMA* 277, 813–817. doi: 10.1001/jama.1997.03540340047031

Wang, M., Ding, F., Deng, S., Guo, X., Wang, W., Iliff, J. J., et al. (2017). Focal solute trapping and global glymphatic pathway impairment in a murine model of multiple microinfarcts. *J. Neurosci.* 37, 2870–2877. doi: 10.1523/JNEUROSCI.2112-16.2017

Wardlaw, J. M., Allerhand, M., Eadie, E., Thomas, A., Corley, J., Pattie, A., et al. (2017). Carotid disease at age 73 and cognitive change from age 70 to 76 years: a longitudinal cohort study. *J. Cereb. Blood Flow Metab.* 37, 3042–3052. doi: 10.1177/0271678X16683693

Wardlaw, J. M., Smith, E. E., Biessels, G. J., Cordonnier, C., Fazekas, F., Frayne, R., et al. (2013). Neuroimaging standards for research into small vessel disease and its contribution to ageing and neurodegeneration. *Lancet Neurol.* 12, 822–838. doi: 10.1016/S1474-4422(13)70124-8

Xie, L., Kang, H., Xu, Q., Chen, M. J., Liao, Y., Thiyagarajan, M., et al. (2013). Sleep drives metabolite clearance from the adult brain. *Science* 342, 373–377. doi: 10.1126/science.1241224

Xu, Z., Xiao, N., Chen, Y., Huang, H., Marshall, C., Gao, J., et al. (2015). Deletion of aquaporin-4 in APP/PS1 mice exacerbates brain Abeta accumulation and memory deficits. *Mol. Neurodegener.* 10:58. doi: 10.1186/s13024-015-0056-1

Conflict of Interest: The authors declare that the research was conducted in the absence of any commercial or financial relationships that could be construed as a potential conflict of interest.

Publisher's Note: All claims expressed in this article are solely those of the authors and do not necessarily represent those of their affiliated organizations, or those of the publisher, the editors and the reviewers. Any product that may be evaluated in this article, or claim that may be made by its manufacturer, is not guaranteed or endorsed by the publisher.

frontiers | Frontiers in Aging Neuroscience

BRIEF RESEARCH REPORT
published: 27 April 2022
doi: 10.3389/fnagi.2022.806000

Functional Screening of Parkinson's Disease Susceptibility Genes to Identify Novel Modulators of α-Synuclein Neurotoxicity in *Caenorhabditis elegans*

Roman Vozdek*, Peter P. Pramstaller and Andrew A. Hicks

Institute for Biomedicine, Eurac Research, Affiliated Institute of the University of Lübeck, Bolzano, Italy

OPEN ACCESS

Edited by:
Natalia Salvadores, Universidad Mayor, Chile

Reviewed by:
Leonidas Stefanis, National and Kapodistrian University of Athens Medical School, Greece
Jolanta Dorszewska, Poznań University of Medical Sciences, Poland

****Correspondence:***
Roman Vozdek
roman.vozdek@eurac.edu

Specialty section:
This article was submitted to Parkinson's Disease and Aging-related Movement Disorders, a section of the journal Frontiers in Aging Neuroscience

Received: *31 October 2021*
Accepted: *18 March 2022*
Published: *27 April 2022*

Citation:
Vozdek R, Pramstaller PP and Hicks AA (2022) Functional Screening of Parkinson's Disease Susceptibility Genes to Identify Novel Modulators of α-Synuclein Neurotoxicity in Caenorhabditis elegans. Front. Aging Neurosci. 14:806000. doi: 10.3389/fnagi.2022.806000

Idiopathic Parkinson's disease (PD) is characterized by progressive loss of dopaminergic (DA) neurons during aging. The pathological hallmark of PD is the Lewy body detected in postmortem brain tissue, which is mainly composed of aggregated α-Synuclein (αSyn). However, it is estimated that 90% of PD cases have unknown pathogenetic triggers. Here, we generated a new transgenic *Caenorhabditis elegans* PD model *erals1* expressing green fluorescent protein- (GFP-) based reporter of human αSyn in DA neurons, and exhibited a nice readout of the developed αSyn inclusions in DA neurons, leading to their degeneration during aging. Using these animals in a preliminary reverse genetic screening of >100-PD genome-wide association study- (GWAS-) based susceptibility genes, we identified 28 orthologs of *C. elegans* and their inactivation altered the phenotype of *erals1*; 10 knockdowns exhibited reduced penetrance of αSyn:Venus inclusions formed in the axons of cephalic (CEP) DA neurons, 18 knockdowns exhibited increased penetrance of disrupted CEP dendrite integrity among which nine knockdowns also exhibited disrupted neuronal morphology independent of the expressed αSyn reporter. Loss-of-function alleles of the five identified genes, such as *sac-2*, *rig-6* or *lfe-2*, *unc-43*, and *nsf-1*, modulated the corresponding *erals1* phenotype, respectively, and supported the RNA interference (RNAi) data. The Western blot analysis showed that the levels of insoluble αSyn:Venus were not correlated with the observed phenotypes in these mutants. However, RNAi of 12 identified modulators reduced the formation of pro-aggregating polyglutamine Q40:YFP foci in muscle cells, suggesting the possible role of these genes in cellular proteotoxicity. Therefore, modulators identified by their associated biological pathways, such as calcium signaling or vesicular trafficking, represent new potential therapeutic targets for neurodegenerative proteopathies and other diseases associated with aging.

Keywords: Parkinson's disease, α-synuclein, GWAS, neurodegeneration, genetic screen, *C. elegans*

INTRODUCTION

Neurotoxicity of disordered α-synuclein (αSyn) is a pathogenetic hallmark of synucleinopathies, including Parkinson's disease [PD; Spillantini et al. (1997)]. There are more than 20 reported genes associated with monogenic parkinsonism, including autosomal dominant *SNCA* encoding alpha-synuclein (αSyn) and *LRRK2* encoding Leucine-rich repeat kinase 2, or autosomal recessive *PRKN* encoding the E3 ubiquitin ligase Parkin and *PINK1* encoding Phosphatase and tensin homologue (PTEN)-induced kinase (Blauwendraat et al., 2020). However, familial PD with the identified genetic variants still accounts for only about 10% of diagnosed PD cases, while pathogenetic triggers in sporadic forms of PD are largely unknown (Reeve et al., 2014). Therefore, it is largely considered to be a complex disease with multifactorial etiology. In recent years, several genome-wide association studies (GWASs) have identified many tens of risk signals associated with sporadic PD surrounded by hundreds of potential susceptibility genes (Nalls et al., 2019). To date, there is little to no published functional validation of genes in these loci. In this study, we examined the role of approximately 100 of these genes in maintaining dopaminergic (DA) neurons upon exogenous expression of human αSyn in a newly constructed *Caenorhabditis elegans* genetic model designed to aid rapid initial functional screening.

The roundworm *C. elegans*, which does not possess the gene for αSyn, has been well-established as a PD model, which can help identify genes that protect against exogenous αSyn-induced degeneration of DA neurons or aggregation of αSyn in muscle cells (Cooper and Van Raamsdonk, 2018; Koopman et al., 2019). The *C. elegans* PD model, expressing αSyn tagged with green fluorescent protein (GFP) in the body wall muscle cells, was used to seek the effectors of αSyn misfolding through reverse genetic screens elicited by RNA interference (RNAi) (Hamamichi et al., 2008; van Ham et al., 2008; Jadiya et al., 2016). In addition, RNAi of 1,673 genes related to neuronal function revealed genes of the endocytic pathway in pan-neuronal αSyn-induced growth/motor abnormalities (Kuwahara et al., 2008). αSyn expressed in nematode DA neurons causes DA neurodegeneration characterized by neuronal loss or abnormal dendritic processing, and also dopamine-mediated locomotion deficits (Lakso et al., 2003; Kuwahara et al., 2006). In addition, in these PD worm models, the expression of human Torsin A and yeast Rab1, which play a role in vesicular trafficking, showed neuroprotective activity against α-synuclein-induced degeneration (Cao et al., 2005; Cooper et al., 2006). Several studies have also demonstrated that fluorescence-based reporters of αSyn expressed in neuronal tissues recapitulate DA neuronal deficits and show the spread of αSyn into the epithelium (Cooper et al., 2018; Sandhof et al., 2020). However, none of these previous nematode models have been used to identify modulators of αSyn aggregation in neurons. Here, we have generated a new nematode model, *erals1*, which allows monitoring of the expression of αSyn in DA neurons *in vivo*, and used these transgenic animals for functional screening of identified PD risk genes.

MATERIALS AND METHODS

Caenorhabditis elegans Strains

Unless otherwise stated, animals were maintained by standard procedures on nematode growth media (NGM) plates. Transgenic strains were generated by germline transformation using microinjection into Bristol strain N2. *C. elegans* constructs for the *eraIs* transgene were generated by direct PCR of the human *SNCA* gene cloned into the pDEST vector in front of, and in frame with, the Venus reporter gene with *unc-54* 3′UTR. The pDEST vectors carrying hSNCA:Venus or mCherry were subsequently recombined with a pENTRY vector carrying the *dat-1* promoter sequence. Transgenic constructs were co-injected at 50 ng/μl, and stable extrachromosomal lines of mCherry- and Venus-positive animals were established. The extrachromosomal array was subsequently integrated by ultraviolet (UV) irradiation, and the lines carrying *eraIs1* were subjected to 5× outcrossing. The strains used were as follows: *eraIs1*, *otIs181*, *eraIs1;otIs181, eraIs1;pdr-1(gk448), eraIs1;pink-1(tm1779), eraIs1;wlzIs3*, *eraIs1;lfe-2(sy326)*, *eraIs1;unc-43(n1186)*, *eraIs1;nsf-1(ty10)*, *eraIs1;sac-2(ok2743)*, *eraIs1;unc-32(e189)*, *eraIs1;rig-6(ok1589)*, and *rmIs133 (unc-54p:Q40:YFP)*.

Reverse Genetic Screen

RNAi was fed to worms to knockdown the respective gene function. Gravid animals carrying *eraIs1*, *otIs181*, or *rmsIs133* transgenes were placed on NGM media containing ampicillin 25 μg/ml and 1 mM IPTG and seeded with bacteria producing the desired double-stranded RNA (dsRNA). Progenies were subsequently grown at 23°C till the fourth larval stage (L4) stage in which the phenotype was scored *via* visual examination. *eraIs1* animals were scored for the disruption of cephalic (CEP) integrity, which was defined by the presence of fluorescent inclusions in the area of the CEP axons (phenotype A) and CEP dendrite blebbing/loss (phenotype B). Both of these phenotypes were selected as being the most tractable by visual inspection due to the bright fluorescence of the αSyn reporter in CEP neurons, which allowed quantification of individual RNAi knockdowns in a relatively high-throughput way. Moreover, assessing animals at the L4 stage revealed modulators of phenotypes A and B. Each population of L4 knockdowns having 0–60% of individuals exhibiting phenotype A and 40–100% of individuals exhibiting phenotype B was classified as modulators. *otIs181* and *rmsIs133* animals were scored for the disruption of CEP integrity, defined by dendrite blebbing/loss and number of fluorescent foci, respectively. At least 20 *eraIs1*, 20 *otIs181*, or 3 *rmsIs133* animals were visually examined for penetrance and fluorescent foci quantification, respectively. Visual examination was done using a fluorescent stereoscope (Nikon SMZ800N) by one researcher with coded plates to ensure blindness of the investigator. The results were recorded and subsequently decoded to reveal the names of RNAi targets. Bacterial clones were obtained from the *C. elegans* RNAi collection—Ahringer (Source: Bioscience).

Locomotor Assay

Animals were grown at 23°C under non-starved conditions. One-day-old adult hermaphrodites were placed on NGM plates and recorded. For the crawling/swimming transition assay, animals were subjected to liquid exposure by dropping 30 µl of M9 buffer on the plate, which was dried within 7–8 min. For the mechanical stimuli assay, animals crawling on the NGM plate with seeded bacteria were stressed by five taps of the plate on the bench. For the foraging assay, well-fed animals were placed 1 cm away from the bacterial lawn. Animal movement was subsequently screened by quantifying body bends in the indicated time intervals of 30 s. During crawling, body bends were scored as head turns for moving forward. During swimming, body bends were scored as C-shaped movements. At least three biological replicates (five animals per assay) were used for statistical analysis. To compare the distribution of animals on and off the food area, 1-day old adults, which were starved for 1 h, were placed 1 cm away from the bacterial lawn on NGM plates, and their position on the plate was scored 30 min later. At least 50 animals for each group (N2 vs. *eraIs1*) with three independent biological replicates were used for statistical analysis.

Statistical Analyses

Data are presented as mean ± standard deviation (SD) with *p*-values calculated by one-way analysis of variance (ANOVA) with Bonferroni correction for multiple comparisons and the Mann–Whitney test for single comparison.

Determination of α-Synuclein Levels

Worms were grown at 23°C as described above and collected as a mixed population of all larval and adult stages. Wet worm pellets were subsequently frozen at −20°C for 4 h to disrupt the nematode cuticle. Worm lysates were prepared by sonication of worm pellets resuspended in M9 buffer containing protease and phosphatase inhibitor cocktail. Crude extracts were immediately centrifuged for 1 h at 4°C and 20,000 *g*, and the supernatants (soluble fraction) and pellets (insoluble fraction) were used for the determination of αSyn:Venus levels in the indicated mutants by the Western blot analysis. Samples were boiled for 10 min in reducing lithium dodecyl sulfate (LDS) sample buffer and submitted to SDS-PAGE (4–12% precast gradient gel). Protein immunodetection was performed by the Western blot using a custom-made mouse monoclonal anti-αSyn antibody (Abnova, MAB5383 1:2,000). Ubiquitin, which was detected using a mouse monoclonal anti-ubiquitin Ab (CellSignal, P4D1 1:2,000), along with an unspecific signal, was used to demonstrate protein loading. Western blot signals were semi-quantified in ImageJ software (Fiji).

Imaging

For confocal imaging, animals were mounted on a 2% agarose pad with 10 mM sodium azide and imaged on a Leica SP8-X confocal laser scanning microscope within 2–10 min. At least three images representing each *C. elegans* strain from three independent biological replicates were analyzed.

RESULTS

To study neuronal genes that mediate proteostasis upon the formation of αSyn inclusions, we have generated a new transgenic *C. elegans* carrying *eraIs1(dat-1p:human SNCA:Venus; dat-1p:mCherry)*. The *eraIs1* transgene uses the *dat-1* promoter to drive the expression of a human *hSNCA:Venus* reporter along with an mCherry reporter specifically in DA neurons consisting of four CEP neurons, two anterior deirids (ADE) in the head, and two posterior deirids (PDE) in the tail. Bright GFP-based reporter Venus of human αSyn allowed us to monitor the spatial and temporal formation of its inclusions (fluorescent foci) in axons, dendrites, and cell bodies (**Figure 1A**). Notably, we observed that expressed mCherry, which is diffusely distributed in the cytosol under standard conditions throughout development and aging, forms inclusions in the presence of αSyn:Venus. Similar to the mCherry reporter, the expression of the untagged Venus reporter alone did not form fluorescent inclusions, indicating that the expression of exogenous human αSyn is crucial for the formation of inclusions (**Figure 1A**). Intriguingly, both αSyn:Venus and mCherry reporters in *eraIs1* can also exhibit aggregated fluorescent signals away from intact neurons (**Figure 1A**). These isolated fluorescent foci of aggregated proteins presumably represent an extruded toxic material as an active neuronal self-maintaining mechanism against disrupted proteostasis rather than cell remnants of degenerated neurons (Melentijevic et al., 2017).

During visual inspection of *eraIs1* animals using a fluorescent stereoscope, we observed that *eraIs1* nematodes exhibit the progressive formation of αSyn:Venus inclusions accompanied by morphological changes of CEP neurons during development, and ultimately the disruption of neuronal integrity in aged animals. The bright Venus fluorescence allowed us to determine which animals developed fluorescent inclusions in the axons of CEP neurons (phenotype A) and pathological morphology (blebbing) of CEP dendrites (phenotype B). We assessed the penetrance of these two phenotypes during animal development and determined that the penetrance of phenotype A increases from 32% at the third larval stage (L3) to 83% at L4, while the penetrance of phenotype B reaches 25% at L4 and 93% at the young adult stage. In 3-day-old adults, CEP neurons exhibited rounded cell bodies accompanied by dendritic disorganization, indicating the process of neurodegeneration associated with aging (**Figures 1B,C**; Chen et al., 2015).

Dopaminergic neurons regulate several animal behaviors, such as locomotory response to food availability (Sawin et al., 2000; Omura et al., 2012), foraging (Hills et al., 2004), or movement transitions between crawling and swimming (Vidal-Gadea et al., 2011). To determine whether *eraIs1* animals exhibit respective behavioral phenotypes due to DA neuronal defects, we exposed 1-day-old adult *eraIs1* and wild-type isolate N2 to various stimuli and compared their locomotor behavior by counting the body bends used for crawling or swimming. First, we exposed well-fed animals, crawling on the bacterial lawn on NGM plates, to M9 buffer. While N2 animals exposed to M9 liquid buffer responded immediately by swimming at the rate of 48 C-shaped body bends per 30 s, *eraIs1* animals failed to

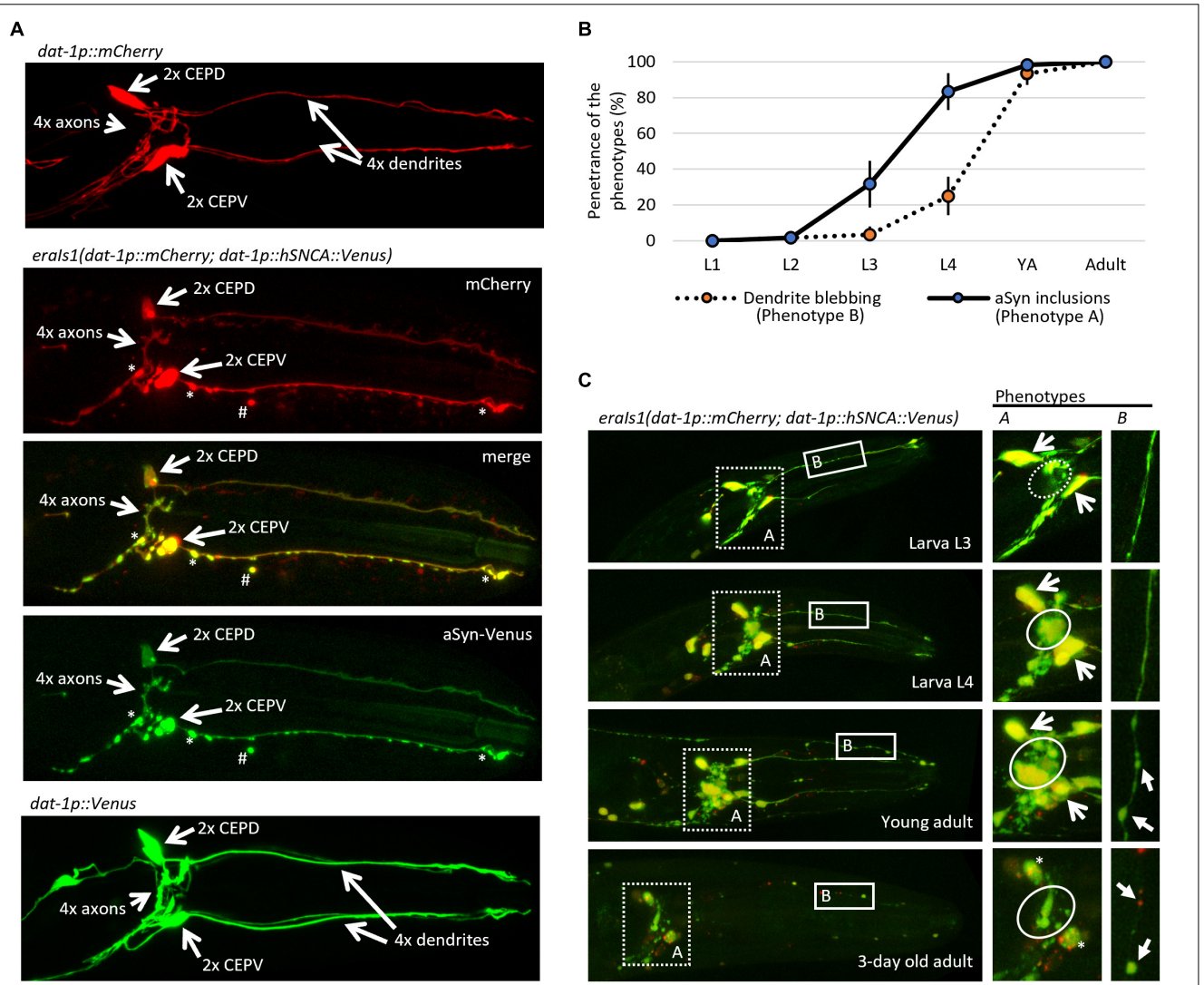

FIGURE 1 | *eraIs1* animals exhibit progressive formation of α-Synuclein (αSyn) inclusions and disruption of the dopaminergic (DA) neuron integrity during aging. **(A)** Representative fluorescent image of the head of third larval stage (L3) animals expressing the mCherry reporter alone, the mCherry reporter with the αSyn:Venus reporter, and the Venus reporter alone in DA neurons. Two head ventral CEPV and two dorsal CEPD neurons and their axons are indicated by open arrows. Stars indicate αSyn:Venus inclusions. Hashtag indicates extruded αSyn:Venus from DA neurons. **(B)** Distribution of phenotypes quantified at distinct developmental stages of *eraIs1* animals. $n \geq 20$ total animals for each group with three independent biological replicates. Mean ± standard deviation (SD) is shown. **(C)** Representative fluorescent images of the head of *eraIs1* animals at different stages of development. Dotted square line highlights the area used for the quantification of phenotype A (αSyn:Venus inclusions) and the solid square line highlights the area used for the quantification of phenotype B [cephalic (CEP) dendrite blebbing]. On the right, there are enlarged images of the phenotypes A and B areas that show the phenotype identifiers for quantification. The circle line defines the area for the evaluation of phenotype A. The dashed circle indicates a normal phenotype, and the solid circle indicates phenotype A. Open arrows indicate CEP cell bodies. Three-day-old adult exhibits rounded CEP cell bodies indicated by the stars. Phenotype B is indicated by arrows.

respond, with an average rate of 3 C-shaped body bends per 30 s (**Figure 2A**). In addition, while crawling locomotion of well-fed *eraIs1* animals was not altered before M9 buffer exposure, it was noticeably reduced after swimming compared to N2 animals (**Figure 2A**). The defective response of *eraIs1* to M9 buffer is not caused by a locomotion defect as both N2and *eraIs1* exhibited a swimming phenotype at the rate of 41 and 46 body bends per 30 s after 5 min in M9 buffer, respectively (**Figure 2A**). Moreover, mechanical stimuli elicited by plate tapping did not reveal significant behavioral changes between N2 and *eraIs1* animals, indicating that the locomotion of *eraIs1* animals is not impaired (**Figure 2B**). Next, we tested whether *eraIs1* animals would exhibit foraging defects. We placed well-fed animals on an NGM plate outside the bacterial lawn and found that *eraIs1* animals exhibit a reduced locomotor response to lack of food (**Figure 2C**). Moreover, when we used starved animals and examined the plates after 30 min, we observed that a greater number of *eraIs1* animals remained outside, but in proximity to, the bacterial lawn, indicating a possible food sensing deficit (**Figure 2D**). Specifically, we observed that only 74% of *eraIs1*

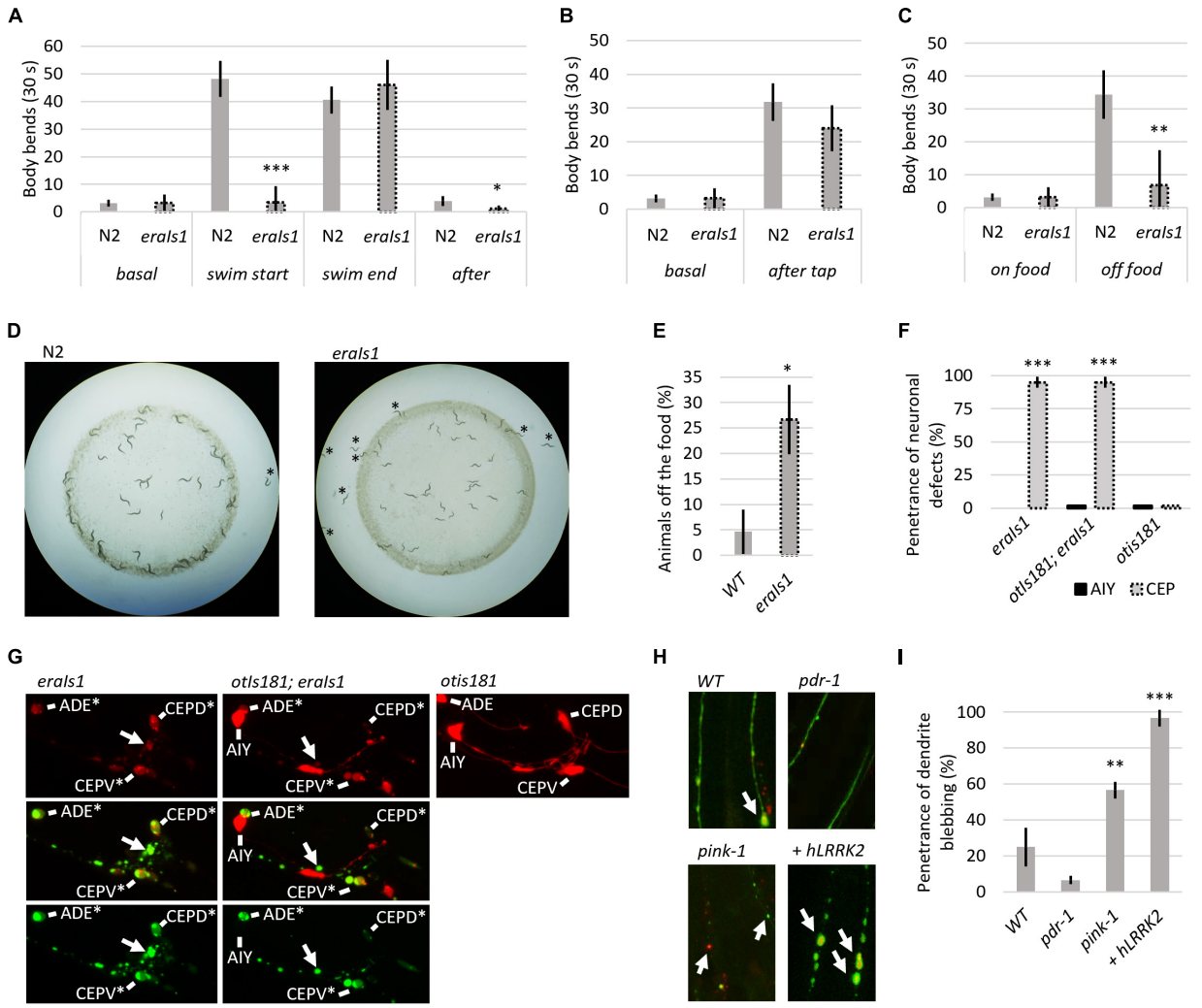

FIGURE 2 | Evaluation of the eralS1 model. **(A)** Locomotor phenotype of the indicated animals placed on a nematode growth media (NGM) plate seeded with OP 50 bacteria (basal), right after exposure to M9 buffer (swim start), 5 min after exposure to M9 (swim end), and right after swimming (after). $n \geq 10$ young adults for each group with three independent biological replicates. During crawling, body bends were scored as head turns for moving forward. During swimming, body bends were scored as C-shaped movements. Mean ± SD is shown. $^{*}p < 0.05$. $^{***}p < 0.001$. **(B)** Locomotory phenotype of the indicated animals localized in the bacterial lawn (basal) and right after being disturbed by tapping (after tap). $n \geq 10$ young adults for each group with three independent biological replicates. Mean ± SD is shown. **(C)** Locomotory phenotype of indicated animals localized in bacterial lawn (on-food) and right after being placed off the bacteria (off-food). $n \geq 10$ young adults for each group with three independent biological replicates. Mean ± SD is shown. $^{**}p < 0.01$. **(D)** Distribution of the indicated animals on the NGM plate seeded with bacteria. Animals starved for 1 h are captured 30 min after being placed 1 cm away from the bacterial lawn. **(E)** Percentage of the indicated animal populations found outside the bacterial lawn. $n \geq 50$ young adults for each group with three independent biological replicates. Mean ± SD is shown. $^{*}p < 0.05$. **(F)** Percentage of young adult *eralS1*, *otIs181;eralS1*, and *otIs181* animals exhibiting αSyn:Venus and mCherry inclusions in CEP and AIY neurons. $n \geq 20$ animals for each group with three independent biological replicates. Mean ± SD is shown. $^{***}p < 0.001$. **(G)** Enlarged fluorescent images of the head of young adult *eralS1*, *eralS1;otIs181*, and *otIs181* animals. Arrows indicate αSyn:Venus inclusions. CEP and AIY cell bodies are indicated. Stars indicate neuronal cell bodies with the αSyn:Venus and mCherry inclusions. **(H)** Representative fluorescent images of CEP dendrites in the indicated *eralS1* animals. *eralS1* wild type (WT), *eralS1;wIzIs3* carrying *human LRRK2 p.G2019S*, and *pdr-1(gk448)* and *pink-1(tm1779)* mutants are shown. Arrows indicate CEP dendrite blebbing. **(I)** The penetrance of dendrite blebbing in the indicated *eralS1* animals. $n \geq 20$ fourth larval stage (L4) animals for each group with three independent biological replicates. Mean ± SD is shown. $^{**}p < 0.01$. $^{***}p < 0.001$.

animals were located inside the bacterial lawn compared to 95% of N2 animals (**Figure 2E**). Taken together, these behavioral data demonstrate that *eraIs1* animals exhibit behavioral characteristics similar to that induced by dopamine deficiency.

We verified the effect of αSyn on neuronal integrity with an independent neuronal mCherry reporter. We used the *otIs181* transgene that uses *dat-1:mCherry* together with *ttx-3:mCherry,* which drives its expression in DA neurons and amphid interneurons (AIY), respectively, and crossed it with *eraIs1*. As expected, *eraIs1* induced neuronal defects of the DA neurons but not the AIY neurons in young adults, suggesting cell-autonomous neurotoxicity of the expressed αSyn (**Figures 2F,G**).

To further validate the PD model *eraIs1*, we tested whether known neurodegenerative triggers, such as loss-of-function of Parkin and PINK1 and gain of function of human LRRK2, which are associated with familial forms of PD, would induce neuronal defects upon αSyn expression (Yao et al., 2010; Blauwendraat et al., 2020). We used loss-of-function alleles of *C. elegans prd-1/Parkin*, *pink-1/PINK1,* and the transgene *wlzIs3* expressing human *LRRK2 p.G2019S* (Saha et al., 2009) and crossed them with *eraIs1*. We assessed the toxicity of αSyn in these mutants at the L4 developmental stage, which allowed us to identify both suppressors of phenotype A and enhancers of phenotype B. In addition, the size of L4 animals reduces experimental bias resulting from impaired traceability of respective phenotypes in younger larval stages and phenotypic variability in adults. We found that dendrite blebbing was exacerbated in animals carrying *pink-1* and *wlzIs3* but not in *pdr-1* mutants (**Figures 2H,I**). These data demonstrate that the phenotype modulated in *eraIs1;pink-1 and eraIs1;wlzIs3* animals could be used as a readout to identify new modulators of αSyn-induced neurodegeneration.

We searched several current GWAS databases, such as iPDGC (Grenn et al., 2020), GWAS catalog (Buniello et al., 2019), and PDgene (Lill et al., 2012; Nalls et al., 2014) for genes associated with sporadic PD. Collectively, we identified 98 risk signals at different levels of statistical significance from 89 independent genomic loci. We selected 131 PD susceptibility genes based on their proximity and position relative to the PD risk signals and analyzed them *in silico* for evolutionary conservation in the *C. elegans* genome based on phylogenetic and structural data information. For 97 of the human-associated potential risk genes, we identified at least one *C. elegans* ortholog, collectively consisting of 127 different worm genes (**Supplementary Table 1**). We set out to perform a preliminary reverse genetic screen of these identified *C. elegans* orthologous genes using an RNA interference by "feeding approach" (genes for which an RNAi clone was not available were not included in the screen), or using previously isolated loss-of-function alleles, for modulated αSyn neurotoxicity in the *eraIs1* strain. Overall, we have visually examined 98 knockdown/mutant animal populations and recorded the penetrance of phenotypes A (αSyn:Venus inclusions in CEP axons) and B (CEP dendrite blebbing/loss) at the L4 developmental stage (**Figure 1C**). The preliminary RNAi data obtained clustered the examined genes into two basic groups: (i) 10 genes whose inactivation reduced the penetrance of phenotype A (**Figure 3A** and **Table 1**) and (ii) 18 genes whose inactivation increased the penetrance of phenotype B (**Figure 3B** and **Table 1**).

We validated each RNAi phenotype with six previously characterized loss-of-function alleles, such as *sac-2, rig-6*, and *unc-32,* whose inactivation reduced the penetrance of phenotype A, and *unc-43, lfe-2*, and *nsf-1,* whose inactivation increased the penetrance of phenotype B. We confirmed reduced penetrance of αSyn:Venus inclusions (phenotype A) formed in *sac-2* and *rig-6* mutants even though confocal imaging of these mutants revealed that the formation of inclusions was not completely suppressed. However, the size of the formed inclusions cannot be recognized by visual inspection using a fluorescent stereoscope compared to the fluorescent inclusions accumulated in wild-type (WT) animals, which explains the observed reduction in penetrance in these mutants (**Figures 3C,D**). Next, we confirmed increased penetrance of dendrite blebbing (phenotype B) in *lfe-2* and *unc-43* that phenocopy *nsf-1* mutants, and confocal imaging revealed the altered integrity of their CEP dendrites (**Figures 3E,F**). These data show that the preliminary results obtained from reverse genetic screening have been validated for five different genes confirming their modulatory role in αSyn neurotoxicity in *C. elegans*.

We investigated whether the altered penetrance of phenotypes A and B in the tested mutants was associated with altered levels, solubility, or processing of expressed αSyn:Venus. We used Western blot analysis to detect the levels of αSyn:Venus in crude, soluble and insoluble *C. elegans* extracts and the amount of αSyn:Venus its soluble and insoluble fractions. We used a detergent-free lysis buffer in which the insoluble αSyn should be composed of both aggregated/fibrillar form and monomeric αSyn bound to the cellular/organelle membrane. First, we did not detect any significant alterations of normalized αSyn levels in crude extracts of the tested mutants, indicating that modulated phenotypes are not mediated through altered expression of αSyn:Venus but rather to altered capability of neurons to cope with the stress induced by αSyn. However, we found various levels of insoluble αSyn among the tested mutants. We normalized the ratio of insoluble/soluble αSyn to WT and detected higher levels of insoluble αSyn in *unc-32* mutants and in strain co-expressing human LRKK2 p.G2019S with increased penetrance of phenotype B. On the other hand, levels of insoluble αSyn were markedly decreased in *rig-6* mutants, in which penetrance of phenotype A was reduced, and in *nsf-1* mutants, in which the penetrance of phenotype B was increased (**Figure 3G**). These data suggest that both modulated phenotypes in *eraIs1* mutants might have various pathogenetic basis that did not have to be necessarily associated with aggregation-related nor membrane-bound-related αSyn toxicity.

To better investigate the role of all identified modulators in cellular proteostasis, we next assessed the RNAi of the 28 identified genes for their capability to modulate the aggregation of the pro-aggregating poly-Glutamine (Q40):YFP protein expressed in muscle cells. We used *rmIs133(unc-54p:Q40:YFP)* animals, in which Q40:YFP progressively forms fluorescent foci during development (van Ham et al., 2008) and are easily tractable by visual inspection under a fluorescent stereoscope. We counted the fluorescent foci at the L4 stage among the tested RNAi conditions and found that nine modulators of phenotype A, such as RNAi of *sac-2, sipa-1, glo-1, C56A3.6, hap-1, F46F11.1, rig-6, ufbp-1*, and *lrk-1*, significantly reduced the number of formed Q40:YFP foci (**Figures 3H,J**). Interestingly, the RNAi against *unc-10*, *seb-3*, and *unc-43*, which were classified as modulators of phenotype B, also reduced the number of Q40:YFP foci (**Figure 3J**). These data suggest that 12 identified mediators of Q40:YFP aggregation may play a role in the maintenance of proteotoxicity, including neurotoxicity induced by the expression of αSyn in *eraIs1* animals.

To evaluate the possibility that the identified modifiers could modulate neuronal integrity independent of αSyn expression,

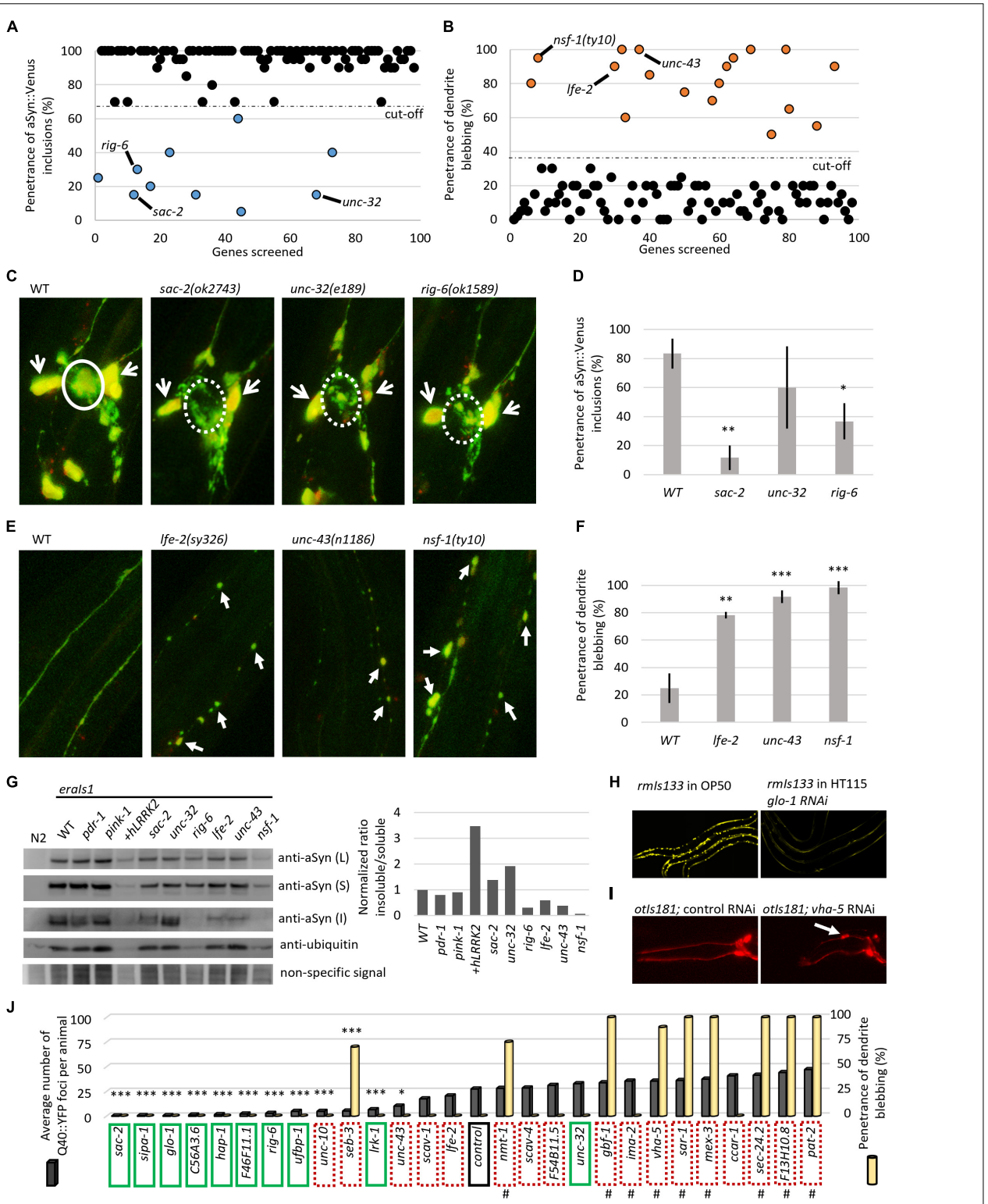

FIGURE 3 | Reverse genetic screening for altered αSyn neurotoxicity in *erals1* animals. **(A)** Distribution of the quantified phenotype of αSyn inclusions (phenotype A) in 98 different knockdowns. **(B)** Distribution of quantified phenotype B (CEP dendrite blebbing) in 98 different knockdowns. **(C)** Representative fluorescent images of CEP cell bodies and their axons of *erals1* mutants at L4 stage. The solid circle line indicates phenotype A while the dotted circle line indicates a normal phenotype. Open arrows indicate CEP cell bodies. **(D)** Penetrance of phenotype A (αSyn:Venus inclusions) in the indicated mutants. $n \geq 20$ L4 animals for each group with three independent biological replicates. Mean ± SD is shown. $^{*}p < 0.05$. $^{**}p < 0.01$. **(E)** Representative fluorescent images of CEP dendrites of *erals1* mutants at the L4

(Continued)

FIGURE 3 | stage. Arrows indicate CEP dendrite blebbing. **(F)** Penetrance of phenotype B (dendrite blebbing) in the indicated mutants. $n \geq 20$ L4 animals for each group with three independent biological replicates. Mean ± SD is shown. $^{**}p < 0.01$. $^{***}p < 0.001$. **(G)** αSyn:Venus protein levels determined by SDS-PAGE followed by western blot using anti-αSyn Ab, and anti-ubiquitin Ab and non-specific signal as a loading control, and the calculated ratio of insoluble/soluble αSyn levels normalized to WT are presented. Animals of mixed stages were collected from three biological replicates and 10 μl of either lysed *Caenorhabditis elegans* pellets of the same density (L) or soluble (S) and insoluble (I) fraction were loaded per lane. *eraIs1* animals carry the following alleles: WT, *pdr-1(gk448)* and *pink-1(tm1779)*, *wIzIs3(snb-1p:hLRRK2 p.G2019S)*, *lfe-2(sy326)*, *unc-43(n1186)*, *nsf-1(ty10)*, *sac-2(ok2743)*, *unc-32(e189)*, and *rig-6(ok1589)*. **(H)** Representative fluorescent images of *rmIs133* animals at the L4 stage expressing Q40:YFP in body wall muscles upon standard (feeding OP50 bacteria) and *glo-1* RNA interference (RNAi). **(I)** Representative fluorescent images of the head of young adult *otIs181* animals upon control and *vha-5* RNAi. **(J)** Quantification of Q40:YFP fluorescent foci in *rmIs133* ($n \geq 3$ L4 animals) and penetrance of CEP dendrite blebbing in *otIs181* animals ($n \geq 20$ L4 animals) among RNAi knockdowns. Green boxes indicate identified modulators of phenotype A (αSyn:Venus inclusions in *eraIs1*), dotted red boxes indicate identified modulators of phenotype B (dendrite blebbing in *eraIs1*). Hashtags indicate knockdowns that fail to propagate (lethal or sterile phenotype). Stars indicate genes whose inactivation reduced Q40:YFP foci. $^{*}p < 0.05$. $^{***}p < 0.001$.

we retested all identified modulators in animals carrying *otIs181(dat-1p:mCherry;ttx-3p:mCherry)* (Flames and Hobert, 2009) expressing an mCherry reporter in DA neurons alone. We found that RNAi against nine genes that were identified as modulators of phenotype B, including *seb-3, sec-24.2, vha-5, sar-1, nmt-1, gbf-1, pat-2, mex-3*, and *F13H10.8*, induced CEP dendrite blebbing in *otIs181* animals, indicating that inactivation of these genes disrupted neuronal integrity independent of neurotoxic αSyn expression (**Figures 3I,J**, and **Table 1**). Notably, RNAi of some of these genes caused sterility, larval arrest, or developmental delay of animals, indicating a widespread effect of gene inactivation on worm health. The complementary screens with *eraIs1* and *otIs181* animals identified 19 genes, whose inactivation modulated αSyn-mediated toxicity, and other nine genes, whose inactivation disrupted the integrity of DA neurons independent of αSyn-mediated toxicity.

DISCUSSION

Several studies over the years have revealed tens of genes that can modulate αSyn aggregation and associated neurodegeneration in various animal and cell model systems. However, a model that allows monitoring of the αSyn processing in neurons *in vivo* in a high-throughput way under various conditions is, until now, somewhat missing. Here, we generated a *C. elegans* model, in which αSyn inclusions and accompanying neuronal morphological processes can be monitored under a fluorescent stereoscope *in vivo*. We showed that the formation of αSyn inclusions was predominantly detected in the axons of CEP neurons at the L4 larval stage, which allowed the screening of inactivated genes that reduced the level of inclusion formation. We also showed that the expression of αSyn in *eraIs1* induced the dendrite blebbing of CEP neurons in adults but was rare in larval stages, which allowed the screening of the genes, whose inactivation induced dendrite blebbing in the larval stages. Therefore, this study provides the first systematic functional screening of the genes identified in the PD GWAS data and reveals new genetic pathways that could mediate PD pathogenesis.

First, we identified 18 genes, whose inactivation exacerbated αSyn:Venus-induced neuronal defect characterized by CEP dendrite blebbing. Notably, RNAi of nine of these modulators induced dendrite blebbing independent of αSyn:Venus expression in these neurons and/or caused impaired propagation of animals, which indicates their crucial role in neuronal cell integrity and *C. elegans* biology. Therefore, we hypothesize that these genes, when misregulated, might induce neuronal defects in other organisms independent of the pathogenicity of αSyn. These data also raise speculation whether some PD GWAS genes could play a role in PD progression in an αSyn-independent manner. Second, we identified 10 genes whose inactivation by RNAi reduced the formation of αSyn:Venus inclusions in CEP axons.

RNAi screening identified a total of 19 genes, which, when inactivated, modulated αSyn-related toxicity; however, our data did not reveal the nature of such toxicity, which could be mediated by aggregation or non-aggregation. The Western blot analysis indicated that the observed neurodegenerative phenotype in *eraIs1* animals does not have to be necessarily related to αSyn aggregation/fibrillation or membrane-bound αSyn as we detected contradicted insoluble αSyn levels among modifiers of phenotype A and among modifiers of phenotype B. In addition, RNAi of 12 identified modulators also reduced the formation of Q40:YFP inclusions in body wall muscle cells, of which three of these caused the dendrite blebbing in *eraIs1* animals. Thus, we cannot exclude the possibility that some genetic conditions that modulated phenotypes of *eraIs1* animals might have opposite consequences in other model systems. Notably, an increasing number of studies have shown that the formation of αSyn inclusions may be a beneficial mechanism for αSyn neurotoxicity (Wong and Krainc, 2017). We should also take into account that RNAi conditions utilizing the vector L4440 in HT115 bacteria might exert phenotype effects independent of the desired RNAi target and thus reduced YFP foci in some animals exposed to RNAi conditions could be an effect of transgene silencing (De-Souza et al., 2019); some RNAi knockdowns exhibited a decreased fluorescent signal of the soluble Q40:YFP reporter compared to animals exposed to standard OP50 bacteria (**Figure 3I**). Further investigations of these observed phenotypes and studying the aggregated vs. non-aggregated-related αSyn toxicity in the *eraIs1* model in follow-up studies are needed. Lastly, it should be noted that other tested PD risk genes, which did not modulate *eraIs1* phenotypes in this study, may play a role in αSyn neurotoxicity under different experimental designs or in other model systems or in humans.

Nonetheless, the physiological roles associated with the identified genes also reveal the biological processes that may constitute pathogenetic pathways in sporadic

TABLE 1 | Identified modulators.

Biological process	Modulators of phenotype A	Presumable function	Modulators of phenotype B	Presumable function
Calcium signaling	*C56A3.6/MICU3*	Regulates mitochondrial Ca2 + uptake (Patron et al., 2019).	*unc-43/CAMK2D*	Regulates Ca2+ homeostatis through targeting T-type calcium channels (Welsby et al., 2003).
			lfe-2/ITPKB	Inhibits Ca2+ release into cytosol from endoplasmic reticulum by metabolizing IP3 (Berridge, 2016).
			*seb-3/CRHR1****	Inhibits T-type calcium channels through GPCR signaling upon binding corticotropin-releasing factor and urocortin (Bonfiglio et al., 2011).
GTPase activity and vesicle trafficking	*lrk-1/LRRK2*	Phosphorylates Rab family of small GTPases (Steger et al., 2016).	*unc-10/RIMS1*	Regulates exocytosis of synaptic vesicle using Ras GTPase activity (Wang and Südhof, 2003).
	glo-1/RAB29	Maintains endosome-trans-Golgi network structure and retrograde trafficking by recruiting LRRK2 (Purlyte et al., 2018).	*sec-24.2/SEC24A****	Mediates protein transport from the endoplasmic reticulum by forming coat of the vesicles (Wendeler et al., 2007).
	unc-32/ATP6V0A1	Transports protons across cellular membranes to acidify various organelles (Aoto et al., 2021).	*vha-5/ATP6V0A1****	Transports protons across cellular membranes to acidify various organelles (Aoto et al., 2021).
	sipa-1/SIPA1L2	Orchestrates retrograde trafficking of amphisomes using Rap GTPase activity (Andres-Alonso et al., 2019).	*nsf-1/NSF*	Promotes fusion of the vesicle with the target membrane using ATPase activity (Zhao et al., 2007).
	sac-2/INPP5F	Regulates endocytic recycling pathway using PI4P 4-phosphatase activity (Nakatsu et al., 2015).	*sar-1/SAR1B****	Initiates coat formation of nascent vesicles using GTPase activity (Hanna et al., 2016).
			*nmt-1/NMT2****	Promotes ARF6 GTPase using its lysine myristoyltransferase activity (Kosciuk et al., 2020).
			*gbf-1/GBF1****	Maintains Golgi network homeostasis using GEF activity toward ARF GTPases (Kawamoto et al., 2002).
Other	*rig-6/CNTN1*	Regulates neurite outgrowth by mediating cell-cell interactions (Falk et al., 2002).	*pat-2/ITGA8****	Regulates neurite outgrowth by mediating cell-cell interactions (Müller et al., 1995).
	ufbp-1/DDRGK1	Regulates reticulophagy (Liang et al., 2020).	*mex-3/MEX3C****	Promotes mRNA decay (Kuniyoshi et al., 2014).
	hap-1/ITPA	Metabolizes ITP and XTP (Simone et al., 2013).	*ccar-1/CCAR2*	Regulates cell cycle and apoptosis (López-Saavedra et al., 2016).
	F46F11.1/PPIP5K2	Maintains IP6 and IP7 levels (Fridy et al., 2007).	*Ima-2/KPNA1*	Imports proteins into nucleosome (Moroianu et al., 1995).
			*F13H10.8/SPTSSB****	Stimulates the activity of serine palmitoyltransferase (Han et al., 2009).
			scav-1 and 4/SCARB2	Serves as lysosomal receptor for protein targeting (Reczek et al., 2007).
			F54B11.5/RNF141	-

****Indicates the genes whose inactivation induced dendrite blebbing also in the control strain otIs181 and thus impaired neuronal integrity independently of exogenously expressed α-Synuclein (αSyn).*

forms of PD. We found that human orthologs of the two identified modulators—*unc-43*/*CAMK2D* and *lfe-2*/*ITPKs*—regulate calcium release from the endoplasmic reticulum into the mitochondria while *C56A3.6*/*MICU3* regulates mitochondrial calcium uptake (**Table 1**). These data are consistent with a recent observation revealing mammalian *ITPKB* as a protective gene against PD-like phenotypes triggered by mitochondrial calcium uptake (Apicco et al., 2021). We thus conclude that intracellular calcium signaling modulates αSyn neurotoxicity in *C. elegans*. In addition, we identified several specific GTPases and their regulators associated with vesicular trafficking, including synaptic, endosomal, ER/Golgi, and autophagosome/lysosome networks, which altered neuronal αSyn processing. The role of vesicular trafficking in PD is well-documented, and its

impairment is one of the leading mechanisms of PD pathogenesis (Hunn et al., 2015). Several genes, such as *sac-2/INPP5F* and *nsf-1/NSF* have been shown to modulate PD-like phenotypes in mouse and fruit fly PD models, respectively (Babcock et al., 2015; Cao et al., 2020). Also, another identified modulator *lrk-1/LRRK2* and its counterpart *glo-1/RAB29* have been previously associated together in PD pathogenesis, but the role of RAB29 in αSyn pathology has not been validated (Kalogeropulou et al., 2020). These findings demonstrate that hypothesis-free identification of candidate PD genes through GWAS can be tracked functionally in a relatively high-throughput way with the *eraIs1* model, to reveal new roles of evolutionary conserved genes in neuronal maintenance upon proteotoxic stress.

Together, reverse genetic screening using a new *C. elegans* PD model system identified 19 functionally interesting PD-risk genes involved in αSyn:Venus toxicity in nematode DA neurons and other nine genes involved in DA neuron maintenance in the αSyn-free system. The obtained data provide a strong foundation for follow-up studies aimed at further characterizing the role of these genes in PD, which represent new potential therapeutic targets for synucleinopathies and other neurodegenerative proteopathies associated with aging.

DATA AVAILABILITY STATEMENT

The original contributions presented in the study are included in the article/**Supplementary Material**, further inquiries can be directed to the corresponding author.

AUTHOR CONTRIBUTIONS

RV designed, performed, and analyzed the experiments and wrote the manuscript. AH designed and analyzed the experiments. All authors acquired funding and reviewed the manuscript.

FUNDING

This project was funded by the European Union's Horizon 2020 Research and Innovation Programme under Grant No. 844497. This research was partly funded by the Department of Educational Assistance, University and Research of the Autonomous Province of Bolzano, Italy, through the Institute for Biomedicine core funding initiative. The authors thank the Department of Innovation, Research University and Museums of the Autonomous Province of Bozen/Bolzano for covering the Open Access publication costs.

ACKNOWLEDGMENTS

We thank the *Caenorhabditis* Genetics Center for *C. elegans* strains and Dengke Ma lab for plasmids.

SUPPLEMENTARY MATERIAL

The Supplementary Material for this article can be found online at: https://www.frontiersin.org/articles/10.3389/fnagi.2022.806000/full#supplementary-material

Supplementary Table 1 | List of human Parkinson's disease (PD) risk genes with respective *Caenorhabditis elegans* orthologs and identified RNA interference (RNAi) phenotype.

REFERENCES

Andres-Alonso, M., Ammar, M. R., Butnaru, I., Gomes, G. M., Acuña Sanhueza, G., Raman, R., et al. (2019). SIPA1L2 controls trafficking and local signaling of TrkB-containing amphisomes at presynaptic terminals. *Nat. Commun.* 10:5448. doi: 10.1038/s41467-019-13224-z

Aoto, K., Kato, M., Akita, T., Nakashima, M., Mutoh, H., Akasaka, N., et al. (2021). ATP6V0A1 encoding the a1-subunit of the V0 domain of vacuolar H+-ATPases is essential for brain development in humans and mice. *Nat. Commun.* 12:2107. doi: 10.1038/s41467-021-22389-5

Apicco, D. J., Shlevkov, E., Nezich, C. L., Tran, D. T., Guilmette, E., Nicholatos, J. W., et al. (2021). The Parkinson's disease-associated gene ITPKB protects against α-synuclein aggregation by regulating ER-to-mitochondria calcium release. *Proc. Natl. Acad. Sci. U.S.A.* 118:e2006476118. doi: 10.1073/pnas.2006476118

Babcock, D. T., Shen, W., and Ganetzky, B. (2015). A neuroprotective function of NSF1 sustains autophagy and lysosomal trafficking in *Drosophila*. *Genetics* 199, 511–522. doi: 10.1534/genetics.114.172403

Berridge, M. J. (2016). The inositol trisphosphate/calcium signaling pathway in health and disease. *Physiol. Rev.* 96, 1261–1296. doi: 10.1152/physrev.00006.2016

Blauwendraat, C., Nalls, M. A., and Singleton, A. B. (2020). The genetic architecture of Parkinson's disease. *Lancet Neurol.* 19, 170–178.

Bonfiglio, J. J., Inda, C., Refojo, D., Holsboer, F., Arzt, E., and Silberstein, S. (2011). The corticotropin-releasing hormone network and the hypothalamic-pituitary-adrenal axis: molecular and cellular mechanisms involved. *Neuroendocrinology* 94, 12–20. doi: 10.1159/000328226

Buniello, A., MacArthur, J. A. L., Cerezo, M., Harris, L. W., Hayhurst, J., Malangone, C., et al. (2019). The NHGRI-EBI GWAS Catalog of published genome-wide association studies, targeted arrays and summary statistics 2019. *Nucleic Acids Res.* 47, D1005–D1012. doi: 10.1093/nar/gky1120

Cao, M., Park, D., Wu, Y., and Camilli, P. D. (2020). Absence of Sac2/INPP5F enhances the phenotype of a Parkinson's disease mutation of synaptojanin 1. *Proc. Natl. Acad. Sci. U.S.A.* 117, 12428–12434. doi: 10.1073/pnas.2004335117

Cao, S., Gelwix, C. C., Caldwell, K. A., and Caldwell, G. A. (2005). Torsin-mediated protection from cellular stress in the dopaminergic neurons of *Caenorhabditis elegans*. *J. Neurosci.* 25, 3801–3812. doi: 10.1523/JNEUROSCI.5157-04.2005

Chen, X., Barclay, J. W., Burgoyne, R. D., and Morgan, A. (2015). Using C. *elegans* to discover therapeutic compounds for ageing-associated neurodegenerative diseases. *Chem. Cent. J.* 9:65. doi: 10.1186/s13065-015-0143-y

Cooper, A. A., Gitler, A. D., Cashikar, A., Haynes, C. M., Hill, K. J., Bhullar, B., et al. (2006). α-Synuclein blocks ER-Golgi traffic and rab1 rescues neuron loss in Parkinson's models. *Science* 313, 324–328. doi: 10.1126/science.1129462

Cooper, J. F., and Van Raamsdonk, J. M. (2018). Modeling Parkinson's disease in C. *elegans*. *J. Parkinsons Dis.* 8, 17–32.

Cooper, J. F., Spielbauer, K. K., Senchuk, M. M., Nadarajan, S., Colaiácovo, M. P., and Van Raamsdonk, J. M. (2018). α-synuclein expression from a single copy transgene increases sensitivity to stress and accelerates neuronal loss in

genetic models of Parkinson's disease. *Exp. Neurol.* 310, 58–69. doi: 10.1016/j.expneurol.2018.09.001

De-Souza, E. A., Camara, H., Salgueiro, W. G., Moro, R. P., Knittel, T. L., Tonon, G., et al. (2019). RNA interference may result in unexpected phenotypes in Caenorhabditis elegans. *Nucleic Acids Res.* 47, 3957–3969. doi: 10.1093/nar/gkz154

Falk, J., Bonnon, C., Girault, J.-A., and Faivre-Sarrailh, C. (2002). F3/contactin, a neuronal cell adhesion molecule implicated in axogenesis and myelination. *Biol. Cell* 94, 327–334. doi: 10.1016/s0248-4900(02)00006-0

Flames, N., and Hobert, O. (2009). Gene regulatory logic of dopamine neuron differentiation. *Nature* 458, 885–889. doi: 10.1038/nature07929

Fridy, P. C., Otto, J. C., Dollins, D. E., and York, J. D. (2007). Cloning and characterization of two human VIP1-like inositol hexakisphosphate and diphosphoinositol pentakisphosphate kinases. *J. Biol. Chem.* 282, 30754–30762. doi: 10.1074/jbc.M704656200

Grenn, F. P., Kim, J. J., Makarious, M. B., Iwaki, H., Illarionova, A., Brolin, K., et al. (2020). The Parkinson's disease genome-wide association study locus browser. *Mov. Disord. Off. J. Mov. Disord. Soc.* 35, 2056–2067. doi: 10.1002/mds.28197

Hamamichi, S., Rivas, R. N., Knight, A. L., Cao, S., Caldwell, K. A., and Caldwell, G. A. (2008). Hypothesis-based RNAi screening identifies neuroprotective genes in a Parkinson's disease model. *Proc. Natl. Acad. Sci. U.S.A.* 105, 728–733. doi: 10.1073/pnas.0711018105

Han, G., Gupta, S. D., Gable, K., Niranjanakumari, S., Moitra, P., Eichler, F., et al. (2009). Identification of small subunits of mammalian serine palmitoyltransferase that confer distinct acyl-CoA substrate specificities. *Proc. Natl. Acad. Sci. U.S.A.* 106, 8186–8191. doi: 10.1073/pnas.0811269106

Hanna, M. G., Mela, I., Wang, L., Henderson, R. M., Chapman, E. R., Edwardson, J. M., et al. (2016). Sar1 GTPase activity is regulated by membrane curvature. *J. Biol. Chem.* 291, 1014–1027. doi: 10.1074/jbc.M115.672287

Hills, T., Brockie, P. J., and Maricq, A. V. (2004). Dopamine and glutamate control area-restricted search behavior in *Caenorhabditis elegans*. *J. Neurosci.* 24, 1217–1225. doi: 10.1523/JNEUROSCI.1569-03.2004

Hunn, B. H. M., Cragg, S. J., Bolam, J. P., Spillantini, M.-G., and Wade-Martins, R. (2015). Impaired intracellular trafficking defines early Parkinson's disease. *Trends Neurosci.* 38, 178–188. doi: 10.1016/j.tins.2014.12.009

Jadiya, P., Fatima, S., Baghel, T., Mir, S. S., and Nazir, A. (2016). A systematic RNAi Screen of neuroprotective genes identifies novel modulators of alpha-synuclein-associated effects in transgenic *Caenorhabditis elegans*. *Mol. Neurobiol.* 53, 6288–6300. doi: 10.1007/s12035-015-9517-3

Kalogeropulou, A. F., Freemantle, J. B., Lis, P., Vides, E. G., Polinski, N. K., and Alessi, D. R. (2020). Endogenous Rab29 does not impact basal or stimulated LRRK2 pathway activity. *Biochem. J.* 477, 4397–4423. doi: 10.1042/BCJ20200458

Kawamoto, K., Yoshida, Y., Tamaki, H., Torii, S., Shinotsuka, C., Yamashina, S., et al. (2002). GBF1, a guanine nucleotide exchange factor for ADP-ribosylation factors, is localized to the cis-Golgi and involved in membrane association of the COPI coat. *Traffic CPH Den.* 3, 483–495. doi: 10.1034/j.1600-0854.2002.30705.x

Koopman, M., Seinstra, R. I., and Nollen, E. A. A. (2019). "C. *elegans* as a model for synucleinopathies and other neurodegenerative diseases: tools and techniques," in *Alpha-Synuclein: Methods and Protocols [Internet]. (Methods in Molecular Biology)*, ed. T. Bartels (New York, NY: Springer), 93–112. doi: 10.1007/978-1-4939-9124-2_9

Kosciuk, T., Price, I. R., Zhang, X., Zhu, C., Johnson, K. N., Zhang, S., et al. (2020). NMT1 and NMT2 are lysine myristoyltransferases regulating the ARF6 GTPase cycle. *Nat. Commun.* 11:1067. doi: 10.1038/s41467-020-14893-x

Kuniyoshi, K., Takeuchi, O., Pandey, S., Satoh, T., Iwasaki, H., Akira, S., et al. (2014). Pivotal role of RNA-binding E3 ubiquitin ligase MEX3C in RIG-I–mediated antiviral innate immunity. *Proc. Natl. Acad. Sci. U.S.A.* 111, 5646–5651. doi: 10.1073/pnas.1401674111

Kuwahara, T., Koyama, A., Gengyo-Ando, K., Masuda, M., Kowa, H., Tsunoda, M., et al. (2006). Familial Parkinson mutant α-synuclein causes dopamine neuron dysfunction in transgenic *Caenorhabditis elegans**. *J. Biol. Chem.* 281, 334–340. doi: 10.1074/jbc.M504860200

Kuwahara, T., Koyama, A., Koyama, S., Yoshina, S., Ren, C.-H., Kato, T., et al. (2008). A systematic RNAi screen reveals involvement of endocytic pathway in neuronal dysfunction in α-synuclein transgenic C . *elegans*. *Hum. Mol. Genet.* 17, 2997–3009. doi: 10.1093/hmg/ddn198

Lakso, M., Vartiainen, S., Moilanen, A.-M., Sirviö, J., Thomas, J. H., Nass, R., et al. (2003). Dopaminergic neuronal loss and motor deficits in *Caenorhabditis elegans* overexpressing human α-synuclein. *J. Neurochem.* 86, 165–172. doi: 10.1046/j.1471-4159.2003.01809.x

Liang, J. R., Lingeman, E., Luong, T., Ahmed, S., Muhar, M., Nguyen, T., et al. (2020). A genome-wide ER-phagy screen highlights key roles of mitochondrial metabolism and ER-resident UFMylation. *Cell* 180, 1160–1177.e20. doi: 10.1016/j.cell.2020.02.017

Lill, C. M., Roehr, J. T., McQueen, M. B., Kavvoura, F. K., Bagade, S., Schjeide, B.-M. M., et al. (2012). Comprehensive research synopsis and systematic meta-analyses in Parkinson's disease genetics: the PDGene database. *PLoS Genet.* 8:e1002548. doi: 10.1371/journal.pgen.1002548

López-Saavedra, A., Gómez-Cabello, D., Domínguez-Sánchez, M. S., Mejías-Navarro, F., Fernández-Ávila, M. J., Dinant, C., et al. (2016). A genome-wide screening uncovers the role of CCAR2 as an antagonist of DNA end resection. *Nat. Commun.* 7:12364. doi: 10.1038/ncomms12364

Melentijevic, I., Toth, M. L., Arnold, M. L., Guasp, R. J., Harinath, G., Nguyen, K. C., et al. (2017). C. *elegans* neurons jettison protein aggregates and mitochondria under neurotoxic stress. *Nature* 542, 367–371. doi: 10.1038/nature21362

Moroianu, J., Hijikata, M., Blobel, G., and Radu, A. (1995). Mammalian karyopherin alpha 1 beta and alpha 2 beta heterodimers: alpha 1 or alpha 2 subunit binds nuclear localization signal and beta subunit interacts with peptide repeat-containing nucleoporins. *Proc. Natl. Acad. Sci. U.S.A.* 92, 6532–6536. doi: 10.1073/pnas.92.14.6532

Müller, U., Bossy, B., Venstrom, K., and Reichardt, L. F. (1995). Integrin alpha 8 beta 1 promotes attachment, cell spreading, and neurite outgrowth on fibronectin. *Mol. Biol. Cell* 6, 433–448. doi: 10.1091/mbc.6.4.433

Nakatsu, F., Messa, M., Nández, R., Czapla, H., Zou, Y., Strittmatter, S. M., et al. (2015). Sac2/INPP5F is an inositol 4-phosphatase that functions in the endocytic pathway. *J. Cell Biol.* 209, 85–95. doi: 10.1083/jcb.201409064

Nalls, M. A., Blauwendraat, C., Vallerga, C. L., Heilbron, K., Bandres-Ciga, S., Chang, D., et al. (2019). Identification of novel risk loci, causal insights, and heritable risk for Parkinson's disease: a meta-analysis of genome-wide association studies. *Lancet Neurol.* 18, 1091–1102. doi: 10.1016/S1474-4422(19)30320-5

Nalls, M. A., Pankratz, N., Lill, C. M., Do, C. B., Hernandez, D. G., Saad, M., et al. (2014). Large-scale meta-analysis of genome-wide association data identifies six new risk loci for Parkinson's disease. *Nat. Genet.* 46, 989–993. doi: 10.1038/ng.3043

Omura, D. T., Clark, D. A., Samuel, A. D. T., and Horvitz, H. R. (2012). Dopamine signaling is essential for precise rates of locomotion by C. *elegans*. *PLoS One* 7:e38649. doi: 10.1371/journal.pone.0038649

Patron, M., Granatiero, V., Espino, J., Rizzuto, R., and De Stefani, D. (2019). MICU3 is a tissue-specific enhancer of mitochondrial calcium uptake. *Cell Death Differ.* 26, 179–195. doi: 10.1038/s41418-018-0113-8

Purlyte, E., Dhekne, H. S., Sarhan, A. R., Gomez, R., Lis, P., Wightman, M., et al. (2018). Rab29 activation of the Parkinson's disease-associated LRRK2 kinase. *EMBO J.* 37, 1–18. doi: 10.15252/embj.201798099

Reczek, D., Schwake, M., Schröder, J., Hughes, H., Blanz, J., Jin, X., et al. (2007). LIMP-2 is a receptor for lysosomal mannose-6-phosphate-independent targeting of beta-glucocerebrosidase. *Cell* 131, 770–783. doi: 10.1016/j.cell.2007.10.018

Reeve, A., Simcox, E., and Turnbull, D. (2014). Ageing and Parkinson's disease: why is advancing age the biggest risk factor? *Ageing Res. Rev.* 14, 19–30. doi: 10.1016/j.arr.2014.01.004

Saha, S., Guillily, M. D., Ferree, A., Lanceta, J., Chan, D., Ghosh, J., et al. (2009). LRRK2 modulates vulnerability to mitochondrial dysfunction in *Caenorhabditis elegans*. *J. Neurosci.* 29, 9210–9218. doi: 10.1523/JNEUROSCI.2281-09.2009

Sandhof, C. A., Hoppe, S. O., Druffel-Augustin, S., Gallrein, C., Kirstein, J., Voisine, C., et al. (2020). Reducing INS-IGF1 signaling protects against non-cell autonomous vesicle rupture caused by SNCA spreading. *Autophagy* 16, 878–899. doi: 10.1080/15548627.2019.1643657

Sawin, E. R., Ranganathan, R., and Horvitz, H. R. (2000). C. *elegans* locomotory rate is modulated by the environment through a dopaminergic pathway and by

experience through a serotonergic pathway. *Neuron* 26, 619–631. doi: 10.1016/s0896-6273(00)81199-x

Simone, P. D., Pavlov, Y. I., and Borgstahl, G. E. O. (2013). ITPA (inosine triphosphate pyrophosphatase): from surveillance of nucleotide pools to human disease and pharmacogenetics. *Mutat. Res.* 753, 131–146. doi: 10.1016/j.mrrev.2013.08.001

Spillantini, M. G., Schmidt, M. L., Lee, V. M.-Y., Trojanowski, J. Q., Jakes, R., and Goedert, M. (1997). α-Synuclein in Lewy bodies. *Nature* 388, 839–840.

Steger, M., Tonelli, F., Ito, G., Davies, P., Trost, M., Vetter, M., et al. (2016). Phosphoproteomics reveals that Parkinson's disease kinase LRRK2 regulates a subset of Rab GTPases. *eLife* 5:e12813. doi: 10.7554/eLife.12813

van Ham, T. J., Thijssen, K. L., Breitling, R., Hofstra, R. M. W., Plasterk, R. H. A., and Nollen, E. A. A. (2008). C. *elegans* model identifies genetic modifiers of α-Synuclein inclusion formation during aging. *PLoS Genet.* 4:e1000027. doi: 10.1371/journal.pgen.1000027

Vidal-Gadea, A., Topper, S., Young, L., Crisp, A., Kressin, L., Elbel, E., et al. (2011). Caenorhabditis elegans selects distinct crawling and swimming gaits via dopamine and serotonin. *Proc. Natl. Acad. Sci. U.S.A.* 108, 17504–17509. doi: 10.1073/pnas.1108673108

Wang, Y., and Südhof, T. C. (2003). Genomic definition of RIM proteins: evolutionary amplification of a family of synaptic regulatory proteins. *Genomics* 81, 126–137. doi: 10.1016/s0888-7543(02)00024-1

Welsby, P. J., Wang, H., Wolfe, J. T., Colbran, R. J., Johnson, M. L., and Barrett, P. Q. (2003). A mechanism for the direct regulation of T-type calcium channels by Ca2+/Calmodulin-dependent kinase II. *J. Neurosci.* 23, 10116–10121. doi: 10.1523/JNEUROSCI.23-31-10116.2003

Wendeler, M. W., Paccaud, J.-P., and Hauri, H.-P. (2007). Role of Sec24 isoforms in selective export of membrane proteins from the endoplasmic reticulum. *EMBO Rep.* 8, 258–264. doi: 10.1038/sj.embor.7400893

Wong, Y. C., and Krainc, D. (2017). α-synuclein toxicity in neurodegeneration: mechanism and therapeutic strategies. *Nat. Med.* 23, 1–13. doi: 10.1038/nm.4269

Yao, C., El Khoury, R., Wang, W., Byrd, T. A., Pehek, E. A., Thacker, C., et al. (2010). LRRK2-mediated neurodegeneration and dysfunction of dopaminergic neurons in a *Caenorhabditis elegans* model of Parkinson's disease. *Neurobiol. Dis.* 40, 73–81. doi: 10.1016/j.nbd.2010.04.002

Zhao, C., Slevin, J. T., and Whiteheart, S. W. (2007). Cellular functions of NSF: not just SNAPs and SNAREs. *FEBS Lett.* 581, 2140–2149. doi: 10.1016/j.febslet.2007.03.032

Conflict of Interest: The authors declare that the research was conducted in the absence of any commercial or financial relationships that could be construed as a potential conflict of interest.

Publisher's Note: All claims expressed in this article are solely those of the authors and do not necessarily represent those of their affiliated organizations, or those of the publisher, the editors and the reviewers. Any product that may be evaluated in this article, or claim that may be made by its manufacturer, is not guaranteed or endorsed by the publisher.

Frontiers in
Aging Neuroscience

Explores the mechanisms of central nervous system aging and age-related neural disease

The third most-cited journal in the field of geriatrics and gerontology, with a focus on understanding the mechanistic processes associated with central nervous system aging.

Discover the latest Research Topics

See more →

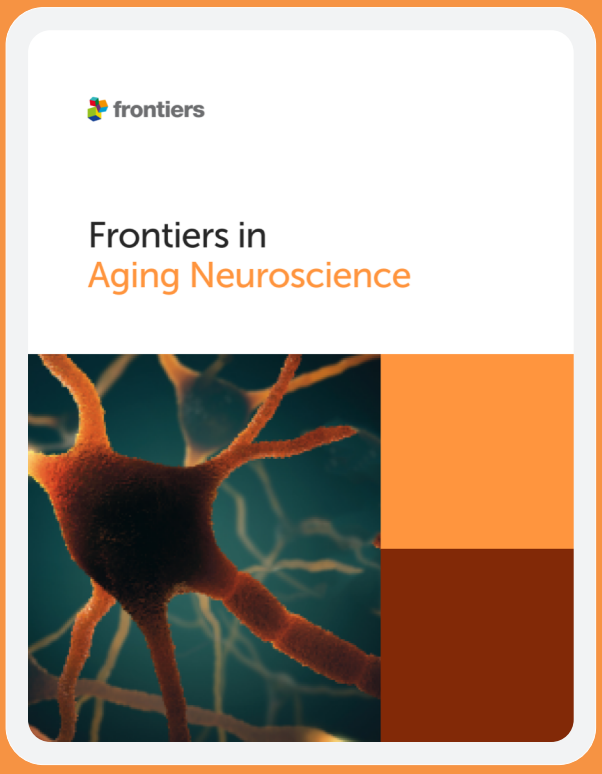

Frontiers

Avenue du Tribunal-Fédéral 34
1005 Lausanne, Switzerland
frontiersin.org

Contact us

+41 (0)21 510 17 00
frontiersin.org/about/contact